ENGINEERING CHANGE NOTICE

Page 1 of 2

1. ECN 659093

Proj. ECN

2. ECN Category (mark one)	3. Originator's Name, Organization, MSIN, and Telephone No.	4. USQ Required?	5. Date
Supplemental ○ Direct Revision ◉ Change ECN ○ Temporary ○ Standby ○ Supersedure ○ Cancel/Void ○	W.L.Cowley, Safety Analysis, R1-44, 376-4567	○ Yes ◉ No	6/20/2000
	6. Project Title/No./Work Order No.: Organic Solvent Safety Issue Resolution	7. Bldg./Sys./Fac. No.: NA	8. Approval Designator: NA
	9. Document Numbers Changed by this ECN (includes sheet no. and rev.): HNF-4240, Rev. 0	10. Related ECN No(s).: NA	11. Related PO No.: NA

12a. Modification Work	12b. Work Package No.	12c. Modification Work Completed	12d. Restored to Original Condition (Temp. or Standby ECNs only)
○ Yes (fill out Blk. 12b) ◉ No (NA Blks. 12b, 12c, 12d)	NA	NA Design Authority/Cog. Engineer Signature & Date	NA Design Authority/Cog. Engineer Signature & Date

13a. Description of Change

13b. Design Baseline Document? ○ Yes ◉ No

Added descriptive narrative to pages 2-1 and 5-29 to close comments from Oregon State ~~Deapstment~~ Department of Ecology. Reprinted entire document and issued as Rev. 1.

14a. Justification (mark one)	14b. Justification Details
Criteria Change ●	
Design Improvement ○	
Environmental ○	
Facility Deactivation ○	
As-Found ○	
Facilitate Const. ○	
Const. Error/Omission ○	
Design Error/Omission ○	

15. Distribution (include name, MSIN, and no. of copies)

See Attached Distribution

RELEASE STAMP

DATE: HANFORD RELEASE ID: 2

STA. 4

JUN 21 2000

ENGINEERING CHANGE NOTICE

Page 2 of 2

1. ECN (use no. from pg. 1): 659093

16. Design Verification Required	17. Cost Impact		18. Schedule Impact (days)
	ENGINEERING	CONSTRUCTION	
○ Yes	Additional ○ $	Additional ○ $	Improvement ○
◉ No	Savings ○ $	Savings ○ $	Delay ○

19. Change Impact Review: Indicate the related documents (other than the engineering documents identified on Side 1) that will be affected by the change described in Block 13. Enter the affected document number in Block 20.

SDD/DD	☐	Seismic/Stress Analysis	☐	Tank Calibration Manual	☐
Functional Design Criteria	☐	Stress/Design Report	☐	Health Physics Procedure	☐
Operating Specification	☐	Interface Control Drawing	☐	Spares Multiple Unit Listing	☐
Criticality Specification	☐	Calibration Procedure	☐	Test Procedures/Specification	☐
Conceptual Design Report	☐	Installation Procedure	☐	Component Index	☐
Equipment Spec.	☐	Maintenance Procedure	☐	ASME Coded Item	☐
Const. Spec.	☐	Engineering Procedure	☐	Human Factor Consideration	☐
Procurement Spec.	☐	Operating Instruction	☐	Computer Software	☐
Vendor Information	☐	Operating Procedure	☐	Electric Circuit Schedule	☐
OM Manual	☐	Operational Safety Requirement	☐	ICRS Procedure	☐
FSAR/SAR	☐	IEFD Drawing	☐	Process Control Manual/Plan	☐
Safety Equipment List	☐	Cell Arrangement Drawing	☐	Process Flow Chart	☐
Radiation Work Permit	☐	Essential Material Specification	☐	Purchase Requisition	☐
Environmental Impact Statement	☐	Fac. Proc. Samp. Schedule	☐	Tickler File	☐
Environmental Report	☐	Inspection Plan	☐		☐
Environmental Permit	☐	Inventory Adjustment Request	☐		☐

20. Other Affected Documents: (NOTE: Documents listed below will not be revised by this ECN.) Signatures below indicate that the signing organization has been notified of other affected documents listed below.

Document Number/Revision	Document Number/Revision	Document Number/Revision
N/A		

21. Approvals

	Signature	Date		Signature	Date
Design Authority			Design Agent		
Cog. Eng.	W. L. Cowley W. L. Cowley	6-21-00	PE		
Cog. Mgr.	R. J. Cash R. J. Cash	6-21-00	QA		
QA			Safety		
Safety			Design		
Environ.			Environ.		
Other	J. E. Meacham J. E. Meacham	6/21/00	Other		

DEPARTMENT OF ENERGY

Signature or a Control Number that tracks the Approval Signature

ADDITIONAL

DISTRIBUTION SHEET

To	From	Page 1 of 1
Distribution	Safety Analysis	Date 6/20/2000
Project Title/Work Order		EDT No. 659093
HNF-4240, Rev. 1, Organic Solvent Topial Report		ECN No.

Name	MSIN	Text With All Attach.	Text Only	Attach./ Appendix Only	EDT/ECN Only
CH2M HILL Hanford Group, Inc.					
R. J. Cash	R1-44	x			
W. L. Cowley	R1-44	5			
J. M. Grigsby	R1-44	x			
J. E. Meacham	R1-49	x			
D. A. Reynolds	R2-11	x			
K. R. Sandgren	R1-49	x			
Fluor Federal Services					
G. W. Ryan	B4-47	x			
R. M. Marusich	B4-47	x			
G&P Consultants					
A. K. Postma		x			
Office of River Protection					
D. H. Irby (advance)	H6-60	x			
Y. G. Noorani (advance)	H6-60	3			
Lockheed Martin Servides, Inc.					
Central Files	B1-07	x			

A-6000-135 (10/97)

S

HNF-4240
Revision 1

Organic Solvent Topical Report

W. L. Cowley
J. E. Meacham
CH2M HILL Hanford Group, Inc.

J. M. Grigsby
A. K. Postma
G&P Consulting

Date Published
June 2000

Prepared for the U.S. Department of Energy
Assistant Secretary for Environmental Management

CH2MHILL
Hanford Group, Inc.

P.O. Box 1500
Richland, Washington

Hanford Management and Integration Contractor for the
U.S. Department of Energy under Contract DE-AC09-96RL14047

Approved for Public Release; Further Dissemination Unlimited

LEGAL DISCLAIMER

This report was prepared as an account of work sponsored by an agency of the United States Government. Neither the United States Government nor any agency thereof, nor any of their employees, nor any of their contractors, subcontractors or their employees, makes any warranty, express or implied, or assumes any legal liability or responsibility for the accuracy, completeness, or any third party's use or the results of such use of any information, apparatus, product, or process disclosed, or represents that its use would not infringe privately owned rights. Reference herein to any specific commercial product, process, or service by trade name, trademark, manufacturer, or otherwise, does not necessarily constitute or imply its endorsement, recommendation, or favoring by the United States Government or any agency thereof or its contractors or subcontractors. The views and opinions of authors expressed herein do not necessarily state or reflect those of the United States Government or any agency thereof.

This report has been reproduced from the best available copy. Available in paper copy and microfiche.

Available electronically at
http://www.doe.gov/bridge. Available for a processing fee to the U.S. Department of Energy and its contractors, in paper, from:
U.S. Department of Energy
Office of Scientific and Technical Information
P.O. Box 62
Oak Ridge, TN 37831-0062
phone: 865-576-8401
fax: 865-576-5728
email: reports@adonis.osti.gov(423) 576-8401

Available for sale to the public, in paper, from:
U.S. Department of Commerce
National Technical Information Service
5285 Port Royal Road
Springfield, VA 22161
Phone: 800-553-6847
fax: 703-605-6900
email: orders@ ntis.fedworld.gov
online ordering:
http://www.ntis.gov/ordering.htm

Printed in the United States of America

Organic Solvent Topical Report

W.L. Cowley & J.E. Meacham, CH2MHill Hanford Group, Inc.
J.M. Grigsby & A.K. Postma, G&P Consulting
Richland, WA 99352
U.S. Department of Energy Contract DE-AC06-96RL13200

EDT/ECN: 659093 UC: N/A
Org Code: 74F00 Charge Code: 101937
B&R Code: EW3120074 Total Pages: 670

Key Words: Organic Solvent, Solvent Fire, Pool Fire

Abstract: This report provides the basis for closing the organic solvent safety issue. Sufficient information is presented to conclude that risk posed by an unmitigated organic solvent fire is within risk evaluation guidelines.

TRADEMARK DISCLAIMER. Reference herein to any specific commercial product, process, or service by trade name, trademark, manufacturer, or otherwise, does not necessarily constitute or imply its endorsement, recommendation, or favoring by the United States Government or any agency thereof or its contractors or subcontractors.

Printed in the United States of America. To obtain copies of this document, contact: Document Control Services, P.O. Box 950, Mailstop H6-08, Richland WA 99352, Phone (509) 372-2420; Fax (509) 376-4989.

Release Approval 6/21/00 Date

DATE: HANFORD RELEASE ID:
STA. 4 2.
JUN 21 2000
Release Stamp

Approved For Public Release

RECORD OF REVISION

(1) Document Number: HNF-4240

Page 1

(2) Title: Organic Solvent Topical Report

Change Control Record

(3) Revision	(4) Description of Change - Replace, Add, and Delete Pages	Authorized for Release (5) Cog. Engr.	(6) Cog. Mgr. Date
0	(7) Initial Issue of complete document, EDT 625112	Y.G.Noorani	G.W.Gault
1 RS	Added descriptive material to resolve comments from Oregon State Department of Ecology.		
	Reprinted entire document and issued. ECN659093	W.L. Cowley	R.J. Cash 6/12/00

A-7320-005 (10/97)

HNF-4240
Revision 1

Organic Solvent Topical Report

W. L. Cowley
J. E. Meacham
CH2M HILL Hanford Group, Inc.

J. M. Grigsby
A. K. Postma
G&P Consulting

Date Published
June 2000

Prepared for the U.S. Department of Energy
Assistant Secretary for Environmental Management

CH2MHILL
Hanford Group, Inc.

P.O. Box 1500
Richland, Washington

Hanford Management and Integration Contractor for the
U.S. Department of Energy under Contract DE-AC09-96RL14047

Approved for Public Release; Further Dissemination Unlimited

LEGAL DISCLAIMER

This report was prepared as an account of work sponsored by an agency of the United States Government. Neither the United States Government nor any agency thereof, nor any of their employees, nor any of their contractors, subcontractors or their employees, makes any warranty, express or implied, or assumes any legal liability or responsibility for the accuracy, completeness, or any third party's use or the results of such use of any information, apparatus, product, or process disclosed, or represents that its use would not infringe privately owned rights. Reference herein to any specific commercial product, process, or service by trade name, trademark, manufacturer, or otherwise, does not necessarily constitute or imply its endorsement, recommendation, or favoring by the United States Government or any agency thereof or its contractors or subcontractors. The views and opinions of authors expressed herein do not necessarily state or reflect those of the United States Government or any agency thereof.

This report has been reproduced from the best available copy. Available in paper copy and microfiche.

Available electronically at
http://www.doe.gov/bridge. Available for a processing fee to the U.S. Department of Energy and its contractors, in paper, from:
U.S. Department of Energy
Office of Scientific and Technical Information
P.O. Box 62
Oak Ridge, TN 37831-0062
phone: 865-576-8401
fax: 865-576-5728
email: reports@adonis.osti.gov(423) 576-8401

Available for sale to the public, in paper, from:
U.S. Department of Commerce
National Technical Information Service
5285 Port Royal Road
Springfield, VA 22161
Phone: 800-553-6847
fax: 703-605-6900
email: orders@ ntis.fedworld.gov
online ordering:
http://www.ntis.gov/ordering.htm

Printed in the United States of America

CONTENTS

1.0 SUMMARY AND CONCLUSIONS 1-1
1.1 SUMMARY HAZARD DESCRIPTION 1-2
1.2 SUMMARY OF ACCIDENT ANALYSIS 1-3
1.3 CONCLUSIONS 1-10
1.3.1 Removal of Tanks 241-C-102 and 241-C-103 from Watch List 1-10
1.3.2 General Conclusions 1-10

2.0 BACKGROUND 2-1
2.1 APPROACH TO RESOLUTION OF THE ORGANIC SOLVENT SAFETY ISSUE . . 2-2
2.2 SOLVENT STREAMS 2-2
2.2.1 Reduction and Oxidation Solvents 2-3
2.2.2 Uranium Recovery Process Solvents 2-3
2.2.3 B Plant Waste Fractionation Process Solvents 2-4
2.2.4 PUREX Process Solvents 2-5
2.3 CHEMICAL AGING OF PROCESS SOLVENTS AND THEIR DEGRADATION PRODUCTS 2-11
2.3.1 Aging of Tributyl Phosphate 2-13
2.3.2 Aging of Normal Paraffin Hydrocarbon 2-13
2.3.3 Aging of Hexone 2-14
2.3.4 Evidence from the Organic Layer of Tank 241-C-103 . . . 2-14
2.3.5 Chemical and Radiological Aging Studies 2-15
2.4 SUMMARY REGARDING SOURCES AND FATE OF HANFORD PROCESS SOLVENTS 2-15
2.4.1 Hexone (Reduction and Oxidation Solvent) 2-15
2.4.2 Uranium Recovery Process Solvents 2-16
2.4.3 B Plant Waste Fractionization Process Solvents 2-16
2.4.4 PUREX Process Solvents 2-16

3.0 HAZARD AND ACCIDENT PHENOMENA 3-1
3.1 DEFLAGRATION IN HEADSPACE AIR 3-1
3.1.1 Key Phenomena 3-2
3.1.2 Calculation of Vapor Contribution to Headspace Flammability 3-3
3.1.3 Conclusion Regarding Solvent Contribution to Headspace Flammability 3-5
3.2 ORGANIC-NITRATE/NITRITE REACTIONS 3-7
3.2.1 Solvent and Solvent Degradation Product Condensed-Phase Reactions with Nitrate/Nitrite 3-8
3.2.2 Solvent Addition to Waste Organic Fuel Value 3-10
3.2.3 Solvent Fire Transition to Condensed-Phase Combustion . 3-10
3.3 COMBUSTION OF ORGANIC LIQUID AS A POOL FIRE 3-10

4.0 PHENOMENOLOGY OF SOLVENT FIRE IGNITION 4-1
4.1 IGNITABILITY OF ORGANIC SOLVENT POOLS, PUDDLES, AND CHANNELS . 4-1
4.1.1 Organic Liquid Pools or Larger Puddles 4-2
4.1.2 Small Solvent Puddles 4-3
4.1.3 Solvent-Filled Channels 4-4
4.2 ORGANIC LIQUIDS ENTRAINED IN WASTE SOLIDS 4-5
4.2.1 Organic Liquid Entrained in Sludge 4-5
4.2.2 Organic Liquid Embedded in Saltcake 4-6

CONTENTS (Continued)

4.3 SMALL SOLVENT FIRES IN ACTIVELY VENTILATED TANKS OR AT MULTIPLE LOCATIONS 4-7
4.3.1 Small Solvent Fires in Actively Ventilated Tanks 4-7
4.3.2 Ignition at Multiple Locations 4-8
4.4 CONCLUSIONS 4-9

5.0 SOLVENT FIRE ACCIDENT PHENOMENA 5-1
5.1 SOLVENT FIRE SEQUENCES CONSIDERED 5-1
5.2 SUMMARY OF SOLVENT FIRE PHENOMENOLOGY 5-2
5.2.1 Ignition 5-2
5.2.2 Fire Spread Rate 5-4
5.2.3 Liquid Burn Rate 5-7
5.2.4 Extinguishment of Pool Fires at Oxygen Flammability Limit 5-8
5.2.5 Heat of Combustion 5-9
5.3 THERMAL HYDRAULIC MODELING OF CONFINED SOLVENT POOL FIRES . . . 5-10
5.3.1 Nodalization of POOLFIRE.4 5-10
5.3.2 Combustion Energy 5-12
5.3.3 Heat Transfer Rate from Gas to Surfaces 5-14
5.3.4 Gas Venting Rate Under Pressure 5-17
5.4 SENSITIVITY ANALYSIS FOR THERMAL HYDRAULIC RESULTS 5-22
5.4.1 Base Case Solvent Fire Parameters 5-22
5.4.2 Effect of Initial Inflamed Area 5-24
5.4.3 Effect of Flame Spread Rate 5-24
5.4.4 Effect of Solvent Pool Area 5-25
5.4.5 Effect of Leak Path Flow Capacity 5-26
5.4.6 Effect of Gas Emissivity 5-26
5.4.7 Effect of Heat Transfer Flux from Flame to Burning Solvent Surface 5-27
5.4.8 Effect of Oxygen Extinguishment Level 5-27
5.4.9 Effect of Combustion Energy of Organic Liquid 5-28
5.4.10 Conclusions from Thermal Hydraulic Sensitivity Analysis 5-29
5.5 PARAMETRIC ANALYSIS OF FIRE PRESSURIZATION 5-29
5.5.1 Methodology 5-29
5.5.2 Solvent Fire Peak Pressures 5-30
5.5.3 Post-Fire Peak Vacuums 5-32

6.0 PHENOMENA AND MODELING OF THE RELEASE OF RADIOACTIVE AND TOXICOLOGICAL MATERIAL DUE TO SOLVENT FIRES 6-1
6.1 KEY ASSUMPTIONS 6-1
6.1.1 Ignition and Flame Spread 6-1
6.1.2 Solvent Pool Area 6-1
6.1.3 Fire Extinguishment 6-1
6.1.4 Tank Parameters 6-2
6.1.5 Tank Structural Integrity 6-2
6.1.6 Carryover of Contaminants with Vented Gas 6-2

CONTENTS (Continued)

6.2 RELEASE OF CONTAMINANTS FROM TANK 6-2
6.2.1 Solvent Smoke 6-4
6.2.2 Headspace Gases 6-5
6.2.3 Aqueous Boiloff 6-5
6.3 RADIOLOGICAL DOSE CONSEQUENCES OF RELEASED CONTAMINATES 6-6
6.4 TOXICOLOGICAL CONSEQUENCES OF RELEASED CONTAMINANTS 6-7

7.0 FREQUENCY OF SOLVENT FIRES 7-1
7.1 SOLVENT FIRE IGNITION FREQUENCIES ON A PER-TANK BASIS 7-1
7.1.1 Electrostatic Sparks 7-5
7.1.2 In-tank Instrumentation (Instrument Faults) 7-5
7.1.3 Welding and Grinding 7-5
7.1.4 Torch Cutting 7-6
7.1.5 Still Camera Photography and Video Camera Operations . . 7-10
7.1.6 Vehicle Fuel Fires 7-11
7.1.7 Lightning Strikes 7-11
7.1.8 Core Sampling 7-15
7.2 NUMBER OF TANKS CONTAINING COMBUSTIBLE SOLVENT 7-17
7.3 POSSIBLE SOLVENT CONFIGURATIONS FOR SINGLE-SHELL, DOUBLE-SHELL, AND DOUBLE-CONTAINED RECEIVER TANKS 7-21
7.4 SOLVENT FIRE ACCIDENT FREQUENCY CATEGORY 7-22

8.0 KEY INPUT DATA FOR CONSEQUENCE CALCULATIONS 8-1
8.1 RADIOLOGICAL DATA 8-1
8.2 TOXICOLOGICAL DATA 8-2
8.2.1 Headspace Gases 8-2
8.2.2 Fire Reaction Products 8-3
8.2.3 Total Particulates 8-4
8.2.4 High-Efficiency Particulate Air Filter Rupture Toxins . 8-4

9.0 SPREADSHEET CALCULATIONS 9-1
9.1 WORKSHEET 1 FINAL SAFETY ANALYSIS REPORT SOLVENT POOL FIRE CASES 9-1
9.2 WORKSHEET 2 DOSE SUMMARY 9-5
9.3 WORKSHEET 3 TOXICOLOGICAL 9-10

10.0 REFERENCES 10-1

APPENDICES

A SCREENING METHODOLOGY FOR SOLVENT FIRE RISK IN WASTE TANKS AT THE HANFORD SITE A-1

B IMPACT OF TURBULENT MIXING OF VENTED GASES ON CALCULATED TOXICOLOGICAL CONSEQUENCES OF SOLVENT POOL FIRES B-1

C SOURCE TERM MITIGATION BY AEROSOL SEDIMENTATION IN POSTULATED SOLVENT POOL FIRES C-1

D FLAMMABILITY OF PUREX SOLVENT VAPOR D-1

CONTENTS (Continued)

E SUMMARY OF LABORATORY SCOPING TESTS RELATED TO ORGANIC SOLVENTS COMBUSTION BY NITRATE OXIDATION AND ORGANIC SOLVENT IGNITABILITY . . E-1

F POWER REQUIRED TO IGNITE A SUSTAINABLE POOL F-1

G FAI/95-17 IGNITABILITY OF ORGANIC SOLVENT IN HANFORD TANK C-103 FOLLOWING INTERIM STABILIZATION G-1

H ANALYSIS OF CONSEQUENCES OF SMALL SOLVENT POOL FIRES IN ACTIVELY VENTILATED WASTE TANKS H-1

I DESCRIPTION OF POOLFIRE.4 . . . . . I-1

J IMPACT OF MULTIPOINT IGNITION ON PREDICTED POOL FIRE CONSEQUENCES . J-1

K SUPPORTING CALCULATIONS FOR SECTION 9.0 . . . . . K-1

L THE AGING OF ORGANIC SOLVENTS L-3

LIST OF FIGURES

3-1. Predicted Percent Lower Flammability Limit of Solvent Vapors in a Passively Ventilated Single-Shell Tank 3-6

5-1. Schematic of Waste Configuration Analyzed 5-3

5-2. Flame Propagation Rate 5-5

5-3. Schematic of POOLFIRE.4 Model 5-11

5-4. Tank Pressurization Predicted for Base Case Solvent Fire 5-23

9-1. Final Safety Analysis Report Solvent Pool Fire Cases 9-2

9-2. Dose Summary Worksheet 9-6

9-3. Toxicological Worksheet 9-11

LIST OF TABLES

1-1. Summary of Consequences and Frequencies of Organic Solvent Fires Without Controls (Unmitigated) 1-9

2-1. Boiling Points of Some Organic Compounds in Tank Wastes 2-4

2-2. Waste Transfers from Anderson (1990) 2-8

2-3. Properties of Shell E-2342, Soltrol-170, and NPH 2-9

2-4. Waste Transfers from Brevick 2-10

2-5. Organic Chemical Constituents of Hanford Single-Shell Tanks Waste Process Solvents 2-12

3-1. Effect of Ventilation Rate on the Predicted Contribution of Solvent Vapor to Flammability For a 1-m^2 Pool and a Headspace Air Temperature of 30 °C 3-4

3-2. Effect of Pool Area on the Predicted Contribution of Solvent Vapor to Flammability at a Headspace Temperature of 30 °C 3-4

3-3. Solvent-Nitrate Combustion Test Results. 3-9

4-1. Results of Sludge Burning Tests 4-5

LIST OF TABLES (Continued)

5-1. Flow Characteristics of Tank 241-C-103 Vent Pipes 5-20

5-2. Vent Flow Rates Calculated for a Tank Pressure of 96.5 kPa (14 psig) 5-21

5-3. Key Parameters for Base Case Solvent Fire 5-22

5-4. Effect of Initial Inflamed Area on Peak Pressure 5-24

5-5. Effect of Flame Spread Velocity on Calculated Peak Pressure . . . 5-24

5-6. Effect of Pool Area on Calculated Peak Pressure 5-25

5-7. Effect of Leak Path Flow Resistance on Calculated Peak Pressure 5-26

5-8. Effect of Emissivity on Calculated Peak Pressure 5-26

5-9. Effect of Flame-Pool Heat Transfer Rate on Predicted Peak Pressure 5-27

5-10. Effect of Oxygen Extinguishment Levels on Calculated Peak Pressure 5-28

5-11. Effect of Combustion Energy on Calculated Peak Pressure 5-28

5-12. Tank Parameters for Parametric Analysis 5-30

5-13. Peak Pressure Predicted for 0.1 cm/s Fire Spread Velocity 5-31

5-14. Peak Pressure Predicted for 1 cm/s Fire Spread Velocity 5-31

5-15. Peak Pressure Predicted for 10 cm/s Fire Spread Velocity 5-32

5-16. Calculated Peak Vacuum for Fire Spread Velocity of 0.1 cm/s . . . 5-33

5-17. Calculated Peak Vacuum for Fire Spread Velocity of 1.0 cm/s . . . 5-33

5-18. Calculated Peak Vacuums for Fire Spread Velocity of 10 cm/s . . . 5-34

7-1. Energy Source Frequencies 7-2

7-2. Solvent Fire Frequencies for Various Organic Solvent Configurations 7-3

7-3. Number of Tanks That May Contain Combustible Solvent 7-18

7-4. Solvent Fire Accident Frequency Categories 7-22

LIST OF TABLES (Continued)

8-1. Radiological Input Data 8-1

8-2. Headspace Gas Data. 8-2

8-3. Reaction Product Toxin Limits. 8-3

8-4. Sum of Fraction Multipliers. 8-4

LIST OF TERMS

AIT	autoignition temperature
AlDBP	aluminum dibutyl phosphate
ARF	aerosol release fraction
AWF	aging waste facility
BIO	Basis for Interim Operation
bp	boiling point
cm	centimeters
cm/s	centimeters per second
DBP	dibutyl phosphate
DCRT	double contained receiver tank
DST	double-shell tank
DTP	dedicated tube propagation
EDTA	ethylenediaminetetraacetic acid
ERPG	emergency response planning guideline
FSAR	final safety analysis report
ft	feet
ft/lb	feet per pound
ft^2	square feet
ft^3/m	cubic feet per minute
ft^3/h	cubic feet per hour
ft^3	cubic feet
FY	fiscal year
g/m^2	grams per square meter
g/L	grams per liter
g/m^3	grams per cubic meter
g/mL	grams per milliliter
g/s	grams per second
g	grams
gal	gallons
HEDTA	N-(hydroxyethyl)-ethylenediaminetriacetic acid
HEPA	high-efficiency particulate air (filter)
HLW	high-level waste
J/g	joules per gram
J	joules
J/kg	joules per kilogram
J/s	joules per second
$kg/min/m^2$	kilograms per minute per square meter
$kg/m^2/min$	kilograms per square meter per minute
kg/s	kilograms per second
kg	kilograms
kgal	kilogallons
kJ	kilojoules
kL	kiloliters
kN	kiloNewtons
kPa	kilopascals
kW/m^2	kilowatts per square meter
$kW/m^2/s$	kilowatts per square meter per second
kW/h	kilowatts per hour
L	liter
lb/in^2	pounds per square inch

LIST OF TERMS (Continued)

lb	pound
lbf	pounds force
LFL	lower flammability limit
LPF	leak path factor
m	meter
m/hr	meters per hour
m/s	meters per second
M	moles per liter
m^2	square meters
m^2/h	square meters per hour
m^2/s	square meters per second
m^3/min	cubic meters per minute
m^3	cubic meters
m^3/sL	cubic meters per second-liter
m^3/hr	cubic meters per hour
m^3/s	cubic meters per second
m^3/min	cubic meters per minute
m^3/hr	cubic meters per hour
max.	maximum
MBP	monobutyl phosphate
MeV	mega-electronvolt
mg/m^3	milligrams per cubic meter
mg/s	milligrams per second
mg/L/h	milligrams per liter per hour
MGy	megagray
min	minute
min.	minimum
MJ/kg	megajoules per kilogram
mL	milliliter
mm	millimeters
$moles/m^3$	moles per cubic meter
moles/s	moles per second
Mrad	megarad
MW	megawatts
NPH	normal paraffin hydrocarbon
OWW	organic wash waste
PEL-TWA	permissible exposure limits-time weighted average
PFP	Plutonium Finishing Plant
PNNL	Pacific Northwest National Laboratory
ppm	parts per million
PR	pressure ratio
psig	pounds per square inch gauge
PUREX	plutonium uranium reduction and extraction
RAG	risk acceptance guideline
REDOX	reduction and oxidation
REG	risk evaluation guideline
RF	respirable fraction
RSST	Reactive Systems Screening Test
s/L	seconds per liter
s/m^3	seconds per cubic meter

LIST OF TERMS (Continued)

s	seconds
scfm	standard cubic feet per minute
sec	second
SpG	specific gravity
SST	single-shell tank
Sv	Sieverts
Sv/kg	Sieverts per kilogram
Sv/L	Sieverts per liter
Svm^3/sL	Sievert cubic meters per second liter
TBP	tributyl phosphate
TOC	total organic carbon
TP	tube propagation
TWRS	Tank Waste Remediation System
ULD	unit liter dose
vol%	volume percent
W/m^2	watts per square meter
W/m	watts per meter
wt%	weight percent
°C	degrees Celsius
°F	degrees Fahrenheit
°K	degrees Kelvin
%	percent
μg	micrograms
μm	micrometers

1.0 SUMMARY AND CONCLUSIONS

This report provides the basis for closing the organic solvent safety issue. Sufficient information is presented to conclude that risk posed by an organic solvent fire is within risk evaluation guidelines. This report updates information contained in *Analysis of Consequences of Postulated Solvent Fires in Hanford Site Waste Tanks*, WHC-SD-WM-CN-032, Rev. 0A, (Cowley et al. 1996). However, this document will not replace Cowley et al. (1996) as the primary reference for the Basis for Interim Operation (BIO) until the recently submitted BIO amendment (Hanson 1999) is approved by the U.S. Department of Energy.

This conclusion is valid for all accident scenarios and does not require use of any controls. This is a significant change from the conclusions presented in Cowley et al. (1996). That calcnote concluded that some organic solvent fire scenarios exceeded risk evaluation guidelines, even with controls imposed.

The conclusions in this report (HNF-4240) differ from Cowley et al. (1996) because the following additional evaluations were performed.

- Cowley et al. (1996) did not include a jet mixing model; this report does. This model applied to the calculation of toxic consequences, but not to the calculation of radiological consequences. The jet mixing model, which is explained in Appendix B, accounts for the effect of turbulent mixing caused by the velocity of the gas stream exiting the tank during a fire. The turbulent mixing dilutes the concentration of toxic substances in the gas stream exiting the tank. Toxicological consequences are based on the peak concentration of toxic substances during the release. Therefore the mixing will affect the calculation of toxicological consequences, because the peak concentration calculated will be different (in this case lower) than the consequences calculated not using a mixing model. The model was not applied to the calculation of radiological consequences because radiological consequences are based on the total mass of material released from the tank, not the concentration. The jet mixing model describes the release concentrations but not the total mass released.

- Cowley et al. (1996) did not include an aerosol retention model; this report does. The model is applied to the calculation of radiological consequences, but not to the calculation of toxicological consequences. Appendix C, "Source Term Mitigation by Aerosol Sedimentation in Postulated Solvent Pool Fires," presents the aerosol retention model and the results of an analysis of aerosol retention in waste tanks. Aerosol retention within a tank is important because it is a naturally-occurring mechanism for mitigating calculated consequences of postulated fire accidents. The retention of aerosols within the tank reduces the total mass of radionuclides released and therefore reduces the radiological consequences of a fire. The aerosol retention model could also be applied to calculation of toxicological consequences. However it

was not, because the toxicological consequences calculated using the jet mixing model were bounding and resulted in toxicological consequences which were less than risk evaluation guidelines.

- This report also contains significant changes in the calculation of both consequences and probability of occurrence for the entrained fire accident. Data included in DOE handbook DOE-HDBK-3010-94, *Airborne Release Fractions/Rates and Respirable Fractions for Nonreactor Nuclear Facilities*, *Volume*, *1*, *Analysis of Experimental Data* and ANSI/ANS-5.10-1998, *Airborne Release Fractions at Nonreactor Nuclear Facilities*, form a basis for changing the Respirable Fraction (RF) used in consequence calculations for entrained fires from 1.0 to 0.5. The consequences for the entrained fire accident presented in Cowley et al. (1996) used an RF of 1.0. The probability of occurrence has been adjusted to account for the fact that the entire surface area of the tanks is not saturated with solvent and that the TBP/NPH mixture in the tanks is much more difficult to ignite than the pure dodecane and pure kerosene used in laboratory ignition tests.

This report contains the technical basis for updating the Tank Waste Remediation System (TWRS) safety analysis for organic solvent fires and supports closure of the organic solvent safety issue. It includes the following:

- descriptions of the calculation methods used to analyze postulated solvent pool fires in Hanford Site Waste Tanks
- specific scientific and engineering information on the nature of the separable-phase organic hazards and the phenomena used to evaluate them
- conservative, deterministic analysis of postulated solvent fire accidents including bounding cases for radiological release and toxicological exposures.

1.1 SUMMARY HAZARD DESCRIPTION

The solvents studied in this report were used in the plutonium uranium reduction and extraction (PUREX) process. The solvents are composed of a mixture of hydrocarbons, typified by alkanes C_{12} to C_{14} and tributyl phosphate (TBP). Because the flash point of the solvents is appreciably higher than the waste temperature, solvent vapors contribute only slightly to headspace flammability. Also, because ignition of a pool fire requires significant heatup of stored solvent, a high-energy ignitor would be required to initiate a pool fire. Because high-energy ignitors are not likely to be introduced into waste tanks, solvent pool fires are low probability accidents.

This report applies to Hanford Site single-shell tanks (SSTs), double-shell tanks (DSTs), and double-contained receiver tanks (DCRTs). Section 2.2 describes the sources of solvents. Some tanks received no solvents, and most solvents that were sent to the tanks have evaporated or

undergone chemical degradation to form organic species that would not be present as a separable, liquid phase. However, tank 241-C-103 is known to have an organic solvent layer floating on the waste surface. Tanks 241-C-102 and 241-BY-108 have headspace concentrations of organic solvents higher than can be explained by any known mechanism other than the presence of liquid phase solvents somewhere in the waste. Because the organic layer in tank 241-C-103 has been sampled and analyzed, its properties are used as reference points and in example calculations throughout this report. Information on tanks 241-C-102 and 241-BY-108 are also used in example calculations.

To date, no solvent pool fires have occurred in Hanford Site waste tanks. The cases analyzed herein are hypothetical, low probability accidents. Potential ignition sources are few and include low frequency incidents of lightning strikes, vehicle fuel spill/ignition accidents, and possibly torch cutting accidents.

Section 3.0 outlines the phenomenology of different accidents involving organic solvents. Section 4.0 describes the ignitability of solvents and the conditions required to support combustion. Section 5.0 provides a thermal hydraulic analysis of the different configurations of solvent fires. Section 6.0 discusses the bases for the toxicological and radiological release calculations used in TWRS accident analysis (Noorani 1997). Section 7.0 describes the development of accident frequencies that are used in the accident analysis. Section 8.0 lists the key parameters and their values used in the accident consequence calculations. Section 9.0 describes the spreadsheet calculations of the radiological and toxicological consequences.

1.2 SUMMARY OF ACCIDENT ANALYSIS

Scenarios have been developed and analyzed for a number of postulated solvent fire accidents. Accident consequences were calculated for many conditions to evaluate solvent fire impact on the tank structure, radiological releases and toxicological exposures. The accidents were evaluated assuming no controls were applied (unmitigated). The bounding consequences were compared to risk evaluation guidelines by assigning the unmitigated cases to accident frequency categories based on a conservative assessment of available ignition sources and estimates on the number of tanks that might contain combustible configurations of solvents. All of the bounding cases are within risk evaluation guidelines without controls (unmitigated).

Accident Scenarios

The organic solvent fire safety analysis evaluates the frequency and consequences of the following three types of fires resulting from combustion of organic solvent with headspace air.

- Pool fires: Pools are either a layer of solvent floating on top of liquid waste or a layer that is trapped in a depression on top of solid waste. In either instance, a pool has an area greater than 1 m^2 (10.8 ft^2). A pool may exist in DCRTs, DSTs, or SSTs.

- Puddle fires: Puddles are less than 1 m^2 (10.8 ft^2) and exist in a depression in a solid waste surface. Puddles should occur mainly in SSTs because many SSTs have a solid surface that can form a depression for solvent to collect in. However, a few DSTs have a floating crust (e.g., tank 241-SY-101) that might form a depression where solvent could collect. Therefore, the analyses include puddles for both DSTs and SSTs.

- Wick-Stabilized Fires: A wick-stabilized fire configuration would consist of a sludge or saltcake that is permeated with solvent. The height of the solvent layer would be equal to the height of the solids level. The sludge or saltcake would act as a wick, and the solvent would burn. Wick-stabilized fires may occur in SSTs. A few DSTs have a floating crust (e.g., tank 241-SY-101) that provide a solids surface where solvent might collect and support a wick-stabilized fire. Therefore, the analyses include wick-stabilized fires for both DSTs and SSTs.

The criterion of 1 m^2 being a pool and anything smaller being a puddle that was developed in Revision 0 is still used. Because of the revised consequence calculations, the size of a puddle could be revised upwards (a bigger puddle would still have consequences below risk evaluation guidelines). However 1 m^2 is still a useful boundary between a pool area that allows a rapid flame front to travel across a large area and produce a high pressure in the tank and a puddle whose rate of fuel consumption results in negligible pressure buildup.

The important distinctions between pool fires and wick-stabilized fires on saltcake or sludge are the rate of flame spread and ease of ignition. A wick-stabilized fire has a much lower flame spread rate and a higher probability of occurrence than a pool fire. The higher flame spread rate leads to higher tank pressures and vent rates. This analysis uses bounding high values for flame spread rate.

Accident Consequences

Because neither the total number of tanks with separable phase organic layers nor the volumes of organic solvent that may be present in these tanks is known with any certainty, it is not possible to use a single scenario to bound this accident. Instead, several scenarios, each of which maximizes a different result, were analyzed. The four results are:

- Maximum tank pressure
- Maximum tank vacuum
- Maximum radiological release
- Maximum toxicological impact.

Each result was calculated for the different combinations of solvent fire type (pool, puddle, and wick-stabilized), tank type (SST, DST, DCRT), and type of ventilation system (active or passive). Twenty-three scenarios were calculated to evaluate different potential combinations and to establish the worst-case scenarios. Section 9.0 provides calculations for all 23 models.

Overpressure. An important assumption embodied in the consequence calculation is that the tank does not suffer dome collapse from the increased internal tank pressure from the fire. A dome collapse would result in larger radiological consequences. The maximum overpressure resulting from a solvent fire in a DST is calculated to be 207 kPa (30 psig). This pressure will not result in DST dome collapse and is documented in *Topical - Structural Integrity and Potential Failure Modes of the Hanford High-Level Waste Tanks* (WHC 1996b). The maximum overpressure calculated for the SST accident is 200 kPa (29 psig), given the SST structure does not fail. The report WHC 1996b predicts that the concrete in the SST dome would crack at a pressure of 76 kPa (11 psig). As the dome cracks, more flow openings are created; hence the pressure is maintained constant until the solvent fire extinguishes because of lack of oxygen. The concrete would maintain adherence to the rebar and the dome would not collapse. The predicted cracking would allow the pressure to vent to the soil above the tank. The approximately 2.4 m (8 ft) of soil on top of the tank would act as a filter and prevent a major release to the atmosphere. The release calculations presented in this report do not take credit for any material that would be filtered from the air stream by the soil. Therefore, the calculated quantity of material released exceeds an actual release quantity.

Eight scenarios bound the potential worst case consequences and are listed below. The letter designator is taken from the spreadsheet used to calculate the consequences; readers may cross reference to the spreadsheet in Section 9.0.

1. Case G represents the bounding radiological accident for an SST fire. Case G is a large pool fire. In this scenario, a pool of solvent burns on the waste surface of an actively ventilated SST. This results in more radioactive material being exhausted from the tank even after the fire has extinguished itself. Actively ventilated SSTs are found in Tank Farms 241-SX and 241-C.

   In this and all pool scenarios, a pool is assumed to be 210 m^2 (2,260 ft^2), which means the flame spread area is not limited before the fire is extinguished by oxygen depletion. Unlimited flame spread produces the largest pressure transient.

   In this scenario, the tank dome does not collapse as a result of the pressure transient (200 kPa [29 psig]) or the vacuum transient(-0.7 kPa [-0.1 psig]). The high pressure is the result of the small vent path through the filter, which is modeled as a 9.5 cm (3.75 in.) orifice. Releases could also occur through risers that do not have covers bolted to the flanges. The fire will burn until the oxygen is depleted consuming 146 kg (321 lb) of solvent.

2. Case H represents the bounding toxicological accident for an SST fire. Case H is a large pool fire and similar to case G except the vent path is modeled as a 9.5 cm (3.75 in.) orifice plus a 1.27 m (50 in.) orifice. The large vent path results in the toxic material in the headspace ejecting from the tank rapidly. Because toxicological guidelines are based on concentration, this case will produce the largest toxicological consequence.

3. Case L represents the bounding radiological and toxicological accident for a DST fire. Case L is a large pool fire. In this scenario, a pool of solvent (210 m^2 [2,260 ft^2]) burns on top of the waste surface. The tank has a powered ventilation system. The vent path is modeled as a 1.27 m (50 in.) orifice and a 0.24 m (9.6 in.) orifice. The large vent path results in the toxic material in the headspace ejecting from the tank rapidly. Because toxicological guidelines are based on concentration, this case produces the largest toxicological consequence.

   The only release path to the environment is through the ventilation system and risers that do not have covers bolted to the flanges. The fire will burn until the oxygen is depleted consuming 92 kg (202 lb) of solvent.

4. Case O represents the bounding radiological and toxicological accident for a DCRT fire. Case O is a large pool fire. The same scenario results in the bounding case for both toxicological and radiological consequences for a DCRT fire. A pool of solvent (34 m^2 [366 ft^2]) burns on top of the waste surface. Thirty-four square meters (366 ft^2) is equal to the maximum waste surface area in the DCRT.

   In this scenario, the DCRT does not structurally fail as a result of the pressure transient (126 kPa [18.3 psig]), or the vacuum transient (-8.3 kPa [-1.2 psig]). The vaults surrounding the DCRTs have powered ventilation systems. Although the vault ventilation system has a duct to the DCRTs, there is no identifiable ventilation inlet to the DCRTs. Therefore, the DCRT is modeled as having a passive ventilation system.[1] The vent path is modeled as a 0.1 m (4 in.) diameter orifice. The pressure transient ruptures the HEPA filter on the vault ventilation system. The only release path to the environment is through the vault ventilation system and risers that do not have covers bolted to the flanges. The fire will burn until the oxygen is depleted consuming 2.12 kg (4.67 lb) of solvent.

5. Case Q represents the bounding radiological accident for SST wick-stabilized fires. It is possible that solvent could intrude into the underlying sludge or saltcake in an SST following saltwell pumping of drainable liquids from a tank. Exposed saltcake, saturated with solvent, could burn like a candle using the sludge or saltcake as a wick. The burning surface would slowly increase and eventually cover approximately 40 m^2 (431 ft^2).

   For a solvent liquid level equal to the solids level in the tank, the flame propagation rate would be approximately 0.1 cm/s. Where a solvent liquid level occurs above the solids level, a pool or

[1] The 244-U DCRT does have an air inlet on the tank. No radioactive material has been transferred through this DCRT. The 244-U DCRT will require additional information on ventilation flows to complete calculations for it. Because any accident involving a DCRT would have smaller consequences than an accident with an SST or DST, 244-U is bounded.

puddle fire would occur; this is addressed later. If the liquid level was below the solids level, ignition would not occur.

The tank does not structurally fail and create a pathway to the environment as a result of the pressure (30.3 kPa [4.4 psig]) or the vacuum (-4.8 kPa [-0.7 psig]) transients. Because of the relatively low pressure, little difference exists between the cases evaluated for active and passive ventilation systems. The case using a powered ventilation system (241-SX or 241-C tank farms) produced the highest radiological and toxicological consequences. The vent path is modeled as a 9.5 cm (3.75 in.) orifice. The only paths to the environment are through a ruptured HEPA filter and risers that do not have covers bolted in place. The fire will burn until oxygen is depleted consuming 130 kg (287 lbs) of solvent.

6. Case Q1 evaluates the releases from a passively ventilated SST. The case is not a maximum in terms of consequences. Cases Q and R produce the bounding consequences. However 133 of the SSTs are passively ventilated and 16 are actively ventilated. When single tank consequences are multiplied by the appropriate number of tanks, the large number of passively ventilated tanks may result in the passively ventilated tanks being in a higher frequency category than the actively ventilated tanks. Therefore separate consequence calculations are needed for passively ventilated SSTs even though the single tank consequences are bounded by actively ventilated tanks.

7. Case R represents the bounding toxicological accident for SST wick-stabilized fires. Case R is similar to case Q except the vent path is modeled as a 9.5 cm (3.75 in.) orifice plus a 1.27 m (50 in.) orifice. The large vent path results in the toxic material in the headspace ejecting from the tank rapidly. Because toxicological guidelines are based on concentration, this case produces the largest toxicological consequence.

8. Case V represents the bounding radiological and toxicological accidents for DST wick-stabilized fires. Only one case is necessary to bound radiological and toxicological consequences because only one vent path exists for an entrained fire that would result in material being released from the tank. The vent path for DSTs is large enough to limit the peak pressure produced by the fire to 0.7 psig, so the flapper valve does not open (assumed opening pressure = 1 psig). Because all DSTs are actively ventilated, no separate case exists for actively and passively ventilated tanks.

   Case V is similar to case Q, except the vent path is a 0.24 m (9.6 in.) orifice, and the only path to the environment is through a ruptured HEPA filter. The fire will burn until oxygen is depleted consuming 120 kg (265 lbs) of solvent.

The likelihood of igniting a DST wick-stabilized fire is assumed to be the same as the likelihood of igniting an SST wick-stabilized fire.

The DST wick-stabilized fire is bounded by case Q, the SST wick-stabilized fire for radiological consequences, and by case R, SST wick-stabilized fire for toxicological consequences. The likelihood of a wick-stabilized fire occurring in a DST is also bounded by the likelihood of occurrence in an SST.

Accident Frequencies

The frequencies with which large energy sources come in contact with waste were estimated by reviewing tank farm equipment, operations, and natural phenomena. These energy source frequencies are combined with ignition probabilities (given the energy source is present) to assign ignition frequencies for solvent fires on a per-tank basis. The number of tanks that might contain combustible solvent configurations are estimated and used as a multiplier for per-tank ignition frequencies. Accident scenario frequencies are assigned to an accident frequency category so that accident consequences can be compared to risk evaluation guidelines.

The evaluation concluded that all solvent pools (floating layers, large pools, small pools, and puddles) require a very robust ignition source. Potential ignition sources for pool fires are few and limited to low frequency incidents of lightning strikes and vehicle fuel spill/ignition accidents. Wick-stabilized fires can be ignited with smaller energy sources. Potential ignition sources for wick-stabilized fires are more numerous and more likely. They include torch cutting accidents and rotary mode core sampling upsets. On a per-tank basis, where a combustible solvent configuration is contained in the tank, the unmitigated frequency of ignition for pool fires is "extremely unlikely" (1×10^{-4} to 1×10^{-6} events per year), and the ignition frequency for wick-stabilized fires is also "extremely unlikely."

The number of tanks containing a combustible solvent configuration is unknown. Only tank 241-C-103 is known to contain a combustible configuration (a floating layer of TBP/normal paraffin hydrocarbon [NPH]). Based on waste transfer records and vapor sampling results, conservative estimates of the number of tanks that could contain separable phase solvents are 14 SSTs and 6 DSTs. Based on the assumption that any tank could contain a combustible solvent unless vapor sampling indicates otherwise, bounding numbers are estimated to be 66 passively ventilated SSTs, 6 actively ventilated SSTs, 28 DSTs, and 6 DCRTs. This is explained in more detail in Section 7.2.

When per-tank ignition frequencies are combined with the conservative estimate of the number of tanks that may contain a combustible solvent configuration, the unmitigated accident frequency category for pool fires becomes "unlikely" (1×10^{-2} to 1×10^{-4} events per year), and the unmitigated frequency category for wick-stabilized fires also becomes "unlikely."

Table 1-1. Summary of Consequences and Frequencies of Organic Solvent Fires Without Controls (Unmitigated).

Accident Case Number	Consequences								Frequency Without controls
	Radiological Sv (rem)				Toxicological SOF				
	Onsite		Offsite		Onsite		Offsite		
	Calculated dose	Risk guideline	Calculated dose	Risk guideline	Calculated SOF	Risk guideline	Calculated SOF	Risk guideline	
Pool fire in 241-C-103	1.55E-02 (1.55)	1.0E-01 (10)	1.36E-05 (1.36E-03)	4.0E-02 (4.0)	0.15	1.0	0.08	1.0	extremely unlikely
G, SST (large pool fire)	1.55E-02 (1.55)	5.0E-02 (5.0)	1.36E-05 (1.36E-03)	5.0E-03 (0.5)	--	--	--	--	unlikely
H, SST (large pool fire)	--	--	--	--	0.94	1 (ERPG-2)	0.35	1 (ERPG-1)	unlikely
L, DST	6.34E-03 (6.34E-01)	5.0E-02 (5.0)	5.44E-06 (5.44E-04)	5.0E-03 (0.5)	0.99	1 (ERPG-2)	0.38	1 (ERPG-1)	unlikely
O, DCRT	2.34E-04 (2.34E-02)	5.0E-02 (5.0)	1.97E-07 (1.97E-05)	5.0E-03 (0.5)	0.30	1 (ERPG-2)	0.01	1 (ERPG-1)	unlikely
Q, Wick-stabilized	8.94E-03 (8.94E-01)	5.0E-02 (5.0)	7.84E-06 (7.84E-04)	5.0E-03 (0.5)	2.32E-01	1 (ERPG-2)	5.68 E-03	1 (ERPG)	unlikely
Q1, Wick-stabilized	2.28E-03 (2.28E-01)	5.0E-02 (5.0)	2E-06 (2E-04)	5.0E-03 (5.0E-01)	1.67E-01	1 (ERPG-2)	4.59 E-03	1 (ERPG-1)	unlikely
R, Wick-stabilized	--	--	--	--	4.11E-01	1 (ERPG-2)	6.93 E-03	1 (ERPG-1)	unlikely

Notes:

DCRT	=	double-contained receiver tank
DST	=	double-shell tank
ERPG	=	emergency response planning guideline
PEL-TWA	=	permissible exposure limits-time weighted average
rem	=	radiation equivalent man
SOF	=	sum of fractions
SST	=	single-shell tank
Sv	=	Sieverts

Comparison to Risk Evaluation Guidelines

Table 1-1 shows the radiological and toxicological consequences for unmitigated (without controls) scenarios. All of the unmitigated accident scenarios are within risk evaluation guidelines. Therefore no controls or TSRs are required.

1.3 CONCLUSIONS

Improvements in the evaluation of the risk posed by solvent fires change the conclusion regarding this hazard from above risk guidelines in Cowley et al. (1996) to below risk guidelines. The key improvements that support this change in conclusion are the incorporation of turbulent jet mixing and aerosol depletion models to predict accident consequences, the change to an RF of 0.5 for entrained fires, and the re-evaluation of probabilities for ignition of entrained fires. Specific conclusions supported by the analysis contained in this calculation note include the following.

1.3.1 Removal of Tanks 241-C-102 and 241-C-103 from Watch List

Tanks 241-C-102 and 241-C-103 were placed on the Watch List because they contain organic solvents (Payne 1994 and Watkins 1991). The analyses in this report show that these tanks do not have a serious potential for release of high-level nuclear waste due to uncontrolled increases of temperature or pressure (Public Law 101-510). Therefore, it is recommended that the U.S. Department of Energy remove these tanks from the Watch List.

The risk posed by the solvent known to exist in tank 241-C-103 is significantly below guidelines. The configuration of the organic solvent in tank 241-C-103 is known to be a large pool.

The risk posed by the solvent that is known to exist in tank 241-C-102 is also significantly below guidelines. The solvent is present either in the form of puddles or entrained in the waste. Both of these forms result in low energy events.

1.3.2 General Conclusions

1. Without controls the risk from solvent pools and wick-stabilized fires is within guidelines, even if conservative assumptions are made regarding the number of tanks that might contain such a combustible configuration (see Section 7.2).

2. A screening methodology has been developed for both passively ventilated and actively ventilated tanks that uses headspace sample data to estimate the maximum solvent pool area that may be present in a specific tank. The screening methodology is described in Appendix A. In Cowley et al. (1996), identification of specific tanks that posed an organic solvent risk was an important program element. The screening was used to determine which tanks required

organic solvent controls and which did not. This report has determined that controls are not necessary, therefore identification of specific tanks is no longer necessary. The screening methodology is still used as one of the methods for identifying the total number of tanks that may contain solvent. The total number of tanks that contains solvent is used to estimate facility risk. Appendix A continues to be included with this report because of its use to help estimate the total number of solvent tanks, and to document work completed and the changes in technical approach as the solvent fire analysis evolves.

3. Cowley et al. (1996) raised a question about small fires that were hypothesized to continue burning using oxygen that was brought into the tank by an active ventilation system. This subject has been addressed in Section 5.0 and Appendix H of this report. It is concluded that if such a fire occurred, its consequences would be bounded by the larger fires analyzed in this report.

4. Review of Cowley et al. (1996) raised a question about the potential consequences of a fire that was ignited at multiple points. Multiple ignition points might result in a fire that spreads faster and therefore, causes higher pressures in the tank. This subject has been addressed in Section 5 and Appendix J of this report. It is concluded that a multi-point fire does not significantly change the results from that of a single point ignition and that the risk of a single point ignition is greater.

5. The bounding cases for wick-stabilized fires in SSTs (cases Q and R) are also bounding for a wick-stabilized fire in a DST. This applies both to consequences and the likelihood of occurrence.

This page intentionally left blank.

2.0 BACKGROUND

Several waste generating processes were operated at the Hanford Site including the bismuth phosphate process, the uranium recovery process, the reduction-oxidation (REDOX) process, the waste fractionization process, the PUREX process, and the processes conducted at the Plutonium Finishing Plant (PFP). The primary goal of these processes was to extract and/or process plutonium. Radioactive wastes from these processes are stored in underground tanks in alkaline slurries (Anderson 1990).

Each waste-generating process had a variety of waste streams (at least 49 different types have been identified), but the following broad categories of waste can be established: 1) cladding (or coating) waste from the removal of the fuel element cladding, 2) metal waste from the processing of the fuel itself to remove the plutonium or other fissile material, 3) decontamination waste from the cleanout of the systems (including N Reactor decontamination waste), and 4) other miscellaneous waste such as laboratory waste. Once the waste was generated and stored in the tanks, other operations were performed including the removal/recovery of substances (e.g., uranium, strontium, and cesium), evaporation, solidification, and settling.

The principal organic compounds sent to the waste tanks were divided into two classes: complexants (for chelating divalent, trivalent, and tetravalent cations) and extraction solvents. This document focuses on the organic extraction solvent hazard; the organic complexant hazard is presented in a separate topical report (Meacham et al. 1997).

The potential risk of burning solvent in the tanks is decreasing with time. The summary of organic solvent aging presented in Section 2.3, and the more detailed discussion given in Appendix L, explain the chemical processes. The key components are NPH and TBP. Aging of the NPH is a key factor in the decreasing risk of a solvent fire. Both theory and field evidence (tank 241-C-103) show that the NPH fragments into lower molecular weight compounds. As the reactions proceed, the reaction products become more soluble in aqueous solution and more volatile. The soluble proudcts will not burn in an aqueous solution. The volatile products are more mobile than the original hydrocarbons and continuously evolve from the waste into the dome space and the atmosphere. As the NPH inventory decreases, the remaining NPH/TBP mixture becomes increasingly difficult to ignite. The increase in ignition difficulty reduces the probability (a component of risk) of a solvent fire.

The TBP also ages. As with NPH, an array of proudcts is evolved that are soluble in aqueous solution or are volatile and escape to the tank dome space and atmosphere. The aging of the TBP, as well as the NPH, reduces the amount of fuel available for a solvent fire. As the quantity of fuel decreases, the potential for damaging the tank due to pressurization decreases. A decrease in fuel burned would also reduce the consequences due to combustion products. As time passes, the risk of a solvent fire decreases because the probability of a fire decreases, the potential for damaging the tank decreases, and the consequences due to release of combustion products decreases.

2.1 APPROACH TO RESOLUTION OF THE ORGANIC SOLVENT SAFETY ISSUE

The approach to resolution of the organic solvent safety issue has matured since the safety analysis on tank 241-C-103 (Postma et al. 1994) was completed in 1994. The original accident scenario assumed catastrophic failure of the tank dome during an organic solvent burn if an SST did not have adequate vent path. Failure of the dome led to radiological consequences above risk evaluation guidelines. Preliminary calculations showed that the solvent pool area would have to be larger than 1 m^2 to create enough pressure to collapse the tank dome. The original approach required identifying tanks containing significant quantities (i.e., greater than a 1 m^2 puddle) of organic solvent (see Appendix A) and ensuring an adequate vent path in those tanks that contain significant organic solvent.

Tank structural integrity was reexamined in 1996 as part of the Authorization Basis upgrade (Noorani 1997a). Analyses (Han 1996) showed that the tank dome would not fail catastrophically under the pressures developed during an organic solvent fire. Instead, the dome would develop cracks and fissures to release the internal pressure and stay mostly intact. Using the information from Han (1998), Cowley et al. (1996) showed radiological consequences within risk evaluation guidelines because radiological consequences were mostly the result of the splash from catastrophic failure of the dome. Ensuring adequate vent path was rendered moot by the tank structural integrity analysis.

Although Cowley et al. (1996) showed that the radiological consequences fell within guidelines, toxicological consequences still exceeded the risk evaluation guidelines. Therefore, the earlier approach still relied on characterization to determine how many solvent tanks existed. If few solvent tanks existed, then the facility-wide accident frequency might be low enough to bring the risk within the evaluation guidelines.

The effects of jet mixing and aerosol depletion (see Section 6.0) are included in the radiological and toxicological consequence calculations (see Section 9.0) in this report. The revised consequence calculations show that the solvent fire hazard falls below risk evaluation guidelines.

2.2 SOLVENT STREAMS

This section reviews Hanford Site tank farm operations and the history of process solvents use and provides insight into the types and amounts of solvent still likely to exist in the waste tanks. A solvent fire hazard is most likely to exist for tanks containing waste from process waste streams 1) that might have contained significant quantities of entrained solvents, 2) that contained solvents because of incomplete phase separations during processing, and 3) for which tank operating histories may have allowed the solvents to persist as a separate phase for many years. The effects of evaporation on the separable phase organics originally sent to the tanks are also discussed in this section.

Four Hanford Site chemical processes used potentially flammable organic solvents: the REDOX process, the uranium recovery process, the B Plant waste fractionation process, and the PUREX process. Mixtures of carbon tetrachloride and cutting oil were used in the PFP. This mixture was nonflammable.

2.2.1 Reduction and Oxidation Solvents

The REDOX process, which was used between 1952 and 1967, was a solvent extraction process that used methyl isobutyl ketone (hexone). Waste from the REDOX Plant (or S Plant) was directed to the S, SX, and U tank farms in the West Area. Aqueous waste that resulted from solvent cleanup processes went through multiple washing and distillations. Solvents were also steam stripped from the high-level waste (HLW) stream before being discharged to the waste tanks. Based on this process history, the concentration of hexone in the waste streams sent to the tank farms is estimated to be less than 0.3 ppm (Borsheim and Kirch 1991 and Prosser 1986).

Hexone, which may have been transferred to the tank farms, is expected to have evaporated during the many years of storage. Hexone is relatively volatile. (Table 2-1 shows the boiling point of hexone and other Hanford Site process solvents.) In addition, most waste tank supernatants have been processed through some form of evaporator to reduce the waste volume, and these evaporation processes would have removed any hexone with the process condensate.

2.2.2 Uranium Recovery Process Solvents

The first chemical separations process used at the Hanford Site was the bismuth phosphate process that recovered plutonium but not uranium. In the 1950s, a short supply of high-grade uranium motivated the recovery of uranium from the bismuth phosphate wastes. This uranium recovery was performed at U Plant from 1952 to 1957 and used a TBP-kerosene solvent similar to TBP-NPH.

The uranium recovery process generated large quantities of waste. The large waste volume resulted in the implementation of several waste volume reduction efforts. These efforts included scavenging soluble cesium from waste supernatants with ferrocyanide and subsequent decanting of the supernatants to cribs. A more widespread waste reduction effort was accomplished by using various evaporation processes. Uranium recovery operations ended in 1957. Since that time, most waste tank supernatants have been processed through some form of evaporative waste reduction process. The evaporation processes would have removed the separable, semivolatile solvents to the condensate streams, and they would have been disposed of along with the condensate (Borsheim and Kirch 1991) to cribs or ponds.

Table 2-1. Boiling Points of Some Organic Compounds in Tank Wastes.

Name	Boiling Point °C[1]
Carbon tetrachloride	77
Methyl isobutyl ketone (hexone)	116
Butanol	117
i-Butyric acid[2]	153
Butyric acid[2]	165
Decane (n)	174
Dodecane (n)	216
Tridecane (n)	234
Tributyl phosphate	289[3]

Notes:
[1]To convert temperature from °C to °F, multiply $T_{°C}$ by 1.8 and add 32.
[2]These compounds will be present in the tanks as sodium salts or acid anions.
[3]Boils with decomposition, boiling point at 37 mm mercury pressure (80 to 81 °C [177 to 178 °F]).

2.2.3 B Plant Waste Fractionation Process Solvents

Although B Plant was used for the bismuth phosphate separation process from 1945 to 1952, the plant was later reconfigured to remove cesium and strontium from the wastes: ^{137}Cs was removed using ion exchange techniques, and ^{90}Sr was separated using a solvent extraction process. This process used a TBP-NPH-di (2-ethylhexyl) phosphoric acid (D2EHPA) solvent mixture and various complexing agents such as ethylenediaminetetraacetic acid (EDTA), N-(hydroxyethyl)-ethylenediaminetriacetic acid (HEDTA), and citrate to prevent transition metal extraction.

The solvent treatment wastes for this process were concentrated in an atmospheric evaporator before they were transferred to the tank farms. Any entrained NPH would have been steam stripped into the concentrator overhead stream and disposed of with the condensate (Borsheim and Kirch 1991) to cribs or ponds.

One receiver of this waste was tank 241-C-106. Tank 241-C-106 is being studied and sampled as part of the preparation for sluicing the waste in the tank and transferring it to tank 241-AY-102. Centrifugation of sludge samples taken during 1996 resulted in the separation of a hitherto unencountered, sludge-associated organic oil that floated on the aqueous layer. All analyses performed on the samples and the conclusions are documented in *Chemical and Chemically-Related Considerations Associated with Sluicing Tank Waste C-106 to Tank AY-102* (WHC 1996a). This organic material is referred to as "sludge oil."

The principal constituent identified by analysis of this organic layer was bis (2-ethylhexyl) phosphoric acid, existing as the sodium salt in the waste. Quoting from WHC (1996a):

> "Minor amounts of TBP, normal paraffin hydrocarbon, and the transesterification products of TBP and 2-ethylhexyl alcohol, or of di(2-ethylhexyl) phosphate and butyl alcohol. This phosphate ester salt was used as a complexing agent in B Plant during the Sr recovery campaigns. The material likely coprecipitated with the sludge when wastes from B Plant were made alkaline before their transfer to the tanks. The absence of a strongly alkaline environment in tank C-106 likely protected this species from hydrolysis."

Samples of the pure sodium salt of bis (2-ethylhexyl) phosphate were tested by Fauske and Associates and are documented in WHC (1996a). The tests showed that the material does not show propagating behavior within the conditions found in tank 241-C-106.

The "sludge oil" consists primarily of phosphate salts with only trace amounts of TBP or NPH. The oil is closely associated with sludge in the tank, which also contains substantial amounts of water. Reactivity tests conducted by Fauske and Associates do not show any reactivity within the conditions found in tank 241-C-106. It is concluded that the "sludge oil" is not relevant to the solvent fire analysis.

Sluicing operations in tank 241-C-106 have released degradation products of the bis-2-ethylhexyl phosphate into the tank headspace. The vapors are removed from the tank by the ventilation system used in conjunction with sluicing. The vapors have no effect on the solvent fire accident, since they do not increase flammability because they are present in very low concentrations, do not increase the length of a fire (length of fire is oxygen limited) or effect the consequences since the combustion products and soot do not change.

2.2.4 PUREX Process Solvents

The PUREX Plant began operations in 1955. The PUREX process used a solvent extraction method based on TBP and diluents. In this report, the properties of the diluents are assumed to be represented by NPH. PUREX ran until 1972 when it was shut down for 11 years. PUREX was then run for several more years until operations ceased in 1990.

Because PUREX operated most recently and used more solvent than the other processes, it has been studied most extensively for possible transfer of solvents to the waste tanks. In *TBP and Diluent Mass Balances in the PUREX Plant at Hanford, 1955-1991*, Sederburg and Reddick (1994) estimated the amount of solvent that was transferred to the tank farms by performing a mass balance between the solvent consumed in the PUREX Plant and six possible effluent streams. The significant findings are given below.

Most organic solvent consumed at PUREX can be tracked to six effluent streams, two of which went to the tank farms. The six solvent effluent streams are:

1. soluble organics in HLW (high-fission product heat load) transferred to the tank farms

2. entrained and soluble solvent (solvent treatment) and degradation products in organic wash wastes transferred to the tank farms

3. disposal to the organic Crib A-2 in early operations, and later briefly to Crib A-31

4. entrained and soluble organic in PUREX process condensate disposed to a crib

5. organic solvents evaporated into the vessel ventilation system and lost as gaseous effluent

6. water or alkali soluble organics in the uranium product stream.

The results of the material balance indicate that 5,260 kL (1,390 kgal) of solvent (TBP plus diluent) were consumed at the PUREX Plant. Of this amount, about 2,480 kL (655 kgal) were estimated to have been discharged in the organic wash waste (OWW) sent to tank farms, 1,560 kL (412 kgal) were in process condensate, 620 kL (164 kgal) were in stack gaseous effluent, 220 kL (59 kgal) were disposed to Crib A-2, 370 kL (98 kgal) were disposed to Cribs A-2 and A-31, and 7 kL (2 kgal) were HLW. The total sent to the tanks farms is therefore estimated to be the sum of OWW (2,480 kL [655 kgal]) and HLW (7 kL [2 kgal]), which equals approximately 2,490 kL (657 kgal).

2.2.4.1 Organic Wash Waste. Normal operations in the PUREX Plant used a solution of TBP in NPH diluent for solvent extraction, with subsequent washing of the TBP-diluent mixture with nitric acid or sodium hydroxide to remove contaminants and degradation products. The washed organic was reused, and the aqueous wash solution was transferred to the tank farms. The wash solution, or OWW, contained TBP degradation products that resulted from acid hydrolysis and radiolysis. Identified degradation products included dibutyl phosphate (DBP), monobutyl phosphate, butanol, butyric acid and phosphoric acid. The diluent (NPH) is more resistant to chemical and radiolytic degradation. In addition to the washed degradation products, the OWW would have contained small amounts of soluble TBP and NPH and larger amounts of entrained TBP and NPH.

The OWW, at least early on (e.g., 1955-1961), was discharged in two components. The bulk of the OWW, also called carbonate waste, was generally transferred to the HLW (self-boiling) tanks (in A-Farm). At times (e.g., when no self-boiling tank was available) the wash wastes and miscellaneous accumulated organic wastes were transferred to nonboiling tanks (apparently, generally in the C-Farm).

Miscellaneous organic waste included separable phase organics that accumulated in PUREX Plant tanks TK-G8 and TK-R8 and perhaps collected in tank F-18 (which included waste collected from cell sumps including the organic wash area). Handling this waste involved decanting operations in which it was necessary to detect the aqueous/organic interface in order to separate the layers. In early operations, accumulated organic in these tanks was deliberately transferred to the tank farms. Later operations involved recovering and reusing the accumulated organic.

During at least a portion of the early PUREX operations, the separable phase organic wastes were transferred to nonboiling tanks because too much organic was being distilled from the HLW (boiling) tanks. High levels of organic were thought to cause percolation problems in the HLW condensate cribs.

During later operations (after 1961), the OWW was sent to nonboiling tanks (Agnew 1994). Later operations also emphasized treatment and reuse of miscellaneous recovered solvents rather than disposal to cribs or transfers to the tank farms.

The OWW was comprised primarily of PUREX solvent degradation products, soluble TBP and diluent, and entrained TBP and diluent. Of the 2,480 kL (655 kgal) of organic estimated to have been sent to the tank farms as OWW, 53 kL (14 kgal) was estimated to have been soluble degradation products, 1,135 L (300 gal) was soluble TBP and diluent, 700 kL (187 kgal) was entrained TBP, and 1,710 kL (453 kgal) was entrained diluent. Therefore, it is estimated that 2,420 kL (640 kgal) of separable phase organic may have been sent to the tank farms during PUREX operations. Although NPH is insoluble in dilute aqueous waste solutions, TBP is soluble. One mL dissolves in approximately 165 mL of water (Merck Index 1989). This estimate is probably high because the mass balance analysis probably underpredicts the degradation products and overpredicts the entrained organics.

The PUREX diluent changed over time. The original diluent was Shell[2] E-2342. Soltrol[3]-170 replaced Shell™ E-2342 in 1961, and NPH replaced Soltrol™-170 in 1966. Table 2-3 shows the properties of these diluents.

2.2.4.2 Estimated Location of Solvents in Single-Shell Tanks. The transfer records for the OWWs have been studied to determine where these organics are expected to be located.

---

[2] Shell is a trademark of the Shell Oil Company, Houston, Texas.

[3] Soltrol is a trademark of the Phillips Chemical Company, Borger, Texas.

Based on a review of waste transfer records documented in Anderson (1990), the following tanks apparently received OWW:

Table 2-2. Waste Transfers from Anderson (1990).

241-AX-101	241-C-102	241-S-110	241-TX-101
241-AX-102	241-C-103	241-SX-103	241-TX-102
241-B-103	241-C-104	241-SX-106	241-TX-104
241-BX-101	241-C-108		214-TX-105
241-BX-102	241-C-110		241-TX-106
241-BX-103	241-C-111		241-TY-102
241-BX-106	241-C-112		241-TY-103
241-BY-109			241-TY-104.
241-BY-111			

Tanks 241-C-102 and 241-C-104 were the main receiving tanks for OWW from PUREX (Agnew 1993). Tank 241-C-102 received 6,940 kL (1,833 kgal) of OWW in the period from 1968 to 1970, and tank 241-C-104 received 19,540 kL (5,163 kgal) from 1970 to 1972. The accumulation of organic layers was first noted in tank 241-C-102 in 1969 (Anderson 1969). Accumulation in tank 241-C-104 was noted in 1972 (Hall 1972).

A good portion of the organic in tanks 241-C-102 and 241-C-104 was evidently transferred into tank 241-C-103 around 1975. Although tank 241-C-103 was used for several years after that time, the floating organic layer apparently remained in the tank. This assumption would be consistent with the use of a submerged turbine pump (P-10 pump) in this tank in the past.

A review of the historical tank content estimates (Brevick et al. 1995, Brevick 1997a and 1997b) indicated the following SSTs contain DBP resulting from the receipt and degradation of OWW wastes. (These wastes may also have contained separable phase organics because of entrainment.)

Table 2-3. Properties of Shell™ E-2342, Soltrol™-170, and NPH. (2 sheets)

	Shell™ E-2342	Soltrol™-170	Normal Paraffin Hydrocarbon (NPH)
Period of use	1955 to 9/1961	9/1961 to 2/1966	2/1966 to 1989
Density at 25 °C (g/mL)	0.801	0.773	0.76 (max.)
Viscosity (centipoise at 25 °C)	1.7	2.3	1.8
Boiling range and midpoint (°C)	--	208-239, (225)	174-252
Flash point	166 °F	192 °F	80 °C (176 °F) min.
Aromatic content	0.1 vol%	Nil	0.2 wt% max as 1,2,3,4 tetrahydronaphthalene
Naphthene content	About 80 vol%	Nil	--
Iodine number	--	<1.1 bromine number	0.1 wt% max. olefins as wt% 1-tetradecene
Solubility in water	<0.004 g/L at 25 °C and 50 °C	very slight	<0.005 g/L between 25 °C and 50 °C
Composition	About 80 vol% 5 and 6 carbon bicyclic saturated paraffin compounds	Mixture of highly branched aliphatic hydrocarbons	Mixture of C10 to C14 straight chain (normal) aliphatic hydrocarbons

Notes:

max. = maximum
min. = minimum

Physical properties for Shell™ E-2342 and Soltrol™-170 are from the Purex Technical Manual (General Electric Company 1955). Composition of Soltrol™-170 is from Walser (1966). Properties of NPH are from the Purex Technical Manual. Composition for Shell™ E-2342 is based on the definition for naphthenes given in Merck Index (1989).

Table 2-4. Waste Transfers from Brevick.

241-A-101	241-BX-110	241-C-102	241-S-101	241-U-102
241-A-102	241-BX-111	241-C-104	241-S-102	241-U-103
241-A-103	241-BY-101	241-C-107	241-S-103	241-U-105
241-A-106	241-BY-102	241-C-109	241-S-105	241-U-106
241-AX-101	241-BY-103		241-S-106	241-U-107
241-AX-102	241-BY-104		241-S-107	241-U-108
241-AX-103	241-BY-105		241-S-108	241-U-109
	241-BY-106		241-S-109	241-U-111.
	241-BY-108		241-S-110	
	241-BY-109		241-S-111	
	241-BY-110		241-S-112	
	241-BY-111		241-SX-101	
	241-BY-112		241-SX-102	
			241-SX-103	
			241-SX-104	
			241-SX-105	
			241-SX-106	

2.2.4.3 Purex Process Waste Storage in Double-Shell Tanks. All SSTs were taken out of service by 1980. Therefore, the wastes generated by PUREX operations between 1983 and 1990 would have been sent to the DSTs. Tank farm specifications existing before the PUREX restart in 1983 did not allow for separable phase organics in the DSTs. The specification for no separable phase was based on a potential fire or explosion hazard in the 242-A Evaporator. This specification was reevaluated, and a basis was developed to allow up to 946 L (250 gal) of separable phase organic to accumulate in the DSTs in the AN or AW Farms (Kirch 1983).

PUREX OWW (solvent treatment waste) was stored in PUREX tanks TK-G8 and TK-R8 and was batch transferred to the 241-AW Tank Farm during the 1980s. A separable phase organic layer was normally present in tanks TK-G8 and TK-R8, but these tanks were equipped with interlocks to automatically terminate transfers to the AW Tank Farm if a <0.9 SpG was detected during sample evaluation (WHC 1994). Some separable phase organic existed in the AW farm, however, as evidenced by the collection of a layer of NPH in the 242-A Evaporator condensate collection tank (TK-C-100) on at least two occasions. The DST operating specification requires a minimum liquid level of 0.9 m (3 ft) above the evaporator feed pump in tank 241-AW-102 to prevent separable phase organics from entering the feed pump.

2.2.4.4 Evaporation of PUREX Process Solvents. As discussed above, a portion of the PUREX organic wastes was sent to the self-boiling, HLW tanks in the A and AX farms. The semivolatile organics would have been distilled or steam stripped from the waste and disposed of with the condensate to cribs. A portion of the organic waste, however, was transferred to nonboiling tanks in C farms and later to DSTs.

Long-term storage of separable phase organics in the tanks enables a significant amount of evaporation to occur particularly under active ventilation conditions.

Tributyl phosphate has a relatively low volatility with a vapor pressure of only 0.0006 mm Hg at 4 °C (25 °F). The vapor pressure increases logarithmically with temperature from 15 mm Hg at 173 °C (343 °F) to 760 mm Hg at 280 °C (536 °F) (Moore 1980). Normal paraffin hydrocarbon also has a relatively low volatility; the vapor pressure is lower than that of water at the same temperature. The vapor pressure of NPH increases from 1.08 mm Hg at 25 °C (77 °F) to 760 mm Hg at 227 °C (441 °F) (Moore 1980).

Although the mixture of NPH and TBP has a relatively low volatility, evaporation will cause the removal of these organics over time. Kirch (1983) estimated that 946 L (250 gal) of NPH would be evaporated in less than a month if stored at 40 °C (104 °F) in an actively ventilated tank (4.25 m^3/min [150 scfm] ventilation rate). In Babad (1996) it is also concluded that light end solvents would have been distilled off by this time.

Under passive ventilation conditions, evaporation would be considerably slower. Over a 6-year period of mostly passive ventilation, 9,369 L (2,475 gal) (a waste level decrease of 0.9 in.) of solvent in tank 241-C-103 is estimated to have evaporated (Postma et al. 1994).

Because of its low volatility but significant chemical reactivity, stored TBP is more likely to react chemically than to evaporate. Chemical aging of process solvents is discussed below.

2.3 CHEMICAL AGING OF PROCESS SOLVENTS AND THEIR DEGRADATION PRODUCTS

This section reviews what is known about how organics in tank wastes are aging, and it identifies major aging products. The information derives from literature precedents, aging experiments with simulated wastes, and analyses of actual tank waste samples. The study of the aging of waste organic chemicals has included both complexants and process solvents. Complexant aging is discussed in Meacham et al. (1997). A detailed discussion of solvent aging is included as Appendix L to this report. Information from Appendix L is summarized in this section.

The study of the aging of solvent components began in 1993 and is less advanced than studies on the aging of complexants. A literature review (Camioni et al. 1996) was performed to gather information about aging reactions. Table 2-5 summarizes the information pertinent to the aging of organic solvents which is discussed in the following paragraphs.

Table 2-5. Organic Chemical Constituents of Hanford Single-Shell Tanks Waste Process Solvents.

Solvents Disposed to Hanford Site Single-Shell Tanks		Quantity (kg)	Inferred Fate of Constituent	Principal Degradation Product		Inferred Fate of Constituent
Name	Chemical Formula			Name	Chemical Formula	
Tributyl phosphate	$C_{12}H_{27}PO_4$	7.2E+05	Partially converted to salt of dibutyl phosphate. Remaining inventory present as immiscible phase floating on supernatant. Sodium dibutyl phosphate ages rapidly under tank conditions	Sodium dibutyl phosphate	$NaC_8H_{18}PO_4$	Partially converted to salt of monobutyl phosphate. Remaining inventory probably present as solute because of high solubility of sodium salt.
				Butyl alcohol	$C_4H_{10}O$	Present as a precipitate if calcium, aluminum or iron salts are stable in caustic, but only in near neutral conditions.
				Sodium Phosphate	$Na3PO_4$	Saponification product of tributyl phosphate with a very high vapor pressure.
Normal paraffin hydrocarbons	Mixture of C_{10} through C_{14} normal hydrocarbons	1.31E+06	Major fraction of inventory probably lost to evaporation. Limited conversion to salts of long chain carboxylic acids.	Salts of long chain carboxylic acids (e.g., sodium dodecanoate)	$NaC_{12}H_{23}O_2$	If formed, the sodium salt would be present as waxes or oils.
Methyl isobutyl ketone (Hexone)	$C_6H_{12}O$	Unknown	Essentially all solvent originally present lost to evaporation. Limited conversion to salts of isobutyric and acetic acids.	Salts of isobutyric acid (e.g., sodium isobutyrate)	$NaC_4H_2O_2$	Like acetic acid, isobutyric acid would be present largely in aqueous phase.
				Ketones	$C_nH_{2n}O$	

2.3.1 Aging of Tributyl Phosphate

Viable thermal and radiolytic pathways exist for degrading TBP. Although TBP is only partly soluble in water, when contacted with alkaline solutions it hydrolyzes to DBP, which is soluble and stable in alkaline solutions (Burger 1955). Rates for alkaline hydrolysis of TBP depend strongly on temperature and hydroxide concentration. Undiluted TBP hydrolyzes in 1 *M* sodium hydroxide with rates of 0.88, 4.4, and 283 mg/L/h at 30 °C, 50 °C, and 90 °C (86 °F, 122 °F, and 194 °F), respectively (Burger 1958 and Kennedy and Grimley 1953). Direct radiolysis of undiluted TBP either by gamma rays or MeV electrons produced dibutyl phosphoric acid and lesser amounts of monobutylphosphoric acid (Wilkinson and Williams 1961, Burger and McClanahan 1958, and Burr 1958). Hydrogen and C1 through C4 hydrocarbon gases are also produced. In addition, polymers are formed but have not been identified. Irradiation of TBP diluted in hydrocarbon solvents also produces DBP and monobutyl phosphate products (Barelko et al. 1966). Hydrogen atoms produced by radiolysis of water and hydrocarbons offer a radiation-inducted path for cleaving alkyl phosphate esters (Camaioni et al. 1996). In this path, the H atom adds to the P=O bond and an alkyl radical cleaves preferentially because the C-O bond is weaker than the H-O bond.

Burger (1958) reports that hydrolysis of TBP under alkaline conditions appears to stop after one butyl group is removed. Accordingly, DBP may accumulate in tank wastes that received PUREX solvent wastes unless radiolytic degradation or metal-catalyzed hydrolysis reactions occur with significant reaction rates. Barney (1994) has extended his organic waste solubility studies to include DBP. Results show that mono- and DBPs have high solubilities in water. Calcium, aluminum, and iron salts are insoluble in water. They will be made soluble in 1 *M* sodium hydroxide (converting to sodium salts) by precipitating iron, calcium, and aluminum hydroxides.

Theoretically, at near neutral conditions, DBP would distribute between the solid and supernatant phases depending on the concentrations of sodium hydroxide and the availabilities of metal ions such as calcium, aluminum, and iron in the tanks. However, under the moderate to highly alkaline conditions found in Hanford Site waste tanks, little DBP will be found in the solid phase.

2.3.2 Aging of Normal Paraffin Hydrocarbon

Radiolysis pathways for NPH aging are probably more important than thermal pathways. Lacking activated C-H bonds, even air oxidation requires elevated temperatures. Direct radiolysis produces saturated hydrocarbons of higher and lower carbon numbers, olefins, and hydrogen (Bugaenko et al. 1993). Alkyl radicals and H atoms are transiently produced (Bugaenko et al. 1993). Hydrogen, HO, and NO_3 radicals, generated via supernatant radiolysis (Neta and Huie 1986 and Buxton et al. 1988), also could attack hydrocarbons, generating alkyl radicals. The fate of radicals and resulting products depends on concentrations of trapping agents: O_2, NO_x, NO_2^-, etc. Combining with O_2, NO_x, and NO_2^- may ultimately produce oxidized products (Camaioni et al. 1996, Meisel et al. 1991 and 1993) but combining with other alkyl radicals could lead to higher molecular weight hydrocarbons.

2.3.3 Aging of Hexone

Hexone, with activated C-H bonds located at tertiary and ß-carbonyl positions, will be amenable to air oxidation and attack by radiolysis radicals. Plausible oxidation products are the salts of isobutyric and acetic acids that would form by oxidative scission of α-carbonyl bonds. Aldol condensation products are not expected to contribute significantly to hexone aging. In practice, the equilibrium between ketone and the condensation product must be driven to obtain product in good yield. This can be accomplished under basic conditions by precipitating the condensation product with an alkaline earth metal (House 1972).

$$CH_3COR + HO^- \rightleftarrows CH_2 = C(O^-)R + H_2O$$

$$CH_2 = C(O^-)R + CH_3COR \rightleftarrows CH_3RC(O^-)CH_2COR$$

$$2\ CH_3RC(O^-)CH_2COR + Ca^{+2} \rightleftarrows [CH_3RC(O^-)CH_2COR]_2Ca.$$

Any hexone that has not evaporated or reacted by the present time will be distributed between aqueous and hydrocarbon phases. Hexone aging products, except for oxalic acid, will be soluble in the tank supernatants (Barney 1994).

2.3.4 Evidence from the Organic Layer of Tank 241-C-103

The floating organic layer in tank 241-C-103 has been sampled and analyzed (Pool and Bean 1994 and Campbell et al. 1994). The floating layer consisted of NPH (25 wt% C12 through C15), TBP (47 wt%), and DBP (2 wt%). Approximately 25 wt% could not be analyzed by gas chromatography. Much of this material appeared to be inorganic. No polymeric or high-molecular-weight materials were identified. Alkaline hydrolysis of TBP is sluggish under the conditions in tank 241-C-103 where the pH is <10 (Pool and Bean 1994) and the temperature is <40 °C (<104 °F).[4]

The ratio of NPH to TBP used in PUREX was 70/30 vol% compared to about 30/70 vol% in tank 241-C-103. The inverted ratio in tank 241-C-103 suggests that a significant portion of NPH has evaporated. Distillation theory also predicts that the low-end NPH components are depleted.

The physical properties of the organic layer in tank 241-C-103 are used for consequence calculations for solvent mixtures in tanks. It is assumed that no solvent mixtures in any tanks retain volatile fractions more flammable than the solvent in tank 241-C-103. Calculations performed by Fauske and Associates (Babad 1996) support this assumption.

[4] Tank 241-C-103's headspace temperature is approximately 38 °C (100 °F) (Grigsby and Postma 1995).

2.3.5 Chemical and Radiological Aging Studies

Chemical and radiological aging studies of organic solvents were performed at Pacific Northwest National Laboratory. The studies involved irradiating a simulated waste containing organic solvent components (dodecane, TBP, DBP, and hexone) and complexants (EDTA and citrate) in an aqueous slurry of hydroxide, nitrate, nitrite, aluminum hydroxide, and a variety of alkali, alkaline earth, and transition metal cations. The results are reported in Camioni et al. (1996). The disappearance of reactants and the appearance of products in both gas and condensed phases are a function of temperature (50 °C to 90 °C [122 °F to 194 °F]) and dose (0.07 MGy to 1.2 MGy [7 Mrad to 120 Mrad]). The results showed hydrogen, nitrous oxide, nitrogen, and ammonia produced while oxygen levels in the headspace fell to a steady-state level, even though the organic material present was sufficient to consume it entirely.

The apparent order of aging was TBP> DBP>>hexone and EDTA>>dodecane. Of these compounds, TBP is most readily degraded in the absence of radiolysis (Burger 1958). The decomposition of the other compounds requires radiolysis. Dodecane and stearate degrade slowly under the applied conditions. Insolubility of dodecane, an NPH compound, and stearic acid, an aging product of NPH, in the aqueous phase probably contributes to their apparent stability. The water-soluble organics are much more effective in scavenging radicals generated by water radiolysis. Dibutyl phosphate recovered from the irradiated simulant was much less than that initially present and showed little variation with dose.

2.4 SUMMARY REGARDING SOURCES AND FATE OF HANFORD PROCESS SOLVENTS

Hundreds of thousands of gallons of waste containing organic solvents have been sent to the underground storage tanks. At first consideration, it seems surprising that only one tank is known to have a separable organic phase on the waste surface. However, evaluating the properties of NPH/TBP components and other solvents such as hexone and looking at the history of tank farm operations indicates that many solvents would have evaporated. The remaining solvents have been subjected to chemical and radiolytic processes that make some soluble in basic solutions and convert some to solid forms. It is concluded that the solvent mixture found in tank 241-C-103 is bounding in terms of flammability, and its properties are used in safety analyses. The following paragraphs summarize which solvents have been included in this study.

2.4.1 Hexone (Reduction and Oxidation Solvent)

The concentration of hexone in the waste streams sent to the tank farms was estimated to be less than 0.3 ppm by Borsheim and Kirch (1991) and Prosser (1986). The hexone that was sent to the tank farms has been in storage for at least 30 years. (Hexone was last used in 1967.) With a moderate boiling point of 116 °C, the remaining hexone should have evaporated. In addition, most tank supernatants have been processed through some form of evaporator to reduce the waste volume. Any evaporation process would have removed residual

hexone in the waste. Hexone should not be a significant waste constituent, and it is not expected to be found in significant quantities as a separable phase in the waste tanks. The results of the headspace sampling in 81 tanks have been reviewed in the TWINS Database (PNNL 1997). No significant quantities of Hexone (2-Hexanone) have been found.

2.4.2 Uranium Recovery Process Solvents

This process used a TBP-kerosene mixture as a solvent. This process was last used in 1957, so the waste has been in storage for at least 39 years. Kerosene, like NPH, is not readily degraded by radiolysis. With its moderate boiling point and chemical and radiolytic stability, kerosene should be more susceptible to evaporation than degradation. Because of the large amount of waste generated by the uranium recovery process, most tank supernatants have been subjected to some evaporative waste reduction processes. The evaporative processes would have removed the kerosene by steam distillation and disposed of it along with the aqueous condensate. Kerosene, or theoretically possible degradation products, should not be a significant waste constituent in an organic liquid phase and is not included in this analysis.

Tributyl phosphate has a high boiling point and is easily hydrolyzed to DBP in basic solutions or converted to di-butyl phosphate by radiolysis. Chemical and radiolytic degradation, rather than evaporation, are expected to be the primary factors affecting TBP. Therefore, TBP is included in this analysis.

2.4.3 B Plant Waste Fractionization Process Solvents

The solvent treatment wastes for this process were concentrated in an atmospheric evaporator before they were transferred to the tank farms. Any entrained NPH would have been steam stripped into the concentrator overhead stream and disposed of with the condensate (Borsheim and Kirch 1991). Therefore, these solvents are not expected to be found, in significant quantities, as a separable phase in the waste tanks.

2.4.4 PUREX Process Solvents

The largest quantities of organic-solvent-containing wastes sent to the tank farms came from the PUREX process. A very conservative estimate (Sederburg and Reddick 1994) was 2,490 kL (657 kgal) of a TBP-diluent mixture. Most of this was in the form of OWW. As previously explained, the primary factor affecting TBP is chemical or radiolytic degradation, and TBP is included in this analysis. All the diluents have relatively high boiling points when compared to hexone or butanol (see Table 2-1). Therefore, it is expected that the diluents lasted long enough that chemical and radiological degradation products are also a factor; therefore, they are included in this analysis.

3.0 HAZARD AND ACCIDENT PHENOMENA

This section describes potential combustion hazards of separable phase organic liquid waste tank storage and concludes that solvent pool fires are the only credible combustion hazard posed by these materials.

3.1 DEFLAGRATION IN HEADSPACE AIR

The waste in SSTs generates flammable gases through three mechanisms:

- radiolysis of the waste which produces hydrogen and ammonia caused by the presence of water, nitrates, and/or nitrites
- corrosion of the steel liner which produces hydrogen
- chemical dissociation or decomposition of organic compounds in the waste which are facilitated by heat, radiation, and the presence of certain catalysts (e.g., the aluminate ion): methane, hydrogen, ammonia, and nitrous oxide are some volatile products of the breakdown.

The gases generated by the waste are generally expected to be released to the tank headspace. Organic liquids in the tank contribute vapors to the headspace through evaporation. These organic liquids are comprised of solvents used in the various Hanford Site chemical separation processes, most notably PUREX.

The hazard posed by flammable gases is the subject of separate evaluation and safety analysis. However, this report evaluates the hazard posed by solvents, and it concludes that organic solvent vapors 1) are not a flammability hazard on their own, and 2) contribute little to headspace flammability. Vapor sampling results from 81 tanks are reported in Huckaby et al. (1997). The highest solvent vapor concentration is found in tank 241-C-103. Tank 241-C-103 data is used in this example.

The evaluation is described in Appendix D and consists of the following:

- reviewing key phenomena that determine headspace vapor concentrations
- calculating vapor contribution to headspace flammability as a function of temperature for a base case situation
- evaluating vapor concentrations that can be expected for various pool sizes and tank ventilation rates through parametric analysis around the base case
- comparing predictions to available measured values
- combining these insights to form a conclusion regarding the tank farm safety analysis assumption.

3.1.1 Key Phenomena

Key phenomena that determine the significance of solvent vapor with respect to headspace flammability are summarized as follows.

3.1.1.1 Vapor-Liquid Equilibria. Solvent vapors originate from solvent liquid. The concentration of vapors at a liquid-air interface represents a boundary condition that affects the transport rate and steady-state concentration of vapors in headspace air. Equilibrium concentration in the vapor phase is determined by the composition of the liquid and the interfacial temperature.

3.1.1.2 Mass Transport Rate from Liquid to Headspace Air. The steady-state airborne concentration of solvent vapors in headspace air is affected by the rate at which vapors are transported from the liquid-air interface into the bulk air volume. The rate of mass transfer depends primarily on the following factors:

- geometry of transport path
- mass transfer rate per unit area of transport path
- concentration gradient between the liquid-air interface and bulk headspace air

3.1.1.3 Vapor Loss Rate by Ventilation. The steady-state airborne concentration of solvent vapor in headspace air is affected by the rate at which vapors are carried out of the tank by ventilation air. The flow rate of ventilation air and the airborne concentration of vapors govern the vapor loss rate from headspace air.

3.1.1.4 Aerosol Formation. Condensation of solvent vapors in headspace air could, under restrictive conditions, cause formation of an aerosol. Aerosols composed of flammable species would contribute to headspace flammability in proportion to the airborne concentration; aerosol particles (diameter $\leq 10\ \mu m$) can be expected to behave similarly to vapors of the same material with respect to a deflagration (Zabetakis 1965). Aerosol mass concentration is therefore the key parameter in assessing the importance of solvent aerosols with respect to headspace flammability.

It should be noted that aerosols can be formed by fragmentation of liquid in processes where mechanical energy is dissipated in a liquid. These means for generating aerosols are discounted for normal interim storage because mechanical energy sources are not present in the tanks during this mode of operation. Waste-intrusive operations involved in characterization activities, equipment installation or removal, or during future waste retrieval operations should be evaluated for their potential to generate aerosols.

3.1.2 Calculation of Vapor Contribution to Headspace Flammability

3.1.2.1 Base Case. The organic vapor contribution to headspace flammability is evaluated by calculating headspace concentrations and determining the percent of the lower flammability limit (LFL) these concentrations represent. Calculations were made for a base case configuration (i.e., a 1-m^2 [10.8-ft^2]) solvent pool in a passively-ventilated tank). The ventilation rate is 17 m^3/h. The results are shown as a function of headspace temperature in Figure 3-1 for two different organic compositions: fresh PUREX solvent and the evaporated PUREX solvent contained in tank 241-C-103. Fresh solvent composition represents an upper bound on volatility (and therefore on percent LFL) because solvents in tanks today would have been stripped of the more volatile component by evaporation into headspace air. The composition of tank 241-C-103 solvent was chosen as one that could typify aged solvents currently in the tanks. Less volatile solvents might also exist in tanks, but their flammability, expressed as percent LFL, would be even lower than calculated for the tank 241-C-103 composition.

The curves of Figure 3-1 indicate that 25 percent of the LFL would be reached at headspace air temperatures of about 97 °C (207 °F) for fresh solvent and approximately 125 °C (257 °F) for tank 241-C-103 solvent. It is predicted that 100 percent of the LFL will be reached at temperatures of 130 °C and 161 °C (266 °F and 322 °F) for fresh and tank 241-C-103 solvent, respectively. The computational approach is discussed in Appendix D.

3.1.2.2 Parametric Result. Parametric variations from the base case for pool area, ventilation rate, and temperature area were analyzed to determine sensitivities and to determine under what conditions solvent vapors could present a significant contribution to head space flammability.

<u>Ventilation Rate</u> - Ventilation rates of tank headspaces affect the predicted percent LFL as discussed in Appendix D.

The impact of ventilation air flow rate on solvent vapor concentration is illustrated by the data in Table 3-1. Typical passive ventilation flow rates decrease the headspace vapor concentration by a factor of about 10 below the case with no ventilation.

Table 3-1. Effect of Ventilation Rate on the Predicted Contribution of Solvent Vapor to Flammability For a 1-m^2 Pool and a Headspace Air Temperature of 30 °C.

Ventilation Rate m^3/h	Predicted Percent of the LFL At Headspace Air Temperature of 30 °C	
	Fresh Solvent	Tank 241-C-103 Solvent
0	4.76	0.69
0.43 (atm. fluctuations alone)	3.64	0.52
1.84 (atm. fluctuations + 50 ft^3/h)	2.04	0.29
17.0 (10 ft^3/min)	0.36	0.049
170.0 (100 ft^3/min)	0.038	0.0053

Pool Area - The effects of pool area on headspace vapor concentration are shown in Table 3-2. These data apply for a ventilation rate of 10 ft^3/min.

Table 3-2. Effect of Pool Area on the Predicted Contribution of Solvent Vapor to Flammability at a Headspace Temperature of 30 °C.

Pool Area m^2	Predicted Percent of the LFL at Headspace Air Temperature of 30 °C	
	Fresh Solvent	C-103 Solvent
411	4.62	0.67
20	2.94	0.42
10	2.13	0.30
1	0.36	0.05
0.1	0.04	0.005

The data in Table 3-2 indicate that a 1-m^2 pool is predicted to generate vapor concentrations that are 8 percent as high as a pool covering the whole tank cross-section, 411 m^2 (4,424 m^2). For the 411-m^2 pool area, headspace air is predicted to be within three percent of the saturated, i.e. upper limit, concentration. The saturated concentrations for fresh and tank 241-C-103 solvents are 4.76 percent LFL and 0.69 percent LFL, respectively, as displayed in Table 3-1 where percent LFL is shown for a hypothetical leak-tight tank (ventilation rate = 0).

Temperature - The temperature at which 100 percent of the LFL is reached corresponds to the flashpoint of a liquid. For the zero ventilation flow case, the methodology used to calculate the data displayed in Figure 3-1 and

Tables 3-1 and 3-2 yields 100 percent of LFL at temperatures of 81 °C and 109 °C (178 °F and 228 °F), respectively, for the fresh and tank 241-C-103 solvents, respectively. These predicted flashpoints agree reasonably with measured flashpoints of 99 °C and 118 °C (210 °F and 244 °F) (Pool and Bean 1994) for a freshly prepared solvent and for solvent removed from tank 241-C-103. The predicted flashpoints are lower than measured, indicating that the methodology used in Appendix D yields conservative predictions; that is, it tends to overpredict interfacial solvent vapor concentrations in the neighborhood of the flashpoint.

For comparison purposes, the highest temperature recorded in the waste in C-103 during the month of September, 1998, was 47 °C (116 °F). The waste temperatures vary by a few degrees each month depending on the season. However it can be seen that the waste temperature doesn't approach the flashpoint.

3.1.3 Conclusion Regarding Solvent Contribution to Headspace Flammability

Based on the parametric analysis described in Appendix D, solvent vapors would only be a significant contributor to headspace flammability (i.e., >25 percent of the LFL) under the following circumstances.

1. The tank contained a significant solvent pool (e.g., >1 m^2 [10.8 ft^2] area) or an even larger solvent lens deeper in the waste solids.

2. The tank ventilation rate is low.

3. The tank headspace temperature is unusually high.

Warmer tanks are less likely to contain significant quantities of solvent vapors because the warm temperatures would have caused increased evaporation of the more volatile components over many years of storage. Tanks with higher heat loads have also been on active ventilation for many years. Cooler tanks may have enabled solvent to persist over many years of storage and are sufficiently cool to limit vapor concentrations to small values as evidenced by tanks 241-C-103 and 241-BY-108. Of the 81 tanks vapor sampled, the largest vapor contribution to headspace flammability is about 2 percent of the LFL.

Based on this evaluation and available headspace vapor sample data, it is reasonable to assume the solvent contribution to headspace flammability is small.

Figure 3-1. Predicted Percent Lower Flammability Limit of Solvent Vapors in a Passively Ventilated Single-Shell Tank.

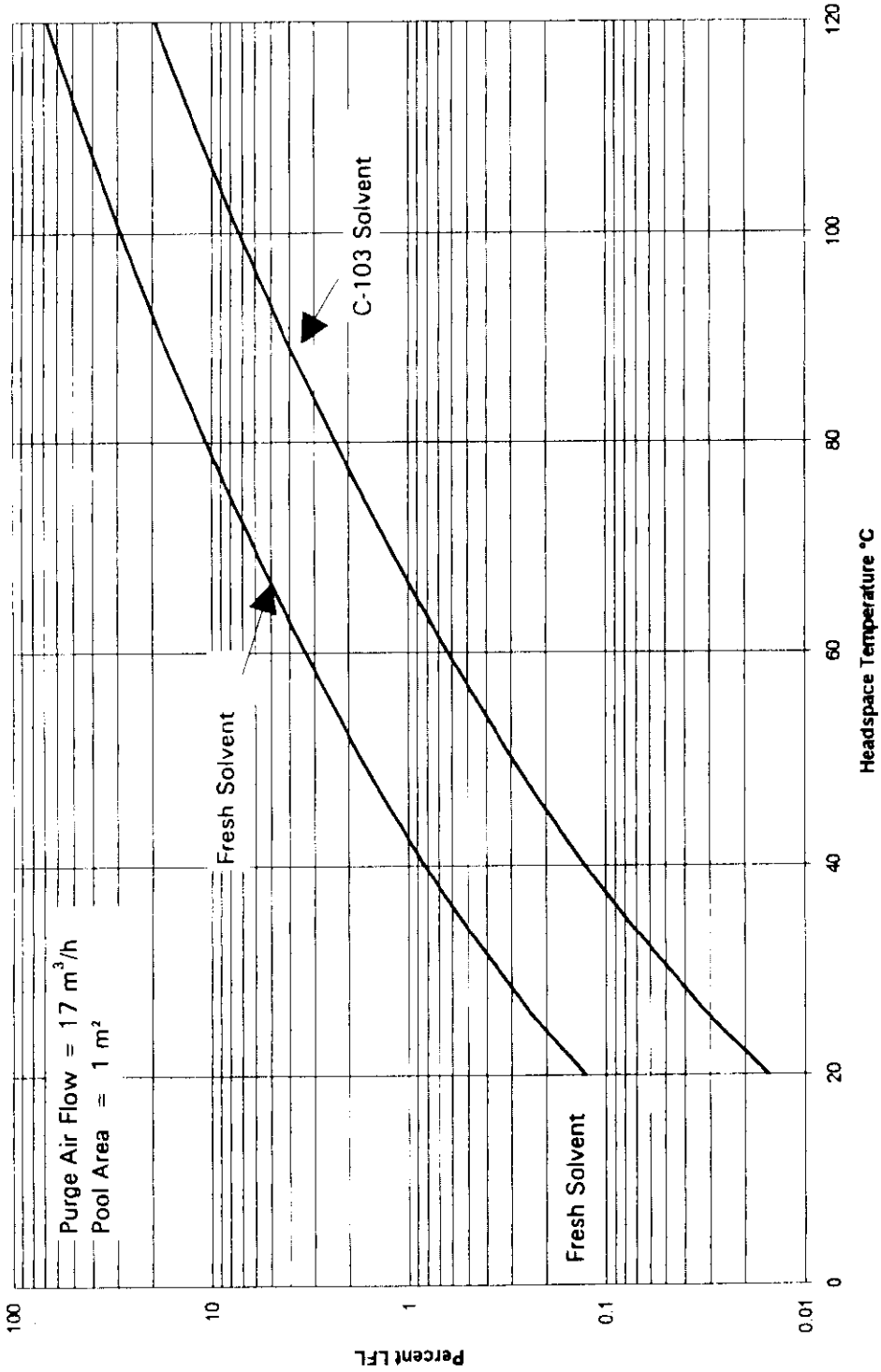

3.2 ORGANIC-NITRATE/NITRITE REACTIONS

Organic nitrate/nitrite, condensed-phase, propagating exothermic reactions are theoretically possible in waste sludges and saltcakes. A hypothetical sequence of events that describes the postulated hazard of organic nitrate/nitrite reactions in the sludges or saltcakes is as follows.

- Aqueous supernatant is lost from the tank through a leak or pumping process, and organic liquid has permeated waste sludges or saltcakes. (An example of this loss of aqueous supernatant is tank 241-BY-108, which was saltwell pumped.)

- The organic liquid is combustible.

- An energetic ignition source is accidently introduced into the tank at the pool-air interface, igniting a pool fire. The pool fire spreads over a large area.

- Heatup of the sludge or saltcake by the burning pool to the reaction onset temperature triggers a propagating organic nitrate reaction in the sludge leading to the release of heat and gases. Vented gases carry entrained material causing the release of radioactive material. Relatively low-developed pressures (about 9 kPa [1.3 psig]) rupture HEPA filters. Tank structural integrity is challenged for higher combustion pressures.

The hypothetical sequence of events described above is possible only if the exothermic reactions in sludge or saltcake release enough thermal energy to support a propagating reaction (i.e., adequate fuel and sufficiently low moisture).

Organic-nitrate propagating exothermic reactions are the subject of separate evaluation and safety analysis (Meacham et al. 1997). This report evaluates the effects on combustion limits and energetics of mixing separable phase organic liquid wastes with condensed phase organic nitrate compounds. Tests and experiments, performed to investigate the potential for process solvents and solvent degradation products to burn with nitrates, have concluded that these compounds do not support propagating exothermic reactions with nitrates or nitrites. The bases for this conclusion are described below and in Appendix E.

The potential for organic compounds to burn with nitrates and/or nitrites is a hazard that has been studied extensively relative to Hanford Site waste tanks. The focus of the hazard evaluation has been the organic complexants such as EDTA, HEDTA, citrate, and their degradation products (e.g., acetate, formate, oxalate, carbonate). These compounds are nonvolatile and can exist as solids at high temperatures when nitrate becomes an effective oxidizer. However, as discussed in Section 2.1, a significant quantity of the organic compounds sent to the tank farms were semivolatile process solvents and their degradation products. Tests were performed to investigate the following potential hazards involving process solvents or their degradation products:

- potential condensed-phase propagating reactions when mixed with sodium nitrate and initiated with an adequate ignition source

- increasing of the fuel value of the waste such that an otherwise nonpropagating mixture (too little organic complexant like sodium acetate) turns into a reactive mixture that can support a propagating reaction given an adequate ignition source

- a surface pool or wicked fire, involving a solvent and headspace air, transition into a condensed-phase combustion regime given adequate organic complexant fuel.

Solvents tested included TBP, a mixture of 30 vol% TBP and 70 vol% NPH. The 70 vol% of NPH is composed of 11.6 percent dodecane, 23.4 percent tridecane and 35 percent tetradecane on a total volume basis. Degradation products tested included DBP and the salt aluminum dibutyl phosphate (AlDBP).

3.2.1 Solvent and Solvent Degradation Product Condensed-Phase Reactions with Nitrate/Nitrite

In contrast to nonvolatile organic complexants, condensed-phase propagating reactions have not been observed with TBP, DBP, PUREX solvent simulants (30 percent TBP, 70 percent NPH), or their salts such as AlDBP or di(2-ethylhexyl)phosphate when mixed with nitrate oxidizer and tested in an adiabatic calorimeter (i.e., Reactive Systems Screening Test [RSST]) or during tube propagation (TP) tests.

The RSST, described in Appendix E, is used to measure the ignition temperature of combustible mixtures. Combustible mixtures of nonvolatile organic complexants (e.g., acetate or citrate) and nitrate exhibit a sharp self-heating rate change. This change occurs when the ignition temperature is reached, and the chemical reaction transitions from a self-heating reaction to a propagating, wave-like combustion reaction. The solvents and degradation products tested with nitrates did not exhibit this transition.

Table 3-3 lists the tested mixtures. The only two mixtures that showed a propagating reaction had sufficient organic salt (sodium citrate) mixed with the oxidizer (sodium nitrate) to support a propagating reaction without dodecane being present. Eight weight percent total organic carbon (TOC) of citrate is the threshold for a propagating reaction. Mixtures that contain less than 8 wt% TOC of citrate will not support a propagating reaction, even if a solvent (dodecane) is added to bring the TOC content to over 8 wt%. The lack of propagating reactions is attributed to the decomposition of these materials in the 150 °C to 200 °C (302 °F to 392 °F) range, which is below the ignition temperature for organic-nitrate mixtures (220 to 300 °C [428 °F to 572 °F]).

Table 3-3. Solvent-Nitrate Combustion Test Results.

Test/Fuel	Propagating Reaction (Yes/No)
RSST - 10 wt% TOC TBP/$NaNO_3$	No
RSST - 28 wt% TOC TBP/$NaNO_3$	No
RSST - 5 wt% TOC DBP/$NaNO_3$	No
RSST - 10 wt% TOC DBP/$NaNO_3$	No
RSST - 22.6 wt% TOC PUREX simulant[1]/saltcake[2]	No
DTP[3]- 8 wt% TOC citrate/$NaNO_3$	Yes
DTP - 11.3 wt% TOC PUREX simulant $NaNO_3$	No
DTP - 8 wt% TOC AlDBP/$NaNO_3$	No
DTP - 5 wt% TOC sodium butyrate/$NaNO_3$	No
DTP - 6 wt% TOC sodium butyrate/$NaNO_3$	No
DTP - 3 wt% TOC citrate, 3 wt% TOC AlDBP/$NaNO_3$	No
DTP - 7 wt% TOC citrate, 8.5 wt% TOC AlDBP/$NaNO_3$	No
Visual bench test - 11 wt% TOC citrate/$NaNO_3$[3] saturated with dodecane	Yes - following pool burning of dodecane

Notes:
[1]PUREX simulant - 30% TBP/70%NPH (11.6% dodecane, 23.4% tridecane, 35% tetradecane)
[2]Tank 241-BY-104 saltcake simulant
[3]8 wt% or greater TOC citrate/$NaNO_3$ will support a propagating reaction without dodecane present.

Tube propagation tests have been carried out to measure combustion temperatures and combustion rates in connection with sustained propagation through cold material when subjected to a large ignition source. Appendix E gives test descriptions. When combustible mixtures are tested, the combustion front travels down the length of the tube as evidenced by rapid temperature spikes observed by thermocouples located along the tube's length. Mixtures of solvents and solvent degradation products and nitrates showed no signs of a propagating reaction during these tube propagation tests. See Meacham et al. 1997, Appendix, C for more discussion of tests.

3.2.2 Solvent Addition to Waste Organic Fuel Value

Waste surrogates that included nitrate oxidizer and a mixture of organic complexant fuel (i.e., sodium citrate) and solvents were prepared. Table 3-3 shows the tested mixtures. Experiments with organic complexant simulants indicate that propagating reactions can be expected when the complexant/nitrate mixture's theoretical heat of reaction exceeds about 1,600 J/g (for dry materials). A complexant/solvent mixture of 3 wt% TOC sodium citrate and 3 wt% TOC AlDBP was tested in a TP test. This mixture has a theoretical heat of reaction of 1,840 J/g but did not show any signs of propagating reactions. A 7 wt% TOC sodium citrate/8.5 wt% TOC dodecane mixture also showed no signs of propagating reactions. Sections 2.0 and 3.0 and Appendix E show the test methods and results.

The absence of a condensed-phase reaction is consistent with previous tests that indicated at least 8 wt% TOC sodium citrate is necessary to support propagating condensed-phase reactions. The dodecane does not appear to contribute to the condensed-phase reaction "fuel value" in any significant way. The conclusion drawn from these experiments is that waste solvents (or their degradation products) do not add to the waste fuel value in terms of supporting propagating reactions.

3.2.3 Solvent Fire Transition to Condensed-Phase Combustion

The test data described above indicate that solvents and their degradation products do not contribute to the waste fuel value regarding condensed-phase reactions. Testing also was performed to investigate the potential for a solvent-air pool fire to transition to a condensed-phase organic complexant-nitrate propagating reaction. Tests were performed with complexant-rich mixtures saturated with dodecane and covered by a shallow pool of dodecane. Visual bench-top tests (detailed in Appendix F) were performed where the pool of dodecane was ignited with a torch. Dodecane-air pool burning occurred in the absence of condensed-phase combustion until the solvent pool was depleted. As long as the pool was present, the temperature in the underlying complexant/nitrate/dodecane mixture remained below condensed-phase reaction initiation temperatures.

After the pool was depleted, dodecane was vaporized from within the solids matrix, the air-vapor combustion raised the exposed complexant-nitrate material to ignition temperature, and the reaction transitioned to condensed-phase combustion. It is concluded that a solvent surface fire could only transition to a condensed-phase reaction if 1) the waste solids are sufficiently fuel rich and dry to support a condensed-phase reaction, and 2) the solvent pool is burned sufficiently to expose waste solids before the pool fire is extinguished because of lack of oxygen.

3.3 COMBUSTION OF ORGANIC LIQUID AS A POOL FIRE

Separable phase organic liquids can form a combustible situation by 1) being present as a free pool (or puddle) on the waste surface or 2) collecting sufficient concentrations entrained in the waste solids to form

a combustible area at the waste surface by capillary or wicking behavior. The subcooled liquid must be heated to flash point, at least, to form a flammable gas phase mixture with the headspace air. A hypothetical sequence of events describing this postulated hazard is as follows.

- Process solvents are transferred to an underground storage tank.
- Conditions in the tank limit evaporation and chemical aging, and solvents persist as a separable phase liquid. The organic liquid is combustible (i.e., will support a sustainable flame when ignited locally).
- Ignition sources are not controlled, and the liquid is ignited locally. Flame spreads over a large area of the pool or wick-saturated waste surface.
- The fire burns until oxygen is extinguished. The fire causes pressure and temperature to rise in the headspace gases. A sufficiently high pressure is reached, and a pressurized release of combustion gases and entrained material takes place to the atmosphere. Relatively low-developed pressure (about 9 kPa [1.3 psig]) ruptures HEPA filters, and pressures of about 75 kPa (11 psig) cause significant dome cracking in SSTs.
- Because the tank pressure is vented and the tank remains intact, a vacuum develops as the tank cools and the headspace gases contract.

Initiating a pool fire over a liquid that is below its flash point requires introducing an ignition source into a flammable air-fuel mixture above the pool and heating liquid (at least locally) to above the flash point. Tank 241-C-103 contains a combustible layer of organic liquid. Although no other tank is currently known to contain a pool of organic liquid, tank characterization data for tanks not yet vapor sampled are not adequate to rule out the possibility of other tanks containing organic liquid pools.

This page intentionally left blank.

4.0 PHENOMENOLOGY OF SOLVENT FIRE IGNITION

This section describes the circumstances under which separable phase organic liquids in the Hanford Waste Tanks may be combustible and the experiments and analyses that have been performed to estimate some of the requirements for ignition. Separable phase organic liquids may be combustible if they 1) exist as a free pool, puddle, or channel on the waste surface, or 2) are sufficiently concentrated and entrained in waste solids, such as sludge or saltcake, to ignite at the waste surface by capillary or wicking behavior.

Ignition requires solvents be heated above their flash points and an energy source to initiate ignition. The flash point of a flammable material is the temperature at which vapors in equilibrium with the material and its air space reach the LFL in air. A spark introduced into combustible vapors at the LFL can ignite a gas-phase deflagration that is perceived as a "flash." Currently, solvent temperatures in waste tanks are well below solvent flash points.

- The solvent in tank 241-C-103 is at a temperature of about 40 °C (104 °F), or about 75 °C (135 °F) below its measured flash point of 118 °C (244 °F).
- The solvent in tank 241-C-102 is about 90 °C (162 °F) below its expected flash point of 118 °C (244 °F).
- The waste surface temperature in tank 241-BY-108 is about 30 °C (54 °F), well below the flash point of evaporated PUREX solvent.

This section also reviews the possibility of solvent fires occurring in actively ventilated tanks or at multiple locations on a pool.

4.1 IGNITABILITY OF ORGANIC SOLVENT POOLS, PUDDLES, AND CHANNELS

Organic liquid in waste tanks (e.g., that currently present in tank 241-C-103) can only be made to burn with great difficulty when the initial liquid temperature is below the flash point. The issue is to determine what energy source is required to ignite cool organic liquid (i.e., many tens of degrees below the flash point.)

In a large pool or puddle, local heating of a liquid layer induces liquid convection because of changes in the surface tension brought on by a rising temperature. Strong convective flows at and near the liquid surface carry heat away from the source (assumed at or above the liquid surface), and lose heat convectively to the tank headspace or atmosphere above. A cool return flow runs countercurrent beneath the liquid surface. This means that large pools or puddle are difficult to ignite. Local heating must be sufficient to bring the local surface to a temperature above the flash point so that ignition can occur. The ignited region must also be large enough to cause flame spreading.

In small puddles, channels, or in sludges and saltcakes where liquid organic is embedded, ignition by local heating is easier. However, ignition can be hindered or possibly prevented by the presence of water in sludges and saltcakes.

Key aspects of solvent ignitability are studied through experiments and theoretical analysis as described in Appendix G and summarized below.

4.1.1 Organic Liquid Pools or Larger Puddles

The conditions for igniting organic liquid pools or larger puddles such as residual layers on top of sludge or water have been investigated experimentally and analytically. Igniting a pool requires 1) an energy source that locally heats the liquid to a temperature above its flash point, 2) enough heat to ignite the vapors, and 3) a sufficiently large locally heated region to sustain combustion (i.e., to prevent flame extinction). Because flame extinction or flame spreading may occur, depending on the region size, the latter condition is equivalent to stating that the energy source must locally heat and ignite a region of sufficient size to allow flame spreading on the remaining cool pool liquid. The following hypothetical events exhibit the conditions to ignite a cool pool.

1. Robust heating of a free pool surface. The heated region must be a sufficient size for a locally-ignited fire to spread to the rest of the subcooled pool. Based on experiments and analyses, the heat source must raise at least a 10-cm (4-in.)-diameter region of solvent above its flash point (see Appendix G). The power applied needs to be sufficient to overcome convective heat losses. The power required can be quantified based on experiments and theory described in FAI (1994). The required power is a function of the solvent depth and increases with depth. Layers less than 2 mm (0.1 in.) in depth have been shown to be non-ignitable. The solvent pulls away from the heat source, exposing the underlying waste or aqueous liquid rather than heating to the flash point.

   Appendix F calculates the energy source power requirements to reach ignition conditions. Assuming dodecane properties (which is conservative for the calculation relative to evaporated PUREX solvent), the power supplied to a layer slightly greater than 2 mm deep and 10 cm in diameter must exceed 200 W to ignite a fire that can spread to the rest of the pool. A 5-mm-deep layer requires at least 1,700 W.

2. Heating and ignition of a confined region. A region of the pool must be confined to prevent convective heat losses to the remaining liquid. The region must also be bulk heated to the liquid flash point to be ignited, and the radiant heat from this region must be sufficient to allow flame spread to the neighboring pool area. The confined region must be sufficiently large that its radiant heat loss causes ignition nearby. This is not likely unless the barrier responsible for fuel layer confinement is removed.

Confined regions from which flame spreading is possible must be 1) at least 10 cm (4 in.) in diameter and greater than 2 mm (0.1 in.) in depth, and 2) gradually and uniformly heated to the flash point. A reasonable bounding minimum energy required to ignite such a contained region is 2 kJ (see Appendix F). The actual initiator energies would be larger if the puddle were deeper than 2 mm.

3. Sustained burning of a large object. A burning object that produces radiant energy equivalent to burning the confined region described above is also sufficient to ignite the adjacent pool. The burning object is considered to have the same characteristic dimension as the burning confined region. A burning object must be at least 10 cm (4 in.) in diameter to cause flame spreading.

4. Spark initiation. Section 3.1.4 of Appendix G evaluates the potential for igniting an organic solvent fire with an electrical spark. It looks at the range of energies that could be produced by a discharge from electrically conductive objects that might be accidentally or deliberately introduced into a waste tank. Spark ignition differs from other initiators by timescale. A spark deposits a large amount of power in a local area for a brief time period, whereas other initiators are more sustained. The rapid transfer of energy to the solvent pool surface may raise the pool surface temperature to the flash point with little heat conducting to lower regions of the pool. Theoretically, the amount of energy needed to create a small flammable vapor cloud above the pool surface may be much less than that required to slowly heat the solvent pool to the flash point. Spark energy must exceed 2 J (0.2 MW spark power) to produce a 10-cm (4-in.)-diameter potentially flammable zone above the pool surface. This energy is well in excess of the maximum theoretical spark energies expected from objects that might enter the tank, considering that a highway tanker truck could conceivably produce a static discharge of 0.45 J (Eckhoff 1991).

4.1.2 Small Solvent Puddles

Small puddles are solvent pools with a diameter of 1 m^2 (10.8 ft^2) or less. As puddle size decreases, the convective flow of solvent away from the heat source becomes constrained, and the heat rejection capability of the puddle reduces. The energy source needed to heat the puddle to the flash point is reduced from the extremely large sources needed to ignite a large pool. Testing performed in a 0.6-m (2-ft)-diameter pan containing solvent indicated that solvent under a heater was not raised to flash point temperatures after absorbing 90 W of radiant heat, the maximum tested (FAI 1994). Ease of ignition for small puddles is, however, bounded by solvent-filled channels and solvent-permeated saltcakes as described below.

4.1.3 Solvent-Filled Channels

Organic solvent in cracks or channels in a sludge surface are confined to a one-dimensional convective flow for heat rejection; therefore, ignition and flame spreading occur more easily than in an open pool. Propagating a fire from a narrow channel into an open pool is subject to the same flame size constraints as for pools. On the other hand, fuel in a large pool connected to a burning channel may continuously supply fuel to the channel. These observations are summarized as follows.

- Relatively small initiators may start fires in narrow channels filled with tank waste solvent.
- These fires may continue as fuel from the pool flows back to the channels.
- Fires in channels cannot propagate into open pool areas unless the characteristic channel size exceeds the pool fire spreading threshold criterion.
- Consequence analysis discussed in Section 6.0 shows that fires in channels with limited surface area could not threaten tank integrity.

For additional information on a one-dimensional version of the thermocapillary convection analysis and on quantitative and qualitative experiments on convection and flame spreading, see Appendix G, Section 3.2.

A series of tests have been performed for relatively narrow (1.3 to 1.5-cm [0.5 to 0.6-in.]) channels (see Appendix G, Section 3.2). Such channels filled with dodecane could not be ignited with a small oxyacetylene torch. Wick-stabilized flames started at one end of the channel failed to cause flame propagation farther up the channel. Testing with radiant heaters determined that a channel filled with solvent could convect significant heat away from a heat source. A few tens of centimeters of channel length were adequate to dissipate more than 30 kW/m^2 of radiant heating applied to one end of a 1.3-cm-wide channel. Igniting the channel required the heated solvent be confined by a barrier to prevent convective cooling. Although small puddles and channels are easier to ignite than a large puddle or pool, a sizeable, sustained heat source is still required to cause ignition.

Igniting small puddles by hot particles and pyrotechnic "electrical matches" has also been attempted (see Appendix E). A test involved 6.3-cm (2.5-in.)-diameter puddles of dodecane. Applying a 138-J electrical match did not result in ignition. Dropping heated steel balls of various sizes into the puddle also did not result in ignition. The steel balls varied in size (1/16, 3/32, and 3/16 in. diameter) and were heated to about 1,300 °C (2,372 °F). This corresponds to energies of 10, 35, and 270 J, respectively.

4.2 ORGANIC LIQUIDS ENTRAINED IN WASTE SOLIDS

Because convective heat loss mechanisms are not effective when liquid organic is embedded in sludge or saltcake, ignition by local heating is easier than for open pools or large puddles. However, ignition can be hindered or possibly prevented by the presence of water in the wastes. The various key aspects of the ignitability of solvents entrained in sludge and saltcake are studied through experiments and theoretical analysis as described in Appendix G and summarized below.

4.2.1 Organic Liquid Entrained in Sludge

The sludge in most tanks, including tank 241-C-103, is expected to retain significant water following saltwell pumping. It is most likely that such a sludge mixture is impossible to ignite because of the preponderance of water relative to entrained or embedded solvent. Solvent ingression experiments conducted with tetradecane/TBP organic on top of water-saturated, kaolin sample materials (FAI 1994), are described below and in Appendix G.

Solvent-permeated sludge simulants were prepared and tested for ignitability. Samples were prepared by mixing moist sludge (moisture was varied) with an organic liquid mixture of 70 percent TBP and 30 percent tetradecane (C_{14}). Table 4-1 summarizes the estimated bounds on the entrained organic content in the sludge on a dry mass basis and by percent of TOC. Note that sludge samples were uniform in color (tan) and appearance (moist), and no free liquid was present on the sample surface or in channels in the (partially consolidated) sludge.

Table 4-1. Results of Sludge Burning Tests.

Test ID	3	7	6	2	5	4
Simulant composition						
sample net (g)	94.8	93.6	95.4	92.7	90.5	97.4
wt% kaolin	70	72	72	72	72	71
wt% water (max./min.)	29/27	23/22	18/16	13/11	8/6	4/2
Organic content (wet basis)						
wt% organic (min./max.)	1/3	5/6	10/12	15/17	20/22	25/27
wt% TOC (min./max.)	1/2	3/4	6/8	9/11	13/14	16/17
Organic content (dry basis)						
wt% organic (min./max.)	2/4	6/8	12/15	17/20	21/24	25/28
wt% TOC (min./max.)	1/3	4/5	7.5/9.5	11/13	13/15	16/18
Nominal % TOC	2	4.5	8.5	12	14	17
Ignitability						
Short-duration flame	N	N	Y	Y	Y	Y
Burn duration (s)	--	--	1	3	5	15

After characterizing the surrogate sludge samples in terms of embedded organic content, an attempt was made to ignite the sludge. Ignition was attempted using a small oxyacetylene torch. Table 4-1 provides these results.

In general, the samples with the most organic (and the least moisture) were the easiest to ignite, but even the sample with 17 percent TOC (nominal) required some effort (prolonged heating) to establish a self-sustained flame. Even then, the flame extinguished after about 15 seconds, and samples with nominal TOC contents of 14, 12, and 8.5 percent burned independently only for about five, three, and one second(s), respectively. With the torch in place, these samples showed visible signs of fuel burning in the vicinity of the torch jet, particularly for higher fuel contents. A self-sustained flame could not be established on the samples with 4.5 and 2 percent TOC, and even with the torch in place there was little, if any, visual evidence of fuel burning.

In summary, the samples that sustained burning did so only briefly, consuming only a fraction of the available fuel before extinguishing. When the torch was applied again, the process was repeated. Samples that contained more than 20 percent water did not ignite at all. The presence of water is likely the most important factor in preventing sustained burning of organic in sludge. It is concluded that sludge containing more than 20 percent water will not ignite and support a sustainable solvent fire.

4.2.2 Organic Liquid Embedded in Saltcake

Waste saltcakes are expected to retain less moisture than sludges and are assumed to be able to contain more solvents in their interstitial pores than sludges. Experiments and analyses of waste simulants and waste samples (Simpson [1994], Jeppson and Wong [1993], Epstein et al. [1994], Toth et al. [1995], Atherton [1974], Handy [1975], Metz [1975a, 1975b, 1976], and Kirk [1980]) show that waste saltcakes are more porous and retain less liquid than waste sludges. Scoping tests with saltcake simulants saturated with kerosene indicated that when a saltcake-kerosene mixture was heated near an open flame, the kerosene ignited after reaching its flash point and burned (Beitel 1977). The saltcake did not participate in the reaction other than to serve as a wick.

Scoping tests indicated that solvent could be ignited above saltcake simulants, where the solvent would wick to the surface and burn in air until the solvent was largely consumed. Ignitability tests were performed to better quantify ignition source requirements for saltcake-solvent mixtures. The results of this testing are described in Appendix E, Section 5.0 and summarized below.

Tests involved introducing a pyrotechnic "electric match" and heated steel balls to a dodecane-saturated saltcake simulant 6.35 cm (2.5 in.) in diameter. Neither the 138-J match nor the heated steel balls (energy ranging from 10 J to 270 J) caused the solvent-saturated saltcake to ignite. It is concluded that small heated objects and sparks cannot ignite solvent-saturated saltcake. A larger, more sustained energy source is required.

4.3 SMALL SOLVENT FIRES IN ACTIVELY VENTILATED TANKS OR AT MULTIPLE LOCATIONS

Questions have been raised about the consequences of small solvent fires in actively ventilated tanks and the simultaneous ignition of a solvent pool or large puddle at more than one location (multipoint ignition). Both scenarios are explored in the subsections below. In both scenarios, results indicate that consequences fall well below the consequences for the bounding cases previously analyzed.

4.3.1 Small Solvent Fires in Actively Ventilated Tanks

The analysis in Section 4.1 for pool fires assumes fires extinguish because of a lack of oxygen. The pressure generated by the fire prevents fresh air from entering the tank to replenish the oxygen supply. Because of questions that have been raised and because of a review of solvent fire methodology (Postma 1996), an analysis has been done for the scenario of a small fire burning at a rate limited by oxygen (incoming ventilation air) and continuing to burn until available fuel is consumed. Such a fire could result in larger masses of solvent being burned (as compared to earlier assessments) because extinguishment would be limited by the fuel inventory rather than the oxygen inventory. Because waste aerosolization is predicted to be proportional to the mass of fuel burned in a fire, it is possible that aerosol release (and accident consequences) could be larger for a small continuing fire than for the larger fires previously analyzed.

This problem can be resolved by quantifying radiological and toxicological consequences for a small continuing fire scenario and comparing them with consequences for the bounding fire scenarios described in Sections 4.1 and 4.2.

The impact of forced ventilation on fire consequences was quantified by analyzing the largest pool fire that could continue to burn <u>if</u> supplied by fresh air at 100 cfm (170 m^3/hr). The methodology used in this analysis is the same as that used to analyze pool and puddle fires, extended to account for air flow into and out of a tank that is actively ventilated. Results of the analysis, in which toxicological consequences are expressed in sums of fractions of guidelines and in which radiological consequences are expressed in radiation doses, can thus be compared to consequences for pool and puddle fires.

Results of the analysis indicate that consequences of a small pool fire in an actively ventilated tank would fall well below consequences for the bounding cases previously analyzed. The HEPA filters in the ventilation system would not suffer over-pressure failure, but would trap particulate contaminants until the filters plugged or available fuel was consumed. As a result of plugging, the ventilation airflow would terminate, and the fire would be extinguished because of low oxygen concentration.

Appendix H contains a complete analysis. In order for the small pool fire described here to exist, some form of physical barrier or waste geometry would have to create a pool that was less than one square meter (and proportional in size to the ventilation rate) in area where the fire burned and had a reservoir of solvent to feed the burning pool. If the burning surface were not constrained, the fire would spread across the available area and be a pool or puddle fire of the same type already analyzed. The oxygen consumption would exceed the supply, and the fire would be extinguished because of oxygen depletion.

4.3.2 Ignition at Multiple Locations

Multipoint ignition is the simultaneous ignition of a solvent pool (or large puddle) at more than one location. Multipoint ignition is possible with lightning as an ignitor; lighting strikes are typically multi-discharge events, and if successive discharges followed different paths to a solvent pool, ignition at more than one point on the pool is possible.

Analyses of pool fire consequences in Section 7.0 are based on ignition at one site on a pool, with subsequent radial spreading of a fire until the entire pool is inflamed or until the fire extinguishes on low oxygen. Ignition at two or more points on the surface of a pool could cause the inflamed area to grow more rapidly than it would for single point ignition. The increase in inflamed area would be reflected in an increase in pressurization rate. Increased pressures in the tank could result in more rapid venting of toxins and would impose larger structural loads on a tank. The degree to which a faster spreading fire, caused by multipoint ignition, increases predicted consequences is analyzed in Appendix J. The impact of multipoint ignition of solvent pool fires on predicted consequences was quantified by analyzing bounding fire cases under the assumption that ignition occurred at three locations simultaneously. The bounding cases examined peak pressurization, toxicological consequences, and radiological consequences. Comparison of consequences for single and multipoint ignitions illustrates how multipoint ignition affects the outcome of postulated solvent fires.

Findings of this study are characterized by the following conclusions and summary statements.

1. Multipoint ignition increases the rate at which the surface of a solvent pool becomes inflamed. The faster burning increases peak pressurization for the large pool cases. No significant effect on puddle fires is expected because even single-point ignition is predicted to cause the entire surface to become inflamed during the first seconds of a burn that continues for many minutes.

2. Peak pressures were predicted to increase from 29 psig (200 kPa) to 32.3 psig (222 kPa) when the number of simultaneous ignition areas was increased from one to three. This increase is too small to change the current evaluation of the structural response of SSTs to pool fires.

3. Toxicological consequences, gauged by onsite sums of fractions for the unlikely frequency category, are calculated to increase from 0.95 to 1.10. The relative insensitivity of predicted toxicological consequences to the number of ignition points indicates that multipoint ignition is not an important issue in assessing toxicological consequences of solvent pool fires.

4. Radiological consequences for the bounding case were predicted to increase by less than one percent when the number of ignition points was increased from one to three. Therefore, multipoint ignition is not an important issue in assessing radiological consequences of solvent pool fires.

4.4 CONCLUSIONS

Liquid organic solvent in the Hanford waste tanks is difficult to ignite in any configuration. It is even more difficult to achieve the conditions necessary for a self-sustaining fire. In theory, it is easier to ignite and sustain an organic solvent fire when the solvent is confined, such as in a small channel. However, laboratory tests show that robust ignition sources are required even for confined cases, such as channels.

Solvents entrained in saltcake or sludge can burn using the saltcake or sludge as a wick. Less energy is required to ignite and sustain a wick-stabilized fire.

The ignition of a solvent fire is already a low probability event. Small solvent fires in actively ventilated tanks are even less likely. Constraining the event further by requiring an unlikely configuration to make the scenario possible removes this scenario from credibility. Therefore, no further development or calculation of consequences for this scenario is included in the main body of this document.

A multipoint ignition is judged to be less probable than a single point ignition. As shown in Appendix J, Section 5.0, the consequences of a multipoint ignition are marginally higher than those of a single point ignition. Risk is a function of consequences and probability. The multipoint ignition would have slightly higher consequences and would be less probable than a single point ignition. The single ignition scenario is judged to be the higher risk scenario. Therefore, no further development or calculation of consequences for this scenario are included in the main body of this document.

This page intentionally left blank.

5.0 SOLVENT FIRE ACCIDENT PHENOMENA

Section 5.0 discusses solvent fire phenomenology and the calculational methodology for analyzing possible consequences of solvent fires in waste tanks. It includes information about 1) the solvent fire sequences that were considered, 2) a summary of solvent fire phenomenology, 3) thermal hydraulic modeling of confined solvent pool fires, 4) a sensitivity analysis for thermal hydraulic results, and 5) a parametric analysis of fire pressurization.

Estimating the consequences of a fire event (see Section 6.0), requires a knowledge of contaminant vent rate and total quantity vented during the course of a fire event. The phenomena discussed in this section are those that affect the venting of contaminated air from a tank.

5.1 SOLVENT FIRE SEQUENCES CONSIDERED

A scenario for an organic solvent fire in a waste tank as described in Sections 4.1 and 4.2 could include the following processes.

1. Local ignition of a fire by means of an accident
2. Spread of the fire from the ignition locale
3. Heating and pressurization of headspace air by the fire
4. Venting of headspace air (and airborne contaminants) from the tank
5. Challenge of tank structural integrity by internal pressure
6. Fire termination on low oxygen level
7. Cooling of headspace air by heat transfer to tank walls and internal structures causing a vacuum with respect to outside air pressure
8. Challenge of tank structural integrity by internal vacuum
9. Inflow of atmospheric air, increasing the oxygen concentration in headspace air
10. Reignition of a fire when fresh air is reintroduced.

The cases to be evaluated were selected to maximize radiological dose, toxicological dose, tank pressure, and tank vacuum.

The maximum pressure and vacuum cases for DSTs and DCRTs have results well within the structural capability of these tanks to withstand. However, for SSTs, some maximum pressure cases resulted in pressures equal to the failure pressure of the SSTs. Based on information provided by the FSAR structural evaluations (WHC 1996b), it was determined that the maximum pressure would not result in a dome collapse of the SST. This conclusion is

due in part to the slow rate of burning for an organic solvent fire compared to a hydrogen deflagration or organic nitrate reaction. Instead of collapse, cracks would develop in the concrete dome and gases would be vented through the cracks, thus preventing dome collapse.

Venting through the soil would filter some of the particulates in the gas stream before it reached the atmosphere. This scenario was not considered well enough developed to attempt to take credit for the reduction in material released. The release calculations used in the safety analyses assumed that all material was released through the vent paths specified in the safety analyses. The peak pressures and vacuums can serve as inputs to structural studies to evaluate the severity of the challenge posed by a fire.

The fire phenomena analyzed here included processes 1, 2, 3, 4, 5, 6, 7, 8, and 9 as listed above. Temperature, pressure, and venting of headspace gases are quantified for a number of cases thought to cover a range of possible outcomes of postulated solvent fires in waste tanks.

Process 10 (reignition) was not included because it appears to be a low-probability outcome of a pool fire, itself a low-probability accident. Extensive studies of confined solvent fires (Malet et al. 1983) provide direct experimental evidence that pool fires extinguish at an oxygen concentration of about 13 percent by volume and do not reignite when air reenters. Reignition was not observed in the six small-scale tests (0.3-m^3 [10-ft^3] vessel) or the nine large-scale tests (400-m^3 [14,125-ft^3] concrete enclosure) reported by Malet et al. (1983).

Figure 5-1 shows the configuration analyzed in this section.

5.2 SUMMARY OF SOLVENT FIRE PHENOMENOLOGY

This section reviews the key phenomena expected to govern the rate of energy production by postulated solvent fires. The objective is to describe a technical basis for quantifying the energy production rates used to predict tank pressurization in Section 5.4.

5.2.1 Ignition

The oxidation reaction that occurs when liquids burn takes place in the gas phase. Ignition requires that combustible material be heated to a temperature sufficient to produce a flammable fuel-air mixture. The flash point of a flammable material is the temperature at which vapors in equilibrium with the material and its air space reach the LFL in air. A spark introduced into combustible vapors at the LFL can ignite a gas-phase deflagration that is perceived as a "flash." The flash is typically not energetic enough to cause additional fuel to vaporize and support a steady flame. A higher temperature, called the "fire point" is required for sustained combustion. As an example, flash point and fire point for dodecane are listed as 74 °C and 103 °C (165 °F and 217 °F), respectively (Thorne 1983). For dodecane, an organic liquid bearing a chemical similarity to organic diluents such as the NPH used in the PUREX process or the solvent in

Figure 5-1. Schematic of Waste Configuration Analyzed.

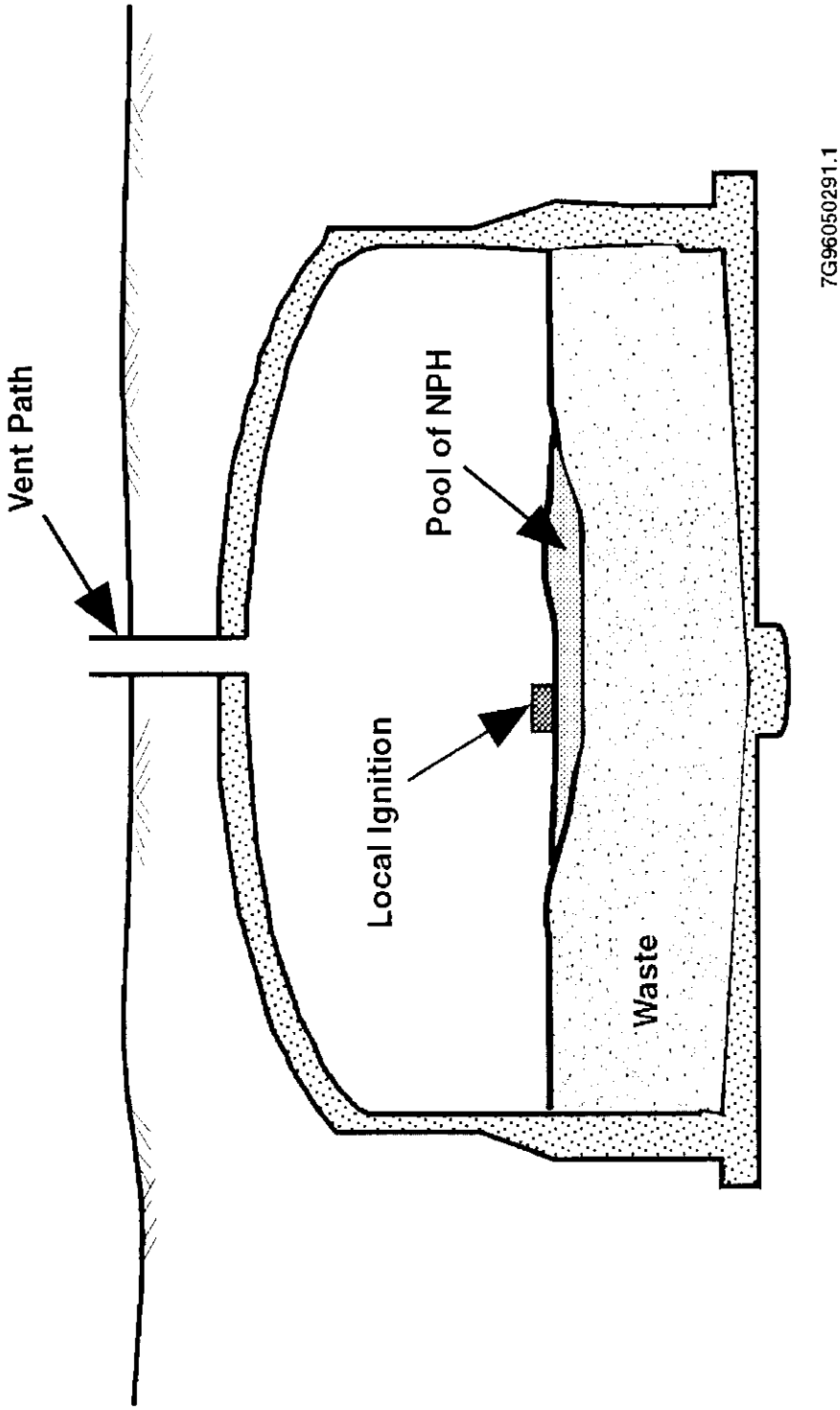

tank 241-C-103, the fire point is approximately 30 °C higher than the flash point. The measured flash point of the tank 241-C-103 solvent is 118 ± 1 °C (Pool and Bean 1994) suggesting a fire point of approximately 118 + 30, or 148 °C (298 °F). Tank 241-C-103 solvent would therefore be expected to support a steady flame only if heated by more than 100 °C from its current temperature of 40 °C (104 °F).

Solvent entrained in porous solids that act as wicks may be more easily ignited than an open pool. The reason is that local heat dissipation in a porous solid may be less rapid than in open liquid pools where convection is an effective heat transfer mechanism (see Section 4.2.2).

In summary, the ignition of a solvent fire requires 1) the creation of a flammable air-fuel mixture, 2) the presence of an ignition source, and 3) fuel and flame conditions that satisfy the requirement that energy transfer from the flame be sufficient to vaporize fuel at a rate fast enough to support a stable flame. The fire analyses described in this report assume that a stable flame is ignited over a specified area.

5.2.2 Fire Spread Rate

A locally-ignited fire can spread if the energy from the burning zone can heat adjacent fuel surfaces to temperatures above the flash point. The spread rate is important in postulated solvent fires because the rate of energy produced by a fire is proportional to the inflamed surface area. The energy production rate affects tank pressurization, venting rate, total quantity vented, and burn time that could result from a solvent pool fire.

No generally-accepted model or correlation currently exists for predicting flame spreading rates easily. In a review of the topic, Quintiere (1988) notes that liquid phase effects control the propagation rate for liquid temperatures below the flash point and gas phase effects control the propagation rate for liquid temperatures above the flash point (see Figure 5-2). As indicated, the spread rate is low and increases with temperature until the liquid is heated to the flash point. Studies of flame spreading rates indicate that liquid properties (e.g., surface tension, viscosity) are of prime importance in this low-temperature region (Glassman and Dryer 1980 and Akita 1973). Above the flash point, the spread rate increases to a maximum that is controlled by flame speeds for premixed vapors. Glassman and Dryer (1980) state the maximum spread velocity is four to five times the laminar burn velocity and is attained when the liquid temperature is high enough to generate vapors that form a stoichiometric mixture above the pool. For tank 241-C-103, solvent temperatures are subcooled by approximately 78 °C (140 °F) (118 °C - 40 °C) compared to the flash point; therefore, liquid properties are expected to control spread rate.

Experimental measurements of spread rates illustrate how spread velocity varies with solvent physical properties. Glassman and Dryer (1980) state that spread rates of kerosene floating on water at room temperature vary from 0.5 to 1.3 cm/s depending on viscosity. Viscosity is controlled by mixing kerosene with a thickening agent (i.e., polyisobutylene). The break point in viscosity is at approximately five centipoise. For lower viscosities, the

Figure 5-2. Flame Propagation Rate.

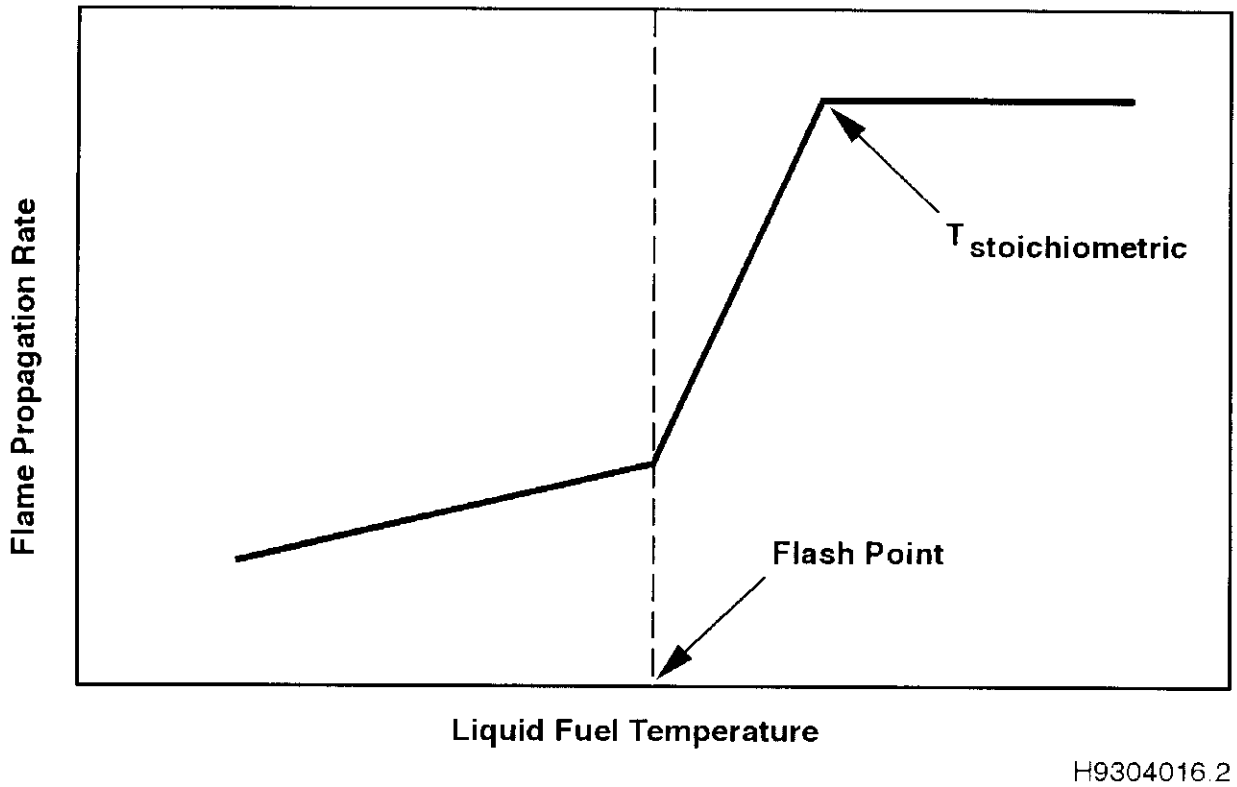

spread rate is approximately 1.3 cm/s. The closed cup flash point of kerosene is reported as 49 °C (120 °F) (NFPA 1988) so the kerosene tested was subcooled by roughly 49-20, or 29 °C (52 °F).

Takeno and Hirano (1986) measure fire spread rates for kerosene/solid admixtures. The highest spread rate (approximately 2 cm/s) is measured when the kerosene depth is 2.2 cm (0.87 in.) above the solids and exposes an open pool to the air atmosphere. The tests are carried out at room temperature so the degree of subcooling with respect to the flash point is similar to the value (29 °C [84 °F]) used in Glassman and Dryer (1980).

Malet et al. (1983) carry out large-scale solvent pool fires in a closed compartment and report fire propagation times. The solvent (a mixture of TBP and NPH, similar to PUREX solvent) is confined in pans that are 0.4 to 4 m^2 (4.3 to 43 ft^2) and is ignited in an electrically-heated local region. Propagation rates estimated from fire propagation times and pan sizes vary from 1.3 cm/s to 3.3 cm/s depending on mean pool temperature. The lower rate (1.3 cm/s) applies to a pool with a mean temperature of 25 °C (77 °F). The flash points of the solvents tested are not reported by Malet et al. (1983), but measurements reported by Pool and Bean (1994) for a 70/30 NPH/TBP mixture yield a flash point of 101 °C (214 °F). Using the 101 °C flash point, the degree of subcooling for the 1.3 cm/s spread rate is estimated to be 101-25, or 74 °C (133 °F). For the higher spread rate (3.3 cm/s), the degree of subcooling is calculated to be 101-53, or 48 °C (86 °F).

The degree of subcooling in waste tanks is illustrated by the known properties of solvents in tank 241-C-103. The solvent pool in tank 241-C-103 is subcooled by 118-40, or 78 °C (140 °F) compared to its flash point. This degree of subcooling is greater than the subcooling in the tests described above; therefore, relatively low spread rates would be projected on the basis of the results of Malet et al (1983) for tank 241-C-103 solvent.

Fire spread rates measured in large-scale open air tests with jet fuel (Leonard et al. 1992) were in the range of 8 cm/s to 10 cm/s for initial fuel temperatures that were 10 °C (18 °F) or more subcooled with respect to the flash point. While the data for jet fuel may not apply directly to confined solvent fires, the tests provide an experimental basis for defining an upper bound of approximately 10 cm/s for spread velocity in waste tanks, because jet fuel is more flammable than fresh PUREX solvent.

It is possible that solvent could intrude into the underlying sludge or saltcake following saltwell pumping of drainable liquids from a tank. For such a case, solvent fire propagation rates would be lower than for open pools because convective transport of heat in the solvent would be greatly reduced. Takeno and Hirano (1986) studies on the propagation rate of flames ignited over kerosene soaked into porous solids show that spread rate diminishes significantly when the thickness of kerosene layer above the top of the solids decreased. For a solids-free depth of 2.2 cm (0.86 in.), the propagation velocity (approximately 2 cm/s) is similar to that of an open pool. When the solids-free depth is reduced to 1 mm, the spread rate is decreased to approximately 0.5 cm/s. For a liquid level equal to the solids level, the

propagation rate varies according to the properties of the solids, but the highest rate measured is approximately 0.1 cm/s, or roughly one-twentieth the open pool spread rate.

Takeno and Hirano (1986) test results are consistent with results reported by Hirano et al. (1984) for flame spread over crude oil sludge. Measured flame-spread rates in Hirano et al. (1984) vary from 0.02 cm/s to 0.4 cm/s, depending on the quantity of n-hexane added to the sludge and on the temperature of the sludge.

The relatively slow flame propagation rates for flammable liquids imbedded in solids can be explained in terms of heat transfer limitations from the flame front to adjacent nonburning material (Takeno and Hirano 1986, Hirano et al. 1984, and Glassman and Dryer 1980). The same limitations are expected to apply to PUREX solvent embedded in sludge or saltcake; therefore, flame-front propagation rates in sludge or saltcake/solvent admixtures are expected to be small compared to spread rates for an open pool of the same solvent.

5.2.3 Liquid Burn Rate

The rate of thermal energy production by a pool or sludge fire is proportional to the burning rate per unit area. For this reason, peak pressures that could be generated by a solvent fire depend on the burning rate. Studies of burning rates indicate that for liquid pools, the burning rate is governed by gas phase heat and mass transport rates. Heat and mass transport in the solid can limit the burning rate for liquid/solid admixtures. Burning rates for liquid pools, expressed as $kg/m^2/min$, increase with pool size to an asymptotic value for large pools. Babrauskas (1988) provides a correlating equation of the form:

$$\dot{m} = \dot{m}_\infty(1 - e^{-kBD}) \qquad (5\text{-}1)$$

where

$\dot{m}$ = burn rate, $kg/m^2/min$.
$\dot{m}_\infty$ = burn rate for a large pool
kB = a constant, m^{-1}
D = pool diameter, m.

For kerosene the kB product is given by Babrauskas (1988) as 3.5 m^{-1}, and based on Equation 5-1, $\dot{m}$ reaches 95 percent of the maximum value for a pool 0.9 m in diameter. This projection, based on experimental data, indicates that data from pools roughly 1 m in diameter would apply reasonably to waste tank solvent fires.

Large-scale pool fire tests using kerosene/TBP mixtures have been carried out in Germany (Jordan and Lindner 1983) and in France (Malet et al. 1983). German tests evaluate the effects of pool size and confinement. French tests evaluate burning rate and the release of contaminants.

Jordan and Lindner (1983) conclude that burning rates increase with pool area for smaller pools; little increase in burn rate is noted when burn area is increased from 0.8 m^2 (8.6 ft^2) to 2 m^2 (21.5 ft^2). This finding agrees with Equation 5-1. Jordan and Lindner (1983) also conclude that burning rates for fires in a pressure-tight steel tank (220 m^3 [7,769 ft^3]) are 40 to 50 percent lower than for fires in open air. Burning rates for large fires in closed containers are estimated at 1 $kg/m^2/min$ to 1.2 $kg/m^2/min$ (Jordan and Lindner 1983).

The large-scale tests reported in Malet et al. (1983) are carried out in a 400-m^3 (14,125-ft^3) concrete enclosure and use pool areas of 0.4 m^2 (4.3 ft^2) to 4 m^2 (43 ft^2). The enclosure in these tests is vented to prevent pressure buildup. Mean combustion rates for nine tests ranged from 1.35 $kg/m^2/min$ to 1.7 $kg/m^2/min$.

An instantaneous burn rate is expected to vary with oxygen concentration. In a confined air space, a specific burn rate would be maximum at an early time (21 percent oxygen) and would decrease with time as the oxygen concentration was lowered by the fire. Burning would cease altogether when oxygen fell to the extinguishment level. Beyler (1997) suggests a simple linear relation between oxygen concentration and burn rate. Based on empirical data, the relationship multiplies the burning rate in air by a fraction, whose value is unity at 21 percent oxygen, and decreases linearly to 0.125 at 12 percent oxygen. Based on this relationship, a specific burning rate would decrease with time by a factor of 8 for a confined fire starting with atmospheric oxygen and extinguishing at 12 percent oxygen.

Burning rates for combustible liquids soaked in inert solids are comparable to open pool burning rates as long as the solids wick the liquid to the surface (Wood et al. 1971). The tests in Wood et al. (1971) show that when the liquid-air interface falls below the top of a sand bed, the burning rate decreases. This behavior is as expected on the basis of additional resistance to heat and mass transfer caused by the porous bed. As applied to saltcake or sludge/solvent admixtures, specific burn rates are expected to be equal to or lower than burning rates for an open pool.

5.2.4 Extinguishment of Pool Fires at Oxygen Flammability Limit

Pool fires in nonventilated compartments extinguish when the oxygen concentration falls below the flammability limit for oxygen. For hydrocarbons, flame propagation is impossible in air-fuel mixtures that contain less than 14.5 vol% oxygen (Lewis and Von Elbe 1987). This limit applies to air-fuel mixtures at one atmosphere pressure and room temperature.

Oxygen extinguishment levels for pool burning of NPH/TBP solvent in nonventilated compartments have been measured in large-scale tests. Jordan and Lindner (1983) report extinguishment levels of 11 to 17.5 percent. A narrower range (13 to 14.5 percent) is reported in Malet et al. (1983) for nine large-scale tests. These results indicate that a solvent fire in a waste tank would extinguish at an oxygen concentration in the range of 11 to

17.5 percent. This extinguishment limits the mass of solvent that can be burned, thereby limiting the thermal energy that can be generated by a solvent fire.

5.2.5 Heat of Combustion

The tank 241-C-103 solvent is composed mainly of hydrocarbons and TBP (Pool and Bean 1994). The combustion energy of the mix can be estimated by adding the contribution due to each of the two main components. The heats of combustion of hydrocarbons are of a similar magnitude when expressed on a mass basis. For example, the heats of combustion of n-decane, n-dodecane, and n-hexadecane are calculated to be 47.6 MJ/kg, 47.5 MJ/kg, and 47.2 MJ/kg, respectively. These values are changes in enthalpy for reactions with oxygen, starting with liquid fuel and forming gaseous CO_2 and liquid H_2O for a reaction temperature of 298 °K (Lewis and Von Elbe 1987). Therefore, the combustion energy of hydrocarbons can be estimated on the basis of a representative component (e.g., dodecane).

Heats of combustion of TBP and NPH are measured in Lee (1974) to be 28.2 MJ/kg and 44.0 MJ/kg, respectively. These values, determined in a bomb calorimeter, indicate the combustion energy of TBP is approximately 65 percent of the value for NPH.

The combustion energy of a mixture of NPH and TBP depends on the mass fraction of each component present in the burning zone. Vapor phase measurements reported by Pool and Bean (1994) for tank 241-C-103 solvent indicate that approximately 16 percent of the vapor mass at 100 °C (212 °F) is attributable to TBP (including di-butyl phosphate with TBP), and the remainder are hydrocarbons. This vapor composition would apply to the solvent before an appreciable fraction had been burned. Because NPH is more volatile than TBP, its concentration would decrease with burn time, and the mix would become progressively enriched in TBP (Jordan and Lindner 1983). The enrichment in the solvent with TBP would cause a decrease in the combustion energy of the mix because TBP has the lower combustion energy of the two components. An upper bound estimate could be based on the initial value and would be realistic for fires that extinguish before an appreciable fraction of the solvent is consumed.

Solvent pool fires result in incomplete combustion (Jordan and Lindner 1983 and Ballinger et al. 1987). For this reason, the thermal energy produced by a solvent fire will be lower than theoretical values based on a complete reaction to form H_2O and CO_2. Combustion efficiencies (i.e., fraction of theoretical heat release) based on experimental results vary from 0.35 for polyvinyl chloride to 1.0 for cellulose (Ayer et al. 1988). Ayer et al. (1988) cite a kerosene combustion efficiency of 0.91. The TBP/NPH mixtures are expected to burn less efficiently than kerosene alone on the basis of the observed heavy smoke production from solvent fires. An upper bound estimate for combustion efficiency is 0.91.

5.3 THERMAL HYDRAULIC MODELING OF CONFINED SOLVENT POOL FIRES

Tanks (particularly SSTs) are gas-tight structures except for several relatively small vent pipes. A combustion of fuels in the confined air volume would heat the air and cause an increase in internal pressure. The peak pressure that can develop from a fire depends on how rapidly heat energy is evolved compared to the rate at which energy can be dissipated through heat transfer to tank surfaces and by gas outflow through leak paths.

Internal gas pressure and temperature were computed as a function of time by performing energy and mass balances on the air inventory in the tank for relatively short (0.1 to 1 second) time steps. Conditions at the end of a time step are used as initial conditions for the next step. Numerical evaluations are accomplished by means of a simple computer program, POOLFIRE.4, written for this specific application. Appendix A describes the model and program. Algorithms used to quantify important parameters in the energy and mass balances are described as follows.

5.3.1 Nodalization of POOLFIRE.4

Figure 5-3 shows the nodalization used in the thermal hydraulic model of solvent pool fires.

Key assumptions and node descriptions are as follows.

5.3.1.1 Gas Phase. The gas phase (tank headspace) is treated as one node. Temperature and pressure are assumed to be uniform throughout the gas phase.

5.3.1.2 Concrete. Exposed concrete is treated as a one-dimensional slab of specified surface area, thickness, and initial temperature. Heat transfer to the side of the slab exposed to the gas phase is calculated at each time step. Transient conduction in concrete is calculated in nodes of uniform area and thickness. Typically, 40 nodes are used to model the concrete dome and exposed cylindrical wall.

5.3.1.3 Waste. Waste is also treated as a one-dimensional slab of specified thickness, area, and initial uniform temperature. The number of nodes for transient conduction calculations in sludge is the same as used for concrete. Waste area is calculated by deducting from the tank cross-sectional area, the area of the solvent pool.

5.3.1.4 Steel Wall. The steel sheeting that lines the cylindrical walls and steel internal structures (risers, thermocouple trees) is treated as a single node of specified area and mass. Heat transfer from the gas to the exposed side of the steel is calculated, but heat loss from the back side of steel sheeting is not addressed.

Figure 5-3. Schematic of POOLFIRE.4 Model.

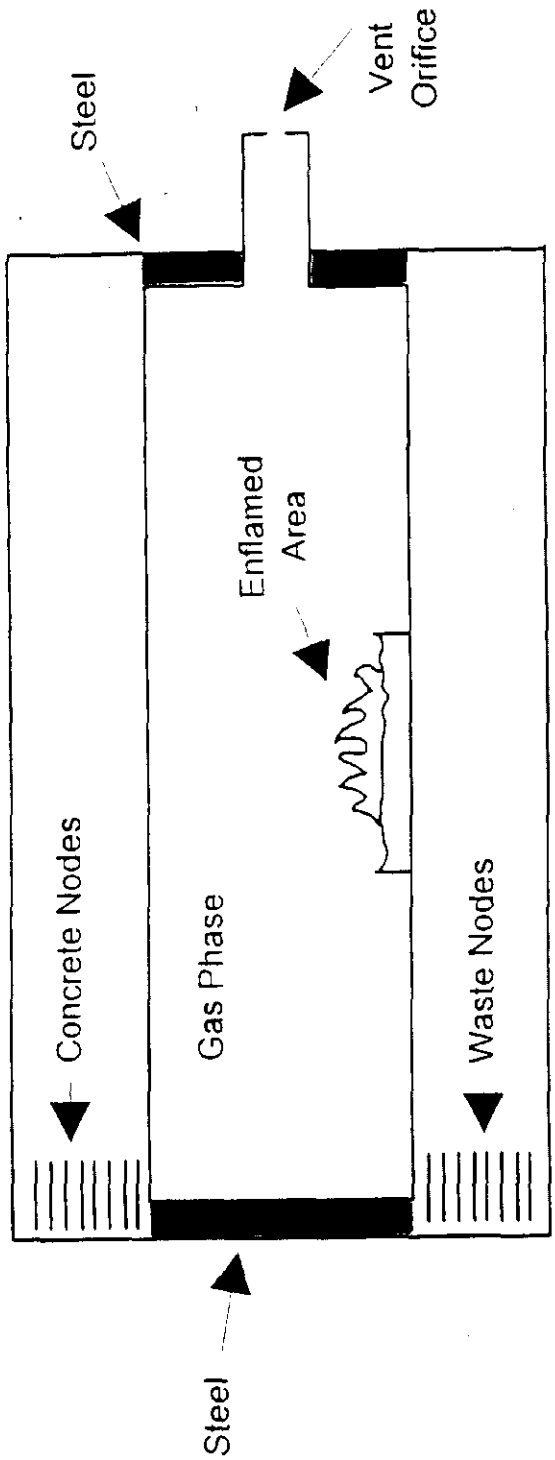

5.3.1.5 Solvent Pool. A solvent pool of prescribed area and depth is treated as one node. Heat transfer from heated gas is accounted for, but heat loss to underlying waste is not addressed. The inflamed area of the pool is calculated at each time step to account for radial spread of a flame, starting at time zero with a specified area.

5.3.1.6 Gas Vent. Gas venting is quantified by specifying an orifice of prescribed diameter and flow coefficient between the tank and the outside atmosphere.

5.3.2 Combustion Energy

The rate of energy production by a solvent fire is computed as the product of specific combustion energy, inflamed area, and specific burning rate:

$$Q_{comb} = \Delta H_c \cdot A_f \cdot \dot{m}_b \qquad (5\text{-}2)$$

where

Q_{comb} = combustion energy rate, J/s
ΔH_c = specific combustion energy, J/kg
A_f = inflamed area, m^2
$\dot{m}_b$ = specified burn rate, $kg/m^2/s$.

The combustion energy quantified in Equation 5-2 is assumed to be added to the gas phase as sensible heat energy. The increase in sensible heat causes an increase in gas temperature and pressure and causes an increase in the heat transfer rate from the gas to the surfaces in the tank.

5.3.2.1 Specific Combustion Energy. The combustion enthalpy (ΔH_c) is a constant for a specific case. It is assigned values on the basis of theoretical values for a complete reaction, multiplied by an efficiency factor. The theoretical value is calculated as the weighted sum of combustion energies for NPH and for TBP:

$$\Delta H_c = 0.84\ \Delta H_c(\text{NPH}) + 0.16\ \Delta H_c(\text{TBP}). \qquad (5\text{-}3)$$

The combustion enthalpy for NPH is taken to be equal to the value for n-dodecane. The ΔH_c for n-dodecane, computed from a combustion enthalpy value, is 44.1 MJ/kg. The combustion enthalpy for TBP is computed from bomb calorimetry analyses (Lee 1974) and amounts to 26.5 MJ/kg.

The mass fractions of NPH and TBP listed in Equation 5-3 (0.84 and 0.16) are based on vapor-phase mass concentrations at 100 °C (212 °F) (Pool and Bean 1994). Increases in the fraction of TBP that would occur as a fire continues (depletion of volatile species) are not addressed. The increase is conservative because the combustion energy of NPH is higher than that of TBP. The theoretical value for combustion enthalpy is thus:

$$\Delta H_c = 0.84\ (44.1) + 0.16\ (26.5) = 41.3\ \text{MJ/kg}. \qquad (5\text{-}4)$$

A best-estimate combustion efficiency of 80 percent is assigned on the basis of a range of values cited by Ayer et al. (1988) for fire events in nuclear fuel cycle facilities. Parametric runs are made using combustion efficiencies of 70 and 91 percent. The higher efficiency (91 percent) is applicable to pools of kerosene (Ayer et al. 1988). The base case combustion energy is 0.8 (41.3) or 33 MJ/kg; higher and lower values used in the sensitivity analysis are 37.6 MJ/kg and 28.9 MJ/kg, respectively.

5.3.2.2 Inflamed Area. Inflamed area is computed as a function of time on the basis of an arbitrarily assigned initial inflamed area and a spread rate. Circular geometry is assumed, leading to the following expression for the radius of the inflamed region:

$$R_f = R_o + V_s t \qquad (5\text{-}5)$$

where

R_f = radius of inflamed circle, m
R_o = radius of initially inflamed area, m
V_s = spread velocity, m/s
t = time from fire ignition, s.

Based on engineering judgement the R_o is assigned a value of 0.15 m (0.5 ft) for the base case, and parametric runs are made with R_o values that are double and half the base case value. The technical basis for starting the fire in a localized area is that ignition of a large pool area is extremely improbable.

An upper limit to R_f is computed for each case analyzed on the basis of a prescribed solvent/air interfacial area. The solvent/air interfacial area in a post-pumped tank is evaluated on a parametric basis with a 10 percent base case value of the tank cross-sectional area. Sensitivity analyses are performed for a broad range of solvent areas.

Flame spread velocity over liquid pools can be related to the degree to which the pool is subcooled with respect to the flash point (see Section 5.2.2). For tank 241-C-103 solvent, a 1.0 cm/s spread velocity was used for consequence calculations. Sensitivity analysis cases are run using spread velocities of 0.1 cm/s, 0.5 cm/s, and 2.0 cm/s.

Flame spread velocities over solids are slow compared to liquids (see Section 5.2.2). Spread velocity falls from approximately 2 cm/s to 0.5 cm/s when the kerosene depth is lowered from 2.2 cm (0.86 in.) to 0.1 cm (0.04 in.) (Takeno and Hirano 1986). Spread velocity falls further to approximately 0.1 cm/s when the liquid interface is at the solid/air interface. Based on these numbers, a best estimate spread velocity over solvent/sludge surfaces is

approximately 0.1 cm/s or less (Takeno and Hirano 1986). The burning of solvent imbedded in inert solids is less important than liquid pool fires because spread velocities of 0.5 cm/s or lower lead to low calculated tank pressures.

5.3.2.3 Specific Burn Rate. The POOLFIRE program predicts the consequences of a solvent fire in a tank. The temporal variation in pressure, temperature, and gas inventory are computed as a result of a series of burn events in which the end state for each time step is used as the initial state for the next time step. Within each time step, mass and energy balances are made to calculate temperature changes, pressure change, and changes in inventory. Within each time step (time steps are typically of the order of 1 sec) thermodynamic process steps are analyzed to determine the temperature and pressure of confined gases.

As discussed in Section 5.2.3, average burn rates are reported in Jordan and Lindner (1983) and Malet et al. (1983) ranging from 1 $kg/m^2/min$ to 1.7 $kg/m^2/min$. Section 5.2.4 discusses oxygen extinguishment levels ranging from 11 to 17.5 percent is reported by Jordan and Lindner (1983) and 13 to 14.5 percent as reported by Malet et al. Experiments reported in Beyler (1997) show that burn rate is a linear function of oxygen concentration. The burn rate varies from a maximum burn at approximately 21 percent oxygen (ambient oxygen fraction) to a minimum burn rate of 0 at the oxygen extinguishment level. Based on the large scale tests reported in Malet et al., an oxygen extinguishment level of 13 percent was selected as the oxygen extinguishment level in this report.

A specific burn rate is needed in POOLFIRE at time t = 0. Section 5.2.3 reports experiments with average burn rates ranging from 1 $kg/m^2/min$ to 1.7 $kg/m^2/min$. The experiments reported in Beyler (1997) (see Figure 5-1, Appendix I) show that the burn rate varies linearly with oxygen concentration. For a linear relationship, the average burn rate is the average of the initial rate and the rate at extinguishment, which is zero. An initial burn rate of 3 $kg/m^2/min$ at t = 0 as selected. The average burn rate is (3 + 0)/2 = 1.5 $kg/m^2/min$. a rate of 1.5 $kg/m^2/min$ is in the range of average burn rates reported in Section 5.2.3.

5.3.3 Heat Transfer Rate from Gas to Surfaces

Sensible heat transfer from the gas to tank surfaces would occur by radiation and convection. Key simplifying assumptions made to model the heat transfer rate from the flame to surrounding gas and from gas to surfaces are as follows.

- The bulk of the gas is assumed to be well-mixed.
- Flame radiation directly to the inflamed solvent is accounted for, but radiation from the flame in other directions is assumed to be absorbed by the bulk gas phase.

These assumptions are expected to cause the model to under-predict heat transfer by radiation because radiation heat transfer rate increases with the

fourth power of absolute temperature. Radiation from regions of higher-than-average temperature would more than offset the reduction in radiation from regions of lower-than-average temperature.

5.3.3.1 Heat Transfer from Flame to Fuel Surface. Heat transfer from flame to the unburned fuel surface provides the energy to volatilize liquid and/or solid fuels and maintain an ongoing flame. Results of empirical studies of flame heat transfer can be used to estimate values for solvent fires in tank 241-C-103. Shinotake et al. (1985) measure the surface heat flux for a heptane pool fire in a burn pan 1 m (3 ft) in diameter. Heat fluxes at the center of the pan peak at approximately 50 kW/m^2 early and hold constant at approximately 35 kW/m^2 for the duration of the fire. Similar behavior is observed at a radial distance 0.4 m (1.3 ft) from the center of the pan, but the heat flux is lower at approximately 30 kW/m^2. Wood et al. (1971) measure fluxes of a similar magnitude for acetone fires. These measured values compare well with the 24.5 kW/m^2 kerosene value (Ayer et al. 1988). For solvent fires, a higher radiation heat transfer rate is expected as compared to pure kerosene because of the higher smoke yield in solvent fires (Jordan and Lindner 1983). The value for burning rubber gloves is 72 kW/m^2 (Ayer et al. 1988), reflecting the much higher soot production from rubber gloves. Soot particles increase the heat transfer rate because they serve as radiators (Siegel and Howell 1989).

A reasonable estimate heat transfer flux of 57 kW/m^2 for solvent fires can be arrived at by interpolating between values of 24.5 kW/m^2 for kerosene and 72 kW/m^2 for rubber gloves on the basis of the fraction of fuel carried off in the form of soot particles. Analyses have also been performed with heat fluxes of 24.5 kW/m^2 and 72 kW/m^2 to illustrate the sensitivity of computed pressure to this parameter.

Radiant heat fluxes to horizontal surfaces outside the inflamed area are appreciable (Yamaguchi and Wakasa 1986) but are not addressed because realistic treatment is beyond the scope of this analysis. Not addressing the radiant heat fluxes is conservative with respect to predicted peak pressure.

5.3.3.2 Radiation Heat Transfer from Bulk Gas to Tank Surfaces. The rate of thermal radiation loss from the gas phase to enclosing tank surfaces is computed by means of the following equation:

$$\frac{q_r}{A} = \sigma \epsilon_g \left(T_g^4 - T_s^4\right) \epsilon_s \qquad (5\text{-}6)$$

where

q_r	=	heat transfer rate due to radiation
A	=	surface area
σ	=	Stefan-Boltzman constant
ϵ_g	=	emissivity of gas
T_g	=	absolute temperature of gas
T_s	=	absolute temperature of surface
ϵ_s	=	emissivity of surface.

The emissivity of the gas is estimated from values of the product of mean beam length and the concentration of emitting species in the gas. Emitting species in the gas phase for this problem include H_2O, CO_2, and soot particles. Before a fire is ignited, water vapor is the main emitting specie. Soot particles significantly increase the emissivity of the gas after a fire is ignited. The emissivity of soot particles and CO_2 is estimated as follows. First, the concentration of airborne particles is estimated from the mass of solvent burned and the fraction emitted as soot. At the point of oxygen extinguishment (13 vol% O_2) stoichiometric calculations indicate that roughly 60 kg (132 lb) of solvent is burned for an initial headspace air volume of 2,660 m^3 (93,936 ft^3). Based on an aerosol production of 15 percent of the solvent combusted (Jordan and Lindner 1983) and a gas phase volume of 2,660 m^3, the concentration of aerosol is 60 x 0.15/2,660 or 3.38 x 10^{-3} kg/m^3. The volume fraction of aerosol, calculated for a density of 870 kg/m^3 (the solvent density), is 3.38 x 10^{-3}/870, or 3.89 x 10^{-6}. The volume fraction multiplied by a mean beam length of 8.1 m (estimated value for a 2,660 m^3 headspace volume) is 3.15 x 10^{-5}. This concentration-beam length product is large compared to values needed to attain an emissivity of approximately unity for a gas-soot suspension at 1,600 °K (Siegel and Howell 1989).

The emissivity of soot alone is greater than 0.5 for soot concentration-path length products greater than approximately 1.0 x 10^{-6} m, for temperatures equal to or greater than 750 °K. If soot and water emissivities were added, total emissivity would be larger than approximately 0.84 (0.5 + 30.4) for tank atmospheres containing only 0.3 percent of the aerosol predicted at the end of the fire. It is therefore concluded that a realistic estimate for gas emissivity for a solvent fire in a waste tank is unity.

The emissivities of tank wall, solvent, and exposed sludge surfaces are expected to be in the range of 0.9 to 1.0 on the basis of typical values (McAdams 1954). Best-estimate radiation heat transfer rates are based on a $\epsilon_g \cdot \epsilon_s$ product of 0.9. Analyses done with emissivity products ($\epsilon_g \cdot \epsilon_s$) of 0.8 and 1.0 to illustrate the sensitivity of predicted peak pressure to this parameter.

5.3.3.3 Convection Heat Transfer from Bulk Gas to Tank Surfaces. Convection heat transfer is computed by means of a heat transfer coefficient and temperature difference:

$$q_c = h_c A (T_g - T_s) \tag{5-7}$$

where

q_c = heat transfer rate due to convection, w
h_c = convection coefficient, w/m^2 °K
A = surface area, m^2
T_g = gas temperature, °K
T_s = surface temperature, °K

The convection coefficient (h_c) is estimated in McAdams (1954) as:

$$\frac{h_c L}{k_f} = 0.13\ [Gr\ Pr]^{1/3} \tag{5-8}$$

where

L = length dimension of surface, m

k_f = thermal conductivity of gas evaluated at film temperature, w/m °K

Gr = Grashov No. evaluated at film properties

Pr = Prandtl No. evaluated at film properties.

The overall heat loss rate from the gas to tank surfaces is the sum of that due to radiation and convection:

$$q_w = q_r + q_c. \tag{5-9}$$

5.3.3.4 Surface Areas for Heat Transfer. Surface areas for heat transfer from the bulk gas phase can be estimated from tank geometry. For example, estimates for tank 241-C-103 (based on tank 241-C-103 data) are summarized as follows. The tank dome and a small segment of the cylindrical wall have exposed concrete surfaces. The areas are estimated to be 476 m^2 (5,124 ft^2). Steel sheeting covers the cylindrical walls from above the cascade pipe to the waste surface. Internal piping and risers also expose steel surfaces to the gas phase. The total steel area is estimated as exposed wall area plus 10 percent to account for internal tank structures. The total is 337 m^2 (3,627 ft^2). The sludge area is computed as the tank area (411 m^2 [4,424 ft^2) minus solvent pool area.

5.3.4 Gas Venting Rate Under Pressure

The venting of gases during a solvent fire would mitigate pressure buildup as compared to a leak-tight vessel. Studies identify a number of known leak paths. These paths include ventilation system pipes and ducts, pit drains, cascade overflow lines, passive breathers (e.g., loop seal pipes and the filter pathways), and saltwell risers that vent through the pump pits. The number and geometry of the vent paths vary from tank to tank and need to be evaluated on a tank-by-tank basis if a tank shows indications of containing significant amounts of solvent. Typical vent paths are discussed as follows in light of information applicable to tank 241-C-103.

Pit Drains: Tank 241-C-103 has three access pits; each is equipped with a floor drain (Postma et al. 1994). The drain line is a sloped, 2-in. Sch. 40 steel pipe. The inlet is in the bottom of a cubical cavity in the floor of

the pit. The outlet terminates in a riser pipe (inside the tank) that has a large diameter compared to the drain line. Two of the pits have drain lines that are approximately 0.61 m (2 ft) in length, and the third has a drain that is approximately 1.52 m (5 ft) in length.

Gases forced from a pressurized tank would enter the pipes, pressurize the pits, and then lift the cover blocks. The internal pressure required to lift a cover block is small--approximately 1.8 kPa (0.26 psig) for a cover block thickness of 7.62 cm (3 in.) of concrete.

The hydraulic resistance attributable to the entrance effect is estimated to be equivalent to 1.52 m (5 ft) of straight pipe (Brown et al. 1950). Resistance at the outlet (the floor drain cavity) is modeled as a long sweep elbow, adding another 0.92 m (3 ft) equivalent length of straight pipe (Brown et al. 1950). Based on these data, two pipes, each having flow areas of 2.17×10^{-3} m^2(0.0233 ft^2), can be modeled as pipes 3.05 m (10 ft) in length. The third pipe, of the same flow area, has an equivalent length of 3.96 m (13 ft).

U-Tube Seal Loop: Passively-ventilated SSTs have a loop seal made of 1.5-in. Sch. 40 steel pipe which is connected to a 4-in. breather pipe above grade. The loop is made from four 90° elbows and short lengths of straight pipe that are approximately 0.46 m (1.5 ft) total. The hydraulic resistance of each elbow is equivalent to a straight pipe length of 1.28 m (4.2 ft) (Brown et al. 1950) so the equivalent length of the U-tube seal is 1.5 + 4(4.2) or 5.58 m (18.3 ft). The internal cross-section area of this pipe is 1.31×10^{-3} m^2 (0.01414 ft^2) (Perry 1963).

Cascade Pipes: A 3-in. Sch. 80 steel pipe connects the headspace of tank 241-C-103 to the headspace of tank 241-C-102. This pipe is approximately 15.2 m (50 ft) in length. Flow resistance caused by the Borda entrance (Brown et al. 1950) is an additional 2.19 m (7 ft), making the equivalent length equal to approximately 17 m (57 ft). The internal cross-section area of this pipe is 4.26×10^{-3} m^2 (0.04587 ft^2) (Perry 1963).

Saltwell Riser: The saltwell riser is a 10-in. Sch. 40 steel pipe that terminates in a pump pit. For tank 241-C-103, the upper flanged end of this riser is thought to be covered by a metal plate held in place by gravity. The plate, a lead sheet 6.35 mm (0.25 in.) in thickness and 2 ft^2 (0.61 m^2) in area, would lift under an internal pressure of approximately 6.89 kPa (1 psig) and pressurize the pit. The pit cover would lift allowing gas to vent.

The flow resistance of this vent pipe is estimated as follows. The length of the solid pipe is estimated at 6 m (20 ft). Below this length, the pipe is connected to a saltwell screen. Two smaller pipes, 0.5 in. and 0.75 in. in nominal diameter and a 2-in. pump support pipe, are located inside the 10-in. pipe and occupy a fraction of the flow area. The hydraulic radius (cross section area/wetted perimeter) is calculated to be 5.26 cm (2.07 in.) from which the equivalent diameter (Perry 1963) is computed to be 4(2.07) = 19.87 cm (8.28 in.). Although resistance to air flow through the screen portion of the 10-in pipe would be small because of the large open area, a pressure drop attributable to a Borda entrance, equivalent to a straight pipe length of approximately 5.8 m (19 ft) (Brown et al. 1950), is added to

account for entrance effects. An exit loss, amounting to roughly the entrance loss is also applicable. Frictional resistance for this vent path is equivalent to that of a straight pipe having an inside diameter of 21 cm (8.28 in.) and a length of 20+19+19 = 17.7 m (58 ft).

High-Efficiency Particulate Air Filter Vent Line: The HEPA filter is connected to a 12-in. riser through a 0.31-m (1-ft) length of 4-in. pipe. A butterfly valve in the section of 4-in. pipe allows the filter to be isolated from headspace air.

The outlet pipe from the HEPA filter is a 180° semicircular section of 4-in. pipe. The flow resistance of the vent is estimated as follows. Entrance loss is estimated as equivalent to 3.35 m (11 ft) of straight pipe (Brown et al. 1950). This loss is applied at the entrance of the 4-in. pipe connected to the 12-in. riser and at the entrance of the 4-in. pipe that vents the HEPA filter housing. The semicircular pipe exiting from the HEPA filter housing is modeled as two long-sweep 90° elbows, adding 2(7) = 4 m (14 ft) of equivalent pipe length. Because it is assumed the filter will rupture from overpressure, the resistance caused by the HEPA filter is not addressed. The flow resistance of the butterfly valve is estimated as equivalent to 1.5 m (5 ft) of straight pipe (Perry 1963). The overall flow resistance of this vent path is equivalent to 12.8 m (42 ft) of 4-in. Sch. 40 steel pipe. The internal diameter of this pipe is 4.026 in. (Perry 1963).

Vent Path Flow Rates: Air flow velocities in vent pipes approach sonic velocities under the pressure gradients that could result from a pool fire. Therefore, flow rate estimates must account for compressibility effects.

Flow rate estimates were based on adiabatic flow of gases in ducts (Lapple 1943 and Brown et al. 1950). First, a resistance factor, N, is computed for each vent path.

$$N = \frac{fL}{D} \tag{5-10}$$

where

f = friction factor
L = pipe length
D = pipe diameter.

For fully developed turbulence (high Reynolds number), the friction factor is a function of the relative roughness of the pipe interior surface (Brown et al. 1950). Table 5-1 lists the estimated values of N for the several vent paths considered here.

A second step is the calculation of the ratio of downstream pressure to upstream pressure:

$$PR = \frac{P_{atm}}{P_o} \tag{5-11}$$

where

PR = pressure ratio
P_{atm} = pressure in outside atmosphere
P_o = pressure in tank.

The pressure ratio (PR) is initially unity (i.e., tank at equilibrium with atmosphere) and has a calculated value of 0.51 at a tank pressure of 96.5 kPa (14 psig), the maximum pressure the tank can safely withstand (July 1994). Evaluating flow resistance at the highest pressure of interest is conservative because compressibility effects limit mass flow rate at high gas velocities.

Table 5-1. Flow Characteristics of Tank 241-C-103 Vent Pipes.

Vent Pipe Description	Equivalent Length (m)	Equivalent Diameter (m)	Friction[1] Factor (f)	$\frac{fL}{D}$
Pump pit drain	3.05	5.25E-2	0.018	1.05
Sluice pit drain	3.05	5.25E-2	0.018	1.05
Heel pit drain	3.96	5.25E-2	0.018	1.36
U-tube seal	5.58	4.09E-2	0.021	2.87
Cascade pipe	17.4	7.37E-2	0.017	4.01
Saltwell riser	17.7	0.21	0.015	1.26
HEPA vent pipe	12.8	0.102	0.016	2.02

Note: [1]For commercial steel roughness see Brown et al. (1950).

Based on PR and pipe resistance factor N (from Equation 5-10), a value of mass flow rate per unit area of flow path may be determined from the solution of the equations of adiabatic flow for compressible gas flow in pipes (Lapple 1943). Numerical results, presented in graphical form by Brown et al. (1950), allow one to determine G/G_{cni} as functions of N and PR. G is the mass flow velocity for the conditions of interest and G_{cni} is the maximum mass flow velocity under isothermal conditions. The latter may be expressed in terms of upstream gas parameters (Brown et al. 1950):

$$G_{cni} = P_o \left(\frac{g_c M}{e RT_o} \right)^{1/2} \qquad (5\text{-}12)$$

where

G_{cni} = maximum mass flow velocity under isothermal pipe flow
P_o = upstream pressure

g_c = dimensional constant, 32.17 lb mass ft/lb force sec^2
M = molecular weight of gas
e = 2.718
R = gas constant
T_o = temperature in gas.

After G is determined, the mass flow rate can be evaluated by multiplying by the flow area:

$$\dot{m} = G \cdot A \tag{5-13}$$

where

$\dot{m}$ = gas flow rate in pipe, kg/s
G = mass velocity, $kg/m^2/s$
A = flow area, m^2

Table 5-2 shows the results of the vent flow rate analysis, and flow rates through each vent path, expressed in volumetric units, computed for a tank pressure of 96.5 kPa (14 psig) and a temperature of 614 °K. The stated temperature (614 °K) was computed as that required to increase tank pressure from its initial value to 96.5 kPa (14 psig) using the ideal gas law.

As indicated in Table 5-2, the saltwell riser is the dominant flow path. The combined flow rate of the six small vents, 3.71 m^3/s, is roughly one-third of calculated flow rate for the saltwell riser. A best estimate base case, vent flow rate for use in the following sensitivity analyses, was based on the following assumptions.

- The six small vents (see Table 5-2) are open at all times.
- The saltwell riser opens only when the riser cap and cover blocks are lifted by a tank pressure exceeding 13.8 kPa (2 psig).

Table 5-2. Vent Flow Rates Calculated for a Tank Pressure of 96.5 kPa (14 psig).

Vent Pipe Description	Vent Flow Rate m^3/s
Pump pit drain	0.46
Sluice pit drain	0.46
Heel pit drain	0.44
U-tube seal	0.22
Cascade pipe	0.65
Saltwell riser	10.17
HEPA vent pipe	1.48
Total	13.88

A simple method for approximating the flow rate predicted from the adiabatic flow equation was used in this analysis. The orifice equation for gases (Perry 1963) was used along with an upper limit to velocity that limited orifice velocity to sonic velocity at the upstream temperature. This method for predicting outflow rates simplified the calculation scheme and yielded outflow rates that were conservative compared to those based on the adiabatic flow equations.

The opening of the saltwell vent path was assumed to begin at the specified lift pressure and be completely open at the lift pressure plus (6.89 kPa [1 psig]). Between these pressure limits, the flow area was linearly related to tank pressure.

5.4 SENSITIVITY ANALYSIS FOR THERMAL HYDRAULIC RESULTS

Peak pressure generated by a pool fire is the major threat to tank structural integrity. This section provides peak pressures for a number of cases. Uncertainties in fire parameters are illustrated by comparing peak pressure for a best-estimate base case with peak pressures computed for a range of possible values of key fire parameters.

5.4.1 Base Case Solvent Fire Parameters

Table 5-3 summarizes the key parameters for the base case fire. Figure 5-4 shows the pressure transient calculated for a solvent fire using base case parameters. Internal tank pressure peaks at (28.3 kPa [4.1 psig]), 162 seconds after fire initiation. Peak pressure is predicted to occur approximately 80 seconds before the fire is terminated by lack of oxygen.

Table 5-3. Key Parameters for Base Case Solvent Fire.

Parameter	Value
Initial inflamed circle diameter	0.305 m
Flame radial spread rate	1 cm/s
Solvent pool area	40.9 m^2
Leak path description	Six small pipes plus saltwell riser open at 13.8 kPa (2 psig) (see Table 5-2)
Emissivity product, $\epsilon_g \times \epsilon_s$	0.9
Oxygen extinguishment level	0.13 mole fraction
Specific burning rate	3.0 kg/min/m^2 @ 21% oxygen to 0 kg/min/m^2 @ 13% oxygen
Combustion enthalpy	33 MJ/kg
Headspace air volume	2,663 m^3

Figure 5-4. Tank Pressurization Predicted for Base Case Solvent Fire.

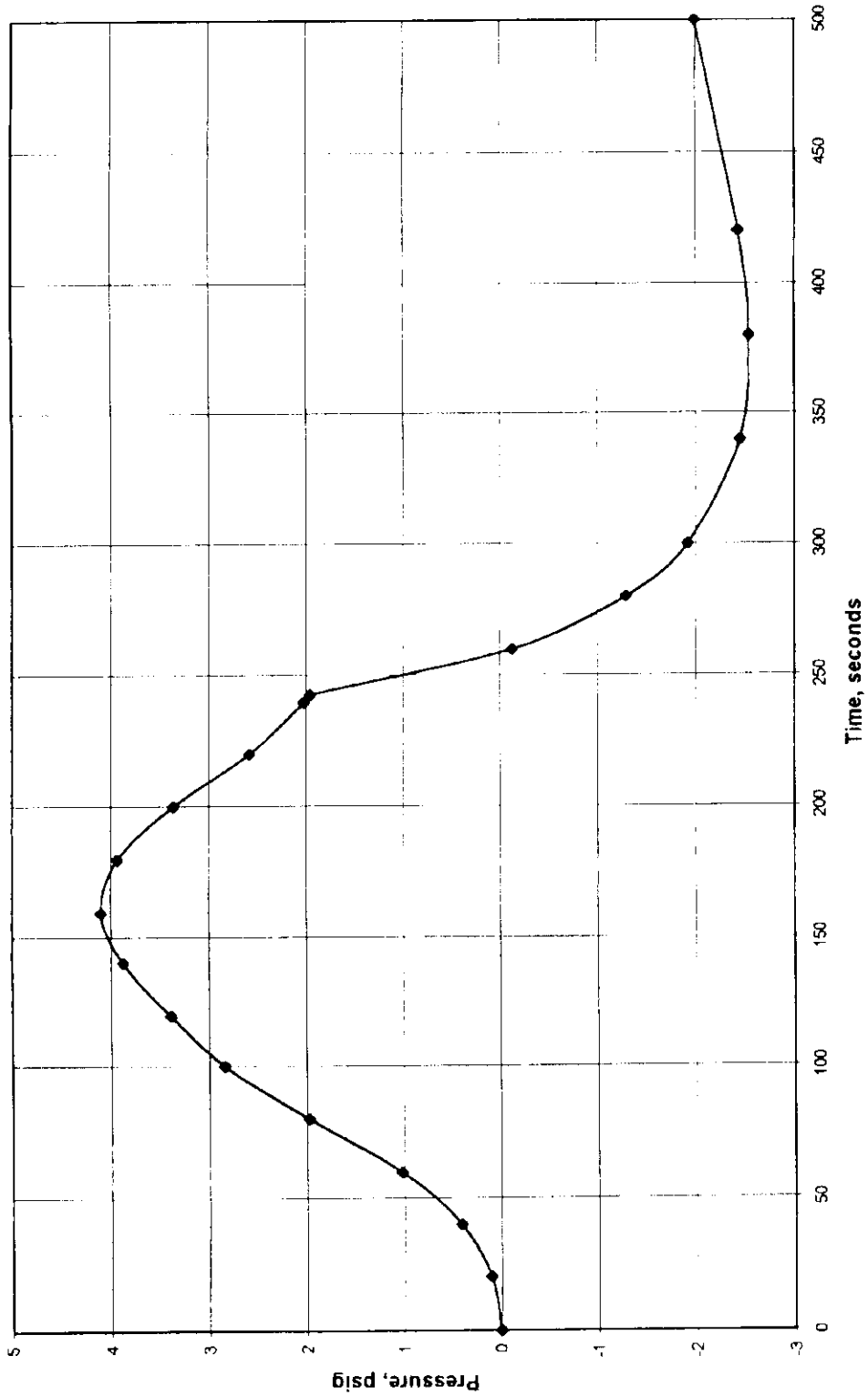

After fire extinguishment, internal pressure falls rapidly as a result of gas venting and heat loss from the gas to tank surfaces. As indicated, tank gauge pressure is calculated to go negative at approximately 260 seconds and reaches a minimum value of 17.5 kPa (-2.5 psig) at approximately 380 seconds. After this minimum, pressure gradually returns to ambient atmospheric pressure. The relatively high vacuum predicted for this case (-2.5 psig) is attributable to the postulated closure of the saltwell riser (the largest vent pipe) when tank pressure falls below 13.8 kPa (2 psig).

5.4.2 Effect of Initial Inflamed Area

As noted in Table 5-3, the initial inflamed area in the base case is 0.31 m (1 ft) in diameter. The effect of the initial inflamed area is evaluated by varying the diameter by a factor of two above and below the base value. Therefore, the initial inflamed area for the two cases is a factor of four above and below the base case area. Table 5-4 shows the results of the analysis, in terms of peak pressure.

Table 5-4. Effect of Initial Inflamed Area on Peak Pressure.

Diameter of Initial Inflamed Area (m)	Peak Pressure kPa (psig)
0.15	28.3 (4.1)
Base Case 0.31	28.3 (4.1)
0.62	28.3 (4.1)

As indicated in Table 5-4, peak pressure is not sensitive to initial inflamed area over the range studied.

5.4.3 Effect of Flame Spread Rate

The base case flame spread rate (1 cm/s) was selected as a realistic estimate for tank 241-C-103 solvent on the basis of available data discussed in Section 5.2.2. The effect of spread rate on peak pressure is quantified by running cases for spread rates of 0.1 cm/s, 0.5 cm/s, 2.0 cm/s, and 10 cm/s. Table 5-5 shows the results of the calculations compared to results for the base case.

Table 5-5. Effect of Flame Spread Velocity on Calculated Peak Pressure.

Fire Spread Velocity (cm/s)	Peak Pressure kPa (psig)
0.1	6.7 (0.98)
0.5	18.6 (2.7)
Base Case 1.0	28.3 (4.1)
2.0	48.3 (7.0)
10	95.1 (13.8)

As indicated in Table 5-5, peak pressures are calculated to vary significantly with fire propagation velocity. The increase in peak pressure with spread velocity is the result of higher overall combustion rates due to the larger inflamed areas computed for higher spread rates.

The high spread rate case, 10 cm/s, results in peak pressures that are appreciably higher than predicted using base case parameters. For this case, the inflamed area is computed to cover 133 m^2 (1,430 ft^2) at the time of fire extinguishment, or roughly one-third of the whole tank cross-section area. From these results, it is concluded that the impact of pool area on calculated peak pressure is closely tied to the fire spread velocity because a larger area can be inflamed by a rapidly spreading fire than can be covered by a slowly spreading fire. Larger inflamed areas result in a higher overall burn rate causing headspace gases to heat more rapidly and diminishing the mitigating effects of heat transfer and gas venting.

5.4.4 Effect of Solvent Pool Area

The base case pool area, 40.9 m^2 (440 ft^2), represents 10 percent of the cross-section area of the tank. The impact of pool area is quantified by varying the pool area from 1 m^2 (10.8 ft^2) to the whole tank cross-section area. An additional case that used 10 cm/s spread velocity and the largest pool area was also run. This case helps evaluate the effect of high-spread velocity for a large pool configuration. Table 5-6 shows the calculated variation of peak pressure with pool area.

Table 5-6. Effect of Pool Area on Calculated Peak Pressure.

Pool Area m^2 (ft^2)	Peak Pressure kPa (psig)
1.0 (10.8)	10.3 (1.5)
4.65 (50)	22.1 (3.2)
9.29 (100)	28.3 (4.1)
18.59 (200)	28.3 (4.1)
Base Case 40.9 (440)	28.3 (4.1)
74.4 (800)	28.3 (4.1)
411 (4,418)	28.3 (4.1)
411 (4,418)	115 (16.7)[1]

Note: [1]This case uses a spread velocity of 10 cm/s.

As indicated in Table 5-6, peak pressure increases with pool area up to an area of approximately 9.3 m^2 (100 ft^2). Larger pool areas do not result in higher peak pressures because overall combustion rate is limited by 1) spread velocity, 2) the reduction in burn rate with oxygen concentration, and 3) fire termination caused by oxygen extinguishment. The calculated pool area at the

time of fire extinguishment for base case fire parameters is 20.8 m^2 (224 ft^2). Solvent areas larger than this do not become inflamed before fire extinguishment (i.e., spread velocity of 1 cm/s). The higher pressure for 10 cm/s spread velocity is attributable to the fire covering a much larger pool area prior to extinguishment resulting in a short burn period with little time for gas venting and heat transfer.

5.4.5 Effect of Leak Path Flow Capacity

The sensitivity of calculated peak pressure to leak path flow capacity can be illustrated by analyzing a case in which the largest path (i.e., saltwell riser) is assumed unavailable. Table 5-7 shows the peak pressure for this case.

Table 5-7. Effect of Leak Path Flow Resistance on Calculated Peak Pressure.

Leak Path Description	Peak Pressure kPa (psig)
6 small pipes + saltwell riser[1] Base Case	28.3 (4.1)
6 small pipes	60.0 (8.7)

Note: [1]Saltwell riser assumed to open at a tank pressure of 2.0 psig (13.8 kPa).

As indicated in Table 5-7, the opening of the saltwell vent has a significant effect on limiting tank pressures. The smaller leak path size case shows significantly higher pressures.

5.4.6 Effect of Gas Emissivity

As indicated in Equation 5-6, radiation heat transfer rate is proportional to the product $\epsilon_g \cdot \epsilon_s$. The base case ascribes a value of 0.9 to this product. Parametric runs can be made by setting this product equal to 0.8 and 1.0 (see Table 5-8).

Table 5-8. Effect of Emissivity on Calculated Peak Pressure.

Numerical Value of $\epsilon_g \cdot \epsilon_s$	Peak Pressure kPa (psig)
1.0	27.6 (4.0)
Base Case .9	28.3 (4.1)
0.8	29.0 (4.2)

As indicated in Table 5-8, the value of the emissivity product $\epsilon_g \cdot \epsilon_s$ has a relatively minor effect on peak pressure over the range covered. Smaller values of emissivity product that cause calculated pressures to be larger do not appear to be realistic.

5.4.7 Effect of Heat Transfer Flux from Flame to Burning Solvent Surface

Heat transfer from the flame to the burning liquid surface is evaluated to have a best-estimate value of 57 kW/m² (see Section 5.3.3.1). The sensitivity of predicted peak pressure to flame-pool surface heat transfer flux is illustrated by assigning parameter values 24.5 kW/m² and 72 kW/m² (Ayer et al. 1988). Table 5-9 shows the results of this calculation.

Table 5-9. Effect of Flame-Pool Heat Transfer Rate on Predicted Peak Pressure.

Flame Pool Heat Transfer Flux (kW/m²)	Peak Pressure kPa (psig)
24.5	29.0 (4.2)
Base Case 57	28.3 (4.1)
72	28.3 (4.1)

As indicated in Table 5-9, calculated peak pressures are insensitive to the flame-pool heat transfer flux over the range studied. This insensitivity is expected because the flame-pool heat transfer rate is small compared to the rate of heat generation by combustion. Because the base case flame pool heat transfer flux (57 kW/m²) amounts to only 8.5 percent of the combustion energy, changes in this parameter have a relatively small effect on the rate of energy transfer from headspace air.

5.4.8 Effect of Oxygen Extinguishment Level

The oxygen extinguishment level determines the maximum quantity of fuel that can be oxidized in the fire. The base case value of 0.13 mole fraction is selected on the basis of large-scale tests (see Section 5.2.4). The impact of the oxygen extinguishment level is evaluated by making parametric runs at 0.11 and 0.175 mole fractions, the range reported in solvent fire tests. Table 5-10 lists the results.

Table 5-10. Effect of Oxygen Extinguishment Levels on Calculated Peak Pressure.

Oxygen Extinguishment Mole Fraction	Peak Pressure kPa (psig)
0.11	28.3 (4.1)
Base Case 0.13	28.3 (4.1)
0.175	27.6 (4.0)

As indicated in Table 5-10, calculated peak pressure is lower for the case where early extinguishment is assumed (O_2 extinguishment level of 0.175 mole fraction). Peak pressure does not increase significantly when the fire is assumed to continue until an oxygen mole fraction of 0.11 is reached. The reason is that peak pressure is reached well before fire extinguishment (see Figure 5-3).

5.4.9 Effect of Combustion Energy of Organic Liquid

As noted in Section 5.3.2.1, the combustion enthalpy for the base case has been assigned a value of 80 percent of the theoretical value for complete combustion. Parametric runs for combustion energies are 91 and 70 percent of the theoretical value (see Table 5-11).

Table 5-11. Effect of Combustion Energy on Calculated Peak Pressure.

Combustion Energy MJ/kg	Calculate Peak Pressure kPa (psig)
28.9	23.4 (3.4)
Base Case 33.0	25.5 (3.7)
41.3	26.9 (3.9)

As indicated in Table 5-11, an increase in combustion energy is reflected in an increase in calculated peak pressure. The increase is relatively small, indicating that uncertainty in combustion efficiency will not significantly affect computed peak pressures.

5.4.10 Conclusions from Thermal Hydraulic Sensitivity Analysis

Findings from the thermal hydraulic sensitivity analysis of postulated solvent fires in SSTs can be summarized as follows.

- The peak pressure predicted for a postulated fire is significantly affected by the tank vent capacity.
- Fire spread rate has significant impact on calculated peak pressure. Fire spread rates over immobile fuel surfaces (e.g., solvent-permeated sludge or saltcake) are much slower than for open liquid pools deeper than a few millimeters. Calculated peak pressures are significantly lower for immobilized solvent than for liquid pools.
- The impact of pool area on peak pressure depends largely on fire spread velocity. For cases where high spread rates may be applicable, bounding values of pool area should be used to assure that predicted peak pressures are not unduly limited by postulated pool area.

5.5 PARAMETRIC ANALYSIS OF FIRE PRESSURIZATION

Peak pressures and post-fire peak vacuums are calculated in this section. The objective is to illustrate how changes in key parameters affect predicted peak pressures and vacuums. Whereas the sensitivity analysis presented in Section 5.4 used tank 241-C-103 parameters, the analyses presented in this section apply to a tank having a bounding headspace air volume.

Bounding high headspace air volumes maximizes oxygen inventory and thus the mass of solvent that can be burned. Solvent burning produces the aerosols and gases that drive the radiological and toxicological hazard. Maximizing the mass burned should lead to bounding predicted consequences for pool fires. Bounding high headspace volumes also yields the minimum in surface to volume ratio, which minimizes the effectiveness of heat loss from the gas phase. To the extent that peak pressure is limited by heat loss during the burn, the effect would be greatest for small headspace volumes. It is also worth noting that peak pressure is not a major driver of predicted consequences because dome cracking relieves pressures in SSTs and predicted peak pressures are well below failure pressures for DSTs and DCRTs.

5.5.1 Methodology

The thermal hydraulic model described in Section 5.3 is used to analyze postulated pool fires in SSTs. Fire parameters studied parametrically are:

- Flame spread velocity
- Vent flow capacity
- Pool area.

These three parameters affect the predicted pressures, and their values are subject to considerable uncertainty. Most other fire parameters were quantified by assigning them the base case values specified in Section 5.3.

Tank parameters for this analysis were specified for the bounding high value of headspace air volume. Table 5-12 summarizes key tank parameters based on information applicable to tank 241-AX-104.

Table 5-12. Tank Parameters for Parametric Analysis.

Parameter	Value
Tank diameter, m (ft)	22.9 (75)
Headspace volume, m^3 (ft^3)	4,816 (170,000)
Concrete area, m^2 (ft^2)	454 (4,885)
Steel area, m^2 (ft^2)	844 (9,080)
Initial temperature, °C (°F)	15.6 (60)
Initial pressure, kPa (psig)	100 (14.5)

5.5.2 Solvent Fire Peak Pressures

Peak pressure was calculated for small and large pools. Small pools are defined as pools smaller than the 1-m^2 (10.8-ft^2) criterion used in the screening methodology (see Appendix A). A large pool is one for which the pool size does not limit flame spread before fire extinguishment on low oxygen. A pool size of 210 m^2 (2,260 ft^2) meets this requirement and was used as the pool area for the large pool case. Flame spread velocity was assigned values of 0.1, 1.0, and 10 cm/s to cover a range of possible values.

Vent flow capacity was quantified on the basis of equivalent orifice diameters ranging from 9.5 cm (3.75 in.) to 0.76 m (30 in.). The smaller orifice mimics the flow capacity of the HEPA vent pipe, and the larger orifice simulates openable risers present on some SSTs. Orifice diameters used to quantify the vent paths applicable to the tank 241-C-103 case (see Tables 5-3 and 5-7) were 0.15 m (5.89 in.) and 0.234 m (9.65 in.), respectively, for the six small pipes and for the saltwell riser.

Table 5-13 summarizes peak pressures predicted for 0.1 cm/s spread rate.

Table 5-13. Peak Pressure Predicted for 0.1 cm/s Fire Spread Velocity.

Vent Orifice Diameter cm (in.)	Peak Pressure kPa (psig)	
	Small Pool (1 m^2)	Large Pool (210 m^2)
9.5 (3.75)	14. 5 (2.1)	30.5 (4.4)
15.2 (6)	8.3 (1.2)	14.5 (2.1)
25.4 (10)	<6.9 (1)	<6.9 (1)
50.8 (20)	<6.9 (1)	<6.9 (1)
76.2 (30)	<6.9 (1)	<6.9 (1)

The highest pressure listed in Table 5-13 is 30.5 kPa (4.4 psig). It is evident that a slowly spreading pool fire could not generate pressures high enough to challenge tank structural integrity.

Table 5-14 lists peak pressures predicted for 1 cm/s spread velocity. The highest pressure listed applies to a large pool and the smallest vent path. Peak pressure falls significantly when vent size is increased, as expected. Peak pressures for small pools fall well below tank structural limits for even the smallest vent studied.

Table 5-14. Peak Pressure Predicted for 1 cm/s Fire Spread Velocity.

Vent Orifice Diameter cm (inches)	Peak Pressure, kPa (psig)	
	Small Pool (1 m^2)	Large Pool (210 m^2)
9.5 (3.75)	2.3 (15.9)	14.8 (103)
15.2 (6)	1.5 (10.3)	12.3 (84.8)
25.4 (10)	1 (< 6.9)	7.7 (53.1)
50.8 (20)	1 (< 6.9)	1.7 (11.7)
76.2 (30)	1 (< 6.9)	1 (< 6.9)

Table 5-15 lists peak pressures predicted for 10 cm/s spread velocity.

Table 5-15. Peak Pressure Predicted for 10 cm/s Fire Spread Velocity.

Vent Orifice Diameter cm (in.)	Peak Pressure, kPa (psig)	
	Small Pool (1 m^2)	Large Pool (210 m^2)
9.5 (3.75)	2.3 (15.9)	28.9 (199)
15.2 (6)	1.5 (10.3)	27.4 (189)
25.4 (10)	1 (<6.9)	23.8 (164)
50.8 (20)	1 (<6.9)	13.9 (95.8)
76.2 (30)	1 (<6.9)	7.2 (49.6)

As evident from a comparison of large pool peak pressures in Tables 5-14 and 5-15, an increase in spread velocity from 1 cm/s to 10 cm/s results in roughly a doubling of peak pressure for the smaller vents. For small pools, peak pressures are unaffected by spread velocity. The reason is that inflamed area is limited by total pool area (1 m^2) for both spread rates.

5.5.3 Post-Fire Peak Vacuums

Venting of gas during a fire, followed by cooling of gas after fire extinguishment, causes a vacuum to develop within the tank. The vacuum imposes a structural loading that could challenge structural tank limits. Conceptually, a worst case corresponds to the opening of a one-way vent that offers little resistance to outward flow, but closes when flow reverses. Some tanks have relatively large risers that are covered with unbolted metal plates. The covers could lift in response to internal tank pressure, then fall back into position, blocking air inflow.

Peak vacuums are studied here by means of the thermal hydraulic code described earlier. Fire and tank parameters used in Section 5.5.2 are used here as well. The fire spread rate and pool area are varied parametrically as described in Section 5.5.2. The vent path configuration is also explored parametrically. A vent orifice of 9.5 cm (3.75 in.) is assumed to exist for two-way flow. This orifice mimics the flow admittance of the HEPA vent pipe. A parallel flow path covered by a flapper valve is also assumed to exist. This flow path opens at a specified pressure difference to simulate the lifting of a riser cover and pit cover blocks. The opening pressure is specified as 13.8 kPa (2 psig), and the path is assumed to be fully open at 20.7 kPa (3 psig). The flow resistance of the fully open vent path is treated parametrically by specifying an equivalent orifice size. The equivalent orifice area is assumed to be proportional to pressure for the range of 13.8 to 20.7 kPa (2 to 3 psig).

Table 5-16 shows calculated vacuums for a 0.1 cm/s fire spread velocity. Fire and tank parameters not specified in Table 5-16 or in Section 5.5.1 are cited in Table 5-3.

Table 5-16. Calculated Peak Vacuum for Fire Spread Velocity of 0.1 cm/s.

Flapper Valve Orifice diameter in (m)	Peak Vacuum, kPa (psig)	
	Small Pool (1 m^2)	Large Pool (210 m^2)
0 (0)	2.76 (0.4)	4.83 (0.70)
6 (0.15)	2.76 (0.4)	11 (1.6)
10 (0.25)	2.76 (0.4)	11 (1.6)
20 (0.51)	2.76 (0.4)	11 (1.6)
30 (0.76)	2.76 (0.4)	11 (1.6)

Peak vacuum for small pool fires is listed as 2.76 kPa (0.4 psig) for all cases. The flapper valve has no effect for small pool fires because the peak pressure is only marginally higher than the pressure required to open the flapper valve. For the large pool case, the flappers hold the peak pressure to just over the opening threshold pressure of 13.8 kPa (2 psig) and vent roughly the same quantity of gas.

In summary, the peak vacuums calculated for a fire spread velocity of 0.1 cm/s are small (<1.6 psig) because relatively little of the headspace gas inventory is vented during the fire.

Table 5-17 shows peak vacuums calculated for a fire spread velocity of 1 cm/s. Fire and tank parameters not specified in Table 5-17 or in Section 5.5.1 are cited in Table 5-3.

Table 5-17. Calculated Peak Vacuum for Fire Spread Velocity of 1.0 cm/s.

Flapper Valve Orifice diameter in (m)	Peak Vacuum, kPa (psig)	
	Small pool (1 m^2)	Large pool (210 m^2)
0 (0)	2.76 (0.4)	0.69 (0.1)
6 (0.15)	2.76 (0.4)	7.58 (1.1)
10 (0.25)	2.76 (0.4)	20 (2.9)
20 (0.51)	2.76 (0.4)	29 (4.2)
30 (0.76)	2.76 (0.4)	29 (4.2)

As shown, results for the small pool case are identical to the results obtained for the lower spread velocity (see Table 5-16). This similarity for small pools is expected because the size of the fire is limited by pool area not spread rate.

For the large pool case, larger openings associated with flapper valve action lead to higher calculated vacuums. This result is as expected because more gas is vented from the tank when larger openings are credited in the calculation.

Table 5-18 shows peak vacuums calculated for a fire spread velocity of 10 cm/s. Fire and tank parameters not specified in Table 5-18 or in Section 5.5.1 are cited in Table 5-3. As indicated by the data of Table 5-18, predicted vacuums for the small pool case are low and identical to values predicted for lower fire spread velocities. This result is expected because pool area controls fire size for the small pool case.

Table 5-18. Calculated Peak Vacuums for Fire Spread Velocity of 10 cm/s.

Flapper Valve Orifice diameter in (m)	Peak Vacuum, kPa (psig)	
	Small pool (1 m²)	Large pool (210 m²)
0 (0)	2.76 (0.4)	0.69 (0.1)
6 (0.15)	2.76 (0.4)	2.76 (1.4)
10 (0.25)	2.76 (0.4)	10.3 (1.5)
20 (0.51)	2.76 (0.4)	29 (4.2)
30 (0.76)	2.76 (0.4)	41.4 (6.0)

For the large pool case, larger openings associated with flapper valve action lead to higher calculated vacuums. The highest peak vacuum is calculated for the largest flapper vent, a 0.76-m (30-in.) orifice. A significant fraction of headspace gas inventory is vented through the large orifice when the tank is pressurized, resulting in a relatively low gas pressure in the tank after cooldown.

In summary, one-way vent openings could result in appreciable post-fire vacuums in waste tanks. The vacuums are small in magnitude for small pools irrespective of fire spread velocity. For large pools, significant vacuums are calculated only for spread velocities higher than 0.1 cm/s. The highest vacuum is predicted for the largest vent orifice (0.76 m [30 in.]) and the highest fire spread velocity (10 cm/s).

6.0 PHENOMENA AND MODELING OF THE RELEASE OF RADIOACTIVE AND TOXICOLOGICAL MATERIAL DUE TO SOLVENT FIRES

This section summarizes the phenomena and methodology for calculating material releases and dose consequences from underground waste tanks caused by postulated solvent fires.

6.1 KEY ASSUMPTIONS

Key assumptions supporting the methodology for quantifying the consequences of solvent pool fires are summarized as follows.

6.1.1 Ignition and Flame Spread

The ignition of a stable flame over a circular area 0.3-m (1-ft)-diameter is postulated as the initial flame configuration. The flame is postulated to spread at a specified radial velocity until the entire pool area is covered by flame or until the fire is extinguished on low oxygen level. A bounding spread velocity is 10 cm/s. Lower spread velocities may be used for specific cases if justified by available information.

6.1.2 Solvent Pool Area

Two cases of pool area may be used to bracket possible pool sizes. First, a pool of 1 m^2 (10.8 ft^2), termed here a puddle, is postulated as a lower limit to be considered. One square meter is the pool area criterion used to screen tanks for the presence of solvent pools (see Appendix A). Second, a large pool is postulated such that inflamed area is not limited by pool size. For SSTs and DSTs a pool area of 210 m^2 (2,260 ft^2) is used to quantify the large pool case. For pools this size and larger, the fire was computed to extinguish on low oxygen level before the entire 210 m^2 became inflamed. For DCRTs, the design that could contain the largest pool was selected (tank 241-244-BX), and the pool was assumed to cover the entire waste surface (34.1 m^2). For the smaller SSTs, a puddle fire case (1 m^2) was analyzed as well as pools that covered the entire tank cross section.

6.1.3 Fire Extinguishment

The fire is assumed to extinguish at an oxygen concentration of 13 percent by volume. This assumption is based on the results of large-scale solvent pool fire tests in ventilated cells. It is recognized that the solvent inventory could limit the quantity of solvent burned for puddle fires, but fire extinguishment attributable to limited solvent inventory is conservatively disregarded.

6.1.4 Tank Parameters

All cases were based on bounding headspace volumes to maximize the oxygen inventory and thereby maximize the mass of solvent burned.

Vent paths were postulated at two extremes to cover possible cases. A minimal vent was postulated to evaluate maximum pressures that could be generated by a pool fire. For SSTs, this minimal vent was based on the HEPA vent pipe. For DSTs and DCRTs, the minimal vent was zero, a conservative default value chosen because a reliable, realistic minimal vent path size was not known. A large vent path case was considered to evaluate maximum vacuum on cooldown. A circular opening, 1.27 m (50 in.) in diameter, covered by a hinged plate was assumed to open at a pressure difference of 1 psi (6.89 kPa). This flapper valve was hypothesized to simulate venting through large risers (in tank pits) that are covered by caps held in place by gravity.

6.1.5 Tank Structural Integrity

All cases considered here are analyzed on the assumption that thermal and mechanical loads imposed on tank structures by the postulated pool fire do not cause collapse of the dome. Thus, radioactive material releases attributable to tank structural failure are not considered. Structural limits are documented in WHC (1996b) and WHC (1996c). Two DCRTs (244-A and 244-CRTK-003) were not analyzed in WHC (1996c). However the other DCRTs were analyzed and determined to have adequate safety margins. It is probable that all of the DCRTs are structurally adequate.

6.1.6 Carryover of Contaminants with Vented Gas

Gaseous contaminants made airborne by the fire may be assumed to be transported as ideal gases. Headspace air is assumed to be perfectly mixed, and the fractional release of gases may be computed on the basis of the fraction of gas vented from the tank. For passively-ventilated tanks, atmospheric releases may be assumed to end when the tank internal pressure falls below the pressure of the outside atmosphere. For actively ventilated tanks, it is assumed that continued operation of ventilation fans would purge all airborne contaminants from the tank. Mitigation of accident consequences by aerosol depletion is computed for all cases. Aerosol depletion by in-tank sedimentation was predicted by means of an aerosol behavior correlation. Particle deposition by mechanisms other than sedimentation was neglected.

6.2 RELEASE OF CONTAMINANTS FROM TANK

The atmospheric source term attributable to postulated solvent pool fires was computed from the following formula.

$$S = M * C * ARF * RF * LPF \qquad (6\text{-}1)$$

where

S = source term, kg

M = mass of material at risk, kg

C = concentration of contaminant in material at risk, kg/kg

ARF = aerosol release fraction (fraction of contaminant in material at risk which is released as an aerosol), dimensionless

RF = respirable fraction of released aerosol, dimensionless

LPF = leak path factor (fraction of aerosol which escapes to the environment), dimensionless

As noted in Section 5.1, some waste material would be released through cracks in the tank dome. The soil covering the tank would act as a filter to remove most of the waste material from the air stream. However, there is no existing model to calculate either the filtering effect of the soil or the fraction of the vented air that would be released through cracks in the tank dome. Therefore, the release calculations assume that all of the vented air is released through tank risers. The release calculations further assume that the initial pressure pulse ruptures any HEPA filters used in the tank ventilation systems and none of the wastes entrained in the escaping air stream are trapped on a filter. Therefore the calculated release quantity exceeds an actual release quantity.

The respirable aerosol fraction, RF, for pool and puddle fires was taken directly from Section 3.3.5 of DOE-HDBK-3010-94. Experiments where TBP and Kerosene mixtures were burned in large surface area pans, with ventilation air passed through the test cells, appear to be a good approximation of the burning conditions that would be found in the tanks. The recommended RF is 1.

Selection of the RF for an entrained solvent fire on saltcake is not as straightforward. Section 3.3.6 of DOE-HDBK reports the result of experiments in a wind tunnel to "...measure the ARF and RF of uranium from various surfaces (sandy soil, sandy soil with vegetation cover, stainless steel, and asphalt) at windspeeds of 1 m/s and 10 m/s." In some experiments with sandy soil, the Uranium Nitrate Hexahydrate (UNH) was air-dried for several days before testing. A gallon of gasoline was poured on the soil and ignited and the ARF and RF were measured. Page 3-49 provides an interpretation of this data. It concludes that aqueous solutions or air-dried salts on a surface that absorbs or holds liquids, including significantly cracked or pitted surfaces (saltcake) has a bounding RF of 0.4. UNH is not one of the main components of the material on the surface of the saltcake in the tanks. However, air dried salts and pitted, cracked surfaces are a very good description of the waste surface. Because of the variability of the numbers, as well as ease in computation, a slightly higher bounding RF of 0.5 is used in this analysis.

Means for quantifying the terms of Equation 6-1 for the several categories of contaminants are described as follows.

6.2.1 Solvent Smoke

The pool fire will cause the airborne release of a fraction of the radionuclide content of the solvent and will result in the formation of toxic combustion products. The radionuclide release was based on the following quantification of terms in Equation 6-1.

M, the mass at risk, was equated to the mass of solvent burned during the course of the fire. This mass was computed by means of the POOLFIRE.4 code for each case analyzed (see Appendix I).

C, the concentration of radionuclides in solvent, was based on measurements performed on a solvent sample retrieved from tank 241-C-103. The analytical measurements are reported by Pool and Bean (1994).

ARF, the aerosol release fraction, was quantified on the basis of empirical results summarized by Mishima (1994). For large pools, which are predicted to burn to oxygen extinction in minutes, a bounding ARF of 0.03 was used. For small pools (puddles), the burn to oxygen extinction is predicted to take many minutes, allowing time for heatup of underlying waste. A higher ARF of 0.1 was selected from (Mishima 1994) for puddle fires.

RF, the respirable aerosol fraction, was conservatively assumed to be unity for pool and puddle fires, as recommended in DOE HDBK-3010-94. An RF OF 0.5 was used for entrained fires, based on information in HDBK-3010-94..

LPF, the leak path transmission factor, was calculated by POOLFIRE.4 for each case analyzed. The fractional leak of aerosolized contaminants was computed to account for incomplete venting of headspace gases during the fire cycle and for in-tank sedimentation losses. Gas venting fractions were computed for each case using the POOLFIRE.4 Code, and aerosol sedimentation was quantified using the correlation published by Epstein and Ellison (1987). The adaptation of this correlation to solvent fire analysis is explained in Appendix C.

Toxic gas species formed by combustion of solvent were assumed to be adequately represented by CO, NO_2, and P_2O_5. For CO and NO_2, emission factors were used to quantify the masses formed by combustion. Emission factors used for CO and NO_2 were 0.0425 and 5.5E-3, respectively (Grigsby and Postma 1995). The emission factor is defined as the mass of pollutant formed per mass of fuel burned. The P_2O_5 formation was quantified by stoichiometry for the oxidation of TBP:

$$C_{12}H_{27}PO_4 + 18\ O_2 = 12\ CO_2 + 13.5\ H_2O + 0.5\ P_2O_5 \qquad (6\text{-}2)$$

Based on Equation 6-2, the mass ratio of P_2O_5 to TBP is 0.27. Tributyl phosphate vapors were assumed to comprise 16 percent by mass of fuel burned. This vapor mass fraction was taken from measurements at 100 °C (212 °F)

reported by Pool and Bean (1994) for solvent samples retrieved from tank 241-C-103. Therefore, an emission factor for P_2O_5 is 0.27(0.16) = 0.0432 kg P_2O_5/kg fuel.

The LPF value computed from POOLFIRE.4 was used for toxic gas releases. The RF was assigned a value of unity.

6.2.2 Headspace Gases

Headspace gases can contain a number of toxic substances. A bounding (worst case), steady state composite was assumed in all cases analyzed here. The composition of headspace gases is quantified by Van Keuren (1996b). The LFP was calculated by POOLFIRE.4, and RF was conservatively assigned a value of unity.

The radioactive content of headspace air before a pool fire was neglected.

6.2.3 Aqueous Boiloff

The pool fire could cause aerosolization of waste by evaporating water or possibly by entrainment caused by air flow. While the pool fire would result in a fire plume that would induce air circulation in the headspace, air velocities near the surface of the waste outside the burning pool are judged to be too low to cause appreciable waste entrainment. Therefore entrainment of waste caused by to air flow at the surface of the waste is discounted. Waste aerosolization caused by moisture evaporation is quantified on the basis of releases from boiling liquids.

The mass of liquid at risk is computed as the mass of water which could be evaporated by heat transferred from the flame to the inflamed surface. Using a flame heat transfer rate of 57 kW/m^2 (an average of values for the burning of rubber gloves and burning of kerosene [Ayer et al. 1988], an average specific burning rate of 1.2 kg/m^2/min [Jordan and Lindner 1983], and a latent heat of water of 2.26 MJ/kg), the mass of water evaporated per mass of fuel burned is:

$$\frac{57\ \text{kJ}}{\text{s m}^2} * \frac{60\ s}{\text{min}} * \frac{m^2\ \text{min}}{1.2\ kg\ fuel} * \frac{1\ kg\ H_2O}{2260\ kJ} = \frac{1.26\ kg\ H_2O}{kg\ fuel}$$

The value of M applicable to aqueous boiloff in Equation 6-1 was computed for each case by multiplying the mass of fuel burned (from POOLFIRE.4) by 1.26.

ARF, the aerosol release fraction, was assigned a value of 0.002 on the basis of release fractions for boiling liquids as recommended by Mishima (1994).

RF, the respirable fraction, was assigned a conservative value of unity for pool and puddle fires. A value of 0.5 was assigned for entrained fires.

LPF, the leak path admittance factor, was computed to account for the fraction of reaction products vented from the tank over the course of the fire and for in-tank aerosol sedimentation.

The concentrations of nuclides in SST, DST, and DCRT liquids, expressed in terms of unit liter doses, were based on values recently reported by Cowley (1996). The concentration of toxic analytes in these liquids was evaluated from sum of fraction per unit release rate data presented by Van Keuren (1996b).

6.3 RADIOLOGICAL DOSE CONSEQUENCES OF RELEASED CONTAMINATES

Onsite dose consequences are calculated on the basis of particle inhalation. The equation used to compute onsite dose is from Van Keuren (1996a):

$$D(Sv) = Q(L) * \frac{\chi}{Q^1} (s/m^3) * R(m^3/s) * ULD(Sv/L) \qquad (6\text{-}3)$$

where

D	=	50 year dose following inhalation, Sv
Q	=	Volume of waste dispersed as an aerosol, L
$\frac{\chi}{Q^1}$	=	Integrated atmospheric dispersion factor, s/m^3
R	=	Breathing rate of individual, m^3/s
ULD	=	Unit liter dose for released waste, Sv/L.

The total dose was calculated to result from releases attributable to three separate sources:

1. Solvent smoke
2. Waste made airborne by aqueous evaporation
3. Rupture of HEPA and pre-filters.

The offsite dose was computed as the sum of inhalation and ingestion exposures.

$$D(Sv) = D_{Inh}(Sv) + D_{Ing}(Sv) \quad (6\text{-}4)$$

The inhalation dose for offsite receptors was computed with Equation 6-3 using appropriate atmospheric dispersion factors and breathing rates. Ingestion dose was computed from (Van Keuren 1996a):

$$D_{Ing}(Sv) = Q(L) * \frac{\chi}{Q^1} (S/m^3) * ULD_G(Sv\ m^3/sL) \quad (6\text{-}5)$$

where

D_{Ing} = 50 year dose due to ingestion, Sv
Q = volume of waste dispersed as an aerosol, L
$\frac{\chi}{Q^1}$ = atmospheric dispersion factor, s/m^3
ULD_G = unit liter dose for ingestion, Sv m^3/sL.

6.4 TOXICOLOGICAL CONSEQUENCES OF RELEASED CONTAMINANTS

The concentrations of toxins in the downwind plume was computed from formulas that quantify the degree of dilution that would occur in the atmosphere between the tank vent and the assumed receptor. Turbulent mixing induced by the momentum and buoyancy of vented gas (see Appendix B) is important in determining dilution at the onsite (100m downstream) receptor location. The following equation is used to compute airborne concentrations at the onsite location:

$$C_{100m} = S * DF_{100m} \quad (6\text{-}6A)$$

where

C_{100m} = toxin concentration at 100m, mg/m^3
S = toxin concentration at tank vent, mg/m^3
DF_{100m} = dilution factor at 100m

Numerical values of DF_{100m} applicable to solvent fires and their technical bases are provided in Appendix B.

Dilution factors for the offsite receptor would be determined primarily by normal atmospheric turbulence. Mixing in the vicinity of the tank vent(s) is neglected in calculating toxin concentrations at the offsite location. The following formula, which applies for continuous releases (Van Keuren 1996b), is used to calculate toxin concentrations at the offsite location.

where

C = peak concentration in plume, mg/m^3

$$C\ (mg/m^3) = \left[\frac{\frac{\chi}{Q^1}\left[\frac{s}{m^3}\right]}{1 + V^1\left[\frac{m^3}{s}\right] * \frac{\chi}{Q^1}\left[\frac{s}{m^3}\right]} \right] * S\left[\frac{mg}{m^3}\right] * V^1\left[\frac{m^3}{s}\right] \qquad (6\text{-}6B)$$

S = gaseous toxic material source concentration, mg/m^3

$\frac{\chi}{Q^1}$ = continuous release atmospheric dispersion factor, s/m^3

V^1 = volume release rate of gaseous source, m^3/s

The concentrations computed from Equations 6-6A and 6-6B were divided by the risk guideline that applies for each toxin:

$$F_i = \frac{C_i}{G_i} \qquad (6\text{-}7)$$

where

F_i = fraction of guideline for i-th toxin, dimmensionless
C_i = concentration of i-th toxin at downwind receptor, mg/m^3
G_i = risk guideline concentration, mg/m^3

Individual chemical toxins were grouped into the following categories by Van Keuren (1996b):

- Total particulates
- Corrosives and irritants
- Systemic poisons
- Central nervous system toxins.

The sum of fractions for each category was computed as the sum of individual fractions:

$$S_c = \sum_{i=1}^{i=n} \frac{C_i}{G_i} \qquad (6\text{-}8)$$

where

S_c = sum of fractions for toxin category, dimensionless
C_i = concentration of i-th toxin in category, mg/m^3
G_i = guideline concentration for i-th toxin in category, mg/m^3

The toxin insult caused by composite materials was evaluated from tabular data presented by Van Keuren (1996b). Composite materials include:

- Waste solids
- Waste liquids.

For these composite materials, the sum of fractions is calculated directly at onsite and offsite locations as a function of the volumetric release rate of these materials. This is illustrated below for a release of 1.27E-5 L of SST solids over a 60s time period. The release rate is:

$$\text{release rate} = 1.27E\text{-}5\ L/60s = 2.12E\text{-}7\ L/s$$

For a frequency range of 10^{-4} - 10^{-6} yr^{-1}, SST solids are characterized by a sum of fractions of 1.0E3 s/L (Van Keuren 1996b) for onsite receptors and 1.7E1 s/L for offsite receptors. The sum of fractions for this specific release of SST solids is calculated as follows:

$$\text{onsite sum} = 2.12E\text{-}7 * 1.0E3 = 2.12E\text{-}4,$$

$$\text{and offsite sum} = 2.12E\text{-}7 * 1.7E1 = 3.6E\text{-}6.$$

The onsite sum of fractions calculated above (2.12E-4) is based on dilution predicted by an atmospheric dispersion factor of 0.0341 s/m^3. This dispersion factor neglects turbulent mixing in the vicinity of the tank vent; therefore, it is overly conservative at the 100m mark. To use the sum of fraction multipliers provided by Van Keuren (1996b), they were adjusted to account for dilution quantified by Equation 6-6A. The sum of fraction multipliers for the onsite location provided by Van Keuren (1996b) were multiplied by $DF_{100m}/(\chi/Q^1 * V^1)$ where the quantities are as defined in Equations 6-6A and 6-6B. See Appendix B for the technical basis for this adjustment. Note that this adjustment factor was used only for calculating onsite toxicological consequences.

The overall insult attributable to toxic chemical releases was computed as the sum of fractions for solvent and for tank waste liquids and solids (composite materials).

$$S_F = \sum_{i=1}^{i=5} S_{ci} \qquad (6\text{-}9)$$

where

S_F = total sum of fractions, dimensionless
S_{ci} = sum of fractions for ith category

To summarize, the five categories of toxic substances included in Equation 6-9 are:

- Total particulates
- Corrosives and irritants
- Systemic poisons
- Central nervous system toxins
- Composite materials (waste solids and liquids).

7.0 FREQUENCY OF SOLVENT FIRES

Risk is a function of consequences and frequency. The previous section evaluated consequences. This section evaluates frequencies. The following summarizes an evaluation of tank farm equipment and operations, including operational upsets and natural phenomena, that might act as initiators for a solvent fire in a waste tank. The energy source frequencies are combined with ignition probabilities, given the energy source is present, to assign ignition frequencies for solvent fires on a per-tank basis. The number of tanks that might contain combustible solvent configurations are then estimated and used as a multiplier for the per tank ignition frequencies. Finally, accident scenario frequencies are assigned to an accident frequency category so that accident consequences can be compared to risk evaluation guidelines.

Operations that were considered in this evaluation are described in Bajwa and Farley (1994). In addition, the tank farm operations procedures described in the computer network-based, online Tank Farms Procedure Information System were reviewed for additional operations that would involve heating potential.

7.1 SOLVENT FIRE IGNITION FREQUENCIES ON A PER-TANK BASIS

The per-tank ignition frequency evaluation was performed in four steps.

1. The operations (normal and upset conditions) and natural phenomena were evaluated to determine which operation could introduce significant energy into the waste tank. Energy must be added to the waste to heat and vaporize a portion of the organic solvent and to create local high temperatures to act as an ignitor.

2. The frequency of the energy being deposited into the waste is estimated, assuming no safety controls are imposed.

3. The probability that the energy source could initiate a sustainable organic fire is estimated. The energy required to ignite a solvent pool or large puddle is quite large, while the energy required to ignite a small puddle or solvent-filled crack is somewhat smaller; the energy required to ignite solvent permeated saltcake is smaller still (see Section 4.1).

4. Controls to prevent or reduce the ignition scenario are identified and the ignition frequencies with controls are estimated. The results of the evaluation are summarized in Tables 7-1 and 7-2 and described in Sections 7.1.1 through 7.1.8.

Table 7-1. Energy Source Frequencies.

Energy Source	Unmitigated Frequency (Events per tank-year)	Mitigated Frequency (Events per tank-year)	Control
Electrostatic sparks between equipment and waste	1	n/a	not needed
Instrumentation faults cause over current in waste	1E-1	n/a	not needed
Welding and grinding sparks fall to waste surface	1E-2	n/a	not needed
Torch cutting	1E-02	prevented	administrative control on torch cutting
Camera and light power supply shorts in waste	1E-3	n/a	not needed
Vehicle fuel spill causes a gasoline fire inside the waste tank	3E-6	prevented	administrative control on vehicle access and fuel tank protection
Lightning strike arcs to waste surface	3E-5[1]	reduced but unquantified	lightning protection measures
Core drill overheating	1E-2	prevented	drill purge and interlocks

Note:
[1]Frequency is for an SST. DSTs and DCRTs are postulated to behave like Faraday cages (see Section 7.1.7). Therefore the frequency of a lightning strike arcing to the waste surface in DSTs or DCRTs is less than for an SST.

Table 7-2. Solvent Fire Frequencies for Various Organic Solvent Configurations. (2 sheets)

Solvent Configuration	Energy Source	Solvent Fire Ignition Probabilities	Unmitigated Solvent Fire Frequency (Events per tank year)	Mitigated Solvent Fire Frequency (Events per tank year)
Floating pool	Electrostatic sparks	0	0	0
	Instrumentation faults	0	0	0
	Welding and grinding sparks	0	0	0
	Torch cutting	0	0	0
	Camera and light power supply shorts	0	0	
	Vehicle fuel fire	1	3E-6	0
	Lightning strikes	1	3E-5	3E-5
	Core drill overheating	0	0	0
		Total	3.3E-5	3E-5
Large puddles	Electrostatic sparks	0	0	0
	Instrumentation faults	0	0	0
	Welding and grinding sparks	0	0	0
	Torch cutting	0	0	0
	Camera and light power supply shorts	0	0	0
	Vehicle fuel fire	1	3E-6	0
	Lightning strikes	1	3E-5	3E-5
	Core drill overheating	0	0	0
		Total	3.3E-5	3E-5
Small puddles/ channels	Electrostatic sparks	0	0	0
	Instrumentation faults	0	0	0
	Welding and grinding sparks	0	0	0
	Torch cutting	0	0	0
	Camera and light power supply shorts	0	0	0
	Vehicle fuel fire	1	3E-6	0
	Lightning strikes	1	3E-5	3E-5
	Core drill overheating	0	0	0
		Total	3.3E-5	3E-5

Table 7-2. Solvent Fire Frequencies for Various Organic Solvent Configurations. (2 sheets)

Solvent Configuration	Energy Source	Solvent Fire Ignition Probabilities	Unmitigated Solvent Fire Frequency (Events per tank year)	Mitigated Solvent Fire Frequency (Events per tank year)
Solvent-permeated sludge	Electrostatic sparks	0	0	0
	Instrumentation faults	0	0	0
	Welding and grinding sparks	0	0	0
	Torch cutting	0	0	0
	Camera and light power supply shorts	0	0	0
	Vehicle fuel fire	1	3E-6	0
	Lightning strikes	1	3E-5	3E-5
	Core drill overheating	0	0	0
		Total	≈3.3E-5	≈3E-5
Solvent-permeated saltcake	Electrostatic sparks	0	0	0
	Instrumentation faults	0	0	0
	Welding and grinding sparks	0	0	0
	Torch cutting	5E-4	5E-6	0
	Camera and light power supply shorts	0	0	0
	Vehicle fuel fire	1	3E-6	0
	Lightning strikes	1	3E-5	3E-5
	Core drill overheating	5E-4	5E-6	0
		Total	≈4.3E-5	≈3E-5

7.1.1 Electrostatic Sparks

Unmitigated — In order for a static electricity discharge to ignite a fire involving combustible liquids, the vapors above the liquid need to be flammable (i.e., the liquid needs to be at or above its flash point), and the spark energy needs to be greater than the minimum ignition energy. Static sparks cannot ignite liquids that are well below their flash point as is the case with the solvent in tank 241-C-103.

Electrostatic charge may build up on an object that is an isolated insulator. The electrostatic spark energy potential is a strong function of the capacitance of the object, which increases with the size of the object. A review of electrostatic spark energies for typical industrial situations indicated that a high-end spark energy is 0.45 J which is attributed to a very large object such as a road tanker or truck. This energy is well in excess of the maximum theoretical spark energies expected from discharge of various types of objects that may be inserted into a waste tank. A spark source initiator must be very large, and therefore, spark sources in the waste tanks other than lightning are not considered to be credible initiators. The probability that an electrostatic spark could ignite the solvent in the tanks is assigned a value of zero.

7.1.2 In-tank Instrumentation (Instrument Faults)

Unmitigated — Various in-tank instrumentation monitors tank and waste conditions, including temperature measurement devices, waste level measurement devices, and often low-power electrical circuits. In-tank instrumentation and equipment failures have been evaluated previously for the potential to ignite flammable gases and vapors (Scaief 1991).

The voltage/current conditions, which have been evaluated, include normal operations and fault conditions. The frequency for fault conditions was not estimated. For this analysis, the frequency is not important but is assigned a conservatively high value of 1.0×10^{-1} per year. The voltages and currents that would be produced, even under fault conditions, is insufficient to ignite flammable vapors. As the solvent is well below the flash point (i.e., no flammable vapors even exist), it is not credible for in-tank instrumentation to heat the solvent and ignite it. The probability of ignition is, therefore, assigned a value of zero.

7.1.3 Welding and Grinding

Unmitigated — For the purposes of this safety analysis, it is postulated that welding and grinding operations could be performed on tank risers. As a result, sparks and hot slag could fall to the waste surface even though welding operations are controlled. (If welding is to be performed outside of a designated welding area, it requires a hot work permit.) It is assumed that every effort would be made to prevent sparks and hot slag from entering the tank, but a human error could still occur. A frequency of 1.0×10^{-2} per operation is assigned to sparks or hot slag entering a tank. Welding and grinding is expected to be performed infrequently, certainly less than once

per year per tank; therefore, the estimated annual frequency of sparks and slag reaching the waste surface is less than 1.0×10^{-2} per tank per year but the conservatively high frequency will be assumed for this analysis.

The temperature of steel mechanical sparks is approximately 1400 °C (2,552 °F) (NFPA 321), but the available energy for ignition is small because the mass of the hot steel flakes is small. Based on the testing described in Section 4.1.2 and 4.1.4, ignition is not produced by introducing hot steel particles (1,300 °C [2,372 °F] containing up to 270 J of available energy) into even small puddles of solvent or onto solvent saturated saltcake. For this analysis, the probability that welding sparks or hot slag will ignite a solvent fire in a waste tank is assigned a value of zero.

7.1.4 Torch Cutting

Unmitigated — Torch cutting differs from welding and grinding in that the use of a torch to cut large bolts, pipes, or other in-tank objects, offers the potential for a relatively large heated object to fall to the solvent pool or solvent entrained waste surface. A relatively large hot object may be able to vaporize solvent and still remain hot enough to ignite the vapors. Smaller objects tend to be cooled as their heat is used to vaporize the solvent.

The size and temperature of an object required to ignite various sized solvent pools or puddles has not been analyzed or tested in detail. The largest hot object tested in solvent ignition tests is a 3/16-in. diameter steel ball heated to 1,300 °C (2,372 °F) or 270 J of available energy. Ignition did not occur with this largest hot object tested. Ignition by significantly larger hot objects than this, however, can not be ruled out. Therefore, it is assumed that a large hot object created during torch cutting could ignite some solvent situations.

For this analysis, the following best estimate assumptions were made regarding ignition by torch cutting.

- The probability of igniting a floating pool is assumed to be zero as the hot object would fall through the floating organic layer and be cooled by the aqueous liquids below.

- The probability of igniting a large pool, a puddle, or a solvent filled channel is assumed to be zero. A series of tests have been performed for relatively narrow (1.3 to 1.5 cm) channels (see Appendix G). Such channels filled with dodecane could not be ignited with a small oxyacetylene torch. Wick-stabilized flames started at one end of the channel failed to cause flame propagation up the channel. If sustained application of a torch flame will not ignite dodecane, it is judged that a piece of metal heated by a torch flame will not ignite the degraded solvent in the tank. Testing with radiant heaters determined that a channel filled with solvent could convect significant heat away from a heat source. A few tens of centimeters of channel length were adequate to dissipate more than 30 kW/m^2 of radiant heating applied to one end of a 1.3-cm-wide channel. Igniting the channel required the heated

solvent be confined by a barrier to prevent convective cooling. Even though small puddles and channels are easier to ignite than a large puddle or pool, a sizeable, sustained heat source is still required to cause ignition.

- The probability of igniting a solvent-permeated sludge is assumed to be zero because testing indicated that even the sustained application of a flaming torch had difficulty igniting solvent/ sludge mixtures.

- The probability of igniting a solvent-permeated saltcake is judged to be greater than zero because the heat transferred to the solvent cannot be dissipated through the waste as easily; therefore, the hot object is more likely to remain above the ignition temperature as solvent is vaporized nearby. The probability is developed in the following paragraphs.

Ignition of solvent-permeated saltcake — This section deals with pieces of metal that fall onto saltcake in a waste tank after being heated by a cutting torch. Experiments reported in Section 5.0, Appendix E of this report show that simple sparks or slag from a welding or grinding process would not initiate an entrained fire on saltcake. However, no experiments were performed for larger pieces of metal cut from a riser with a cutting torch.

The first assumption needed to calculate the probability of igniting an entrained fire on saltcake is how many times torch cutting will be performed directly on a tank in a location where a piece of hot, cut metal could fall on the waste surface. In order for a piece of metal to fall on the waste surface, cutting would have to be performed directly on or over a tank riser that gives vertical access to the tank. Cutting with torches in such locations is not a routine activity. Risers have bolted flanges and equipment is attached to the tanks using the flanges. Some welding and grinding may be performed after equipment is installed, but work requiring cutting torches is performed in shops as part of the fabrication process. Much of the equipment that is installed over tanks consists of pump out lines, ventilation systems, and instrumentation. Most of these components do not have direct, vertical access to the waste surface. A spool piece is bolted to a riser, and a bolted connection is made between the spool piece and the equipment item. However, using a torch to cut a riser has occurred. Two risers were cut with torches as part of a project to install a new ventilation system. Because the torch cutting has occurred in the last few years and could happen again, a frequency category of anticipated is assigned. However, because the use of high temperature torches is normally a shop fabrication process, and most attachments to risers use bolt on flanges, a specific frequency of 1E-2 is believed to be a reasonable number. Since there are 149 SSTs, this would result in a facility frequency of 149 x 1E-2 = 1.49, or approximately 1.5 occurrences per year.

The second assumption is whether solvent saturated saltcake capable of being ignited is in the spot where the hot metal falls. The location of the entrained solvent is independent of the location of the risers. Wastes were added to the tanks using "distributors" in a pump pit. Distributors were long

pipes and nozzles that were turned by hand so that waste pumped to the tanks could be distributed into different areas of the tank so that the tanks would fill evenly. The riser in a pump pit is only one of the many risers on a tank. And even in the case of the pump pit riser, the distributor deposited the waste out of line with the pump pit riser. Information about the potential surface area of solvent saturated saltcake can be taken from Huckaby and Sklarew (1997). The report gives information about the surface area of solvent that must be exposed to the atmosphere in the tank to evaporate the quantity of solvent found in the headspace by sampling. The largest estimated pool/puddle size, exclusive of tank C-103 which has a top layer composed entirely of solvent, is approximately 11 square meters. The information in Huckaby and Sklarew (1997) is for a pool/puddle on the surface of the waste, or for an entrained quantity of solvent that provides total evaporation equal to the pool/puddle size. Solvent can only burn at the waste surface because oxygen is needed. An entrained fire assumes that capillary action brings entrained solvent to the surface where it can burn. The vertical distance that capillary action can move solvent is limited. It is assumed that solvent that can be transported by capillary action is near the surface of the waste. If it is near the surface, then the surface area of the entrained material will not be significantly larger than the surface area of a puddle whose size has been calculated by Huckaby and Sklarew (1997). From this it is concluded that if the largest pool/puddle size measured is 11 square meters, then it is reasonable to use 20 square meters as an upper limit for the size of the area in a tank that could be ignited by a piece of hot metal falling into the tank.

The surface area of waste in a tank is 400 square meters. If a maximum of 20 meters is in a combustible configuration, then the probability of hot metal falling on that 20 square meters is **20/400 = 5E-2**.

The third assumption is whether the entrained solvent in the saltcake actually ignites if a piece of hot metal falls onto it. Test results reported in Section 5.0, Appendix E of this report show that neither hot steel particles (1300° C) nor an electric match which releases 138 J over a three to five millisecond period resulted in sustained combustion when applied to dodecane in lab tests. Dodecane is more flammable than the solvent mixture in the tanks. However the specific configuration of a larger piece of metal heated by a cutting torch was not tested. It is hypothesized that a piece of metal is cut from a riser with a cutting torch and has a free vertical fall to the waste. The metal lands edge on in the saltcake such that part of it extends into the saltcake and part into the tank atmosphere. Because the entrained solvent in the saltcake cannot conduct heat away as quickly as a pool or puddle of solvent, it is assumed that some solvent could be vaporized. It is further assumed that there is sufficient residual heat left in the piece of metal exposed to the tank atmosphere that it can ignite the solvent vapor before the metal cools. For the fire to self-propagate, the energy of the resulting burning vapor must be sufficient to both vaporize additional solvent and ignite it. Considering that the very hot particles and electrical match could not initiate a self-sustaining fire when applied directly to dodecane, it does not seem reasonable that the edge of a piece of metal could ignite a self-sustaining fire after it has fallen to the waste surface, cooling as it falls. The sequence of events hypothesized above is also tenuous. Having a piece of metal land upright so that it is in saltcake and air, having the metal not cool during its fall, and being able to ignite a solvent mixture

that is less flammable (lower vapor pressure) than dodecane is remote. Because the configuration has not been directly tested, this scenario is not dismissed. A frequency category of anticipated is assigned to it. However because of the factors discussed above, a best estimate of one chance in one hundred, 1E-2, is assigned.

The probability of initiating an entrained fire in saltcake by torch cutting on a tank is:

1E-2 (torch cutting events per year) x 5E-2 (chance of hitting entrained solvent) x 1E-2 (probability of ignition) = 5E-6 per tank.

Several additional uncertainties are associated with the configuration of the tanks and solvent that were not included in the above calculation. The additional uncertainties have not been quantified because the accident can be shown to be within risk evaluation guidelines using only the information presented above. If the following uncertainties were quantified and included in the above calculations, it would show that a fire is even more unlikely.

- All of the ignition tests were performed using either dodecane or kerosene. The mixture in the tanks is TBP and NPH. The TBP/NPH mixture is significantly more difficult to ignite than either pure dodecane or kerosene.

- Measurements using neutron detection show that in many SSTs the liquid level is well below the saltcake, in some cases by several feet. Capillary action would not raise solvent several feet to the surface of the saltcake to burn.

- With over 8,000 tank-years of history, no solvent fires have occurred in Hanford Site tanks. During the earlier years, there was much more solvent in the tanks than there is now. There were also many more in-tank activities involving different energy sources and more transfers from tank to tank. The fact that there were no fires in the past is not an indicator that there will be no fires in the future. However no previous fires over 8,000 tank-years certainly lends credence to the estimation that the accident belongs in the unlikely range (10E-2 to 10E-4 occurrences per year).

Mitigated — An administrative control on torch cutting is included in the TSRs. It requires installing a barrier or devices before torch cutting to prevent hot metal/slag from falling to the waste surface in a tank with potential organic-solvent hazards (solvent-permeated saltcake). This prevents the ignition scenario by stopping hot debris (ignition source) from contacting the solvent-permeated saltcake.

7.1.5 Still Camera Photography and Video Camera Operations

Unmitigated — The still camera system used is a standard 70-mm still camera and flash unit mounted in a metal frame. The system is suspended in the tank by a flexible support hose containing wiring to the camera and flash unit. Power to the flash unit is supplied by a portable generator on the ground surface above the tank. The wiring is sealed but not intrinsically safe. The camera and flash unit are manually lowered into the tank to a level controlled by an adjustable safety stop ("top hat") at the top of the riser.

The video equipment consists of a standard video camera with pan and tilt capabilities and a quartz halogen light source. The in-tank portion of the video system operates on 12 volt direct current. An auxiliary light source can be installed in a second riser to provide more illumination. The auxiliary light source uses a high-pressure sodium bulb and operates on 120 volts alternating current. The light is enclosed in an impact-resistant polycarbonate cover. The entire video camera unit is connected to a support stem. The camera system is supported by a shield plug that limits the length the system can intrude into the tank.

Upset conditions include breaking a light and allowing the hot filament to fall to the waste surface or lowering the camera and light system to the waste surface with subsequent shorting of the electrical supply in or near the solvent. The potential for a hot filament to ignite the subcooled solvent is negligible because there is insufficient energy to heat solvent and ignite it.

The frequency of shorting power cables in or near the solvent is estimated to be 0.001 per tank per year. This estimate is based on the following.

- Only a few in-tank photographic or video operations are anticipated to be performed in a tank.
- A top hat (i.e., a shield plug that has a top flange larger in diameter than the riser inside diameter) is required for photography and video imaging to be performed effectively and is required by procedure. The top hat acts as a safety stop preventing the unit from being lowered to the waste surface
- The electrical wiring is not likely to short even if immersed in the solvent or sludge because it is sealed from the outside environment.

Shorting the power supply in or near the solvent could possibly dissipate electrical energy in the solvent if the wires remained in a pool or puddle for a period of time and not trip the over current protector. The energy dissipation (ohmic heating) in the solvent is expected to be low because the solvent is not expected to be very electrically conductive and little current, if any, would flow through the solvent. Conversely, if the wires were to enter sludge or saltcake, ohmic heating would be small because of the low resistivity of the aqueous brine contained in the waste.

Electrical sparks that might be produced by two wires touching together are bounded by welding sparks and slag as discussed above. It is concluded that shorting of the electrical power supply could not ignite pools, puddles, or solvent permeated sludges or saltcakes.

7.1.6 Vehicle Fuel Fires

Unmitigated — A number of vehicles are used in the tank farms for construction, surveillance, sampling, and maintenance activities. Two incidents in the last several years have raised a concern about motor vehicles that enter the tank farms. An accident could occur that results in 1) vehicle fuel entering a waste storage tank and igniting or 2) fuel igniting followed by the burning fuel entering the tank.

In Lindberg (1996), it is assumed one collision per year occurs between a vehicle and a riser. Therefore, there are 1/177 = 5.6E-3 collisions per tank per year. Because a collision alone is not sufficient to start a fire, the following factors are also included: the probability of the riser breaking (0.5), the probability that the fuel tank ruptures and fuel enters the tank (0.1), the probability fuel is ignited from the accident as it enters the waste tank (0.01), and the probability that the burning fuel ignites organic solvent if present in the tank (1.0).

Therefore, the probability of having an organic solvent fire, if solvent is present in the tank, is:

P(organic fire) = (5.6E-3) (0.5) (0.1) (0.01) = 2.8E-6 per tank per year

Mitigated — The controls specified in the TSRs prevent the accident by protecting the vehicle fuel tanks from being punctured. Although a collision may occur, no fuel would be released and the accident scenario would not occur unless the fuel tank was punctured.

7.1.7 Lightning Strikes

Thunderstorms can produce lightning strikes that discharge the electrical potential between the atmosphere and the ground. Although rare, ash fall and dust storms can also produce lightning.

Operational records do not report any lightning strikes on a tank riser or appurtenance in the 50-year history of the Hanford Site. Records do indicate a number of lightning strikes have hit 200 East and 200 West Area structures, power poles, and transformers. Recent research on lightning as a potential accident initiator at the tank farms is reported in *Probability, Consequences, and Mitigation for Lightning Strikes to Hanford Site High-Level Waste Tanks* (Zach 1996). This report establishes that, after conservatively accounting for detection frequency and uncertainties, the observed lightning strike frequency at the tank farms is 0.06 strikes/yr/km^2

(0.16 strikes/yr/mi^2). The report discusses a number of factors necessary for a lightning strike to initiate an accident including the following:

- Lightning must strike a tank riser, appurtenance, or the ground in the immediate vicinity of a tank farm.
- The tank must contain a combustible configuration of organic solvent.
- The discharge must pass from the riser or appurtenance into the tank through conduction paths such as instrumentation lines or other equipment connected to the tank riser or by arcing across nonconductive segments.
- The discharge must have sufficient energy to create a large arc or cause ohmic heating to temperatures high enough to ignite the solvent.

Unmitigated — Using the observed 0.06 strikes/yr/km^2 (0.02 strikes/yr/mi^2) as an estimate of lightning strike frequency and considering the cross section area of a large underground tank to be bounded by 500 m^2 (5,400 ft^2), the likelihood of a direct strike over a particular tank is 3E-5/yr, that is, "extremely unlikely."

The likelihood of and the amount of lightning current that will enter a waste tank differs significantly between SSTs and DSTs because DSTs contain a closed steel liner, and the risers are welded to this steel liner. These factors make the buried DSTs effective Faraday cages (Cowley and Stepnewski 1994). Therefore, electrically noncontinuous paths through the tank that can result in arcing would only exist when a tank activity (such as installing long length equipment with a crane) opens a riser and inserts a conductor through the Faraday cage of the tank liner.

The structure of the SSTs, the rebar in the concrete, and the fact that the tank is buried, gives SSTs some properties of a Faraday cage. However, SSTs lack a closed steel liner, and this makes SSTs less effective as a Faraday cage than DSTs. In addition, construction drawings do not indicate that any effort was made during construction to make electrical connections between risers and the rebar in the concrete. There are, therefore, electrically noncontinuous paths through the tank that can result in arcing at all times.

Discussions with Dr. Martin Uman indicate that a lighting strike that "hits" the top of a tank could be expected to create high electrical potentials (voltages) between the risers and ground. These high voltages could cause lightning current to arc from the risers and installed equipment (or equipment in the process of being installed or removed from the tank, especially when using a crane) into the waste and to ground (through the tank side walls or bottom). As lightning strikes are often comprised of multiple strokes (stepped leader, return stroke, dart leader, etc.), and each stroke can have multiple ground connections, it is quite possible that lightning current and arcing could occur through multiple paths (e.g., risers). As a conservative safety analysis assumption, the frequency of lightning

current arcing to the waste surface in SSTs is assumed to be equal to the frequency that lightning strikes the top of the tank, or 3 x 10-5 per year per SST. This value is considered appropriate for use as an organic solvent initiator where a comparatively high energy is required to ignite the solvent.

Solvent Fire Ignition: The probability that arcing lightning current would cause ignition is evaluated below. The arc-producing scenario would occur when lightning current travels down equipment suspended above the waste surface (i.e., risers), and the current arcs from the end of the suspended object to the waste surface. The arc or lightning current channel (the bright lighting bolt) is a very hot channel of air (>20,000 °K) that has been turned into a plasma. The channel is fairly narrow (perhaps a centimeter in diameter) but causes significant heating of surrounding air. Radiative and convective heating of the waste surface (e.g., solvent pool) can be expected. In the arc-gap scenario, the energy deposition at the point of contact with the waste is concentrated. The energy deposition in the waste where the arc hits is estimated below according to Cowley and Stepnewski (1994):

First, a very high density energy deposition takes place at the point of contact. The energy deposition associated with arcing between gas and solid phases is different from ohmic heating. It is proportional to the time integral of the current rather than, as in ohmic heating, the integral of the square of the current. The electrical power generated as a function of time at a metal arc interface is roughly $V_c I(t)$ after the initial breakdown (which will provide energy to heat gas to tens of thousands of °K), where V_c is the contact potential difference between the metal and the arc, typically 5 to 10 volts, and I(t) is the time-varying current flow in the arc. The total energy generated is roughly $V_c Q$, where Q is the total charge traversing the arc. The energy appears as heated gas and heated and melted electrode material. A typical lightning transfers 25 coulombs of charge and could liberate 250 J of energy at the arc spot, in a volume of less than 1 cubic centimeter, perhaps less than a cubic millimeter. However, it is not likely that all of the lightning charge will flow across a single interior gap in a SST because of the many parallel paths available to the lightning current.

Once the current moves somewhat beyond the arc contact point, the energy may be dissipated by ohmic heating. The energy deposition is described by:

$$E = \frac{10^4}{sRo} \text{ joules}$$

where

s = conductivity of the waste
Ro = radius of arc spot, m

The electrical conductivity of the solvent has not been measured. The resistivity of organic liquids can be much higher than that of waste aqueous liquids and solids. The resistivity of transformer oil and capacitor mineral oil is in the range of 1.0 to 100.0 x 10^{10} ohm-m, with water contamination

causing a reduction of about two orders of magnitude (Fink and Beatty 1976). The discharge of lightning current through a high resistivity fluid could cause significant heating. If the arc were to strike an organic pool, the high resistivity of the solvent could cause significant energy deposition (many MJs) in the pool. It would be difficult to conclude that such an arc-gap scenario would not vaporize a significant amount of solvent and form and ignite a vapor cloud sufficiently large (10-15 cm in diameter) to ignite a pool fire.

The probability that arcing lightning current will strike a solvent pool or puddle is not known because the presence, size, and location of solvent pools has not been determined for many of the tanks. However, a review of tank waste photographs for interim stabilized tanks indicates that puddles (either solvent or more likely aqueous liquids) appear likely to form under risers. This may be due to equipment installation or flushing operations that cause depressions in the waste under the risers. For this analysis, it is assumed 1) the equipment arc-gap configurations result from risers or equipment installed in a riser and 2) the probability of a solvent puddle being formed in a waste depression under a riser is one-- given the tank contains liquid pools and significant solvent. The probability that a lightning strike to in-tank equipment would ignite a solvent fire is assigned a value based on the following.

- The probability that the resistance between the struck object and ground is high (assumed to be 1.0 unless field measurements indicate otherwise, or the object is verified to be immersed in aqueous liquid which would be grounded through the tank bottom), times

- The probability that the equipment-to-waste arc path passes through a solvent pool or combustible solvent permeated saltcake. This is assumed to be 1.0 if the tank contains significant amounts of solvent unless other data indicate otherwise, times

- The probability that the lightning arc has sufficient energy and duration to ignite a solvent fire. This is assumed to be 1.0 unless further analysis or testing indicates that solvent ignition by lightning strike is not likely.

The probability of lightning initiated solvent fires, therefore, is conservatively assumed to be equal to the frequency of lightning strikes on the tank or 3 x 10-5 per tank per year, assuming the tank contains a combustible configuration of solvent.

Mitigated — Controls on crane use during thunderstorms are included in the TSR administrative controls. The administrative controls require stopping activities in dome intrusive and waste intrusive locations of tanks that have a potential organic solvent hazard when lightning is identified within a 48-km (30-mi) radius of the tank farm. In addition, equipment is secured in lowest position if lightning is identified within 48-km (30-mi) of the tank farm. This decreases the likelihood of an organic solvent fire by removing potential lightning dissipation paths in the tanks.

In addition, a program has been implemented to improve the lighting protection provided the tanks by installing the following:

- grounded air terminals, grounding tank risers, and bonding permanently installed instrumentation to risers to promote the dissipation of lightning energy outside waste volume

- grounding grids to promote the dissipation of lightning energy outside waste volume.

Although lightning-related controls have been identified, their ability to prevent ignition of organic solvents or otherwise mitigate the scenario is unquantifiable. Therefore, the frequency of the scenario with controls is conservatively represented by the scenario without controls.

7.1.8 Core Sampling

The waste characterization effort obtains waste samples by core sampling. Core sampling trucks are designed to obtain full-depth samples in one of two modes: push mode only or push mode or rotary mode. Push mode-sampling works well for soft waste materials where a core sample is obtained using hydraulic pressure to push the samplers through the waste. Rotary-mode sampling is used is used for hard waste materials.

Unmitigated — Because push-mode core sampling generates very little heat, it is not considered a credible source for heating wastes and cannot cause solvent fire ignition. Keller (1991) reports the results of testing the 5.7-cm-diameter core drill string to determine the effect of frictional heating on both the drill face surface and the waste simulant. The testing was conducted on three simulants: a sludge, a soft saltcake, and a hard saltcake. The results from the test indicated the following: no temperature increase on the drill face surface from push-mode sampling the sludge material, a 6 °C increase in the soft saltcake, and a 22 °C increase in the hard saltcake. These tests are considered enveloping because they were done at higher insertion rates than can be accomplished in the field (i.e., rather than stopping every 48.3 cm to retrieve a sample, the testing pushed continuously as fast as possible). Based on these results, it is concluded that push-mode core sampling has no potential to ignite organic solvent pools or solvent permeated waste sludges or saltcakes.

Rotary-mode core sampling can generate significant heat from friction at the drill bit–waste interface. High temperatures have been experienced during testing with waste simulants when drill bit progress through the simulant is slow or stopped. In this situation, the heat generated is deposited in nearby waste for an extended period of time. When the bit is progressing through the waste as designed, the bit and waste remain relatively cool because the bit continually moves down through and contacts cool waste.

High temperatures are produced when a drill bit has difficulty drilling through hard wastes. High temperatures would not be produced while drilling in surface pools or puddles or within a few centimeters of the waste surface. Ignition of pools and puddles and solvent-filled channels by rotary drill core

sampling is judged not credible; therefore the probability of a drill overheating scenario to ignite solvent pools, puddles, or solvent-filled channels is assigned a value of zero.

Ignitability testing of sludges indicated the sludge must contain a significant amount of solvent to support combustion. Such a sludge, however, would not contain any interstitial air. Overheating is not likely in a solvent-saturated sludge because such a material is likely to be soft. Finally, burning with tank headspace air would not be possible if the ignition source is tens of centimeters below the waste surface. Ignition and sustained burning of solvent-permeated sludges by rotary core drill sampling is judged not credible; therefore, the probability that core drill upsets could cause a solvent fire in sludges is assigned a value of zero.

The frequency with which core drill overheating could cause a solvent fire in solvent-permeated saltcake is conservatively estimated to be 5E-6 per year as follows.

- The frequency of drill overheating is assumed to be 0.01 per year. This is a subjective estimate based on the drill encountering hard waste where the subsequent friction heats the waste above the solvent flash point because the purge system fails.

- The probability that an overheating drill could cause solvent ignition is assigned a conservatively high probability of 0.01. This is based on the judgment that creating a flammable solvent vapor/air mixture in the waste solids near the drill bit and heating this mixture to the autoignition temperatures (AIT) is unlikely. It is judged the heat generated by the drill bit would vaporize the solvent which would displace air that may be in the waste solids. It is also judged likely the vapors in the interstitial pores would exceed the upper flammability limit before the AIT was reached, and the vaporization of the solvent would cool the bit waste interface. Finally, high temperatures that are produced tens of centimeters below the waste surface would not cause a fire that could burn with headspace air. Ignition would need to occur at or near the waste surface.

- The final assumption is whether solvent saturated saltcake capable of being ignited is in the spot where the core drill is used. Information about the potential surface area of solvent saturated saltcake can be taken from Huckaby and Sklarew (1997). The report gives information about the surface area of solvent that must be exposed to the atmosphere in the tank to evaporate the quantity of solvent found in the headspace by sampling. The largest estimated pool/puddle size, exclusive of tank C-103 which has a top layer composed entirely of solvent, is approximately 11 square meters. The information in Huckaby and Sklarew (1997) is for a pool/puddle on the surface of the waste, or for an entrained quantity of solvent that provides total evaporation equal to the pool/puddle size. Solvent can only burn at the waste surface because oxygen is needed. After the drill bit has penetrated a few centimeters into the waste, there will not be oxygen available to support combustion at the

heated surfaces of the drill bit. If combustion can only take place near the surface, then the surface area of the entrained material will not be significantly larger than the surface area of a puddle whose size has been calculated by Huckaby and Sklarew (1997). From this it is concluded that if the largest pool/puddle size measured is 11 square meters, then it is reasonable to use 20 square meters as an upper limit for the size of the area in a tank that could be ignited by core drilling. The surface area of waste in a tank is 400 square meters. If a maximum of 20 meters is in a combustible configuration, then the probability of the core drill contacting 20 square meters solvent permeated saltcake **20/400 = 5E-2**.

Mitigated - To eliminate the possibility of heating waste to high temperatures and initiating waste combustion accidents (e.g., organic salt-nitrate reactions), the core drill system was modified to provide bit cooling by nitrogen purge and interlocks to shut down the system if key drilling parameters (bit down force and rotational speed) are exceeded.

A safety envelope was developed through testing and thermal analyses so that operation within the envelope (nitrogen purge on, bit down force below 5.2 kN [1,170 lbf], and rotational speed below 55 revolutions per minute) would maintain cool waste temperatures. Operation outside the envelope would be prevented by shutdown interlocks that stop drilling operations. For this analysis, it will be assumed that overheating conditions are credible if the interlocks were not in place (see unmitigated above).

The possibility of rotary core drill overheating and igniting waste organic solvents has not been included in the rotary core sampling safety envelope development and testing program. It would seem unlikely that rotary core sampling could cause solvent ignition because the solvents would tend to vaporize when the waste surrounding the drill bit is heated. This vaporization would tend to cool the waste and remove the solvent as a fuel. Demonstrating the acceptability of drilling without nitrogen purge or shutdown interlocks would appear to require rotary drill testing in solvent-permeated waste simulants. The safety of drilling in solvent-permeated waste is assured by the safety envelope developed for fuel-nitrate hazards.

The safety envelope parameters ensure the drill bit temperature will not increase more than 57 °C. This value is based on the drill bit reaching a maximum temperature of 150 °C in the highest measured temperature tank waste. This temperature provides a safety margin below the AIT for waste solvents which is estimated to be over 200 °C based on a review of hydrocarbon AIT. This review indicated that the straight chain hydrocarbons, such as found in NPH, have some of the lowest AITs of the values reported for hydrocarbons. The minimum AITs for n-decane are 210 °C and 230 °C for kerosine (Kuchta 1985). Tetradecane has an AIT of 202 °C (Lewis and Von Elbe 1987).

7.2 NUMBER OF TANKS CONTAINING COMBUSTIBLE SOLVENT

The solvent fire frequencies developed in Section 7.1 are based on a per-tank basis, assuming that a tank contains organic solvent in a combustible configuration. To convert to a tank farm accident frequency which can be

compared to risk evaluation guidelines, the per-tank frequencies are multiplied by the number of tanks that contain each combustible solvent configuration (e.g., floating layer, large pool, solvent permeated-saltcake), then summed over all configurations. The results are summarized in Table 7-3 for several different assumptions described below.

Table 7-3. Number of Tanks That May Contain Combustible Solvent.

Tank Type	Solvent Configuration	Basis	Number of Tanks
SSTs	Large pool	Known - 241-C-103	1
SSTs passive vent	Large pool or solvent permeated waste	Vapor sampling and transfer records	14
SSTs passive vent	Large pool or solvent-permeated waste	Bounding	66
SSTs active vent	Large pool or solvent-permeated waste	Bounding	6
DSTs	Large pool or solvent-permeated crust	Waste process history and transfer records	6
DCRTs	Large pool	Bounding	6

The number of waste tanks that may contain separable organic solvent phases is not known. Not all tanks received solvents, and most solvents that were sent to the tanks have evaporated or undergone chemical degradation to form organic species that would not be present as a separable, liquid phase. However, tank 241-C-103 is known to have an organic solvent layer floating on the waste surface. Other tanks have vapor space concentrations of organic solvent vapor higher than can be explained except by the presence of liquid phase solvents somewhere in the waste.

An additional factor that must be taken into account is that SSTs may be either passively ventilated or actively ventilated. Fifteen SSTs are actively ventilated, and 134 are passively ventilated. Process Engineering has determined that there is no solvent in 9 SX farm tanks which are actively ventilated. Six actively ventilated SSTs may contain solvent.

A screening test has been developed that uses the results of the ongoing tank vapor space sampling program to predict the presence of significant quantities of separable phase solvents in tanks. The screening tests identify specific tanks as having or not having any remaining separable organic solvent phase. The screening methodology uses vapor characterization data in conjunction with an evaporation model to estimate the size of solvent pools that feed vapors into tank headspaces. The screening test predicts that a pool may be present or not present. If the screen predicts that a pool may be present, it is assumed a pool is present unless an alternate method of

confirming or dismissing its presence is used. If the screen predicts that a pool is not present, it is a positive test that a pool is not present. As of August 1997, the vapor spaces of 81 tanks have been sampled. None of the actively ventilated SSTs have not been sampled. When the screening criteria was applied to the 81 tanks, 13 tanks were identified as potentially having solvent pools or a large subsurface layer of solvent. The 13 tanks are 241-B-103, 241-BX-103, 241-BX-104, 241-BY-107, 241-BY-108, 241-C-101, 241-C-102, 241-C-103, 241-C-110, 241-C-201, 241-C-204, 241-T-111, and 241-TY-103. The results of the vapor space sampling and the screening are documented in Huckbay et al. (1997).

As noted above, the actual number of tanks that contain solvent is not known. However, for the purposes of comparing accident consequences to risk evaluation guidelines, an approximate number of tanks is needed.

The following estimates predict a specific number of tanks that may contain a separable organic solvent phase under increasing conservative assumptions. This number is used as a multiplier to estimate facility-based accident frequencies.

Known to Contain Combustible Solvent—Tank 241-C-103 is known to have an organic solvent layer floating on the waste surface. No other tank is known to contain a combustible solvent. Other SSTs may or may not contain a combustible configuration.

Based on Transfer Records and Vapor Samples-Before 1980, wastes containing immiscible organic solvents were transferred to SSTs. Although the bulk of the solvents were not sent to the tanks, some solvent was entrained with the aqueous phase which was sent. Using historical records, 67 SSTs were identified as potential receivers of organic solvent (WHC-MR-0132, *A History of the 200 Area Tank Farms*; WHC-SD-WM-ER-349, *Historical Tank Content Estimate for the Northeast Quadrant of the Hanford 200 East Areas*; WHC-SD-WM-ER-352, *Historical Tank Content Estimate for the Southwest Quadrant of the Hanford 200 West Areas*; and WHC-SD-WM-ER-351, *Historical Tank Content Estimate for the Northwest Quadrant of the Hanford 200 West Areas*). The vapor space sampling program has sampled and screened 81 SSTs. There are 56 tanks in common between the historical list of receiver tanks and the list of tanks that have been vapor sampled. Eighty-four percent (56/67) of the tanks that potentially received organic solvent have been vapor sampled.

Of the 81 SSTs that have been sampled, thirteen have shown a positive result. Six of the 13 tanks (241-BX-104, 241-BY-107, 241-C-101, 241-C-201, 241-C-204, and 241-T-111) are not on the historical list of potential solvent receivers. However, tanks 241-BY-107 and 241-C-101 are connected by cascade lines to tanks 241-BY-108 and 241-C-103, respectively. Both tanks 241-BY-108 and 241-C-103 are on the historical list of solvent receivers and show very strong solvent signatures in the vapor sampling. It is reasonable to expect that tanks 241-BY-107 and 241-C-101 would also show a positive vapor signature coming from tanks 241-BY-108 and 241-C-103 respectively, even if they do not contain a separable phase organic pool. Therefore, tanks 241-BX-104, 241-C-201, 241-C-204, and 241-T-111 are the only tanks that show a positive vapor sample that is neither on the historical receiver list nor is connected to a tank that is a historical receiver of organic solvent.

Seven of 13 tanks that show a positive vapor sample result are on the historical list of solvent receivers. Because 84 percent of the historical receivers have been sampled, it is reasonable to use a simple linear extrapolation (7/56 = x/67) to estimate the total number of historical receivers that might still contain solvent. This extrapolation predicts a total of 8.4 tanks, which is rounded 8 tanks. In addition to the 8 tanks predicted by the extrapolation, 6 tanks (identified above as non-historical receivers with positive screenings) are added for a total of 14 SSTs that potentially contain organic solvent. There may be additional tanks in the group of non-historical receivers that have not been vapor sampled.

Two activities resulted in organic solvents being sent to DSTs: the transfer of waste streams containing entrained solvents directly from PUREX to the tanks farms and the pumping of supernate from SSTs to DSTs.

After 1980, the SSTs did not receive waste, and they were isolated. PUREX wastes, including entrained organic solvents, were sent to DSTs. The waste stream containing solvents, identified as organic wash waste, indicate the waste was collected in PUREX tanks G-8 and R-8. These two tanks were periodically transferred to tanks 241-AW-103, 241-AW-104, and 241-AW-105. Some supernate from these tanks was pumped to the 242-A Evaporator for volume reduction. Evaporator feed sampling of the AW tanks did not indicate floating organics. Any solvent that was evaporated as part of the waste would have been collected as condensate in tank 241-C-100 and ultimately transferred to low-level disposal facilities. Since restart of the 242-A Evaporator in 1994, no organic solvents have been detected in tank 241-C-100. Therefore, it is not likely that solvents sent to the AW tanks ended up in other DSTs. However, tanks 241-AW-103, 241-AW-104, and 241-AW-105 potentially contain some separable phase organic solvent.

Three DSTs potentially contain a separable organic solvent phase because they were the receivers for transfers from SSTs that received organic solvents. Tank 241-AN-101 received saltwell liquor from 241-A, 241-AX, 241-B, 241-BX, and 241-BY tank farms. Tank 241-SY-102, the staging tank for transfers from 200 West to 200 East Areas, received saltwell liquor from 200 West Area tanks that had received organic solvents. Tank 241-AY-101 received liquid from the saltwell pumping of tanks 241-C-102, 241-C-107, and 241-C-110. All three 241-C tank farm tanks were historical receivers of wastes containing organic solvent.

A total of six DSTs (241-AW-103, 241-AW-104, 241-AW-105, 241-SY-102, 241-AY-101 and 241-AN-101) may contain separable phase organic solvent.

Bounding Estimate—Given that vapor sampling indicated some non-historical receivers may contain combustible solvents, a bounding value for the number of tanks that may contain solvents can be determined by assuming all tanks that have not been verified by vapor sampling as containing solvent, do contain solvent. This is a "assume guilt unless proven innocent" approach. It does not mean the tanks do contain solvent, but it provides a bounding approach which is very robust if the risk is acceptable even given this conservative, bounding assumption.

Sixty-eight passively ventilated SSTs have been verified as not containing a significant solvent pool by vapor sample results (81 total samples - 13 samples that indicated that solvent pools may be present). Another 68 SSTs have not been vapor space sampled. Included in the 68 are the 15 actively ventilated SSTs. Therefore there are 53 (68-15) plus 13 (contain solvent per vapor space screening) or 66 passively ventilated tanks that may contain solvent. Nine of the 15 actively ventilated tanks have been determined not to contain solvents. Therefore there are 6 actively ventilated tanks that may contain solvent.

There are 28 DSTs (including AWF tanks). Because wastes are transferred between DSTs, the theoretical bounding assumption is that all DSTs could contain solvent pools (although this is very unlikely).

Six DCRTs are used to support waste transfer operations.

7.3 POSSIBLE SOLVENT CONFIGURATIONS FOR SINGLE-SHELL, DOUBLE-SHELL, AND DOUBLE-CONTAINED RECEIVER TANKS

Possible solvent configurations depend on the waste surface. Tanks containing a aqueous supernate could only have a pool of solvent floating on the aqueous supernate. Tanks with solids at the surface (sludge, saltcake or crusts) could contain large pools or small puddles in depressions in the waste surface. Tanks that have a porous solids surface (saltcake or crusts) may contain solvent permeated in the solids which could support a wick-stabilized fire. Therefore, the applicable solvent configurations and fire scenarios are as follows:

- Pool fires: Pools are a layer of solvent floating on top of liquid waste or a layer that is trapped in a depression on top of solid waste. A pools has an area greater than 1 m^2 (10.8 ft^2). A pool may exist in SSTs, DSTs or DCRTs.

- Puddle fires: Puddles are less than 1 m^2 (10.8 ft^2) in area and exist in a depression in a solid waste surface. Puddles should occur mainly in SSTs because many SSTs have a solid surface that can form a depression for solvent to collect in. However, a few DSTs have a floating crust (e.g., tank 241-SY-101) that might form a depression where solvent could collect. Therefore, the analyses include puddles for both DSTs and SSTs.

- Wick-Stabilized Fires: A wick-stabilized fire configuration would consist of a sludge or saltcake that is permeated with solvent. The height of the solvent layer would be equal to the height of the solids level. The sludge or saltcake would act as a wick, and the solvent would burn. Wick-stabilized fires may occur in SSTs. A few DSTs have a floating crust (e.g., tank 241-SY-101) that provides a solids surface where solvent might collect and support a wick-stabilized fire. Therefore, the analyses include wick-stabilized fires for SSTs and DSTs.

7.4 SOLVENT FIRE ACCIDENT FREQUENCY CATEGORY

The per-tank ignition frequency (see Table 7-2) is multiplied by the number of tanks that may contain combustible solvent (see Table 7-3) to assign an accident frequency category. The two solvent scenarios of most interest are pool fires and wick-stabilized fires. As indicated in Section 7.1, the ignition frequency for pool fires (floating layer, large puddle, small puddle) are similar but differ significantly from the ignition frequency of a wick-stabilized fire involving a solvent-permeated saltcake. The solvent-permeated saltcake is more easily ignited. Accident frequency categories for various assumptions are shown in Table 7-4. Although tank 241-C-103 currently contains a floating layer of organic solvent and cannot support a wick-stabilized fire, this fact is ignored in the wick-stabilized fire frequencies estimated here. This is conservative and supports the future saltwell pumping of this tank and addresses the condition that might arise if the tank supernate were to leak from the tank.

Table 7-4. Solvent Fire Accident Frequency Categories. (2 sheets)

Scenario	Per Tank Ignition Frequency	Number of Tanks	Basis	Accident Frequency (Frequency Category)
Pool Fire - unmitigated	3.3E-5/yr	1	Known (241-C-103)	3.3E-5/yr (extremely unlikely)
Pool Fire - unmitigated	3.3E-5/yr	20 (14 SSTs + 6 DSTs)	Vapor sampling and transfer records	6.6E-4/yr (unlikely)
Pool Fire - unmitigated	3.3E-5/yr	109 (81 SSTs + 28 DSTs)	Bounding number	3.6E-3/yr (unlikely)
Wick-stabilized fire - unmitigated passive SST vent	4.3E-5/yr	20 (14 SSTs + 6 DSTs)	Vapor sampling and transfer records	8.6E-4 (unlikely)
Wick-stabilized fire - unmitigated passive SST vent	4.3E-5/yr	94 (66 SSTs + 28 DSTs)	Bounding number	4.0E-3 unlikely
Wick-stabilized fire - unmitigated active SST vent	4.3E-5/yr	34 (6 SSTs + 28 DSTs)	Bounding number	1.5E-3 (unlikely)

Conclusions regarding solvent fire frequency categories — The mitigated and unmitigated solvent fire accident frequency for tank 241-C-103, known to contain a combustible solvent floating layer, is "extremely unlikely."

Unmitigated and mitigated frequencies for pool fires are dominated by lightning as the initiator which places both scenarios in the category of "unlikely." The "unlikely" category is applicable over a large variation in the number of tanks assumed to contain combustible solvent pools.

The unmitigated frequency category for wick-stabilized fires is "unlikely" (10E-2 to 10E-4 events per year), and is dominated by lightning. If the accident was mitigated using controls to reduce the frequency of the initiators, the accident would still be "unlikely". The frequency would still be dominated by lightning as an initiator, which cannot be controlled.

This page intentionally left blank.

8.0 KEY INPUT DATA FOR CONSEQUENCE CALCULATIONS

This section specifies key inputs used to quantify consequences of postulated fires. These inputs are used in Section 9.0, which describes the actual consequence calculations using an EXCEL[1] spreadsheet.

8.1 RADIOLOGICAL DATA

Table 8-1 lists key data used to compute radiological doses.

Table 8-1. Radiological Input Data. (2 sheets)

Parameter	Units	Numerical Value	Reference
Atmospheric dispersion factor, onsite	s/m^3	3.41E-2	Van Keuren (1996a)
Atmospheric dispersion factor, offsite	s/m^3	2.83E-5	Van Keuren (1996a)
Breathing rate, onsite	m^3/s	3.3E-4	Van Keuren (1996a)
Breathing rate, offsite	m^3/s	3.3E-4	Van Keuren (1996a)
ULD, inhalation, SST solids	Sv/L	2.2E5	Cowley (1996)
ULD, inhalation, SST liquids	Sv/L	1.1E4	Cowley (1996)
ULD, inhalation, DST liquids	Sv/L	6.1E3	Cowley (1996)
ULD, inhalation, AWF liquids	Sv/L	1.4E3	Cowley (1996)
ULD, inhalation, Solvent liquid	Sv/kg	2.83	Cowley (1996)
ULD, ingestion, SST solids	$Svm^{3/}sL$	4.1	Cowley (1996)
ULD, ingestion, SST liquids	$Svm^{3/}sL$	0.052	Cowley (1996)
ULD, ingestion, DST liquids	$Svm^{3/}sL$	0.068	Cowley (1996)
ULD, ingestion, AWF liquids	$Svm^{3/}sL$	0.092	Cowley (1996)
SST solids inventory on ventilation system, passive SST	L	1.27E-2	VanVleet (1996)
SST solids inventory on ventilation system, active SST	L	2.0 (rounded)	Himes (1998)
AWF liquids inventory on ventilation system, DST, and AWF systems	L	3.7 (rounded)	Himes (1998)

[1] EXCEL is a trademark of Microsoft Corporation, Redmond, Washington.

Table 8-1. Radiological Input Data. (2 sheets)

Parameter	Units	Numerical Value	Reference
SST liquids inventory on ventilation system, DCRT	L	2.27E-1	VanVleet (1996)
Airborne release fraction for ventilation system releases	None	1E-03	Mishima (1994)
Respirable fraction (RF), pool and puddle fires	None	1.0	Mishima (1994)
Respirable fraction (RF) entrained fires	None	0.5	Mishima (1994)

Note:
The ULD for DCRT liquids was assumed to be the same as the ULD for SST liquids (Cowley 1996).

8.2 TOXICOLOGICAL DATA

Toxicological consequences were quantified in terms of a sum of fractions, where the fraction is the downwind concentration of each toxin divided by the limit for that toxin. This section includes the data to compute the fraction; the calculational method is described in Section 6.4.

8.2.1 Headspace Gases

Table 8-2 summarizes headspace gas concentrations and guideline concentrations used in this study and taken from (Van Keuren 1996b).

Table 8-2. Headspace Gas Data. (2 sheets)

Analyte	Toxic Category	Headspace Conc, mg/m^3	ERPG-3 mg/m^3	ERPG-2 mg/m^3	ERPG-1 mg/m^3	PEL-TWA mg/m^3
Benzene	central nervous system	1.32	3130	1,565	78	3
Butanol	central nervous system	164	7,500	750	75	75
Dodecane	central nervous system	296	7,330	1,450	37	37
2-hexanone	central nervous system	2.68	5,000	500	50	20
Nitrous oxide	central nervous system	2,340	36,000	18,000	270	90

Table 8-2. Headspace Gas Data. (2 sheets)

Analyte	Toxic Category	Headspace Conc, mg/m^3	ERPG-3 mg/m^3	ERPG-2 mg/m^3	ERPG-1 mg/m^3	PEL-TWA mg/m^3
Tridecane	central nervous system	388	7,330	1,450	37	37
Acetonitrile	systemic poison	21.8	60	20	3	3
Propane nitrile	systemic poison	10.5	60	20	3	3
Ammonia	corrosive and irritant	1,300	680	140	17	17
1,3 butadiene	corrosive and irritant	0.19	11,000	110	22	22
Methylene chloride	corrosive and irritant	21.76	17,400	3,480	700	174
Tributyl phosphate	corrosive and irritant	11.6	50	15	3	2.5

The guideline limit for onsite workers was taken as ERPG-3, and the offsite limit was taken as ERPG-2. These limits are applicable to extremely unlikely accidents in the frequency range of 10^{-4} to 10^{-6} per year (Van Keuren 1996b). For the unlikely frequency category, onsite and offsite guidelines are ERPG-2 and ERPG-1, respectively; and for the anticipated frequency category, onsite and offsite receptors are ERPG-1 and PEL-TWA, respectively.

8.2.2 Fire Reaction Products

Table 8-3 summarizes guideline limits for reaction products, taken from (Van Keuren 1996b).

Table 8-3. Reaction Product Toxin Limits.

Analyte	Toxic Category	ERPG-3 mg/m^3	ERPG-2 mg/m^3	ERPG-1 mg/m^3	PEL-TWA mg/m^3
Phosphorus pentoxide	corrosive and irritant	100	25	5	1
Nitrogen dioxide	corrosive and irritant	94	47	3.8	3.5
Carbon monoxide	systemic poison	1,360	690	230	40

8.2.3 Total Particulates

Aerosol mass produced by the postulated solvent fire was computed as the sum of soot and P_2O_5. Based on data from Jordan and Linder (1983), soot production was evaluated as 20 percent of solvent burned. The P_2O_5 production was computed as 4.32 percent of solvent burned (see Section 3.3). The guideline limits for total particulate mass was taken as 500, 50, 30, and 10 g/m^3 for ERPG-3, ERPG-2, ERPG-1 and PEL-TWA, respectively (Van Keuren 1996b).

8.2.4 High-Efficiency Particulate Air Filter Rupture Toxins

The toxicological consequences of HEPA filters rupturing were computed on the basis of waste release volumes and an ARF of 1E-3(see Table 8-1), a release duration of 60 seconds, and the sum of fraction multipliers (Van Keuren 1996b). Table 8-4 summarizes the sum of fraction multipliers applicable to solvent fires.

For an example calculation of the toxicological impact of HEPA filters rupturing, see Section 6.4.

Table 8-4. Sum of Fraction Multipliers.

		Sum of Fraction Multiplier (s/L)					
		Onsite	Offsite	Onsite	Offsite	Onsite	Offsite
Filter Type	Contaminant	10^{-4}-10^{-6} year^{-1}	10^{-4}-10^{-6} year^{-1}	10^{-2}-10^{-4} year^{-1}	10^{-2}-10^{-4} year^{-1}	10^{-0}-10^{-2} year^{-1}	10^{-0}-10^{-2} year^{-1}
SST-passive	SST solids	1.0E-3	1.7E-1	2.1E-4	3.3E-1	4.0E-4	9.4E-1
SST-active	SST solids	1.0E-3	1.7E-1	2.1E-3	3.3E-1	4.0E-4	9.4E-1
DST-active	DST liquids	2.1E-2	6.2E-1	7.5E-2	8.4E-0	1.0E-4	8.4E-0
DCRT-active	SST liquids	2.0E-2	6.2E-1	7.5E-2	8.0E-0	9.6E-3	8.0E-0

9.0 SPREADSHEET CALCULATIONS

Twenty-two solvent pool fire cases were evaluated in an effort to quantify unmitigated bounding consequences for SSTs, DSTs, and DCRTs. The analysis was performed with the aid of the EXCEL™ program. Calculations were carried out in three work sheets. The worksheets are described below.

9.1 WORKSHEET 1 FINAL SAFETY ANALYSIS REPORT SOLVENT POOL FIRE CASES

Figure 9-1 shows this worksheet (WS1). Each entry is described as follows.

Column A

Assigns case numbers on an alphabetic lettering sequence. Case letters carry over as the first column on each page of the workbook.

Column B

Identifies the type of waste tank considered for each case.

SST	=	single-shell tank
DST	=	double-shell tank
DCRT	=	double-contained receiver tank
55 kgal SST	=	55,000 gallon single-shell tank

Column C

Describes the size of pool analyzed for each case.

Column D

Lists the pool surface area assumed for each case.

Column E

Identifies the parameter (a consequence of a fire) that is maximized for the stated case. For example, Cell E3 identifies "*pressure*" as the parameter. The highest pressure for the puddle fire (case A) results from assuming the minimal vent path (the HEPA vent) for this case. The parameter "*vacuum*" indicates that vent path configuration was selected to cause the highest possible tank vacuum following fire extinction and the cooldown of headspace gases.

"*Radiological*" and "*toxicological*" descriptors indicate the cases were designed to yield bounding radiological and toxicological consequences, respectively.

The descriptor "passive vent" in Cell E20 indicates that this case was run to evaluate the passive ventilation case, even though it does not represent a maximum.

Figure 9-1. Final Safety Analysis Report Solvent Pool Fire Cases.

	A	B	C	D	E	F	G	H	I	J	K	L	M	N	O	P	Q	R
1	Case	Tank Type	Solvent Pool Description	Pool Area m²	Bounding Parameters	Ventilation Flow	Vent Description	Poolfire.4 Peak Pressure psig (kPa)	Poolfire.4 Peak Vacuum psig (kPa)	Poolfire.4 Solvent Burned kg	Solvent Aerosol Release Factor ARF	Poolfire.4 Leak Path Factor LPF	Aerosol Depletion Factor ADF	Solvent Atmosphere Release Basis kg	Aqueous Boiloff kg	Aerosol Release Factor for Aqueous ARF	Aqueous Atmospheric Release kg	Aqueous Unit Liter Dose Sv/L
2																		
3	a	SST	puddle	1.0	pressure	passive	hepa	3.1 (21.4)	0.5 (3.45)	126	0.1	0.0747	1.00E+00	9.56E-01	161.26	0.002	2.41E-02	1.10E+04
4	b	SST	puddle	1.0	vacuum	passive	hepa/ flapper[2]	1.0 (6.89)	0.5 (3.45)	124	0.1	0.0399	1.00E+00	4.95E-01	155.24	0.002	1.25E-02	1.10E+04
5	c	SST	puddle	1.0	radiological	100 cfm (0.047 m³/s)	hepa	3.1 (21.4)	0.5 (3.45)	126	0.1	1.0	1.60E-01	2.05E+00	161.26	0.002	5.16E-02	1.10E+04
6	d	SST	puddle	1.0	toxicological	100 cfm (0.047 m³/s)	hepa	3.1 (21.4)	0.5 (3.45)	126	0.1	1.0	1.60E-01	2.05E+00	161.26	0.002	5.16E-02	1.10E+04
7	e	SST	large	210	pressure	passive	hepa	29 (200)	0.1 (0.69)	146	0.03	0.146	8.85E-01	5.66E-01	183.96	0.002	4.75E-02	1.10E+04
8	f	SST	large	210	vacuum	passive	hepa/ flapper	1.8 (12.4)	6.8 (46.9)	64	0.03	0.3	1.00E+00	7.56E-01	105.64	0.002	6.35E-02	1.10E+04
9	g	SST	large	210	radiological	100 cfm (0.047 m³/s)	hepa	29 (200)	0.1 (0.69)	146	0.03	1.0	2.31E-01	1.01E+00	183.96	0.002	8.50E-02	1.10E+04
10	h	SST	large	210	toxicological	passive	hepa/ flapper	1.8 (12.4)	6.8 (46.9)	64	0.03	0.3	1.00E+00	7.56E-01	105.64	0.002	6.35E-02	1.10E+04
11	i	DST	large	210	pressure	sealed tank	none	30.8 (212)	0 (0)	162	0.03	0.0	1.00E+00	0.00E+00	204.12	0.002	0.00E+00	6.10E+03
12		DST	large	210	vacuum	passive	flapper	2.1 (14.5)	8 (55.2)	92.5	0.03	0.31	1.00E+00	8.60E-01	116.55	0.002	7.23E-02	6.10E+03
13	k	DST	puddle	1.0	radiological	100 cfm (0.047 m³/s)	vent pipe[3]	0.9 (6.21)	0.1 (0.69)	132	0.1	1.0	1.33E-01	1.76E+00	166.32	0.002	4.42E-02	6.10E+03
14	l	DST	large	210	toxicological	100 cfm (0.047 m³/s)	flapper/ vent pipe	2.0 (13.8)	5.2 (35.9)	92.1	0.03	1.0	3.60E-01	1.05E+00	116.046	0.002	8.82E-02	6.10E+03
15	m	DCRT	large	34.1	pressure	sealed tank	none	30.5 (210)	0 (0)	2.47	0.03	0.00	1.00E+00	0.00E+00	3.1122	0.002	0.00E+00	1.10E+04
16	n	DCRT	large	34.1	vacuum	passive	4" (0.1m) orifice	18.3 (126)	1.2 (8.27)	2.12	0.03	0.31	1.00E+00	1.97E-02	2.6712	0.002	1.66E-03	1.10E+04
17	o	DCRT	large	34.1	radiological	passive	4" (0.1m) orifice	18.3 (126)	1.2 (8.27)	2.12	0.03	0.31	1.00E+00	1.97E-02	2.6712	0.002	1.66E-03	1.10E+04
18	p	DCRT	large	34.1	toxicological	passive	4" (0.1m) orifice	18.3 (126)	1.2 (8.27)	2.12	0.03	0.31	1.00E+00	1.97E-02	2.6712	0.002	1.66E-03	1.10E+04
19	q	SST	entrained	40.0	radiological	100 cfm (0.047 m³/s)	hepa[1]	4.4(30.5)	0.7(4.8)	130	0.1	1	1.95E-01	2.54E+00	163.8	0.002	6.39E-02	1.10E+04
20	q1	SST	entrained	40.0	passive vent	passive	hepa[1]	4.4(30.5)	0.7(4.8)	130	0.1	0.11	1.00E+00	1.43E+00	163.8	0.002	3.60E-02	1.10E+04
21	r	SST	entrained	40.0	toxicological and vacuum	100 cfm (0.047 m³/s)	hepa/ flapper	1.0 (6.89)	2.1 (14.5)	113	0.1	1	2.21E-01	2.50E+00	142.38	0.002	6.29E-02	1.10E+04
22	s	55 kgal SST	large	29.2	pressure	passive	hepa[4]	23.9 (165)	75 (5.2)	6.54	0.03	0.22	1.00E+00	4.32E-02	6.2404	0.002	3.63E-03	1.10E+04
23	t	55 kgal SST	large	29.2	toxicological and vacuum	passive	hepa/ flapper[4]	2.0 (13.8)	5.3 (13.8)	4	0.03	0.3	1.00E+00	3.60E-02	5.04	0.002	3.02E-03	1.10E+04
24	u	55 kgal SST	puddle	1.0	pressure	passive	hepa[4]	6.0 (41.4)	1.1 (7.52)	5.76	0.1	0.156	1.00E+00	9.10E-02	7.2576	0.002	2.29E-03	1.10E+04
25	v	DST	entrained	40.0	toxicological and radiological	100 cfm (0.047 m³/s)	flapper/ vent pipe[3]	0.7(4.83)	1.1 (7.58)	120	0.1	1	2.10E-01	2.52E+00	151.2	0.002	6.35E-02	6.10E+03
26		(1) HEPA Vent Modeled as 3.75" (9.5 mm) orifice																
27		(2) Flapper is 50 in. (1.27 m) orifice opening at 1 psid (6.89 kPa)																
28		(3) Vent Pipe on DST Modeled as 9.6 in. (0.24 m) orifice																
29		(4) HEPA Vent for 55 kgal tanks is 3.42" (.087m) orifice. Flapper is 17" orifice.																

Column F

Describes the type of ventilation assumed for each case. "*Passive*" applies to SSTs and DCRTs where ventilation is caused by atmospheric breathing and natural convection. The ventilation flow for actively ventilated tanks is listed as "100 cfm (0.047 m^3/s)". This flow rate designator was used to remind the analyst that ventilation flow rates in actively ventilated tanks are in the order of 100 cfm under normal conditions. This flow rate number is used when estimating aerosol depletion by in-tank sedimentation.

Column G

Lists the type of vent path assumed for each case. Footnotes 1 through 4 quantify the size of the equivalent orifice used in POOLFIRE.4 calculations.

Cases I and M are specified to have "none." Because available information is insufficient to characterize the minimal vent opening for DSTs and DCRTs, a default value of zero was assumed for these cases. Peak pressures computed for these cases is a conservative upper bound on pressures which could be generated by pool fires in these tanks.

Column H

Lists the peak pressure computed by POOLFIRE.4 for each case. As noted in Appendix A, POOLFIRE.4 calculates specific burning rate as a function of oxygen concentration in headspace air. All cases analyzed here use a bounding high value of 10 cm/s for fire spread velocity.

Column I

Lists the peak vacuum inside the tank referenced to the outside atmosphere for each case. Headspace air pressure is computed as a function of time by POOLFIRE.4, and the numbers in column I are minimum gauge pressures from runs with POOLFIRE.4.

Column J

Lists the mass of solvent burned from fire initiation to fire extinguishment at an oxygen level of 13 mole percent for each case. These numbers come from runs with POOLFIRE.4. Note that cases with small vents result in the highest mass of solvent burned. The venting of oxygen from the tank leaves less oxygen in the tank to oxidize fuel; therefore, less fuel burns when larger vent paths are specified.

Column K

Lists aerosol release fraction (ARF) for each case analyzed. Puddle fires use ARF = 0.1 and large pool fires use ARF = 0.03. Section 6.2.1 describes the bases for these values.

Column L

Lists the leak path factor (LPF), defined as the fraction of reaction products released from the tank during the course of a pool fire, for each case. For passively ventilated tanks, the numbers in this column are values calculated by POOLFIRE.4. For actively ventilated tanks, a default value of unity is assumed. This factor is calculated on the basis of zero depletion, i.e., on ideal gas behavior.

Column M

Lists the aerosol depletion factor (ADF), defined as the ratio of aerosol mass leaked to the mass of aerosol which would leak if no deletion took place, for each case. The ADF is a transmission factor for aerosol mass. An ADF of 1.0 indicates that no depletion by aerosol deposition is predicted; a value of 0.16 indicates that in-tank sedimentation is calculated to reduce leaked aerosol mass to 16 percent of the mass leaked based on ideal gas behavior.

The LPF (see column L), the fractional leakage of contaminants based on ideal gas behavior times ADF is the fractional leakage of particulate contaminants predicted for solvent fires. For information on the methodology used to predict ARF for each fire case, see Appendix C.

Column N

Calculates from Equation 6-1 the solvent release from the tank to the environs (mass in kg) and assigns C a default value of unity.

$$S = M * 1 * ARF * LPF$$

The EXCEL™ equation for Cell N3 is:

$$N3 = J3 * K3 * L3 * M3.$$

This equation is reproduced in all rows by advancing the row number appropriately. The release of contaminants in the solvent may be quantified by multiplying their concentrations by the solvent mass releases calculated in column N. This mass release is also the appropriate mass to be used for computing doses using ULD values as indicated in Equation 6-3.

Column O

Calculates the mass of water evaporated as explained in Section 6.2.3;

$$\text{aqueous mass} = \text{fuel burned} * 1.26$$

The EXCEL™ equation, for Cell O3, is:

$$O3 = 1.26 * J3$$

Column P

Assigns a value of 0.002 to the ARF for water evaporation for all cases. This ARF is cited as a bounding value for boiling liquids by Mishima (1994).

Column Q

Calculates from Equation 6-1 the atmospheric release of aqueous waste caused by evaporation and assigns C a default value of unity:

$$S = M * 1 * ARF * LPF.$$

The EXCEL™ equation for Cell Q3 is:

$$Q3 = O3 * P3 * L3 * M3.$$

This equation is reproduced in all rows by advancing the row number appropriately. The ADF has been included to account for in-tank sedimentation of particulate contaminants.

Column R

Lists the unit liter doses for liquid waste, the waste subject to evaporative release for each case. The values in column R are those given in Table 8-1.

9.2 WORKSHEET 2 DOSE SUMMARY

Figure 9-2 shows this worksheet (WS2). Each entry is described as follows.

Columns A Through G

These columns are repeated from WS1 to remind the analyst of case descriptions.

HNF-4240 Rev. 1

Figure 9-2. Dose Summary Worksheet.

	A	B	C	D	E	F	G	H	I	J	K	L
1	Case	Tank Type	Solvent Pool Description	Pool Area m²	Bounding Parameters	Ventilation Flow	Vent Description	On Site Solvent Smoke Dose, Sv	Onsite Aqueous Boiloff Dose, Sv	HEPA Rupture Dose Onsite Sv	Total Onsite Dose Sv	Total Offsite Dose Sv
2												
3	a	SST	puddle	1.0	pressure	passive	hepa[1]	3.04E-05	2.98E-03	3.14E-05	3.04E-03	2.67E-06
4	b	SST	puddle	1.0	vacuum	passive	hepa/ flapper[2]	1.58E-05	1.54E-03	3.14E-05	1.59E-03	1.39E-06
5	c	SST	puddle	1.0	radiological	100 cfm (0.047 m³/s)	hepa	6.52E-05	6.39E-03	4.95E-03	1.14E-02	1.00E-05
6	d	SST	puddle	1.0	toxicological	100 cfm (0.047 m³/s)	hepa	6.52E-05	6.39E-03	4.95E-03	1.14E-02	1.00E-05
7	e	SST	large	210	pressure	passive	hepa	1.80E-05	5.88E-03	3.14E-05	5.93E-03	5.20E-06
8	f	SST	large	210	vacuum	passive	hepa/ flapper	2.41E-05	7.86E-03	3.14E-05	7.91E-03	6.94E-06
9	g	SST	large	210	radiological	100 cfm (0.047 m³/s)	hepa	3.22E-05	1.05E-02	4.95E-03	1.55E-02	1.36E-05
10	h	SST	large	210	toxicological	passive	hepa/ flapper	2.41E-05	7.86E-03	3.14E-05	7.91E-03	6.94E-06
11	i	DST	large	210	pressure	sealed tank	none	0.00E+00	0.00E+00	0.00E+00	0.00E+00	0.00E+00
12	j	DST	large	210	vacuum	passive	flapper	2.74E-05	4.96E-03	8.72E-07	4.99E-03	4.28E-06
13	k	DST	puddle	1.0	radiological	100 cfm (0.047 m³/s)	vent pipe[3]	5.59E-05	3.04E-03	2.54E-04	3.35E-03	2.87E-06
14	l	DST	large	210	toxicological	100 cfm (0.047 m³/s)	flapper/ vent pipe	3.34E-05	6.05E-03	2.54E-04	6.34E-03	5.44E-06
15	m	DCRT	large	34.1	pressure	sealed tank	none	0.00E+00	0.00E+00	0.00E+00	0.00E+00	0.00E+00
16	n	DCRT	large	34.1	vacuum	passive	4" (0.1m) orifice	6.28E-07	2.05E-04	2.81E-05	2.34E-04	1.97E-07
17	o	DCRT	large	34.1	radiological	passive	4" (0.1m) orifice	6.28E-07	2.05E-04	2.81E-05	2.34E-04	1.97E-07
18	p	DCRT	large	34.1	toxicological	passive	4" (0.1m) orifice	6.28E-07	2.05E-04	2.81E-05	2.34E-04	1.97E-07
19	q	SST	entrained	40.0	radiological	100 cfm (0.047 m³/s)	hepa[1]	4.04E-05	3.95E-03	4.95E-03	8.94E-03	7.84E-06
20	q1	SST	entrained	40.0	passive vent	passive	hepa[1]	2.28E-05	2.23E-03	3.14E-05	2.28E-03	2.00E-06
21	r	SST	entrained	40.0	toxicological and vacuum	100 cfm (0.047 m³/s)	hepa/ flapper	3.98E-05	3.89E-03	4.95E-03	8.88E-03	7.79E-06
22	s	55 kgal SST	large	29.2	pressure	passive	hepa[4]	1.37E-06	4.49E-04	3.14E-05	4.81E-04	4.22E-07
23	t	55 kgal SST	large	29.2	toxicological and vacuum	passive	hepa/ flapper[4]	1.15E-06	3.74E-04	3.14E-05	4.07E-04	3.57E-07
24	u	56 kgal SST	puddle	1.0	pressure	passive	hepa[4]	2.90E-06	2.84E-04	3.14E-05	3.18E-04	2.79E-07
25	v	DST	entrained	40.0	toxicological and radiological	100 cfm (0.047 m³/s)	flapper/ vent pipe[3]	8.02E-05	4.36E-03	2.54E-04	4.69E-03	4.11E-06
26		[1] HEPA Vent Modeled as 3.75" (9.5 mm) orifice										
27		[2] Flapper is 50 in. (1.27 m) orifice opening at 1 psid (6.89 kPa)										
28		[3] Vent Pipe on DST Modeled as 9.6 in. (0.24 m) orifice										
29		[4] HEPA Vent for 55 kgal tanks is 3.42" (.087m) orifice. Flapper is 17" orifice.										

Column H

Calculates from Equation 6-3 the onsite dose attributable to solvent smoke. The product of $\frac{\chi}{Q^1}$ and R is entered as a constant:

$$\frac{\chi}{Q^1} * R = 0.0341 \frac{s}{m^3} * 3.3E-4 \frac{m^3}{s} = 1.125E-5.$$

The dose is calculated from:

$$D(Sv) = Q(L) * 1.125E-5 * ULD(Sv/L).$$

The EXCEL™ equation for Cell H3 is:

$$H3 = N3\ (WS1) * 1.125E-5 * 2.83$$

A factor of 0.5 is inserted into cells in column H, for rows 19, 20, and 21. This reflects the use of a respirable fraction (RF) of 0.5 for the entrained fire cases. All of the other cases use an RF of 1.0. The EXCEL™ equation for the entrained fire case 20 is:

$$H20 = N20\ (WS1) * 1.125E-5 * 2.83 * 0.5$$

The ULD for solvent is expressed in Sv/kg units (see Table 8-1); therefore, the Q(L) is also expressed in kg (see column N of WS1).

Column I

Computes doses attributable to aqueous boiloff from:

$$D(Sv) = Q(L) * 1.125E-5 * ULD(Sv/L).$$

Q(L) and ULD(Sv/L) are calculated in WS1; therefore, the EXCEL™ equation for Cell I3 is:

$$I3 = Q3\ (WS1) * R3\ (WS1) * 1.125E-5$$

A factor of 0.5 is inserted into cells in column I, for rows 19, 20, and 21. This reflects the use of a respirable fraction (RF) of 0.5 for the entrained fire cases. All of the other cases use an RF of 1.0. The EXCEL™ equation for the entrained fire case 20 is:

$$I20 = Q20\ (WS1) * R20\ (WS1) * 1.12E\text{-}5 * 0.5$$

Note that Q3 (WSI) is the mass in kilograms of aqueous waste released. The volume of waste in liters, the quantity needed to match with ULD values expressed on a per liter basis, is the mass in kilograms divided by density in kg/L. A conservative default density of 1.4 kg/L has been used here.

Column J

Lists the onsite radiological dose caused by HEPA filter rupture. The doses for Column J are calculated separately and entered in Column J. A spreadsheet titled Calculate Onsite Rad Dose calculates the dose and is included as Appendix K to this document. The onsite doses are calculated with the following formula:

$$D = Q \times ARF \times ULD \times \frac{X}{Q} \times BR$$

here:

BR = breathing rate = 3.3×10^{-4} m^3/sec.

X/Q = 3.4×10^{-2} sec/m^3

ULD = unit liter dose = different values of Sv/L for different waste.

ARF = aerosol release factor, a dimensionless factor. Taken from Mishima (1994). Section 5.4 of Mishima (1994) gives ARFs for HEPA filters. An ARF of 1×10^{-2} is for blast effects. An ARF of 2×10^{-6} is for shock effects. The overpressure resulting from a solvent burn is best characterized as a shock effect. A conservative extrapolation between the two values is 1x10-3.

Q = Liters of waste loaded on the filters taken from document HNF-SD-WM-CN-099, Rev. 1A. For these calculations, 1.98 L was rounded to 2.0 L, and 3.66 L was rounded to 3.7 L.

The HEPA rupture doses calculated in the spreadsheet from Appendix K are entered in column J of the Dose Summary spreadsheet. Values used in the above equation are given in Table 8-1.

Column K

Computes total onsite dose by summing doses caused by solvent smoke, aqueous boiloff, and HEPA rupture. The EXCEL™ equation for Row 3 is:

$$K3 = H3 + I3 + J3.$$

Column L

Calculates offsite doses as the sum of inhalation and ingestion doses. Combining Equations 6-3, and 6-4, and 6-5 and performing algebraic manipulations, offsite dose can be expressed as:

$$\text{total dose} = \text{inhalation dose} * \left[1 + \frac{ULD_G}{R * ULD_I}\right]$$

where

total dose	=	inhalation dose + ingestion dose
ULD_G	=	unit liter ingestion dose, Sv m^3/sL
R	=	breathing rate, m^3/s
ULD_I	=	unit liter inhalation dose, Sv/L

Further, offsite inhalation dose can be expressed in terms of onsite inhalation dose and a ratio of atmospheric dispersion factors:

$$\text{offsite inhalation dose} = \text{onsite inhalation dose} * \frac{\frac{\chi}{Q^1}\text{offsite}}{\frac{\chi}{Q^1}\text{onsite}}.$$

The ratio of atmospheric dispersion factors is:

$$\text{offsite/onsite} = 2.83E\text{-}5/3.41E\text{-}2 = 8.30E\text{-}4.$$

For SST solids, the ratio $ULD_G/R * ULD_I$ is calculated on the basis of Table 8-1 data as:

$$4.1/(3.3E\text{-}4 * 2.2E5) = 0.0565.$$

The EXCEL™ equation for Cell L3 is:

$$L3 = K3 * 8.3E-4(1 + 0.0565)$$

The ratio $ULD_G/R * ULD_I$ is assigned a value of 0.0565 for all SST cases. For DSTs, the ratio is calculated to be 0.0338 using Table 8-1 data for DST liquids. The DCRT releases are based on SST liquids, for which the $ULD_G/R * ULD_I$ ratio is calculated to be 0.0143.

9.3 WORKSHEET 3 TOXICOLOGICAL

Figure 9-3 shows this worksheet (WS3) which quantifies the toxicological consequences of fires. The calculation steps are explained in detail as follows.

Columns A through G

These columns repeated from WS1 remind the analyst of particulars for each case being analyzed.

Column H

Lists the headspace air volume assumed for each case. In general, bounding high values were assumed to maximize the oxygen inventory, thereby maximizing the quantity of solvent which could be burned.

Column I

Lists the time period for which the pool fire is calculated to cause tank pressurization and outflow from the tank. The word "maximum" is included in the label descriptor because vent rate is a factor in quantifying the concentration of toxins in the downwind plume. The average vent rate during the fire-induced outflow period was found to be larger than the active ventilation flow rate (assumed to be 100 cfm) so the limiting toxicological consequences are associated with the outflow period listed in column I.

For puddle fires, outflow is calculated to end well before the fire extinguishes. For case A, outflow stops at 2,500 seconds, but the fire burns for 5,018 seconds before extinguishment. Gas heatup, caused by the relatively high specific burning rate computed for high oxygen concentrations, is sufficient to pressurize the atmosphere for 2,500 seconds. For a longer time, the reduced burning rate is insufficient to increase gas temperature, and venting ceases for tanks not connected to a forced ventilation system.

Column J

Lists the masses of solvent burned during the outflow period. These numbers are smaller than the total solvent burned (column J of WS1) for puddle fires. For large pools, outflow continues for the whole of the

HNF-4240 Rev. 1

Figure 9-3. Toxicological Worksheet. (9 sheets)

	A	B	C	D	E	F	G	H	I	J	K	L	M	N	O	P	Q	R
1	Case	Tank Type	Solvent Pool Description	Pool Area m^2	Bounding Parameters	Ventilation Flow	Vent Description	Tank Gas Volume m^3	Poolfire.4 Maximum Vent duration s	Poolfire.4 Solvent Burned in Vent kg	Poolfire.4 Reaction Gas Fraction	Poolfire.4 Headspace Gas Fraction	Source Conc. P_2O_5 mg/m^3	Source Conc. CO mg/m^3	Source Conc. NO_2 mg/m^3	Atmospheric Dilution Factor at 100m Dimensionless	Aqueous Vent Rate L/s	Van's Onsite Limit Ex. Unlikely s/L
2																		
3	a	SST	puddle	1.0	pressure	passive	hepa[1]	4.82E+03	2.50E+03	8.73E+01	1.10E-01	2.30E-01	3.75E+02	3.67E+02	4.76E+01	2.60E-03	1.42E-05	2.00E+02
4	b	SST	puddle	1.0	vacuum	passive	hepa/ flapper[2]	4.82E+03	1.70E+03	6.51E+01	7.56E-02	2.40E-01	1.84E+02	1.80E+02	2.34E+01	8.70E-03	1.39E-05	2.00E+02
5	c	SST	puddle	1.0	radiological	100 cfm (0.047 m^3/s)	hepa	4.82E+03	2.50E+03	8.73E+01	1.10E-01	2.30E-01	3.75E+02	3.67E+02	4.76E+01	2.60E-03	1.42E-05	2.00E+02
6	d	SST	puddle	1.0	toxicological	100 cfm (0.047 m^3/s)	hepa	4.82E+03	2.50E+03	8.73E+01	1.10E-01	2.30E-01	3.75E+02	3.67E+02	4.76E+01	2.60E-03	1.42E-05	2.00E+02
7	e	SST	large	210	pressure	passive	hepa	4.82E+03	1.30E+03	1.46E+02	1.46E-01	1.58E-01	1.21E+03	1.19E+03	1.54E+02	2.60E-03	4.13E-05	2.00E+02
8	f	SST	large	210	vacuum	passive	hepa/ flapper	4.82E+03	6.70E+01	8.40E+01	3.00E-01	6.00E-01	3.77E+02	3.69E+02	4.78E+01	1.30E-02	9.48E-04	2.00E+02
9	g	SST	large	210	radiological	100 cfm (0.047 m^3/s)	hepa	4.82E+03	1.30E+03	1.46E+02	1.46E-01	1.58E-01	1.21E+03	1.19E+03	1.54E+02	2.60E-03	4.13E-05	2.00E+02
10	h	SST	large	210	toxicological	passive	hepa/ flapper	4.82E+03	6.70E+01	8.40E+01	3.00E-01	6.00E-01	3.77E+02	3.69E+02	4.78E+01	1.30E-02	9.48E-04	2.00E+02
11	i	DST	large	210	pressure	sealed tank	none	5.30E+03	8.30E+01	1.62E+02	0.00E+00	0.00E+00	NA	NA	NA	0.00E+00	0.00E+00	
12	j	DST	large	210	vacuum	passive	flapper	5.30E+03	7.00E+01	9.25E+01	3.10E-01	6.10E-01	3.83E+02	3.75E+02	4.87E+01	1.30E-02	1.03E-03	2.10E+02
13	k	DST	puddle	1.0	radiological	100 cfm (0.047 m^3/s)	vent pipe[3]	5.30E+03	1.20E+03	5.00E+01	8.10E-02	2.50E-01	1.32E+02	1.29E+02	1.68E+01	2.00E-03	2.25E-05	2.10E+02
14	l	DST	large	210	toxicological	100 cfm (0.047 m^3/s)	flapper/ vent pipe	5.30E+03	7.00E+01	9.21E+01	3.10E-01	6.10E-01	3.82E+02	3.74E+02	4.85E+01	1.30E-02	1.03E-03	2.10E+02
15	m	DCRT	large	34.1	pressure	sealed tank	none	8.01E+01	1.95E+01	2.47E+00	0.00E+00	0.00E+00	NA	NA	NA	0.00E+00	0.00E+00	2.00E+02
16	n	DCRT	large	34.1	vacuum	passive	4" (0.1m) orifice	8.01E+01	3.30E+01	2.12E+00	3.10E-01	4.10E-01	8.64E+02	8.47E+02	1.10E+02	2.00E-03	5.02E-05	2.00E+02
17	o	DCRT	large	34.1	radiological	passive	4" (0.1m) orifice	8.01E+01	3.30E+01	2.12E+00	3.10E-01	4.10E-01	8.64E+02	8.47E+02	1.10E+02	2.00E-03	5.02E-05	2.00E+02
18	p	DCRT	large	34.1	toxicological	passive	4" (0.1m) orifice	8.01E+01	3.30E+01	2.12E+00	3.10E-01	4.10E-01	8.64E+02	8.47E+02	1.10E+02	2.00E-03	5.02E-05	2.00E+02
19	q	SST	entrained	40.0	radiological	100 cfm (0.047 m^3/s)	hepa[1]	4.82E+03	1.70E+03	1.30E+02	1.10E-01	2.10E-01	6.11E+02	5.99E+02	7.76E+01	2.60E-03	2.12E-05	2.00E+02
20	q1	SST	entrained	40.0	passive vent	passive	hepa[1]	4.82E+03	1.70E+03	1.30E+02	1.10E-01	2.10E-01	6.11E+02	5.99E+02	7.76E+01	2.60E-03	2.12E-05	2.00E+02
21	r	SST	entrained	40.0	toxicological and vacuum	100 cfm (0.047 m^3/s)	hepa/ flapper	4.82E+03	1.46E+03	1.13E+02	1.00E-01	3.10E-01	3.27E+02	3.20E+02	4.15E+01	8.70E-03	1.95E-05	2.00E+02
22	s	55 kgal SST	large	29.2	pressure	passive	3.42" (.087m) orifice	2.27E+02	8.20E+01	6.54E+00	2.20E-01	2.70E-01	1.01E+03	9.94E+02	1.29E+02	2.60E-03	4.42E-05	2.00E+02
23	t	55 kgal SST	large	29.2	toxicological and vacuum	passive	hepa/ flapper[4]	2.27E+02	2.32E+01	4.00E+00	3.00E-01	6.00E-01	3.81E+02	3.73E+02	4.83E+01	8.70E-03	1.30E-04	2.00E+02
24	u	55 kgal SST	puddle	1.0	pressure	passive	hepa[4]	2.27E+02	1.57E+02	4.81E+00	1.90E-01	3.50E-01	4.97E+02	4.87E+02	6.31E+01	2.60E-03	1.75E-05	2.00E+02
25	v	DST	entrained	40.0	toxicological and radiological	100 cfm (0.047 m^3/s)	flapper/ vent pipe[3]	5.30E+03	1.36E+03	1.07E+02	1.12E-01	3.50E-01	2.79E+02	2.74E+02	3.54E+01	2.00E-03	2.49E-05	2.10E+02
26		[1] HEPA Vent Modeled as 3.75" (9.5 mm) orifice																
27		[2] Flapper is 50 in. (1.27 m) orifice opening at 1 psid (6.89 kPa)																
28		[3] Vent Pipe on DST Modeled as 9.6 in. (0.24 m) orifice																
29		[4] HEPA Vent for 55 kgal tanks is 3.42" (.087m) orifice. Flapper is 17" orifice.																

Figure 9-3. Toxicological Worksheet. (9 sheets)

	A	S	T	U	V	W	X	Y	Z	AA	AB	AC	AD	AE	AF	AG	AH	AI
1	Case	Van's Offsite Limit Ex. Unlikely s/L	Van's Onsite Limit Unlikely s/L	Van's Offsite Limit Unlikely s/L	Van's Onsite Limit Anticipated s/L	Van's Offsite Limit Anticipated s/L	Onsite Sum of Fractions Aqueous Boiloff Ex.Unlikely	Offsite Sum of Fractions Aqueous Boiloff Ex.Unlikely	Vent Rate of Gas m^3/s	Onsite Conc. P_2O_5 mg/m^3	Onsite Conc. CO mg/m^3	Onsite Conc. NO_2 mg/m^3	Onsite Normalized Conc. (1 mg/m^3 at source)	Source Soot Conc. mg/m^3	Onsite Total Particulate mg/m^3	Offsite Total Particulate mg/m^3	Particulate Limit ERPG-3 mg/m^3	Particulate Limit ERPG-2 mg/m^3
2																		
3	a	6.20E-01	7.50E+02	8.00E+00	9.60E+03	8.00E+00	2.84E-03	8.80E-06	4.43E-01	9.74E-01	9.54E-01	1.24E-01	2.60E-03	1.73E+03	5.48E+00	2.64E-02	500	50
4	b	6.20E-01	7.50E+02	8.00E+00	9.60E+03	8.00E+00	2.78E-03	8.62E-06	6.80E-01	1.60E+00	1.57E+00	2.03E-01	8.70E-03	8.52E+02	9.01E+00	1.99E-02	500	50
5	c	6.20E-01	7.50E+02	8.00E+00	9.60E+03	8.00E+00	2.84E-03	8.80E-06	4.43E-01	9.74E-01	9.54E-01	1.24E-01	2.60E-03	1.73E+03	5.48E+00	2.64E-02	500	50
6	d	6.20E-01	7.50E+02	8.00E+00	9.60E+03	8.00E+00	2.84E-03	8.80E-06	4.43E-01	9.74E-01	9.54E-01	1.24E-01	2.60E-03	1.73E+03	5.48E+00	2.64E-02	500	50
7	e	6.20E-01	7.50E+02	8.00E+00	9.60E+03	8.00E+00	8.26E-03	2.56E-05	5.85E-01	3.15E+00	3.08E+00	4.00E-01	2.60E-03	5.60E+03	1.77E+01	1.13E-01	500	50
8	f	6.20E-01	7.50E+02	8.00E+00	9.60E+03	8.00E+00	1.90E-01	5.88E-04	4.31E+01	4.90E+00	4.80E+00	6.22E-01	1.30E-02	1.74E+03	2.76E+01	2.59E+00	500	50
9	g	6.20E-01	7.50E+02	8.00E+00	9.60E+03	8.00E+00	8.26E-03	2.56E-05	5.85E-01	3.15E+00	3.08E+00	4.00E-01	2.60E-03	5.60E+03	1.77E+01	1.13E-01	500	50
10	h	6.20E-01	7.50E+02	8.00E+00	9.60E+03	8.00E+00	1.90E-01	5.88E-04	4.31E+01	4.90E+00	4.80E+00	6.22E-01	1.30E-02	1.74E+03	2.76E+01	2.59E+00	500	50
11	i	6.20E-01	7.50E+02	8.40E+00	1.00E+04	8.40E+00	0.00E+00	0.00E+00	0.00E+00	#VALUE!	#VALUE!	#VALUE!	0.00E+00	NA	#VALUE!	#VALUE!	500	50
12	j	6.20E-01	7.50E+02	8.40E+00	1.00E+04	8.40E+00	2.17E-01	6.40E-04	4.62E+01	4.98E+00	4.88E+00	6.33E-01	1.30E-02	1.77E+03	2.80E+01	2.82E+00	500	50
13	k	6.20E-01	7.50E+02	8.40E+00	1.00E+04	8.40E+00	4.72E-03	1.39E-05	1.10E+00	2.64E-01	2.59E-01	3.35E-02	2.00E-03	6.11E+02	1.49E+00	2.32E-02	500	50
14	l	6.20E-01	7.50E+02	8.40E+00	1.00E+04	8.40E+00	2.16E-01	6.37E-04	4.62E+01	4.96E+00	4.86E+00	6.30E-01	1.30E-02	1.77E+03	2.79E+01	2.80E+00	500	50
15	m	6.20E-01	7.50E+02	8.00E+00	9.60E+03	8.00E+00	0.00E+00	0.00E+00	0.00E+00	#VALUE!	#VALUE!	#VALUE!	0.00E+00	NA	#VALUE!	#VALUE!	500	50
16	n	6.20E-01	7.50E+02	8.00E+00	9.60E+03	8.00E+00	1.00E-02	3.11E-05	9.95E-01	1.73E+00	1.69E+00	2.20E-01	2.00E-03	4.00E+03	9.73E+00	1.37E-01	500	50
17	o	6.20E-01	7.50E+02	8.00E+00	9.60E+03	8.00E+00	1.00E-02	3.11E-05	9.95E-01	1.73E+00	1.69E+00	2.20E-01	2.00E-03	4.00E+03	9.73E+00	1.37E-01	500	50
18	p	6.20E-01	7.50E+02	8.00E+00	9.60E+03	8.00E+00	1.00E-02	3.11E-05	9.95E-01	1.73E+00	1.69E+00	2.20E-01	2.00E-03	4.00E+03	9.73E+00	1.37E-01	500	50
19	q	6.20E-01	7.50E+02	8.00E+00	9.60E+03	8.00E+00	4.24E-03	1.31E-05	5.95E-01	7.94E-01	1.56E+00	2.02E-01	2.60E-03	1.41E+03	4.47E+00	2.89E-02	500	50
20	q1	6.20E-01	7.50E+02	8.00E+00	9.60E+03	8.00E+00	4.24E-03	1.31E-05	5.95E-01	7.94E-01	1.56E+00	2.02E-01	2.60E-03	1.41E+03	4.47E+00	2.89E-02	500	50
21	r	6.20E-01	7.50E+02	8.00E+00	9.60E+03	8.00E+00	3.90E-03	1.21E-05	1.02E+00	1.42E+00	2.79E+00	3.61E-01	8.70E-03	7.57E+02	8.01E+00	2.66E-02	500	50
22	s	6.20E-01	7.50E+02	8.00E+00	9.60E+03	8.00E+00	8.84E-03	2.74E-05	7.47E-01	2.64E+00	2.58E+00	3.35E-01	2.60E-03	4.70E+03	1.48E+01	1.21E-01	500	50
23	t	6.20E-01	7.50E+02	8.00E+00	9.60E+03	8.00E+00	2.61E-02	8.08E-05	5.87E+00	3.31E+00	3.25E+00	4.21E-01	8.70E-03	1.76E+03	1.86E+01	3.56E-01	500	50
24	u	6.20E-01	7.50E+02	8.00E+00	9.60E+03	8.00E+00	3.50E-03	1.09E-05	5.05E-01	1.29E+00	1.27E+00	1.64E-01	2.60E-03	2.30E+03	7.27E+00	4.00E-02	500	50
25	v	6.20E-01	7.50E+02	8.40E+00	1.00E+04	8.40E+00	5.23E-03	1.54E-05	1.36E+00	5.58E-01	5.47E-01	7.09E-02	2.00E-03	1.29E+03	3.14E+00	6.06E-02	500	50
26																		
27																		
28																		
29																		

HNF-4240 Rev. 1

Figure 9-3. Toxicological Worksheet. (9 sheets)

	A	AJ	AK	AL	AM	AN	AO	AP	AQ	AR	AS	AT	AU	AV	AW	AX	AY	AZ	BA
1	Case	Particulate Limit ERPG-1 mg/m³	Particulate Limit PEL-TWA mg/m³	Ex. Un. Onsite Total Particulate Fraction	Ex. Un. Offsite Total Particulate Fraction	Offsite Normalized Conc. (1mg/m³)	Ammonia Headspace Conc. mg/m³	Ammonia ERPG-3 mg/m³	Ammonia ERPG-2 mg/m³	Ammonia ERPG-1 mg/m³	Ammonia PEL-TWA mg/m³	1,3 Buta Headspace Conc. mg/m³	1,3 Buta ERPG-3 mg/m³	1,3 Buta ERPG-2 mg/m³	1,3 Buta ERPG-1 mg/m³	1,3 Buta PEL-TWA mg/m³	meth. chl. Headspace conc. mg/m³	meth. chl. ERPG-3 mg/m³	meth. chl. ERPG-2 mg/m³
2																			
3	a	30	10	1.10E-02	5.29E-04	1.25E-05	1300	680	140	17	17	0.19	11,000	110	22	22	21.76	17,400	3480
4	b	30	10	1.80E-02	3.98E-04	1.92E-05	1300	680	140	17	17	0.19	11,000	110	22	22	21.76	17,400	3480
5	c	30	10	1.10E-02	5.29E-04	1.25E-05	1300	680	140	17	17	0.19	11,000	110	22	22	21.76	17,400	3480
6	d	30	10	1.10E-02	5.29E-04	1.25E-05	1300	680	140	17	17	0.19	11,000	110	22	22	21.76	17,400	3480
7	e	30	10	3.54E-02	2.26E-03	1.66E-05	1300	680	140	17	17	0.19	11,000	110	22	22	21.76	17,400	3480
8	f	30	10	5.51E-02	5.17E-02	1.22E-03	1300	680	140	17	17	0.19	11,000	110	22	22	21.76	17,400	3480
9	g	30	10	3.54E-02	2.26E-03	1.66E-05	1300	680	140	17	17	0.19	11,000	110	22	22	21.76	17,400	3480
10	h	30	10	5.51E-02	5.17E-02	1.22E-03	1300	680	140	17	17	0.19	11,000	110	22	22	21.76	17,400	3480
11	i	30	10	NA	NA	0.00E+00	1300	680	140	17	17	0.19	11,000	110	22	22	21.76	17,400	3480
12	j	30	10	5.61E-02	5.63E-02	1.31E-03	1300	680	140	17	17	0.19	11,000	110	22	22	21.76	17,400	3480
13	k	30	10	2.97E-03	4.65E-04	3.12E-05	1300	680	140	17	17	0.19	11,000	110	22	22	21.76	17,400	3480
14	l	30	10	5.58E-02	5.61E-02	1.31E-03	1300	680	140	17	17	0.19	11,000	110	22	22	21.76	17,400	3480
15	m	30	10	NA	NA	0.00E+00	1300	680	140	17	17	0.19	11,000	110	22	22	21.76	17,400	3480
16	n	30	10	1.95E-02	2.74E-03	2.82E-05	1300	680	140	17	17	0.19	11,000	110	22	22	21.76	17,400	3480
17	o	30	10	1.95E-02	2.74E-03	2.82E-05	1300	680	140	17	17	0.19	11,000	110	22	22	21.76	17,400	3480
18	p	30	10	1.95E-02	2.74E-03	2.82E-05	1300	680	140	17	17	0.19	11,000	110	22	22	21.76	17,400	3480
19	q	30	10	8.94E-03	5.79E-04	1.68E-05	1300	680	140	17	17	0.19	11,000	110	22	22	21.76	17,400	3480
20	q1	30	10	8.94E-03	5.79E-04	1.68E-05	1300	680	140	17	17	0.19	11,000	110	22	22	21.76	17,400	3480
21	r	30	10	1.80E-02	5.32E-04	2.89E-05	1300	680	140	17	17	0.19	11,000	110	22	22	21.76	17,400	3480
22	s	30	10	2.97E-02	2.42E-03	2.12E-05	1300	680	140	17	17	0.19	11,000	110	22	22	21.76	17,400	3480
23	t	30	10	3.73E-02	7.12E-03	1.66E-04	1300	680	140	17	17	0.19	11,000	110	22	22	21.76	17,400	3480
24	u	30	10	1.45E-02	7.99E-04	1.43E-05	1300	680	140	17	17	0.19	11,000	110	22	22	21.76	17,400	3480
25	v	30	10	6.28E-03	1.21E-03	3.86E-05	1300	680	140	17	17	0.19	11,000	110	22	22	21.76	17,400	3480
26																			
27																			
28																			
29																			

Figure 9-3. Toxicological Worksheet. (9 sheets)

	A	BB	BC	BD	BE	BF	BG	BH	BI	BJ	BK	BL	BM	BN	BO	BP	BQ	BR	BS
1	Case	meth. chl. ERPG-1 mg/m³	meth. chl. PEL-TWA mg/m³	TBP Headspace Conc. mg/m³	TBP ERPG-3 mg/m³	TBP ERPG-2 mg/m³	TBP ERPG-1 mg/m³	TBP PEL-TWA mg/m³	P_2O_5 Headspace Conc. mg/m³	P_2O_5 ERPG-3. mg/m³	P_2O_5 ERPG-2. mg/m³	P_2O_5 ERPG-1. mg/m³	P_2O_5 PEL-TWA mg/m³	NO_2 Headspace Conc. mg/m³	NO_2 ERPG-3 mg/m³	NO_2 ERPG-2 mg/m³	NO_2 ERPG-1 mg/m³	NO_2 PEL-TWA mg/m³	Acetonit. Headspace conc. mg/m³
2																			
3	a	700	174	11.6	50	15	3	2.5	3.75E+02	100	25	5	1	4.76E+01	94	47	3.8	3.5	21.81
4	b	700	174	11.6	50	15	3	2.5	1.84E+02	100	25	5	1	2.34E+01	94	47	3.8	3.5	21.81
5	c	700	174	11.6	50	15	3	2.5	3.75E+02	100	25	5	1	4.76E+01	94	47	3.8	3.5	21.81
6	d	700	174	11.6	50	15	3	2.5	3.75E+02	100	25	5	1	4.76E+01	94	47	3.8	3.5	21.81
7	e	700	174	11.6	50	15	3	2.5	1.21E+03	100	25	5	1	1.54E+02	94	47	3.8	3.5	21.81
8	f	700	174	11.6	50	15	3	2.5	3.77E+02	100	25	5	1	4.78E+01	94	47	3.8	3.5	21.81
9	g	700	174	11.6	50	15	3	2.5	1.21E+03	100	25	5	1	1.54E+02	94	47	3.8	3.5	21.81
10	h	700	174	11.6	50	15	3	2.5	3.77E+02	100	25	5	1	4.78E+01	94	47	3.8	3.5	21.81
11	i	700	174	11.6	50	15	3	2.5	0.00E+00	100	25	5	1	0.00E+00	94	47	3.8	3.5	21.81
12	j	700	174	11.6	50	15	3	2.5	3.83E+02	100	25	5	1	4.87E+01	94	47	3.8	3.5	21.81
13	k	700	174	11.6	50	15	3	2.5	1.32E+02	100	25	5	1	1.68E+01	94	47	3.8	3.5	21.81
14	l	700	174	11.6	50	15	3	2.5	3.82E+02	100	25	5	1	4.85E+01	94	47	3.8	3.5	21.81
15	m	700	174	11.6	50	15	3	2.5	0.00E+00	100	25	5	1	0.00E+00	94	47	3.8	3.5	21.81
16	n	700	174	11.6	50	15	3	2.5	8.64E+02	100	25	5	1	1.10E+02	94	47	3.8	3.5	21.81
17	o	700	174	11.6	50	15	3	2.5	8.64E+02	100	25	5	1	1.10E+02	94	47	3.8	3.5	21.81
18	p	700	174	11.6	50	15	3	2.5	8.64E+02	100	25	5	1	1.10E+02	94	47	3.8	3.5	21.81
19	q	700	174	11.6	50	15	3	2.5	3.05E+02	100	25	5	1	7.76E+01	94	47	3.8	3.5	21.81
20	q1	700	174	11.6	50	15	3	2.5	3.05E+02	100	25	5	1	7.76E+01	94	47	3.8	3.5	21.81
21	r	700	174	11.6	50	15	3	2.5	1.63E+02	100	25	5	1	4.15E+01	94	47	3.8	3.5	21.81
22	s	700	174	11.6	50	15	3	2.5	1.01E+03	100	25	5	1	1.29E+02	94	47	3.8	3.5	21.81
23	t	700	174	11.6	50	15	3	2.5	3.81E+02	100	25	5	1	4.83E+01	94	47	3.8	3.5	21.81
24	u	700	174	11.6	50	15	3	2.5	4.97E+02	100	25	5	1	6.31E+01	94	47	3.8	3.5	21.81
25	v	700	174	11.6	50	15	3	2.5	2.79E+02	100	25	5	1	3.54E+01	94	47	3.8	3.5	21.81
26																			
27																			
28																			
29																			

Figure 9-3. Toxicological Worksheet. (9 sheets)

	A	BT	BU	BV	BW	BX	BY	BZ	CA	CB	CC	CD	CE	CF	CG	CH	CI	CJ	CK
1	Case	Acetonit. ERPG-3 mg/m³	Acetonit. ERPG-2 mg/m³	Acetonit. ERPG-1 mg/m³	Acetonit. PEL-TWA mg/m³	prop. nit. Headspace conc. mg/m³	prop. nit. ERPG-3 mg/m³	prop. nit. ERPG-2 mg/m³	prop. nit. ERPG-1 mg/m³	prop. nit. PEL-TWA mg/m³	CO Headspace conc. mg/m³	CO ERPG-3 mg/m³	CO ERPG-2 mg/m³	CO ERPG-1 mg/m³	CO PEL-TWA mg/m³	benezene Headspace conc. mg/m³	benezene ERPG-3 mg/m³	benezene ERPG-2 mg/m³	benezene ERPG-1 mg/m³
2																			
3	a	60	20	3	3	10.47	60	20	3	3	3.67E+02	1360	690	230	40	1.32	3130	1565	78
4	b	60	20	3	3	10.47	60	20	3	3	1.80E+02	1360	690	230	40	1.32	3130	1565	78
5	c	60	20	3	3	10.47	60	20	3	3	3.67E+02	1360	690	230	40	1.32	3130	1565	78
6	d	60	20	3	3	10.47	60	20	3	3	3.67E+02	1360	690	230	40	1.32	3130	1565	78
7	e	60	20	3	3	10.47	60	20	3	3	1.19E+03	1360	690	230	40	1.32	3130	1565	78
8	f	60	20	3	3	10.47	60	20	3	3	3.69E+02	1360	690	230	40	1.32	3130	1565	78
9	g	60	20	3	3	10.47	60	20	3	3	1.19E+03	1360	690	230	40	1.32	3130	1565	78
10	h	60	20	3	3	10.47	60	20	3	3	3.69E+02	1360	690	230	40	1.32	3130	1565	78
11	i	60	20	3	3	10.47	60	20	3	3	0.00E+00	1360	690	230	40	1.32	3130	1565	78
12	j	60	20	3	3	10.47	60	20	3	3	3.75E+02	1360	690	230	40	1.32	3130	1565	78
13	k	60	20	3	3	10.47	60	20	3	3	1.29E+02	1360	690	230	40	1.32	3130	1565	78
14	l	60	20	3	3	10.47	60	20	3	3	3.74E+02	1360	690	230	40	1.32	3130	1565	78
15	m	60	20	3	3	10.47	60	20	3	3	0.00E+00	1360	690	230	40	1.32	3130	1565	78
16	n	60	20	3	3	10.47	60	20	3	3	8.47E+02	1360	690	230	40	1.32	3130	1565	78
17	o	60	20	3	3	10.47	60	20	3	3	8.47E+02	1360	690	230	40	1.32	3130	1565	78
18	p	60	20	3	3	10.47	60	20	3	3	8.47E+02	1360	690	230	40	1.32	3130	1565	78
19	q	60	20	3	3	10.47	60	20	3	3	5.99E+02	1360	690	230	40	1.32	3130	1565	78
20	q1	60	20	3	3	10.47	60	20	3	3	5.99E+02	1360	690	230	40	1.32	3130	1565	78
21	r	60	20	3	3	10.47	60	20	3	3	3.20E+02	1360	690	230	40	1.32	3130	1565	78
22	s	60	20	3	3	10.47	60	20	3	3	9.94E+02	1360	690	230	40	1.32	3130	1565	78
23	t	60	20	3	3	10.47	60	20	3	3	3.73E+02	1360	690	230	40	1.32	3130	1565	78
24	u	60	20	3	3	10.47	60	20	3	3	4.87E+02	1360	690	230	40	1.32	3130	1565	78
25	v	60	20	3	3	10.47	60	20	3	3	2.74E+02	1360	690	230	40	1.32	3130	1565	78
26																			
27																			
28																			
29																			

Figure 9-3. Toxicological Worksheet. (9 sheets)

	A	CL	CM	CN	CO	CP	CQ	CR	CS	CT	CU	CV	CW	CX	CY	CZ	DA	DB	DC
1	Case	benezene PEL-TWA mg/m³	butanol Headspace conc. mg/m³	butanol ERPG-3 mg/m³	butanol ERPG-2 mg/m³	butanol ERPG-1 mg/m³	butanol PEL-TWA mg/m³	dodecane Headspace conc. mg/m³	dodecane ERPG-3 mg/m³	dodecane ERPG-2 mg/m³	dodecane ERPG-1 mg/m³	dodecane PEL-TWA mg/m³	2-hexano Headspace conc. mg/m³	2-hexano ERPG-3 mg/m³	2-hexano ERPG-2 mg/m³	2-hexano ERPG-1 mg/m³	2-hexano PEL-TWA mg/m³	N_2O Headspace conc. mg/m³	N_2O ERPG-3 mg/m³
2																			
3	a	3	164.13	7500	750	75	75	296	7330	1450	37	37	2.68	5000	500	50	20	2340	36000
4	b	3	164.13	7500	750	75	75	296	7330	1450	37	37	2.68	5000	500	50	20	2340	36000
5	c	3	164.13	7500	750	75	75	296	7330	1450	37	37	2.68	5000	500	50	20	2340	36000
6	d	3	164.13	7500	750	75	75	296	7330	1450	37	37	2.68	5000	500	50	20	2340	36000
7	e	3	164.13	7500	750	75	75	296	7330	1450	37	37	2.68	5000	500	50	20	2340	36000
8	f	3	164.13	7500	750	75	75	296	7330	1450	37	37	2.68	5000	500	50	20	2340	36000
9	g	3	164.13	7500	750	75	75	296	7330	1450	37	37	2.68	5000	500	50	20	2340	36000
10	h	3	164.13	7500	750	75	75	296	7330	1450	37	37	2.68	5000	500	50	20	2340	36000
11	i	3	164.13	7500	750	75	75	296	7330	1450	37	37	2.68	5000	500	50	20	2340	36000
12	j	3	164.13	7500	750	75	75	296	7330	1450	37	37	2.68	5000	500	50	20	2340	36000
13	k	3	164.13	7500	750	75	75	296	7330	1450	37	37	2.68	5000	500	50	20	2340	36000
14	l	3	164.13	7500	750	75	75	296	7330	1450	37	37	2.68	5000	500	50	20	2340	36000
15	m	3	164.13	7500	750	75	75	296	7330	1450	37	37	2.68	5000	500	50	20	2340	36000
16	n	3	164.13	7500	750	75	75	296	7330	1450	37	37	2.68	5000	500	50	20	2340	36000
17	o	3	164.13	7500	750	75	75	296	7330	1450	37	37	2.68	5000	500	50	20	2340	36000
18	p	3	164.13	7500	750	75	75	296	7330	1450	37	37	2.68	5000	500	50	20	2340	36000
19	q	3	164.13	7500	750	75	75	296	7330	1450	37	37	2.68	5000	500	50	20	2340	36000
20	q1	3	164.13	7500	750	75	75	296	7330	1450	37	37	2.68	5000	500	50	20	2340	36000
21	r	3	164.13	7500	750	75	75	296	7330	1450	37	37	2.68	5000	500	50	20	2340	36000
22	s	3	164.13	7500	750	75	75	296	7330	1450	37	37	2.68	5000	500	50	20	2340	36000
23	t	3	164.13	7500	750	75	75	296	7330	1450	37	37	2.68	5000	500	50	20	2340	36000
24	u	3	164.13	7500	750	75	75	296	7330	1450	37	37	2.68	5000	500	50	20	2340	36000
25	v	3	164.13	7500	750	75	75	296	7330	1450	37	37	2.68	5000	500	50	20	2340	36000
26																			
27																			
28																			
29																			

Figure 9-3. Toxicological Worksheet. (9 sheets)

	A	DD	DE	DF	DG	DH	DI	DJ	DK	DL	DM	DN	DO	DP	DQ	DR	DS	DT	DU
1	Case	N_2O ERPG-2 mg/m³	N_2O ERPG-1 mg/m³	N_2O PEL-TWA mg/m³	tridecane Headspace conc. mg/m³	tridecane ERPG-3 mg/m³	tridecane ERPG-2 mg/m³	tridecane ERPG-1 mg/m³	tridecane PEL-TWA mg/m³	Ex.Unlikely Onsite Corrosives and Irritants Fraction	Ex. Unlikely Offsite Corrosives and Irritants Fraction	Unlikely Onsite Corrosives and Irritants Fraction	Unlikely Offsite Corrosives and Irritants Fraction	Anticipated Onsite Corrosives and Irritants Fraction	Anticipated Offsite Corrosives and Irritants Fraction	Ex. Unlikely Onsite Systemic Poisons Fraction	Ex. Unlikely Offsite Systemic Poisons Fraction	Unlikely Onsite Systemic Poisons Fraction	Unlikely Offsite Systemic Poisons Fraction
2																			
3	a	18000	270	90	388	7330	1450	37	37	1.66E-02	3.27E-04	6.78E-02	2.10E-03	4.36E-01	5.89E-03	2.10E-03	2.69E-05	5.58E-03	1.55E-04
4	b	18000	270	90	388	7330	1450	37	37	3.68E-02	3.45E-04	1.56E-01	2.37E-03	1.07E+00	5.23E-03	5.83E-03	3.61E-05	1.63E-02	2.22E-04
5	c	18000	270	90	388	7330	1450	37	37	1.66E-02	3.27E-04	6.78E-02	2.10E-03	4.36E-01	5.89E-03	2.10E-03	2.69E-05	5.58E-03	1.55E-04
6	d	18000	270	90	388	7330	1450	37	37	1.66E-02	3.27E-04	6.78E-02	2.10E-03	4.36E-01	5.89E-03	2.10E-03	2.69E-05	5.58E-03	1.55E-04
7	e	18000	270	90	388	7330	1450	37	37	4.13E-02	1.02E-03	1.61E-01	6.01E-03	9.43E-01	2.21E-02	3.67E-03	5.52E-05	8.67E-03	2.64E-04
8	f	18000	270	90	388	7330	1450	37	37	8.35E-02	3.19E-02	3.40E-01	2.05E-01	2.19E+00	5.75E-01	1.05E-02	2.62E-03	2.79E-02	1.51E-02
9	g	18000	270	90	388	7330	1450	37	37	4.13E-02	1.02E-03	1.61E-01	6.01E-03	9.43E-01	2.21E-02	3.67E-03	5.52E-05	8.67E-03	2.64E-04
10	h	18000	270	90	388	7330	1450	37	37	8.35E-02	3.19E-02	3.40E-01	2.05E-01	2.19E+00	5.75E-01	1.05E-02	2.62E-03	2.79E-02	1.51E-02
11	i	18000	270	90	388	7330	1450	37	37	0.00E+00	0.00E+00	0.00E+00	0.00E+00	0.00E+00	0.00E+00	0.00E+00	0.00E+00	0.00E+00	0.00E+00
12	j	18000	270	90	388	7330	1450	37	37	8.44E-02	3.45E-02	3.44E-01	2.22E-01	2.21E+00	6.24E-01	1.06E-02	2.82E-03	2.81E-02	1.62E-02
13	k	18000	270	90	388	7330	1450	37	37	7.29E-03	4.91E-04	3.14E-02	3.47E-03	2.22E-01	6.81E-03	1.27E-03	5.63E-05	3.60E-03	3.54E-04
14	l	18000	270	90	388	7330	1450	37	37	8.42E-02	3.44E-02	3.43E-01	2.21E-01	2.20E+00	6.22E-01	1.06E-02	2.81E-03	2.80E-02	1.62E-02
15	m	18000	270	90	388	7330	1450	37	37	0.00E+00	0.00E+00	0.00E+00	0.00E+00	0.00E+00	0.00E+00	0.00E+00	0.00E+00	0.00E+00	0.00E+00
16	n	18000	270	90	388	7330	1450	37	37	2.39E-02	1.32E-03	9.40E-02	7.95E-03	5.64E-01	2.75E-02	2.32E-03	8.00E-05	5.68E-03	4.07E-04
17	o	18000	270	90	388	7330	1450	37	37	2.39E-02	1.32E-03	9.40E-02	7.95E-03	5.64E-01	2.75E-02	2.32E-03	8.00E-05	5.68E-03	4.07E-04
18	p	18000	270	90	388	7330	1450	37	37	2.39E-02	1.32E-03	9.40E-02	7.95E-03	5.64E-01	2.75E-02	2.32E-03	8.00E-05	5.68E-03	4.07E-04
19	q	18000	270	90	388	7330	1450	37	37	1.57E-02	4.03E-04	6.22E-02	2.73E-03	4.21E-01	6.88E-03	2.54E-03	4.18E-05	6.45E-03	2.25E-04
20	q1	18000	270	90	388	7330	1450	37	37	1.57E-02	4.03E-04	6.22E-02	2.73E-03	4.21E-01	6.88E-03	2.54E-03	4.18E-05	6.45E-03	2.25E-04
21	r	18000	270	90	388	7330	1450	37	37	3.67E-02	5.05E-04	1.52E-01	3.58E-03	1.08E+00	7.42E-03	6.73E-03	6.01E-05	1.81E-02	3.51E-04
22	s	18000	270	90	388	7330	1450	37	37	3.55E-02	1.13E-03	1.39E-01	6.71E-03	8.24E-01	2.39E-02	3.30E-03	6.46E-05	7.94E-03	3.19E-04
23	t	18000	270	90	388	7330	1450	37	37	5.62E-02	4.37E-03	2.29E-01	2.81E-02	1.47E+00	7.90E-02	7.07E-03	3.58E-04	1.87E-02	2.06E-03
24	u	18000	270	90	388	7330	1450	37	37	2.02E-02	4.47E-04	8.13E-02	2.81E-03	5.11E-01	8.52E-03	2.33E-03	3.31E-05	6.03E-03	1.84E-04
25	v	18000	270	90	388	7330	1450	37	37	1.06E-02	8.49E-04	4.40E-02	5.62E-03	2.91E-01	1.43E-02	1.48E-03	7.76E-05	4.02E-03	4.61E-04
26																			
27																			
28																			
29																			

HNF-4240 Rev. 1

Figure 9-3. Toxicological Worksheet. (9 sheets)

	A	DV	DW	DX	DY	DZ	EA	EB	EC	ED	EE	EF	EG	EH	EI	EJ	EK	EL
1	Case	Anticipated Onsite Systemic Poisons Fraction	Anticipated Offsite Systemic Poisons Fraction	Ex. Unlikely Onsite Nervous system Fraction	Ex. Unlikely Offsite Nervous system Fraction	Unlikely Onsite Nervous system Fraction	Unlikely Offsite Nervous system Fraction	Anticipated Onsite Nervous system Fraction	Anticipated Offsite Nervous system Fraction	Ex. Unlikely Onsite Particulate Fraction	Ex. Unlikely Offsite Particulate Fraction	Unlikely Onsite Particulate Fraction	Unlikely Offsite Particulate Fraction	Anticipated Onsite Particulate Fraction	Anticipated Offsite Particulate Fraction	Ex. Unlikely Onsite HEPA Fraction	Ex. Unlikely Offsite HEPA Fraction	Unlikely Onsite HEPA Fraction
2																		
3	a	3.21E-02	2.50E-04	4.71E-04	1.04E-05	2.15E-03	3.69E-04	7.65E-02	5.92E-04	1.10E-02	5.29E-04	1.10E-01	8.81E-04	1.83E-01	2.64E-03	2.12E-04	3.60E-06	4.45E-03
4	b	1.00E-01	2.94E-04	1.58E-03	1.59E-05	7.19E-03	5.66E-04	2.56E-01	9.09E-04	1.80E-02	3.98E-04	1.80E-01	6.64E-04	3.00E-01	1.99E-03	2.12E-04	3.60E-06	4.45E-03
5	c	3.21E-02	2.50E-04	4.71E-04	1.04E-05	2.15E-03	3.69E-04	7.65E-02	5.92E-04	1.10E-02	5.29E-04	1.10E-01	8.81E-04	1.83E-01	2.64E-03	3.33E-02	5.67E-04	7.00E-02
6	d	3.21E-02	2.50E-04	4.71E-04	1.04E-05	2.15E-03	3.69E-04	7.65E-02	5.92E-04	1.10E-02	5.29E-04	1.10E-01	8.81E-04	1.83E-01	2.64E-03	3.33E-02	5.67E-04	7.00E-02
7	e	4.14E-02	6.69E-04	4.71E-04	1.37E-05	2.15E-03	4.87E-04	7.65E-02	7.83E-04	3.54E-02	2.26E-03	3.54E-01	3.76E-03	5.90E-01	1.13E-02	2.12E-04	3.60E-06	4.45E-03
8	f	1.61E-01	2.44E-02	2.36E-03	1.01E-03	1.07E-02	3.59E-02	3.82E-01	5.76E-02	5.51E-02	5.17E-02	5.51E-01	8.62E-02	9.19E-01	2.59E-01	2.12E-04	3.60E-06	4.45E-03
9	g	4.14E-02	6.69E-04	4.71E-04	1.37E-05	2.15E-03	4.87E-04	7.65E-02	7.83E-04	3.54E-02	2.26E-03	3.54E-01	3.76E-03	5.90E-01	1.13E-02	3.33E-02	5.67E-04	7.00E-02
10	h	1.61E-01	2.44E-02	2.36E-03	1.01E-03	1.07E-02	3.59E-02	3.82E-01	5.76E-02	5.51E-02	5.17E-02	5.51E-01	8.62E-02	9.19E-01	2.59E-01	2.12E-04	3.60E-06	4.45E-03
11	i	0.00E+00	0.00E+00	0.00E+00	0.00E+00	0.00E+00	0.00E+00	0.00E+00	0.00E+00	NA	NA	0.00E+00	0.00E+00	0.00E+00	0.00E+00	0.00E+00	0.00E+00	0.00E+00
12	j	1.61E-01	2.63E-02	2.36E-03	1.08E-03	1.07E-02	3.84E-02	3.82E-01	6.17E-02	5.61E-02	5.63E-02	5.61E-01	9.39E-02	9.35E-01	2.82E-01	4.45E-05	1.31E-07	1.59E-04
13	k	2.26E-02	4.37E-04	3.62E-04	2.58E-05	1.65E-03	9.19E-04	5.88E-02	1.48E-03	2.97E-03	4.65E-04	2.97E-02	7.74E-04	4.96E-02	2.32E-03	1.30E-02	3.82E-05	4.63E-02
14	l	1.61E-01	2.62E-02	2.36E-03	1.08E-03	1.07E-02	3.84E-02	3.82E-01	6.17E-02	5.58E-02	5.61E-02	5.58E-01	9.35E-02	9.31E-01	2.80E-01	1.30E-02	3.82E-05	4.63E-02
15	m	0.00E+00	0.00E+00	0.00E+00	0.00E+00	0.00E+00	0.00E+00	0.00E+00	0.00E+00	NA	NA	#VALUE!	#VALUE!	#VALUE!	#VALUE!	0.00E+00	0.00E+00	0.00E+00
16	n	2.89E-02	9.00E-04	3.62E-04	2.33E-05	1.65E-03	8.28E-04	5.88E-02	1.33E-03	1.95E-02	2.74E-03	1.95E-01	4.57E-03	3.24E-01	1.37E-02	7.57E-04	2.35E-06	2.84E-03
17	o	2.89E-02	9.00E-04	3.62E-04	2.33E-05	1.65E-03	8.28E-04	5.88E-02	1.33E-03	1.95E-02	2.74E-03	1.95E-01	4.57E-03	3.24E-01	1.37E-02	7.57E-04	2.35E-06	2.84E-03
18	p	2.89E-02	9.00E-04	3.62E-04	2.33E-05	1.65E-03	8.28E-04	5.88E-02	1.33E-03	1.95E-02	2.74E-03	1.95E-01	4.57E-03	3.24E-01	1.37E-02	7.57E-04	2.35E-06	2.84E-03
19	q	3.47E-02	4.33E-04	4.71E-04	1.39E-05	2.15E-03	4.95E-04	7.65E-02	7.95E-04	8.94E-03	5.79E-04	8.94E-02	9.65E-04	1.49E-01	2.89E-03	3.33E-02	5.67E-04	7.00E-02
20	q1	3.47E-02	4.33E-04	4.71E-04	1.39E-05	2.15E-03	4.95E-04	7.65E-02	7.95E-04	8.94E-03	5.79E-04	8.94E-02	9.65E-04	1.49E-01	2.89E-03	2.12E-04	3.60E-06	4.45E-03
21	r	1.06E-01	5.42E-04	1.58E-03	2.39E-05	7.19E-03	8.50E-04	2.56E-01	1.37E-03	1.60E-02	5.32E-04	1.60E-01	8.87E-04	2.67E-01	2.66E-03	3.33E-02	5.67E-04	7.00E-02
22	s	3.92E-02	7.53E-04	4.71E-04	1.75E-05	2.15E-03	6.22E-04	7.65E-02	9.99E-04	2.97E-02	2.42E-03	2.97E-01	4.03E-03	4.95E-01	1.21E-02	2.12E-04	3.60E-06	4.45E-03
23	t	1.08E-01	3.34E-03	1.58E-03	1.37E-04	7.19E-03	4.89E-03	2.56E-01	7.85E-03	3.73E-02	7.12E-03	3.73E-01	1.19E-02	6.21E-01	3.56E-02	2.12E-04	3.60E-06	4.45E-03
24	u	3.35E-02	3.28E-04	4.71E-04	1.18E-05	2.15E-03	4.20E-04	7.65E-02	6.75E-04	1.45E-02	7.99E-04	1.45E-01	1.33E-03	2.42E-01	4.00E-03	2.12E-04	3.60E-06	4.45E-03
25	v	2.39E-02	6.79E-04	3.62E-04	3.19E-05	1.65E-03	1.14E-03	5.88E-02	1.82E-03	6.28E-03	1.21E-03	6.28E-02	2.02E-03	1.05E-01	6.06E-03	1.30E-02	3.82E-05	4.63E-02
26																		
27																		
28																		
29																		

Figure 9-3. Toxicological Worksheet. (9 sheets)

	A	EM	EN	EO	EP	EQ	ER	ES	ET	EU	EV	EW	EX	EY	EZ	FA
1	Case	Unlikely Offsite HEPA Fraction	Anticipated Onsite HEPA Fraction	Anticipated Offsite HEPA Fraction	Ex. Un. Onsite Sum of Fractions Aqueous Boiloff	Ex. Un. Offsite Sum of Fractions Aqueous Boiloff	Unlikely Onsite Sum of Fractions Aqueous Boiloff	Unlikely Offsite Sum of Fractions Aqueous Boiloff	Anticipated Onsite Sum of Fractions Aqueous Boiloff	Anticipated Offsite Sum of Fractions Aqueous Boiloff	Ex. Un. Onsite Total Sum Of Fractions	Ex. Un. Offsite Total Sum Of Fractions	Unlikely Onsite Total Sum Of Fractions	Unlikely Offsite Total Sum Of Fractions	Anticipated Onsite Total Sum Of Fractions	Anticipated Offsite Total Sum Of Fractions
2																
3	a	6.99E-06	8.47E-03	1.99E-05	4.88E-04	8.80E-06	1.83E-03	1.14E-04	2.34E-02	1.14E-04	3.09E-02	9.05E-04	1.91E-01	3.63E-03	7.60E-01	9.50E-03
4	b	6.99E-06	8.47E-03	1.99E-05	1.04E-03	8.62E-06	3.91E-03	1.11E-04	5.01E-02	1.11E-04	6.35E-02	8.08E-04	3.68E-01	3.94E-03	1.79E+00	8.56E-03
5	c	1.10E-03	1.33E+00	3.13E-03	4.88E-04	8.80E-06	1.83E-03	1.14E-04	2.34E-02	1.14E-04	6.40E-02	1.47E-03	2.57E-01	4.72E-03	2.08E+00	1.26E-02
6	d	1.10E-03	1.33E+00	3.13E-03	4.88E-04	8.80E-06	1.83E-03	1.14E-04	2.34E-02	1.14E-04	6.40E-02	1.47E-03	2.57E-01	4.72E-03	2.08E+00	1.26E-02
7	e	6.99E-06	8.47E-03	1.99E-05	1.08E-03	2.56E-05	4.04E-03	3.31E-04	5.17E-02	3.31E-04	8.21E-02	3.38E-03	5.34E-01	1.09E-02	1.71E+00	3.52E-02
8	f	6.99E-06	8.47E-03	1.99E-05	1.68E-03	5.88E-04	6.28E-03	7.58E-03	8.04E-02	7.58E-03	1.53E-01	8.78E-02	9.41E-01	3.50E-01	3.74E+00	9.23E-01
9	g	1.10E-03	1.33E+00	3.13E-03	1.08E-03	2.56E-05	4.04E-03	3.31E-04	5.17E-02	3.31E-04	1.15E-01	3.94E-03	6.00E-01	1.20E-02	3.03E+00	3.83E-02
10	h	6.99E-06	8.47E-03	1.99E-05	1.68E-03	5.88E-04	6.28E-03	7.58E-03	8.04E-02	7.58E-03	1.53E-01	8.78E-02	9.41E-01	3.50E-01	3.74E+00	9.23E-01
11	i	0.00E+00	0.00E+00	0.00E+00	0.00E+00	0.00E+00	0.00E+00	0.00E+00	0.00E+00	0.00E+00	0.00E+00	0.00E+00	0.00E+00	0.00E+00	0.00E+00	0.00E+00
12	j	1.78E-06	2.12E-03	1.78E-06	1.79E-03	6.40E-04	6.39E-03	8.67E-03	8.52E-02	8.67E-03	1.55E-01	9.53E-02	9.50E-01	3.79E-01	3.77E+00	1.00E+00
13	k	5.18E-04	6.17E-01	5.18E-04	2.50E-04	1.39E-05	8.95E-04	1.89E-04	1.19E-02	1.89E-04	2.51E-02	1.09E-03	1.14E-01	6.23E-03	9.82E-01	1.18E-02
14	l	5.18E-04	6.17E-01	5.18E-04	1.78E-03	6.37E-04	6.36E-03	8.63E-03	8.48E-02	8.63E-03	1.68E-01	9.50E-02	9.93E-01	3.78E-01	4.38E+00	1.00E+00
15	m	0.00E+00	0.00E+00	0.00E+00	#DIV/0!	0.00E+00	#DIV/0!	0.00E+00	#DIV/0!	0.00E+00	0.00E+00	0.00E+00	0.00E+00	0.00E+00	0.00E+00	0.00E+00
16	n	3.03E-05	3.63E-02	3.03E-05	5.92E-04	3.11E-05	2.22E-03	4.01E-04	2.84E-02	4.01E-04	4.74E-02	4.20E-03	3.01E-01	1.42E-02	1.04E+00	4.39E-02
17	o	3.03E-05	3.63E-02	3.03E-05	5.92E-04	3.11E-05	2.22E-03	4.01E-04	2.84E-02	4.01E-04	4.74E-02	4.20E-03	3.01E-01	1.42E-02	1.04E+00	4.39E-02
18	p	3.03E-05	3.63E-02	3.03E-05	5.92E-04	3.11E-05	2.22E-03	4.01E-04	2.84E-02	4.01E-04	4.74E-02	4.20E-03	3.01E-01	1.42E-02	1.04E+00	4.39E-02
19	q	1.10E-03	1.33E+00	3.13E-03	5.43E-04	1.31E-05	2.04E-03	1.70E-04	2.61E-02	1.70E-04	6.15E-02	1.62E-03	2.32E-01	5.68E-03	2.04E+00	1.43E-02
20	q1	6.99E-06	8.47E-03	1.99E-05	5.43E-04	1.31E-05	2.04E-03	1.70E-04	2.61E-02	1.70E-04	2.84E-02	1.05E-03	1.67E-01	4.59E-03	7.16E-01	1.12E-02
21	r	1.10E-03	1.33E+00	3.13E-03	9.73E-04	1.21E-05	3.65E-03	1.56E-04	4.67E-02	1.56E-04	9.53E-02	1.70E-03	4.11E-01	6.93E-03	3.08E+00	1.53E-02
22	s	6.99E-06	8.47E-03	1.99E-05	9.02E-04	2.74E-05	3.38E-03	3.54E-04	4.33E-02	3.54E-04	7.01E-02	3.66E-03	4.54E-01	1.20E-02	1.49E+00	3.82E-02
23	t	6.99E-06	8.47E-03	1.99E-05	1.13E-03	8.08E-05	4.25E-03	1.04E-03	5.44E-02	1.04E-03	1.04E-01	1.21E-02	6.36E-01	4.80E-02	2.52E+00	1.27E-01
24	u	6.99E-06	8.47E-03	1.99E-05	5.29E-04	1.09E-05	1.99E-03	1.40E-04	2.54E-02	1.40E-04	3.83E-02	1.31E-03	2.41E-01	4.89E-03	8.97E-01	1.37E-02
25	v	5.18E-04	6.17E-01	5.18E-04	2.25E-04	1.54E-05	8.03E-04	2.09E-04	1.07E-02	2.09E-04	3.20E-02	2.22E-03	1.60E-01	9.96E-03	1.11E+00	2.36E-02
26																
27																
28																
29																

burn period, and masses burned during the vent are equal to the total mass burned for all but the puddle fire cases. Mass burned is a calculated output of POOLFIRE.4, as detailed in Appendix I.

Column K

Lists the fraction of reaction products vented during the outflow period for each case. The CO_2 is a reaction product tracked in POOLFIRE.4, and the fractional release from the tank is computed at each time step. The CO_2 release fraction, computed from POOLFIRE.4 output, is listed in this column.

Column L

Lists the headspace gas fraction, defined as the fraction of headspace vented from the tank during the outflow period for each fire case. The numbers are computed from POOLFIRE.4 output. The fraction of headspace gases vented is larger than the fraction of reaction products vented. The difference is that reaction products are formed during the burn, whereas headspace gases are present at maximum concentration at the beginning of the vent cycle.

Column M

The source concentration of P_2O_5, defined as the mass of P_2O_5 vented divided by the volume of gas vented, is calculated for each case. The mass of P_2O_5 formed was calculated as 4.32 percent of solvent mass burned (see Section 6.2.1). The EXCEL™ formula for Cell M3 is:

$$M3 = 0.0432 * J3 * K3 * 1E6\ (mg/kg)/(H3 * L3)$$

This formulation yields the average concentration during the release period. No attempt is made to compute the instantaneous release rate as a function of time.

Column N

The average source concentration of CO, defined as the mass of CO vented divided by the volume of gas vented, is calculated for each case. Based on an emission factor of 0.0425 kg/kg (Grigsby et al. 1995), the mass of CO formed is calculated to be 98 percent of the P_2O_5 mass. The EXCEL™ formula for Cell N3 is:

$$N3 = 0.98 * M3$$

Column O

Calculates the average source concentration of NO_2 vented divided by the volume of gas vented for each case. Based on an emission factor of

5.5E-3 kg/kg, (Grigsby et al. 1995), the mass of NO_2 formed is calculated to be 12.7 percent of the mass of P_2O_5 formed. The EXCEL™ formula for Cell O3 is:

$$O3 = 0.127 * M3$$

Column P

Lists atmospheric dilution factors at 100 m for each case. This factor accounts for turbulent mixing in the vicinity of the tank vent. For case A, the dilution factor is 2.60E-3 indicating that the airborne concentration at 100 m downwind would be 2.60E-3 times the concentration in vented gases. The basis for the dilution factors listed in this column are described in Appendix B.

Column Q

The carryover rate of aqueous waste, defined as mass vented divided by the time of the vent, is calculated for each case. The EXCEL™ equation for Cell Q3 is:

$$Q3 = O3\ (WSI) * 0.002 * K3/(I3 * 1.0)$$

The units of column Q are L/s; therefore, the above equation is based on the assumption of an aqueous density of 1.0 kg/L. This is conservative because actual waste liquids will be slightly more dense than water (dissolved material causes an increase in density).

The ARF has been assigned a value of 0.002. In terms of Equation 6-1 nomenclature, this EXCEL™ equation can be written as:

$$S/time = M * ARF * RF/(time * 1.0)$$

A multiplier of 0.5 was inserted into Cells Q19, Q20, and Q21 to reflect RF = 0.5 for aqueous boiloff.

Column R

Lists sums of fraction multipliers for aqueous waste for onsite exposure. These values are obtained from Table 3-8 of Van Keuren (1996b). These multipliers apply to a frequency range of 10E-4 to 10E-6 events per year which is extremely unlikely.

Column S

Lists sums of fraction multipliers for aqueous waste for offsite exposure. These values are obtained from Table 3-8 of Van Keuren (1996b). These multipliers apply to a frequency range of 10E-4 to 10E-6 events per year which is extremely unlikely.

Column T

Lists sums of fraction multipliers for aqueous waste for onsite exposure for a frequency range of 10^{-2} - 10^{-4} $year^{-1}$ which is unlikely. These values are obtained from Table 3-8 of Van Keuren (1996b).

Column U

Lists sums of fraction multipliers for aqueous waste for offsite exposure for a frequency range of 10^{-2} - 10^{-4} $year^{-1}$ which is unlikely. These values are obtained from Table 3-8 of Van Keuren (1996b).

Column V

Lists sum of fraction multipliers for aqueous waste for onsite exposure for a frequency range of 10^{0} - 10^{-2} $year^{-1}$ (anticipated). These values are obtained from Table 3-8 of Van Keuren (1996b).

Column W

Lists sums of fraction multipliers for aqueous waste for offsite exposure for a frequency range of 10^{0} - 10^{-2} $year^{-1}$ (anticipated). These values are obtained from Table 3-8 of Van Keuren (1996b).

Column X

Lists computed values of sums of fractions for aqueous waste, for an onsite receptor, for the extremely unlikely (10^{-4} - 10^{-6}) frequency category. Implicit in this calculation is the minimal atmospheric dilution factor based on a χ/Q^1 value of 0.0341. This χ/Q^1 value was used by Van Keuren (1996b) in quantifying the sum of fraction multipliers listed in columns R through W. The sums of fractions shown in this column are baseline values that are adjusted at a later stage in the calculation to account for turbulent mixing in the vicinity of the tank vent. The EXCEL™ equation for Cell X3 is:

$$X3 = Q3 * R3$$

Column Y

Lists computed values of sums of fractions for aqueous waste, for an offsite receptor, for the extremely unlikely (10^{-4} - 10^{-6}) frequency category. The EXCEL™ equation for Cell Y3 is:

$$Y3 = Q3 * S3$$

Column Z

The vent rate of gas from the tank, m^3/s, is calculated as the volume vented divided by the time of venting. The EXCEL™ equation for Cell Z3 is:

$$Z3 = H3 * L3/I3$$

Columns AA, AB, and AC

Compute onsite concentrations for P_2O_5, CO, and NO_2 by multiplying headspace concentrations by the atmospheric dilution factor. The EXCEL™ equations are:

$$AA3 = M3 * P3$$

$$AB3 = N3 * P3$$

$$AC3 = O3 * P3$$

A factor of 0.5 was inserted in Column AA, rows 19, 20, and 21 to reflect an RF = 0.5 for entrained fire cases. The EXCEL™ equation is:

$$AA20 = M3 * P3 * 0.5$$

Columns M, N, and O are source concentrations of these three contaminants, and column P lists atmospheric dilution factors at 100 m.

Column AD

A normalized onsite concentration is computed on the basis of a source concentration of 1 mg/mg^3. The EXCEL™ equation for Cell AD3 is:

$$AD3 = MIN(1 * P3, 0.0341 * 1 * Z3/(1 + Z3 * 0.0341))$$

This calculation selects the minimum value of downwind concentrations based on either the atmospheric dilution factors in column P or the dilution factor based on Equation 6-6B. As evident from comparing numbers in column P and column AD, atmospheric dilution factors in column P are selected as the minimum in every case.

Column AE

Computes soot concentration in vented gas as the mass of soot vented divided by the volume of gas vented. Soot formation is calculated as 20 percent of mass of solvent burned. The EXCEL™ equation for Cell AE3 is:

AE3 = 0.2 * J3 * K3 * 1E6 (mg/kg)/(H3 * L3)

A factor of 0.5 was inserted in Column AE, rows 19, 20, and 21 to reflect RF = 0.5 for entrained fire cases. The Excel™ equation is:

AE20 = 0.5 * 0.2 * J20 * K20 * 1E6 (mg/kg)/(H20*J20)

Note that column J contains masses of solvent burned.

Column AF

Computes onsite total particulate concentration as the sum of onsite concentrations of soot and P_2O_5. The EXCEL™ equation for Cell AF3 is:

AF3 = AA3 + AD3 * AE3

Note that column AA contains onsite concentrations of P_2O_5.

Column AG

Computes offsite total particulate concentration from Equation 6-6b, accounting for soot and P_2O_5. The EXCEL™ equation for Cell AG3 is:

AG3 = 2.83E-5 * (M3 + AE3) * Z3/(1 + Z3 * 2.83E-5)

A factor of 0.5 was introduced into the formula for column AG for rows 19, 20, and 21. The factor multiplies column M values which represent concentrations of P_2O_5. This change reflects RF = 0.5 for P_2O_5. The EXCEL™ equation is:

AG20 = 0.5 * 2.83E-5 * (M20 + AE20)*Z20/(1 + Z20 * 2.83E-5)

Columns AH, AI, AJ and AK.

List the onsite and offsite total particulate guideline limits. These guideline values are from Van Keuren (1996b).

Column AL

Calculates the ratio of onsite particle concentration to the extremely unlikely guideline limit ERPG-3 for each case. The EXCEL™ equation for Cell AL3 is:

AL3 = AF3/AH3

Column AM

Calculates the ratio of offsite particle concentration to the extremely unlikely guideline limit (ERPG-2) for each case. The EXCEL™ equation for Cell AM3 is:

AM3 = AG3/AI3

Column AN

Computes offsite concentration for a source concentration of 1 mg/m^3 using Equation 6-6b. The EXCEL™ equation for Cell AN3 is:

AN3 = 2.83E-5 * 1 * Z3/(1 + Z3 * 2.83E-5)

Columns AO Through BR

List assumed headspace concentrations before a solvent fire and ERPG-3, ERPG-2, ERPG-1, and PEL-TWA guidelines for gases in the corrosives and irritants category. These data are from Van Keuren (1996b).

Column BI lists the headspace concentration of P_2O_5 and repeats column M. It is repeated to collect all corrosives and irritants into one section for easy comparison. Likewise, column BN lists the headspace concentration of NO_2, repeating column O. Note that P_2O_5 and NO_2 are reaction products, but other gases in this category are headspace gases that were present before a fire.

Columns BS through CG

List the headspace concentrations and guideline limits for the identified analytes in the systemic poison category. These numbers are from Van Keuren (1996b). Column CC repeats column N and lists source concentrations of CO for each case. The CO, a fire reaction product, is listed in this column to bring all systemic poisons together for easy comparison.

Columns CH through DK

List headspace concentrations before a fire and guideline limits for identified analytes in the central nervous system toxin category. These numbers are from Van Keuren (1996b).

Column DL

Calculates the sum of fractions for corrosives and irritants onsite using Equation 6-8. Onsite concentration is calculated by multiplying source concentration by the onsite normalized concentration (calculated in column AD). The EXCEL™ equation for Cell DL3 is:

$$DL3 = AD3 * (AO3/AP3 + AT3/AU3 + AY3/AZ3 + BD3/BE3 + BI3/BJ3 + BN3/BO3)$$

The denominator in each fraction is the ERPG-3 value. This sum of fractions is appropriate for onsite and a frequency range of 10^{-4} - 10^{-6} year^{-1}, the extremely unlikely category.

Column DM

Calculates the sum of fractions for corrosives and irritants offsite using Equation 6-8. Offsite concentration is calculated by multiplying source concentration by the offsite normalized concentration (calculated in column AN). The EXCEL™ equation for Cell DM3 is:

$$DM3 = AN3 * (AO3/AQ3 + AT3/AV3 + AY3/BA3 + BD3/BF3 + BI3/BK3 + BN3/BP3)$$

The denominator in each fraction is the ERPG-2 value. This sum of fractions is appropriate for offsite and a frequency range of 10^{-4} - 10^{-6} year^{-1}, the extremely unlikely category.

Column DN

Calculates the sum of fractions for corrosives and irritants onsite, unlikely (10^{-2} - 10^{-4} year^{-1}), frequency category. The EXCEL™ equation for Cell DN3 is:

$$DN3 = AD3 * (AO3/AQ3 + AT3/AV3 + AY3/BA3 + BD3/BF3 + BI3/BK3 + BN3/BP3)$$

The denominator in each fraction is the ERPG-2 value, which is the appropriate guideline for the unlikely, onsite category.

Column DO

Calculates the sum of fractions for corrosives and irritants for the offsite, unlikely (10^{-2} - 10^{-4} year^{-1}), frequency category. The EXCEL™ equation for Cell DO3 is:

$$DO3 = AN3 * (AO3/AR3 + AT3/AW3 + AY3/BB3 + BD3/BG3 + BI3/BL3 + BN3/BQ3)$$

The denominator in each fraction is the ERPG-1 value, the appropriate guideline for the unlikely, offsite category.

Column DP

Calculates the sum of fractions for corrosives and irritants for the onsite, anticipated (10^{-0} - 10^{-2} year^{-1}), frequency category. The EXCEL™ equation for Cell DP3 is:

$$DP3 = AD3 * (AO3/AR3 + AT3/AW3 + AY3/BB3 + BD3/BG3 + BI3/BL3 + BN3/BQ3)$$

The denominator in each fraction is the ERPG-1 value, the appropriate guideline for the anticipated, onsite category.

Column DQ

Calculates the sum of fractions for corrosives and irritants for the offsite, anticipated (10^{-0} - 10^{-2} year^{-1}), frequency category. The EXCEL™ equation for Cell DQ3 is:

$$DQ3 = AN3 * (AO3/AS3 + AT3/AX3 + AY3/BC3 + BD3/BH3 + BI3/BM3 + BN3/BR3)$$

The denominator in each fraction is the PEL-TWA value, the appropriate guideline for the anticipated, offsite category.

Column DR

Calculates the sum of fractions for systemic poisons onsite, using Equation 6-8. Onsite concentration is calculated by multiplying source concentration by the onsite normalized concentration (calculated in column AD). The EXCEL™ equation for Cell DR3 is:

$$DR3 = AD3 * (BS3/BT3 + BX3/BY3 + CC3/CD3)$$

The denominator in each fraction is the ERPG-3 value. This sum of fractions is appropriate for onsite and a frequency range of 10^{-4} - 10^{-6} year^{-1}, the extremely unlikely category.

Column DS

Calculates the sum of fractions for systemic poisons offsite, using Equation 6-8. Offsite concentration is calculated by multiplying source concentration by the offsite normalized concentration(calculated in column AN). The EXCEL™ equation for Cell DS3 is:

DS3 = AN3 * (BS3/BU3 + BX3/BZ3 + CC3/CE3)

The denominator in each fraction is the ERPG-2 value. This sum of fractions is appropriate for offsite and a frequency range of 10^{-4} - 10^{-6} $year^{-1}$, the extremely unlikely category.

Column DT

Calculates the sum of fractions for systemic poisons for the onsite, unlikely (10^{-2} - 10^{-4} $year^{-1}$) frequency category. The EXCEL™ equation for Cell DT3 is:

DT3 = AD3 + (BS3/BU3 + BX3/BZ3 + CC3/CE3)

The denominator in each fraction is the ERPG-2 value, the appropriate guideline for the unlikely, onsite category.

Column DU

Calculates the sum of fractions for systemic poisons for the offsite, unlikely (10^{-2} - 10^{-4} $year^{-1}$) frequency category. The EXCEL™ equation for Cell DU3 is:

DU3 = AN3 * (BS3/BV3 + BX3/CA3 + CC3/CF3)

The denominator in each fraction is the ERGP-1 value, the appropriate guideline for the unlikely, offsite category.

Column DV

Calculates the sum of fractions for systemic poisons for the onsite, anticipated (10^{-0} - 10^{-2} $year^{-1}$) frequency category. The EXCEL™ equation for Cell DV3 is:

DV3 = AD3 * (BS3/BV3 + BX3/CA3 + CC3/CF3)

The denominator in each fraction is the ERPG-1 value, the appropriate guideline for the anticipated, onsite category.

Column DW

Calculates the sum of fractions for systemic poisons for the offsite, anticipated (10^{-0} - 10^{-2} $year^{-1}$) frequency category. The EXCEL™ equation for Cell DW3 is:

$$DW3 = AN3 * (BS3/BW3 + BX3/CB3 + CC3/CG3)$$

The denominator in each fraction is the PEL-TWA value, the appropriate guideline for the anticipated, offsite category.

Column DX

Calculates the sum of fractions for central nervous system toxins onsite, using Equation 6-8. Onsite concentration is calculated by multiplying source concentration by the onsite normalized concentration (calculated in column AD). The EXCEL™ equation for Cell DX3 is:

$$DX3 = AD3 * (CH3/CI3 + CM3/CN3 + CR3/CS3 + CW3/CX3 + DB3/DC3 + DG3/DH3)$$

The denominator in each fraction is the ERPG-3 value. This sum of fractions is appropriate for onsite and a frequency range of 10^{-4} - 10^{-6} $year^{-1}$, the extremely unlikely category.

Column DY

Calculates the sum of fractions for central nervous system toxins offsite, using Equation 6-8. Offsite concentration is calculated by multiplying source concentration by offsite normalized concentration (calculated in column AN). The EXCEL™ equation for Cell DY3 is:

$$DY3 = AN3 * (CH3/CJ3 + CM3/CO3 + CR3/CT3 + CW3/CY3 + DB3/DD3 + DG3/DI3)$$

The denominator in each fraction is the ERPG-2 value. This sum of fractions is appropriate for offsite and a frequency range of 10^{-4} - 10^{-6} $year^{-1}$, the extremely unlikely category.

Column DZ

Calculates the sum of fractions for central nervous system toxins for the onsite, unlikely (10^{-2} - 10^{-4} $year^{-1}$) frequency category. The EXCEL™ equation for Cell DZ3 is:

$$DZ3 = AD3 * (CH3/CJ3 + CM3/CO3 + CR3/CT3 + CW3/CY3 + DB3/DD3 + DG3/DI3)$$

The denominator in each fraction is the ERPG-2 value, the appropriate guideline for the unlikely, onsite category.

Column EA

Calculates the sum of fractions for central nervous system toxins for the offsite, unlikely (10^{-2} - 10^{-4} year^{-1}) frequency category. The EXCEL™ equation for Cell EA3 is:

$$EA3 = AN3 * (CH3/CK3 + CM3/CP3 + CR3/CU3 + CW3/CZ3 + DB3/DE3 + DG3/DJ3)$$

The denominator in each fraction is the ERPG-1 value, the appropriate guideline for the unlikely, offsite category.

Column EB

Calculates the sum of fractions for central nervous system toxins for the onsite, anticipated (10^{-0} - 10^{-2} year^{-1}) frequency category. The EXCEL™ equation for Cell EB3 is:

$$EB3 = AD3 * (CH3/CK3 + CM3/CP3 + CR3/CU3 + CW3/CZ3 + DB3/DE3 + DG3/DJ3)$$

The denominator in each fraction is the ERPG-1 value, the appropriate guideline for the anticipated, onsite category.

Column EC

Calculates the sum of fractions for central nervous system toxins for the offsite, anticipated (10^{-0} - 10^{-2} year^{-1}) frequency category. The EXCEL™ equation for Cell EC3 is:

$$EC3 = AN3 * (CH3/CL3 + CM3/CQ3 + CR3/CV3 + CW3/DA3 + DB3/DF3 + DG3/DK3)$$

The denominator in each fraction is the PEL-TWA value, the appropriate guideline for the anticipated, offsite category.

Column ED

Repeats column AL and lists onsite, extremely unlikely particulate fraction for each case. This column is repeated to exhibit the particulate fraction on the same page where other toxin categories are

summed. This fraction is calculated using ERPG-3 limits; therefore, this column applies to a frequency range of 10^{-4} - 10^{-6} $year^{-1}$, the extremely unlikely category.

Column EE

Repeats of column AM and lists offsite, extremely unlikely particulate fraction for each case. This column is repeated to exhibit the particulate fraction on the same page where other toxin categories are summed. This fraction was based on ERPG-2 values; therefore, this column applies to a frequency range of 10^{-4} - 10^{-6} $year^{-1}$ the extremely unlikely category.

Column EF

Calculates the sum of fractions for total particulate toxin for the onsite, unlikely (10^{-2} - 10^{-4} $year^{-1}$) frequency category. The EXCEL™ equation for Cell EF3 is:

EF3 = AF3/AI3

This equation calculates the ratio of onsite total particulate concentration (column AF) to ERPG-2 guideline concentration (column AI). ERPG-2 is the applicable guideline for the onsite, unlikely frequency category.

Column EG

Calculates the sum of fractions for total particulate toxin for the offsite, unlikely (10^{-2} - 10^{-4} $year^{-1}$) frequency category. The EXCEL™ equation for Cell EG3 is:

EG3 = AG3/AJ3

This equation calculates the ratio of offsite total particulate concentration (column AG) to ERPG-1 guideline concentration (column AJ). ERPG-1 is the applicable guideline for the offsite, unlikely frequency category.

Column EH

Calculates the sum of fractions for total particulate toxin for the onsite, anticipated (10^{-0} - 10^{-2} $year^{-1}$) frequency category. The EXCEL™ equation for Cell EH3 is:

EH3 = AF3/AJ3

This equation calculates the ratio of onsite total particulate concentration (column AF) to ERPG-1 guideline concentration (column AJ). ERPG-1 is the applicable guideline for the onsite, anticipated frequency category.

Column EI

Calculates the sum of fractions for total particulate toxin for the offsite, anticipated (10^{-0} - 10^{-2} $year^{-1}$) frequency category. The EXCEL™ equation for Cell EI3 is:

$$EI3 = AG3/AK3$$

This equation calculates the ratio of offsite total particulate concentration (column EI) to PEL-TWA guideline concentration (column AK). PEL-TWA is the applicable guideline for the offsite, anticipated frequency category.

Columns EJ through EO

The sum of fractions (SOFs) for HEPA filter ruptures are listed in Columns EJ through EO. To change the total SOFs to reflect the new ventilation system inventories, change columns EJ through EO. The new sums of fractions for HEPA filter rupture are calculated on a spreadsheet titled Calculate New SOFs, which is included in Appendix K of this document. The new SOFs are entered in columns EJ through EO of the main spreadsheet in Section 9.0 of this document. The SOFs are calculated using the following formula:

$$SOF = SOF\ multiplier \times release\ rate$$

where:

SOF	=	Sum of fractions is a dimensionless number.
SOF Multiplier	=	Has different values in seconds/liter for different wastes. Values taken from Table 8-4 in this document.
Release Rate	=	Calculated by dividing volume of waste released by release time. Units are Liters/seconds. In all cases a release time of 60 sec is used. Release volumes are taken from document HNF-SD-WM-CN-099, Rev. 1A, and are rounded to 2.0 L and 3.7 L.

Column EJ

Lists the onsite, extremely unlikely sum of fractions for HEPA rupture.

The sum of fraction multipliers used to calculate the listed fractions apply to an accident frequency of 10^{-4} - 10^{-6} year^{-1}; therefore, the results shown in this column apply to the onsite extremely unlikely category.

Column EK

Lists the offsite, extremely unlikely sum of fractions for HEPA rupture.

The sum of fraction multipliers used to calculate the listed fractions apply to an accident frequency of 10^{-4} - 10^{-6} year^{-1}; therefore, the results shown in this column apply to the offsite extremely unlikely category.

Column EL

Lists the sum of fractions for HEPA rupture, onsite, for a frequency range of 10^{-2} - 10^{-4} year^{-1}, the unlikely category.

The sum of fraction multipliers used to calculate the listed fractions apply to the onsite, unlikely category; therefore, the results listed in column EL apply to the onsite, unlikely (10^{-2} - 10^{-4} year^{-1}) frequency category.

Column EM

Lists the sum of fractions for HEPA rupture, offsite, for a frequency range of 10^{-2} - 10^{-4} year^{-1}, the unlikely category.

The sum of fraction multipliers used to calculate the listed fractions apply to the offsite, unlikely category. Thus the results listed in column EM apply to the offsite, unlikely (10^{-2} - 10^{-4} year^{-1}) frequency category.

Column EN

Lists the sums of fractions for HEPA rupture, onsite, for the anticipated category.

The sum of fraction multipliers used to calculate the listed fractions apply to the onsite, anticipated (10^{-0}- 10^{-2} year^{-1}) frequency category.

Column EO

Lists the sums of fractions for HEPA rupture, offsite, for the anticipated category. The sum of fraction multipliers used to calculate the listed fractions apply to the offsite, anticipated (10^{-0} - 10^{-2} year^{-1}) frequency category.

Column EP

Lists the sum of fractions for aqueous boil off, onsite, for a frequency range of 10^{-4} - 10^{-6} $year^{-1}$. The concentration of aerosolized waste at the 100 m downwind location has been calculated to account for turbulent mixing in the atmosphere in the vicinity of the tank vent. The EXCEL™ formula for Cell EP3 is:

$$EP3 = X3 * P3/(Z3 * 0.0341)$$

The value of Cell X3 is the sum of fractions for aqueous waste based on a χ/Q^1 atmospheric dispersion factor of 0.031 s/m^3, applied to a waste release rate expressed in L/s. The quantity that multiplies X3, P3/(Z3 * 0.0341), adjusts the sum of fractions, X3, to account for dilution based on jet mixing. The technical basis for this adjustment factor is presented in Appendix B.

Column EQ

Lists the sum of fractions for aqueous boiloff, offsite, for a frequency range of 10^{-4} - 10^{-6} $year^{-1}$. The numbers shown are copied from Column Y and are reproduced here to exhibit the aqueous boiloff sum of fractions on the same page where other toxin category sums are shown.

Offsite sums of fractions were not recalculated to reflect jet mixing in the vicinity of the tank vent.

Column ER

This column calculates sums of fractions for aqueous boiloff toxins for the onsite, unlikely category. The EXCEL™ equation for Cell ER3 is:

$$ER3 = Q3 * T3 * P3/(Z3 * 0.0341)$$

This formula accounts for jet mixing in the vicinity of the tank vent (column P factor). The technical basis for this formula is described in Appendix B. The sum of fractions multiplier (column T) used in this column applies to the onsite, unlikely (10^{-2} - 10^{-4} $year^{-1}$) frequency category.

Column ES

Calculates sums of fractions for aqueous boiloff toxins for the offsite, unlikely category. The EXCEL™ equation for Cell ES3 is:

$$ES3 = Q3 * U3$$

Q3 is the vent rate in L/s, and U3 is the sum of fractions multiplier (s/L) for the offsite, unlikely (10^{-2} - 10^{-4} $year^{-1}$) frequency category. The turbulent mixing in the vicinity of the tank vent has not been accounted for in calculating offsite consequences.

Column ET

Calculates sums of fractions for aqueous boiloff toxins for the onsite, anticipated category. The EXCEL™ equation for Cell ET3 is:

$$ET3 = Q3 * V3 * P3/(Z3 * 0.0341)$$

This formula accounts for jet mixing in the vicinity of the tank vent (column P factor). The technical basis for this formula is described in Appendix B. The sum of fraction multiplier (column V) applies to the onsite, anticipated (10^{-0} - 10^{-2} $year^{-1}$) frequency category.

Column EU

Calculates sums of fractions for aqueous boiloff toxins for the offsite, anticipated category. The EXCEL™ equation for Cell EU3 is:

$$EU = Q3 * W3$$

Q3 is the vent rate in L/s, and W3 is the sum of fractions multiplier (s/L) for the offsite, anticipated (10^{-0} - 10^{-2} $year^{-1}$) frequency category. The turbulent mixing in the vicinity of the tank vent has not been accounted for in calculating offsite consequences.

Column EV

Sums the sums of fractions for toxins in the several classes for the onsite, extremely unlikely (10^{-4} - 10^{-6} $year^{-1}$) category. The EXCEL™ equation for Cell EV3 is:

$$EV3 = DL3 + DR3 + DX3 + ED3 + EJ3 + EP3$$

The several classes of toxins are:

Column DL: corrosives and irritants
Column DR: systemic poisons
Column DX: central nervous system poisons
Column ED: total particulates
Column EJ: HEPA filter released contaminants
Column EP: Aqueous Waste Boiloff

Each column cited above applies to the onsite, extremely unlikely category.

Column EW

Sums the sums of fractions for the offsite, extremely unlikely (10^{-4} - 10^{-6} $year^{-1}$) frequency category. The EXCEL™ equation for Cell EW3 is:

$$EW3 = DM3 + DS3 + DY3 + EE3 + EK3 + EQ3$$

Each column listed in the equation above applies to the offsite, extremely unlikely frequency category. The toxin classes are those identified in the text that describes column EV.

Column EX

Sums the sums of fractions for the onsite, unlikely (10^{-2} - 10^{-4} $year^{-1}$) frequency category. The EXCEL™ equation for Cell EX3 is:

$$EX3 = DN3 + DT3 + DZ3 + EF3 + EL3 + ER3$$

Each column listed in the equation for column EX applies to the onsite, unlikely frequency category. The toxin classes are those identified in the text that describes column EV.

Column EY

Sums the sums of fractions for the offsite, unlikely (10^{-2} - 10^{-4} $year^{-1}$) frequency category. The EXCEL™ equation for Cell EY3 is:

$$EY3 = DO3 + DU3 + EA3 + EG3 + EM3 + ES3$$

Each column listed in the equation for column EY applies to the offsite, unlikely frequency category. The toxin classes are those identified in the text that describes column EV.

Column EZ

Sums the sums of fractions for the onsite, anticipated (10^{-0} - 10^{-2} $year^{-1}$) frequency category. The EXCEL™ equation for Cell EZ3 is:

$$EZ3 = DP3 + DV3 + EB3 + EH3 + EN3 + ET3$$

Each column listed in the equation for column EZ applies to the onsite, anticipated category. The toxin classes are those identified in the text that describes column EV.

Column FA

Sums the sums of fractions for the offsite, anticipated (10^{-0} - 10^{-2} yr^{-1}) frequency category. The EXCEL™ equation for Cell FA3 is:

$$FA3 = DQ3 + DW3 + EC3 + EI3 + EO3 + EU3$$

Each column listed in the equation for column FA applies to the offsite, anticipated category. The toxin classes are those identified in the text that describes column EV.

This page intentionally left blank.

10.0 REFERENCES

Agnew, S. F., 1993, *Tank History Analysis: C-Farm and 103-C*, LAUR-93-1989, Los Alamos National Laboratory, Los Alamos, New Mexico.

Agnew, S. F., 1994, *Hanford Defined Wastes: Chemical and Radionuclide Compositions*, LAUR-94-2657, Rev. 2, Los Alamos National Laboratory, Los Alamos, New Mexico.

Akita, K., 1973, "Some Problems of Flame Spread Along a Liquid Surface," in *Fourteenth Symposium (International) on Combustion Proceedings*, The Combustion Institute, Pittsburgh, Pennsylvania.

Anderson, T. D., 1969, *Organics in 102-C Tank*, (internal letter to W. L. Godfrey, October 2), Atlantic Richfield Hanford Company, Richland, Washington.

Anderson, J. D., 1990, *A History of the 200 Area Tank Farms*, WHC-MR-0132, Westinghouse Hanford Company, Richland, Washington.

ANSI, 1998, *Airborne Release Fractions at Non-Reactor Nuclear Facilities*, ANSI/ANS-5.10, American Nuclear Society, LaGrange Park, Illinois.

Atherton, J. A., 1974, *Prediction of Liquor Retention in Saltcakes and Sludges*, ARH-CD-230, Atlantic Richfield Hanford Company, Richland, Washington.

Ayer, J. E., A. T. Clark, P. Loysen, M. Y. Ballinger, J. Mishima, P. Z. Owczarski, W. S. Gregory, and B. D. Nichols, 1988, *Nuclear Fuel Cycle Facility Accident Analysis Handbook*, NUREG 1320, U.S. Nuclear Regulatory Commission, Washington, D.C.

Babad, H., 1996, *Modeling Solvent Low End Vapor Losses During Waste Storage*, (internal letter 74E10-96-005 to E. J. Lipke, February 5), Westinghouse Hanford Company, Richland, Washington.

Babrauskas, V., 1988, *Burning Rates*, SFPE Handbook of Fire Protection Engineering, First Edition, National Fire Protection Association, Quincy, Massachusetts.

Ballinger, M. Y., P. C. Owczarski, K. Hashimoto, G. Nishio, S. Jordan, and W. Lindner, 1987, "Aerosols Released in Accidents in Reprocessing Plants," *Nuclear Technology*, Vol. 81, pp. 278-292.

Bajwa, J. K., and W. G. Farley, 1994, *Construction, Maintenance, and Operation Accident Analysis*, WHC-SD-WM-SARR-009, Rev. 0, Westinghouse Hanford Company, Richland, Washington.

Barelko, E. P., I. P. Solyanina, and Z. I. Tsvetkova, 1966, "Radiation-Chemical Stability of TBP in Hydrocarbon Solutions," *Atomic. Energy*. Vol. 21(4), pp. 281-5.

Barney, G. S., 1994, *The Solubilities of Significant Organic Compounds in HLW Tank Supernate Solutions*, WHC-SA-2565-FP, Westinghouse Hanford Company, Richland, Washington.

Beitel, G. A., 1977, *Exothermic Potential of Sodium Nitrate Saltcake*, ARH-LD-163, Atlantic Richfield Hanford Company, Richland, Washington.

Beyler, C., *and M. J. Peatross, 1997, Ventilation Effects on Compartment Fire Characterization*, Fire Safety Science-Proceedings of the Fifth International Symposium.

Borsheim, G. L., and N. W. Kirch, 1991, *Summary of Single-Shell Tank Waste Stability*, WHC-EP-0347, Westinghouse Hanford Company, Richland, Washington.

Braun, D. J., 1992, *Risk Assessment of Nitrogen Purge System for Rotary Mode Sampling Truck*, WHC-SD-WM-RA-006, Westinghouse Hanford Company, Richland, Washington.

Brevick, C. H., L. A. Gaddis, and W. W. Pickett, 1995, *Historical Tank-Content Estimate for the Northeast Quadrant of the Hanford 200 East Areas*, WHC-SD-WM-ER-349, Rev. 0A, Westinghouse Hanford Company, Richland, Washington.

Brevick, C.H., J. W. Funk, and J. L. Stroup, 1997a, *Historical Tank-Content Estimate for the Southwest Quadrant of the Hanford 200 West Area*, HNF-SD-WM-ER-352, Rev. 1, Fluor Daniel Northwest Inc. for Fluor Daniel Hanford, Inc., Richland, Washington.

Brevick, C.H., J. W. Funk, and J. L. Stroup, 1997b, *Historical Tank-Content Estimate for the Northwest Quadrant of the Hanford 200 West Area*, HNF-SD-WM-ER-351, Rev. 1, Fluor Daniel Northwest, Inc. for Fluor Daniel Hanford, Inc., Richland, Washington.

Brown, G. G., A. S. Foust, D. L. Katz, R. Schneidewind, R. R. White, W. P. Wood, G. M. Brown, L. E. Brownell, J. J. Martin, G. B. Williams, J. T. Banchero, and J. L. York, 1950, *Unit Operations*, John Wiley & Sons, Inc., New York, New York.

Bugaenko, L. T., M. G. Kuzmin, and L. S. Polak, 1993, *High Energy Chemistry*, Ellis Howood PTR, Prentice Hall, New York, New York.

Burger, L. L., 1955, *The Chemistry of Tributyl Phosphate - A Review*, HW-40910, General Electric Company, Richland, Washington.

Burger, L. L., 1958, "The Decomposition Reactions of Tributyl Phosphate and its Diluents and Their Effect on Uranium Recovery Processes," in *Progress in Nuclear Energy*, Series III, Vol. 2, Process Chemistry, Pergamon Press, New York, New York.

Burger, L. L., and E. D. McClanahan, 1958, "Tributyl Phosphate and Its Diluent Systems," *Industrial Engineering Chemistry*, Vol. 50(2), pp. 153-56.

Burr, J. G., 1958, "The Radiolysis of Tributyl Phosphate," *Radiation Research*, Vol. 8, p. 214.

Buxton, G. V., C. L. Greenstock, W. P. Helman, and A. B. Ross, 1988, "Critical Review of Rate Constants for Reactions of Hydrated Electrons, Hydrogen Atoms, and Hydroxyl Radicals (HO·/O-·) in Aqueous Solution," *Journal of Chemical Reference Data.*, Vol. 17(2), pp. 513-886.

Camaioni, D. M., W. D. Samuels, B. D. Lenihan, S. A. Clauss, A. K. Sharma, K. L. Wahl, and J. A. Campbell, 1996, *Organic Tanks Safety Program FY 96 Waste Aging Studies*, PNL-11312, Pacific Northwest National Laboratory, Richland, Washington.

Campbell, J. A., S. A. Clauss, K. E. Grant, F. V. Hoopes, B. D. Lerner, R. B. Lucke, G. M. Mong, J. K. Rau, and R. T. Steele, 1994, *Flammable Gas Safety Program; Analytical Methods Development: FY 1993 Progress Report*, PNL-9062, Pacific Northwest Laboratory, Richland, Washington.

Cowley, W. L, and D. D. Stepnewski, 1994, *Evaluation of Hazards to Tank Farm Facilities from Lightning Strikes*, WHC-SD-WM-SARR-027, Rev. 0, Westinghouse Hanford Company, Richland, Washington.

Cowley, W. L., 1996, *Development of Radiological Concentrations and Unit Liter Doses for TWRS FSAR Radiological Consequence Calculations*, WHC-SD-WM-SARR-037, Rev. 0, Westinghouse Hanford Company, Richland, Washington.

Cowley, W. L., and A. K. Postma, 1996, *Consequences of Postulated Solvent Fires in Hanford Site Waste Tanks*, WHC-SD-WM-CN-032, Rev. 0A, Westinghouse Hanford Company, Richland, Washington.

Eckhoff, 1991, *Dust Explosions in the Process Industries*, Butterworth-Heinemann, Oxford, England.

Epstein, M., and P.G. Ellison, 1988, "Correlations of the Rate of Removal of Coagulating and Depositing Aerosols for Application to Nuclear Reactor Safety Problems," *Nuclear Engineering & Design*, North Holland, Amsterdam.

Epstein, M., H. K. Fauske, M. D. Crippen, D. R. Dickinson, J. D. McCormack, R. J. Cash, J. E. Meacham, and C. S. Simmons, 1994, *Ferrocyanide Safety Program: Assessment of the Possibility of Ferrocyanide Sludge Dryout*, WHC-EP-0816, Westinghouse Hanford Company, Richland, Washington.

FAI, 1994, *Hazardous Assessment Techniques for Hanford Waste Tanks Presently or Previously Containing Liquid Organic Layers*, FAI/94-91, Fauske and Associates, Inc., Burr Ridge, Illinois.

FDH, 1999, *Organic Solvent Fire Authorization Basis Change Package, Contract Number DE-AC06-96RL13200*, (letter FDH-9950067 to J. C. Hall, February 2), Fluor Daniel Hanford, Inc., Richland, Washington.

Fink, D. G., and W. H. Beatty, 1976, *Standard Handbook for Electrical Engineers*, 12th Edition, McGraw-Hill, New York, New York.

General Electric Company, 1955, *Purex Technical Manual*, HW-31000, Richland, Washington.

Grigsby, J. M., and A. K. Postma, 1995, *Risk from Organic Solvent Fires in C-103 following Interim Stabilization*, WHC-SD-WM-SARR-001, Supplement 1, Rev. 0A, Westinghouse Hanford Company, Richland, Washington.

Glassman, I., and F. L. Dryer, 1980, "Flame Spreading Across Liquid Fuels," *Fire Safety Journal*, Vol. 3, pp. 123-138, Elsevier Sequoia S. A., Lausanne - Printed in the Netherlands.

Hall, J. C., 1972, *Safety Analysis - Storage of Organic Liquid in Underground Storage Tanks*, (internal letter to R. C. Roal, June 27), Atlantic Richfield Hanford Company, Richland, Washington.

Han, F.C., 1996, *Structural Integrity and Potential Failure Modes of Hanford High-Level Waste Tanks*, WHC-SD-TWR-RPT-002, Westinghouse Hanford Company, Rev. 0, Richland, Washington.

Handy, L. L., 1975, *Flow Properties of Saltcake for Interstitial Liquid Removal/Immobilization Development Program*, ARH-C-6, Atlantic Richfield Hanford Company, Richland, Washington.

Himes, D. A., 1998, *Radiological and Toxicological Analyses of Tank 241-C-106 Ventilation Systems*, HNF-SD-WM-CN-099, Rev. 1A, Fluor Daniel Northwest, Inc., Richland, Washington.

Hirano, T., T. Suzuki, J. Sato, and H. Ohtani, 1984, "Flame Spread Over Crude Oil Sludge," in *Twentieth Symposium (International) on Combustion Proceedings*, 1984 Symposium, The Combustion Institute, Pittsburgh, Pennsylvania.

House, H. O., 1972, *Modern Synthetic Reactions*, 2nd ed., The Organic Chemistry Monograph Series, Benjamin/Cummings Publishers, Menlo Park, California.

Huckaby, J. L., and D. S. Sklarew, 1997, *Screening for Organic Solvents in Hanford Waste Tanks Using Organic Vapor Concentrations*, PNNL-11698, Pacific Northwest National Laboratory, Richland, Washington.

Jeppson, D. w., and J. J. Wong, 1993, *Ferrocyanide Waste Simulant Characterization*, WHC-EP-0631, Westinghouse Hanford Company, Richland, Washington.

Jordan, S., and W. Lindner, 1983, "The Behavior of Burning Kerosene, Aerosol Formation and Consequences," in *CSNI Specialist Meeting on Interaction of Fire and Explosion with Ventilation Systems in Nuclear Facilities Proceedings*, April 25-28, 1983, Los Alamos, New Mexico.

Julyk, L. J., 1994, *Static Internal Pressure Capacity of Hanford Single-Shell Waste Tanks*, WHC-SD-WM-TI-623, Rev. 0, Westinghouse Hanford Company, Richland, Washington.

Keller, C. M., 1991, *Push Mode Core Sample Test Report*, WHC-SD-WM-TRP-048, Rev. 0, Westinghouse Hanford Company, Richland, Washington.

Kennedy, J., and S. S. Grimley, 1953, *Radioactive Studies with Phosphorus-32 Labelled Tri-n-butyl Phosphates*, CE/R-1284, Atomic Energy Research Enterprise, Harwell, United Kingdom.

Kirch, N. W., 1983, *PUREX Organic Waste*, SD-WM-TI-076, Rev. 0, Rockwell Hanford Operations, Richland, Washington.

Kirk, J. J., 1980, *Permeability, Porosity, and Capillarity of Hanford Waste Material and Its Limits of Pumpability*, RHO-CD-925, Rev. 2, Rockwell Hanford Operations, Richland, Washington.

Kuchta, J. M, 1985, *Investigation of Fire and Explosion Accidents in the Chemical, Mining, and Fuel Related Industries - A Manual*, Bulletin 680, U.S. Department of Interior, Bureau of Mines, Washington, D.C.

LANL, 1995, *A Safety Assessment for Prepared Pump Mixing Operations to Mitigate Episodic Gas Released in Tank 241-SY-101*, Rev. 14, Los Alamos National Laboratory, Los Alamos, New Mexico.

Lapple, C. E, 1943, "Isothermal Adiabataic Flow of Compressible Fluids," *Transactions American Institute Chemical Engineers*, Vol. 39, p. 385.

Lee, H. A., 1974, *Final Report - Program for Fire Protection, Caves, Canyons, and Hot Cells*, ARH-ST-104, Atlantic Richfield Hanford Company, Richland, Washington.

Leonard, J. T., C. R. Fulper, R. Darwin, G. G. Back, R. E. Burns, and R. Ouelette, 1992, *Fire Hazards of Mixed Fuels on the Flight Deck*, Naval Research Laboratory, Washington, D.C.

Lewis, B., and G. Von Elbe, 1987, *Combustion, Flames and Explosions of Gases*, Third Edition, Academic Press, Inc. New York, New York.

Lindberg, S. E., 1996, *Frequency Analysis of Vehicle Fuel Release Resulting in Waste Tank Fire*, WHC-SD-WM-CN-037, Rev. 0, Westinghouse Hanford Company, Richland, Washington.

Malet, J. C., G. Duverger de Cuy, R. Gasteiger, and K. Janberg, 1983, "Solvent Pool Fire Testing," in *CNI Specialist Meeting on Interaction of Fire and Explosion with Ventilation Systems in Nuclear Facilities Proceedings*, April 25-28, 1983, Los Alamos, New Mexico.

McAdams, W. H., 1954, *Heat Transmission*, McGraw-Hill, New York, New York.

Meacham, J. E., A. B. Webb, N. W. Kirch, J. A. Lechelt, D. A. Reynolds, G. S. Barney, D. M. Camaioni, F. Gao, R. T. Hallen, and P. G. Heasler, 1997, *Organic Complexant Topical Report*, HNF-SD-WM-CN-058, Rev. 1A, DE&S Hanford, Inc. for Fluor Daniel Hanford Inc., Richland, Washington.

Meisel, D., H. Diamond, E. P. Horwitz, M. S. Matheson, M. C. Sauer Jr., and J. C. Sullivan, 1991, *Radiation Chemistry of Synthetic Waste*, ANL-91/40, Argonne National Laboratory, Argonne, Illinois.

Meisel, D., C. D. Jonah, S. Kapoor, M. S. Matheson, and M. C. Sauer Jr., 1993, *Radiolytic and Radiolytically Induced Generation of Gases from Synthetic Wastes*, ANL-93/43, Argonne National Laboratory, Argonne, Illinois.

Merck & Company, 1989, *The Merck Index*, Eleventh Edition, Rahway, New Jersey.

Metz, W. P, 1975a, *Capillarity Demonstration*, (internal memorandum to R. C. Roal, March 26), atlantic Richfield Hanford Company, Richland, Washington.

Metz, W. P., 1975b, *Preliminary Evaluation of the Affects of Capillary Forces on Stabilizing Hanford Waste Saltcakes and Sludges*, (internal memorandum to R. J. Thompson, September 9), Atlantic Richfield Hanford Company, Richland, Washington.

Metz, W. P., 1976, *A Topical Report on Interstitial Liquid Removal from Hanford Saltcakes*, ARH-CD-545, Atlantic Richfield Hanford Company, Richland, Washington.

Mishima, J, 1994, *Recommended Values and Technical Bases for Airborne Release Fractions, Airborne Release Rates and Respirable Fractions for Materials from Accidents in DOE Fuel Cycle, Ex-Reactor Facilities*, DOE-HDBK-3010-94, Rev. 2, U.S. Department of Energy, Washington, D.C.

Moore, J. D. 1980, *PUREX Technical Manual*, RHO-MA-116, Rockwell Hanford Operations, Richland, Washington.

Noorani, Y. G., 1997a, *Tank Waste Remediation System Basis for Interim Operation*, HNF-SD-WM-BIO-001, Rev. 0-F, DE&S Hanford, Inc. for Fluor Daniel Hanford, Inc., Richland, Washington.

Noorani, Y. G., 1997b, *TWRS Technical Safety Requirements*, HNF-SD-WM-TSR-006, Rev. 0I, DE&S Hanford, Inc. for Fluor Daniel Hanford, Inc., Richland, Washington.

Neta, P., and R. E. Huie, 1986, "Rate Constants for Reactions of NO_3 Radicals in Aqueous Solutions," *Journal of Physical Chemistry*, Vol. 90, pp. 4,644-4,648.

NFPA, 1988, *SFPE Handbook of Fire Protection Engineering*, First Edition, National Fire Protection Association, Quincy, Massachusetts.

NFPA, 1991, *Standard on Basic Classification of Flammable and Combustible Liquids*, 321, National Fire Protection Association, Quincy, Massachusetts.

Pacific Northwest National Laboratory (PNNL). December 19, 1997. Tank Characterization Database, Version 2.1b.

Payne, M. A., 1994, *Revision of Organic Tanks Watch List*, letter #9453328 to R. E. Gerton, DOE-RL, May 13), Westinghouse Hanford Company, Richland, Washington.

Perry, J. H., Editor, 1963, *Chemical Engineers' Handbook*, Fourth Edition, McGraw-Hill, New York, New York.

Pool, K. H., and R. M. Bean, 1994, *Waste Tank Safety Project: Analysis of Liquid Samples from Hanford Waste Tank 241-C-1-3*, PNL-9403, Pacific Northwest Laboratory, Richland, Washington.

Postma, A. K., 1996, *Refinement of Solvent Fire Analysis Methodology*, LR-GP-96-068, G&P Consulting, Inc., Richland, Washington.

Postma, A. K., D. B. Bechtold, G. L. Borsheim, J. M. Grigsby, R. L. Guthrie, M. Kummerer, M. G. Plys, and D. A. Turner, 1994, *Safety Analysis of Exothermic Reaction Hazards Associated With the Organic Liquid Layer in Tank 241-C-103*, WHC-SD-WM-SARR-001, Rev. 0, Westinghouse Hanford Company, Richland, Washington.

Prosser, R. D., 1986, *Potential Hazards Associated with the Storage and Disposal of Hexone*, (letter R86-3175 to J. D. White, U. S. Department of Energy, Richland Operations Office, July 28), Rockwell Hanford Operations, Richland, Washington.

Public Law 101-510, 1990, "Safety Measures for Waste Tanks at Hanford Nuclear Reservation," Section 3137 of the *National Defense Authorization Act for Fiscal Year 1991*.

Quintiere, J. G., 1988, "Surface Flame Spread," *SFPE Handbook of Fire Protection Engineering*, National Fire Protection Association, Quincy, Massachusetts.

Scaief, C. C., 1991, *Hydrogen Ignition Capability of Tank Farm Instrumentation and Electrical Equipment*, WHC-SD-WM-ES-176, Rev. 0, Westinghouse Hanford Company, Richland, Washington.

Sederburg, J. P., and J. A. Reddick, 1994, *TBP and Diluent Mass Balances in the PUREX Plant at Hanford 1955 - 1991*, WHC-MR-0483, Rev. 0, Westinghouse Hanford Company, Richland, Washington.

Shinotake, A., S. Koda, and K. Akita, 1985, *An Experimental Study of Radiative Properties of Pool Fires of an Intermediate Scale*, Combustion Science and Technology, Vol. 43, pp. 85-97.

Siegel, R., and J. R. Howell, 1989, *Thermal Radiation Heat Transfer, Third Edition*, Hemisphere Publishing Corporation, Washington, D.C.

Simpson, B. C., 1994, *Tank 241-T-111 Characterization Report*, WHC-EP-0806, Westinghouse Hanford Company, Richland, Washington.

Takeno, K., and T. Hirano, 1986, "Flame Spread Over Porous Solids Soaked With a Combustible Liquid," in *Twenty-First Symposium (International) on Combustion Proceedings*, The Combustion Institute, Pittsburgh, Pennsylvania.

Thorne, P. F., 1983, "Principles of Fire and Explosion Protection," in *CSNI Specialist Meeting on Interaction of Fire and Explosion with Ventilation Systems in Nuclear Facilities Proceedings*, April 25-28, 1983, Los Alamos, New Mexico.

Toth, J. J., P. G. Heasler, M. E. Lerchen, J. G. Hill, and P. D. Whitney, 1995, *Analysis of Organic Carbon and Moisture in Hanford Single-Shell Tank Waste*, Pacific Northwest Laboratory, Richland, Washington.

Van Keuren, J. C., 1996a, *Tank Waste Compositions and Atmospheric Dispersion Coefficients for Use in Safety Analysis Consequence Assessments*, WHC-SD-WM-SARR-016, Rev. 2, Westinghouse Hanford Company, Richland, Washington.

Van Keuren, J. C., 1996b, *Toxic Chemical Considerations for Tank Farm Releases*, WHC-SD-WM-SARR-011, Rev. 2, Westinghouse Hanford Company, Richland, Washington.

Van Vleet, R. J., 1996, *Waste Tank Ventilation System Waste Material Accumulations*, WHC-SD-WM-CN-054, Rev. 0, Westinghouse Hanford Company, Richland, Washington.

Watkins, J. D., 1991, *Report to United States Congress on Waste Tank Safety Issues at the Hanford Site*, (letter to D. Quayle, President of the Senate, July 16), U.S. Department of Energy, Washington, D.C.

Walser, R. L., 1966, *Interim Evaluation of Purex Process Test - Normal Paraffin Hydrocarbon Diluent*, ISO-584, Isochem Inc., Richland, Washington.

WHC, 1994, *242-A Evaporator/Crystallizer Final Safety Analysis Report*, WHC-SD-WM-SAR-023, Rev. 2, Westinghouse Hanford Company, Richland, Washington.

WHC, 1996a, *Chemical and Chemically-Related Issues Associated with Sluicing Tank-C-106 Waste to Tank AY-102*, WHC-SD-WM-TI-756, Rev. 1, Westinghouse Hanford Company, Richland, Washington.

WHC, 1996b, *Structural Integrity and Potential Failure Modes of the Hanford High-Level Waste Tanks*, WHC-SD-TWR-RPT-002, Rev. 0, Westinghouse Hanford Company, Richland, Washington.

WHC, 1996c, *Structural Assessment of Accident Loads*, WHC-SD-WM-TI-775, Rev. 0, Westinghouse Hanford Company, Richland, Washington.

WHC-CM-4-46, *Nuclear Reactor Safety Analysis Manual*, Westinghouse Hanford Company, Richland, Washington.

Wilkinson, R. W., and T. F. Williams, 1961, "The Radiolysis of Tri-n-alkyl Phosphates," *Journal of the Chemical Society* (September), p. 4098.

Wood, B. D., P. L. Blackshear, Jr., and E. R. G. Eckert, 1971, "Mass Fire Model: An Experimental Study of the Heat Transfer to Liquid Fuel Burning from a Sand-Filled Pan Burner," *Combustion Science and Technology*, Vol. 4, pp. 113-129.

Yamaguchi, T., and K. Wakasa, 1986, *Oil Pool Fire Experiment*, *in Fire Safety Science*, *Proceedings of the First International Symposium*, 1986, pp. 11-918, Editors, C. E. Grant and P. J. Pagni, Hemisphere Publishing Corporation, a subsidiary of Harper and Row, Publishers, Inc., Washington, New York, and London.

Zabetakis, M. G., 1965, "Flammability Characteristics of Combustible Gases and Vapors," Bulletin 627, U.S. Department of the Interior, Bureau of Mines, Washington, D.C.

Zach, J. J., 1996, *Probability*, *Consequences and Mitigation for Lightning Strikes to Hanford Waste Tanks*, WHC-SD-WM-ES-387, Rev. 0, Westinghouse Hanford Company.

This page intentionally left blank.

APPENDIX A

SCREENING METHODOLOGY FOR SOLVENT FIRE RISK IN WASTE TANKS AT THE HANFORD SITE

This page intentionally left blank.

CONTENTS

1.0 INTRODUCTION A-5

2.0 SUMMARY AND CONCLUSIONS A-5
2.1 SUMMARY A-5
2.2 CONCLUSIONS A-6

3.0 OBJECTIVE AND SCOPE A-6
3.1 OBJECTIVE A-6
3.2 SCOPE A-6

4.0 TECHNICAL APPROACH A-7

5.0 SOLVENT POOL FIRE HAZARD PHENOMENOLOGY A-7

6.0 TRANSPORT MODELING OF SOLVENT EVAPORATION INTO HEADSPACE AIR A-8
6.1 WASTE CONFIGURATION ANALYZED A-8
6.2 MASS TRANSFER RATE OF VAPORS INTO HEADSPACE AIR A-10
6.2.1 Vapor Diffusion in Saltcake A-10
6.2.2 Mass Transport in Tank Headspace A-11
6.3 ESTIMATION OF POOL AREA A-12
6.3.1 Surface Pool Versus Submerged Liquid Lens A-12
6.3.2 Interfacial Concentration of Solvent Vapors A-13
6.3.3 Temperature at Solvent/Air Interface A-15
6.3.4 Mass Transfer Coefficient at Solvent-Air Interface . . . A-17
6.3.5 Ventilation Flow Rate A-19

7.0 RESULTS OF SCREENING A-20

8.0 REFERENCES A-20

LIST OF FIGURES

6-1 Schematic of Waste Configuration Analyzed A-9

LIST OF TABLES

6-1 Estimated Composition of NPH Components in Tank 241-C-103 Solvent . A-14

6-2 Constants for Equation A-9 . . . . . A-15

This page intentionally left blank.

1.0 INTRODUCTION

This appendix describes a means for identifying single-shell waste tanks (SSTs) that could contain a solvent pool larger than 1 m^2. The methodology involves using vapor characterization data and an evaporation model to estimate the size of solvent pools that feed vapors into tank vapor spaces. For tanks that fall below a derived pool area criterion, postulated pool fires could not challenge tank structural limits and would have consequences that fall below risk guidelines for the unlikely frequency category.

The solvents that are fire hazards originated from PUREX processing at the Hanford Site from 1955 to 1986 (Sederburg and Reddick 1994). The solvents were mixtures of hydrocarbon liquids (called diluents) and tributyl phosphate (TBP). Spent solvents ended up in a number of SSTs as waste products.

Recently obtained vapor characterization data (Huckaby and Sklarew 1997a) have shown that a number of hydrocarbon species initially present in diluents are present in tank headspaces. An implication of this finding is that a liquid phase is present in the tanks and is the source of a fraction of the organic compounds in tank headspaces.

The methodology described in this appendix was developed to identify which tanks pose an acceptably small pool fire risk and which tanks require more study to quantify the pool fire risk. Tanks that meet a screening criterion can be judged to meet applicable risk evaluation guidelines (REGs) without additional evaluation. Tanks that fail the screening criterion may require additional evaluation to quantify the solvent fire risk.

2.0 SUMMARY AND CONCLUSIONS

2.1 SUMMARY

The methodology described in this appendix was developed to screen waste tanks with respect to solvent pool fire risk. The technical basis for screening rests on the following key assumptions:

1. The consequences of a postulated pool fire fall below REGs if the pool area is below a definable criterion.

2. Pool area in a tank can be estimated from tank and solvent parameters and measured concentrations of organic vapors in headspace air.

The first of these assumptions is supported by consequence analyses (Figures 9-2 and 9-3 of the main body of this report) which shows consequences fall below guidelines for the unlikely frequency category for pool areas smaller than 1 m^2. The second assumption is validated by the technical analysis presented in Section 6.0 of this Appendix.

Pool fire analyses applicable to SSTs were carried out to quantify a pool size associated with fire-generated pressures well below those that would challenge tank structural integrity. A pool area of 1 m^2 (10.8 ft^2) was determined to be a conservative criterion and was used as a basis for the screening methodology presented here.

To determine pool area size in specific tanks, a simple solvent vapor transport model was developed by equating vapor outflow rate in ventilation air to pool evaporation rate. In the resulting equation, pool area is correlated with the concentration of solvent vapors in headspace air. Important parameters in the model include headspace ventilation rate, temperature at the pool surface, mass transfer coefficient for solvent evaporation, volatility of the solvent at a specified temperature, and the concentration of solvent vapors in headspace air.

2.2 CONCLUSIONS

The following conclusions characterize the findings of the study described in this appendix.

1. A simple solvent vapor transport model can be used to estimate the air-solvent interfacial area from measured headspace organic concentration and other predictable tank parameters.

2. A pool area of 1 m^2 is a conservative criterion for screening tanks for solvent pool fire risk. Pools this size and smaller could not threaten tank structural integrity if ignited and burned to oxygen extinguishment. Also, consequences of pools this size and smaller fall below guidelines for the unlikely frequency category.

3.0 OBJECTIVE AND SCOPE

3.1 OBJECTIVE

The objective of this study is to develop a screening methodology, based on measured headspace temperature and organic vapor concentration, that can be used to help assess the solvent fire hazard in Hanford Site waste tanks.

3.2 SCOPE

The hazard of focus in this study is a postulated solvent-air fire that could cause tank pressurization and the release of airborne contaminants to the environment. The methodology is applicable to SSTs and double-shell tanks (DSTs) for which headspace air samples yield an estimate of solvent vapor concentration.

4.0 TECHNICAL APPROACH

The technical approach used to develop screening criteria for the solvent fire hazard is based on the following justifiable postulates.

1. Solvent liquids exert an equilibrium vapor pressure at the liquid-air interface. Diffusion and convection cause solvent vapors to enter headspace air on a continual basis.

2. The steady-state concentration of solvent vapors in headspace air results from a dynamic equilibrium in which the evaporation rate from liquid is balanced by ventilation outflow.

3. An analysis of mass transfer rates quantifies the interfacial liquid area required to cause a specified concentration of solvent vapor in headspace air.

4. The risk posed by solvent air fires is acceptably small if the solvent pool area is below a size that would generate fire pressures that would challenge tank structural limits or lead to consequences that exceed applicable guidelines.

5.0 SOLVENT POOL FIRE HAZARD PHENOMENOLOGY

Previous studies of pool fire hazard phenomenology (Grigsby 1995) have identified three significant factors to the present study.

1. Solvent fires are low-probability accidents because ignition frequency is very low.

2. Consequences of solvent fires fall within REGs, provided that the tank is not structurally damaged and the fire does not trigger significant condensed-phase reactions. The chief threat to tank structural integrity is internal gas pressure developed by the fire.

3. Peak pressures generated by fires depend heavily on pool surface area, fire spread rate (for large pools), headspace air volume, and the flow capacity of tank vents. Because the present study considers small pools only, spread velocity is relatively unimportant.

A conservative estimate of the pool area required for significant tank pressurization was obtained for this study by analyzing a postulated fire in a 3,785-kL (1,000,000-gal) tank with minimal vent openings. Constraints used in the analysis included the following.

- The fire was initiated on a circle 0.3 m (1 ft) in diameter.

- The fire spread radially at a velocity of 10 cm/s.

- Vent paths were limited to the U-tube seal on the high-efficiency particulate air (HEPA) vent riser.
- The duration of the fire was limited by oxygen extinguishment at 13 percent O_2.
- Peak pressure was limited to 5 psig, or roughly half the 11 psig capability (Julyk 1994) of the 3,785-kL tanks.

This analysis of pressurization, together with an analysis of consequences (radiological and toxicological) of postulated fires covering an area of 1 m^2 (10.8 ft^2) (Section 10 of the main body of this report), indicate that an SST with a solvent pool area of 1 m^2 or less poses an acceptably small solvent fire risk. Therefore, a 1-m^2 area can be used as a preliminary screen to identify tanks that pose a deminimus solvent fire risk. Facility solvent fire risk can be evaluated by considering fires in tanks that have pools larger than 1 m^2.

6.0 TRANSPORT MODELING OF SOLVENT EVAPORATION INTO HEADSPACE AIR

This section describes the transport models used to estimate solvent interfacial area on the basis of the temperature and concentration of solvent vapors in headspace air.

6.1 WASTE CONFIGURATION ANALYZED

Figure 6-1 shows the waste-solvent configuration analyzed. Key assumptions of the modeled waste configuration are as follows.

- Headspace air is ventilated by atmospheric air.
- Headspace air is well mixed by natural convection driven by the transport of decay heat across the headspace.
- A solvent pool or submerged liquid lens of an arbitrary plan area is submerged beneath the waste surface by a distance H.
- Heat and mass transfer rates in waste are adequately modeled by one-dimensional models.
- Headspace characterization data, including temperature and the concentration of solvent vapors, are available.

Figure 6-1. Schematic of Waste Configuration Analyzed.

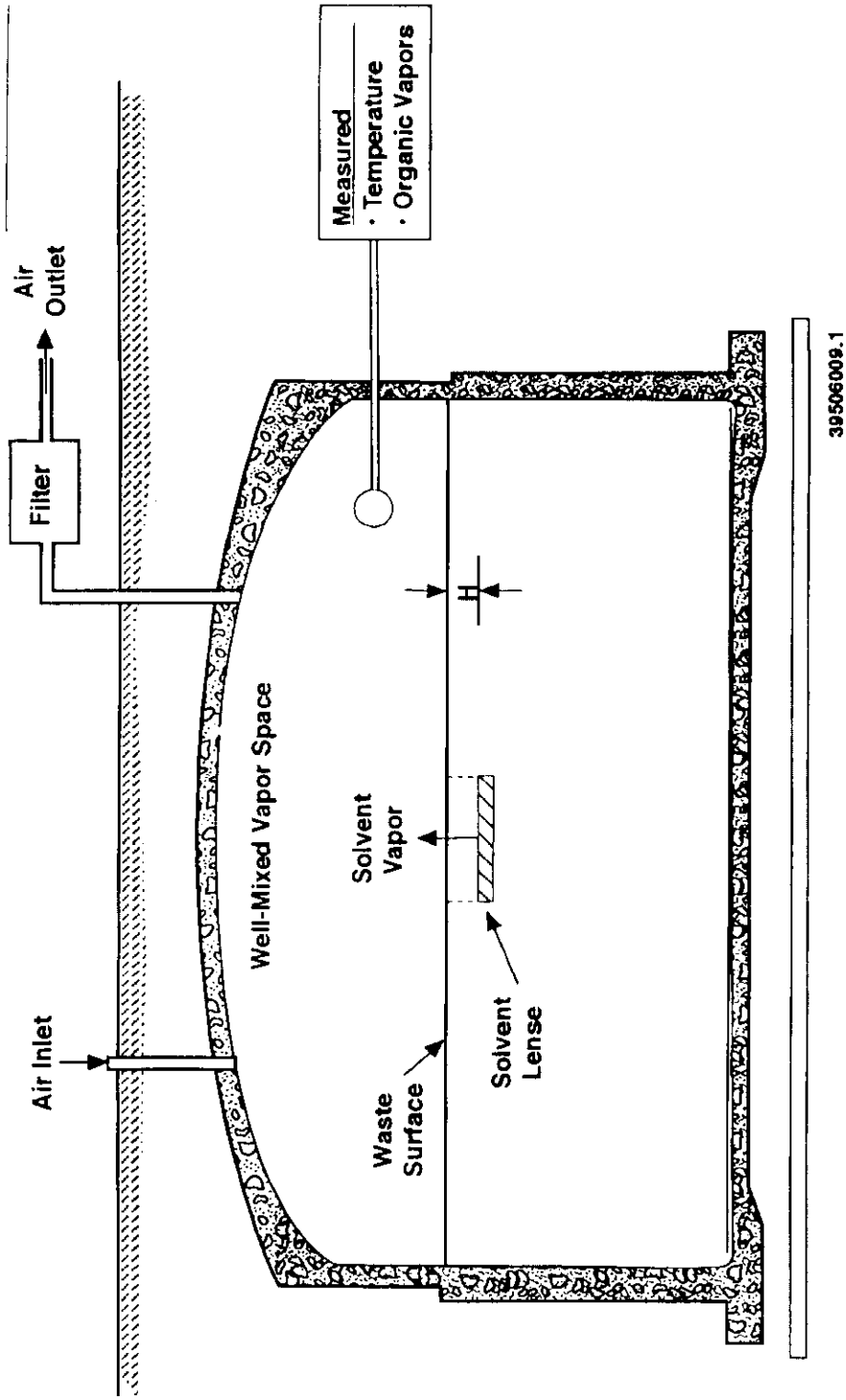

6.2 MASS TRANSFER RATE OF VAPORS INTO HEADSPACE AIR

Solvent vapors enter the headspace by diffusion from a liquid-air interface. Diffusional transport from an interface, through a porous medium, then into headspace air is quantified as follows.

6.2.1 Vapor Diffusion in Saltcake

The steady-state diffusion flux of organic vapors within a pore of constant cross section can be expressed:

$$N_A = -cD_{AB} \frac{dX_A}{dy} + X_A (N_A + N_B) , \qquad \text{(A-1)}$$

where

N_A = molar flux of A (moles/s m²)
c = total gas concentration (moles/m³)
D_{AB} = diffusivity of A in B (m²/s)
X_A = mole fraction of A in gas (A + B)
y = distance measured in direction of flux (m)
N_B = molar flux of B (moles/s m²).

This equation is taken from Bird et al. (1960).

Component A is specified as solvent vapor. Component B is specified as the remainder of the gas including air, water vapor, and trace levels of radiolytic gases (H_2, NH_3, N_2O, etc).

The first term on the right side of Equation A-1 is the flux caused by diffusion. The second term represents the flux caused by bulk flow of the total gas. The magnitude of the bulk flow term, estimated to be small, is disregarded in this analysis.

A simplified form of Equation A-1 may be derived by neglecting the bulk flow term [X_A (N_A + N_B)]; by replacing the product of CX_A by the species concentration, C_A; by evaluating the gradient, dC_A/dy, as a difference in concentration divided by the diffusion path length; and by introducing porosity and tortuosity factors to account for the diffusional resistance of porous media. The resulting equation may be expressed as follows.

$$N_A = \frac{D_{AB}\, \epsilon\, (C_e - C_s)}{\tau H} , \qquad \text{(A-2)}$$

where

ϵ	=	porosity of saltcake (dimensionless)
τ	=	tortuosity factor for diffusion (dimensionless)
H	=	submergence depth (m)
C_e	=	solvent vapor concentration in equilibrium with liquid at depth H (g/m^3)
C_s	=	solvent vapor concentration at waste surface (g/m^3).

Porosity accounts for the fraction of the solid that is open to gas diffusion, and tortuosity accounts for diffusional resistance caused by nonuniformities in the pore spaces (Sherwood et al. 1975).

The total transport rate of vapor by diffusion in saltcake is the flux, N_A, multiplied by the projected horizontal area of the liquid-air interface.

$$W_A = N_A A \ , \qquad \text{(A-3)}$$

where

W_A	=	diffusional transport rate (g/s)
A	=	area of liquid lens (m^2).

6.2.2 Mass Transport in Tank Headspace

A mass balance on solvent vapor in headspace air may be used to relate headspace vapor concentration to the controlling parameters. The rate at which solvent vapors enter headspace air is

$$\text{input rate} = k_c(C_s - C_b)A \ , \qquad \text{(A-4)}$$

where

k_c	=	mass transfer coefficient at waste surface (m/s)
C_b	=	bulk concentration of solvent vapor in headspace air (g/m^3).

The rate at which solvent vapors leave the tank headspace because of ventilation air flow is

$$\text{output rate} = QC_b \ ,$$

where

Q	=	ventilation rate (m^3/s).

Under steady-state conditions (equilibrium conditions in headspace air), input rate equals output rate.

$$k_c(C_s - C_b)A = QC_b \ , \qquad \text{(A-6)}$$

The concentration of solvent vapor at the waste surface, C_s, can be eliminated as a variable in the analysis by solving Equation A-2, Equation A-3, and Equation A-6 simultaneously. The result may be expressed as

$$\frac{C_b}{C_e} = \frac{k_c A}{k_c A + Q\left[1 + \dfrac{k_c \tau H}{\epsilon\ D_{AB}}\right]} \ . \qquad \text{(A-7)}$$

The ratio C_b/C_e expressed in Equation A-7 represents the fractional approach of solvent to saturation. In a perfectly sealed tank ($Q = 0$), the righthand side of Equation A-7 goes to unity, and the vapors are calculated to be saturated. For waste tanks, the ventilation rate is not zero, and C_b/C_e will always be less than unity. This allows the interfacial area, A, to be estimated.

Inspection of Equation A-7 reveals that estimating A requires that all other parameters be estimable by independent means. Means for estimating the parameters of Equation A-7 are discussed in the following section.

6.3 ESTIMATION OF POOL AREA

6.3.1 Surface Pool Versus Submerged Liquid Lens

As evident from Equation A-7, the interfacial area, A, (computed on the basis of known or calculable values of C_b/C_e, k_c, Q, τ, ϵ and D_{AB}), depends on submergence depth, H. Therefore, for a given tank, the measured solvent vapor concentration could be the result of a surface pool ($H = 0$) or a submerged lens of larger area. Because it is assumed that information on H is not available, H must be assigned a default value that is consistent with a conservative assessment of the solvent fire hazard. The default value is $H = 0$; i.e., it is assumed that the liquid solvent exists as an open pool at the surface of the waste. By setting $H = 0$, the need to quantify the parameters τ and ϵ exhibited in Equation A-7 is eliminated.

The assumption that solvent exists as a single surface pool (or surface wetted by wick action) is conservative for the following reasons.

- The ignition of a submerged lens appears to be of much lower probability than the ignition of an open pool or a wick-wetted surface.
- The fire spread rate for liquids submerged in inert porous solids is significantly slower than for surface pools (Wood et al. 1971 and Takeno and Hirano 1986).
- The specific burning rate (kg/m² s) is slower for submerged pools than for surface pools (Wood et al. 1971).

The conservative assumption of H = 0 allows pool area A to be related to measured or calculable tank parameters. It is recognized that, even though high concentrations of organic vapors are present in a tank, a solvent fire hazard might not exist because the source of the vapors could be submerged liquid that is incapable of supporting a persistent flame. Additional evaluation could be used to show the absence or presence of a surface pool that could sustain a fire.

6.3.2 Interfacial Concentration of Solvent Vapors

The mass concentration of solvent vapor in equilibrium with liquid, C_e, depends on temperature and the composition of the solvent liquid. Because experimental data on the present composition of solvents generally are not available, an indirect means must be used to estimate C_e. A suitably conservative surrogate solvent with a known vapor concentration—temperature curve is needed. A candidate surrogate is solvent removed from tank 241-C-103 in 1993 (Pool and Bean 1994). This solvent, a 70:30 mixture (on a mass basis) of TBP and normal paraffin hydrocarbon (NPH), is stripped of lighter and more volatile fractions and is expected to represent other solvents that may be present in SSTs.

Pool and Bean (1994) measured equilibrium vapor concentrations over tank 241-C-103 liquid at temperatures of 40 °C, 70 °C, and 100 °C (104 °F, 158 °F, and 212 °F). These concentration-temperature data were fitted to an integrated form of the Clausius—Clapeyron equation. The resulting equation may be expressed as follows.

$$\log C_e = 10.232 - \frac{3152.78}{T} , \qquad \text{(A-8)}$$

where

C_e = equilibrium solvent vapor concentration (g/m³)
T = temperature (°K)
log = base 10 logarithm.

Equation A-8 can be used to compute C_e for any tank for which the interfacial temperature, T, is known.

An alternative, more conservative (because lower vapor concentration is predicted, resulting in larger predicted pool area) estimate of equilibrium vapor concentration may be obtained by calculating vapor concentrations from Rauolt's Law and pure component vapor pressures for tank 241-C-103 liquid. The following liquid composition has been derived from measurements reported by Pool and Bean (1994) by grouping unidentified alkanes with identified alkanes having similar chromatographic elution times.

Table 6-1. Estimated Composition of NPH Components in Tank 241-C-103 Solvent.

Component	Molecular Fraction
Dodecane	0.0564
Tridecane	0.2231
Tetradecane	0.1225
Pentadecane	0.0131
Tributyl phosphate	0.5845
TOTAL	0.9996

Note:
NPH = normal paraffin hydrocarbon

Vapor pressures for each compound listed in Table 6-1 may be computed from a three parameter fitting equation:

$$\log p = A - B/(T + C) , \qquad \text{(A-9)}$$

where

p	=	vapor pressure (torr)
A,B,C	=	fitting constants
T	=	temperature (°C)
log	=	base 10 logarithm.

Values of the constants A, B, and C are available from Dreisbach (1959) for the alkanes and from Schulz et al. (1984) for TBP. Table 6-2 lists the constants that yield vapor pressures in torr (mm Hg).

Table 6-2. Constants for Equation A-9.

Compound	Molecular Weight	A	B	C
Dodecane	170.3	7.3157	1830.0	198.3
Tridecane	184.4	7.3147	1881.7	190.9
Tetradecane	198.4	7.3143	1930.4	183.8
Pentadecane	212.4	7.3123	1973.3	176.6
Tributyl phosphate	266.3	8.916	3359	273.16

Equilibrium vapor concentrations predicted on the basis of compositions listed in Table 6-1 and the fitting constants listed in Table 6-2 are approximately 50 percent of the values predicted from Equation A-8. The difference in predicted and measured vapor concentrations highlights the uncertainty involved in predicting the equilibrium vapor compositions for solvents in waste tanks. For a discussion of how solvent composition (volatility) affects screening criteria, refer to Huckaby and Sklarew (1997).

6.3.3 Temperature at Solvent/Air Interface

Temperature is key in evaluating the mass transfer coefficient at the waste surface and in determining vapor pressure of solvent at the solvent-air interface. The temperature of interest for the preliminary screening is the surface temperature because the headspace organic concentration is being modeled in terms of a surface pool. To attempt to estimate the size of a submerged pool, the temperature at the solvent interface at the submergence depth would be of interest. Because waste surface temperature is the lowest temperature in the waste, and because equilibrium vapor concentrations increase with temperature, the use of surface temperature to compute pool size will always result in the largest pool estimate. This can be seen from Equation A-7 where calculated pool area decreases with increasing C_e. The use of surface temperature is conservative in the preliminary screening step. To estimate the area of a submerged pool, the temperature gradient in the waste would have to be known as well as applicable values of tortuosity and porosity.

6.3.3.1 Passivately Ventilated Tanks. Temperature at the waste surface is higher than bulk gas temperature because a gradient in temperature is linked to the transport of decay heat upward from the waste to the abovegrade atmosphere. The average heat flux in the upward direction can be computed from the mean difference in temperature between the tank headspace and the atmosphere (Crowe et al. 1993).

$$\frac{q}{A} = \frac{k_s \left(T_{vap} - T_{air}\right)}{\Delta Z} , \qquad \text{(A-10)}$$

where

$\frac{q}{A}$ = heat flux (W/m²)

T_{vap} = annual average bulk headspace air temperature (°K)
T_{air} = annual average atmospheric temperature (°K)
k_s = thermal conductivity of soil overburden (W/m °K)
ΔZ = average depth of soil overburden (m).

The formulation expressed in Equation A-10 neglects the small temperature differences that would exist from headspace to dome and from soil surface to atmospheric air. On the basis of information in Crowe et al. (1993), T_{air} is ~56.3 °F (286.7 °K), the soil thermal conductivity is 0.1 W/m °K (~0.6 Btu/h-ft °F), and the average effective depth of soil overburden is 4.02 m (~13.2 ft).

The bulk vapor temperature in all SSTs varies with time in response to the annual weather cycle. The annual average tank temperature occurs on approximately July 15 and January 15 (Crowe et al. 1993). Between these dates, tank temperatures experience a sinusoidal variation above and below the average. The maximum and minimum temperatures occur on approximately October 15 and April 15 respectively. The peaks and valleys differ from the yearly average by ~5 °F (2.8 °K) (Crowe et al. 1993). By accounting for the seasonal variation, a value of T_{vap} applicable to Equation A-10 may be computed from a value measured at the time of headspace sampling.

The temperature difference (waste surface—dome surface) that is associated with the heat flux quantified in Equation A-10 may be computed on the basis of standard textbook heat transfer relationships. The flux is equal to a coefficient multiplied by a temperature difference.

$$\frac{q}{A} = (h_c + h_r)\Delta T , \qquad \text{(A-11)}$$

where

h_c = convection heat transfer coefficient (W/m² °K)
h_r = radiation heat transfer coefficient (W/m² °K)
ΔT = temperature difference between waste surface and tank dome (°K).

Numerical evaluations in by Crowe et al. (1993) indicate the temperature drop across the headspace (waste surface to dome surface) is relatively small, amounting to a few degrees Kelvin or less. Because the gas temperature is intermediate between dome and waste surface temperatures, the surface of a solvent pool will be warmer than the gas temperature by a few degrees or less. Although this temperature difference is small, it may not be negligible, because vapor pressures are highly sensitive to liquid temperature (see Equation A-8). In this study, the liquid interface temperature is computed by subtracting from the bulk gas temperature half of the ΔT ($T_{surface} - T_{dome}$) computed from Equation A-11.

6.3.3.2 Actively Ventilated Tanks. Air flow removes a substantial fraction of decay heat load in actively ventilated tanks. Heat flux at the waste surface may be estimated from the total heat load in the tank:

$$\frac{q}{A} = f\frac{Q}{A_T} \qquad \text{(A-12)}$$

where

f = fraction of total decay heat that is transported through the headspace, dimensionless

Q = total decay heat load, watts

A_T = cross section area, m^2.

Estimated values of f, the fraction of decay heat transported upward through the headspace, are provided by Crowe et al. (1993) as a function of tank size and waste depth. Total decay heat loads for actively ventilated SSTs and DSTs, Q, are listed by Kummerer (1994).

Equation A-12 can be used to calculate the heat flux at the surface of a pool. Equation A-11 then can be used to estimate the temperature drop across the solvent-air interface. Surface temperature can be computed by adding the calculated temperature difference to headspace air temperature.

6.3.4 Mass Transfer Coefficient at Solvent-Air Interface

The mass transfer coefficient at the waste-air interface (k_c in Equation A-7) can be estimated on the basis of the Chilton-Colburn analogy (Sherwood et al. 1975) by using a correlation of natural convection heat transfer coefficients. For naturally convected heat transfer from heated planar surfaces facing upward, the Nusselt number can be correlated with the Grashov and Prandtl numbers (McAdams 1954). A simplified form of this correlation that applies to large Grashov numbers (large surfaces) and normal air temperatures and pressures is presented as the following dimensional equation (McAdams 1954).

$$h_c = 1.52\ \Delta T^{1/3}, \qquad \text{(A-13)}$$

where

h_c = convective heat transfer coefficient (W/m² °K)
ΔT = temperature difference between surface and bulk air (°K).

A numerical value of h_c can be computed from Equation A-12 by using a temperature difference, ΔT, evaluated for a specific tank as described in Section 6.3.3.

The mass transfer coefficient, k_c, may be computed from the heat transfer coefficient, h_c, on the basis of the Chilton–Colburn analogy (Sherwood et al. 1975).

$$k_c = \frac{h_c D_{AB}}{k} \left(\frac{Sc}{Pr}\right)^{1/3}, \qquad \text{(A-14)}$$

where

k_c = mass transfer coefficient (m/s)
h_c = heat transfer coefficient (W/m² °K)
D_{AB} = diffusivity of solvent vapor (m²/s)
k = thermal conductivity of gas (W/m °K)
Sc = Schmidt number (dimensionless)
Pr = Prandtl number (dimensionless).

Diffusivity of solvent vapor can be estimated from handbook correlations (Perry 1950) as can other gas properties needed to evaluate the parameters of Equation A-13. The use of Equations A-10 through A-14 allows k_c to be computed as a function of tank headspace temperature and decay heat load.

Equations A-13 and A-14 apply as long as temperature decreases with elevation in the headspace. This condition will persist for tanks that have sufficiently high decay heat loads, but an adverse gradient (temperature increases with elevation) could develop in low-heat tanks during summer months. If the adverse gradient existed, then turbulent natural convection would be suppressed, and neither the assumption of a well-mixed headspace nor the applicability of Equations A-13 and A-14 would be assured. Crowe (1996) has performed an analysis of heat cycles in soil covering waste tanks and identified seasonal dates when an adverse temperature gradient could exist. His analysis shows that tanks with heat loads below about 1 kW could experience adverse temperature gradients during summer months. Tank screening should not be based on samples withdrawn from low heat tanks during the periods identified by Crowe (1996).

6.3.5 Ventilation Flow Rate

Ventilation air flow rate is an important parameter in Equation A-7. The predicted pool area is proportional to ventilation air flow rate.

For actively ventilated tanks, the ventilation rate is obtainable from pitot tube measurements. Data presented in HNF-SD-WM-CN-117, Rev.0 indicate that flow rates vary with time and from tank to tank. Flow rates for most tanks fall in the range of 50 to 200 cfm (85 to 340 m^3/h). Two requirements for screening with respect to solvent pool area are that the flow rate be known and that the flow rate be reasonably constant for a time period corresponding to several purge times. A purge time is defined as the headspace volume divided by the ventilation flow rate. These conditions are required to validate the steady-state assumption used to derive Equation A-7.

Ventilation flow rates in passively ventilated tanks are not routinely measured and are subject to considerable uncertainty. Recent measurements of headspace concentrations of hydrogen and injected tracer gases have provided information on ventilation rates for a number of passively ventilated tanks.

Wilkins et al. (1996) used the decay rate of hydrogen in headspace air to compute ventilation rates. Hydrogen is released from waste into headspace air during so-called gas release events. Hydrogen mixes rapidly in headspace air and is gradually purged from the headspace by atmospheric air. The rate of decay of hydrogen is a measure of the purge rate, i.e., the passively-induced ventilation rate. Ventilation rates calculated from hydrogen decay data in seven passively ventilated tanks fell within the range of 2 to 11 cfm (3.4 to 18.7 m^3/h).

Huckaby et al. (1997b) report results of tests in which the concentration of injected tracer gases (helium and sulfur hexafluoride) was measured as a function of time from injection. The rate of decay of the tracers is a measure of headspace ventilation rate. Calculated ventilation rates for seven passively ventilated SSTs fell in the range of 1.1 to 24.7 cfm (1.9 to 4 m^3/h).

Most measured ventilation rates are higher than the sum of atmospheric breathing (~0.2 cfm) and instrument purge air (~1 cfm), indicating that natural convection governs ventilation rate in most passively ventilated tanks. Therefore, estimates of ventilation rates in passively ventilated tanks for which no rate data are available must account for natural convection.

An estimated value is required to apply the screening methodology to tanks that do not have ventilation rate measurements. Because predicted pool area increases with ventilation flow rate, it is important that the rate not be substantially underestimated. To this end, a flow rate of 10 cfm (17 m^3/h) is suggested for screening purposes in tanks where data are unavailable. This flow rate is the maximum value used to evaluate hydrogen generation rates in the flammable gas program (HNF-SD-WM-CN-116, Rev. 0).

7.0 RESULTS OF SCREENING

To date, 81 passively ventilated tanks have been sampled, and screened with respect to solvent pool area (Huckaby and Sklarew 1997). Key results are:

- 13 tanks have pool areas > 1 m^2
- 8 tanks have pool areas > 5 m^2
- 68 tanks have pool areas of 1 m^2 or less.

Based on these results, it is concluded that for 68 of 81 tanks, a solvent pool fire, if ignited, would neither threaten the structural integrity of a tank nor emit enough airborne contaminants to exceed guidelines. For the 13 tanks which are indicated to have pools larger than 1 m^2, additional evaluations would be required to determine whether a pool >1 m^2 was actually present or, alternatively, whether the organic vapors emanated from a submerged solvent lens.

A discussion of how uncertainties in screening parameters affects predicted pool area is given by Huckaby and Sklarew (1997).

8.0 REFERENCES

Bird, R. B, W. E. Stewart, and E. N. Lightfoot, 1960, *Transport Phenomena*, John Wiley & Sons, Inc., New York, New York.

Crowe, R. D., 1996, *Simple Method to Predict a Temperature Inversion in a Waste Tank Vapor Space*, WHC-SD-WM-CN-027, Rev. 0, Westinghouse Hanford Company, Richland, Washington.

Crowe, R. D., M. Kummerer, and A. K. Postma, 1993, *Estimation of Heat Load in Waste Tanks Using Average Vapor Space Temperatures*, WHC-EP-0709, Westinghouse Hanford Company, Richland, Washington.

Dreisbach, R. R., 1959, "Physical Properties of Chemical Compounds," *Advances in Chemistry Series*, No. 22, American Chemical Society, Washington, D.C.

Grigsby, J. M., 1995, *Safety Analysis of Exothermic Reaction Hazards Associated with the Organic Liquid Layer in Tank 241-C-103 - Supplement 1: Risk From Organic Solvent Fires in C-103 Following Interim Stabilization*, WHC-SD-WM-SARR-001, Rev. 0A, Supplement 1, Westinghouse Hanford Company, Richland, Washington.

Huckaby, J. L., and D. S. Sklarew, 1997a, *Screening for Organic Solvents in Hanford Waste Tanks Using Organic Vapor Concentrations*, PNNL-11490, Pacific Northwest National Laboratory, Richland, Washington.

Huckaby, J. L., J. C. Evans, K. B. Olsen, K. M. Remund, D. S. Sklavew, 1997b, *Measurements of Waste Tank Pasive Ventilation Rates Using Tracer Gases*, PNNL-11683, Pacific Northwest National Laboratories, Richland, Washington.

Julyk, L. J., 1994, *Static Internal Pressure Capacity of Hanford Single-Shell Waste Tanks*, WHC-SD-WM-TI-623, Rev. 0, Westinghouse Hanford Company, Richland, Washington.

Kummerer, M, 1994, *Topical Report on Heat Removal Characteristics of Waste Storage Tanks*, WHC-SD-WM-SARR-010, Rev. 0, Westinghouse Hanford Company, Richland, Washington.

McAdams, W. H., 1954, *Heat Transmission*, McGraw-Hill, Inc., New York, New York.

Perry, R. H., 1950, *Chemical Engineers' Handbook*, McGraw-Hill, Inc., New York, New York.

Pool, K. H., and R. M. Bean, 1994, *Waste Tank Safety Project: Analysis of Liquid Samples from Hanford Waste Tank 241-C-1-3*, PNL-9403, Pacific Northwest Laboratory, Richland, Washington.

Schulz, W. W., J. D. Navratil, and A. E. Talbot, 1984, *Science and Technology of Tributyl Phosphate, Volume I Synthesis, Properties, Reactions and Analysis*, CRC Press, Inc., Boca Raton, Florida.

Sederburg, J. P., and J. A. Reddick, 1994, *TBP and Diluent Mass Balances in the PUREX Plant at Hanford 1955—1991*, WHC-MR-0483, Westinghouse Hanford Company, Richland, Washington.

Sherwood T. K., R. L. Pigford, and C. R. Wilke, 1975, *Mass Transfer*, McGraw Hill, Inc., New York, New York.

Takeno, K., and T. Hirano, 1986, "Flame Spread Over Porous Solids Soaked With a Combustible Liquid," in *Twenty-First Symposium (International) on Combustion*, The Combustion Institute, Pittsburgh, Pennsylvania.

Wilkins, N. E., R. E. Bauer, and D. M. Ogden, 1996, *Results of Vapor Space Monitoring of Flammable Gas Watch List Tanks*, HNF-SD-WM-TI-797, DE&S Hanford, Inc. for Fluor Daniel Hanford, Inc., Richland, Washington.

Wood, B. D., P. L. Blackshear, Jr., and E. R. G. Eckert, 1971, "Mass Fire Model: An Experimental Study of the Heat Transfer to Liquid Fuel Burning from a Sand-Filled Pan Burner," *Combustion Science and Technology*, vol. 4, pp. 113—129.

This page intentionally left blank.

APPENDIX B

IMPACT OF TURBULENT MIXING OF VENTED GASES ON CALCULATED TOXICOLOGICAL CONSEQUENCES OF SOLVENT POOL FIRES

This page intentionally left blank.

CONTENTS

1.0 INTRODUCTION B-5

2.0 OBJECTIVE AND SCOPE B-5

3.0 SUMMARY AND CONCLUSIONS B-6
3.1 SUMMARY B-6
3.2 CONCLUSIONS B-6

4.0 ANALYSIS OF ATMOSPHERIC DILUTION OF VENTED GASES B-7
4.1 DESCRIPTION OF VENT CONFIGURATIONS ANALYZED B-7
4.1.1 Exhaust Stack on Actively Ventilated Tanks B-7
4.1.2 Open Riser in Uncovered Pit B-7
4.1.3 Levitated Concrete Coverblocks B-9
4.1.4 Passive HEPA Vent B-9
4.1.5 Other Vent Paths B-9
4.2 PREDICTED DILUTION OF SOURCE GAS AT 100 m B-10
4.2.1 Dilution Factors for Characterized Vents B-10
4.2.2 Dilution Factors for Analyzed Pool Fire Cases B-12

5.0 RECALCULATION OF TOXICOLOGICAL CONSEQUENCES B-16
5.1 GASEOUS RELEASES B-17
5.2 RELEASE OF COMPOSITE MATERIALS B-18
5.2.1 Rupture of HEPA Filter on Passively Ventilated Tanks . . B-22
5.2.2 Rupture of HEPA Filters on Actively Ventilated SSTs . . B-22
5.2.3 Rupture of HEPA Filters on Actively Ventilated DSTs . . B-23
5.2.4 Rupture of HEPA Filters Associated with DCRTs B-23
5.2.5 Rupture of HEPA Filters on 55 kgal SSTs B-24
5.2.6 Aqueous Waste Carryover B-24
5.3 RECALCULATED TOXICOLOGICAL CONSEQUENCES B-25

6.0 COMPARISON OF RECALCULATED CONSEQUENCES WITH CONSEQUENCES BASED ON FSAR METHODOLOGY B-36

7.0 REFERENCES B-37

LIST OF FIGURES

4-1 Schematic Drawings Illustrating Four Waste Tank Vent Geometries of Interest B-8

LIST OF TABLES

4-1 Initial Conditions for the Numerical Calculations B-11

4-2 Predicted Plume Height and Normalized Concentration at 100 m Downwind from Source B-12

5-1 Spread Sheet for Solvent Pool Fire Cases - Toxicological B-26

6-1 Comparison of Bounding Cases with Previous Assessment B-36

1.0 INTRODUCTION

This report summarizes the findings of an analysis of the impact of turbulent mixing on calculated toxicological consequences of hypothetical solvent fires in Hanford Site waste tanks. Results of this analysis are important because predicted onsite consequences are significantly lowered when turbulent mixing in the vicinity of the tank vent is accounted for.

Postulated solvent pool fires are predicted to generate toxic gases and particles, and to vent a fraction of these to the environment. A previous analysis (Cowley and Postma 1996) which neglected atmospheric mixing induced by vented gases, indicated that an individual at the closest onsite distance (100 m) could be briefly exposed to toxin concentrations higher than guidelines. The need to re-analyze fire consequences using a more realistic atmospheric mixing model was noted by Cowley et al. 1997 as one of the improvements required to properly assess solvent fire risk. The present report was prepared to provide a more realistic accounting for near-field turbulent mixing of gases vented from tanks.

The impact of near-field mixing on toxicological consequences was quantified by re-calculating onsite toxin concentrations for the 21 pool fire cases previously analyzed (Cowley and Postma 1996). The only change from previous methodology was the introduction of jet mixing models that predicted dilution factors for vented toxins at 100 m downwind. The dilution factors used here were based on a supporting study carried out by M. Epstein of FAI, Inc. (Epstein 1997). Epstein (1997) is included as Attachment A of Appendix B.

This study was focussed on toxicological consequences for an individual at 100 m downwind. No effort was made to reanalyze toxic consequences at the offsite location because the previous analyses (Cowley and Postma 1996) indicated that consequences fell below guidelines for offsite individuals. A reanalysis that accounted for near-field turbulent mixing could reduce calculated off-site consequences, but there is little incentive to reduce calculated consequences that presently fall below guidelines.

2.0 OBJECTIVE AND SCOPE

The objective of this study is to quantify the impact of jet mixing on predicted toxicological consequences for hypothetical solvent fires in waste tanks. Pool fire scenarios and accident methodology used herein are based on the earlier analysis of Cowley and Postma (1996). The earlier analysis is modified by accounting for near-field turbulent mixing caused by vented gases, and toxin concentrations at 100 m downwind are re-calculated to account for turbulent mixing. All other aspects of the earlier analysis are used without change.

3.0 SUMMARY AND CONCLUSIONS

3.1 SUMMARY

Hypothetical solvent pool fires were re-analyzed to account for turbulent mixing induced by vented gases. The objective was to obtain a more realistic estimate of toxin concentrations at the location of the onsite receptor, 100 m downwind. An earlier analysis (Cowley and Postma 1996) used an extremely conservative dispersion model that projected onsite toxicological consequences that were above guidelines. The need for more realistic treatment of near-field atmospheric mixing was cited to Cowley et al. (1997) as one of the improvements needed to properly assess solvent fire risk. This report is responsive to the need cited by Cowley et al. (1997).

The twenty one hypothetical solvent pool fire cases described by Cowley and Postma (1996) were reanalyzed using atmospheric dilution factors at 100 m downwind predicted by Epstein (1997). The reanalysis was accomplished by modifying the spreadsheet used previously. The modifications needed to account for near-field mixing are described in detail herein. Likewise, onsite consequences are computed and compared with onsite consequences projected earlier (Cowley and Postma 1996).

3.2 CONCLUSIONS

The following conclusions and summary statements characterize the findings of this study.

1. Toxicological consequences of solvent pool fires are predicted to fall below risk acceptance guidelines when turbulent mixing induced by vented gases is accounted for.

2. Turbulent mixing induced by vented gases is predicted to significantly dilute toxins between the point of release and 100 m downwind. This dilution is particularly important for fire cases involving high vent rates because earlier methodology predicted little dilution for high vent rate cases. High vent rate cases are bounding with respect to toxicological consequences.

3. Four different vent geometries thought to characterize potential tank vents were analyzed herein. These include 1. a passive HEPA vent pipe that is directed downward, 2. a vertical stack employed on actively ventilated tanks, 3. a vertical discharge from a riser in a pit, and 4. slot-like openings formed by levitated pit covers. The minimum dilution factor predicted was for a slot-like opening with a horizontal discharge. For this case, toxin concentrations at 100 m were predicted to be 1.3% of concentrations in vented gases. This 1.3% compared to 61% predicted in the earlier methodology (Cowley and Postma 1996). The reduction from 61% to 1.3% reduces calculated toxicological consequences by a factor of 47.

4. The dispersion formula used earlier does not account for turbulent mixing induced by vented gases, and its use results in a significant overprediction of toxicological consequences at the onsite receptor location. This overprediction results for all accident scenarios in which gas is vented under significant (>1 psig) pressure.

5. It is recommended that onsite dilution be revisited for all accident scenarios (hydrogen burns, etc.) which cause tanks to be pressurized and where predicted toxicological consequences exceed guidelines.

4.0 ANALYSIS OF ATMOSPHERIC DILUTION OF VENTED GASES

This section describes the analysis methodology used to quantify mixing and dilution of vented gas from the point of release to a point 100 m downwind.

4.1 DESCRIPTION OF VENT CONFIGURATIONS ANALYZED

The degree of atmospheric mixing induced by vented gases depends on the shape, size and elevation of the vent and on the angle with respect to grade surface. Vent paths considered in previous analyses (Cowley and Postma 1996) are described and quantified in this section.

4.1.1 Exhaust Stack on Actively Ventilated Tanks

DSTs, DCRTs, and a fraction of SSTs are connected to active ventilation systems. Steel ducting connects tank headspaces to HEPA filter banks, thence to an exhaust fan, and finally to a vertically oriented exhaust stack. Tank ventilation exhaust stacks are typically in the neighborhood of 16 in. (0.41 m) in diameter and 10 to 12 feet (3.1 to 3.7 m) in height. Headspace gases and debris released from a ruptured HEPA would enter the atmosphere as a vertically directed circular jet. This vent path configuration is illustrated as Type 1 in Figure 4-1. Note that while materials released from ruptured HEPAs would exit through this stack, headspace gases could escape through other paths as well. Other potential leak paths are described as follows.

4.1.2 Open Riser in Uncovered Pit

Most SSTs and DSTs have pump pits in which tank riser pipes terminate. The pits are normally covered by means of concrete cover block or by steel plates. The risers, which are located beneath the pit covers, may be covered by unbolted metal plates. Tank internal pressure of a relatively low magnitude (a few psig or less) could lift an unbolted riser cover, and cause the pit to be pressurized. Internal pressure in the pit could then lift the pit cover, allowing headspace gases to escape to the atmosphere. If both riser cover and pit cover were dislodged laterally, the riser could vent

Figure 4-1. Schematic Drawings Illustrating Four Waste Tank Vent Geometries of Interest. (Epstein 1997)

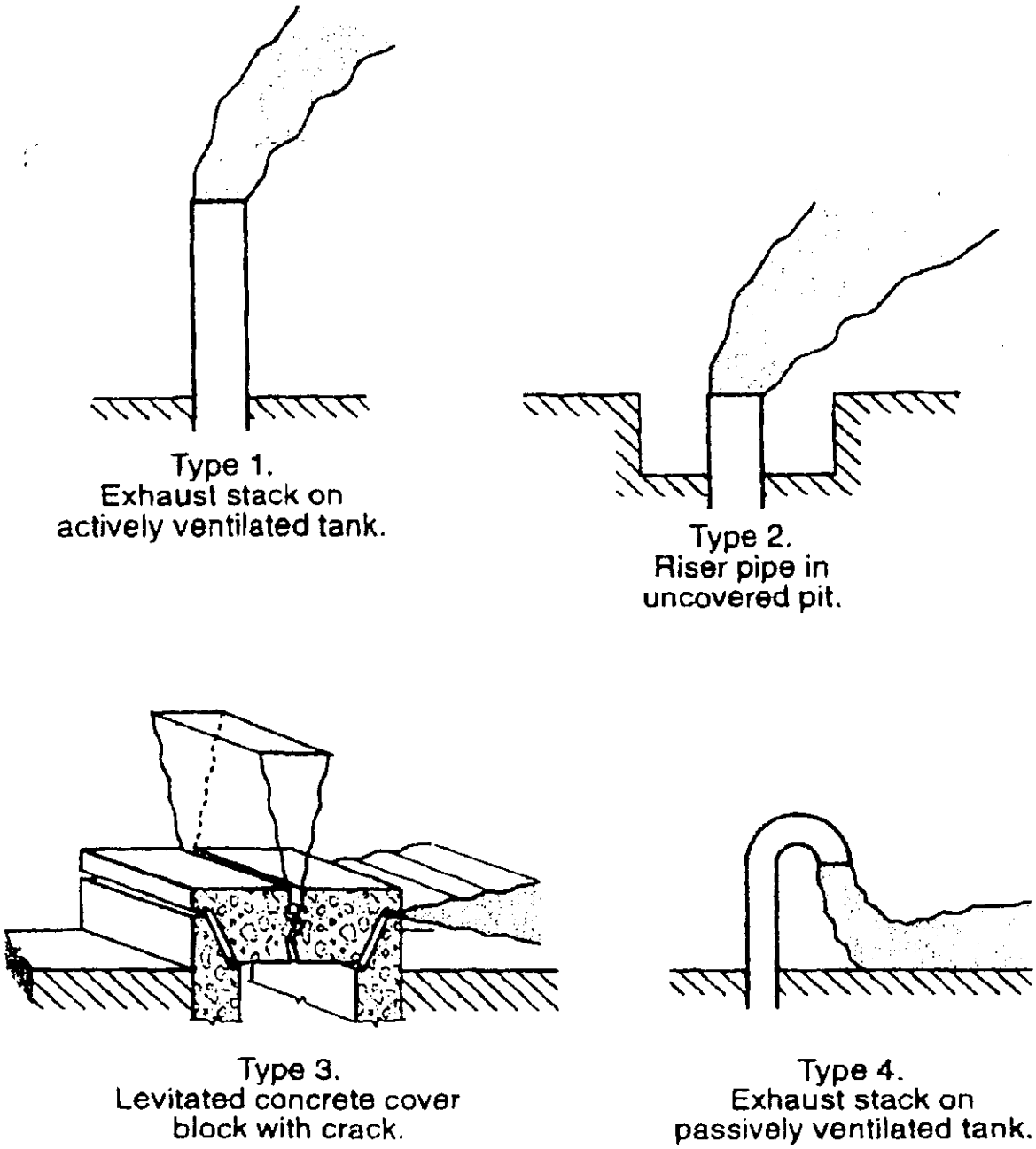

directly to the atmosphere. For this case, the vented gas would exit as a vertically directed circular jet. This vent configuration is depicted schematically as Type 2 in Figure 4-1.

This vent type differs from Type 1 in that the jet starts at grade level (or slightly below grade in the pit) and riser diameters could be as large as 42 in. (1.1 m) in diameter. The Type 1 vent (exhaust stack) is elevated and smaller in diameter than the Type 2 vent.

4.1.3 Levitated Concrete Coverblocks

If pit covers were not displaced laterally to the extent that a riser was uncovered, then vented gas would escape through gaps between the pit support walls and pit covers. This vent configuration is depicted schematically in Figure 4-1 as Type 3. The angle of the venting jet(s) could vary from horizontal to vertical depending on how coverblocks lifted in response to pressure in the pits. A single discharge opening is extremely unlikely because lifted pit covers would expose gaps between adjacent cover blocks and between cover blocks and pit walls. Gases would likely be discharged in several directions through a number of rectangular openings having widths that are small with respect to their lengths.

4.1.4 Passive HEPA Vent

The vent pipe from the HEPA filter housing on passively ventilated tanks is pointed downward to prevent rainwater intrusion. The discharge pipe is typically 4 in. (0.1 m) in diameter and terminates roughly 4 feet (1.2 m) above grade. Gases vented from this path would exit as a downwardly directed circular jet. This vent configuration is illustrated schematically as Type 4 in Figure 4-1. The jet would impact the ground and then spread laterally as it moved downwind.

4.1.5 Other Vent Paths

In addition to the four vent paths described above, leakage could occur from imperfectly sealed riser flanges and caps on equipment hatches. Also, vented gases could enter the headspaces of tanks connected by cascade pipes or by ventilation ducting. Neglect of leakage from the other possible paths is expected to result in conservative estimates of downwind toxin concentrations. Reasons for this judgment are as follows:

- Gases vented to other tanks would not be expelled to the atmosphere during the peak vent period, and
- Gas vented from small cracks (leaking gaskets, etc.) would be diluted to a greater extent than calculated for the bounding case of the four vent paths described in Sections 4.1.1 through 4.1.4.

4.2 PREDICTED DILUTION OF SOURCE GAS AT 100 m

The degree to which vented gases are diluted by the time they reach the receptor at 100 m downwind is important because it is the concentration of toxins that is used to compute toxicological consequences. In this report the degree of dilution is expressed as the onsite normalized concentration:

$$N = \frac{\text{toxin concentration at 100 m downwind}}{\text{toxin concentration in headspace air}}$$

where

N = normalized onsite concentration.

For N = 0.01, toxin concentrations at 100 m are 1% of the value at the tank vent. The words "dilution factor" are also used in the following discussion in place of "normalized onsite concentration". Both terms refer to the value of N as defined above.

4.2.1 Dilution Factors for Characterized Vents

Dilution of vented gases by atmospheric air between the vent and 100 m downwind was quantified for the four vent configurations described in Section 4.1. The analysis is described in detail in Epstein 1997. Three cases of initial conditions for each vent configuration were analyzed to illustrate how initial conditions affect calculated dilution factors. Each of the four vent configurations shown in Figure 4-1 has a defined direction of discharge, discharge height above grade, and discharge opening (area). The tanks are grouped by these parameters rather than by DST, SST, or DCRT, for this analysis. The poolfire spreadsheet was examined and a representative range of temperatures and pressures was selected from the tanks that have a given vent configuration (vent configuration can be determined from column G of the spreadsheet). The different temperature/pressure combinations are designated a, b, and c. For some configurations there is little or no variation in the temperatures and pressures. The selected temperatures and pressures are entered in Table 4-1. The angle of jet discharge for levitated concrete coverblocks was varied from horizontal to vertical to cover the possible range. Initial conditions for the twelve vent cases analyzed are listed in Table 4-1.

The data of Table 4-1 are described as follows. The left column identifies the case descriptor. Case number refers back to Figure 4-1. $Z_{cl,0}$ is the height of the nozzle above ground level. u_0 is the initial jet velocity. T_0 is the temperature of vented gases. θ_0 is the angle of the jet with respect to horizontal: $\pi/2$ is a vertically oriented jet and 0.0 is a horizontally oriented jet. A_0 is the cross sectional area of the jet. W_0 is the half-length of the slot-type jet. For example for **Case 3A**, the slot is 6 inches wide by 10 feet long (0.152 m by 3.05 m).

Dilution of source gas by atmospheric air was computed as a function of distance downwind by solving the continuity, momentum, and energy equations for a gas jet discharged into a 1 m/s crosswind. Entrainment of surrounding air into the jet was quantified by means of empirical correlations for entrainment velocity. A description of technical details is given by Epstein 1997. Results of the dilution calculations at 100 m are summarized in Table 4-2.

Table 4-1. Initial Conditions for the Numerical Calculations.[1]

Vent Type & Case	$Z_{cl,0}$ (m)	u_0 (m s^{-1})	T_0 (K)	θ_0 (radians)	A_0 (m^2)	W_0 (m)
1A	3.3	90.0	755.0	$\pi/2$	0.13	-
1B	3.3	3.7	310.0	$\pi/2$	0.13	-
1C	3.3	45.0	530.0	$\pi/2$	0.13	-
2A	0.0	90.0	505.0	$\pi/2$	0.894	-
2B	0.0	15.0	505.0	$\pi/2$	0.894	-
2C	0.0	15.0	310.0	$\pi/2$	0.073	-
3A	0.61	120.0	505.0	0.0	0.465	0.152
3B	0.61	120.0	505.0	$\pi/2$	0.465	0.152
3C	0.61	120.0	505.0	0.0	7.74×10^{-2}	0.152
4A	1.22	180.0	755.0	$-\pi/2$	8.11×10^{-3}	-
4B	1.22	90.0	505.0	$-\pi/2$	8.11×10^{-3}	-
4C	1.22	30.0	310.0	$-\pi/2$	8.11×10^{-3}	-

[1] Epstein (1997)

Table 4-2. Predicted Plume Height and Normalized Concentration at 100 m Downwind from Source.[1]

Case	Discharge Direction	Vent Geometry	Height of Lower Plume Boundary (m)	Normalized Concentration
1A	Upward	Circular	32.0	8×10^{-4}
1B	Upward	Circular	8.4	2×10^{-3}
1C	Upward	Circular	25.0	10^{-3}
2A	Upward	Circular	45.0	2.9×10^{-3}
2B	Upward	Circular	28.4	1.5×10^{-3}
2C	Upward	Circular	6.6	2.4×10^{-3}
3A	Horizontal	Slit	0.0	1.8×10^{-2}
3B	Upward	Slit	26.0	2×10^{-3}
3C	Horizontal	Slit	0.0	8.7×10^{-3}
4A	Downward	Circular	0.0	2.6×10^{-3}
4B	Downward	Circular	0.0	3.9×10^{-3}
4C	Downward	Circular	0.0	5.2×10^{-3}

[1] Epstein (1997)

Key results of the plume dispersion calculation are presented in the two right-most columns of Table 4-2. The height of the lower boundary of the plume at 100 m downwind is indicated to be well above breathing height for all vertically directed jets. Only the horizontal and downward directed jets are predicted to expose people at the 100 m distance.

Normalized concentrations at 100 m vary from 1.8E-2 for the widest horizontal slit considered (**Case 3A**) to 8E-4 for the highest velocity vertically directed jet considered (**Case 1A**). The largest normalized concentration, 1.8E-2, is small compared to the largest normalized concentration, 0.61, used in the earlier analysis of toxicological consequences (Cowley and Postma 1996). A reanalysis using the normalized concentrations of Table 4-2 will clearly result in lower calculated toxicological consequences at the onsite location.

4.2.2 Dilution Factors for Analyzed Pool Fire Cases

Onsite normalized concentrations that are applicable to specific pool fire cases are quantified in this section. This is done by matching postulated vent configurations for each of the previously analyzed cases (Cowley and Postma 1996) with the results of dilution predictions listed in Table 4-2. Dilution factors so determined will be used to re-calculate onsite consequences. This step maps the dilution factors for the different vent

configurations back into the poolfire cases that are based on tank type (SSTs, DSTs, and DCRTs) and fire type (pool, puddle, or entrained). This will be done by modifying the spreadsheet of Cowley and Postma 1996. Details that characterize each pool fire case are listed in the revised spreadsheet (Table 5-1) presented in Section 5.3 of this report.

Case a. SST Puddle Fire, Passive HEPA Vent

For this case the postulated vent path is the passive HEPA vent pipe. Peak pressure for this case (Cowley and Postma 1996) is 3.1 psig (21.4 kPa), which is high enough to expel gas from the vent at velocities of hundreds of feet per second. **Case 4A** of Table 4-2 has vent characteristics that closely resemble those for this case, so a normalized concentration of 2.6E-3 is applicable. This value is shown in cell P3 of Table 5-1.

Case b. SST Puddle Fire, Passive HEPA + Flapper Vent

This case differs from **Case a** because venting is postulated to occur from a pump pit as well as from the HEPA filter vent pipe. It is assumed that an unbolted riser cover in a pump pit is lifted by tank pressure. Pressure in the pit is postulated to lift pit cover blocks, allowing venting from the pit. Internal tank pressure for this case is just enough to lift cover blocks to expose a small leak path. Dominant leak paths would be the HEPA vent pipe and cracks between pit cover blocks and between cover block and the pit support wall. The vent with the highest normalized concentration (the most conservative) for those potential vent configurations is Case 3C in Table 4-2. The normalized concentration for this case, 8.7E-3 is selected as a conservative bound. This value is shown in cell P4 of Table 5-1.

Case c. SST Puddle Fire, Actively Ventilated

For this hypothetical case, a passive HEPA vent was assumed to be present on an actively ventilated tank. The passive vent was assumed to control venting during the pressurized portion of the fire cycle, and the active vent was assumed to purge tank headspace air after fire extinguishment. This unlikely arrangement is conservate from a radiological standpoint (it maximizes radiological releases), and is considered here as a hypothetical case. Since the HEPA vent has a higher normalized concentration than the exhaust stack associated with an active ventilation system (see Table 4-2), the HEPA vent is selected as bounding for this case. An onsite normalized concentration os 2.6E-3 is used to analyze this case, as indicated by the numerical value in Cell P5 of Table 5-1.

Case d. SST Puddle Fire, Actively Ventilated

Tank vents for this case are identical to those for **Case c** discussed above. Therefore the same dilution factor applies. An N value of 2.6E-3 is entered for this case in Cell P6 of Table 5-1.

Case e. SST Large Pool Fire, Passive HEPA Vent

This case was postulated to yield bounding tank pressurization and therefore is based on a large solvent pool combined with a minimal vent. High velocity gases would be expelled from the HEPA vent pipe. By reference to Table 4-2, Case 4A closely resembles this vent configuration. An onsite normalized concentration of 2.6E-3 is appropriate for this case, and this value is entered into Cell P7 of Table 5-1.

Case f. SST Large Pool Fire, Passive HEPA + Flapper Vent

This case was postulated to yield bounding vacuum on cooldown after fire extinguishment. The assumed flapper valve is a riser with an unbolted cover plate that lifts during pressurization, and then falls back into place over the riser during cooldown. For this case gases would vent from rectangular openings associated with levitated pit cover blocks and from the HEPA vent pipe. Multiple vent paths from levitated cover blocks, with various discharge angles would be expected for this case. The maximum crack width that could expel gases horizontally is assumed to be at most a few inches, so a bounding dilution factor would be intermediate between those for Cases 3A and 3C of Table 4-2. An average value for these two cases, (1.8E-2 + 8.7E-3)/2 = 1.3E-2, is judged to be appropriately conservative for this case. This value, 1.3E-2, is entered in Cell P8 of Table 5-1.

Case g. SST Large Pool Fire, Actively Ventilated

This case differs from **Case c** only in the postulated pool area. Vent configurations are identical to those of **Case c**, so the same dilution factor is appropriate. An N value of 2.6E-3 is selected and entered in Cell P9 of Table 5-1.

Case h. SST Large Pool Fire, Passive HEPA + Flapper Vent

This case was designed to yield bounding toxicological consequences for SST pool fires. Vents are the same as for **Case f,** so the dilution factor identified for **Case f**, 1.3E-2, applies for this case. This value is entered into Cell P10 of Table 5-1.

Case i. DST Large Pool Fire, Sealed Tank

Parameters for this hypothetical case were selected to yield bounding estimates of tank pressurization. Since the bounding vent for this case is a sealed tank, no venting is calculated. Dilution factors are not meaningful for this case and zero is entered in Cell P11 of Table 5-1.

Case j. DST Large Pool Fire, Passive HEPA + Flapper Vent

Parameters for this case were selected to yield bounding estimates of tank vacuum after fire extinguishment. The flapper vent would allow air to escape from levitated pit cover blocks. Cover block venting is assumed to be identical to **Case f**, so the same dilution factor, 1.3E-2, is appropriate. This value is entered into Cell P12 of Table 5-1.

Case k. DST Puddle Fire, Actively Ventilated

For this case the vent path is assumed to be the active ventilation system which terminates in a vertical stack. Case 1B of Table 4-2 has the largest normalized concentration at 100 m and the lowest plume height at 100 m. A bounding dilution factor of 2.0E-3, the value for Case 1B of Table 4-2, is selected and entered into Cell P13 of Table 5-1. It is recognized that a realistic analysis would find no exposure to the onsite receptor because the plume boundary is well above breathing level for a person on the ground at 100 m. The value used herein will clearly result in conservative toxicological predictions for this case.

Case l. DST Large Pool Fire, Actively Ventilated + Flapper Vent

A large riser in a pit is postulated to open and discharge headspace air from levitated pit cover blocks. Pit venting for this case is identical to that for **Case f**, for which an N value of 1.3E-2 was applicable. This value is selected and entered into Cell P14 of Table 5-1.

Case m. DCRT Large Pool Fire, Sealed Tank

This hypothetical no-vent case was designed to yield a bounding tank pressure estimate. Since no venting occurs, a dilution factor is not meaningful, and a zero is entered into Cell P15 of Table 5-1 for this case.

Cases n, o, p. DCRT Large Pool fire, Vent Pipe

The vent path for DCRTs is via a 4 inch (0.1m) diameter steel pipe into an active ventilation system. The active ventilation system discharges to the atmosphere through a vertical stack. For vertically directed, elevated vents, Case 1B of Table 4-2 yields the highest normalized concentration at 100 m. An N value of 2.E-3 is selected for these cases and this value is entered into cells P16, P17 and P18 of Table 5-1. It is recognized that a realistic analysis of onsite toxicological consequences would find negligible consequences because the plume boundary is well above breathing level for a person on the ground. The N value used herein will clearly result in conservative toxicological predictions for these cases.

Case q. SST Entrained Fire, Passive HEPA Vent

The vent for this case is the downwardly directed jet from the passive HEPA outlet. This vent is identical to that of **Case a**, for which an N value of 2.6E-3 was applicable. This same value is entered in Cell P19 of Table 5-1 for this case.

Case r. SST Entrained Fire, Passive HEPA + Flapper Vent

Vent paths for this case are identical to those for **Case b**, for which an N value of 8.7E-3 was applicable. This same value is entered into cell P20 of Table 5-1 for this case.

Case s. 55 kgal SST Large Pool Fire, Passive HEPA Vent

The passive HEPA vent on the 55 kgal SSTs is assumed to be identical to HEPA vents on the standard 75-ft diameter SSTs. Therefore, this case is similar to **Case a**, for which an N value of 2.6E-3 is appropriate. This same value is entered in Cell P21 of Table 5-1 for this case.

Case t. 55 kgal SST Large Pool Fire, Passive HEPA + Flapper Vent

This case differs from **Case** s in that riser cover plates and pit cover blocks are assumed to lift when the tank is pressurized. Vent rates are calculated to be comparatively slow for the 55 kgal SSTs, so only a narrow slot would provide adequate vent capacity. The postulated vent configuration is similar to **Case 3c** of Table 4-2. Therefore an N value of 8.7E-3 is appropriate for this case and this value is entered into Cell P22 of Table 5-1.

Case u. 55 kgal SST Puddle Fire, Passive HEPA Vent

The vent for this case is the passive HEPA vent pipe. Vent parameters for this case are similar to those for **Case a**, for which an appropriate value of N is 2.6E-3. This same value is entered into Cell P23 of Table 5-1 for this case.

5.0 RECALCULATION OF TOXICOLOGICAL CONSEQUENCES

This section describes the technical basis for changes made to spreadsheet formulae to re-compute onsite toxicological consequences for the 21 solvent fire cases analyzed.

5.1 GASEOUS RELEASES

Toxicological consequences are gauged by comparing airborne toxin concentrations at 100 m downwind to guideline concentrations. For each toxin present, a fraction of the limit is computed:

$$F_i = \frac{C_i}{G_i} \tag{1}$$

where

F_i = fraction of guidelines for i-th toxin,
C_i = concentration of i-th toxin in air, mg/m^3,
G_i = risk guideline concentration for i-th toxin, mg/m^3.

The overall toxicological consequence is then computed as the sum of individual fractions:

$$S = \sum_{i=1}^{i=n} F_i \tag{2}$$

where

S = sum of fractions,
n = number of toxins in vented air.

Toxicological consequences fall within guidelines if S is unity or smaller.

The reanalysis performed herein involves the re-computation of toxin concentrations, C_i values, at the 100 m distance downwind. Guideline concentrations, G_i values, remain the same as used by Cowley and Postma 1996. The onsite toxin concentration was computed from the defining equation for N:

$$C_i = C_{oi} * N \tag{3}$$

where

C_i = concentration of i-th toxin at 100 m, mg/m^3,
C_{oi} = concentration of i-th toxin at tank vent, mg/m^3,
N = normalized concentration at 100 m.

C_{oi} was computed earlier by Cowley and Postma (1996) and the same values were used herein. N, the normalized concentration for gaseous releases were quantified in Section 4.2 of this report on the basis of Epstein's jet diffusion analysis (Epstein 1997).

Equation (3) replaces the atmospheric equation used previously by Cowley and Postma (1996). The equation used previously was one recommended by Van Keuren (1995) for FSAR evaluations of toxicological consequences for gaseous releases. The previously used equation, which is now replaced by Equation (3), is:

$$C_i = \left(\frac{\frac{\chi}{Q}}{1 + V * \frac{\chi}{Q}} \right) * C_{oi} V \qquad (4)$$

where

$\frac{\chi}{Q}$ = atmospheric dispersion factor, s/m^3,

V = gas vent rate, m^3/s.

The atmospheric dispersion factor, χ/Q, was assigned a numerical value of 0.0341 s/m^3 in the previous analysis (Cowley and Postma 1996). This dispersion formula predicts that dilution of vented gases becomes minimal when vent rate becomes large. For the highest vent rate case (**Case j**) reported by Cowley and Postma (1996), V has a value of 46.2 m^3/s, and the toxin concentration at 100 m is predicted to be 61.2% of the concentration at the source. For the case with the lowest vent flow rate (**Case a**), V has a value of 0.443 m^3/s, and the toxin concentration at 100 m is predicted to be 1.49% of the concentration at the source. The latter value (0.0149) is not too far different than some of the N values based on Epstein's analysis (Epstein 1997) (Section 4.2.2 values) but the value for the high vent rate case (0.612) is unrealistically large and causes toxicological consequence to be significantly overpredicted.

5.2 RELEASE OF COMPOSITE MATERIALS

Stored waste is a complex mixture of chemical species. The toxicological potency of various wastes have been assessed by assigning sum of fraction multipliers that treat the wastes as composites (Van Keuren et al. 1995). Sum of fraction multipliers used by Cowley and Postma (1996) need to be recalculated to account for realistic dilution of toxins between the tank vent and the 100 m downwind distance. The following discussion describes how sum of fraction multipliers of Van Keuren et al. (1995) were adjusted for use herein.

For a specific composite material, the toxicological impact is computed as a sum of fractions:

$$S_c = R_c M_c \tag{5}$$

where

S_c = sum of fraction for composite,
R_c = release rate of composite, L/s,
M_c = multiplier for composite, s/L.

Cowley and Postma (1996) used M_c values published by Van Keuren, et al. (1995) to compute toxicological impacts of waste releases attributable to solvent pool fires. The release rate multiplier for a single chemical species was quantified by Van Keuren, et al. (1995) on the basis of the following atmospheric dispersion formula:

$$C_i = R_i \frac{\chi}{Q} \tag{6}$$

where

C_i = airborne concentration of i-th toxin at 100 m downwind, L/m^3,
R_i = release rate of i-th toxin, L/s,
$\frac{\chi}{Q}$ = atmospheric dispersion factor, s/m^3,

The toxicological sum of fractions for a composite material is calculated by adding the fractions for each chemical specie. Combining Equations (1), (2), and (6) the sum may be expressed as follows.

$$S_c = \sum_{i=1}^{i=n} \frac{C_i}{G_i} = \sum_{i=1}^{i=n} \frac{R_i \frac{\chi}{Q}}{G_i} = \frac{\chi}{Q} \sum_{i=1}^{i=n} \frac{R_i}{G_i} \tag{7}$$

where

S_c = sum of fractions for composite,
G_i = guideline concentration for i-th toxin, L/m^3.

The total release of a composite is the sum of the parts; for a total composite release rate of R_c, Equation (7) may be written as:

$$S_c = \frac{X}{Q}\sum_{i=1}^{i=n} \frac{R_c Y_i}{G_i} = R_c \frac{X}{Q} \sum_{i=1}^{i=n} \frac{Y_i}{G_i} \tag{8}$$

where

R_c = total composite release rate, L/s,
Y_i = volume fraction of i-th toxin in composite.

Equations (5) and (8) both define the sum of fractions for composite materials, and provide a basis for defining the sum of fractions multiplier, M_c, of Equation (5). Dividing Equation (5) by (8) and then solving for M_c, the result is:

$$M_c = \frac{X}{Q} \sum_{i=1}^{i=n} \frac{Y_i}{G_i} \tag{9}$$

Equation (9) quantifies the sum of fractions multiplier based on the atmospheric dispersion formula, Equation (6). This is the formula used by Van Keuren, et al. (1995) to develop the M_c values used by Cowley and Postma (1996) to calculate toxicological consequences of solvent fires. Since atmospheric dispersion is a factor in M_c, and since the present analysis uses a different atmospheric dilution model, M_c must be recalculated to reflect the atmospheric dilution factors used herein.

Combining Equations (3), (1), and (2), the composite sum of fractions may be written as:

$$S_c = \sum_{i=1}^{i=n} \frac{C_i}{G_i} = \sum_{i=1}^{i=n} \frac{C_{oi} * N}{G_i} = C_{oc}\, N \sum_{i=1}^{i=n} \frac{Y_i}{G_i} \tag{10}$$

where

C_{oi} = airborne concentration of i-th toxin at source, L/m^3,
C_{oc} = airborne concentration of composite at source, L/m^3,
Y_i = volume fraction of i-th toxin in composite,
N = normalized concentration at 100 m.

If Equation (10) is multiplied and divided by gas volumetric rate, V, an equation comparable to Equation (9) can be obtained.

$$S_c = C_{oc} N \frac{V}{V} \sum_{i=1}^{i=n} \frac{Y_i}{G_i} = R_c \frac{N}{V} \sum_{i=1}^{i=n} \frac{Y_i}{G_i} \tag{11}$$

This formulation for the sum of fractions due to composites is based on the atmospheric dilution formula used in the reanalysis, Equation (3). The sum of fractions multiplier implicit in Equation (11) is definable by comparing Equations (11) and (5-5). M_c is found to be:

$$M_c = \frac{N}{V} \sum_{i=1}^{i=n} \frac{Y_i}{G_i} \tag{12}$$

This equation defines a sum of fractions multiplier for composites that accommodates the new atmospheric dilution analysis. The ratio of new to old M_c values can be found by dividing Equation (12) by (9). The resulting ratio is:

$$\frac{M_{c2}}{M_{ci}} = \frac{\frac{N}{V}}{\frac{\chi}{Q}} \tag{13}$$

where

M_{c2} = multiplier based on Equation (3) dilution,
M_{c1} = multiplier based on Equation (6) dilution,
N = onsite normalized concentration,
V = gas vent rate, m^3/s,
$\frac{\chi}{Q}$ = atmospheric dispersion factor, s/m^3,

This equation provides a basis for recalculating toxicological consequences of composite material releases to account for more realistic atmospheric dilution between the tank and 100 m downwind. Application of this equation does not change guideline concentrations; the only change is in predicted airborne toxin concentrations at the 100 m mark. Means for applying this equation to the composite materials released in postulated pool fires are detailed in the following report section.

5.2.1 Rupture of HEPA Filter on Passively Ventilated Tanks

The application of Equation (13) requires that values of N and V be quantified for each release of composite chemical toxins. The value of N, the normalized onsite concentration, is 2.6E-3 as discussed for **Case a** of Section 4.2.2. The applicable gas vent rate, V, was estimated on the basis of a pressure drop of 1 psi across the HEPA vent line. It is reasoned that this pressure drop will yield a minimum flow rate associated with HEPA rupture because smaller pressure drops would not cause HEPA rupture. Use of a lower bound for V is conservative with respect to consequences because V is a denominator factor in Equation (13); higher values of V lead to lower predicted consequences. Based on an equivalent orifice diameter of 3.75 in. (0.1 m) (Cowley and Postma 1996), a flow rate of 0.475 m^3/s is computed. The ratio expressed in Equation (13) is quantified as:

$$\frac{M_{c2}}{M_{c1}} = \frac{2.6E-3}{0.475 * 0.0341} = 0.161$$

The value of χ/Q used above, 0.0341 s/m^3, is the value used to evaluate onsite HEPA rupture consequences in the previous analysis (Cowley and Postma 1996). Toxicological consequences of rupturing HEPA filters installed on passively ventilated SSTs was quantified by multiplying the sum of fractions given in Cowley and Postma (1996) by 0.161. This done in Columns DJ and DL of the spreadsheet (see Table 5-1) of Section 5.3.

5.2.2 Rupture of HEPA Filters on Actively Ventilated SSTs

Materials discharged by the rupture of HEPA filters on actively ventilated SSTs would exit from the ventilation exhaust stack. The applicable value of N for stack discharge, as discussed for **Case k** of Section 4.2.2 is 2.0E-3. A gas vent rate corresponding to a pressure drop of 1 psi (6.9 kPa) across the ventilation duct was projected as the minimum that could be associated with HEPA filter rupture. Based on an equivalent orifice diameter of 9.2 in. (0.23 m) (Cowley and Postma 1996) an air vent rate of 2.86 m^3/s was estimated. The ratio expressed in Equation (13) is quantified as follows.

$$\frac{M_{c2}}{M_{c1}} = \frac{2E-3}{2.86 * 0.0341} = 0.0205$$

Toxicological consequences for HEPA filters rupture in actively ventilated SSTs was quantified by multiplying the sum of fractions in Cowley and Postma (1996) by 0.0205. This is done in Columns DJ and DL of the spreadsheet presented as Table 5-1.

5.2.3 Rupture of HEPA Filters on Actively Ventilated DSTs

Material released from ruptured HEPA filters on actively ventilated DSTs would be vented to the atmosphere through the ventilation stack. The applicable value of N for stack discharge is conservatively estimated to be 2.0E-3 as discussed for **Case k** of Section 4.2.2. A gas vent rate corresponding to a pressure drop of 1 psi (6.9 kPa) across the ventilation duct was projected as the minimum that could be associated with HEPA filter rupture. Based on an equivalent orifice diameter of 9.6 in. (0.24 m) (Cowley and Postma 1996), a vent rate of 2.98 m^3/s was estimated. The ratio expressed in Equation (13) is quantified as:

$$\frac{M_{c2}}{M_{c1}} = \frac{2.0E-3}{2.98 * 0.0341} = 0.0197$$

Toxicological consequences for HEPA filter rupture in actively ventilated DSTs were recalculated by multiplying the sum of fractions given in Cowley and Postma (1996) by 0.0197. This is done in Columns DJ and DL of the spreadsheet presented as Table 5-1.

5.2.4 Rupture of HEPA Filters Associated with DCRTs

All DCRTs are vented to the atmosphere through a HEPA filter system. Therefore, any material released as a result of filter rupture would be discharged to the atmosphere through a vertically oriented exhaust stack. A conservative value of N for stack discharge is 1.0E-3. A gas vent rate corresponding to a pressure drop of 1 psi (6.9 kPa) was projected as the minimum that could be associated with HEPA rupture. Based on an equivalent orifice diameter of 4 in. (0.1 m) (Cowley and Postma 1996) a vent rate of 0.54 m^3/s was calculated. The ratio expressed in Equation (13) is quantified as:

$$\frac{M_{c2}}{M_{c1}} = \frac{2.0E-3}{0.54 * 0.0341} = 0.109$$

Toxicological consequences for the rupture of HEPA filters associated with DCRTs were recalculated by multiplying sums of fractions given in Cowley and Postma (1996) by 0.109. This is done in Columns DJ and DL of the spreadsheet presented as Table 5-1.

5.2.5 Rupture of HEPA Filters on 55 kgal SSTs

Small (55 kgal) SSTs are equipped with passive breathing HEPA filters, similar to those used on 75 ft. diameter SSTs. The HEPA filters are assumed to be the same as those used on passively ventilated SSTs. The applicable value of N for passive HEPAs is 2.6E-3 as discussed for **Case a** of Section 4.2.2. A gas vent rate corresponding to a pressure drop of 1 psi across the HEPA vent pipe was calculated as the minimum that could be associated with HEPA rupture. Based on an equivalent orifice diameter of 3.42 in. (0.09 m) (Cowley and Postma 1996) a vent rate of 0.395 m^3/s was calculated. The ratio expressed in Equation (13) is quantified as:

$$\frac{M_{c2}}{M_{c1}} = \frac{2.6E-3}{0.395\ (0.0341)} = 0.193$$

Toxicological consequences for the rupture of HEPA filters on passively ventilated SSTs were recalculated by multiplying sums of fractions given in Cowley and Postma (1996) by 0.193. This is done in Columns DJ and DL of the spreadsheet presented as Table 5-1.

5.2.6 Aqueous Waste Carryover

Aerosolization of waste attributable to a solvent pool fire is quantified by means of an empirical model of entrainment based on measured values for boiling liquids (Cowley and Postma 1996). Aerosols in headspace air would be vented along with other airborne contaminants. Recalculation of toxicological consequences was done by evaluating the ratio expressed in Equation (13) for each fire case analyzed in Table 5-1. The terms of Equation (13) were evaluated as follows.

- N, the normalized downwind concentration was assigned values appropriate for the particular vent configuration that applies to a case. These values were quantified in Section 4.2.2 for each case and are listed in Column P of Table 5-1.

- V, the gas vent rate, was assigned the value calculated by Cowley and Postma (1996) for each fire case analyzed. The vent rate is listed in Column X of Table 5-1.

- χ/Q was assigned the value used in the previous analysis (Cowley and Postma 1996), 0.0341 s/m^3.

Toxicological consequences of aqueous waste carryover were computed for each fire case by multiplying sums of fractions given in Cowley and Postma (1996) by the ratio expressed in Equation (13). This is done in Columns DN and DP of Table 5-1.

5.3 RECALCULATED TOXICOLOGICAL CONSEQUENCES

Toxicological consequences for 21 fire cases were recalculated by changing the spreadsheet formulas to account for the jet mixing in the vicinity of the tank vent. The changes required to account for dilution at the 100 m distance were described in detail in Sections 5.1 and 5.2. Results of the calculations are summarized in the spreadsheet, included here as Table 5-1.

Key results are shown in Columns DR and DT which display total onsite sums of fractions for the extremely unlikely and unlikely frequency categories. The largest fractions are 0.95, and apply to the unlikely frequency category for large pool fires in SSTs and DSTs postulated to be vented via a large flapper valves. No cases have fractions greater than unity so consequences fall beneath guidelines.

Table 5-1. Spread Sheet for Solvent Pool Fire Cases - Toxicological. (10 sheets)

	A	B	C	D	E	F	G	H	I	J	K	L	M
1	Case	Tank Type	Solvent Pool Description	Pool Area m^2	Bounding Parameters	Ventilation Flow	Vent Description	Tank Gas Volume m^3	Poolfire.4 Maximum Vent duration s	Poolfire.4 Solvent Burned in Vent kg	Poolfire.4 Reaction Gas Fraction	Poolfire.4 Headspace Gas Fraction	Source Conc. P_2O_5 mg/m^3
3	a	SST	puddle	1.0	pressure	passive	hepa[1]	4.82E+03	2.50E+03	8.73E+01	1.10E-01	2.30E-01	3.75E+02
4	b	SST	puddle	1.0	vacuum	passive	hepa/flapper[2]	4.82E+03	1.70E+03	6.51E+01	7.56E-02	2.40E-01	1.84E+02
5	c	SST	puddle	1.0	radiological	100 cfm (0.047 m^3/s)	hepa	4.82E+03	2.50E+03	8.73E+01	1.10E-01	2.30E-01	3.75E+02
6	d	SST	puddle	1.0	toxicological	100 cfm (0.047 m^3/s)	hepa	4.82E+03	2.50E+03	8.73E+01	1.10E-01	2.30E-01	3.75E+02
7	e	SST	large	210	pressure	passive	hepa	4.82E+03	1.30E+03	1.46E+02	1.46E-01	1.58E-01	1.21E+03
8	f	SST	large	210	vacuum	passive	hepa/flapper	4.82E+03	6.70E+01	8.40E+01	3.00E-01	6.00E-01	3.77E+02
9	g	SST	large	210	radiological	100 cfm (0.047 m^3/s)	hepa	4.82E+03	1.30E+03	1.46E+02	1.46E-01	1.58E-01	1.21E+03
10	h	SST	large	210	toxicological	passive	hepa/flapper	4.82E+03	6.70E+01	8.40E+01	3.00E-01	6.00E-01	3.77E+02
11	i	DST	large	210	pressure	sealed tank	none	5.30E+03	8.30E+01	1.62E+02	0.00E+00	0.00E+00	NA
12	j	DST	large	210	vacuum	passive	flapper	5.30E+03	7.00E+01	9.25E+01	3.10E-01	6.10E-01	3.83E+02
13	k	DST	puddle	1.0	radiological	100 cfm (0.047 m^3/s)	vent pipe[3]	5.30E+03	1.20E+03	5.00E+01	8.10E-02	2.50E-01	1.32E+02
14	l	DST	large	210	toxicological	100 cfm (0.047 m^3/s)	flapper vent pipe	5.30E+03	7.00E+01	9.21E+01	3.10E-01	6.10E-01	3.82E+02
15	m	DCRT	large	34.1	pressure	sealed tank	none	8.01E+01	1.95E+01	2.47E+00	0.00E+00	0.00E+00	NA
16	n	DCRT	large	34.1	vacuum	passive	4" (0.1m) orifice	8.01E+01	3.30E+01	2.12E+00	3.10E-01	4.10E-01	8.65E+02
17	o	DCRT	large	34.1	radiological	passive	4" (0.1m) orifice	8.01E+01	3.30E+01	2.12E+00	3.10E-01	4.10E-01	8.65E+02
18	p	DCRT	large	34.1	toxicological	passive	4" (0.1m) orifice	8.01E+01	3.30E+01	2.12E+00	3.10E-01	4.10E-01	8.65E+02
19	q	SST	entrained	40.0	radiological	100 cfm (0.047 m^3/s)	hepa[1]	4.82E+03	1.70E+03	1.30E+02	1.10E-01	2.10E-01	6.11E+02
20	r	SST	entrained	40.0	toxicological and vacuum	100 cfm (0.047 m^3/s)	hepa/flapper	4.82E+03	1.46E+03	1.13E+02	1.00E-01	3.10E-01	3.27E+02
21	s	55 kgal SST	large	29.2	pressure	passive	3.42" (.087m) orifice	2.27E+02	8.20E+01	6.54E+00	2.20E-01	2.70E-01	1.01E+03
22	t	55 kgal SST	large	29.2	toxicological and vacuum	passive	hepa/flapper[4]	2.27E+02	2.32E+01	4.00E+00	3.00E-01	6.00E-01	3.81E+02
23	u	55 kgal SST	puddle	1.0	pressure	passive	hepa[4]	2.27E+02	1.57E+02	4.81E+00	1.90E-01	3.50E-01	4.97E+02

Table 5-1. Spread Sheet for Solvent Pool Fire Cases - Toxicological. (10 sheets)

	A	B	N	O	P	Q	R	S	T	U	V	W	X	Y	Z	AA
1	Case	Tank Type	Source Conc CO mg/m^3	Source Conc. NO_2 mg/m^3	Atmospheric Dilution Factor at 100m Dimensionless	Aqueous Vent Rate L/s	Van's Onsite Limit Ex Unlikely s/L	Van's Offsite Limit Ex. Unlikely s/L	Van's Onsite Limit Unlikely s/L	Van's Offsite Limit Unlikely s/L	Onsite Sum of Fractions Aqueous Boiloff	Offsite Sum of Fractions Aqueous Boiloff	Vent Rate of Gas m^3/s	Onsite Conc. P_2O_5 mg/m^3	Onsite Conc. CO mg/m^3	Onsite Conc. NO_2 mg/m^3
3	a	SST	3.67E+02	4.76E+01	2.60E-03	1.42E-05	2.00E+02	6.20E-01	7.50E+02	8.00E+00	2.84E-03	8.80E-06	4.43E-01	9.74E-01	9.54E-01	1.24E-01
4	b	SST	1.80E+02	2.34E+01	8.70E-03	1.39E-05	2.00E+02	6.20E-01	7.50E+02	8.00E+00	2.78E-03	8.62E-06	6.80E-01	1.60E+00	1.57E+00	2.03E-01
5	c	SST	3.67E+02	4.76E+01	2.60E-03	1.42E-05	2.00E+02	6.20E-01	7.50E+02	8.00E+00	2.84E-03	8.80E-06	4.43E-01	9.74E-01	9.54E-01	1.24E-01
6	d	SST	3.67E+02	4.76E+01	2.60E-03	1.42E-05	2.00E+02	6.20E-01	7.50E+02	8.00E+00	2.84E-03	8.80E-06	4.43E-01	9.74E-01	9.54E-01	1.24E-01
7	e	SST	1.19E+03	1.54E+02	2.60E-03	4.13E-05	2.00E+02	6.20E-01	7.50E+02	8.00E+00	8.26E-03	2.56E-05	5.85E-01	3.15E+00	3.08E+00	4.00E-01
8	f	SST	3.69E+02	4.78E+01	1.30E-02	9.48E-04	2.00E+02	6.20E-01	7.50E+02	8.00E+00	1.90E-01	5.88E-04	4.31E+01	4.90E+00	4.80E+00	6.22E-01
9	g	SST	1.19E+03	1.54E+02	2.60E-03	4.13E-05	2.00E+02	6.20E-01	7.50E+02	8.00E+00	8.26E-03	2.56E-05	5.85E-01	3.15E+00	3.08E+00	4.00E-01
10	h	SST	3.69E+02	4.78E+01	1.30E-02	9.48E-04	2.00E+02	6.20E-01	7.50E+02	8.00E+00	1.90E-01	5.88E-04	4.31E+01	4.90E+00	4.80E+00	6.22E-01
11	i	DST	NA	NA	0.00E+00	0.00E+00		6.20E-01	7.50E+02	8.40E+00	0.00E+00	0.00E+00	0.00E+0	#VALUE!	#VALUE!	#VALUE!
12	j	DST	3.75E+02	4.87E+01	1.30E-02	1.03E-03	2.10E+02	6.20E-01	7.50E+02	8.40E+00	2.17E-01	6.40E-04	4.62E+01	4.98E+00	4.88E+00	6.33E-01
13	k	DST	1.29E+02	1.68E+01	2.00E-03	2.25E-05	2.10E+02	6.20E-01	7.50E+02	8.40E+00	4.72E-03	1.39E-05	1.10E+00	2.64E-01	2.59E-01	3.35E-02
14	l	DST	3.74E+02	4.85E+01	1.30E-02	1.03E-03	2.10E+02	6.20E-01	7.50E+02	8.40E+00	2.16E-01	6.37E-04	4.62E+01	4.96E+00	4.86E+00	6.30E-01
15	m	DCRT	NA	NA	0.00E+00	0.00E+00	2.00E+02	6.20E-01	7.50E+02	8.00E+00	0.00E+00	0.00E+00	0.00E+00	#VALUE!	#VALUE!	#VALUE!
16	n	DCRT	8.47E+02	1.10E+02	2.00E-03	5.02E-05	2.00E+02	6.20E-01	7.50E+02	8.00E+00	1.00E-02	3.11E-05	9.95E-01	1.73E+00	1.69E+00	2.20E-01
17	o	DCRT	8.47E+02	1.10E+02	2.00E-03	5.02E-05	2.00E+02	6.20E-01	7.50E+02	8.00E+00	1.00E-02	3.11E-05	9.95E-01	1.73E+00	1.69E+00	2.20E-01
18	p	DCRT	8.47E+02	1.10E+02	2.00E-03	5.02E-05	2.00E+02	6.20E-01	7.50E+02	8.00E+00	1.00E-02	3.11E-05	9.95E-01	1.73E+00	1.69E+00	2.20E-01
19	q	SST	5.99E+02	7.76E+01	2.60E-03	2.12E-05	2.00E+02	6.20E-01	7.50E+02	8.00E+00	4.24E-03	1.31E-05	5.95E-01	1.59E+00	1.56E+00	2.02E-01
20	r	SST	3.20E+02	4.15E+01	8.70E-03	1.95E-05	2.00E+02	6.20E-01	7.50E+02	8.00E+00	3.90E-03	1.21E-05	1.02E+00	2.84E+00	2.79E+00	3.61E-01
21	s	55 kgal SST	9.94E+02	1.29E+02	2.60E-03	4.42E-05	2.00E+02	6.20E-01	7.50E+02	8.00E+00	8.84E-03	2.74E-05	7.47E-01	2.64E+00	2.58E+00	3.35E-01
22	t	55 kgal SST	3.73E+02	4.83E+01	8.70E-03	1.30E-04	2.00E+02	6.20E-01	7.50E+02	8.00E+00	2.61E-02	8.08E-05	5.87E+00	3.31E+00	3.25E+00	4.21E-01
23	u	55 kgal SST	4.87E+02	6.31E+01	2.60E-03	1.75E-05	2.00E+02	6.20E-01	7.50E+02	8.00E+00	3.50E-03	1.09E-05	5.05E-01	1.29E+00	1.27E+00	1.64E-01

Table 5-1. Spread Sheet for Solvent Pool Fire Cases - Toxicological. (10 sheets)

	A	B	AB	AC	AD	AE	AF	AG	AH	AI	AJ	AK	AL	AM
1	Case	Tank Type	Onsite Normalized Conc. (1 mg/m^3)	Source Soot Conc. mg/m^3	Onsite Total Particulate mg/m^3	Offsite Total Particulate mg/m^3	Particulate Limit ERPG-3 mg/m^3	Particulate Limit ERPG-2 mg/m^3	Particulate Limit ERPG-1 mg/m^3	Ex. Un. Onsite Total Particulate Fraction	Ex. Un. Offsite Total Particulate Fraction	Offsite Normalized Conc. (1 mg/m^3)	Ammonia Headspace Conc. mg/m^3	Ammonia ERPG-3 mg/m^3
3	a	SST	2.60E-03	1.73E+03	5.48E+00	2.64E-02	500	50	30	1.10E-02	5.29E-04	1.25E-05	1300	680
4	b	SST	8.70E-03	8.52E+02	9.01E+00	1.99E-02	500	50	30	1.80E-02	3.99E-04	1.92E-05	1300	680
5	c	SST	2.60E-03	1.73E+03	5.48E+00	2.64E-02	500	50	30	1.10E-02	5.29E-04	1.25E-05	1300	680
6	d	SST	2.60E-03	1.73E+03	5.48E+00	2.64E-02	500	50	30	1.10E-02	5.29E-04	1.25E-05	1300	680
7	e	SST	2.60E-03	5.60E+03	1.77E+01	1.13E-01	500	50	30	3.54E-02	2.26E-03	1.66E-05	1300	680
8	f	SST	1.30E-02	1.74E+03	2.76E+01	2.59E+00	500	50	30	5.51E-02	5.17E-02	1.22E-03	1300	680
9	g	SST	2.60E-03	5.60E+03	1.77E+01	1.13E-01	500	50	30	3.54E-02	2.26E-03	1.66E-05	1300	680
10	h	SST	1.30E-02	1.74E+03	2.76E+01	2.59E+00	500	50	30	5.51E-02	5.17E-02	1.22E-03	1300	680
11	i	DST	0.00E+00	NA	#VALUE!	#VALUE!	500	50	30	NA	NA	0.00E+00	1300	680
12	j	DST	1.30E-02	1.77E+03	2.80E+01	2.82E+00	500	50	30	5.61E-02	5.63E-02	1.31E-03	1300	680
13	k	DST	2.00E-03	6.11E+02	1.49E+00	2.32E-02	500	50	30	2.97E-03	4.65E-04	3.12E-05	1300	680
14	l	DST	1.30E-02	1.77E+03	2.79E+01	2.80E+00	500	50	30	5.58E-02	5.61E-02	1.31E-03	1300	680
15	m	DCRT	0.00E+00	NA	#VALUE!	#VALUE!	500	50	30	NA	NA	0.00E+00	1300	680
16	n	DCRT	2.00E-03	4.00E+03	9.73E+00	1.37E-01	500	50	30	1.95E-02	2.74E-03	2.82E-05	1300	680
17	o	DCRT	2.00E-03	4.00E+03	9.73E+00	1.37E-01	500	50	30	1.95E-02	2.74E-03	2.82E-05	1300	680
18	p	DCRT	2.00E-03	4.00E+03	9.73E+00	1.37E-01	500	50	30	1.95E-02	2.74E-03	2.82E-05	1300	680
19	q	SST	2.60E-03	2.83E+03	8.94E+00	5.79E-02	500	50	30	1.79E-02	1.16E-03	1.68E-05	1300	680
20	r	SST	8.70E-03	1.51E+03	1.60E+01	5.32E-02	500	50	30	3.20E-02	1.06E-03	2.89E-05	1300	680
21	s	55 kgal SST	2.60E-03	4.70E+03	1.48E+01	1.21E-01	500	50	30	2.97E-02	2.42E-03	2.12E-05	1300	680
22	t	55 kgal SST	8.70E-03	1.76E+03	1.86E+01	3.56E-01	500	50	30	3.73E-02	7.12E-03	1.66E-04	1300	680
23	u	55 kgal SST	2.60E-03	2.30E+03	7.27E+00	4.00E-02	500	50	30	1.45E-02	7.99E-04	1.43E-05	1300	680

Table 5-1. Spread Sheet for Solvent Pool Fire Cases - Toxicological. (10 sheets)

	A	B	AN	AO	AP	AQ	AR	AS	AT	AU	AV	AW	AX	AY	AZ	BA
1	Case	Tank Type	Ammonia ERPG-2 mg/m^3	Ammonia ERPG-1 mg/m^3	1,3 Buta Headspace Conc. mg/m^3	1,3 Buta ERPG-3 mg/m^3	1,3 Buta ERPG-2 mg/m^3	1,3 Buta ERPG-1 mg/m^3	meth. chl. Headspace conc. mg/m^3	meth. chl. ERPG-3 mg/m^3	meth. chl. ERPG-2 mg/m^3	meth. chl. ERPG-1 mg/m^3	TBP Headspace Conc. mg/m^3	TBP ERPG-3 mg/m^3	TBP ERPG-2 mg/m^3	TBP ERPG-1 mg/m^3
3	a	SST	140	17	0.19	11,000	110	22	21.76	17,400	3480	700	11.6	50	15	3
4	b	SST	140	17	0.19	11,000	110	22	21.76	17,400	3480	700	11.6	50	15	3
5	c	SST	140	17	0.19	11,000	110	22	21.76	17,400	3480	700	11.6	50	15	3
6	d	SST	140	17	0.19	11,000	110	22	21.76	17,400	3480	700	11.6	50	15	3
7	e	SST	140	17	0.19	11,000	110	22	21.76	17,400	3480	700	11.6	50	15	3
8	f	SST	140	17	0.19	11,000	110	22	21.76	17,400	3480	700	11.6	50	15	3
9	g	SST	140	17	0.19	11,000	110	22	21.76	17,400	3480	700	11.6	50	15	3
10	h	SST	140	17	0.19	11,000	110	22	21.76	17,400	3480	700	11.6	50	15	3
11	i	DST	140	17	0.19	11,000	110	22	21.76	17,400	3480	700	11.6	50	15	3
12	j	DST	140	17	0.19	11,000	110	22	21.76	17,400	3480	700	11.6	50	15	3
13	k	DST	140	17	0.19	11,000	110	22	21.76	17,400	3480	700	11.6	50	15	3
14	l	DST	140	17	0.19	11,000	110	22	21.76	17,400	3480	700	11.6	50	15	3
15	m	DCRT	140	17	0.19	11,000	110	22	21.76	17,400	3480	700	11.6	50	15	3
16	n	DCRT	140	17	0.19	11,000	110	22	21.76	17,400	3480	700	11.6	50	15	3
17	o	DCRT	140	17	0.19	11,000	110	22	21.76	17,400	3480	700	11.6	50	15	3
18	p	DCRT	140	17	0.19	11,000	110	22	21.76	17,400	3480	700	11.6	50	15	3
19	q	SST	140	17	0.19	11,000	110	22	21.76	17,400	3480	700	11.6	50	15	3
20	r	SST	140	17	0.19	11,000	110	22	21.76	17,400	3480	700	11.6	50	15	3
21	s	55 kgal SST	140	17	0.19	11,000	110	22	21.76	17,400	3480	700	11.6	50	15	3
22	t	55 kgal SST	140	17	0.19	11,000	110	22	21.76	17,400	3480	700	11.6	50	15	3
23	u	55 kgal SST	140	17	0.19	11,000	110	22	21.76	17,400	3480	700	11.6	50	15	3

Table 5-1. Spread Sheet for Solvent Pool Fire Cases - Toxicological. (10 sheets)

	A	B	BB	BC	BD	BE	BF	BG	BH	BI	BJ	BK	BL	BM	BN	BO	BP
1	Case	Tank Type	P_2O_5 Headspace Conc. mg/m^3	P_2O_5 ERPG-3, mg/m^3	P_2O_5 ERPG-2, mg/m^3	P_2O_5 ERPG-1, mg/m^3	NO_2 Headspace Conc. mg/m^3	NO_2 ERPG-3 mg/m^3	NO_2 ERPG-2 mg/m^3	NO_2 ERPG-1 mg/m^3	Acetonit. Headspace conc. mg/m^3	Acetonit. ERPG-3 mg/m^3	Acetonit. ERPG-2 mg/m^3	Acetonit. ERPG-1 mg/m^3	prop. nit. Headspace conc. mg/m^3	prop. nit. ERPG-3 mg/m^3	prop. nit. ERPG-2 mg/m^3
3	a	SST	3.75E+02	100	25	5	4.76E+01	94	47	3.8	21.81	60	20	3	10.47	60	20
4	b	SST	1.84E+02	100	25	5	2.34E+01	94	47	3.8	21.81	60	20	3	10.47	60	20
5	c	SST	3.75E+02	100	25	5	4.76E+01	94	47	3.8	21.81	60	20	3	10.47	60	20
6	d	SST	3.75E+02	100	25	5	4.76E+01	94	47	3.8	21.81	60	20	3	10.47	60	20
7	e	SST	1.21E+03	100	25	5	1.54E+02	94	47	3.8	21.81	60	20	3	10.47	60	20
8	f	SST	3.77E+02	100	25	5	4.78E+01	94	47	3.8	21.81	60	20	3	10.47	60	20
9	g	SST	1.21E+03	100	25	5	1.54E+02	94	47	3.8	21.81	60	20	3	10.47	60	20
10	h	SST	3.77E+02	100	25	5	4.78E+01	94	47	3.8	21.81	60	20	3	10.47	60	20
11	i	DST	0.00E+00	100	25	5	0.00E+00	94	47	3.8	21.81	60	20	3	10.47	60	20
12	j	DST	3.83E+02	100	25	5	4.87E+01	94	47	3.8	21.81	60	20	3	10.47	60	20
13	k	DST	1.32E+02	100	25	5	1.68E+01	94	47	3.8	21.81	60	20	3	10.47	60	20
14	l	DST	3.82E+02	100	25	5	4.85E+01	94	47	3.8	21.81	60	20	3	10.47	60	20
15	m	DCRT	0.00E+00	100	25	5	0.00E+00	94	47	3.8	21.81	60	20	3	10.47	60	20
16	n	DCRT	8.65E+02	100	25	5	1.10E+02	94	47	3.8	21.81	60	20	3	10.47	60	20
17	o	DCRT	8.65E+02	100	25	5	1.10E+02	94	47	3.8	21.81	60	20	3	10.47	60	20
18	p	DCRT	8.65E+02	100	25	5	1.10E+02	94	47	3.8	21.81	60	20	3	10.47	60	20
19	q	SST	6.11E+02	100	25	5	7.76E+01	94	47	3.8	21.81	60	20	3	10.47	60	20
20	r	SST	3.27E+02	100	25	5	4.15E+01	94	47	3.8	21.81	60	20	3	10.47	60	20
21	s	55 kgal SST	1.01E+03	100	25	5	1.29E+02	94	47	3.8	21.81	60	20	3	10.47	60	20
22	t	55 kgal SST	3.81E+02	100	25	5	4.83E+01	94	47	3.8	21.81	60	20	3	10.47	60	20
23	u	55 kgal SST	4.97E+02	100	25	5	6.31E+01	94	47	3.8	21.81	60	20	3	10.47	60	20

Table 5-1. Spread Sheet for Solvent Pool Fire Cases - Toxicological. (10 sheets)

	A	B	BQ	BR	BS	BT	BU	BV	BW	BX	BY	BZ	CA	CB	CC	CD	CE
1	Case	Tank Type	prop. nit. ERPG-1 mg/m^3	CO Headspace conc. mg/m^3	CO ERPG-3 mg/m^3	CO ERPG-2 mg/m^3	CO ERPG-1 mg/m^3	benezene Headspace conc. mg/m^3	benezene ERPG-3 mg/m^3	benezene ERPG-2 mg/m^3	benezene ERPG-1 mg/m^3	butanol Headspace conc. mg/m^3	butanol ERPG-3 mg/m^3	butanol ERPG-2 mg/m^3	butanol ERPG-1 mg/m^3	dodecane Headspace conc. mg/m^3	dodecane ERPG-3 mg/m^3
3	a	SST	3	3.67E+02	1360	690	230	1.32	3130	1565	78	164.13	7500	750	75	296	7330
4	b	SST	3	1.80E+02	1360	690	230	1.32	3130	1565	78	164.13	7500	750	75	296	7330
5	c	SST	3	3.67E+02	1360	690	230	1.32	3130	1565	78	164.13	7500	750	75	296	7330
6	d	SST	3	3.67E+02	1360	690	230	1.32	3130	1565	78	164.13	7500	750	75	296	7330
7	e	SST	3	1.19E+03	1360	690	230	1.32	3130	1565	78	164.13	7500	750	75	296	7330
8	f	SST	3	3.69E+02	1360	690	230	1.32	3130	1565	78	164.13	7500	750	75	296	7330
9	g	SST	3	1.19E+03	1360	690	230	1.32	3130	1565	78	164.13	7500	750	75	296	7330
10	h	SST	3	3.69E+02	1360	690	230	1.32	3130	1565	78	164.13	7500	750	75	296	7330
11	i	DST	3	0.00E+00	1360	690	230	1.32	3130	1565	78	164.13	7500	750	75	296	7330
12	j	DST	3	3.76E+02	1360	690	230	1.32	3130	1565	78	164.13	7500	750	75	296	7330
13	k	DST	3	1.29E+02	1360	690	230	1.32	3130	1565	78	164.13	7500	750	75	296	7330
14	l	DST	3	3.74E+02	1360	690	230	1.32	3130	1565	78	164.13	7500	750	75	296	7330
15	m	DCRT	3	0.00E+00	1360	690	230	1.32	3130	1565	78	164.13	7500	750	75	296	7330
16	n	DCRT	3	8.47E+02	1360	690	230	1.32	3130	1565	78	164.13	7500	750	75	296	7330
17	o	DCRT	3	8.47E+02	1360	690	230	1.32	3130	1565	78	164.13	7500	750	75	296	7330
18	p	DCRT	3	8.47E+02	1360	690	230	1.32	3130	1565	78	164.13	7500	750	75	296	7330
19	q	SST	3	5.99E+02	1360	690	230	1.32	3130	1565	78	164.13	7500	750	75	296	7330
20	r	SST	3	3.20E+02	1360	690	230	1.32	3130	1565	78	164.13	7500	750	75	296	7330
21	s	55 kgal SST	3	9.94E+02	1360	690	230	1.32	3130	1565	78	164.13	7500	750	75	296	7330
22	t	55 kgal SST	3	3.73E+02	1360	690	230	1.32	3130	1565	78	164.13	7500	750	75	296	7330
23	u	55 kgal SST	3	4.87E+02	1360	690	230	1.32	3130	1565	78	164.13	7500	750	75	296	7330

Table 5-1. Spread Sheet for Solvent Pool Fire Cases - Toxicological. (10 sheets)

	A	B	CF	CG	CH	CI	CJ	CK	CL	CM	CN	CO	CP	CQ	CR	CS
1	Case	Tank Type	dodecane ERPG-2 mg/m^3	dodecane ERPG-1 mg/m^3	2-hexano Headspace conc. mg/m^3	2-hexano ERPG-3 mg/m^3	2-hexano ERPG-2 mg/m^3	2-hexano ERPG-1 mg/m^3	N2O Headspace conc. mg/m^3	N2O ERPG-3 mg/m^3	N2O ERPG-2 mg/m^3	N2O ERPG-1 mg/m^3	tridecane Headspace conc. mg/m^3	tridecane ERPG-3 mg/m^3	tridecane ERPG-2 mg/m^3	tridecane ERPG-1 mg/m^3
3	a	SST	1450	37	2.68	5000	500	50	2340	36000	18000	270	388	7330	1450	37
4	b	SST	1450	37	2.68	5000	500	50	2340	36000	18000	270	388	7330	1450	37
5	c	SST	1450	37	2.68	5000	500	50	2340	36000	18000	270	388	7330	1450	37
6	d	SST	1450	37	2.68	5000	500	50	2340	36000	18000	270	388	7330	1450	37
7	e	SST	1450	37	2.68	5000	500	50	2340	36000	18000	270	388	7330	1450	37
8	f	SST	1450	37	2.68	5000	500	50	2340	36000	18000	270	388	7330	1450	37
9	g	SST	1450	37	2.68	5000	500	50	2340	36000	18000	270	388	7330	1450	37
10	h	SST	1450	37	2.68	5000	500	50	2340	36000	18000	270	388	7330	1450	37
11	i	DST	1450	37	2.68	5000	500	50	2340	36000	18000	270	388	7330	1450	37
12	j	DST	1450	37	2.68	5000	500	50	2340	36000	18000	270	388	7330	1450	37
13	k	DST	1450	37	2.68	5000	500	50	2340	36000	18000	270	388	7330	1450	37
14	l	DST	1450	37	2.68	5000	500	50	2340	36000	18000	270	388	7330	1450	37
15	m	DCRT	1450	37	2.68	5000	500	50	2340	36000	18000	270	388	7330	1450	37
16	n	DCRT	1450	37	2.68	5000	500	50	2340	36000	18000	270	388	7330	1450	37
17	o	DCRT	1450	37	2.68	5000	500	50	2340	36000	18000	270	388	7330	1450	37
18	p	DCRT	1450	37	2.68	5000	500	50	2340	36000	18000	270	388	7330	1450	37
19	q	SST	1450	37	2.68	5000	500	50	2340	36000	18000	270	388	7330	1450	37
20	r	SST	1450	37	2.68	5000	500	50	2340	36000	18000	270	388	7330	1450	37
21	s	55 kgal SST	1450	37	2.68	5000	500	50	2340	36000	18000	270	388	7330	1450	37
22	t	55 kgal SST	1450	37	2.68	5000	500	50	2340	36000	18000	270	388	7330	1450	37
23	u	55 kgal SST	1450	37	2.68	5000	500	50	2340	36000	18000	270	388	7330	1450	37

Table 5-1. Spread Sheet for Solvent Pool Fire Cases - Toxicological. (10 sheets)

	A	B	CT	CU	CV	CW	CX	CY	CZ	DA	DB	DC	DD
1	Case	Tank Type	Ex. Unlikely Onsite Corrosives and Irritants Fraction	Ex. Unlikely Offsite Corrosives and Irritants Fraction	Unlikely Onsite Corrosives and Irritants Fraction	Unlikely Offsite Corrosives and Irritants Fraction	Ex. Unlikely Onsite Systemic Poisons Fraction	Ex. Unlikely Offsite Systemic Poisons Fraction	Unlikely Onsite Systemic Poisons Fraction	Unlikely Offsite Systemic Poisons Fraction	Ex. Unlikely Onsite Nervous system Fraction	Ex. Unlikely Offsite Nervous system Fraction	Unlikely Onsite Nervous system Fraction
3	a	SST	1.66E-02	3.27E-04	6.78E-02	2.10E-03	2.10E-03	2.69E-05	5.58E-03	1.55E-04	4.71E-04	1.04E-05	2.15E-03
4	b	SST	3.68E-02	3.45E-04	1.56E-01	2.37E-03	5.83E-03	8.07E-05	1.63E-02	2.22E-04	1.58E-03	1.59E-05	7.19E-03
5	c	SST	1.66E-02	3.27E-04	6.78E-02	2.10E-03	2.10E-03	1.78E-03	5.58E-03	1.55E-04	4.71E-04	1.04E-05	2.15E-03
6	d	SST	1.66E-02	3.27E-04	6.78E-02	2.10E-03	2.10E-03	1.78E-03	5.58E-03	1.55E-04	4.71E-04	1.04E-05	2.15E-03
7	e	SST	4.13E-02	1.02E-03	1.61E-01	6.01E-03	3.67E-03	1.17E-04	8.67E-03	2.64E-04	4.71E-04	1.37E-05	2.15E-03
8	f	SST	8.35E-02	3.19E-02	3.40E-01	2.05E-01	1.05E-02	3.24E-03	2.79E-02	1.51E-02	2.36E-03	1.01E-03	1.07E-02
9	g	SST	4.13E-02	1.02E-03	1.61E-01	6.01E-03	3.67E-03	1.82E-03	8.67E-03	2.64E-04	4.71E-04	1.37E-05	2.15E-03
10	h	SST	8.35E-02	3.19E-02	3.40E-01	2.05E-01	1.05E-02	3.24E-03	2.79E-02	1.51E-02	2.36E-03	1.01E-03	1.07E-02
11	i	DST	0.00E+00	0.00E+00	0.00E+00	0.00E+00	0.00E+00	5.81E-05	0.00E+00	0.00E+00	0.00E+00	0.00E+00	0.00E+00
12	j	DST	8.44E-02	3.45E-02	3.44E-01	2.22E-01	1.06E-02	3.52E-03	2.81E-02	1.62E-02	2.36E-03	1.08E-03	1.07E-02
13	k	DST	7.29E-03	4.91E-04	3.14E-02	3.47E-03	1.27E-03	1.28E-04	3.60E-03	3.54E-04	3.62E-04	2.58E-05	1.65E-03
14	l	DST	8.42E-02	3.44E-02	3.43E-01	2.21E-01	1.06E-02	3.51E-03	2.80E-02	1.62E-02	2.36E-03	1.08E-03	1.07E-02
15	m	DCRT	0.00E+00	0.00E+00	0.00E+00	0.00E+00	0.00E+00	3.69E-05	0.00E+00	0.00E+00	0.00E+00	0.00E+00	0.00E+00
16	n	DCRT	2.39E-02	1.32E-03	9.40E-02	7.95E-03	2.32E-03	1.48E-04	5.68E-03	4.07E-04	3.62E-04	2.33E-05	1.65E-03
17	o	DCRT	2.39E-02	1.32E-03	9.40E-02	7.95E-03	2.32E-03	1.48E-04	5.68E-03	4.07E-04	3.62E-04	2.33E-05	1.65E-03
18	p	DCRT	2.39E-02	1.32E-03	9.40E-02	7.95E-03	2.32E-03	1.48E-04	5.68E-03	4.07E-04	3.62E-04	2.33E-05	1.65E-03
19	q	SST	2.36E-02	6.09E-04	9.40E-02	3.75E-03	2.54E-03	1.79E-03	6.45E-03	2.25E-04	4.71E-04	1.39E-05	2.15E-03
20	r	SST	5.10E-02	6.94E-04	2.09E-01	4.53E-03	6.73E-03	1.81E-03	1.81E-02	3.51E-04	1.58E-03	2.39E-05	7.19E-03
21	s	55 kgal SST	3.55E-02	1.13E-03	1.39E-01	6.71E-03	3.30E-03	1.28E-04	7.94E-03	3.19E-04	4.71E-04	1.75E-05	2.15E-03
22	t	55 kgal SST	5.62E-02	4.37E-03	2.29E-01	2.81E-02	7.07E-03	4.75E-04	1.87E-02	2.06E-03	1.58E-03	1.37E-04	7.19E-03
23	u	55 kgal SST	2.02E-02	4.47E-04	8.13E-02	2.81E-03	2.33E-03	8.00E-05	6.03E-03	1.84E-04	4.71E-04	1.18E-05	2.15E-03

Table 5-1. Spread Sheet for Solvent Pool Fire Cases - Toxicological. (10 sheets)

	A	B	DE	DF	DG	DH	DI	DJ	DK	DL	DM
1	Case	Tank Type	Unlikely Offsite Nervous System Fraction	Ex. Unlikely Onsite Particulate Fraction	Ex. Unlikely Offsite Particulate Fraction	Unlikely Onsite Particulate Fraction	Unlikely Offsite Particulate Fraction	Ex. Unlikely Onsite HEPA Fraction	Ex. Unlikely Offsite HEPA Fraction	Unlikely Onsite HEPA Fraction	Unlikely Offsite HEPA Fraction
3	a	SST	3.69E-04	1.10E-02	5.29E-04	1.10E-01	8.81E-04	3.41E-04	3.60E-05	7.16E-03	7.00E-05
4	b	SST	5.66E-04	1.80E-02	3.99E-04	1.80E-01	6.64E-04	3.41E-04	3.60E-05	7.16E-03	7.00E-05
5	c	SST	3.69E-04	1.10E-02	5.29E-04	1.10E-01	8.81E-04	0.002091	1.74E-03	4.41E-02	3.37E-03
6	d	SST	3.69E-04	1.10E-02	5.29E-04	1.10E-01	8.81E-04	0.002091	1.74E-03	4.41E-02	3.37E-03
7	e	SST	4.87E-04	3.54E-02	2.26E-03	3.54E-01	3.76E-03	3.41E-04	3.60E-05	7.16E-03	7.00E-05
8	f	SST	3.59E-02	5.51E-02	5.17E-02	5.51E-01	8.62E-02	3.41E-04	3.60E-05	7.16E-03	7.00E-05
9	g	SST	4.87E-04	3.54E-02	2.26E-03	3.54E-01	3.76E-03	0.002091	1.74E-03	4.41E-02	3.37E-03
10	h	SST	3.59E-02	5.51E-02	5.17E-02	5.51E-01	8.62E-02	3.41E-04	3.60E-05	7.16E-03	7.00E-05
11	i	DST	0.00E+00	NA	NA	#VALUE!	#VALUE!	0	5.81E-05	0.00E+00	7.87E-04
12	j	DST	3.84E-02	5.61E-02	5.63E-02	5.61E-01	9.39E-02	3.88E-04	5.81E-05	1.38E-03	7.87E-04
13	k	DST	9.19E-04	2.97E-03	4.65E-04	2.97E-02	7.74E-04	3.88E-04	5.81E-05	1.38E-03	7.87E-04
14	l	DST	3.84E-02	5.58E-02	5.61E-02	5.58E-01	9.35E-02	3.88E-04	5.81E-05	1.38E-03	7.87E-04
15	m	DCRT	0.00E+00	NA	NA	#VALUE!	#VALUE!	0.00E+00	3.69E-05	0.00E+00	4.76E-04
16	n	DCRT	8.28E-04	1.95E-02	2.74E-03	1.95E-01	4.57E-03	1.30E-03	3.69E-05	4.86E-03	4.76E-04
17	o	DCRT	8.28E-04	1.95E-02	2.74E-03	1.95E-01	4.57E-03	1.30E-03	3.69E-05	4.86E-03	4.76E-04
18	p	DCRT	8.28E-04	1.95E-02	2.74E-03	1.95E-01	4.57E-03	1.30E-03	3.69E-05	4.86E-03	4.76E-04
19	q	SST	4.95E-04	1.79E-02	1.16E-03	1.79E-01	1.93E-03	0.002091	1.74E-03	4.41E-02	3.37E-03
20	r	SST	8.50E-04	3.20E-02	1.06E-03	3.20E-01	1.77E-03	0.002091	1.74E-03	4.41E-02	3.37E-03
21	s	55 kgal SST	6.22E-04	2.97E-02	2.42E-03	2.97E-01	4.03E-03	4.09E-04	3.60E-05	8.59E-03	7.00E-05
22	t	55 kgal SST	4.89E-03	3.73E-02	7.12E-03	3.73E-01	1.19E-02	4.09E-04	3.60E-05	8.59E-03	7.00E-05
23	u	55 kgal SST	4.20E-04	1.45E-02	7.99E-04	1.45E-01	1.33E-03	4.09E-04	3.60E-05	8.59E-03	7.00E-05

Table 5-1. Spread Sheet for Solvent Pool Fire Cases - Toxicological. (10 sheets)

	A	B	DN	DO	DP	DQ	DR	DS	DT	DU
1	Case	Tank Type	Ex. Un. Onsite Sum of Fractions Aqueous Boiloff	Ex. Un. Offsite Sum of Fractions Aqueous Boiloff	Unlikely Onsite Sum of Fractions Aqueous Boiloff	Unlikely Offsite Sum of Fractions Aqueous Boiloff	Ex. Un. Onsite Total Sum Of Fractions	Ex. Un. Offsite Total Sum Of Fractions	Unlikely Onsite Total Sum Of Fractions	Unlikely Offsite Total Sum Of Fractions
3	a	SST	4.88E-04	8.80E-06	1.83E-03	1.14E-04	3.10E-02	9.38E-04	1.94E-01	3.69E-03
4	b	SST	1.04E-03	8.62E-06	3.91E-03	1.11E-04	6.36E-02	8.85E-04	3.71E-01	4.01E-03
5	c	SST	4.88E-04	8.80E-06	1.83E-03	1.14E-04	3.27E-02	4.39E-03	2.31E-01	6.99E-03
6	d	SST	4.88E-04	8.80E-06	1.83E-03	1.14E-04	3.27E-02	4.39E-03	2.31E-01	6.99E-03
7	e	SST	1.08E-03	2.56E-05	4.04E-03	3.31E-04	8.23E-02	3.47E-03	5.37E-01	1.09E-02
8	f	SST	1.68E-03	5.88E-04	6.28E-03	7.58E-03	1.54E-01	8.85E-02	9.44E-01	3.50E-01
9	g	SST	1.08E-03	2.56E-05	4.04E-03	3.31E-04	8.40E-02	6.88E-03	5.74E-01	1.42E-02
10	h	SST	1.68E-03	5.88E-04	6.28E-03	7.58E-03	1.54E-01	8.85E-02	9.44E-01	3.50E-01
11	I	DST	#DIV/0!	0.00E+00	#DIV/0!	0.00E+00	0.00E+00	0.00E+00	#VALUE!	0.00E+00
12	j	DST	1.79E-03	6.40E-04	6.39E-03	8.67E-03	1.56E-01	9.61E-02	9.51E-01	3.80E-01
13	k	DST	2.50E-04	1.39E-05	8.95E-04	1.89E-04	1.25E-02	1.18E-03	6.87E-02	6.50E-03
14	l	DST	1.78E-03	6.37E-04	6.36E-03	8.63E-03	1.55E-01	9.58E-02	9.48E-01	3.79E-01
15	m	DCRT	#DIV/0!	0.00E+00	#DIV/0!	0.00E+00	0.00E+00	0.00E+00	#VALUE!	0.00E+00
16	n	DCRT	5.92E-04	3.11E-05	2.22E-03	4.01E-04	4.80E-02	4.30E-03	3.03E-01	1.46E-02
17	o	DCRT	5.92E-04	3.11E-05	2.22E-03	4.01E-04	4.80E-02	4.30E-03	3.03E-01	1.46E-02
18	p	DCRT	5.92E-04	3.11E-05	2.22E-03	4.01E-04	4.80E-02	4.30E-03	3.03E-01	1.46E-02
19	q	SST	5.43E-04	1.31E-05	2.04E-03	1.70E-04	4.71E-02	5.33E-03	3.28E-01	9.94E-03
20	r	SST	9.73E-04	1.21E-05	3.65E-03	1.56E-04	9.44E-02	5.35E-03	6.02E-01	1.10E-02
21	s	55 kgal SST	9.02E-04	2.74E-05	3.38E-03	3.54E-04	7.03E-02	3.75E-03	4.58E-01	1.21E-02
22	t	55 kgal SST	1.13E-03	8.08E-05	4.25E-03	1.04E-03	1.04E-01	1.22E-02	6.41E-01	4.80E-02
23	u	55 kgal SST	5.29E-04	1.09E-05	1.99E-03	1.40E-04	3.85E-02	1.38E-03	2.46E-01	4.95E-03

[1] HEPA Vent Modeled as 3.75" (9.5 mm) orifice
[2] Flapper is 50 in. (1.27 m) orifice opening at 1 psid (6.89 kPa)
[3] Vent Pipe on DST Modeled as 9.6 in. (0.24 m) orifice
[4] HEPA Vent for 55 kgal tanks is 3.42" (.087m) orifice. Flapper is 17" orifice.

6.0 COMPARISON OF RECALCULATED CONSEQUENCES WITH CONSEQUENCES BASED ON FSAR METHODOLOGY

Toxin concentrations at the onsite (100 m) receptor location are predicted herein to be significantly lower than those predicted by Cowley and Postma (1996) using FSAR methodology. The reason is that FSAR methodology does not realistically account for near-field mixing that is induced by vented gases. Since toxicological consequences are directly proportional to toxin concentration at 100 m downwind, the neglect of near-field dilution results in an overstatement of toxicological consequences.

Pool fires that have the highest calculated toxicological consequences are those that are assumed to vent gases horizontally from levitated pit cover blocks. This vent configuration yields the least dilution of the vent paths considered. In reality, multiple vent paths would likely exist and not all vented gas would exit as a horizontal slot jet pointed downwind. These factors would enhance near-field dilution as compared to the dilution assumed herein. Therefore, the bounding toxicological cases presented herein are conservative; more realistic analyses would reduce predicted consequences. The author believes that consequences of postulated pool fires are not as close to risk acceptance guidelines as indicated by the predicted sum of fractions of 0.95.

Bounding toxicological consequences are predicted for large pools in SSTs and DSTs that have the postulated flapper vent. Results for two bounding cases are compared with previous calculations (Cowley and Postma 1996) in Table 6-1.

Table 6-1. Comparison of Bounding Cases with Previous Assessment.

Pool Fire Case	Unlikely, Onsite Sum of Fractions	
	This report	Cowley and Postma 1996
h-SST Large Pool, Flapper Vent	0.94	43
ℓ-DST Large Pool, Flapper Vent	0.95	45

The sums of fractions listed in Table 6-1 illustrate the significant findings of this study: the more realistic treatment of near-field dilution of vented gases causes calculated toxicological consequences to fall beneath risk acceptance guidelines. The previous analysis based on FSAR methodology had overestimated toxicological consequences by a significant factor.

7.0 REFERENCES

Cowley, W. L., J. E. Meacham, J. M. Grigsby, and A. K. Postma, 1997, *Organic Solvent Topical*, HNF-SD-WM-SARR-036, Rev. 1, Duke Engineering and Services Hanford, Inc., Richland, Washington.

Cowley, W. L., and A. K. Postma, 1996, *Analysis of Consequences of Postulated Solvent Fires in Hanford Site Waste Tanks*, WHC-SD-WM-CN-032, Rev. 0, Westinghouse Hanford Company, Richland, Washington.

Epstein, M., 1997, *Downwind Dispersion of Toxic Combustion Products Escaping from a Hanford Site Waste Tank*, FAI/97-45, Fauske & Associates, Inc., Burr Ridge, Illinois.

Van Keuren, J. C., J. S. Davis, and M. L. Dentler, 1995, *Toxic Chemical Considerations for Tank Farm Releases*, WHC-SD-WM-SARR-011, Rev. 1, Westinghouse Hanford Company, Richland, Washington.

This page intentionally left blank.

ATTACHMENT A

FAI/97-45
DOWNWIND DISPERSION OF TOXIC COMBUSTION PRODUCTS ESCAPING FROM A HANFORD SITE WASTE TANK

This page intentionally left blank.

Fauske & Associates, Inc.

April 21, 1997

Mr. J. E. Meacham
Duke Engineering & Services Hanford
S7-14
P.O. Box 350
Richland, WA 99352-0350

Dear Joe:

SUBJECT: *FAI/97-45, "Downwind Dispersion of Toxic Combustion Products Escaping from a Hanford Site Waste Tank," by Michael Epstein*

Please find enclosed three copies of the subject report. In this report a model is described for predicting the atmospheric concentrations of radioactive (toxic) materials arising from the release of combustion product gases or aerosols from a Hanford Site waste tank within which a liquid-organic chemical fire is postulated to occur. Substantial dilution of the combustion product plumes are noted at 100 m downwind of the waste tank.

The submittal of this report completes Task Order No. 9-MAA-SLB-A25777. Please call Mike Epstein (630) 887-5210 if any questions should arise.

Sincerely yours,

Hans K. Fauske
President

HKF:lak
Enclosure

cc: M. Epstein, FAI
A. K. Postma, G&P Consultants, Inc.

16W070 West 83rd Street • Burr Ridge, Illinois 60521 • (630) 323-8750
Telefax (630) 986-5481 • E-Mail - fai@fauske.com

FAI/97-45
DOWNWIND DISPERSION OF TOXIC COMBUSTION PRODUCTS ESCAPING FROM A HANFORD SITE WASTE TANK

Submitted To:
Duke Engineering & Services Hanford
Richland, Washington

Prepared By:
Michael Epstein
Fauske & Associates, Inc.
16W070 West 83rd Street
Burr Ridge, Illinois 60521
TEL: (630) 323-8750
FAX: (630) 986-5481

April, 1997

TABLE OF CONTENTS

		Page
1.0	INTRODUCTION	1-1
2.0	PHYSICAL MODEL	2-1
3.0	ENTRAINMENT EQUATIONS	3-1
4.0	AIRBORNE JET ZONE	4-1
5.0	EQUATIONS FOR GROUND-LEVEL JETS	5-1
6.0	ATMOSPHERIC VELOCITY DISTRIBUTION AND EQUATION OF STATE	6-1
7.0	RESULTS	7-1
8.0	DISCUSSION OF VALIDITY OF MODEL	8-1
9.0	CONCLUSIONS	9-1
10.0	NOMENCLATURE	10-1
11.0	REFERENCES	11-1
	APPENDIX A	A-1

LIST OF FIGURES

Page

Figure 1 Schematic diagram of plume model for circular and rectangular plumes 2-3

Figure 2 Schematic drawings illustrating four waste tank vent geometries of interest 7-3

Figure 3 Predicted plume profile for Case 1A (see Table 4); vertical discharge from 3.3-m tall circular stack 7-4

Figure 4 Normalized concentration of released species versus distance downwind for Case 1A (see Table 4); vertical discharge from 3.3-m tall circular stack 7-5

Figure 5 Predicted plume profile for Case 3B (see Table 4); vertical discharge from long slit 0.61 m above ground

Figure 6 Normalized concentration of released species versus distance downwind for Case 3B (see Table 4); vertical discharge from long slit 0.61 m above ground 7-7

Figure 7 Predicted plume profile for Case 3A (see Table 4); horizontal discharge from long slit 0.61 m above ground 7-10

Figure 8 Normalized concentration of released species versus distance downwind for Case 3A (see Table 4); horizontal discharge from long slit 0.61 m above ground 7-11

Figure 9 Predicted plume profile in vicinity of release location for Case 4A. (see Table 4); downward discharge from circular stack 1.22 m above ground 7-12

Figure 10 Normalized concentration of released species versus distance downwind for Case 4A (see Table 4); downward discharge from circular stack 1.22 m above ground 7-14

Figure 11 Normalized concentration profiles for elevated, circular, pure-momentum jets; comparison of numerical model with exact solution 8-3

LIST OF FIGURES - (Cont'd)

Page

Figure 12 Normalized concentration profiles for elevated, rectangular, pure-momentum jets; comparison of numerical model with exact solution 8-4

Figure 13 Normalized concentration profiles for ground-level, rectangular, pure-momentum jets; comparison of numerical model with exact solution 8-5

Figure 14 Predicted plume profile illustrating final plume rise at low wind speed in stable atmosphere 8-8

Figure 15 Predicted plume profile illustrating final plume rise at moderate wind speed in stable atmosphere 8-9

Figure 16 Comparison of numerical model plume rise predictions with the semi-empirical plume rise correlation of Briggs (1984) 8-10

LIST OF TABLES

Page

Table 1 Values for Constants for ay and az in Eq. (8) 3-4

Table 2 Values of the Exponent p in Eq. (55) for Six Stability Classes and Two Surface Roughness 6-1

Table 3 Temperature Gradient in a Potential Atmosphere in K m~i for Six Stability Classes 6-2

Table 4 Initial Conditions for the Numerical Calculations 7-2

Table 5 Predicted Plume Heights and Normalized Species Concentrations at 100 m Downwind 7-9

1.0 INTRODUCTION

A model is presented here for predicting the downwind transport and dispersion of radioactive (toxic) gases and aerosols released to the atmosphere from a rupture or vent opening connected to an underground Hanford Site waste tank during a postulated, tank-internal organic-chemical pool fire. In the model it is assumed that for some rather large distance downwind of the release location (in some cases of the order of hundreds of meters), the effects of buoyancy and atmospheric turbulence on the inflow of atmospheric air into the toxic jet (plume) is negligible in comparison with the effects of turbulence generated by the jet. This assumption is what distinguishes the present model from most of the previous modeling efforts on hazardous species releases, which are based on the notion that downward transport and dispersion are controlled by the wind and atmospheric turbulence, respectively, and represented by the Gaussian-plume model, beginning at or above the release location. It is important to recognize that the velocity of a jet that emanates from a waste tank pressurized internally by a chemical fire may be of the order of one hundred meters per second (224 mph) and well above the prevailing wind speed. Generally, therefore, Gaussian models will overpredict hazardous species concentrations in the near field of a "high pressure release" because of the dominance of the jet's self-generated turbulence.

Jets that are warm relative to the atmosphere and/or directed upward with high initial momentum will rise to heights that are much greater than their initial release height. This jet rise behavior is included in the Gaussian models by using the plume rise equations recommended by Briggs (1984).* Interestingly enough, his equations are based on plume trajectory calculations which assume plume mixing with the atmosphere by the plume's self-generated turbulence. However, the significant dilution of the radioactive species during plume rise is ignored in the Gaussian model of the plume rise. Various ad hoc approaches have been used in Gaussian models to terminate the plume rise and begin the Gaussian plume of horizontal

*A jet is usually defined as a plume with no initial buoyancy. Most of the releases of practical interest have both initial momentum and initial buoyancy and therefore should be referred to as plumes. However, in this report we do not distinguish between jets and plumes and we use these terms interchangeably.

trajectory. The difficulty with this approach is that the plume trajectory may not in fact become horizontal within any distance of practical interest. Moreover, none of the available plume rise models appear to be applicable to the situation of a gas at high pressure released to the atmosphere at a non-vertical angle of inclination.

Here an integral model for the prediction of the spreading and rising of buoyant and/or high momentum toxic jets in the near and far fields is introduced. The model is based on the fundamental conservation equations of fluid mechanics. To close the system of equations it is necessary to adopt empirical models of the rate of entrainment of ambient air by the jet. However, this empirical input is well identifiable and is based on experimental evidence or physical reasoning.

2.0 PHYSICAL MODEL

A schematic representation of a hazardous gas jet being released through a breach or vent that leads from an underground waste-tank headspace subjected to a chemical fire is shown in Fig. 1. The underground waste tank is not shown in the figure. The jet may be vertical or inclined at the vent and is released at or above ground level. The equations are written to take account of a temporarily steady flow of waste tank combustion product gas (air) and a steady horizontal wind. The wind direction does not change with horizontal distance x or altitude z. The jet lies in the x,z plane. In developing the jet dispersion model it is necessary to divide the jet into two regions: (i) an airborne (unbounded) jet zone in which the trajectory and dilution of the jet is predicted and (ii) a ground-level jet behavior zone which always occurs (far from the vent)when certain weather conditions are present and is likely to occur in the vicinity of the vent when the release is directed toward the ground. It is assumed that the release-gas flow is sufficiently subsonic so that it is fully depressurized to atmospheric pressure just outside the vent opening.

Over the distance the jet is airborne its cross-section is taken to be circular when the jet is released from a circular vent (Fig. 1a). The cross-section of an airborne jet released from a slit-like opening is assumed to be rectangular (Fig. 1b). In both cases the radius R of the jet is assumed to be small compared with its centerline radius of curvature (slender plume approximation). The cross-section of the ground-level jet is rectangular. The half-width of the rectangular jet W at ground contact is calculated by setting the area of the ground-level jet equal to that of the elevated jet. This ensures that in the post-ground contact region the mass and momentum fluxes within the jet are conserved and that the continuity and smoothness of toxin concentration and jet temperature with distance are preserved. A discontinuous change from radius R to width W occurs when an initially circular plume contacts the ground.

In the present model only two distinct regimes of jet entrainment behavior are considered: mixing by the jet's self-generated turbulence in the near field and mixing by environmental turbulence in the far field. Moreover a fairly sharp transition point at which near-field entrainment behavior changes to far-field behavior is assumed. The intermediate regime

involving the combined modes of mixing into the jet is regarded as insignificant. We begin the description of the jet model with a discussion of the entrainment equations.

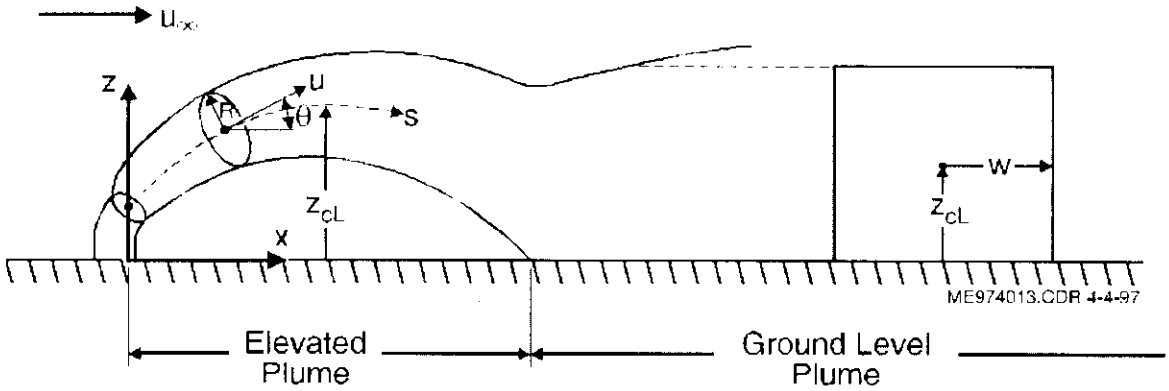

(a) Plume released from circular vent

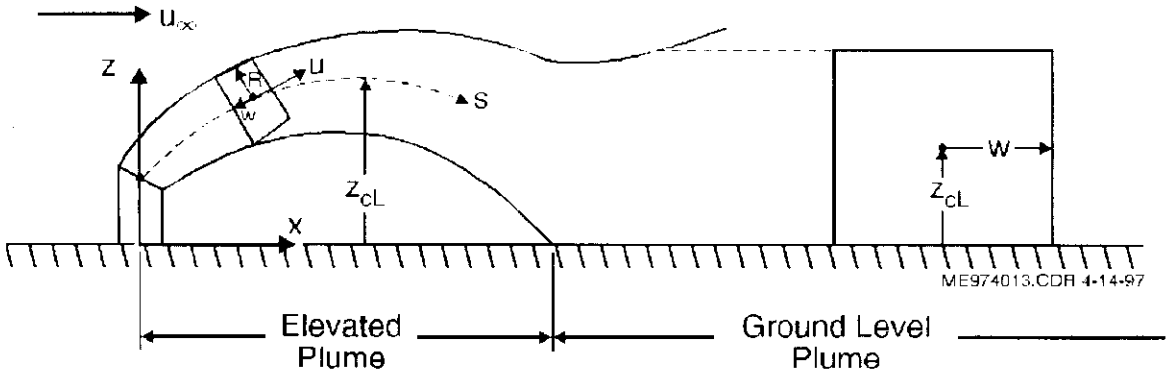

(b) Plume released from rectangular (slit) vent

Figure 1 Schematic diagrapm of plume model for circular and rectangular plumes.

3.0 ENTRAINMENT EQUATIONS

Hirst (1971) performed an analysis on a limited set of experimental data on buoyant jet flow discharged into a uniform cross stream to determine the jet entrainment velocity due to the jet's self-generated turbulence. Using the form suggested by Morton et al. (1956) as a basis, he constructed a correlation for the entrainment velocity v_{en}. For jets with a two-dimensional trajectory, his expression becomes

$$v_{en} = \left(\frac{\rho}{\rho_\infty}\right)^{1/2} \left(E_0 |u - u_\infty \cos\theta| + E_1 u_\infty |\sin\theta|\right) \tag{1}$$

where the term $|u - u_\infty \cos\theta|$ represents the relative velocity of the jet with respect to the wind. Actually, Eq. (1) is a combination of the entrainment model proposed by Hirst and the entrainment model of Ricou and Spalding (1961) for vastly different jet and ambient densities, ρ and ρ_∞, respectively. Equation (1) reduces to the entrainment function of Hirst in the limit $\rho \to \rho_\infty$. The constants of proportionality E_0 and E_1 are called the entrainment coefficients. Ricou and Spalding have verified through measurements that for pure momentum jets injected into a quiescent ambient ($u_\infty = 0$) values of E_0 lie within the range 0.06 to 0.12.

Morton (1959) found that if a uniform velocity profile is used $E_0 = 0.12$ results in the best agreement between theory and experiment. From data on buoyant water jets discharged at varying angles into flowing aqueous salt solutions, Hirst (1971) specified the values $E_0 = 0.057$ and $E_1 = 0.513$. His value of E_0 is consistent with the lower end of the range recommended by Ricou and Spalding for pure momentum jets ($u_\infty = 0$). Hoult et al. (1969) suggested, also on the basis of experiments with salt solutions and water, $E_0 = 0.12$ and $E_1 = 0.6$. Their E_0 is in agreement with the upper end of the range 0.06 to 0.12. In the calculations which follow, we shall adopt Eq. (1) and use values of E_0 and E_1 of 0.1 and 0.5, respectively.

In the far field the energy-containing eddies of environmental turbulence dominate mixing, and the jet growth (expansion) is strictly due to the action of the wind. A number of different ways have been proposed to relate the entrainment velocity to ambient turbulence. Most of these rely on knowledge of one or a combination of the following atmospheric

quantities: the turbulent diffusivity, the root-mean-square-velocity, and the energy dissipation rate. Unfortunately, measurements of these microphysical properties of atmospheric turbulence usually are totally lacking. An alternative approach is to use the measured Gaussian dispersion coefficients to obtain a formula for entrainment due to atmospheric turbulence effects (Epstein et al., 1990).

In the very far field the released species mass continuity equation and the overall mass continuity equation for the jet are

$$\frac{d}{dx}(Y\rho_\infty u_\infty A) = 0 \tag{2}$$

$$\frac{d}{dx}(\rho_\infty u_\infty) = \rho_\infty v_{en} C \tag{3}$$

where Y is the mass fraction of the released (hazardous) species (gas or aerosol). The meanings of all the symbols in this report are given in Section 10. Solving Eq. (2) we have

$$\dot{m}_r = Y\rho_\infty u_\infty A \tag{4}$$

where $\dot{m}_r$ is the mass rate of release of the hazardous species. Substituting this result into Eq. (3) gives the following expression for the entrainment velocity as a function of the inverse concentration gradient d(1/Y)/dx:

$$v_{en} = \frac{\dot{m}_r}{\rho_\infty C}\frac{d}{dx}\left(\frac{1}{Y}\right) \tag{5}$$

Now far downwind from the source, where the jet (plume) has become very dilute, the Gaussian plume equation for the centerline concentration is

$$Y = \frac{\dot{m}_r}{\pi\rho_\infty u_\infty \sigma_y(x)\sigma_z(x)} \tag{6}$$

where $\sigma_y(x)$ and $\sigma_z(x)$ are the Gaussian dispersion coefficients in the y- and z-directions, respectively. Identifying Y in Eq. (6) with Y in Eq. (5) gives an equation for the entrainment velocity due to atmospheric turbulence in the far field; namely,

$$v_{en} = \frac{u_*}{C} \frac{d}{dx} \left[\sigma_y(x)\sigma_z(x)\right] \tag{7}$$

While this expression has been derived for passive (Gaussian) plume behavior in the very far field we will assume here that the rate of entrainment due to atmospheric turbulence is given by Eq. (7) regardless of the distance from the source. That is, we are assuming that the manner in which ambient turbulence contributes to the entrainment velocity is independent of whether the plume is transported only by the wind or whether plume buoyancy and momentum control the motion of the plume. It is important to note in this regard that the use of Eq. (7) does not imply Gaussian plume behavior. Equation (7) provides the additional closure (entrainment) assumption that is required to proceed with the predicting of the motion of the plume after ambient turbulence becomes more important than the plume's self-generated turbulence but well before passive plume behavior is established. Of course, choosing Eq. (7) as a closure law guarantees that the jet model will tend towards the desired Gaussian behavior (with respect to centerline concentration) in the very far field.

Close to the source, the entrainment velocity given by Eq. (1) greatly exceeds that given by Eq. (7) and vice versa at distances far from the source. One would expect, therefore, a fairly definite transition point (or perhaps a short transition zone) at which the character of the jet changes when the near- and far-field entrainment velocities are comparable. Therefore, during the course of a calculation a switch is made from Eq. (1) to Eq. (7) at the location in which both equations predict the same entrainment velocity, thereby merging the internally generated turbulence mixing model with the ambient turbulence mixing model.

Some remarks with regard to the calculation of the dispersion coefficients are in order. Values of σ_y and σ_z as functions of distance x from the release location are available from the air pollution literature and are commonly referred to as the Pasquill-Gifford curves. Many of the analytical fits to these curves can be represented by the power-law expressions

$$\sigma_y = a_i x^{b_i} \quad \sigma_z = c_i x^{d_i} \tag{8}$$

where i denotes the atmospheric stability class A through F. The coefficients and exponents a_i, b_i, c_i, and d_i used in the present work are the same as those recommended by Tadmor and Gur (1969) and employed in the MACCS code system (Jow et al., 1986) and are given in Table 1. The values of x, σ_y and σ_z in Eq. (8) are expressed in meters.

Table 1

Values for Constants for σ_y and σ_z in Eq. (8)

Stability Class		Constant			
P-G	**i**	a_i	b_i	c_i	d_i
A	1	0.3658	0.9031	0.00025	2.125
B	2	0.2751	0.9031	0.0019	1.6021
C	3	0.2089	0.9031	0.2	0.8543
D	4	0.1474	0.9031	0.3	0.6532
E	5	0.1046	0.9031	0.4	0.6021
F	6	0.0722	0.9031	0.2	0.6020

Stability classes A through C represent three unstable states of the atmosphere. Stability class D refers to a neutral atmosphere, and stability classes E and F refer to two stable atmospheric conditions. The classification of stability states is based on the reaction of a parcel of air to a small vertical displacement from some initial height at which it is in thermal equilibrium with the atmosphere. The rate of change of the parcel temperature with vertical displacement distance is known as the adiabatic temperature gradient: $-g/c_p \approx -0.01$ K m^{-1}. If the adiabatic temperature gradient is greater than the actual atmospheric temperature gradient the density of the parcel upon upward displacement will be less than that of the atmosphere and the parcel will continue to accelerate upward. If the parcel is displaced downward its density will be greater than that of the atmosphere and its downward acceleration will continue. Thus the parcel is accelerated away from its original equilibrium position regardless of which direction

it is displaced and the atmosphere is regarded as unstable. By similar arguments one can demonstrate that if the adiabatic temperature gradient $-g/c_p$ is less than the atmospheric temperature gradient the displaced air parcel will return to its equilibrium position and the atmosphere is regarded as stable. In a neutral atmosphere the atmospheric temperature gradient equals $-g/c_p$ and the density of the displaced parcel remains the same as that of the atmosphere. The stability of the atmosphere is not only important with respect to the values of σ_y and σ_z, that is with respect to plume diffusion in the atmosphere, but is also important in determining the trajectory of the plume. In general, plume dilution decreases with increasing atmospheric stability. Therefore, to err on the conservative side only the class F stability coefficients in Table 1 are used in the present model.

Now that the closure laws (for plume entrainment) have been derived, the jet behavior can be determined from the (jet) conservation equations for mass, momentum and energy. The plume (jet) conservation equations are the subject of the next two sections.

4.0 AIRBORNE JET ZONE

The centerline of the airborne but unbounded jet makes an angle θ with the horizontal (see Fig. 1), s is the distance along the jet, A is the cross-sectional area of the jet, and C is the perimeter of the cross-section. The location s = 0 for the airborne jet refers to the plane of the rupture opening. Given the complexity of the problem that we are dealing with it is sufficient to assume that inside the jet the velocity, gas and aerosol concentrations, and temperature are uniform in the crosswind plane. That is, each variable is assumed to have "top-hat" form with a certain value inside the plume and another value outside the plume, and a discontinuity at the plume boundaries. Top-hat profiles have yielded good results for buoyant plumes (Morton et al., 1956 and Hoult et al., 1969).

The equations for the conservation of mass of a representative hazardous gas or aerosol species escaping from the waste tank headspace and the conservation of total jet mass (headspace gas plus outside air entrained by the jet) are

$$\frac{d}{ds}(\rho u A Y) = 0 \tag{9}$$

$$\frac{d}{ds}(\rho u A) = \rho_{\infty} v_{en} C \tag{10}$$

The momentum equation in the vertical direction is a balance between jet momentum and mass:

$$\frac{d}{ds}(\rho A u^2 \sin\theta) = g(\rho_{\infty} - \rho)A \tag{11}$$

The momentum equation in the horizontal direction is a balance between jet momentum and momentum entrained:

$$\frac{d}{ds}(\rho A u^2 \cos\theta) = u_{\infty}\frac{d}{ds}(\rho A u) \tag{12}$$

Conservation of heat may be written in the following form

$$\frac{d}{ds}(\rho u A h) = \rho_a v_{en} C h \tag{13}$$

where h is the overall enthalpy of the mixture within the jet. In writing Eq. (13) we have neglected the kinetic and potential energy terms. The former quantity may not be small very close to the source of a high velocity relatively cold jet, within a few vent opening diameters, but is negligible at distances from the source of practical interest.

In evaluating the mixture properties within the jet we ignore the presence of the hazardous species (gas + aerosol) on the basis that these materials are always present in the headspace gas in trace amounts. Thus we can express the overall density and the overall enthalpy of the mixture as the sum of the densities and enthalpies of only the air and headspace reacted gas components. Further simplification is possible by making the defensible assumption that the reacted headspace gas mixture may be treated as air. The energy equation, Eq. (13), may be readily converted from enthalpy to temperature as the dependent variable by introducing the thermodynamic relation h(T) for air, assuming the air to be ideal. The pressure within the jet is equal to the atmospheric pressure P_a this requirement together with the ideal gas law gives

$$P_a = \rho R_a T \tag{14}$$

It is worth mentioning at this point that the thermodynamic properties of the atmosphere, namely P_a, ρ_a, and T_a are not constant but vary with altitude z. We will return to this issue later on.

The height z_{cl} of the jet centerline above ground level can be related to the distance s along the jet and the jet angle θ by the differential relation

$$\frac{dz_{cl}}{ds} = \sin\theta \tag{15}$$

and, similarly, the horizontal distance x from the vent opening is given by

$$\frac{dx}{ds} = \cos\theta \tag{16}$$

When the cross-section of the elevated jet is taken to be circular, the radius R, circumference C and cross-sectional area A are related by the expressions

$$C = 2\pi R = 2(\pi A)^{1/2} \tag{17}$$

For a jet of rectangular cross section the circumference C is a function of both the cross-sectional area A and the half-width W of the jet: that is

$$C = \frac{A}{W} + 4W \tag{18}$$

The "radius" R (see Fig. 1b) of the rectangular plume is related to A and W by

$$R = \frac{A}{4W} \tag{19}$$

Now the rectangular plume geometry requires one additional equation to describe the expansion of the jet's half-width W. This equation is given by the kinematic condition

$$u \frac{dW}{ds} = v_{en} \tag{20}$$

which allows the plume to spread by entrainment in the direction normal to the x-z plane in Fig. 1b.

The above equations express the mathematical consequences of the airborne jet model and, together with an equation of state for the atmosphere, are sufficient to determine the coupled unknown quantities, ρ, Y, u, A, T, z_{cl} and θ as functions of the horizontal coordinate x. These quantities are subject to the following initial conditions at the release location x = 0:

$$\rho = \rho_o \quad , \quad Y = Y_o \quad , \quad W = W_o \quad , \quad u = u_o \tag{21}$$

$$T = T_o \quad , \quad A = A_o \quad , \quad z_{cl} = z_{cl,o} \quad , \quad \theta = \theta_o \tag{22}$$

where $z_{el,o}$ is the height of the vent opening above ground and θ_o is the angle of the release relative to the horizontal at the vent.

5.0 EQUATIONS FOR GROUND-LEVEL JETS

In unstable air (stability classes A through D) with light winds the plume exhibits the purely airborne behavior described mathematically in the previous section. In fact, plume rise in this case is unlimited and nothing prevents the plume from reaching the upper levels of the atmosphere, much like a thundercloud. The atmosphere, however, is not always unstable everywhere. Changes in solar radiation from night to day set up a cycle of stable and unstable situations. During the night air is normally stably stratified and the condition of the atmosphere is well-described by stability classes E or F. In such stable air, often referred to as a ground-based inversion, plume rise is limited because of the negative buoyancy acquired by entraining ambient air and transporting it to levels of higher atmospheric temperature (actually potential temperature; see Section 6). During the day the air may be unstable near the ground but above some height an inversion layer of stable air is present. The interaction of plumes with elevated inversions is not easy to predict. Plumes may penetrate the inversion layer if the layer is thin or close to the ground. The approach employed in the present model is a conservative one in that the assumption is made that the atmosphere is always stable from the ground up and represented by stability class F. Fortunately, plume behavior for this case can be modeled.

Horizontal or downward-directed releases into moderate-to-strong winds, usually results in the plume making contact with the ground before significant plume rise occurs. Predicting plume behavior beyond the point of touchdown is not an easy matter. The plume may retain enough buoyancy so that at some location it lifts off the ground and once again becomes an elevated plume. Or, the plume may be prevented from leaving the ground as a consequence of down drafts. Or ambient turbulence may "withdraw" so much vertical momentum and buoyancy from the jet that its behavior after ground contact is that of a grounded, near-passive wind-driven plume. Apparently, no criterion is available to predict which one of these behaviors is favored in a given situation, but the latter grounded plume scenarios are more easily modeled and will serve adequately to predict conservative downwind concentrations of radioactive species.

In the present model, the ground-level plume is handled in the same way as the rectangular elevated jet, except that the momentum equations, Eqs. (11) and (12), and the

kinematic equations, Eqs. (15) and (16), are modified to account for the presence of the ground. Specifically, Eq. (11) is omitted from the equation set and θ in Eq. (12) is set equal to zero if ground contact is made. Thus the jet is assumed to lose its buoyancy and its vertical momentum as a result of contact with the ground so that its ground-level motion and dispersion are strictly controlled by axial momentum and entrainment. Equations can be written that account for gravity-controlled compaction/expansion and sideways spreading of a ground-level plume (see, e.g. Epstein et al., 1990). However the present application requires the coupling of these equations with the equations for the stability of the atmosphere and their derivation and implementation in a computer routine are beyond the scope of the present effort.

The plume is assumed to feel the presence of the ground when the elevation z_{cl} of the centerline of the plume is equal to its radius R. Note that beyond ground-contact z_{cl} still represents the vertical distance from the ground to the centerline of the plume (see Fig. 1). The height (vertical thickness) and radius (half-width) of the ground-level plume are, respectively, $2z_{cl}$ and W. Beyond ground contact, Eq. (17) for the perimeter of the circular elevated or Eq. (18) for the perimeter of the elevated rectangular jet are replaced by the expression

$$C = \frac{A}{W} + 2W \tag{23}$$

this relation for the rectangular ground-level plume is derived by not allowing entrainment to occur at the jet-ground boundary. The half-width W of the plume at ground contact is calculated by setting the vertical distance z_{cl} and area A of the rectangular plume equal to those of the elevated plume (circular or rectangular). As mentioned previously, this ensures that in the post contact region the mass, momentum and energy fluxes within the jet are conserved and that the continuity and smoothness of concentrations- and temperature-with-distance are preserved. A discontinuity in W will exist when a circular plume contacts the ground; its value at ground contact is

$$W = \frac{A}{4z_{cl}} \tag{24}$$

The above equation is valid beyond the location of plume touchdown and is used to calculate the vertical distance z_{cl} to the grounded plume's centerline. Thus Eq. (24) replaces Eq. (15) for the airborne plume.

Some additional points with respect to the computation of ground-level plume behavior are worth noting. If the plume's self-generated turbulence is still causing entrainment after plume touchdown, the cross-wind component of the entrainment velocity is set equal to zero by demanding that $\theta = 0$ in Eq. (1). In other words ground-level plumes are regarded as quasi-horizontal with boundary-layer-like behavior. After the transition to a ground-level plume is made the horizontal distance x is related to the distance s along the plume via the differential geometric relationship

$$\frac{dx}{ds} = \left[1 - \left(\frac{dz_{cl}}{ds}\right)^2\right]^{1/2} \tag{25}$$

This equation replaces Eq. (16) for the free elevated plume.

6.0 ATMOSPHERIC VELOCITY DISTRIBUTION AND EQUATION OF STATE

In order to complete the equations of plume behavior described in the foregoing, we need to specify relations for the wind velocity u , ambient pressure P , ambient density ρ , and ambient temperature T , all as a function of plume altitude z_{cl}.

It was found by Blasius (see Schlichting, 1968) and others that the mean velocity distribution in a turbulent boundary layer could well be described by the empirical law

$$u_{\infty} = u_{\infty,ref} \left(\frac{z_{cl}}{z_{ref}} \right)^{p} \tag{26}$$

where p is an exponent whose value depends on the roughness of the surface. This law seems to have found wide acceptance also in meteorological work (Hanna, 1982). In this application the reference windspeed $u_{\infty,ref}$ is usually evaluated at the reference height z_{ref} = 10 m, and the exponent p depends on stability class as well as surface roughness. The values of p are taken from Hanna (1982) and are given in Table 2. Recall that here we are only concerned with stability class F.

Table 2

Values of the Exponent p in Eq. (26) for Six Stability Classes and Two Surface Roughness

Stability Class	A	B	C	D	E	F
Urban Surfaces	0.15	0.15	0.20	0.25	0.40	0.60
Rural Surfaces	0.07	0.07	0.10	0.15	0.35	0.55

As demonstrated by Briggs (1984) and Plate (1971), in order for the equation of state of the atmosphere to be compatible with the incompressible conservation equations** for atmospheric boundary layers or plumes, the equation of state must be based on the potential temperature distribution $T_{\theta}(z)$ of the atmosphere rather than the actual temperature distribution $T_{atm}(z)$ of the atmosphere. The potential temperature is defined in such a way that its gradient is equal to the actual atmospheric temperature gradient minus the temperature gradient $-g/c_p$ produced by air in adiabatic vertical motion; namely,

$$\frac{dT_{\theta}}{dz} = \frac{dT_{atm}}{dz} + \frac{g}{c_p} \tag{27}$$

The atmospheric temperature gradient and, therefore, the potential temperature gradient are assumed to be constant with altitude. The U.S. Nuclear Regulatory Commission Guide 1.23 (1972) specifies ranges for dT_{atm}/dz for the six atmospheric stability classes A through F. The values of dT_{θ}/dz given below were obtained from Eq. (27), using the midpoint values of the dT_{atm}/dz ranges and the fact that $g/c_p \approx 0.01 K\ m^{-1}$. These values are listed in Table 3 where the constant derivative dT_{θ}/dz is denoted by the symbol β.

Table 3

Temperature Gradient in a Potential Atmosphere in K m^{-1} for Six Stability Classes

Stability Class	A	B	C	D	E	F
$\beta = dT_{\theta}/dz$	-0.01	-0.008	-0.006	0.0	0.015	0.0375

Again, here we only use the value of β associated with stability class F. It can be readily shown by application of the equation of state for an ideal gas and the hydrostatic equation that the vertical variations of temperature, pressure and density with plume altitude in a potential atmosphere are given by the following differential equations

**The conservation equations employed here are based on the Boussinesq approximation that density differences due to compressibility are unimportant except in the buoyant-force terms.

$$\frac{dT_{\cdot}}{ds} = \beta \frac{dz_{cl}}{ds} \tag{28}$$

$$\frac{d\rho_{\cdot}}{ds} = - \frac{(\beta + g/R_a)\ \rho_{\cdot}}{T_{\cdot}} \bullet \frac{dz_{cl}}{ds} \tag{29}$$

$$\frac{dP_{\cdot}}{ds} = - \rho_{\cdot} g \bullet \frac{dz_{cl}}{ds} \tag{30}$$

7.0 RESULTS

From the system of equations presented in the previous sections we can compute the released species and entrained air concentrations, jet temperature, jet velocity, jet density and jet centerline and boundaries as a function of distance from the release location. To utilize available numerical integration schemes, the equations were converted to an equivalent system of first-order ordinary differential equations by expanding the derivatives in Eqs. (9)-(13). Numerical integration was performed using Euler's elementary method and a forward integration step size $\Delta s = 10^{-4}$ m.

Four different Hanford waste-tank-vent geometries are of interest and are treated here. The four vent geometries are illustrated schematically in Fig. 2 and for purposes of identification in this report are assigned numbers (types) ranging from 1 to 4. Three cases were considered for each vent type and are denoted by A, B, or C. The initial conditions for each of the twelve numerical cases, namely 1A, 1B,.....,4B, 4C, are summarized in Table 4. The vent type recommendations as well as the initial values for each case were provided by Postma (1997). All the numerical cases are for a windspeed $u_{,ref} = 1.0$ m s^{-1} (2.24 mph) and for the following atmospheric thermodynamic conditions at the elevation of the vent relative to the ground: $T_{,0} = 285.0$K, $\rho_{,0} = 1.224$ kg m^{-3}, and $P_{,0} = 10^5$ Pa. The stability of the atmosphere is regarded as stable so that the potential temperature gradient $\beta = 0.0375$ K m^{-1} (see Table 3) and the exponent in the windspeed velocity distribution function, Eq. (26), is $p = 0.55$ (see Table 2). From a toxicological point of view, the normalized hazardous species concentration (Y/Y_0) at 100 m downwind of the vent is of major interest.

The predicted plume profiles and hazardous species concentrations for Cases 1A and 3B are shown in Figs. 3 to 6. The plume profiles in Figs. 3 and 5 include the upper and lower plume boundaries and the plume centerline as a function of horizontal distance. In both cases the waste tank combustion-product gas is discharged vertically upward. In Case 1A the gas vents to the atmosphere through a 0.407-m (16-in) diameter stack. In Case 3B the gas vents through a 3.04-m (10-ft) long slit of opening "diameter" 0.153 m (6.0″). Over the 100-m downwind distance of interest the spreading of the plumes is caused by self-generated turbulence

Table 4

Initial Conditions for the Numerical Calculations

Vent Type & Case	$z_{cl,0}$ (m)	u_0 (m s^{-1})	T_0 (K)	θ_0 (radians)	A_0 (m^2)	W_0 (m)
1A	3.3	90.0	755.0	$\pi/2$	0.13	-
1B	3.3	3.7	310.0	$\pi/2$	0.13	-
1C	3.3	45.0	530.0	$\pi/2$	0.13	-
2A	0.0	90.0	505.0	$\pi/2$	0.894	-
2B	0.0	15.0	505.0	$\pi/2$	0.894	-
2C	0.0	15.0	310.0	$\pi/2$	0.073	-
3A	0.61	120.0	505.0	0.0	0.465	1.52
3B	0.61	120.0	505.0	$\pi/2$	0.465	1.52
3C	0.61	120.0	505.0	0.0	7.74×10^{-2}	1.52
4A	1.22	180.0	755.0	$-\pi/2$	8.11×10^{-3}	-
4B	1.22	90.0	505.0	$-\pi/2$	8.11×10^{-3}	-
4C	1.22	30.0	310.0	$-\pi/2$	8.11×10^{-3}	-

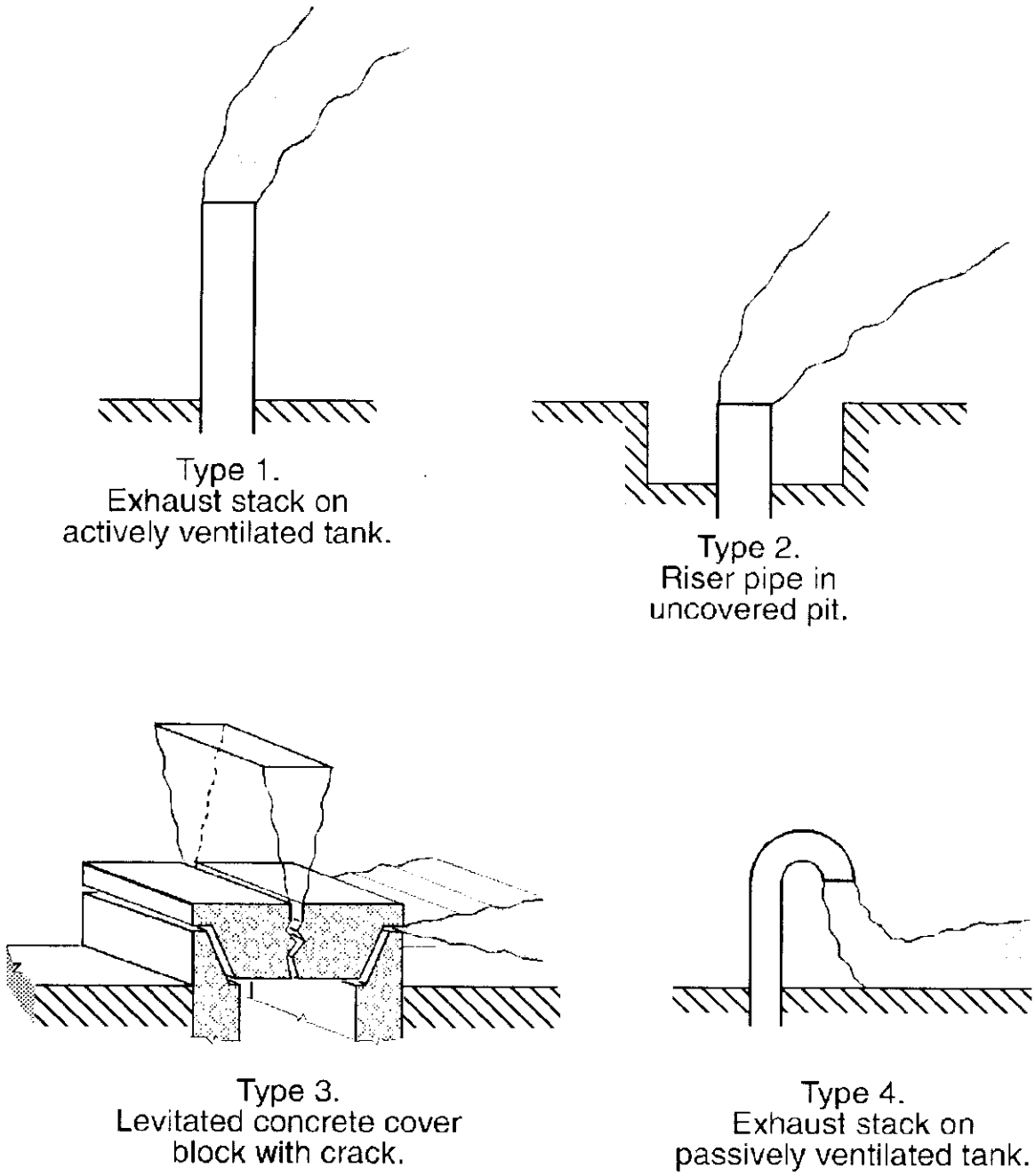

Figure2 Schematic drawings illustrating four waste tank vent geometries of interest.

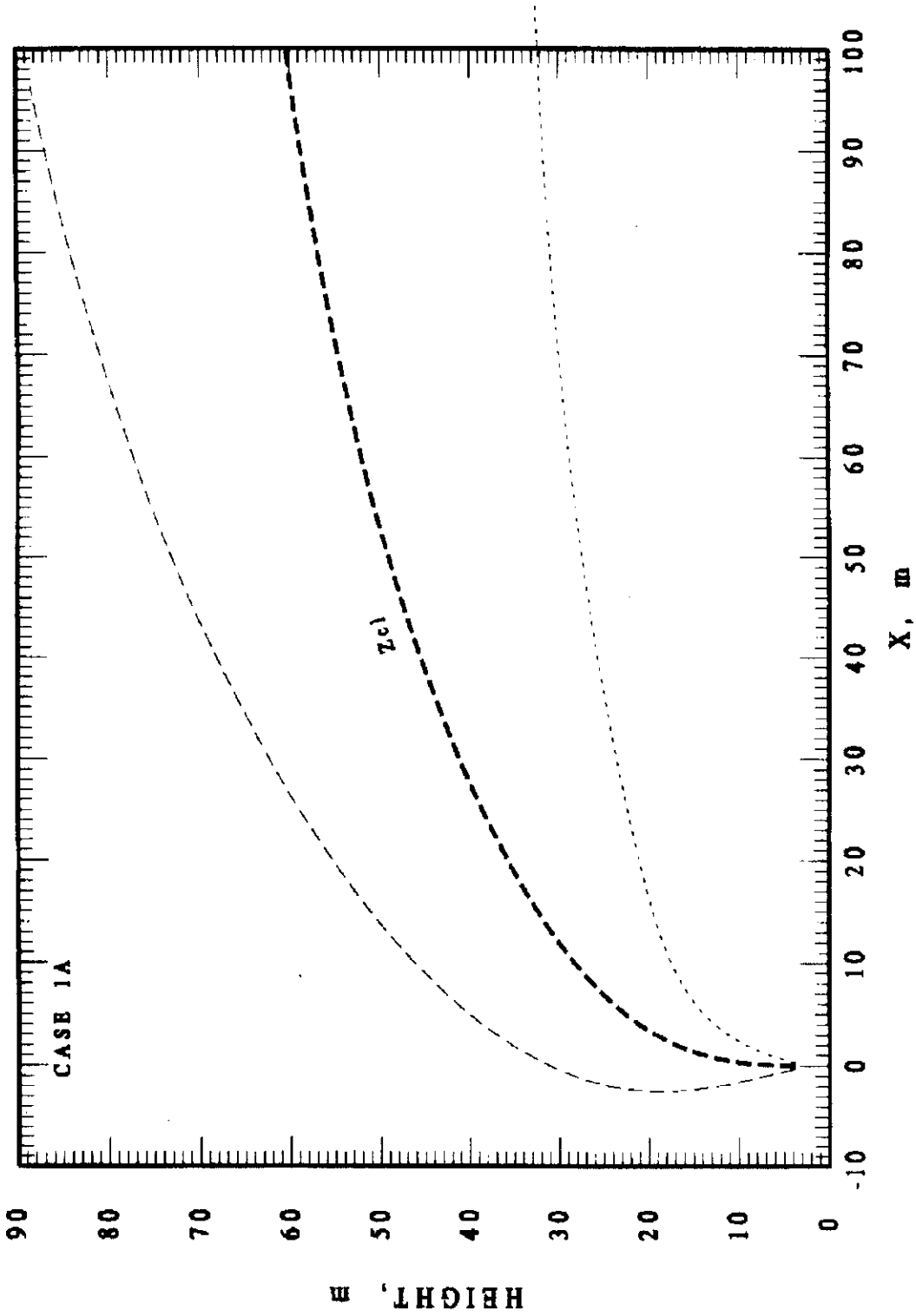

Figure 3 Predicted plume profile for Case 1A (see Table 4); vertical discharge from 3.3-m tall circular stack.

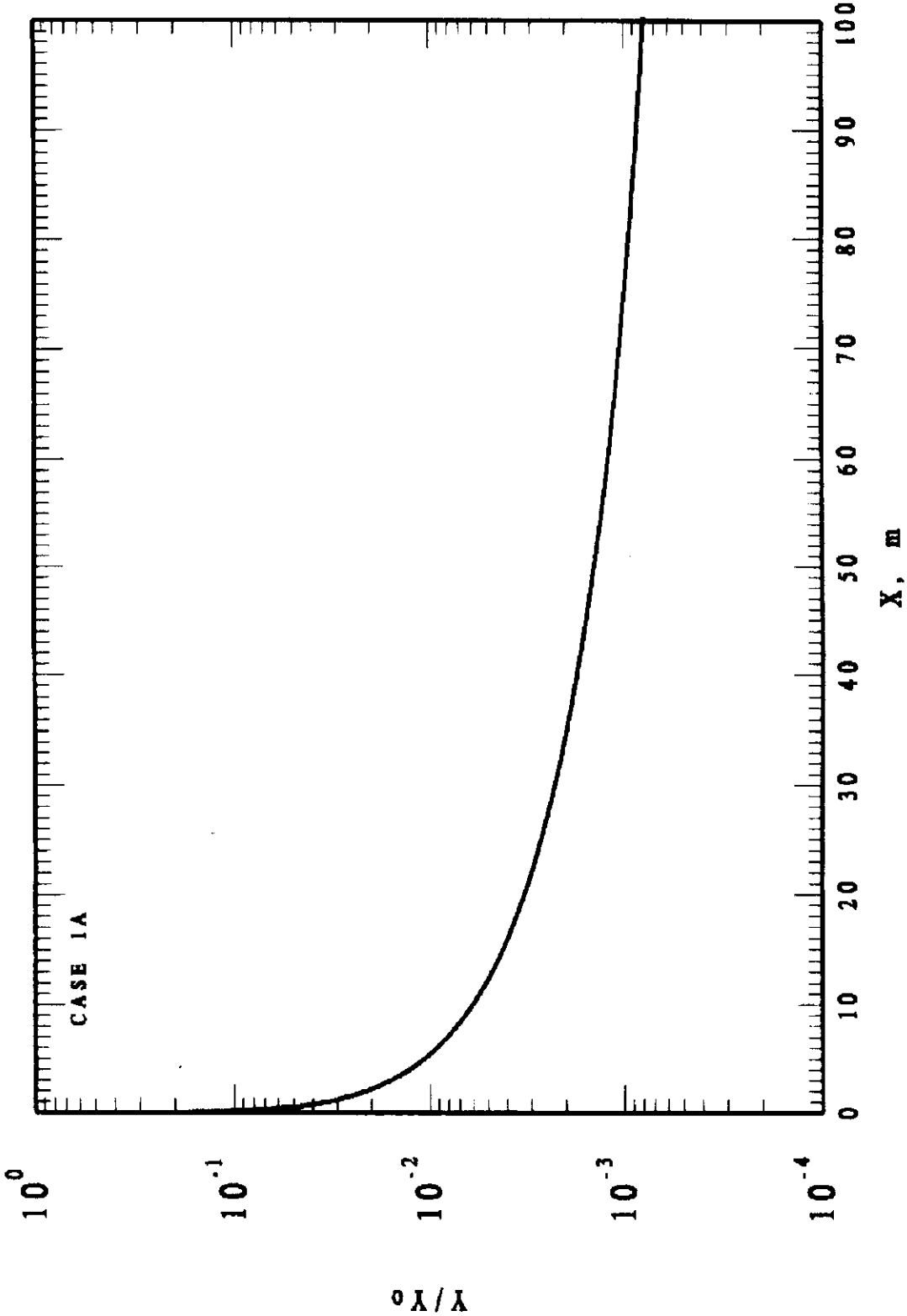

Figure 4 Normalized concentration of released species versus distance downwind for Case 1A (see Table 4); vertical discharge from 3.3-m tall circular stack.

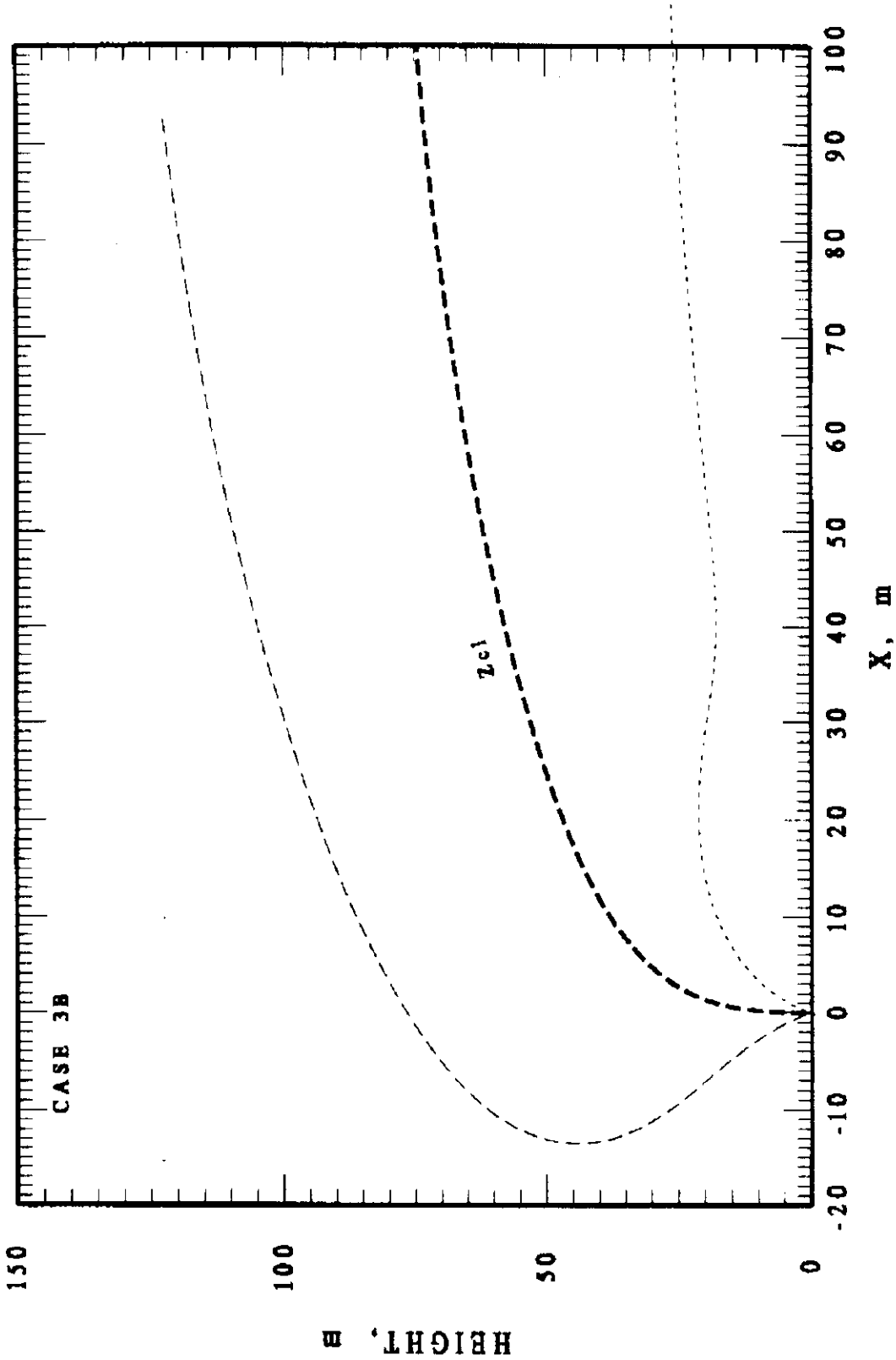

Figure 5 Predicted plume profile for Case 3B (see Table 4): vertical discharge from long slit 0.61 m above ground.

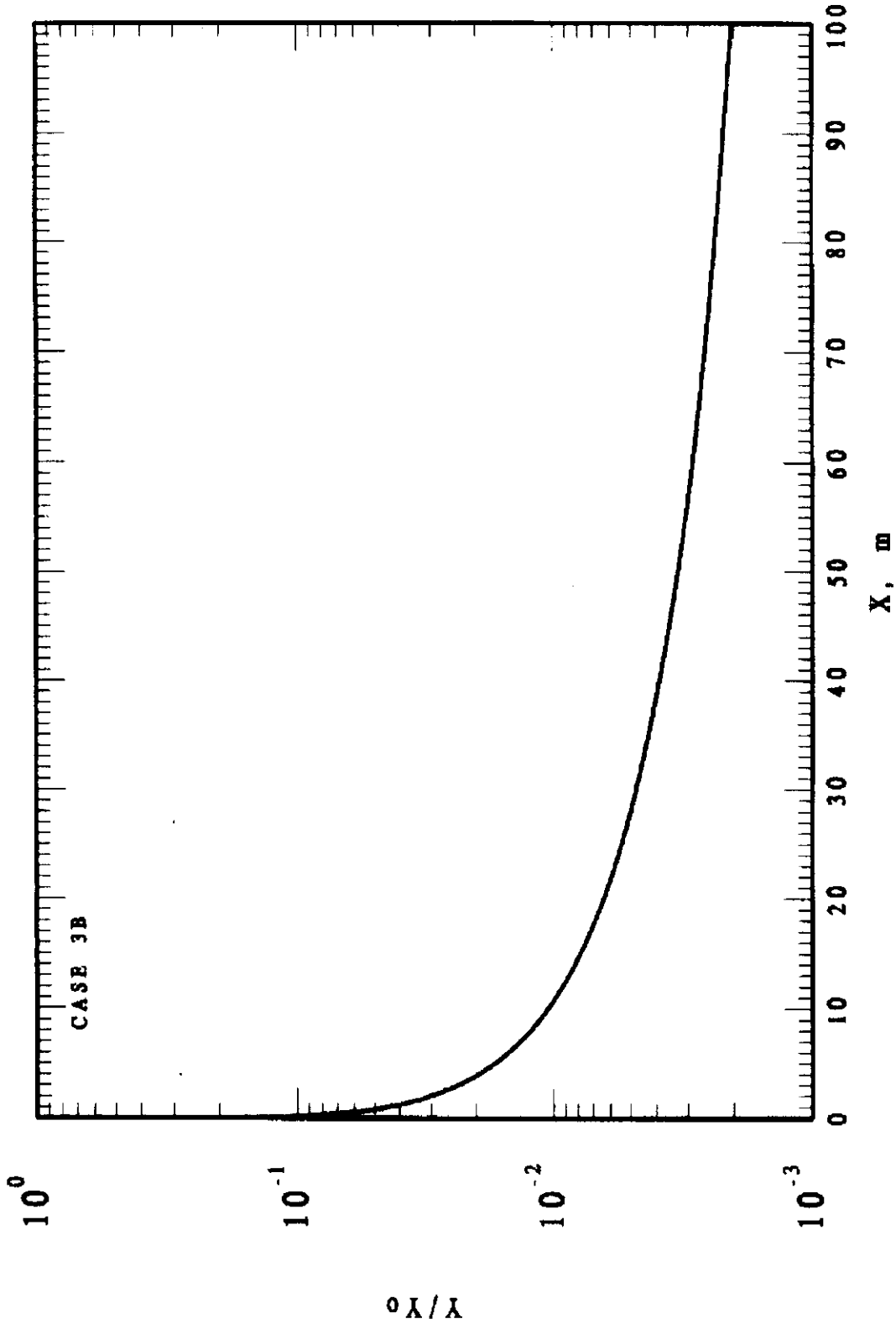

Figure 6 Normalized concentration of released species versus distance downwind fro Case 3B (see Table 4); vertical discharge from long slit 0.61 m above ground.

- i.e., entrainment by ambient turbulence does not occur. Also, the plumes do not make contact with the ground and their lower boundaries remain well above ground level at the 100-m distance from the source. The plume dilution ratios Y/Y_0 at this location are 8×10^{-4} and 2×10^{-3} for the circular vent (Case 1A) and the slit vent (Case 3B), respectively. Qualitatively similar results were obtained for all the other numerical cases involving plumes discharged vertically upward. Such plumes pose no hazard to people on the ground, at least up to 100 m from the source. The predicted plume dilution ratios Y/Y_0 and the predicted heights above the ground of the plumes' lower boundaries are given in Table 5.

Figures 7 and 8 show, respectively, the profile and dilution as a function of distance for a jet issuing horizontally from a slit located 0.61 m above the ground (Case 3A). Following release, plume spreading is rapid and touchdown occurs at about 2.2 m downwind of the slit vent. From this point on the plume, by assumption, exhibits zero-buoyancy, passive behavior and expands sufficiently so that at 100 m downwind its vertical thickness exceeds 30.0 m. It should be kept in mind, however, that buoyancy in a stable atmosphere may limit the vertical spreading of the plume and decrease plume dilution. In a stably stratified atmosphere denser ambient air entrained and carried upward by the jet as it expands "absorbs" the horizontal jet momentum and cause the jet to slow down. This effect is probably not too important over the 100-m downwind distance of interest but it should be checked.

Figure 9 shows the predicted plume profile in the vicinity of a downfacing Type 4 vent (see Fig. 2) for Case 4A. Since we are dealing with a very light wind, the plume does not bend over before it feels the presence of the ground (as dictated by the criterion $z_{cl} = R$). Nevertheless, the present model assumes that after ground contact the plume's momentum is directed downwind so that the plume behaves as if it were discharged horizontally. Obviously an alternative and, perhaps, aesthetically more pleasing model could be developed which allows the plume to spread radially after ground contact in the form of a cylindrically symmetric ground current. It is not clear as to which model would yield a lower hazardous species concentration at the 100 m position, although the ground concentrations predicted with the two models should not be too different from one another. The radially spreading plume has a large cross-sectional area which tends to enhance plume dilution relative to the plume that travels downwind.

Table 5

Predicted Plume Heights and Normalized Species Concentrations at 100 m Downwind

Case	Discharge Direction	Vent Geometry	Height of Lower Plume Boundary (m)	Y/Y_0
1A	Upward	Circular	32.0	8×10^{-4}
1B	Upward	Circular	8.4	2×10^{-3}
1C	Upward	Circular	25.0	10^{-3}
2A	Upward	Circular	45.0	2.9×10^{-3}
2B	Upward	Circular	28.4	1.5×10^{-3}
2C	Upward	Circular	6.6	2.4×10^{-3}
3A	Horizontal	Slit	0.0	1.8×10^{-2}
3B	Upward	Slit	26.0	2×10^{-3}
3C	Horizontal	Slit	0.0	8.7×10^{-3}
4A	Downward	Circular	0.0	2.6×10^{-3}
4B	Downward	Circular	0.0	3.9×10^{-3}
4C	Downward	Circular	0.0	5.2×10^{-3}

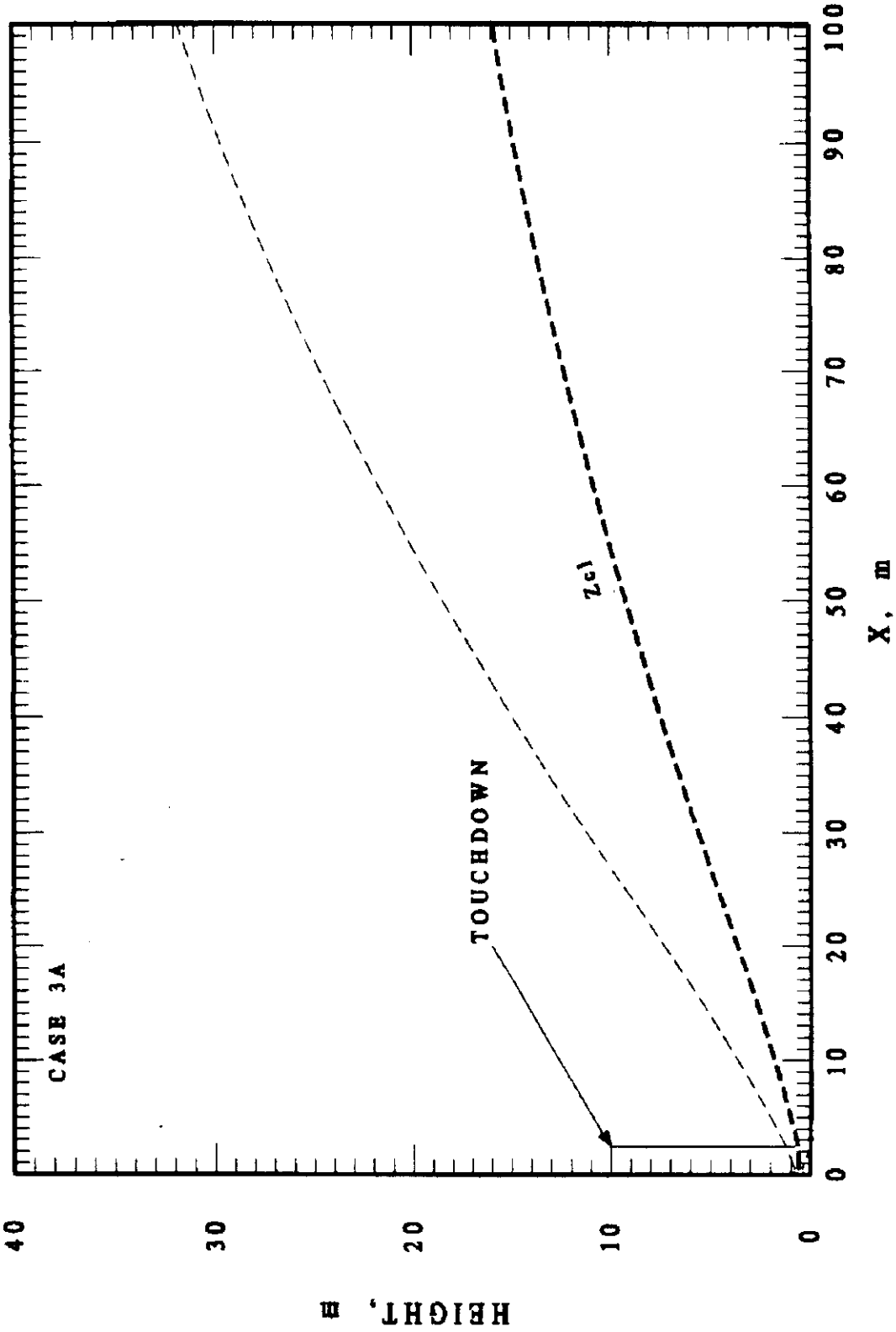

Figure 7 Predicted plume profile for Case 3A (see Table 4); horizontal discharge from long slit 0.61 m above ground.

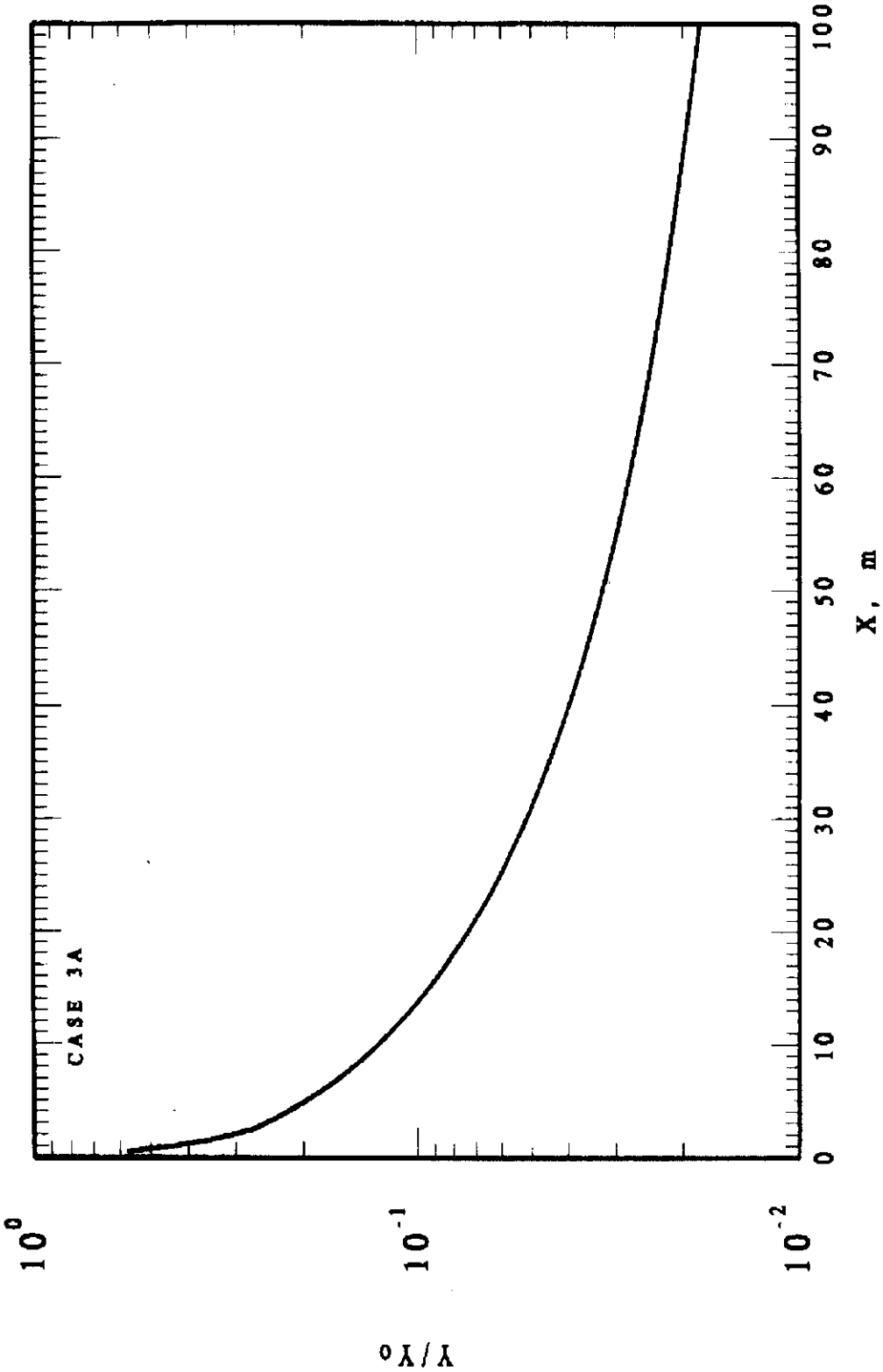

Figure 8 Normalized concentration of released species versus distance downwind for Case 3A (see Table 4): horizontal discharge from long slit 0.61 m above ground.

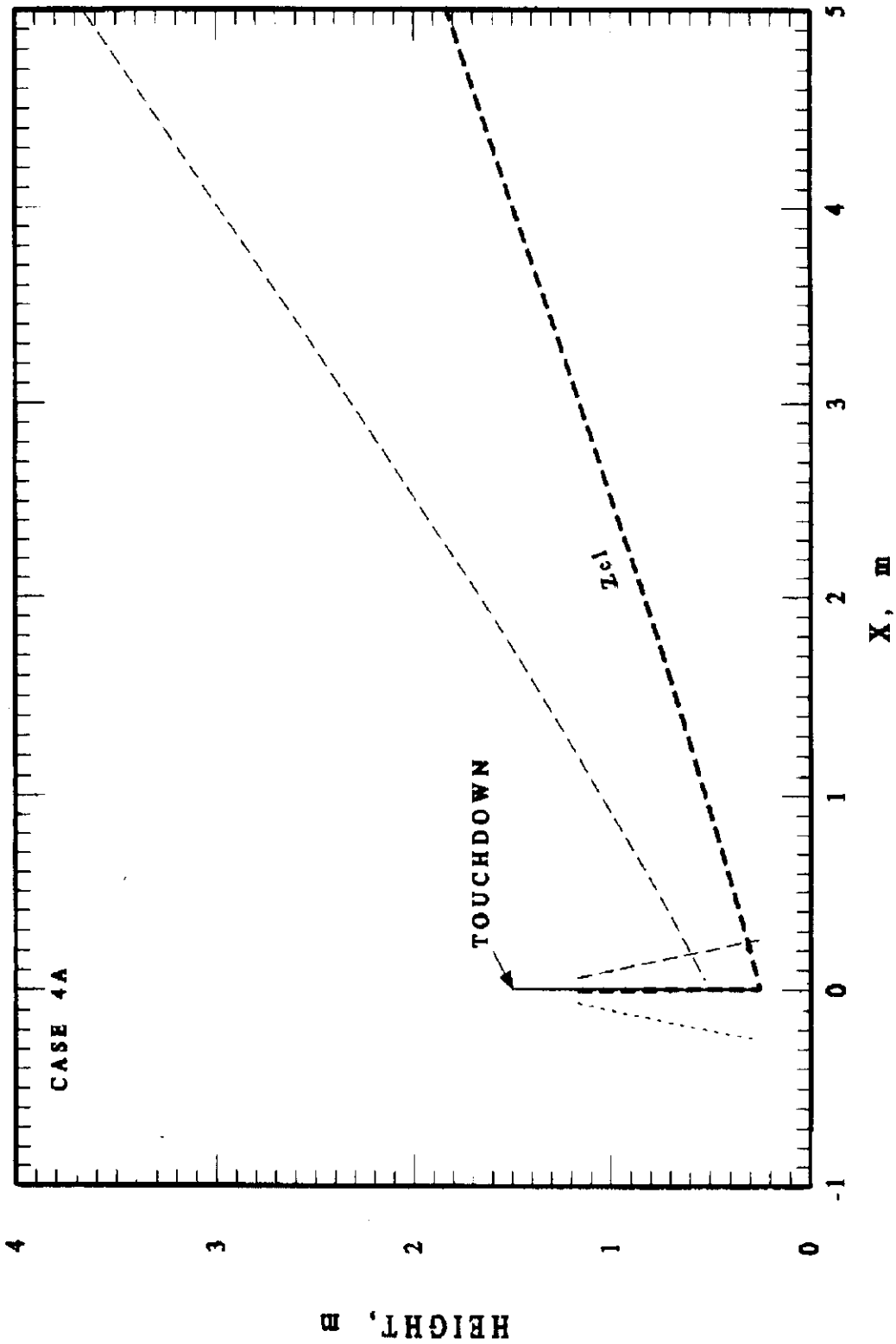

Figure 9 Predicted plume profile in vicinity of release location for Case 4A (see Table 4); downward discharge from circular stack 1.22 m above ground.

However, the local velocity within the radial plume is low which tends to decrease its dilution rate compared with the downwind plume. The radial spreading ground-level plume is perhaps another area that is worthy of future modeling work. Figure 10 gives the normalized species concentration as a function of distance for Case 4A. The discontinuous decrease in plume concentration at x = 0 is due to the entrainment of ambient just below the vent where the plume is airborne and directed vertically downward.

The predicted normalized species concentrations for all the numerical cases are summarized in Table 5. It is of interest to note that, over the downwind distance 0 to 100 m, the model predicts a transition from the jet-induced turbulence regime to the atmospheric turbulence regime of jet dilution in only two cases, namely Cases 4B and 4C for a downward facing vent. The predicted transitions occur 91.5 m and 43.8 m downwind of the vent for these cases, respectively.

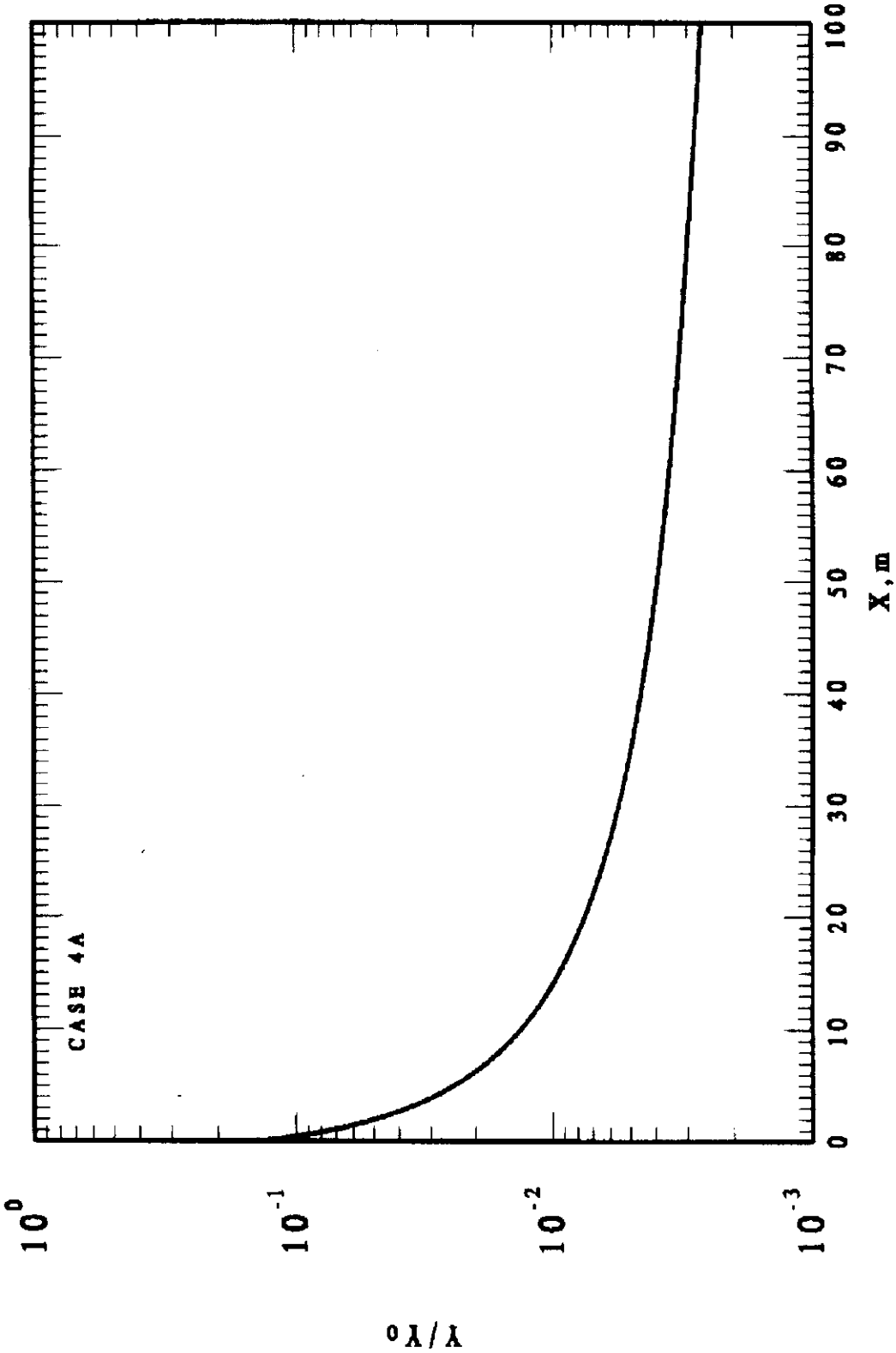

Figure 10 Normalized concentration of released species versus distance downwind for Cade 4A (see Table 4); downward discharge from circular stack 1.22 m above ground.

8.0 DISCUSSION OF VALIDITY OF MODEL

To gain confidence in the present plume dispersion model, it is prudent to explicitly consider the implications of our approximations and the correctness of the equations and method of solution.

The reliability of the numerical technique can be established by comparing its predictions to the small number of analytical solutions to the plume equations. Of course, these exact solutions pertain to much less general plume/jet problems than those treated in Sections 4.0 and 5.0. Thus we will check the model equations when applied to purely momentum dominated, elevated jets of circular cross-section and ground-level and elevated jets of rectangular cross section.

When the effects of gravity and atmospheric turbulence are neglected and the gas is discharged horizontally into the direction of the wind then Eqs. (1), (9)-(12) and (17) simplify to yield the jet species dilution law for a circular jet (see Appendix A):

$$\frac{Y}{Y_0} = \frac{1}{1 + \frac{u_0}{u_{\infty,ref}} \left\{ \left[1 + 3\, E_0 \left(\frac{\rho_\infty}{\rho_0} \right)^{1/2} \left(1 + \frac{u_0}{u_{\infty,ref}} \right) \frac{x\, u_{\infty,ref}}{u_0 R_0} \right]^{2/3} - 1 \right\}} \tag{31}$$

where x is the horizontal distance over which the jet remains elevated. Note from Eq. (31) that far downwind of the source the concentration of the released species obeys an $x^{-2/3}$ power-law dependence on distance. In the absence of a horizontal wind, $u_{\infty,ref} = 0$ and Eq. (31) reduces to

$$\frac{Y}{Y_0} = \frac{1}{1 + 2\, E_0 \left(\frac{\rho_\infty}{\rho_0} \right)^{1/2} \frac{x}{R_0}} \tag{32}$$

Thus, according to the theory, in the initial phase of jet behavior, where the jet's self-generated turbulence is the dominant mixing agency, the presence of wind acts to reduce the dilution rate of the jet from that predicted in a quiescent atmosphere. Of course in the final phase of jet behavior, far downwind of the source, the energy containing eddies of environmental turbulence dominate mixing and the jet growth is strictly due to the action of the wind. It may be of

interest to point out that Eqs. (31) and (32) for pure momentum jets are valid for arbitrary values of the environment-to-release density ratio ρ_∞/ρ_0 or, equivalently, for arbitrary values of the released species mass fraction Y_0.

Unlike a circular jet, a closed-form solution for the dilution of a rectangular jet can only be obtained by invoking the assumptions of zero wind speed ($u_{\infty,ref} = 0$) and trace quantities of the released species ($Y_0 << 1$). Again ignoring gravity, Eqs. (1), (9)-(12), (18) or (23), and (20) for a rectangular airborne or ground-level jet reduce to the dilution law (see Appendix A)

$$\frac{Y}{Y_0} = \frac{1}{\left(1 + \frac{E_0 x}{W_0}\right)\left[1 + \frac{2bW_0^2}{A_0}\ln\left(1 + \frac{E_0 x}{W_0}\right)\right]^{1/2}} \tag{33}$$

where b = 4 for an airborne jet and b = 2 for a ground-level jet.

Elevated, pure momentum jets of circular cross section were simulated numerically by releasing the jet horizontally at elevation $z_{cl,0} = z_{ref}$ where the wind speed is $u_{\infty,ref}$ (see Eq. 26). The jet release density ρ_0 was set equal to the atmospheric density ρ_∞ to eliminate jet buoyancy, thereby ensuring that the jet elevation remained horizontal at elevation $z_{cl} = z_{ref}$. Numerical solutions for ground-level, pure momentum jets were also achieved by demanding that $\rho_0 = \rho_\infty$ and by considering only perfectly calm conditions ($u_{\infty,ref} = 0$). Ground-level plumes were initiated at x = 0 from rectangular vents with ground-level lower boundaries. The numerical solutions (solid curves) of the governing equations are compared with the appropriate closed form solutions (circles) in Figs. 11, 12, and 13. As shown in the figures the numerical solutions for jet dilution versus horizontal distance faithfully pass through the points generated by the closed form solutions in the parametric extreme of pure momentum jets. This agreement

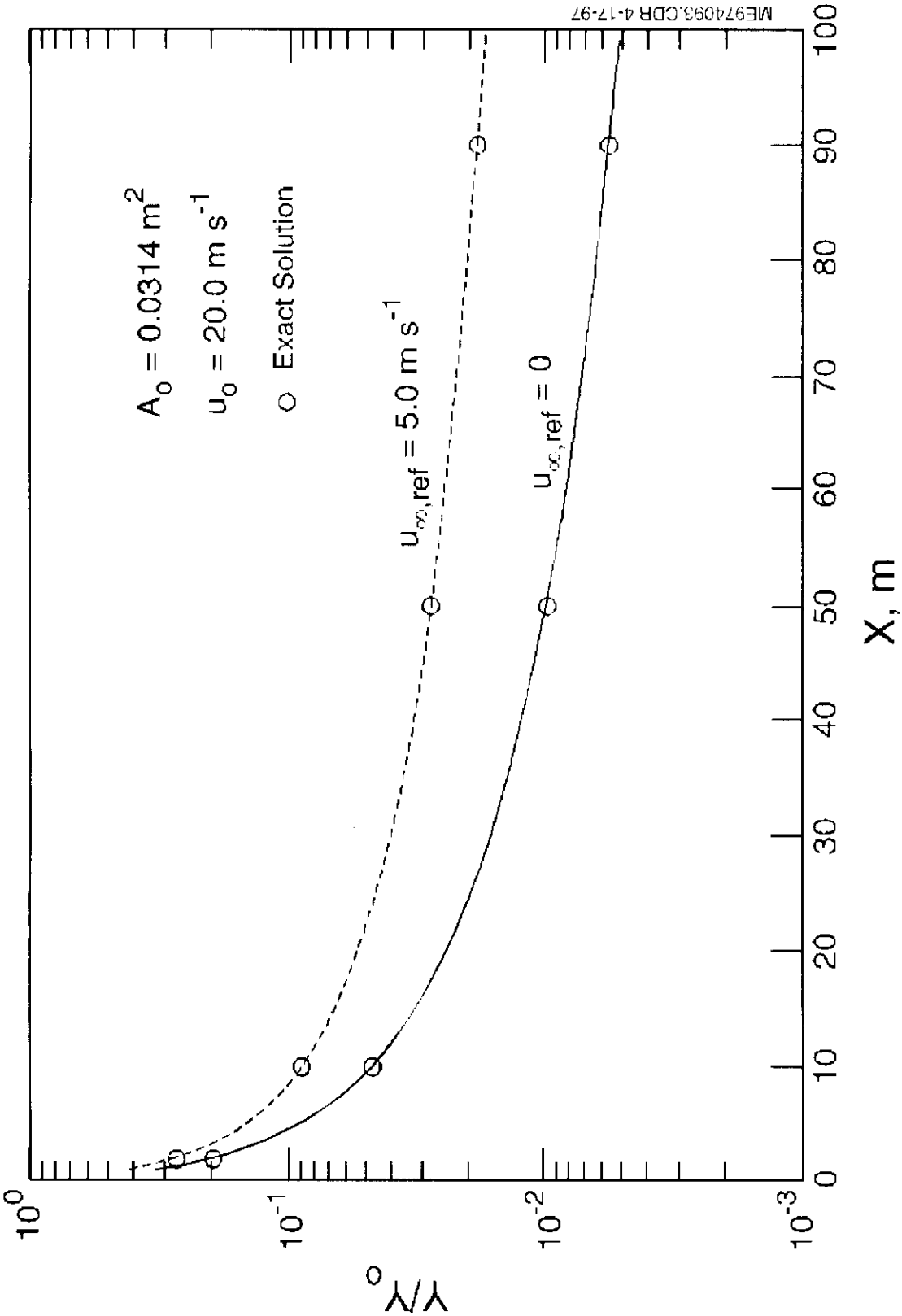

Figure 11 Normalized concentration profiles for elevated, circular, pure-momentum jets; comparison of numberical model with exact solution.

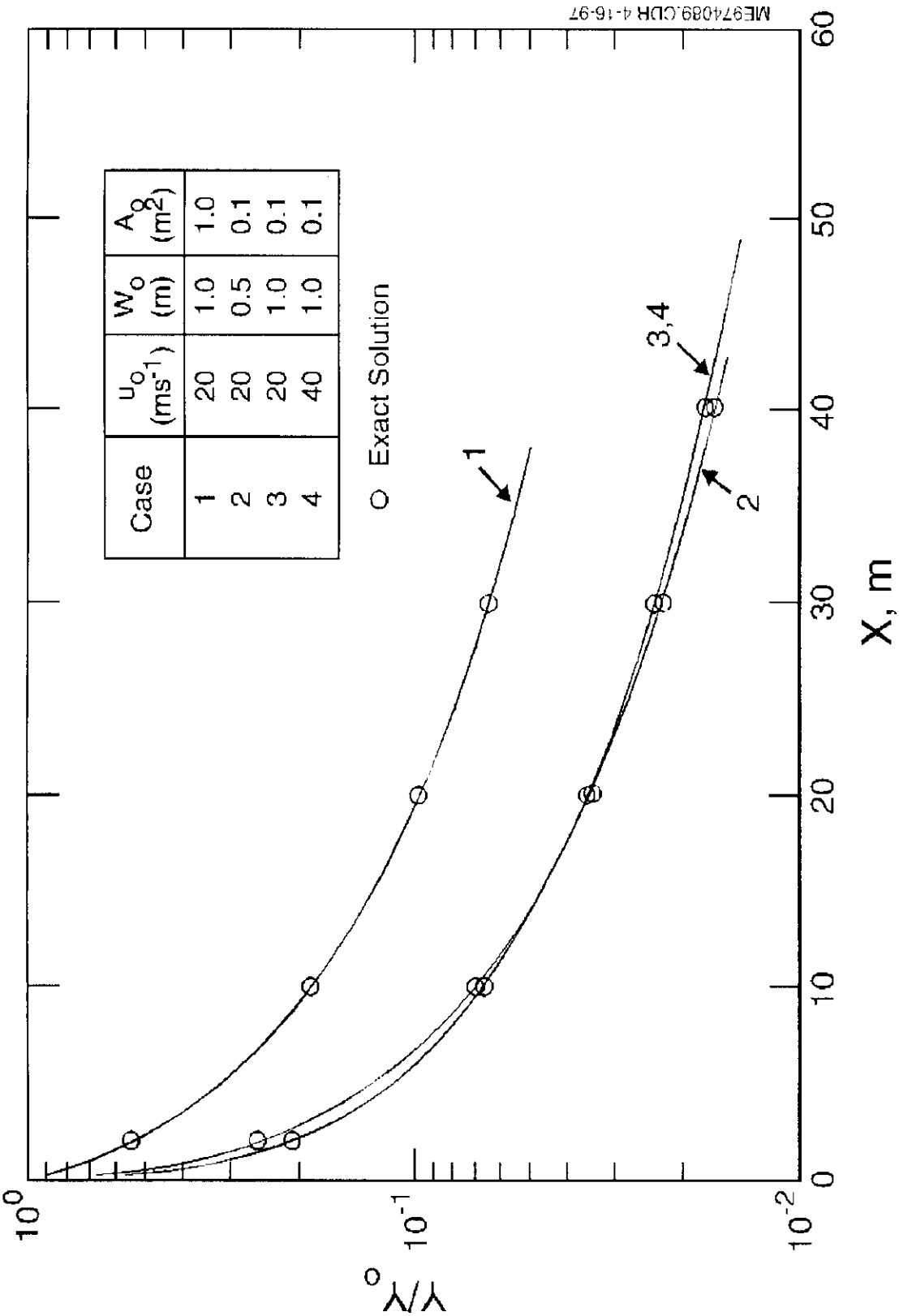

Figure 12 Normalized concentration profiles for elevated, rectangular, pure-momentum jets: comparison of numerical model with exact solution.

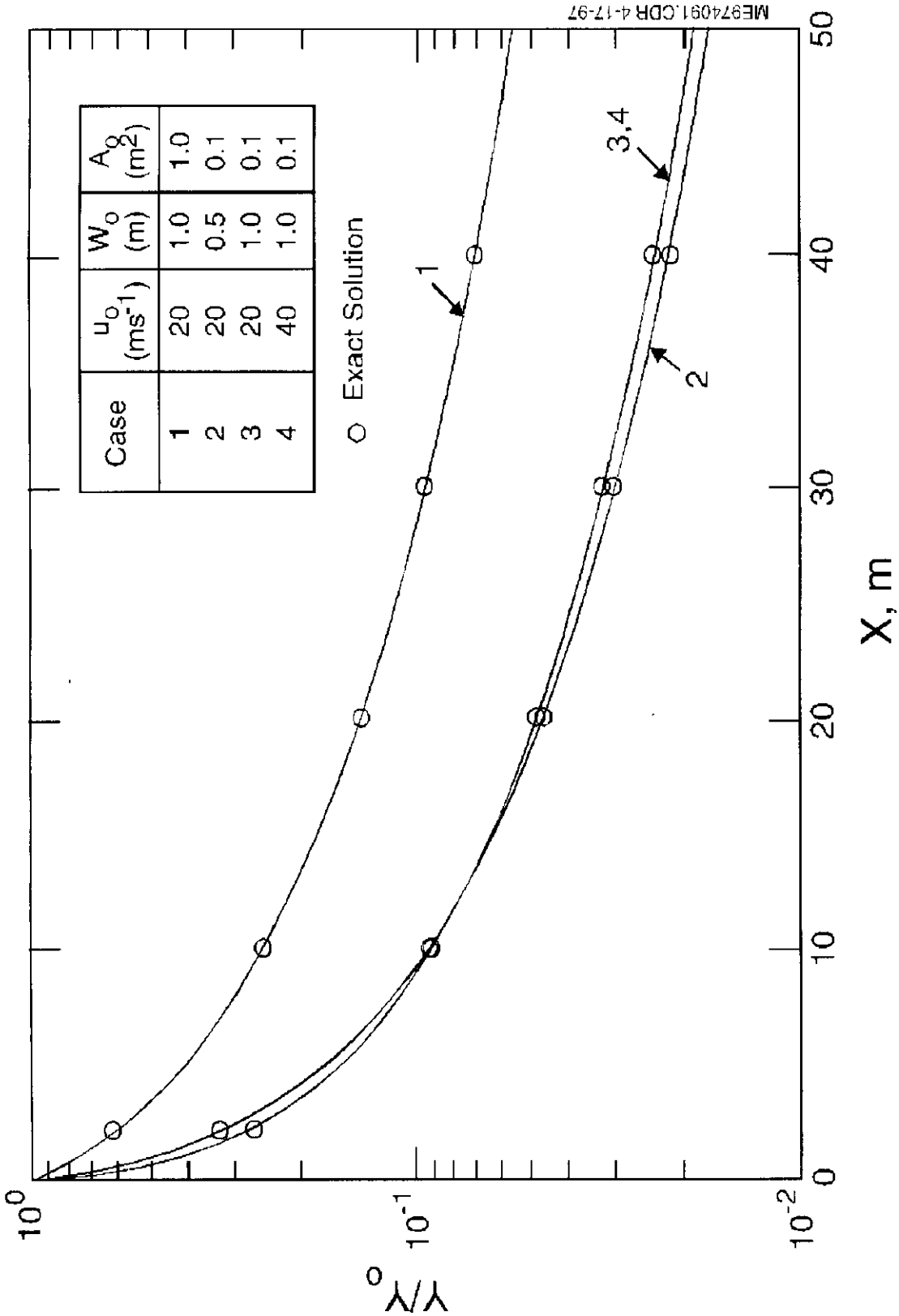

Figure 13 Normalized concentration profiles for ground-level, rectangular, pure-momentum jets; comparison of numerical model with exact solution.

suggests that the equations were programmed correctly for numerical solution and that the simple numerical scheme exploited here is more than adequate.

Of course, it is of interest to test the present plume dispersion model by comparison with field observations. Ground concentration data for stable and unstable conditions are available (see, e.g., Moore, 1974), but are not too useful for testing the model since the ground samples were usually located so far from the source that the atmospheric/plume conditions only approximate those of the far-field Gaussian-based dispersion models. Near-field test data are available for pressurized liquids released horizontally in the direction of the wind (Goldwire, et al., 1985; Goldwire, 1986; and Blewitt et al., 1987). These releases of volatile liquid chemicals result in the formation of high-momentum flashed jets with liquid phases comprised of extremely fine droplets, and beyond some not very significant distance from the release point the liquid phase is consumed by evaporation into the entrained air. The resulting cold, chemical vapor/air jet is heavier than the surrounding air. Obviously, the present model can not treat such two-phase releases. However, a model similar in structure to and employing the same entrainment laws as the present model has been developed to treat pressurized liquid releases (Epstein et al., 1990). Suffice it to say that the model is capable of reproducing the released chemical, peak concentration measurements within a factor of three at distances downwind of the source of up to 3000 m. At 100 m from the source the results were especially encouraging, with the model representing the data to better than 20.0 percent.

An alternative to comparison of the model with ground concentration data is to test whether the model can correctly predict "plume rise observations". This procedure tests the mass, momentum and energy conservation equations as well as the entrainment relations, since plume rise predictions depend on the correctness of all the airborne plume model components. On the basis of many observations of plume rise in a stably stratified atmosphere, most of them of power plant plumes, Briggs (1984) recommended the following semi-empirical formula:

$$\Delta z_{cl} = 1.8 \left[\frac{T_{atm}(T_0 - T_{atm})\ u_0 A_0}{T_0\ \beta\ \bar{u}_{.}} \right]^{1/3} \tag{34}$$

where Δz_{cl} is final rise (vertical height) of the plume centerline above the vertical location $z_{cl,0}$ of the source vent. The wind speed $\bar{u}$ in this formula is an average value between the heights $z_{cl,0}$ and $z_{cl,0} + \Delta z_{cl}$.

The predicted plume profiles for a fixed set of release conditions and wind speeds $u_\infty = 1.0, 5.0$ m s^{-1} are shown in Figs. 14 and 15. In the F stability atmosphere considered here the air is stably stratified and an inversion layer exists from the ground up. As can be seen from Figs. 8-1 and 8-2 plume rise is limited. This is because ambient air at a given level of the atmosphere is entrained by the plume which rises to levels of higher ambient potential temperature (or less dense ambient air). The plume loses its buoyancy and asymptotically approaches a final height. The plume may overshoot its asymptotic height, that is become temporarily negatively buoyant and behave as a damped oscillator. As can be seen from Fig. 14, such oscillatory behavior is particularly evident at low wind speeds. We also note from Figs. 14 and 15 that maximum plume rise is achieved beyond the 100-m downwind distance of interest in the waste tank organic-pool-fire-plume problem.

Some predictions of plume rise obtained from the present model are compared with Eq. (34) in Fig. 16. Equation (26) was used to evaluate $\bar{u}$ in Eq. (34) in the placement of the numerical solution data in Fig. 16. We may conclude from this comparison that the model is consistent with many observations of power-plant plume rise.

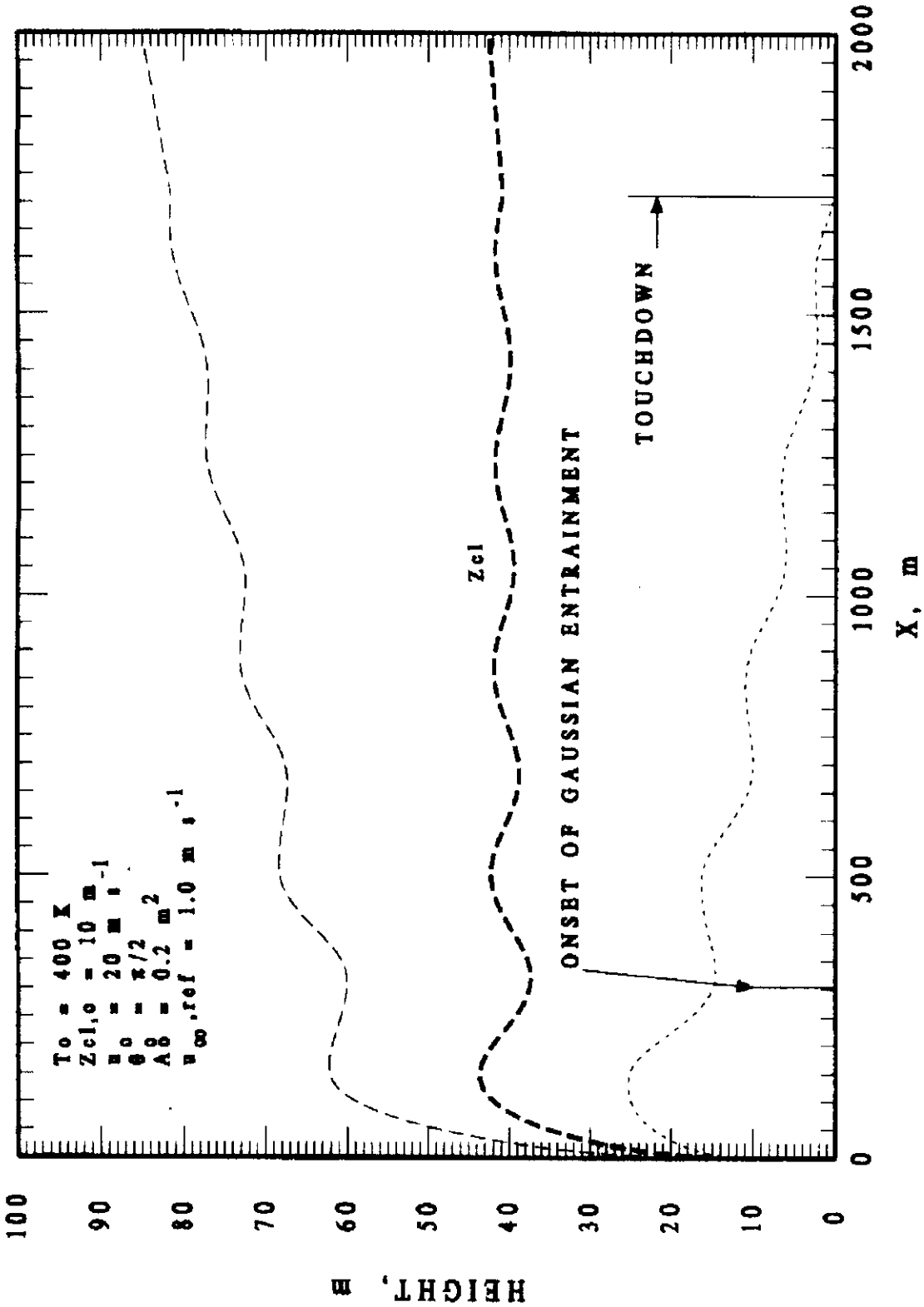

Figure 14 Predicted plume profile illustrating final plume rise at low wind speed in stable atmosphere.

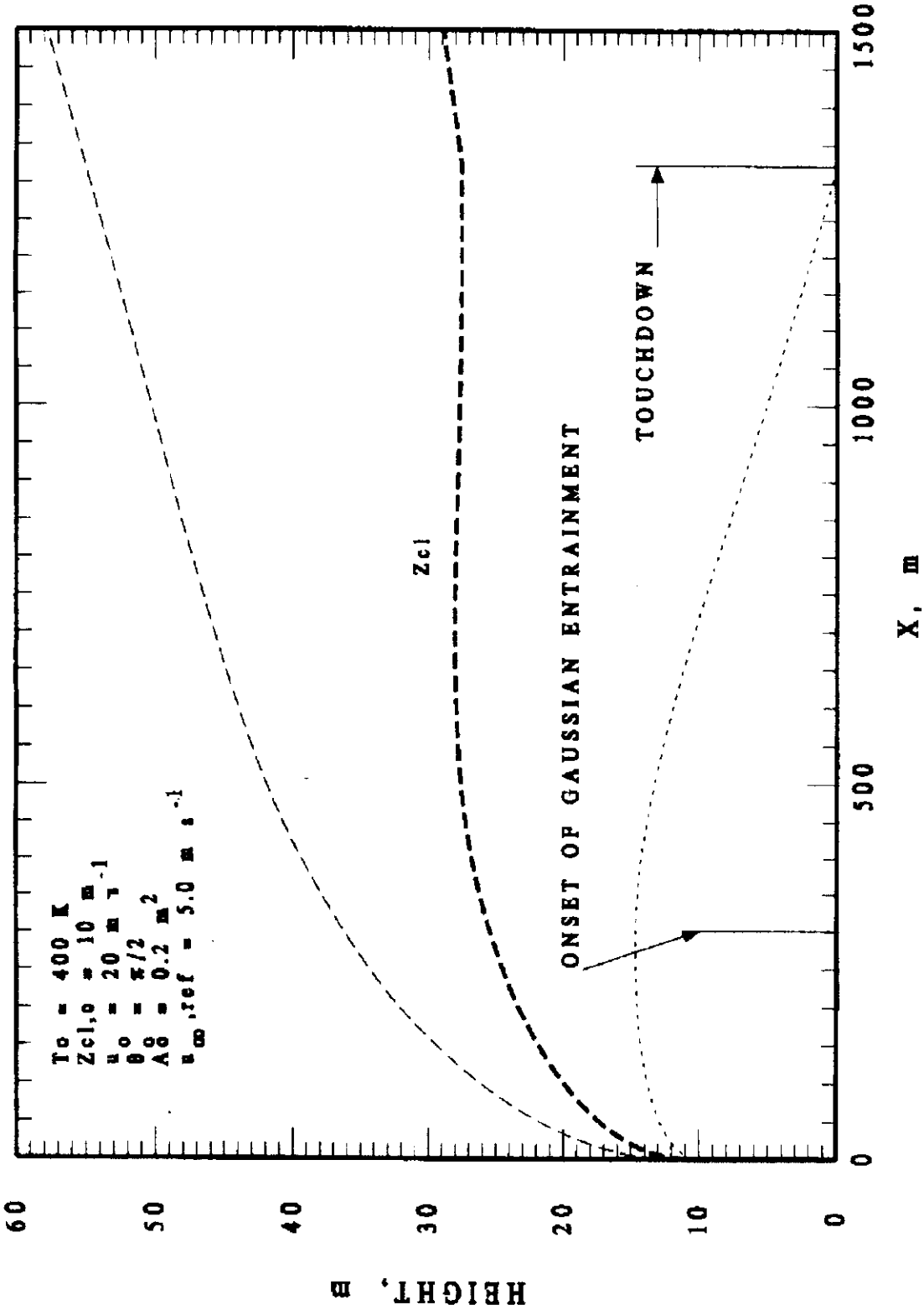

Figure 15 Predicted plume profile illustrating final plume rise at moderate wind speed in stable atmosphere.

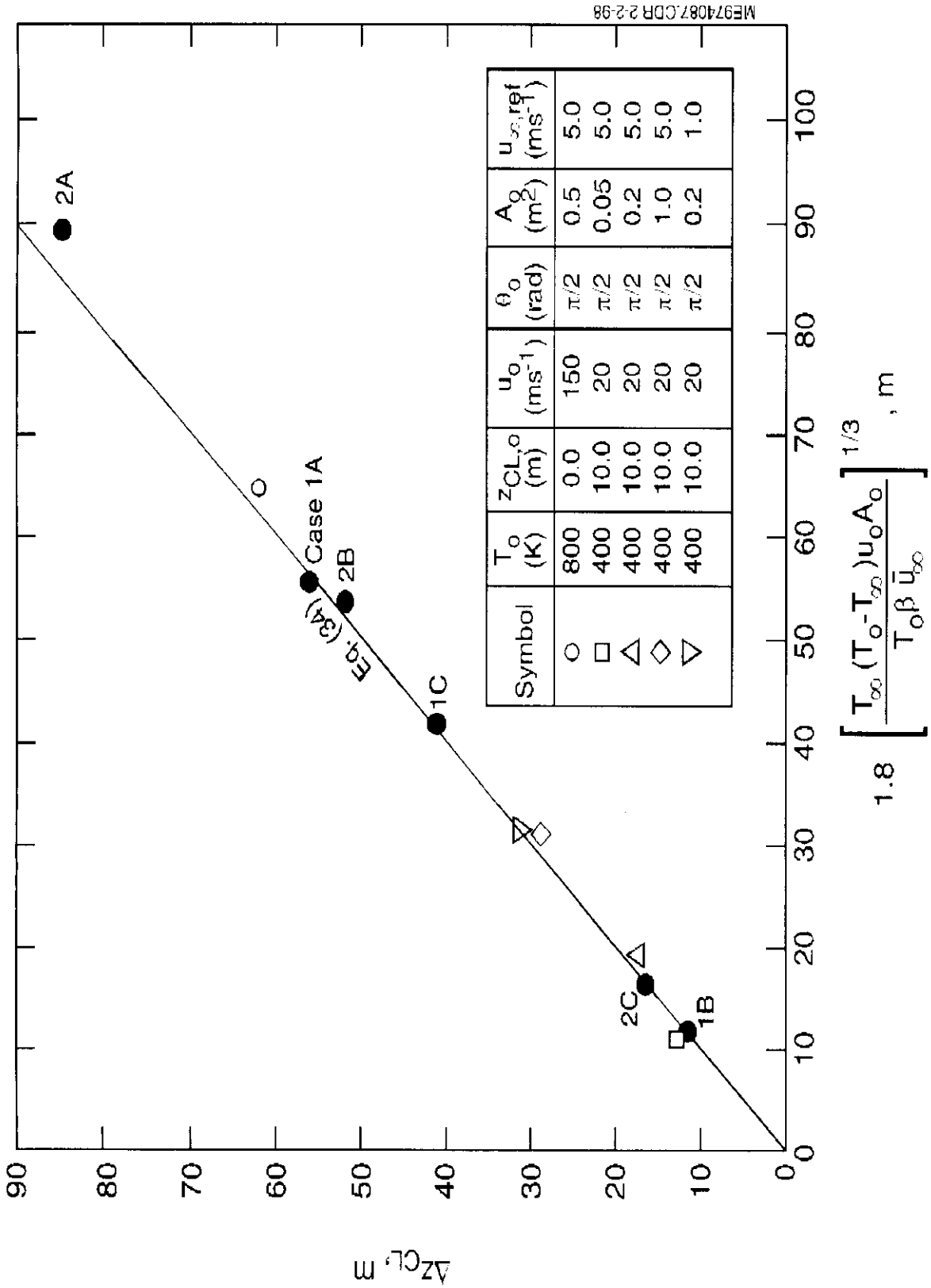

Figure 16 Comparison of numerical model plume rise predictions with the semi-empirical plume rise correlation of Briggs (1984).

9.0 CONCLUSIONS

In this report a model was described for predicting the atmospheric concentrations of radioactive (toxic) materials arising from the release of combustion product gases or aerosols from a Hanford Site waste tank within which a liquid-organic chemical fire is occurring. The dilution of the combustion product plume (or jet) produced by the release has been modeled by a direct application of the conservation equations combined with two turbulent entrainment models. Two regimes of jet behavior are incorporated into the model: an integral model in curvilinear coordinates for describing a free elevated jet and an integral wall-jet model for describing ground-level behavior. The ground-level jet model does not include the effects of buoyancy, nor does it allow for purely radial jet flow in the case of downward directed discharges into very light winds. It is felt that both of these effects are not likely to influence jet dilution behavior by more than about a factor of two, but this conclusion may require justification.

Predictions of the normalized hazardous species concentration Y/Y_0 at 100 m downwind of the waste tank vent were made for four different vent geometries. Jets released upward from exhaust stacks on actively ventilated tanks, from riser pipes in uncovered pits or from cracks in concrete cover blocks persist as elevated plumes out to 100 m and beyond. The normalized species concentration within these airborne plumes at 100 m is about $Y/Y_0 \approx 2 \times 10^{-3}$. Jets directed downward from exhaust stacks on passively ventilated tanks are diluted to about $Y/Y_0 \approx 4 \times 10^{-3}$ at the 100-m position. Finally, jets discharged horizontally from levitated concrete cover blocks have a ground-level concentration of about $Y/Y_0 \approx 10^{-2}$ at 100 m.

10.0 NOMENCLATURE

a_i	coefficient in expression for σ_y; Eq. (8)
A	cross-sectional area of plume
A_0	area of release (vent or rupture opening)
b_i	exponent in expression for σ_y; Eq. (8)
c_i	coefficient in expression for σ_z; Eq. (8)
c_p	heat capacity of atmosphere
C	circumference of plume through which entrainment occurs
d_i	exponent in expression for σ_z; Eq. (8)
E_0, E_1	entrainment constants; Eq. (1)
g	gravitational acceleration
h	mean plume enthalpy
$\dot{m}_r$	mass rate of release of radioactive (hazardous) species
M_0	mass rate of flow integration constant; Eq. (A-6)
p	exponent in wind distribution expression; Eq. (26)
P_∞	pressure of potential atmosphere
R	radius of circular plume or rectangular plume; Fig. 1
R_a	ideal gas constant for air
R_0	radius of circular vent
s	distance measured from the source along the centerline of the plume
T	mean temperature inside plume
T_{atm}	actual temperature of atmosphere
u	mean velocity inside plume
u_∞	wind speed
$u_{\infty,ref}$	reference wind velocity; Eq. (26)
$\bar{u}_\infty$	average wind speed in plume rise formula; Eq. (34)
v_{en}	entrainment velocity
W	half-width of rectangular jet; Fig. 1
x	distance measured from the source along the ground
Y	mass fraction of released species

Y_0 mass fraction of released species at vent

z vertical distance coordinate measured from ground

z_{cl} distance measured from ground to plume centerline

z_{ref} distance above ground where $u_{,ref}$ is measured (usually z_{ref} = 10 m); Eq. (26)

$z_{cl,o}$ height of release (rupture or vent opening) above ground

Greek Letters

β temperature gradient in potential atmosphere; dT_∞/dz

Δz_{cl} maximum rise height of plume centerline in stable atmosphere

ρ mean plume or jet density

ρ_∞ density of potential atmosphere

θ angle plume centerline makes with the horizontal

θ_0 angle of jet at release location

σ_y, σ_z Gaussian dispersion coefficients in the y- and z-directions

Subscripts

o initial conditions at vent

∞ pertains to the potential atmosphere or wind speed

11.0 REFERENCES

Blewitt, D. N., Yohn, J. F., Koopman, R. P., and Brown, T. C., 1987, "Conduct of Anhydrous Hydrofluoric Acid Spill Experiments," in Int. Conf. on Vapor Cloud Modeling, November 2-4, Cambridge, Massachusetts, (Ed. J. Woodward), pp. 1-38.

Briggs, G. A., "Plume Rise and Buoyancy Effects," 1984, in Atmospheric Science and Power Production, D. Randerson, Ed., DOE/TIC-27601, available from National Technical Information Service, Springfield, VA.

Epstein, M., Fauske, H. K., and Hauser, G. M., 1990, "A Model of the Dilution of a Forced Two-Phase Chemical Plume in a Horizontal Wind," J. Loss Prev. Process Ind. 3, pp. 280-290.

Goldwire, Jr., H. C., 1986, "Large-Scale Ammonia Spill Tests," Chem. Eng. Prog., April, pp. 35-41.

Goldwire, Jr., H. C., McRae, T. G., Johnson, G. W., and Hipple, D. L. et al., 1985, "Desert Tortoise Series Data Report - 1983 Pressurized Ammonia Spills," Lawrence Livermore National Laboratories Report UCID-20562, December.

Hanna, S. R., Briggs, G. A., and Hosker, R. P., Jr., 1982, Handbook on Atmospheric Diffusion, DOE/TIC-11223, U.S. Department of Energy, Washington, D.C.

Hirst, E. A., 1971, "Analysis of Round, Turbulent, Buoyant Jets Discharged to Flowing Stratified Ambients," Oak Ridge National Laboratory Report ORNL-4685.

Hoult, D. P., Fay, J. A., and Forney, L. J., 1969, "A Theory of Plume Rise Compared with Field Observations," J. Air Pollution Control Assoc. 19, pp. 585-590.

Jow, H. N., Spring, J. L., Rollstin, J. A., Ritchie, L. T., and Chanin, D., I., 1986, "MELCOR Accident Consequence code System (MACCS)," Sandia National Laboratories Report, NUREG/CR-4691, SAND 86-1562 Vol. 2.

Moore, D. J., 1974, "Observed and Calculated Magnitudes and Distances of Maximum Ground Level Concentration of Gaseous Effluent Material Downwind of a Tall Stack," in Advances in Geophysics Ser. B, Vol. 18B, Academic Press, New York, pp. 201-222.

Morton, B. R., Taylor, G. I., and Turner, J. S., 1956, "Turbulent Gravitational Convection from Maintained and Instantaneous Sources," Proc. Royal Soc. London, Ser. A 234, pp. 1-23.

Morton, B. R., 1959, "Forced Plumes," J. Fluid Mechanics 5, pp. 151-163.

Plate, E. J., 1971, "Aerodynamic Characteristics of Atmospheric Boundary Layers," U.S. Atomic Energy Commission, Div. Tech. Info., Oak Ridge, Tennessee.

Postma, A., 1997, Personal Communications, March 11 and April 8.

Ricou, F. B. and Spalding, D. B., 1961, "Measurements of Entrainment of Axisymmetrical Turbulent Jets," J. Fluid Mechanics 11, pp. 21-32.

Schlichting, H., 1968, Boundary Layer Theory, 6th ed., McGraw-Hill, Inc., New York.

Tadmor, J. and Gur, Y., 1969, "Analytical Expressions for the Vertical and Lateral Dispersion Coefficients in Atmospheric Diffusion," Atmospheric Environment, Pergamon Press, Vol. 3, Great Britain, p. 688.

U.S. Nuclear Regulatory Commission, Regulatory Guide 1.23, 1972, U.S. Nuclear Regulatory Commission, Washington, D.C.

APPENDIX A

Derivation of Eq. (31) for a Pure-Momentum Circular Jet

For the case of a circular jet released horizontally in the direction of the wind, and ignoring the influence of gravity and atmospheric turbulence, the conservation equations (9), (10), and (12) become (see also Eqs. 1 and 17)

$$\frac{d}{dx}(\rho u R^2 Y) = 0 \tag{A-1}$$

$$\frac{d}{dx}(\rho u R^2) = 2\rho_\infty E_0 R(\rho/\rho_\infty)^{1/2}(u - u_{\infty,ref}) \tag{A-2}$$

$$\frac{d}{dx}(\rho u^2 R^2) = u_{\infty,ref}\frac{d}{dx}(\rho u R^2) \tag{A-3}$$

We emphasize that the formulation given above holds for the near-field high-momentum regime only, since the entrainment velocity is given by Eq. (1) (with $\theta = 0$). An examination of Eqs. (A-1) to (A-3) reveals four unknown variables, namely, ρ, u, R, and Y. In order to determine all of these quantities as functions of horizontal distance x from the source, the equation of energy must be added to the above equation set. Fortunately, the species concentration Y(x) and the jet velocity u(x) may be found from Eqs. (A-1) to (A-3) without invoking the energy equation. This is because the jet density ρ and radius R appear in the equations only as the product ρR^2, or, equivalently as $\rho^{1/2}R$, which may be regarded as a single variable, thereby reducing the number of unknown from four to three.

The solution of Eqs. (A-1) and (A-3), subject to the initial conditions $\rho = \rho_0$, $u = u_0$, $Y = Y_0$, and $R = R_0$ [$R_0 = (A_0/\pi)^{1/2}$] at $x = 0$, is

$$\rho u R^2 Y = M_0 \tag{A-4}$$

$$\rho u R^2 (u - u_{\infty,ref}) = (u_0 - u_{\infty,ref}) M_0 \tag{A-5}$$

where M_0 is an integration constant that is proportional to the mass rate of release of the hazardous species:

$$M_0 = \rho_0 u_0 R_0^2 Y_0 \tag{A-6}$$

Dividing Eq. (A-5) by Eq. (A-4) gives

$$u = u_{\infty,ref} + (u_0 - u_{\infty,ref})\, Y \tag{A-7}$$

Eliminating u between Eqs. (A-5) and (A-7) and taking the square-root of the result yields

$$\rho^{1/2} R = \left[\frac{M_0}{Y[u_{\infty,ref} + (u_0 - u_{\infty,ref})Y]} \right]^{1/2} \tag{A-8}$$

Combining equations (A-2), (A-4), (A-7), and (A-8) results in the following differential equation for the inverse of the species mass fraction Y as a function of distance from the source

$$\frac{d}{dx}\left(\frac{1}{Y}\right) = \frac{2\, E_0 \left(\frac{\rho_\infty}{\rho_0}\right)^{1/2} \left(1 - \frac{u_{\infty,ref}}{u_0}\right)}{R_0 \left[\frac{u_{\infty,ref}}{u_0}\left(\frac{1}{Y} - 1\right) + 1\right]^{1/2}} \tag{A-9}$$

Integration of this equation gives Eq. (31).

Derivation of Eq. (33) for a Pure-Momentum Rectangular Jet

In addition to the assumption of a nonbuoyant jet, the derivation of a closed form solution for the pure-momentum rectangular-jet dispersion process requires that; (i) the atmosphere is stagnant (i.e., $u_{\infty,ref} = 0$) and (ii) the hazardous gas is present in only trace quantities upon release to the environment (i.e. $Y_0 << 1$), so that ρ is approximately constant and equal to ρ_∞. Subject to these assumptions, the conservation equations (Eqs. 9, 10, 12, and 20) simplify to

$$\frac{d}{dx}(uAY) = 0 \tag{A-10}$$

$$\frac{d}{dx}(uA) = E_0 C u \tag{A-11}$$

$$\frac{d}{dx}(Au^2) = 0 \tag{A-12}$$

$$u \frac{dW}{dx} = E_0 u \tag{A-13}$$

where the jet perimeter C is related to the jet cross-sectional area A by

$$C = \frac{A}{W} + bW \tag{A-14}$$

In the above equation b = 4 for an elevated rectangular jet (see Eq. 18) and b = 2 for a ground-level rectangular jet (see Eq. 23).

Equations (A-10), (A-12), and (A-3) can be integrated immediately to obtain

$$uAY = u_0 A_0 Y_0 \tag{A-15}$$

$$Au^2 = A_0 u_0^2 \tag{A-16}$$

$$W = W_0 + E_0 x \tag{A-17}$$

where W_0 is the initial half-width of the jet. Dividing Eq. (A-16) by Eq. (A-15):

$$\frac{u}{u_0} = \frac{Y}{Y_0} \tag{A-18}$$

From the above equation and Eq. (A-15) we get

$$\frac{A}{A_0} = \left(\frac{Y_0}{Y}\right)^2 \tag{A-19}$$

Dividing Eq. (A-11) by Eq. (A-13) and using Eqs. (A-18) and (A-19) to eliminate u and A from the result in favor of Y yields the following differential equation for Y as a function of W:

$$\frac{d}{dW}\left(\frac{1}{Y}\right) = -\frac{CY}{A_0 Y_0^2} \tag{A-20}$$

Now Eq. (A-14) for the jet perimeter C may be expressed in terms of W and Y via Eq. (A-19), as follows:

$$C = \frac{A_0}{W}\left(\frac{Y_0}{Y}\right)^2 + bW \tag{A-21}$$

Eliminating C between Eqs. (A-20) and (A-21) results in a differential equation for Y as a function of W only, namely

$$\frac{dY}{dW} = -\frac{Y}{W} - \frac{bWY^3}{A_0 Y_0^2} \tag{A-22}$$

Let us make in Eq. (A-22) the transformation

$$\xi = YW \tag{A-23}$$

from which we obtain

$$W\frac{d\xi}{dW} = -\frac{b\xi^3}{A_0 Y_0^2} \tag{A-24}$$

Integrating this result:

$$\frac{1}{\xi^2} = \frac{1}{\xi_0^2} + \frac{2b}{A_0 Y_0^2}\ln\left(\frac{W}{W_0}\right) \tag{A-25}$$

Finally, using Eq. (A-23) to replace ξ with Y, we get

$$\frac{Y}{Y_0} = \frac{1}{\frac{W}{W_0}\left[1 + \frac{2bW_0^2}{A_0}\ln\left(\frac{W}{W_0}\right)\right]^{1/2}} \tag{A-26}$$

Substituting Eq. (A-17) for W into the above equation gives the desired result, namely Eq. (33).

This page intentionally left blank.

APPENDIX C

SOURCE TERM MITIGATION BY AEROSOL SEDIMENTATION IN POSTULATED SOLVENT POOL FIRES

This page intentionally left blank.

CONTENTS

1.0 INTRODUCTION C-5

2.0 OBJECTIVE AND SCOPE C-5

3.0 SUMMARY AND CONCLUSIONS C-5
3.1 SUMMARY C-5
3.2 CONCLUSIONS C-6

4.0 PHENOMENOLOGY OF AEROSOL RETENTION IN TANKS C-6
4.1 AEROSOL PARTICLE FORMATION C-6
4.2 PARTICLE GROWTH BY AGGLOMERATION C-7
4.3 PARTICLE DEPLETION MECHANISMS C-8
4.4 INFORMATION REQUIRED TO QUANTIFY IN-TANK PARTICLE RETENTION IN POOL FIRES C-9

5.0 METHODOLOGY C-10
5.1 THERMAL HYDRAULIC CONDITIONS C-10
5.2 AEROSOL BEHAVIOR MODEL C-10
5.2.1 Correlation for Source Period C-10
5.2.2 Correlation for Decay Period C-12
5.2.3 Calculation of Aerosol Leakage C-13
5.3 COMPARISON OF CORRELATION WITH NUMERICAL SOLUTION C-14
5.3.1 Hypothetical Fog Formation in Tank C-103 . . . . . C-14
5.3.2 Aerosol Sedimentation In Hypothetical Pool Fire C-20

6.0 RESULTS OF AEROSOL TRANSPORT ANALYSIS C-23

7.0 REFERENCES C-28

LIST OF TABLES

5-1 Listing of AEROSOL.GAS Program C-15

5-2 Input Parameters for MAEROS2 Analysis of Fog Formation in Tank C-103. . . . . C-19

5-3 Equilibrium Fog Concentration Predicted by MAEROS2 and AEROSOL.GAS C-19

5-4 Predicted Aerosol Parameters for Period 1 at 2500S C-21

5-5 Predicted Aerosol Parameters for Period 2 . . . . . C-21

5-6 Predicted Aerosol Parameters for Period 3 . . . . . C-22

6-1 Aerosol Depletion Factors for Solvent Pool Fires. C-24

6-2 Dose Consequences for Solvent Pool Fires C-26

6-3 Effect of Ventilation Rate on Aerosol Depletion Factor and Predicted Doses C-27

1.0 INTRODUCTION

This appendix presents the results of an analysis of aerosol retention in waste tanks under postulated solvent pool fire conditions. Aerosol retention within a tank is potentially important because it is a naturally-occurring mechanism for mitigating calculated consequences of postulated fire accidents. Dose consequences predicted on the basis of negligible aerosol depletion are slightly higher than guidelines for accident scenarios which postulate the operation of a ventilation system which purges airborne contaminants from the tank (Cowley et al. 1997). Aerosol retention was cited by Cowley et al. (1997) as a phenomenon that needed to be accounted for to obtain more realistic estimates of pool fire consequences. The work presented in this appendix is responsive to the need cited by Cowley et al. 1997.

2.0 OBJECTIVE AND SCOPE

The objective of this study is to quantify the impact of aerosol depletion on predicted releases of particulate contaminants from solvent pool fires. This information is to be used to more realistically quantify the predicted dose consequences of pool fires.

The scope of this work was limited to an evaluation of in-tank sedimentation losses in 21 pool fire cases described herein.

3.0 SUMMARY AND CONCLUSIONS

3.1 SUMMARY

An aerosol retention factor was estimated for each of 21 solvent pool fire cases analyzed in this document. The retention factor quantifies the degree to which aerosol fallout inside a waste tank mitigates the radiological consequences of analyzed accidents.

The retention factor was estimated on the basis of sedimentation losses of particulate material to the floor of a waste tank. Particulate matter which settles out is unavailable for leakage with gases which escape from the tank as a result of fire-generated pressures or as a result of fan operation.

Aerosol agglomeration, fallout, and leakage were predicted by means of a correlation (Epstein and Ellison 1987) which accounts for agglomeration of particles inside the tank. The correlation has been shown to agree well with experimental data and with numerical solutions to the differential equations that govern aerosol behavior in a confined volume (Epstein and Ellison 1987).

The correlation was used herein because it greatly simplified the analysis of the many cases analyzed here as compared to an analysis based on the MAEROS2 Code (Gelbard 1996), the numerical code available for analyzing aerosol behavior.

The applicability of the correlation to the solvent pool fire cases was demonstrated by comparing the aerosol retention factor predicted by the correlation with the retention factor based on MAEROS2 Code predictions. The fire case analyzed by the two methods was representative of the fire cases for which significant retention was predicted; the two methods yielded very similar results.

3.2 CONCLUSIONS

Results of this work are characterized by the following conclusions and summary statements.

1. Sedimentation is predicted to reduce the carry-over of particulate materials by factors ranging from one to seven.

2. The higher retention factors apply to puddle fires in actively ventilated tanks; for these cases, predicted dose consequences fall well below guidelines when aerosol depletion is accounted for. Doses fall slightly above guidelines for actively ventilated cases when aerosol deposition is ignored.

3. Aerosol retention was predicted to be negligible for fire cases where the fire duration was brief in time and the venting rate was large. Too little time was available to allow much aerosol fallout for those cases. Predicted dose consequences for these passively ventilated cases had previously fallen below guidelines and remain unchanged as a result of this analysis of aerosol behavior.

4.0 PHENOMENOLOGY OF AEROSOL RETENTION IN TANKS

This section is a brief discussion of phenomena that govern the retention of particulate contaminants generated by a pool fire in a tank.

4.1 AEROSOL PARTICLE FORMATION

Incomplete combustion of solvent causes the formation of soot particles, visible as smoke. The combustion of solvent vapor occurs in the gas phase in a mixing zone above the surface of the pool. Combustion products that are non-volatile condense out in the gas phase as small particles, i.e., as soot. The small primary particles rapidly coagulate, forming agglomerates. Agglomerates are larger particles composed of many smaller primary particles. Experiments on solvent pool fires (Jordan) indicate that primary particles are a fraction of a micrometer in diameter. Agglomeration processes cause the

small primary particles to grow in size to an extent that is determined mainly by particle mass concentration (kg of particles per cubic meter of gas) and time.

In addition to carbonaceous particles, oxides of phosphorous are formed by the combustion of tributylphosphate (TBP) which is present in solvent. Phosphorous oxide, typified by P_2O_5, is of relatively low volatility and is highly deliquescent. It would be expected to be present in smoke as fine droplets of phosphoric acid, by reacting with water vapor.

Waste material in a tank is subject to aerosolization by means of mechanical forces or volatilization. Aerosolized waste materials that are non-volatile in headspace gases would be present in particulate form and represent a third source of aerosols generated by a pool fire. This source is important with respect to dose consequences because aerosolized waste is the source of radioactive material that is predicted to be vented from a tank as a result of a pool fire.

The three aerosol species described above would be present at the same time in headspace air and would co-agglomerate. It is assumed herein that co-agglomeration would cause all aerosol species to behave similarly. Thus, the behavior of radioactive particles is assumed to be the same as soot particles which are predicted to constitute the major fraction of aerosol mass. The co-agglomeration assumption employed herein is commonly used in accident analyses and is supported by experimental data from large scale aerosol tests conducted at Hanford (Hilliard et al. 1987 and McCormack et al. 1987).

4.2 PARTICLE GROWTH BY AGGLOMERATION

Agglomeration of small particles into larger ones increases particle settling velocity and thereby increases the fallout rate by sedimentation. Key mechanisms for agglomeration are the following.

- Brownian diffusion: This mechanism is most important for submicron particles. Brownian diffusion would cause primary particles to agglomerate into micron-sized clumps in the fire plume.

- Gravity agglomeration: This mechanism reflects capture of smaller particles by larger ones due to differences in settling velocity. It would occur throughout the headspace volume, and becomes increasingly effective for large particles and high mass concentrations.

- Other mechanisms: Fluid turbulence and water vapor uptake are other mechanisms that can cause particle growth. These mechanisms are believed to be of secondary importance for solvent pool fire conditions, and have been neglected in this study.

4.3 PARTICLE DEPLETION MECHANISMS

A number of different mechanisms can cause the removal of airborne particles during fire accidents. These are briefly discussed as follows.

Sedimentation

Sedimentation is the fallout of particles due to gravity onto surfaces that face upward. This mechanism is typically observed to be the dominant means of aerosol depletion in large scale tank-type, aerosol tests (Hilliard et al. 1979, 1983, 1987 and McCormack et al. 1987). Since particle settling velocity varies as the square of particle diameter, particle size must be known to predict sedimentation rate.

Other Mechanisms

Other mechanisms for particle deposition that would contribute to retention, but which have been neglected in this study are briefly described as follows.

- **Thermophoresis**

  Thermal gradients in a gas cause particles to migrate down the gradient. In a poolfire incident, particles would migrate to the tank walls because headspace air, heated by the fire, would be at a higher temperature than the walls. Thermophoretic deposition is neglected herein on the basis that this mechanism was found to be of secondary importance in large scale sodium pool fire tests carried out at Hanford (Hilliard et al. 1979).

- **Brownian Diffusion**

  Brownian diffusion causes particle migration down the particle concentration gradient that exists near surfaces. This mechanism is neglected on the basis of large scale aerosol test results (Hilliard et al. 1979) that showed that plateout on surfaces (due to all plateout mechanisms, including Brownian diffusion) was of secondary importance as compared to sedimentation.

- **Diffusiophoresis**

  Diffusiophoresis is particle migration driven by molecular weight gradients in the suspending gas. It could be important under conditions where water vapor condensed in significant quantity on tank walls. None of the fire cases analyzed herein involve significant condensation of water vapor on tank walls, so diffusiophoresis is judged to be negligible and is neglected herein.

- **Inertial Deposition**

  Inertial deposition could be important in enhancing wall plateout from turbulent boundary layer flow and from gases vented from tortuous leak paths. Plateout due to turbulence in wall boundary layers has been neglected on the basis that such deposition was relatively unimportant in sodium pool fire tests (Hilliard et al. 1979). Inertial impaction in vent paths has been neglected for two reasons: (1) retention in the leak path would probably reduce particle carryover by less than a factor of two, and (2) a credible analysis of leak path retention is beyond the scope of the present study.

4.4 INFORMATION REQUIRED TO QUANTIFY IN-TANK PARTICLE RETENTION IN POOL FIRES

The fractional retention of particles in a tank during a pool fire sequence is calculable on the basis of a material balance which compares particle depletion rates attributable to leakage and sedimentation. Leakage rate at any instant in time can be calculated as follows:

$$L = C_g * Q \tag{1}$$

where

L = particle leak rate, kg/s,
C_g = aerosol concentration, kg/m^3,
Q = gas leak rate, m^3/s.

Sedimentation rate of particulate material is calculable from the following equation:

$$S = C_g * U_s * A_s \tag{2}$$

where

S = sedimentation rate, kg/s,
C_g = aerosol concentration, kg/m^3,
U_s = mean settling velocity, m/s,
A_s = sedimentation surface area, m^2.

U_s, the mean sedimentation velocity, depends on particle size, which is dependent on the extent to which particles agglomerate in the tank headspace. An aerosol agglomeration model is needed to predict mean sedimentation

velocity as a function of time. Key parameters needed to quantify aerosol depletion due to sedimentation are:

- gas leakage rate, m^3/s,
- sedimentation surface area, m^2,
- aerosol concentration, g/m^3,
- aerosol agglomeration model to predict U_s.

5.0 METHODOLOGY

This section describes calculational methodology used to estimate the impact of in-tank aerosol sedimentation on mitigating the release of radioactive particles from a tank under postulated pool fire accident conditions.

5.1 THERMAL HYDRAULIC CONDITIONS

Thermal hydraulic conditions for the pool fire cases analyzed herein were obtained by means of the POOLFIRE.4 Code. This code, and key results from it, are described elsewhere in this report. Key thermal hydraulic parameters used in the aerosol analysis are the following:

- solvent burn rate vs. time,
- gas venting rate vs. time,
- gas temperature vs. time,
- physical dimensions of tank.

5.2 AEROSOL BEHAVIOR MODEL

A correlation of aerosol agglomeration, sedimentation, and leakage was used to analyze aerosol behavior in pool fires. The correlation (Epstein and Ellison 1987) has been shown to yield predictions that agree well with numerical solutions and large scale experimental test results (Epstein and Ellison 1987). The applicability of the Epstein and Ellison (1987) correlation to the present situation was checked by analyzing one typical pool fire case by both the correlation and the MAEROS2 Code (Gelbard 1996). The two methods gave answers that agreed well, and this agreement supports the validity of the correlation for analyzing aerosol behavior in pool fires.

5.2.1 Correlation for Source Period

The aerosol removal rate constant for removal due to sedimentation and leakage during a time period when an aerosol source is present is given by Epstein and Ellison (1987) as:

$$\lambda_{TOT} = (\lambda_{SED} + \frac{1}{3}\lambda_L)\left[1 + \left(\frac{\lambda_L}{\lambda_{SED} + \frac{1}{3}\lambda_L}\right)^{4.5}\right]^{0.222} \quad (3)$$

where

λ_{TOT} = combined removal rate constant, s^{-1},
λ_{SED} = removal rate constant for sedimentation, s^{-1},
λ_L = removal rate constant for leakage, s^{-1}.

The sedimentation removal rate constant, λ_{SED}, is related to airborne mass concentration by the following correlation. First, a dimensionless constant, Λ_{SED} is defined:

$$\Lambda_{SED} = \left(\frac{\gamma\chi^2\mu h^2\epsilon_o}{\alpha K_o g\rho}\right)^{\frac{1}{2}} * \lambda_{SED} \quad (4)$$

where

Λ_{SED} = dimensionless removal rate constant,
γ = collision shape factor, dimensionless,
χ = particle settling shape factor, dimensionless,
μ = gas viscosity, kg/ms,
h = effective height of compartment (volume/deposition area), m,
ϵ_o = particle capture efficiency, dimensionless,
α = density correction factor, dimensionless,
K_o = normalized Brownian collision coefficient, $4kT_\infty/3\mu$,
k = Boltzmann constant, J/°K
T_∞ = bulk gas temperature, °K,
g = gravitational constant, m/s^2,
ρ = density of particle material, kg/m^3.

The dimensionless removal lambda is correlated to mass concentration as follows.

$$\Lambda_{SED} = 0.226M^{0.282}(1 + 0.189M^{0.8})^{0.695} \quad (5)$$

where

M = dimensionless mass concentration.

M is related to aerosol mass concentration by:

$$M = \left(\frac{\gamma^9 g h^4 \epsilon_o^5}{\alpha^3 K_o \rho^3 \mu} \right)^{1/4} \cdot m \tag{6}$$

where

m = airborne mass concentration, kg/m^3.

λ_L, the removal rate constant due to leakage is simply the fraction of the tank's volume leaked per second:

$$\lambda_L = \frac{Q}{V} \tag{7}$$

where

Q = gas leak rate, m^3/s,
V = headspace volume, m^3.

Equations (3) through (7) define removal rate constants for sedimentation and leakage when a source of aerosols is present. For pool fires, the particle source is the fire, so Equations (3) through (7) are used for the period when the fire is burning.

5.2.2 Correlation for Decay Period

For times beyond the point where the aerosol source is terminated, λ_{TOT} is calculated as the sum of λ_{SED} and λ_L (Epstein and Ellison 1987):

$$\lambda_{TOT} = \lambda_{SED} + \lambda_L . \tag{8}$$

λ_L has the same form as defined in Equation (7) but λ_{SED} has a different correlation for the decay period. For decay, Λ_{SED} is correlated to dimensionless concentration, M, as follows:

$$\Lambda_{SED} = 0.528M^{0.235} (1 + 0.473M^{0.754})^{0.786} \tag{9}$$

Equations (8) and (9) define sedimentation and leakage decay constants for times after the fire is extinguished.

5.2.3 Calculation of Aerosol Leakage

In order to apply the aerosol correlation defined by Equations (3) through (9), the airborne concentration must be computed as a function of time. This is done by making a material balance: the change in concentration is calculated as the difference between input and output rates.

$$\text{input rate} = s \tag{10}$$

$$\text{output rate} = \lambda_{TOT}\, C_g\, V \tag{11}$$

$$\text{accumulation rate} = \frac{d}{dt}(VC_g) \tag{12}$$

Equating accumulation rate to the difference between input and output rates, Equations (10, (11) and (12) may be combined to yield the following predictive equation for airborne concentration:

$$V\frac{dC_g}{dt} = S - \lambda_{TOT} C_g\, V \tag{13}$$

where

s = particle source rate, kg/s.

Equation (13) was integrated by simply approximating the differentials in Equation (13) by finite differences. Very small time steps were used to assure that the change in C_g as small compared to its absolute value. For each time step, aerosol mass leaked was computed from:

$$\text{aerosol mass leaked} = C_g Q \Delta t \tag{14}$$

where

C_g = average concentration over time step, kg/m^3,
Q = vent flow rate, m^3/s,
Δt = length of time step, s.

Mass leaked computed for each time step (Equation (14)) was summed to obtain the total mass leaked over time.

Equation (13) was also integrated for a non-sedimenting species having the same mass generation rate and leakage that applied to the aerosol. The mass leaked for a non-sedimenting specie serves as a baseline to calculate an aerosol depletion factor:

$$\text{ADF} = \text{aerosol depletion factor} = \frac{\text{mass of aerosol leaked}}{\text{mass of non-sedimenting specie leaked}} \quad (15)$$

The aerosol factor was then used as a multiplier in the spreadsheet used to quantify radiological consequences. The spread sheet consequences were earlier based on non-sedimeting species behavior, so multiplying by the aerosol factor shown in Equation (15) yields an estimate of mass leaked that accounts for aerosol sedimentation.

The calculation of aerosol leakage was done by means of a simple BASIC[1] program. A copy of the program listing is given in Table 5-1.

5.3 COMPARISON OF CORRELATION WITH NUMERICAL SOLUTION

Aerosol behavior predicted by the correlation described in Section 5.2 was compared with predictions based on the MAEROS2 Code to confirm its applicability to the problem at hand and to verify that the AEROSOL.GAS program yielded numerically correct results. Two aerosol cases were analyzed with each Code. Results are described as follows.

5.3.1 Hypothetical Fog Formation in Tank C-103

A bounding case of organic aerosol formation in the headspace of tank C-103 was analyzed by means of the MAEROS2 Code (Postma et al. 1994) as part of the hazards analysis of tank C-103. The MAEROS2 Code was used to predict the maximum aerosol concentration that could build in the headspace given specific aerosol generation rates. Key aerosol and tank parameters used in the MAEROS2 runs are reproduced in Table 5-2.

[1] Basic is a trade mark of Microsoft Corp, Redmond, Washington.

Table 5-1. Listing of AEROSOL.GAS Program. (4 sheets)

```
10 CLS
20 REM          THIS PROGRAM IS CALLED  " AEROSOL.GAS"
30 REM          THIS PROGRAM CALCULATES AEROSOL DECAY DUE TO
40 REM           AEROSOL SOURCE, SEDIMENTATION AND LEAKAGE
99 REM
100 REM         INPUT VARIABLES ARE DEFINED AS FOLLOWS
101 REM
102 REM         ALPHA = AEROSOL FACTOR, DIMENSIONLESS
103 REM
104 REM         CHI = AEROSOL FACTOR, DIMENSIONLESS
105 REM
106 REM         GAMMA = AEROSOL FACTOR, DIMENSIONLESS
107 REM
108 REM         EO = COAGULATION EFFICIENCY, DIMENSIONLESS
109 REM
110 REM         MU = VISCOSITY OF GAS IN TANK, KG/M S
111 REM
112 REM         G = ACCELERATION OF GRAVITY, M/S^2
113 REM
114 REM         TG= GAS TEMPERATURE, K
115 REM
116 REM         BOLTZ = BOLTZMANN'S CONSTANT, JOULE/K
117 REM
118 REM         RHO = PARTICLE DENSITY, KG/M^3
119 REM
120 REM         GVOL = GAS VOLUME IN TANK, M^3
121 REM
122 REM         ASED = HORIZONTAL AREA FOR SEDIMENTATION, M^2
123 REM
124 REM         LEAK = LEAK RATE , M^3/S
125 REM
150 DATA     1.0    ,   1.0  ,    1.0    ,  .3333 ,  2.0E-5 ,  9.81 ,  330
152 READ   ALPHA    ,  CHI   ,   GAMMA   ,   EO   ,   MU    ,   G   ,   TG
160 DATA    1.39E-23, 1000   ,  4820     ,  411   ,  0.001  ,  0.0472
162 READ    BOLTZ   ,   RHO  ,  GVOL     ,  ASED  ,  TEST   ,  LEAK
163 REM
200 REM         VARIABLES ARE DEFINED AS FOLLOWS
201 REM
210 REM         H = EFFECTIVE HEIGHT = GVOL/ASED
212 H= GVOL/ASED
213 REM
214  PRINT "H=";H
220 REM KO = VISCOSITY GROUP = 4*K*T/3* MU
222 KO=4* BOLTZ* TG/(MU*3)
223 REM
224  PRINT "KO=";KO
240 REM         B = DIMENSIONAL CONSTANT FOR SUSPENDED MASS
241 REM
242 B=((GAMMA^9*G*H^4*EO^5)/(ALPHA^3*KO*RHO^3*MU))^.25
243 REM
```

Table 5-1. Listing of AEROSOL.GAS Program. (4 sheets)

```
250 REM          C = DIMENSIONAL CONSTANT FOR AEROSOL DECAY
251 REM
252 C=((GAMMA*CHI^2*MU*H^2*E0)/(ALPHA*K0*G*RHO))^.5
253 REM
255 PRINT "A=";A;"B=";B;"C=";C
260 LAMLEAK=LEAK/GVOL
300 REM THIS SECTION ENTERS KEYBOARD INPUTS
302 PRINT " "
305 INPUT "INITIAL CONCENTRATION, KG/M^3";M0
307  PRINT " "
310 INPUT "AEROSOL GENERATION RATE, KG/SEC";MDOT
311 MDOT=MDOT/GVOL
312 PRINT " "
320 INPUT "TIME DURATION OF AEROSOL SOURCE, SEC";TSOURCE
322 PRINT " "
330 INPUT "LENGTH OF TIME STEP, SEC";DT
332 PRINT " "
340 INPUT "TOTAL TIME FOR PROBLEM, SEC";TIMTOT
342 PRINT " "
350 INPUT "TIME INTERVAL FOR PRINTING, SEC";TIMP
352 PRINT " "
400 REM  THIS SECTION PRINTS KEY INPUTS FOR PROBLEM
402 PRINT " "
410 PRINT " THIS PROGRAM IS CALLED --AEROSOL.GAS--"
412 PRINT" "
420 PRINT "THIS PROGRAM COMPUTES AEROSOL BUILDUP AND DECAY DUE TO A SOURCE,
ACCOUNTING FOR SEDIMENTATION AND LEAKAGE USING EPSTEIN'S CORRELATION"
422 PRINT " "
424 PRINT "INITIAL CONCENTRATION=";M0;" KG/M^3 "
426 PRINT " "
427 M00=M0
428 M0GAS=M0
430 PRINT "CHAMBER VOLUME=";GVOL; " M^3"
432  PRINT " "
438 MTOT= TSOURCE*MDOT*GVOL+M0*GVOL
440 PRINT "TOTAL AEROSOL MASS INJECTED OVER WHOLE TIME PERIOD=";MTOT;"KG"
442 PRINT " "
450 PRINT "TIME DURATION OF SOURCE= ";TSOURCE; "SEC"
452 PRINT " "
460 PRINT "LEAK RATE=";LEAK;" M^3/S"
462 PRINT " "
470 PRINT "THIS CASE RUN AT ";TIME$; " ON ";DATE$
472 PRINT " "
500 REM  THIS SECTION PRINTS HEADING FOR RESULTS
510 PRINT"    TIME,SEC    CONC.,KG/M^3   MASS LEAKED,KG   GAS LEAKED,KG
DEPL.FACT."
512 PRINT " "
600 REM  THIS SECTION PRINTS INITIAL CONDITIONS
605 FAIRBORN=1
610 PRINT USING "   ##.###^^^^  ";TIM;M00;SUMLEAK;SUMLEAKGAS;FRACTL
800 REM  THIS SECTION IS EXECUTIVE
810 TIM=TIM+DT
820 GOSUB 1000
830 GOSUB 2000
```

Table 5-1. Listing of AEROSOL.GAS Program. (4 sheets)

```
840 GOTO 3000
1000 REM THIS SUB APPLIES TO SOURCE PERIOD
1010 IF TIM > TSOURCE THEN RETURN
1020 MAVG=M0+DT*(MDOT-LAMTOT*M0)/2
1025 M1GAS=M0GAS+DT*(MDOT-LAMLEAK*M0GAS)
1026 MAVGGAS=(M0GAS+M1GAS)/2
1028 M1GAS=M0GAS+DT*(MDOT-LAMLEAK*MAVGGAS)
1030 GOSUB 1500
1040 GOSUB 1800
1050 MAVG=(M0+M1)/2
1060 GOSUB 1500
1070 GOSUB 1800
1075 MAVG=(M0+M1)/2
1080 M0=M1
1085 M0GAS=M1GAS
1090 MLEAK=LEAK*MAVG*DT
1095 MLEAKGAS=LEAK*MAVGGAS*DT
1100 SUMLEAK=SUMLEAK+MLEAK
1105 SUMLEAKGAS=SUMLEAKGAS+MLEAKGAS
1110 FRACTL=SUMLEAK/(MDOT*TIM*GVOL+M00*GVOL)
1120 FAIRBORN=M1/(MDOT*TIM+M00)
1200 RETURN
1500 REM THIS SUB COMPUTES LAMTOT FOR SOURCE PERIOD
1510 M=B*MAVG
1520 CAPLAMSED=.226*M^.282
1525 CAPLAMSED=CAPLAMSED*(1+.189*M^.8)^.695
1530 LAMSED=CAPLAMSED/C
1540 LAMTOT=(LAMSED+LAMLEAK/3)*(1+(LAMLEAK/(LAMSED+LAMLEAK /3))^4.5)^.222
1590 RETURN
1800 REM THIS SUB COMPUTES M1
1810 M1=M0+DT*(MDOT-LAMTOT*MAVG)
1890 RETURN
2000 REM THIS SECTION APPLIES AFTER SOURCE SHUTOFF
2005 IF TIM=< TSOURCE THEN RETURN
2010 MAVG=M0-DT*LAMTOT*M0/2
2015 M1GAS=M0GAS*(1-DT*LAMLEAK)
2020 GOSUB 2500
2030 GOSUB 2800
2040 MAVG=(M0+M1)/2
2045 MAVGGAS=(M0GAS+M1GAS)/2
2050 GOSUB 2500
2060 GOSUB 2800
2065 MAVG=(M0+M1)/2
2070 M0=M1
2075 M0GAS=M1GAS
2080 MLEAK=LEAK*MAVG*DT
2085 MLEAKGAS=LEAK*MAVGGAS*DT
2090 SUMLEAK=SUMLEAK+MLEAK
2095 SUMLEAKGAS=SUMLEAKGAS+MLEAKGAS
2100 FRACTL=SUMLEAK/(MDOT*GVOL*TSOURCE+M00*GVOL)
2110 FAIRBORN=M1*GVOL/(MDOT*TSOURCE+M00*GVOL)
2200 RETURN
2500 REM THIS SUB COMPUTES LAMTOT
2510 M=B*MAVG
```

Table 5-1. Listing of AEROSOL.GAS Program. (4 sheets)

```
2520 CAPLAMDEC=(.528*M^.235)*(1+.473*M^.754)^.786
2530 LAMSED=CAPLAMDEC/C
2540 LAMTOT=LAMSED+LAMLEAK
2590 RETURN
2800 REM THIS SUB RETURNS M1
2810 M1=MO-DT*LAMTOT*MAVG
2900 RETURN
3000 REM  THIS SUB PRINTS AND STOPS
3005 DEPL=SUMLEAK/SUMLEAKGAS
3010 DELTIM=DELTIM+DT
3020 IF DELTIM+.1>TIMP THEN GOTO 3100
3030 GOTO 800
3100 PRINT USING "   ##.###^^^^  ";TIM;M1;SUMLEAK;SUMLEAKGAS;DEPL
3110 DELTIM=0
3120 IF TIM+.1>TIMTOT THEN END
3130 GOTO 800
```

Table 5-2. Input Parameters for MAEROS2 Analysis of Fog Formation in Tank C-103.[a]

Parameter	Units	Value
gas volume	m^3	2560
sedimentation area	m^2	411
gas temperature	°K	317
source rate	kg/s	1.21E-6, 1.21E-5, 1.21E-7
γ, collision shape factor	dimensionless	1
χ, settling shape factor	dimensionless	1
α, density correction factor	dimensionless	1
gas leak rate	m^3/s	0
source mean diameter	m	1.3E-7
source geo. std. dev.	dimensionless	2
gas pressure	pascal	101325
smallest diameter	m	1E-7
largest diameter	m	1E-5
no. of sections	dimensionless	16

Note:
[a]Postma et al. (1994)

This same case was analyzed with the AEROSOL.GAS program that is based on the correlation of Epstein and Ellison (1987) described in Section 5.2. AEROSOL.GAS does not require size information for the aerosol source. Parameters needed for AEROSOL.GAS that are not listed in Table 5-2 are capture efficiency, ϵ_o, gas viscosity, μ, and gravitational constant, g. These three parameters were assigned values of: ϵ_o = 0.333; μ = 2.0E-5 kg/ms; g = 9.81 m/s^2. A capture efficiency value of 1 is sometimes used. However discussion with Mr. Epstein resulted in the selection of a more conservative value of 0.33 for this application. The value for air viscosity is for a gas temperature of 411° Kelvin. Maximum aerosol concentrations predicted by the two methods are compared in Table 5-3.

Table 5-3. Equilibrium Fog Concentration Predicted by MAEROS2 and AEROSOL.GAS

Particle Source Rate kg/s	Predicted Equilibrium Concentration kg/m^3	
	MAEROS2	AEROSOL.GAS
1.21E-6	4.2E-5	4.2E-5
1.2E-7	8E-6	7E-6
1.2E-5	2.2E-4	2.4E-4

Equilibrium concentrations predicted by the two methods, as quantified in Table 5-3, agree very well. This agreement supports the use of the correlation as a simple alternative to the numerical solution of agglomeration equations performed by the MAEROS2 Code.

5.3.2 Aerosol Sedimentation In Hypothetical Pool Fire

Aerosol particle capture by in-tank sedimentation was analyzed by both the correlation and the MAEROS2 Code for a postulated pool fire in a single shell tank. Parameters for this case include the following:

- tank type : SST
- puddle area : $1 m^2$
- vent path : hepa
- ventilation flow : 100 cfm.

Parameters that govern predicted aerosol transport for this case are quantified as follows. Note that thermal hydraulic conditions have been taken from calculations made with the POOLFIRE.4 Code for Case C of the spreadsheet (Table 6-2) which summarizes fire consequences.

Three time periods may be used to model aerosol behavior for this case. Key parameters for each are quantified as follows.

Period 1, 0 to 2500S

This period covers the pressurized venting of headspace air in response to the fire. During this period, 87.3 kg of fuel is predicted to burn, and the average vent rate of gas is 0.443 m^3/s. Aerosol generation rate is estimated as follows:

$$S = \frac{87.3\text{kg fuel}}{2500S} * \frac{0.265\text{kg aerosol}}{\text{kg fuel}} = 9.25E\text{-}3 \text{ kg/s}$$

Aerosol formation is calculated as the sum of soot (20% of fuel burned) P_2O_5 (4.32% of fuel burned) and water (50% of P_2O_5) sufficient to form H_3PO_4.

Source particle size was characterized by a mass mean diameter of 0.4 μm and a geometric standard deviation of 2. This size distribution is representative of particle sizes measured in solvent fires (Jordan and Lindner, 1983).

Average temperature for period 1 is 372°K, chamber volume is 4820 m^3 and floor area is 411 m^2. Particle shape factors (α, γ, χ) were all assigned values of unity.

Predicted aerosol concentrations and mass leaked at the end of period 1 are listed in Table 5-4.

Table 5-4. Predicted Aerosol Parameters for Period 1 at 2500S.

Parameter	Predicted Value	
	MAEROS2	AEROSOL.GAS
Aerosol concentration, kg/m^3	4.28E-3	4.25E-3
Leaked mass, for period 1, kg	2.448	2.46
Mean particle diameter, μm	1.1	---
Geometric std. deviation	1.6	---

The data of Table 5-4 show that values of airborne concentration and leaked mass predicted by the correlation are essentially identical to the values predicted by the numerical solution. Particle size parameters predicted by MAEROS2 are needed as input for period 2 for MAEROS2. Particle size is not an explicit input or output for the correlation.

Period 2, 2500S to 5000S

This period covers the burn to oxygen extinguishment while the headspace is ventilated at 100 cfm (0.0472 m^3/s). During this period, 40.7 kg of fuel is calculated to burn. The source rate is calculated as follows:

$$S = \frac{40.7\text{kg fuel}}{2500\text{s}} * \frac{0.265\text{kg aerosol}}{\text{kg fuel}} = 4.31\text{E-3kg/s}$$

Source particle size is the same as for period 1, e.g. mean diameter = 0.4μm, geometric standard deviation = 2.0. Initial mass concentrations for period 2 are the values depicted in Table 5-4. Average gas temperature for this period is 355°K, and vent rate is 0.0472 m^3/s. Particle shape factors were assigned values of unity for period 2, identical to values used for period 1.

Predicted aerosol concentrations and masses leaked for period 2 are listed in Table 5-5.

Table 5-5. Predicted Aerosol Parameters for Period 2.

Parameter	Predicted Value	
	MAEROS2	AEROSOL.GAS
Aerosol concentration @ 5000S, kg/m^3	6.31E-3	5.73E-3
Leaked mass for period 2, kg	0.605	0.592
Mean particle diameter @ 5000s, μm	2.0	--
Geometric std. deviation	1.6	--

The data of Table 5-5 show that the correlation predicts concentrations and leaked masses that are close to values predicted by the numerical solution.

Period 3, 5000s to 200,000s

During this period the aerosol is depleted through sedimentation and leakage. The fire is out, so there is no aerosol source. Average temperature for this period is 311°K. Initial particle size parameters are the values predicted for the end of period 2, and are listed in Table 5-5. The total time (200,000s) is arbitrarily set at a long enough time so that virtually all aerosol is removed (leaked + settled) from the headspace.

Predicted aerosol concentrations and leaked masses for period 3 are listed in Table 5-6.

Table 5-6. Predicted Aerosol Parameters for Period 3.

Parameter	Predicted Value	
	MAEROS2	AEROSOL.GAS
Aerosol concentration @ 200,000s kg/m^3	1.5E-6	2.4E-6
Leaked mass for period 3, kg	2.647	2.27

Total mass leaked over the course of the pool fire event is the sum of masses leaked for the three periods. For MAEROS2 the total is:

$$\text{total leaked} = 2.448 + 0.605 + 2.647 = 5.70\text{kg}$$

The total mass leaked predicted by AEROSOL.GAS is:

$$\text{total leaked} = 2.46 + 0.592 + 2.27 = 5.32\text{kg}.$$

The difference in these values, 5.70 - 5.32 = 0.38kg is 6.7% of the value predicted by MAEROS2. This small difference is believed to be within the accuracy bounds required for analysis of low probability accidents.

6.0 RESULTS OF AEROSOL TRANSPORT ANALYSIS

The mass of aerosol leaked from the tank over the course of a pool fire scenario was computed for each of the 21 cases analyzed in this report. This aerosol mass was divided by the leaked mass for a non-sedimenting specie. The ratio forms an aerosol depletion factor (ADF) as illustrated in Equation (15). Since calculated doses are proportional to leaked aerosol mass, the ADF can be used as a factor in dose calculations performed in the spreadsheet.

Aerosol depletion factors calculated for 21 pool fire cases by means of AEROSOL.GAS are presented in Column M of Table 6-1.

Review of aerosol depletion factors (ADFs) listed in Column M of Table 6-1 shows that aerosol sedimentation is a significant factor only for actively ventilated cases. Agglomeration and fallout are apparently too slow to cause much depletion during the burn and pressurized vent phase of most fire cases analyzed. However, it is the actively ventilated cases that have the highest calculated doses, so aerosol depletion is a significant factor in limiting consequences for the bounding radiological cases. The ADF (Table 6-1, Column M) is 0.16, 0.16, 0.23, 0.13, 0.38, 0.20, and 0.22 for Cases c, d, g, k, l, q, and r respectively, all of which are actively ventilated at 100 cfm after the pressurized venting portion of the fire cycle.

Dose consequences for the 21 fire cases have been recalculated to account for aerosol depletion. Results are summarized in Table 6-2. The highest calculated onsite dose listed in Table 6-2, Column L, is 0.0257 Sv and applies to Case g. This dose falls below guidelines (0.05 Sv) for the unlikely frequency category. The main contributor to this dose is the HEPA rupture dose, 0.0152 Sv, as listed in Column J of Table 6-2. The maximum dose predicted earlier on the basis of zero aerosol depletion is a 0.0609 Sv, also for Case g (Cowley and Postma 1996). Thus, the quantification of aerosol depletion reduces calculated onsite dose by a factor of 2.4 (0.0609/0.0257) from slightly above guidelines to below guidelines.

Table 6-1. Aerosol Depletion Factors for Solvent Pool Fires. (2 sheets)

	A	B	C	D	E	F	G	H	I	J
1	Case	Tank Type	Solvent Pool Description	Pool Area m^2	Bounding Parameters	Ventilation Flow	Vent Description	Poolfire 4 Peak Pressure psig (kPa)	Poolfire 4 Peak Vacuum psig (kPa)	Poolfire 4 Solvent Burned kg
3	a	SST	puddle	1.0	pressure	passive	hepa[a]	3.1 (21.4)	0.5 (3.45)	128
4	b	SST	puddle	1.0	vacuum	passive	hepa/flapper[b]	1.0 (6.89)	0.5 (3.45)	124
5	c	SST	puddle	1.0	radiological	100 cfm (0.047 m^3/s)	hepa	3.1 (21.4)	0.5 (3.45)	128
6	d	SST	puddle	1.0	toxicological	100 cfm (0.047 m^3/s)	hepa	3.1 (21.4)	0.5 (3.45)	128
7	e	SST	large	210	pressure	passive	hepa	29 (200)	0.1 (0.69)	146
8	f	SST	large	210	vacuum	passive	hepa/ flapper	1.8 (12.4)	6.8 (46.9)	84
9	g	SST	large	210	radiological	100 cfm (0.047 m^3/s)	hepa	29 (200)	0.1 (0.69)	146
10	h	SST	large	210	toxicological	passive	hepa/flapper	1.8 (12.4)	6.8 (46.9)	84
11	i	DST	large	210	pressure	sealed tank	none	30.8 (212)	0 (0)	162
12	j	DST	large	210	vacuum	passive	flapper	2.1 (14.5)	8 (55.2)	92.5
13	k	DST	puddle	1.0	radiological	100 cfm (0.047 m^3/s)	vent pipe[c]	0.9 (6.21)	0.1 (0.69)	132
14	l	DST	large	210	toxicological	100 cfm (0.047 m^3/s)	flapper/vent pipe	2.0 (13.8)	5.2 (35.9)	92.1
15	m	DCRT	large	34.1	pressure	sealed tank	none	30.5 (210)	0 (0)	2.47
16	n	DCRT	large	34.1	vacuum	passive	4" (0.1m) orifice	18.3 (126)	1.2 (8.27)	2.12
17	o	DCRT	large	34.1	radiological	passive	4" (0.1m) orifice	18.3 (126)	1.2 (8.27)	2.12
18	p	DCRT	large	34.1	toxicological	passive	4" (0.1m) orifice	18.3 (126)	1.2 (8.27)	2.12
19	q	SST	entrained	40.0	radiological	100 cfm (0.047 m^3/s)	hepa[a]	4.4(30.5)	0.7(4.8)	130
20	r	SST	entrained	40.0	toxicological and vacuum	100 cfm (0.047 m^3/s)	hepa/flapper	1.0 (6.89)	2.1 (14.5)	113
21	s	55 kgal SST	large	29.2	pressure	passive	hepa[d]	23.9 (165)	.75 (5.2)	6.54
22	t	55 kgal SST	large	29.2	toxicological and vacuum	passive	hepa/flapper[d]	2.0 (13.8)	5.3 (13.8)	4
23	u	55 kgal SST	puddle	1.0	pressure	passive	hepa[d]	6.0 (41.4)	1.1 (7.52)	5.76

Table 6-1. Aerosol Depletion Factors for Solvent Pool Fires. (2 sheets)

	A	B	K	L	M	N	O	P	Q	R
1	Case	Tank Type	Solvent Aerosol Release Factor ARF	Poolfire 4 Leak Path Factor LPF	Aerosol Depletion Factor ADF	Solvent Atmosphere Release Basis kg	Aqueous Boiloff kg	Aerosol Release Factor for Aqueous ARF	Aqueous Atmospheric Release kg	Aqueous Unit Liter Dose Sv/L
3	a	SST	0.1	0.0747	1.00E+00	9.56E-01	161.28	0.002	2.41E-02	1.10E+04
4	b	SST	0.1	0.0399	1.00E+00	4.95E-01	156.24	0.002	1.25E-02	1.10E+04
5	c	SST	0.1	1.0	1.60E-01	2.05E+00	161.28	0.002	5.16E-02	1.10E+04
6	d	SST	0.1	1.0	1.60E-01	2.05E+00	161.28	0.002	5.16E-02	1.10E+04
7	e	SST	0.03	0.146	8.85E-01	5.66E-01	183.96	0.002	4.75E-02	1.10E+04
8	f	SST	0.03	0.3	1.00E+00	7.56E-01	105.84	0.002	6.35E-02	1.10E+04
9	g	SST	0.03	1.0	2.31E-01	1.01E+00	183.96	0.002	8.50E-02	1.10E+04
10	h	SST	0.03	0.3	1.00E+00	7.56E-01	105.84	0.002	6.35E-02	1.10E+04
11	i	DST	0.03	0.0	1.00E+00	0.00E+00	204.12	0.002	0.00E+00	6.10E+03
12	j	DST	0.03	0.31	1.00E+00	8.60E-01	116.55	0.002	7.23E-02	6.10E+03
13	k	DST	0.1	1.0	1.33E-01	1.76E+00	166.32	0.002	4.42E-02	6.10E+03
14	l	DST	0.03	1.0	3.80E-01	1.05E+00	116.046	0.002	8.82E-02	6.10E+03
15	m	DCRT	0.03	0.00	1.00E+00	0.00E+00	3.1122	0.002	0.00E+00	1.10E+04
16	n	DCRT	0.03	0.31	1.00E+00	1.97E-02	2.6712	0.002	1.66E-03	1.10E+04
17	o	DCRT	0.03	0.31	1.00E+00	1.97E-02	2.6712	0.002	1.66E-03	1.10E+04
18	p	DCRT	0.03	0.31	1.00E+00	1.97E-02	2.6712	0.002	1.66E-03	1.10E+04
19	q	SST	0.1	1	1.95E-01	2.54E+00	163.8	0.002	6.39E-02	1.10E+04
20	r	SST	0.1	1	2.21E-01	2.50E+00	142.38	0.002	6.29E-02	1.10E+04
21	s	55 kgal SST	0.03	0.22	1.00E+00	4.32E-02	8.2404	0.002	3.63E-03	1.10E+04
22	t	55 kgal SST	0.03	0.3	1.00E+00	3.60E-02	5.04	0.002	3.02E-03	1.10E+04
23	u	55 kgal SST	0.1	0.158	1.00E+00	9.10E-02	7.2576	0.002	2.29E-03	1.10E+04

Notes:

[a]HEPA Vent modeled as 3.75" (9.5 mm) orifice

[b]Flapper is 50 in. (1.27 m) orifice opening at 1 psid (6.89 kPa)

[c]Vent Pipe on DST Modeled as 9.6 in. (0.24 m) orifice

[d]HEPA Vent for 55 kgal tanks is 3.42" (.087m) orifice. Flapper is 17" orifice.

Table 6-2. Dose Consequences for Solvent Pool Fires.

	A	B	C	D	E	F	G	H	I	J	K	L
1	Case	Tank Type	Solvent Pool Description	Pool Area m²	Bounding Parameters	Ventilation Flow	Vent Description	On Site Solvent Smoke Dose, Sv	Onsite Aqueous Boiloff Dose, Sv	HEPA Rupture Ddose Onsite Sv	Total Onsite Dose Sv	Total Offsite Dose Sv
3	a	SST	puddle	1.0	pressure	passive	hepa[a]	3.04E-05	2.98E-03	3.14E-04	3.33E-03	2.92E-06
4	b	SST	puddle	1.0	vacuum	passive	hepa/flapper[b]	1.58E-05	1.54E-03	3.14E-04	1.87E-03	1.64E-06
5	c	SST	puddle	1.0	radiological	100 cfm (0.047 m[c]/s)	hepa	6.52E-05	6.39E-03	1.52E-02	2.17E-02	1.90E-05
6	d	SST	puddle	1.0	toxicological	100 cfm (0.047 m[c]/s)	hepa	6.52E-05	6.39E-03	1.52E-02	2.17E-02	1.90E-05
7	e	SST	large	210	pressure	passive	hepa	1.80E-05	5.88E-03	3.14E-04	6.21E-03	5.45E-06
8	f	SST	large	210	vacuum	passive	hepa/flapper	2.41E-05	7.86E-03	3.14E-04	8.20E-03	7.19E-06
9	g	SST	large	210	radiological	100 cfm (0.047 m[c]/s)	hepa	3.22E-05	1.05E-02	1.52E-02	2.57E-02	2.26E-05
10	h	SST	large	210	toxicological	passive	hepa/flapper	2.41E-05	7.86E-03	3.14E-04	8.20E-03	7.19E-06
11	i	DST	large	210	pressure	sealed tank	none	0.00E+00	0.00E+00	0.00E+00	0.00E+00	0.00E+00
12	j	DST	large	210	vacuum	passive	flapper	2.74E-05	4.96E-03	8.90E-05	5.08E-03	4.35E-06
13	k	DST	puddle	1.0	radiological	100 cfm (0.047 m[c]/s)	vent pipe[c]	5.59E-05	3.04E-03	8.90E-05	3.18E-03	2.73E-06
14	l	DST	large	210	toxicological	100 cfm (0.047 m[c]/s)	flapper/vent pipe	3.34E-05	6.05E-03	8.90E-05	6.17E-03	5.30E-06
15	m	DCRT	large	34.1	pressure	sealed tank	none	0.00E+00	0.00E+00	0.00E+00	0.00E+00	0.00E+00
16	n	DCRT	large	34.1	vacuum	passive	4" (0.1m) orifice	6.28E-07	2.05E-04	4.40E-04	6.46E-04	5.43E-07
17	o	DCRT	large	34.1	radiological	passive	4" (0.1m) orifice	6.28E-07	2.05E-04	4.40E-04	6.46E-04	5.43E-07
18	p	DCRT	large	34.1	toxicological	passive	4" (0.1m) orifice	6.28E-07	2.05E-04	4.40E-04	6.46E-04	5.43E-07
19	q	SST	entrained	40.0	radiological	100 cfm (0.047 m[c]/s)	hepa[a]	8.07E-05	7.91E-03	1.52E-02	2.32E-02	2.03E-05
20	r	SST	entrained	40.0	toxicological and vacuum	100 cfm (0.047 m[c]/s)	hepa/flapper	7.95E-05	7.79E-03	1.52E-02	2.31E-02	2.02E-05
21	s	55 kgal SST	large	29.2	pressure	passive	hepa[d]	1.37E-06	4.49E-04	3.14E-04	7.64E-04	6.70E-07
22	t	55 kgal SST	large	29.2	toxicological and vacuum	passive	hepa/flapper[d]	1.15E-06	3.74E-04	3.14E-04	6.89E-04	6.05E-07
23	u	55 kgal SST	puddle	1.0	pressure	passive	hepa[d]	2.90E-06	2.84E-04	3.14E-04	6.01E-04	5.27E-07

Notes:

[a]HEPA Vent Modeled as 3.75" (9.5 mm) orifice

[b]Flapper is 50 in. (1.27 m) orifice opening at 1 psid (6.89 kPa)

[c]Vent Pipe on DST Modeled as 9.6 in. (0.24 m) orifice

[d]HEPA Vent for 55 kgal tanks is 3.42" (.087m) orifice. Flapper is 17" orifice.

As noted in Column F_v of Tables 6-1 and 6-2, ventilation flow was set equal to 100 cfm (0.0472m^3/s) for the actively ventilated cases. Recent field data (HNF-SD-WM-CN-117 Rev. 0) indicate that ventilation rates in actively ventilated DSTs and SSTs vary with time and may be higher or lower than 100 cfm. Because leak rate is an important parameter in determining in-tank sedimentation losses, aerosol depletion factors were re-evaluated for higher and lower ventilation flow rates. This was done for Case g of Table 6-2, the fire case that has the highest calculated dose, and in this sense is bounding. This case was re-analyzed for assumed ventilation flow rates ranging from 0 to 1000 cfm. Results of this analysis are summarized in Table 6-3.

Table 6-3. Effect of Ventilation Rate on Aerosol Depletion Factor and Predicted Doses.

Leak Rate		Aerosol Depletion Factor	Calculated Onsite Dose
CFM	m^3/s		
0	0	0.161	2.26(-2)
10	0.004721	0.169	2.29(-2)
20	0.009443	0.176	2.32(-2)
50	0.02361	0.198	2.42(-2)
100	0.04721	0.231	2.57(-2)
200	0.09443	0.287	2.83(-2)
500	0.2361	0.408	3.38(-2)
1000	0.4721	0.532	3.95(-2)

Several aspects of the calculated results shown in Table 6-3 are noteworthy. First, leak rates in the range of 0 to 10 cfm have little impact on the predicted aerosol depletion factor and hence have little impact on predicted onsite dose. The reason is that most airborne mass is retained by in-tank sedimentation, and the quantity which leaks (from a dose standpoint) is small in comparison with dose attributed to HEPA filter rupture. Second, doses predicted for ventilation rates of 50 to 200 cfm (a range that brackets most SSTs) differ from the dose for the baseline flow rate of 100 cfm by (.0283-0.0257)=0.0026 or less. This amounts to 10% at most and does not significantly affect the comparison of predicted dose with the guideline. Third, while predicted dose increases noticeably with ventilation rates higher than 200 cfm, the dose calculated for 1000 cfm, 0.0395 Sv, falls below the guideline of 0.05 Sv applicable to the onsite, unlikely frequency category.

In summary, it is concluded that variations in ventilation flow rate from the nominal value of 100 cfm used to quantify the aerosol depletion factors listed in Tables 6-3 and 6-2 will not significantly affect the comparison of predicted doses with guidelines.

7.0 REFERENCES

Cowley, W.L., J. E. Meacham, J. M. Grigsby, and A. K. Postma, 1996, "*Organic Solvent Topical*," HNF-SD-WM-SARR-036, Rev. 1, DE&S Hanford, Inc. for Fluor Daniel Hanford, Inc., Richland, Washington.

Cowley, W. L. and A. K. Postma, 1996, *"Analysis of Consequences of Postulated Solvent Fires in Hanford Site Waste Tanks,"* WHC-SD-WM-CN-032, Rev. 0, Westinghouse Hanford Company, Richland, Washington.

Epstein, M., and P. G. Ellison, 1987, "Correlations of the Rate of Removal of Coagulating and Depositing Aerosols for Application to Nuclear Reactor Safety Problems," *Nuclear Engineering and Design 107 (1988) 327-344*.

Gelbard, F., Sandia National Laboratories, October 10, 1996, *"MEROS2 Program Files, User No. 222"*, Personal Communication with A.K. Postma, G&P Consulting, Inc., P.O. Box 576, Richland, Washington.

Hilliard, R. K., J. D. McCormack, and A. K. Postma, 1983, *"Results and Code Predictions for Abcove Aerosol Code Validation -- Test AB5"*, HEDL-TME-83-16, Westinghouse Hanford Company, Richland, Washington.

Hilliard, R. K., L. D. Muhlestein, and T. J. Albiol, 1987, *"Final Report of Experimental Results of LACE Test LA2 -- Failure to Isolate Containment"*, LACE TR-007, Westinghouse Hanford Company, Richland, Washington.

Hilliard, R. K., J. D. McCormack, and A. K. Postma. 1989, *"Aerosol Behavior During Sodium Pool Fires in a Large Vessel -- CSTF Tests AB1 and AB2"*, HEDL-TME 79-28, Westinghouse Hanford Company, Richland, Washington.

Jordan, S., and W. Lindner, 1983, "The Behavior of Burning Kerosene, Aerosol Formation and Consequences," in *CSNI Specialist Meeting on Interaction of Fire and Explosion with Ventilation Systems in Nuclear Facilities Proceedings*, April 25-28, 1983, Los Alamos, New Mexico.

McCormack, J. D., R. K. Hilliard, and J. M. Salgado, 1987, "*Final Report of Experimental Results of LACE Test LA4 -- Late Containment Failure with Overlapping Aerosol Injection Periods*" LACE TR-025, Westinghouse Hanford Company, Richland, Washington.

Postma, A. K., D. B. Bechtold, G. L. Borsheim, J. M. Grigsby, R. L. Guthrie, M. Kummerer, M. G. Plys, and D. A. Turner, 1994, *Safety Analysis of Exothermic Reaction Hazards Associated With the Organic Liquid Layer in Tank 241-C-103*, WHC-SD-WM-SARR-001, Rev. 0, Westinghouse Hanford Company, Richland, Washington.

APPENDIX D

FLAMMABILITY OF PUREX SOLVENT VAPOR

This page intentionally left blank.

Formerly Appendix E of
HNF-SD-WM-SARR-036 REV 1A

FLAMMABILITY OF PUREX SOLVENT VAPOR

This page intentionally left blank.

CONTENTS

1.0 INTRODUCTION D-7

2.0 PHENOMENOLOGY OF HAZARD D-7
2.1 HAZARD DESCRIPTION D-7
2.2 KEY PHENOMENA D-7
2.2.1 Vapor-Liquid Equilibria D-8
2.2.2 Mass Transport Rate from Liquid to Headspace Air D-8
2.2.3 Vapor Loss Rate by Ventilation D-8
2.2.4 Aerosol Formation D-8

3.0 METHODOLOGY D-9

4.0 ANALYSIS OF SOLVENT VAPOR FLAMMABILITY D-10
4.1 INTERFACIAL VAPOR CONCENTRATIONS D-10
4.2 TEMPERATURE AT SOLVENT-AIR INTERFACE D-11
4.3 SOLVENT VAPORIZATION RATE D-13
4.4 STEADY-STATE SOLVENT VAPOR CONCENTRATION IN HEADSPACE AIR . . . D-14
4.5 COMPARISON OF SOLVENT VAPOR CONCENTRATIONS TO LOWER FLAMMABILITY LIMITS D-15
4.6 POTENTIAL FOR AEROSOL FORMATION D-19

5.0 REFERENCES D-21

LIST OF FIGURES

4-1 Predicted Percent Low Flammability Limit of Solvent Vapors in a Passively-Ventilated Single-Shell Tank D-18

LIST OF TABLES

4-1 Solvent Volatility Parameters D-11

4-2 LFL Values at 25 °C D-15

4-3 Effect of Pool Area on the Predicted Contribution of Solvent Vapor to Flammability at a Headspace Temperature of 30 °C D-17

4-4 Effect of Ventilation Rate on the Predicted Contribution of Solvent Vapor to Flammability For a 1-m² Pool and a Headspace Air Temperature of 30 °C D-17

This page intentionally left blank.

1.0 INTRODUCTION

The potential contribution of solvent vapors to headspace flammability in waste tanks is analyzed in this section. The airborne concentrations of solvent vapors are predicted from a mass transfer analysis, and the concentrations are then compared with the lower flammability limit (LFL) in order to quantify the percent LFL. Headspace temperature, pool area, solvent composition and ventilation rate are varied parametrically to illustrate how variations in these parameters could affect the contribution of solvent vapors to percent LFL in a given tank.

This Appendix quantifies the potential contribution of PUREX solvent vapors to the flammability of tank headspace air. Equilibrium vapor concentrations in the headspace of passively ventilated SSTs are calculated for solvent compositions, pool areas, and ventilation rates that illustrate the possible contribution of solvent vapors to combustible gas concentrations. Except where specified otherwise, physical properties and constants used for calculations are taken from standard literature and handbooks.

2.0 PHENOMENOLOGY OF HAZARD

2.1 HAZARD DESCRIPTION

The hazard of concern is a deflagration in a fuel-air mixture in the tank headspace. Following is a hypothetical sequence of events that qualitatively describes the hazard.

- Solvent vapors, in addition to other flammable species (H_2, NH_3, etc.) build to a flammable concentration in headspace air.
- A flammable mixture is ignited by an accident.
- A deflagration in headspace air causes tank pressurization and the ensuing release of radioactive airborne material to the environs.

The deflagration cited above is impossible if the total concentration of flammable species falls below the lower flammability limit (LFL). The focus of this appendix is to quantify the possible contribution of solvent vapor to the LFL for a range of tank conditions of interest.

2.2 KEY PHENOMENA

Key phenomena that determine the significance of solvent vapor with respect to headspace flammability are described as follows.

2.2.1 Vapor-Liquid Equilibria

Solvent vapors originate from solvent liquid. The concentration of vapors at a liquid-air interface represents a boundary condition that affects the transport rate and steady-state concentration of vapors in headspace air. The concentration of solvent vapors at the interface is determined by the composition of the liquid and the interfacial temperature.

2.2.2 Mass Transport Rate from Liquid to Headspace Air

The steady-state airborne concentration of solvent vapors in headspace air is affected by the rate at which vapors are transported from the liquid-air interface into the bulk air volume. The rate of mass transfer is primarily dependent on the following factors:

- Geometry of transport path
- Mass transfer rate per unit area of transport path
- Concentration gradient of vapor between the liquid-air interface and bulk headspace air.

2.2.3 Vapor Loss Rate by Ventilation

The steady-state airborne concentration of solvent vapor in headspace air is affected by the rate at which vapors are carried out of the tank by ventilation air. The flow rate of ventilation air and the airborne concentration of vapors govern the vapor loss rate from headspace air. Condensation of vapor on the tank dome would occur if the dew point of vapors were higher than the dome temperature. The small pools considered at the screening level of interest in this appendix yield solvent vapor concentrations predicted to be well below saturation (at headspace temperature), so condensation is discounted as an important vapor loss mechanism in this study.

2.2.4 Aerosol Formation

Condensation of solvent vapors within headspace air could, under restrictive conditions, cause the formation of an aerosol. Aerosols composed of flammable species would contribute to headspace flammability in proportion to the airborne mass concentration; aerosol particles (diameter $\leq 10\ \mu m$) can be expected to behave similarly to vapors of the same material with respect to a deflagration (Zabetakis 1965). Therefore, aerosol mass concentration is the key parameter in assessing the importance of solvent aerosols with respect to headspace flammability.

Aerosols can also be formed by fragmentation of liquid in processes where mechanical energy is dissipated within a liquid. This means for generating aerosols is discounted because no such mechanism is evident in waste tanks considered herein.

3.0 METHODOLOGY

The contribution of solvent vapor and aerosol mass to headspace flammability was evaluated on the basis of the following work steps and key assumptions.

Solvent Liquid Composition. Two solvent compositions were selected to cover a range of possible solvent compositions. The first was a solvent composition (Beary 1970) that typified fresh solvents in terms of volatility. The second, tank 241-C-103 solvent, is of lower volatility because the most volatile components have been stripped by ventilation air during the several decades of storage time that have elapsed since the solvent entered the tank farm. The tank 241-C-103 solvent is probably a reasonable surrogate for solvent currently stored in other tanks because stripping of volatiles will have occurred in all tanks. The fresh solvent composition was included as a bounding case with respect to solvent volatility.

Interfacial Vapor Concentration. The concentration of solvent vapors at the liquid-air interface was computed as a function of liquid temperature. For the fresh solvent, Rauolt's law was used to compute partial pressures. Partial pressures were expressed as mass concentrations on the basis of the ideal gas law and the molecular weight of each species.

Temperature at Solvent-Air Interface. Temperature at the waste-air interface was computed as a function of headspace air temperature. The temperature difference between air and surface was computed as the value required to dissipate decay heat.

Liquid-air interface temperature was equated to computed waste surface temperature. Although liquids submerged beneath the waste surface would be at higher temperatures (because of the temperature gradient in waste), a vapor path to the surface would cool vapors to the surface temperature before they entered the tank air space. Therefore, the appropriate temperature for computing solvent evaporation rates into headspace air appears to be the waste-air interface temperature. Headspace air temperature was assigned values on a parametric basis to cover a range of possible values for waste tanks.

Geometry of Solvent-Air Interface. The rate of mass transfer of vapors from the liquid-air interface into headspace air was modeled on the basis of a pool of liquid, of prescribed surface area, exposed to headspace air. Pool area was assigned a range of values to illustrate its relative importance. Also, a base case value of 1 m^2 (10 ft^2), taken from tank screening criteria (Appendix A), was used to illustrate the possible contribution of solvent vapors to the LFL for tanks that contain a 1-m^2 solvent pool.

Ventilation Rate of Headspace Air. Headspace air ventilation rate was assigned a base case value of 17 m^3/h (10 cfm). The effect of ventilation rate on predicted vapor concentration was illustrated by varying the rate over a range of interest.

Impact of Solvent Vapor Aerosols. The potential contribution of solvent aerosols was examined by comparing tank conditions with conditions necessary to form condensation aerosols. An upper limit to aerosol concentration was projected on the basis of aerosol behavior predicted earlier for tank 241-C-103.

4.0 ANALYSIS OF SOLVENT VAPOR FLAMMABILITY

The potential contribution of solvent vapors to headspace flammability in waste tanks is analyzed in this section. The airborne concentrations of solvent vapors are predicted from a mass transfer analysis, and the concentrations are then compared with the lower flammability limit (LFL) in order to quantify the percent LFL. Headspace temperature, pool area, solvent composition, and ventilation rate are varied parametrically to illustrate how variations in these parameters could affect the contribution of solvent vapors to percent LFL in a given tank.

4.1 INTERFACIAL VAPOR CONCENTRATIONS

The interfacial composition of vapors was computed on the basis of equilibrium between liquid and gas at the interface. For the fresh solvent, a liquid composition was computed assuming a typical 30%/70% mix of tributyl phosphate (TBP) and normal paraffin hydrocarbon (NPH) on a volumetric basis. The composition of the mix, based on an NPH composition given by Beary (1970) is listed in Table 4-1. The vapor pressure of each component was then computed from Raoult's law:

$$P_i = X_i P_{oi} \tag{4-1}$$

where

P_i = partial pressure of component i,

X_i = liquid mole fraction of i,

P_{oi} = vapor pressure of pure component i.

Vapor pressures of the normal paraffins were computed as a function of temperature using a three-parameter vapor pressure equation and the vapor pressure constants presented by Dreisbach (1959). The vapor pressure equation is:

$$\log_{10}P = A - \frac{B}{T + C} \tag{4-2}$$

where

P = vapor pressure, mm Hg,

T = temperature, °C,

A, B, C = constants.

The vapor pressure of TBP was computed using Equation 4-2 with constants recommended by Schulz et al. (1984).

Mass concentrations in gas at the interface were computed from partial pressures assuming ideal gas behavior. Vapor pressure constants and molecular weights of solvent components are summarized in Table 4-1.

Table 4-1. Solvent Volatility Parameters.

Component	Mole Wt.	Mole Fraction		A[3]	B[3]	C[c]
		Fresh[1]	Aged[2]			
Decane, $C_{10}H_{22}$	142.3	0.02881	0	7.33883	1719.86	213.8
Undecane, $C_{11}H_{24}$	156.3	0.2416	0	7.3225	1776.4	206
Dodecane, $C_{12}H_{26}$	273.8	0.2113	0.0564	7.3157	1830	198.3
Tridecane, $C_{13}H_{28}$	184.4	0.1618	0.2231	7.3147	1881.7	190.9
Tetradecane, $C_{14}H_{30}$	198.4	0.09531	0.1225	7.3143	1930.4	183.8
Pentadecane, $C_{15}H_{32}$	212.4	0	0.0131	7.3123	1973.3	176.6
TBP, $C_{12}H_{27}PO_4$	266.3	0.2613	0.5845	8.916	3359	273.16

Note:
1 Composition from Beary (1970)
2 Composition from Pool and Bean (1994)
3 Vapor pressure constants for alkanes from Dreisbach (1959), and from Schulz et al. (1984) for TBP

4.2 TEMPERATURE AT SOLVENT-AIR INTERFACE

Temperature of the solvent-air interface was equated to temperature at the waste-air interface as noted in Section 3. The average temperature at the air-waste interface is higher than bulk headspace air temperature because a gradient in temperature is linked to the transport of decay heat upward from the waste to the above-grade atmosphere. The heat flux in the upward direction can be computed from the mean difference in temperature between tank headspace air and the outside atmosphere (Crowe et al. 1993):

$$\frac{q}{A} = \frac{k_s(T_{vap} - T_{air})}{\Delta Z} \tag{4-3}$$

where

$\frac{q}{A}$ = heat flux, W/m^2,

T_{vap} = annual average bulk vapor temperature, °K,

T_{air} = annual average atmospheric temperature, °K,

k_s = thermal conductivity of soil overburden, W/m °K,

ΔZ = average depth of soil overburden, m.

The formulation expressed in Equation 4-3 neglects the small temperature drops that would exist from vapor to dome and from soil surface to atmospheric air. On the basis of information presented by Crowe et al. (1993), T_{air} is approximately 56.3 °F (286.7 °K), the soil thermal conductivity is approximately 0.1 W/m °K, and the average depth of soil overburden is approximately 4.02 m (13.2 ft).

The bulk vapor temperature in all SSTs varies with time in response to the annual weather cycle. The annual average occurs on approximately July 15 and January 15 (Crowe et al. 1993). Between these dates, tank temperatures experience a sinusoidal variation above and below the average. The maximum and minimum temperatures occur on approximately October 15 and April 15 respectively. The peaks and valleys differ from the yearly average by approximately 5 °F (2.8 °K) (Crowe et al. 1993).

The temperature difference (waste surface-dome surface) that is required to drive the heat flux quantified in Equation 4-3 was computed on the basis of standard textbook heat transfer relationships. The flux is equal to a coefficient multiplied by a temperature difference:

$$\frac{q}{A} = (h_c + h_r)\Delta T \tag{4-4}$$

where

h_c = convection heat transfer coefficient, W/m^2 °K, (heat transfer resistance at two interfaces),

h_r = radiation heat transfer coefficient, W/m^2 °K,

ΔT = temperature difference between waste surface and tank dome, °K.

Numerical evaluations presented by Crowe et al. (1993) indicate that the temperature drop across the headspace is relatively small, amounting to a few degrees Kelvin or less. Because the gas temperature is intermediate between dome and waste surface temperatures, the surface of a solvent pool will be warmer than the gas temperature by a few degrees or less. While this

temperature difference is small, it may not be negligible because vapor pressures are highly sensitive to liquid temperature, as illustrated in Equation 4-2. In this study, the liquid interface temperature is computed by subtracting from the bulk gas temperature, half of the ΔT ($T_{surface} - T_{dome}$) computed from Equation 4-4.

Because the heat flux increases with headspace air temperature (Equation 4-3), the ΔT computed from Equation 4-4 will increase with headspace air temperature. Headspace air temperature was assigned values on a parametric basis to cover a range applicable to SSTs.

4.3 SOLVENT VAPORIZATION RATE

The rate at which solvent vapors entered bulk headspace air was computed on the basis of an interfacial area, a mass transfer coefficient, and a concentration driving force:

$$W = k_c (C_s - C_b) A \tag{4-5}$$

where

W = vaporization rate, g/s,

k_c = mass transfer coefficient, m/s,

c_s = vapor concentration at solvent surface, g/m³,

c_b = vapor concentration in bulk air, g/m³,

A = interfacial area, m².

The mass transfer coefficient at the waste-air interface (k_c in Equation 4-5) may be estimated on the basis of the Chilton-Colburn analogy (Sherwood et al. 1975) using a correlation of natural convection heat transfer coefficients. For naturally convected heat transfer from heated planar surfaces facing upward, the Nusselt number can be correlated with the Grashov and Prandt numbers (McAdams 1954). A simplified form of this correlation that applies for large Grashov numbers (large surfaces) and normal air temperatures and pressures, is presented as the following dimensional equation.

$${}_c h_k = 1.52\ \Delta T^{1/3} \tag{4-6}$$

where

${}_c h_k$ = convective heat transfer coefficient, W/m² °K.

ΔT = temperature difference between surface and bulk air, °K.

A numerical value of ${}_c h_k$ can be computed from Equation 4-6 using a temperature difference, ΔT, evaluated as a function of headspace air temperature.

The mass transfer coefficient, k_c, may be computed from the heat transfer coefficient, ${}_ch_k$, on the basis of the Chilton-Colburn analogy (Sherwood et al. 1975):

$$k_c = \frac{{}_ch_k \; D_{AB}}{k} \left(\frac{Sc}{Pr}\right)^{1/3} \tag{4-7}$$

where

k_c = mass transfer coefficient, m/s,

${}_ch_k$ = heat transfer coefficient, W/m² °K,

D_{AB} = diffusivity of solvent vapor, m²/s,

k=thermal conductivity of gas, W/m °K,

Sc = Schmidt no., dimensionless,

Pr = Prandtl no., dimensionless.

Diffusivity of solvent vapor can be estimated from handbook correlations (Perry 1950), as can other gas properties needed to evaluate the parameters of Equation 4-7.
Values of W (Equation 4-5) were computed for each of the component species listed in Table 4-1.

Interfacial area, A, was assigned a value of 1 m² (10.8 ft^2) as a base case. This area is a value used in the screening analysis (Appendix A) and corresponds to an open pool area for which postulated solvent fires do not pose a threat to tank structural integrity. The impact of solvent pool area on the concentration of solvent vapors was illustrated by means of sensitivity calculations.

4.4 STEADY-STATE SOLVENT VAPOR CONCENTRATION IN HEADSPACE AIR

The steady-state concentration of solvent vapors in headspace air was computed by equating inflow rate (Equation 4-5) to outflow rate. Outflow rate was calculated by multiplying bulk vapor concentration by ventilation flow rate. On this basis, the steady-state concentration of solvent vapors is:

$$C_b = C_s \frac{k_c \; A}{k_c \; A + Q} \tag{4-8}$$

where

C_b = concentration in bulk air phase, g/m³,

C_s = concentration at liquid-gas interface, g/m³,

k_c = mass transfer coefficient, m/s,

A = area of liquid-gas interface, m²,

Q = flow rate of ventilation air, m³/s.

As indicated by Equation 4-8, C_b, the concentration of vapors in headspace air tends to its maximum value, C_s, as Q tends toward small values. A conservative (upper limit) estimate of C_s can be made by assigning Q a minimum value. A minimum value may be estimated on the basis of natural breathing: based on a pressure variation of 0.45 percent per day (Crippen 1993) and a headspace air volume of 2,266 m³ (80,000 ft³), atmospheric pressure fluctuations induce a flow of 0.43 m³/h (0.25 cfm). A base case value of 10 cfm (17 m³/h) was assigned on the basis of available data on headspace ventilation rates (see Section 6.3.5 of Appendix A).

4.5 COMPARISON OF SOLVENT VAPOR CONCENTRATIONS TO LOWER FLAMMABILITY LIMITS

The contribution of solvent vapors to headspace flammability can be quantified by dividing concentrations by the LFL. The LFL decreases with temperatures as indicated by Equation 4-9 (Zabetakis 1965):

$$L_t = L_{25}\left[1-7.85\ E\text{-}4\ (T - 25)\right] \qquad (4\text{-}9)$$

where

L_t = LFL at temperature, T, g/m³,

L_{25} = LFL at 25 °C, g/m³,

T = temperature, °C.

Values of the LFL, expressed in g/m³, are listed in Table 4-2 for solvent vapor species.

Table 4-2. LFL Values at 25 °C. (2 sheets)

Vapor Specie	LFL @ 25 °C, g/m³
n - decane	48[1]
n - undecane	48[1]
n - dodecane	46[1]
n - tridecane	46[1]
n - tetradecane	44[1]

Table 4-2. LFL Values at 25 °C. (2 sheets)

Vapor Specie	LFL @ 25 °C, g/m³
n - pentadecane	44[1]
TBP	65

Note: [1] Zabetakis (1965)

As noted, LFL values for the paraffin hydrocarbons were taken from Zabetakis (1965). The LFL for TBP was estimated on the basis of vapor concentration at an assumed flashpoint of 135 °C. This flashpoint temperature falls at the lower end of measured values (Appendix A of Postma et al. 1994). The LFL based on this flashpoint is expected to be a conservatively small value.

The fractional approach to the LFL for a mixture containing a number of flammable gas species can be estimated by summing the fractions for each specie (Kuchta 1985):

$$\text{Fraction LFL} = \sum_{n=1}^{n=n} \frac{C_i}{LFL_i} \qquad (4\text{-}10)$$

where

Fraction LFL = fractional approach to LFL for mixture,

C_i = concentration of specie i,

LFL_i = LFL for specie i,

n = number of flammable species in mixture.

Equation 4-10, a form of LeChatliers law (Kuchta 1985), was used to calculate the contribution of solvent vapors to the LFL. Steady-state vapor concentrations in bulk air (Equation 4-8) were divided by L_t values computed from Equation 4-9, which used Table 4-2 LFL values at 25 °C, adjusted for headspace air temperature.

The contribution of solvent vapors to headspace flammability is quantified in Figure 4-1 for fresh solvent and for tank 241-C-103 solvent. Base case assumption of a pool area of 1 m² and a purge air flow of 17.0 m³/h apply to this figure.

The curves of Figure 4-1 indicate that 25 percent of the LFL would be reached at headspace air temperatures of ~97 °C (207 °F) for fresh solvent and 125 °C (257 °F) for tank 241-C-103 solvent.

The impact of pool surface area and ventilation air flow rate on solvent vapor concentration was evaluated by repeating the prediction with different

values of these two parameters. The effect of assumed pool area is illustrated in Table 4-3 where solvent vapor concentration, expressed as a percent of LFL, is shown as a function of pool area.

Table 4-3. Effect of Pool Area on the Predicted Contribution of Solvent Vapor to Flammability at a Headspace Temperature of 30 °C.

Pool Area m^2	Predicted Percent of the LFL at Headspace Air Temperature of 30 °C	
	Fresh Solvent	C-103 Solvent
411	4.62	0.67
20	2.94	0.42
10	2.13	0.30
1	0.36	0.05
0.1	0.04	0.005

The data in Table 4-3 indicate that a 1-m^2 pool is predicted to generate vapor concentrations that are 8 percent as high as a pool covering the whole tank cross-section, 411 m^2 (4,424 m^2). For the 411-m^2 pool area, headspace air is predicted to be within three percent of the saturated, i.e. upper limit, concentration. The saturated concentrations for fresh and tank 241-C-103 solvents are 4.76 percent LFL and 0.69 percent LFL, respectively, as displayed in Table 4-4 where percent LFL is shown for a hypothetical leak-tight tank (ventilation rate = 0).

The impact of ventilation air flow rate on solvent vapor concentration is illustrated by the data in Table 4-4.

Table 4-4. Effect of Ventilation Rate on the Predicted Contribution of Solvent Vapor to Flammability For a 1-m^2 Pool and a Headspace Air Temperature of 30 °C.

Ventilation Rate m^3/h	Predicted Percent of the LFL At Headspace Air Temperature of 30 °C	
	Fresh Solvent	Tank 241-C-103 Solvent
0	4.76	0.69
0.43 (atm. fluctuations alone)	3.64	0.52
1.84 (atm. fluctuations + 50 ft^3/h)	2.04	0.29
17.0 (10 ft^3/min)	0.36	0.049
170.0 (100 ft^3/min)	0.038	0.0046

Figure 4-1. Predicted Percent Low Flammability Limit of Solvent Vapors in a Passively-Ventilated Single-Shell Tank.

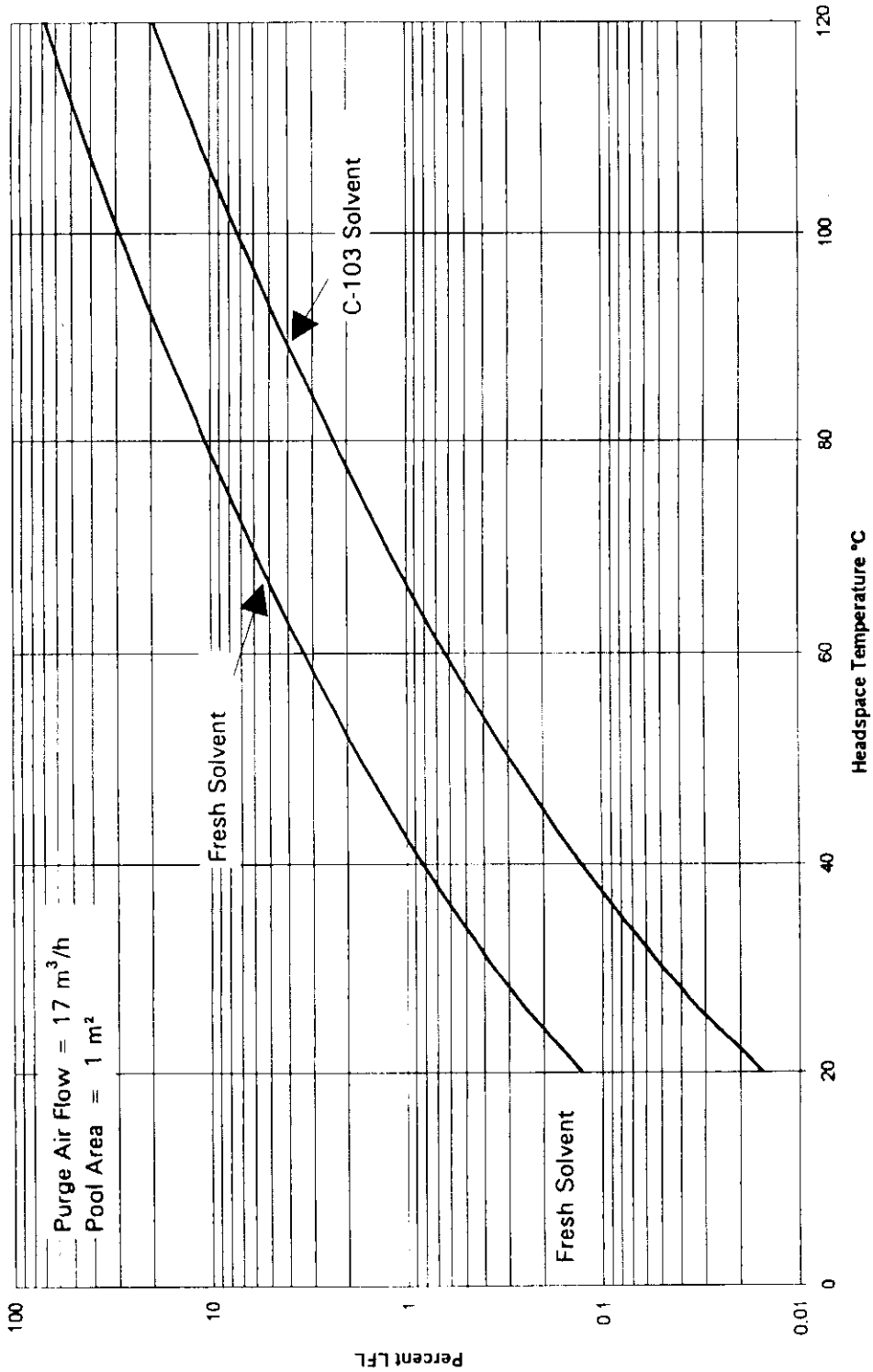

As indicated by the data in Table 4-4, headspace solvent vapor concentrations are predicted to decrease with increasing ventilation air flow rate. The perfectly sealed case (0 m^3/h) represents the saturated condition; saturation is predicted in sealed tanks for pools of any size as an equilibrium level. The 0-m^3/h case is an upper bound on solvent vapor concentration. Ventilation by atmospheric pressure fluctuations alone is predicted to lower equilibrium solvent vapor concentration to 76 percent (3.64 * 100/4.76) of the saturated level. When a purge air flow rate of 1.4 m^3/h (50 ft^3/h) is added, the equilibrium concentration is predicted to fall to 43 percent (2.04 * 100/4.76) of the saturation value. The base case has a ventilation flow rate of 17 m^3/h (10 ft^3/m). As indicated, a ventilation flow of 17 m^3/h (10 ft/m) is predicted to lower the equilibrium vapor concentration to 7.5 percent (0.36 * 100/4.76) of the saturated level. This level, 7.5 percent, applies for a tank containing a 1-m^2 pool; for larger pools, solvent vapor concentration would be higher. A sensitivity case at 100 cfm (170 m^3/h is also shown in Table 4-4. Predicted LFL varies approximately inversely with ventilation flow rate, for rates higher than a 10 cfm (17 m^3/h).

The temperature at which 100 percent of the LFL is reached corresponds to the flashpoint of a liquid. For the zero ventilation flow case, the methodology used to calculate the data displayed in Figure 4-1 and Tables 4-3 and 4-4 yields 100 percent of LFL at temperatures of 81 °C and 109 °C (178 °F and 228 °F), respectively, for the fresh and tank 241-C-103 solvents, respectively. These predicted flashpoints agree reasonably with measured flashpoints of 99 °C and 118 °C (210 °F and 244 °F) (Pool and Bean 1994) for a freshly prepared solvent and for solvent removed from tank 241-C-103. The predicted flashpoints are lower than measured, indicating that the methodology used in this appendix yields conservative predictions; that is, it tends to overpredict interfacial solvent vapor concentrations in the neighborhood of the flashpoint.

4.6 POTENTIAL FOR AEROSOL FORMATION

The potential for condensation of solvent vapor to form liquid aerosol has been evaluated for tank 241-C-103 (Postma et al. 1994). The concern is that thermal gradients in headspace air could produce condensation aerosols on a continuing basis, causing aerosol mass concentration to reach a value high enough to significantly increase fuel concentration as compared to saturated vapor alone. Based on the tank 241-C-103 study, the contribution of aerosols to flammability can be discounted for almost all tanks. Reasons for discounting aerosols as a flammability hazard are explained as follows.

Vapor Saturation Requirement. Aerosols can form and persist only if the atmosphere is slightly supersaturated with condensable vapor, as compared to a planar surface at the same temperature. For any atmosphere in which vapors are subsaturated, aerosol formation is impossible. This condition applies to most, if not all, waste tanks.

Hypothetical Peak Aerosol Concentration. A theoretical analysis of aerosol buildup in tank C-103 (Postma et al. 1994) predicted a maximum aerosol concentration of 0.043 g/m^3, or about 0.1 percent of the LFL. This

concentration is a steady-state level based on a projected generation rate of 1.2 mg/s. Sensitivity calculations based on generation rates of 12 mg/s and 0.12 mg/s yielded peak aerosol concentrations of 0.22 g/m^3 and 0.008 g/m^3 respectively. It was concluded that condensation aerosols could not contribute significantly to the LFL for tank 241-C-103.

In summary, aerosols formed by the condensation of solvent vapors can be totally discounted for tanks in which headspace air is subsaturated with vapor. For tank 241-C-103 predicted peak aerosol concentrations (under hypothetical sealed tank conditions) were shown to be small compared to 1 percent of the LFL. This tank 241-C-103 result is expected to bound the aerosol concentration for any tank that has a temperature at or below the temperature of tank 241-C-103. Therefore, the aerosol issue remains open only for tanks whose headspace is saturated with solvent vapors and whose temperature is higher than that of tank 241-C-103 (~40 °C [104 °F]).

5.0 REFERENCES

Beary, M. M., 1970, *Solvent Improvement Resulting from the Use of NPH in the Hanford PUREX Plant*, ARH-SA-73, Atlantic Richfield Hanford Company, Richland, Washington.

Crippen, M. D., 1993, *Barometric Pressure Variations*, WHC-EP-0651, Westinghouse Hanford Company, Richland, Washington.

Crowe, R. D., M. Kummerer, and A. K. Postma, 1993, *Estimation of Heat Load in Waste Tanks Using Average Vapor Space Temperatures*, WHC-EP-0709, Westinghouse Hanford Company, Richland, Washington.

Dreisbach, R. R., 1959, *Physical Properties of Chemical Compounds*, (pp 161-167), No. 22, *Advances in Chemistry Series*, American Chemical Society, Washington, D.C.

Kuchta, J. M., 1985, "Investigation of Fire and Explosion Accidents in the Chemical, Mining, and Fuel-Related Industries - A Manual," Bulletin 680, Bureau of Mines, U.S. Department of Interior, Washington, D.C.

McAdams, W. H., 1954, *Heat Transmission*, McGraw-Hill, Inc., New York.

Perry, R. H., 1950, "Chemical Engineers' Handbook", McGraw-Hill, Inc., New York, New York.

Pool, K. H., and R. M. Bean, 1994, *Waste Tank Safety Project: Analysis of Liquid Samples from Hanford Waste Tank 241-C-1-3*, PNL-9403, Pacific Northwest Laboratory, Richland, Washington.

Postma, A. K., D. B. Bechtold, G. L. Borsheim, J. M. Grigsby, R. L. Guthrie, M. Kummerer, M. G. Plys, and D. A. Turner, 1994, *Safety Analysis of Exothermic Reaction Hazards Associated With the Organic Liquid Layer in Tank 241-C-103*, WHC-SD-WM-SARR-001, Rev. 0, Westinghouse Hanford Company, Richland, Washington.

Schulz, W. W., J. D. Navratil, and A. E. Talbot, 1984, *Science and Technology of Tributyl Phosphate, Volume I Synthesis, Properties, Reactions and Analysis*, CRC Press, Inc., Boca Raton, Florida, pp. 27—28.

Sherwood T. K., R. L. Pigford, and C. R. Wilke, 1975, *Mass Transfer*, McGraw-Hill, Inc., New York, New York.

Zabetakis, M.G., 1965, *Flammability Characteristics of Combustible Gases and Vapors*, Bulletin 627, Washington, U.S. Department of the Interior, Bureau of Mines.

This page intentionally left blank.

APPENDIX E

SUMMARY OF LABORATORY SCOPING TESTS RELATED TO ORGANIC SOLVENTS COMBUSTION BY NITRATE OXIDATION AND ORGANIC SOLVENT IGNITABILITY

This page intentionally left blank.

HNF-4240 Rev. 1

Formerly Appendix C of
HNF-SD-WM-SARR-036 REV 1A

Summary of Laboratory Scoping Tests Related to Organic Solvents Combustion by Nitrate Oxidation and Organic Solvent Ignitability

Submitted To:

Westinghouse Hanford Company
Richland, Washington

Prepared By:

Fauske & Associates, Inc.
16W070 West 83rd Street
Burr Ridge, Illinois 60521

June, 1995

This page intentionally left blank.

TABLE OF CONTENTS

1.0 INTRODUCTION AND SUMMARY E-7

2.0 THE POTENTIAL FOR ORGANIC SOLVENTS OR THEIR SALTS AS FUEL FOR CONDENSED PHASE PROPAGATING REACTIONS E-9

2.1 RSST Tests E-9

2.2 Tube Propagation Tests E-17

3.0 THE POTENTIAL FOR ORGANIC SOLVENTS OR THEIR SALTS AS SUPPLEMENTAL FUEL TO COMPLEXANT-NITRATE PROPAGATING REACTIONS E-25

4.0 THE POTENTIAL FOR SURFACE VAPOR COMBUSTION TRANSITION TO CONDENSED-PHASE COMBUSTION E-27

5.0 ORGANIC SOLVENT IGNITABILITY TESTS E-29

LIST OF FIGURES

Figure 2-1 Reactive System Screening Tool (RSST) containment and test cell E-10

Figure 2-2 Transition from a homogenous runaway reaction to a self-propagating reaction occurring at about 300°C E-11

Figure 2-3 Self-heat rate data with 10 wt.% TOC TBP/$NaNO_3$ E-12

Figure 2-4 Self-heat rate data with 28 wt.% TOC TBP/$NaNO_3$ E-13

Figure 2-5 Self-heat rate data with 5 wt.% TOC DBP/$NaNO_3$ illustrating repeatability E-14

Figure 2-6 Self-heat rate data with 10 wt.% TOC DBP/$NaNO_3$ E-15

Figure 2-7 Self-heat rate data with 22.6 wt.% TOC 30% TBP - 70% NPH/104-BY salt case simulant E-16

Figure 2-8 Illustration of tube propagation test cell E-18

Figure 2-9 Illustration of sustained combustion with 8 wt.% TOC NaCitrate/$NaNO_3$ mixtures E-19

Figure 2-10 Illustration of absence of sustained combustion with 11.3 wt.% TOC 30% TBP - 70% NPH/$NaNO_3$ mixture E-20

Figure 2-11 Illustration of absence of condensed-phase combustion with 8% TOC AℓDBP/$NaNO_3$ mixture E-21

Figure 2-12 Repeat test; illustration of absence of condensed-phase combustion with 8% TOC AℓDBP/$NaNO_3$ mixture E-22

Figure 2-13 Illustration of temperature data with 5 wt.% TOC NaButyrate/$NaNO_3$ mixture. Igniter on-time ~ 200 s E-23

Figure 2-14 Illustration of temperature data with 6 wt.% TOC NaButyrate/$NaNO_3$ mixture E-24

Figure 3-1 Illustration of absence of condensed-phase combustion with 6 wt.% TOC (3% NaCitrate + 3% AℓDBP)/$NaNO_3$ mixture . E-26

Figure 5-1 Ignition potential and effect of volatile organic E-30

Figure 5-2 Ignition potential and the effect of free water E-31

1.0 INTRODUCTION AND SUMMARY

This report summarizes laboratory scoping tests completed to date with various organic solvents including dibutyl phosphate (DBP), tributyl phosphate (TBP), 30% TBP - 70% NPH (11.6% dodecane, 23.4% tridecane and 35% tetradecane) and the salt AℓDBP to address the following questions

- can these materials when mixed together with an oxidizer like $NaNO_3$ support condensed-phase propagating reactions given an adequate ignition source,
- can these materials make an otherwise non-propagating mixture (too little organic complexant fuel like NaAcetate, NaHEDTA etc.) into a reactive propagating mixture given an adequate ignition source,
- can an initial organic solvent pool surface fire or wicked surface fire transition into a condensed-regime combustion phase given adequate organic complexant fuel like NaAcetate, NaHEDTA etc., and
- are credible ignition sources available to ignite organic solvent pools or organic solvent permeated salt cakes etc.

The observations made to date can be summarized as follows

- The above organic solvents as well as the AℓDBP salt do not exhibit condensed-phase combustion when mixed with $NaNO_3$. The mixtures tested cover theoretical chemical energy releases well in excess of that required for sustained condensed-phase combustion with non-volatile organic complexants like Na Acetate and Na HEDTA. [See FAI/94-103.]
- Adding an organic solvent or a salt like AℓDBP do not make an otherwise non-reactive waste (too little non-volatile organic complexant) into a combustible condition.
- Surface vapor combustion (an initial pool fire or wicked fire) can only transition into condensed-phase combustion if the non-volatile complexant TOC level for condensed-phase burning is satisfied. (Note that surface vapor combustion with less than saturated soaked salt cake condition appears to be the requirement for transition to condensed-phase combustion, i.e., if an organic solvent pool still exists following loss of head space oxygen, further combustion will not occur even if the organic complexant TOC level for condensed-phase combustion is satisfied.)
- Subjecting 2.5 inch diameter dodecane puddles or 2.5 inch dodecane saturated saltcakes to 1/16, 3/32 and 3/16 inch steel

particles heated to about 1300°C, resulting in energy levels of 10, 35 and 270 J did not result in sustained ignition. Applying the 138 J match (energy release time of about 3 ms) to the same conditions also resulted in no sustained ignition.

Therefore in terms of waste tank safety assessment, the organic solvents and their degradation products represent a potential combustion hazard only with the head space air, given the presence of a sufficient ignition source. The above ignition sources would appear to envelope all credible sources (in-tank instrumentation, welding and grinding, hot filament and shorting electrical wires) with the exception of lightning.

2.0 THE POTENTIAL FOR ORGANIC SOLVENTS OR THEIR SALTS AS FUEL FOR CONDENSED PHASE PROPAGATING REACTIONS

In contrast to the non-volatile organic complexants (FAI/94-103) condensed-phase propagating reactions were not observed with any of the non-salt volatile organic compounds like tributyl phosphate (TBP), dibutyl phosphate (DBP), 30% TBP/70% NPH, or their salts like AℓDBP when mixed with nitrate oxidizer and subjected to a large ignition source. This behavior can be related to early decomposition of these compounds (150-200°C temperature range) with or without the presence of nitrate oxidizer. Both RSST and dedicated tube propagation tests have been performed and are summarized below.

2.1 RSST Tests

The Reactive System Screening Tool (RSST) is being used to measure the ignition temperature. The RSST (Figure 2-1) consists of a spherical glass reaction vessel, its surrounding jacket heater and insulation, thermocouple (imbedded in sample) and a pressure transducer, a stainless steel containment vessel, and, not shown, a magnetic stirrer base, a control box containing the heater power supply, temperature/pressure amplifiers, and a data acquisition and control panel. The sample cell volume is 10 mℓ and the containment volume is 350 mℓ. A key feature of the apparatus is its low effective heat capacity relative to that of the sample whose value, expressed as the capacity ratio, is ~ 1.04 (i.e., quite adiabatic).

Typically, a sample (~ 10 gm) is heated at a constant rate of about 1°C per minute and the sample self-heat rate dT/dt is found as a function of sample temperature under essentially zero heat loss condition. Figure 2-2 is an example of reaction kinetics for an initially solid waste surrogate of sodium acetate and sodium nitrate with a sodium acetate concentration of 24 wt% (or 7 wt% total organic carbon (TOC) content). Significant exothermic activity is noted at about 200°C which leads to a runaway reaction exhibiting an Arrhenius type dependence on temperature up to about 300°C; at this temperature a dramatic step change in the rate of temperature rise is observed. This is interpreted as a threshold for rapid wave-like reaction propagation and the temperature of 300°C is referred to as the ignition temperature.

The transitions to propagating reactions were not observed when the non-volatile organic complexants were replaced with various organic solvents. For the TBP/$NaNO_3$ and DBP/$NaNO_3$ mixtures significant exothermic activity is noted about 150°C which leads to a runaway reaction exhibiting an Arrhenius type dependence on temperature (see Figures 2-3 to 2-6). An example of good repeatability is illustrated in Figure 2-5. The effect of increased volatility is illustrated by the data in Figure 2-7. The previously noted exothermic activity at about 150°C is tempered by the increased volatility of 30% TBP - 70% NPH mixture and is effectively delayed until the temperature reaches about 250°C. The 70% NPH consisted of 11.6% dodecane (B.P. ≈ 216°C), 23.4% tridecane (B.P. ≈ 235.4°C) and 35% tetradecane (B.P. ≈ 253.5°C).

Figure 2-1 Reactive System Screening Tool (RSST) containment and test cell.

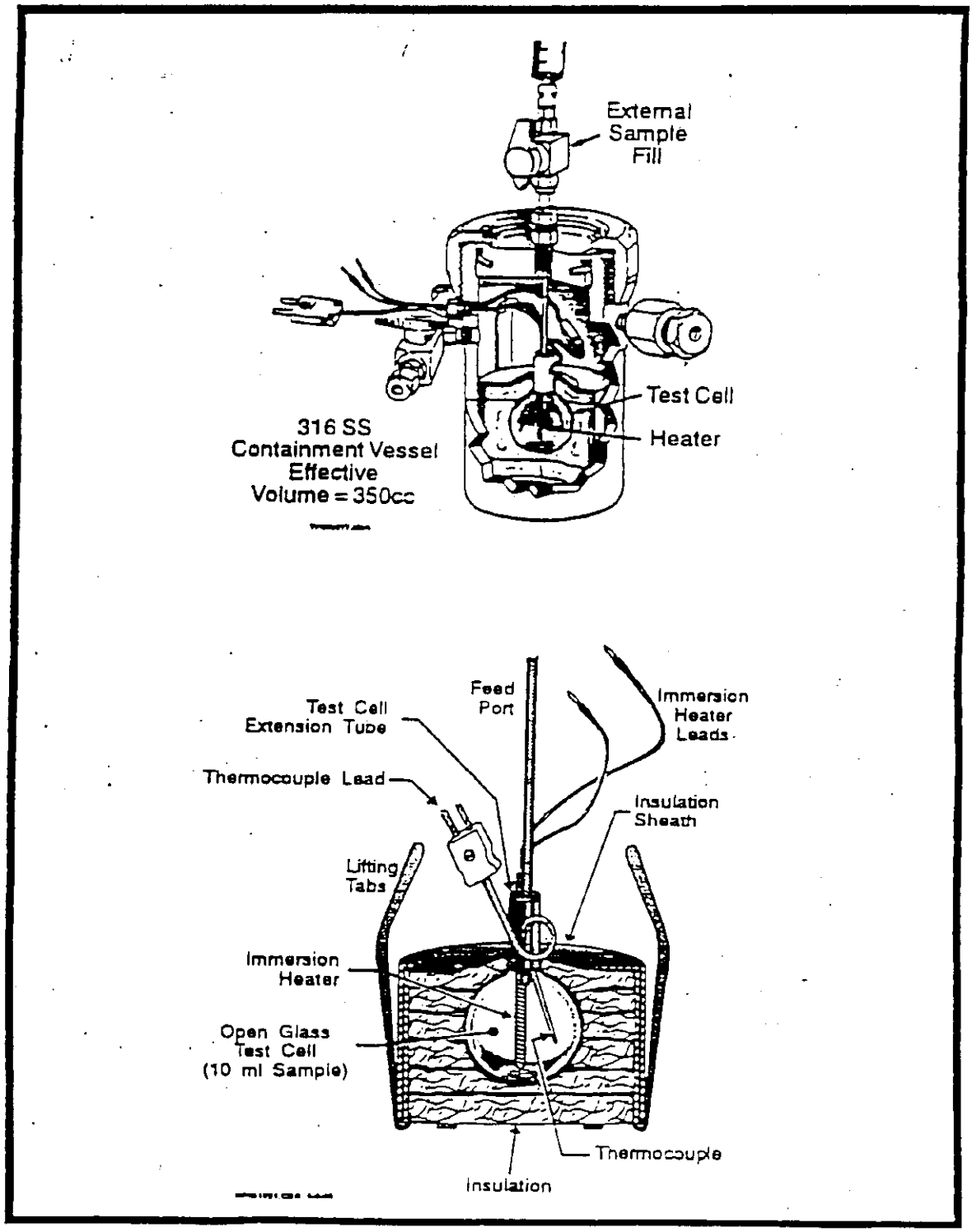

Figure 2-2 Transition from a homogeneous runaway reaction to a self-propagating reaction occurring at about 300°C.

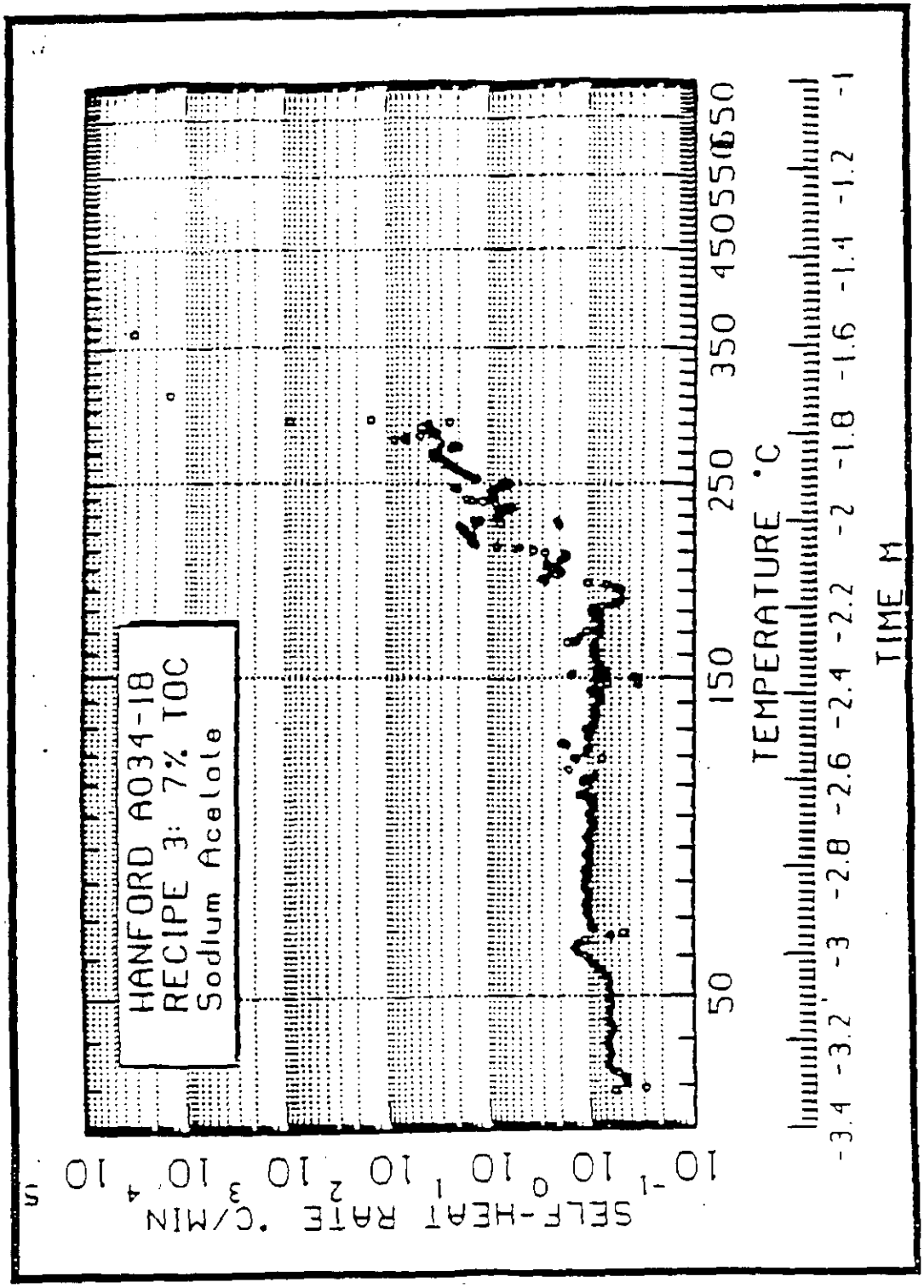

Figure 2-3 Self-heat rate data with 10 wt.% TOC TBP/$NaNO_3$.

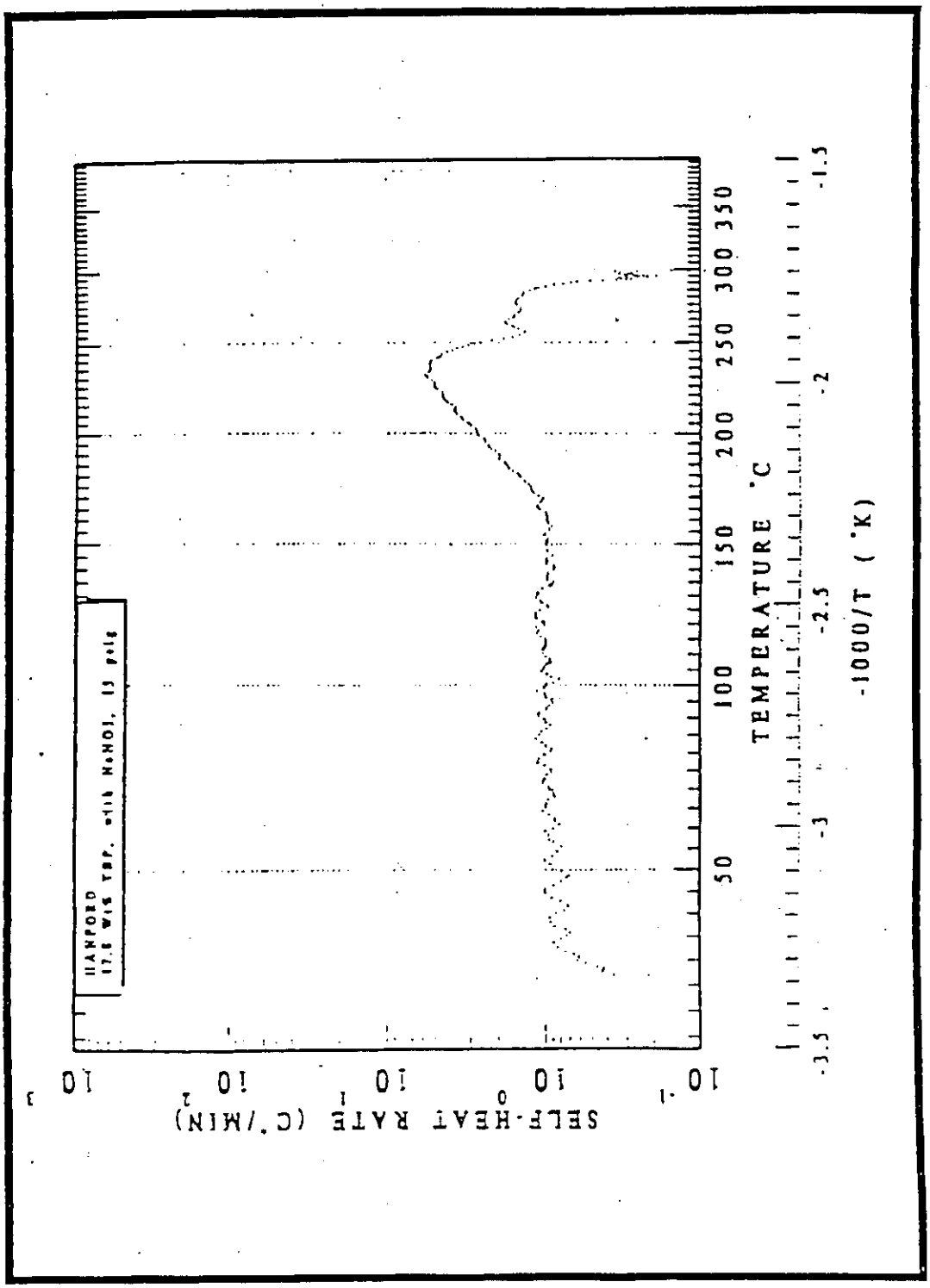

Figure 2-4 Self-heat rate data with 28 wt.% TOC TBP/$NaNO_3$.

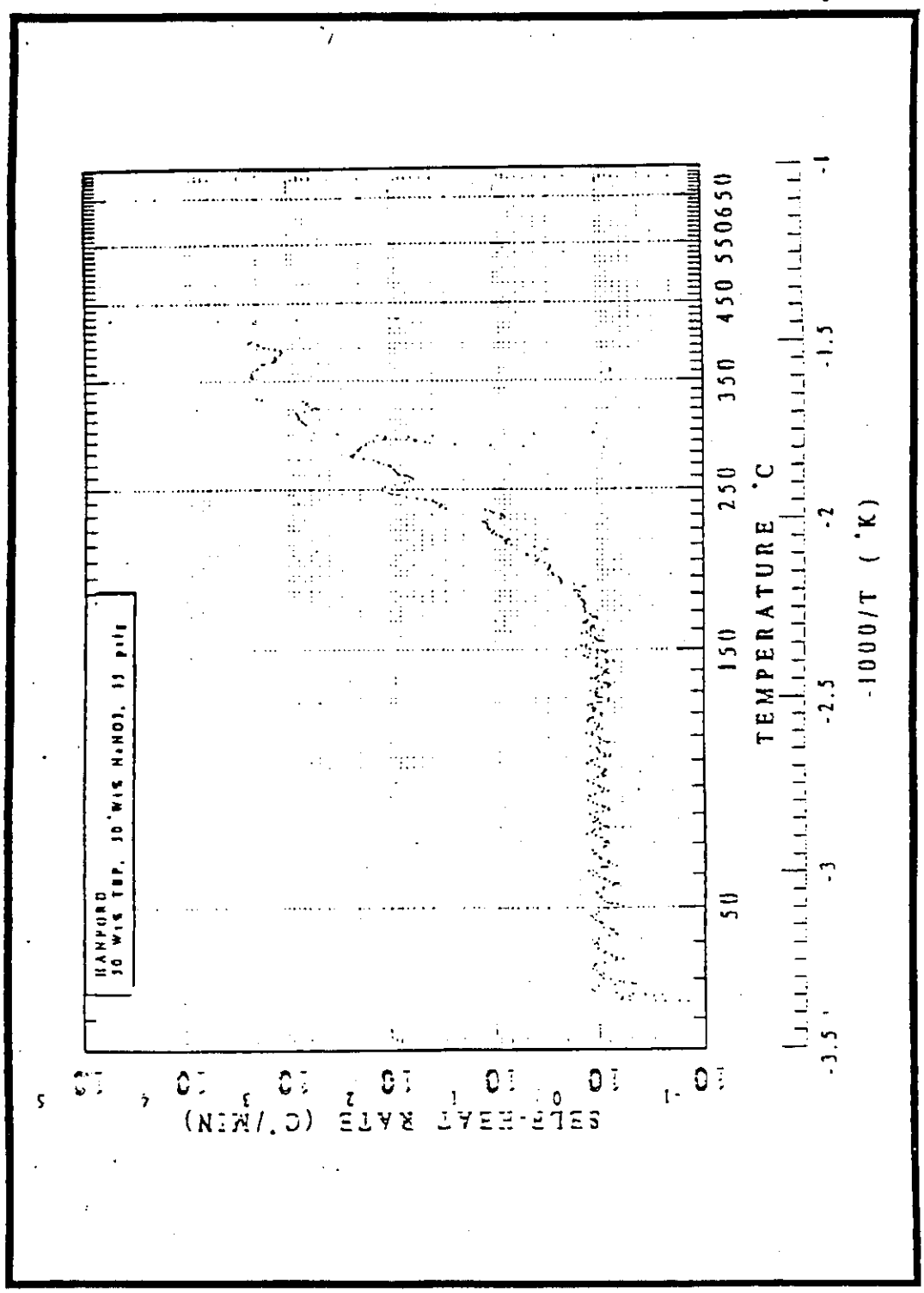

Figure 2-5 Self-heat rate data with 5 wt.% TOC DBP/$NaNO_3$ illustrating repeatability.

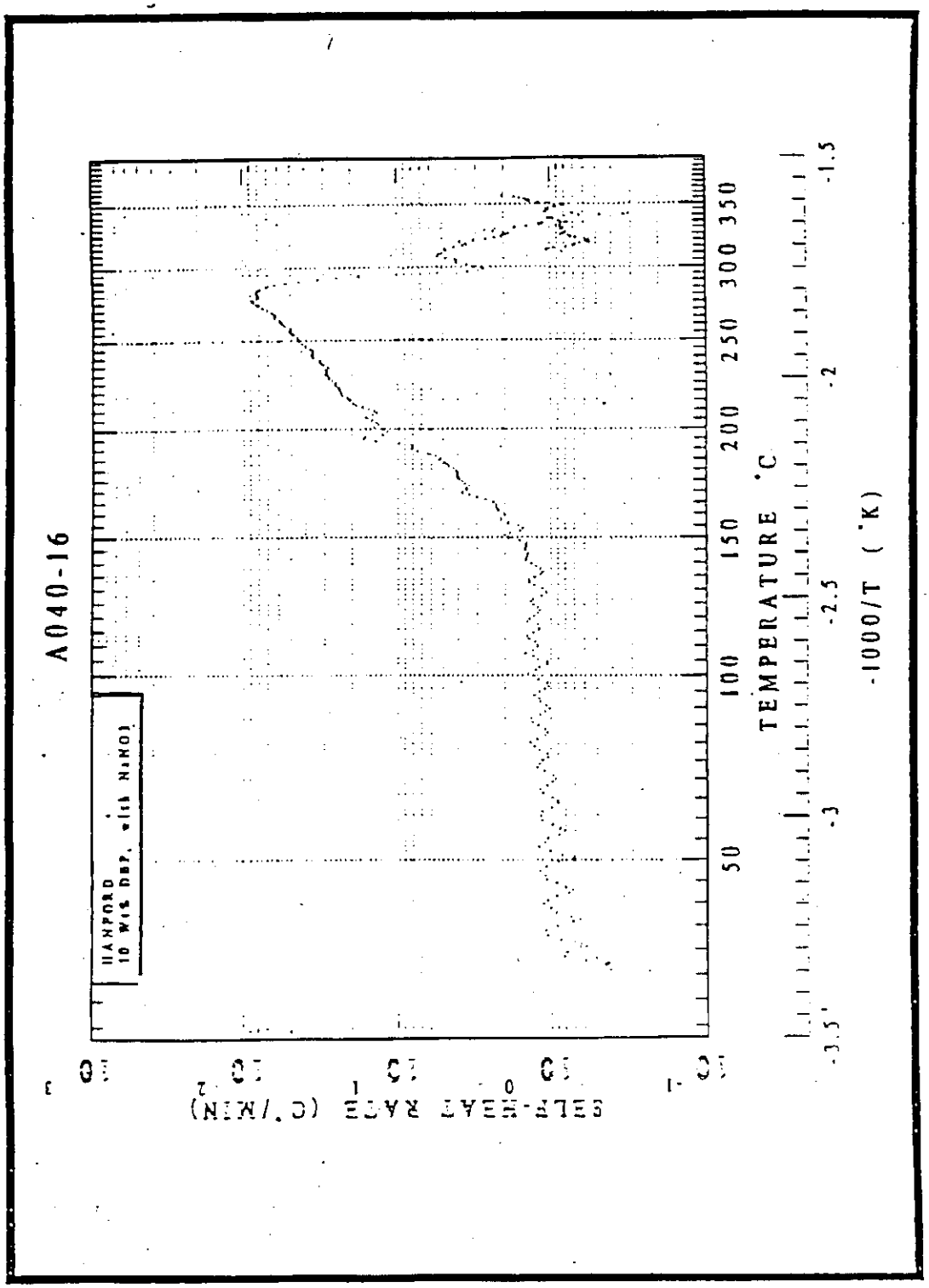

Figure 2-6 Self-heat rate data with 10 wt.% TOC DBP/$NaNO_3$.

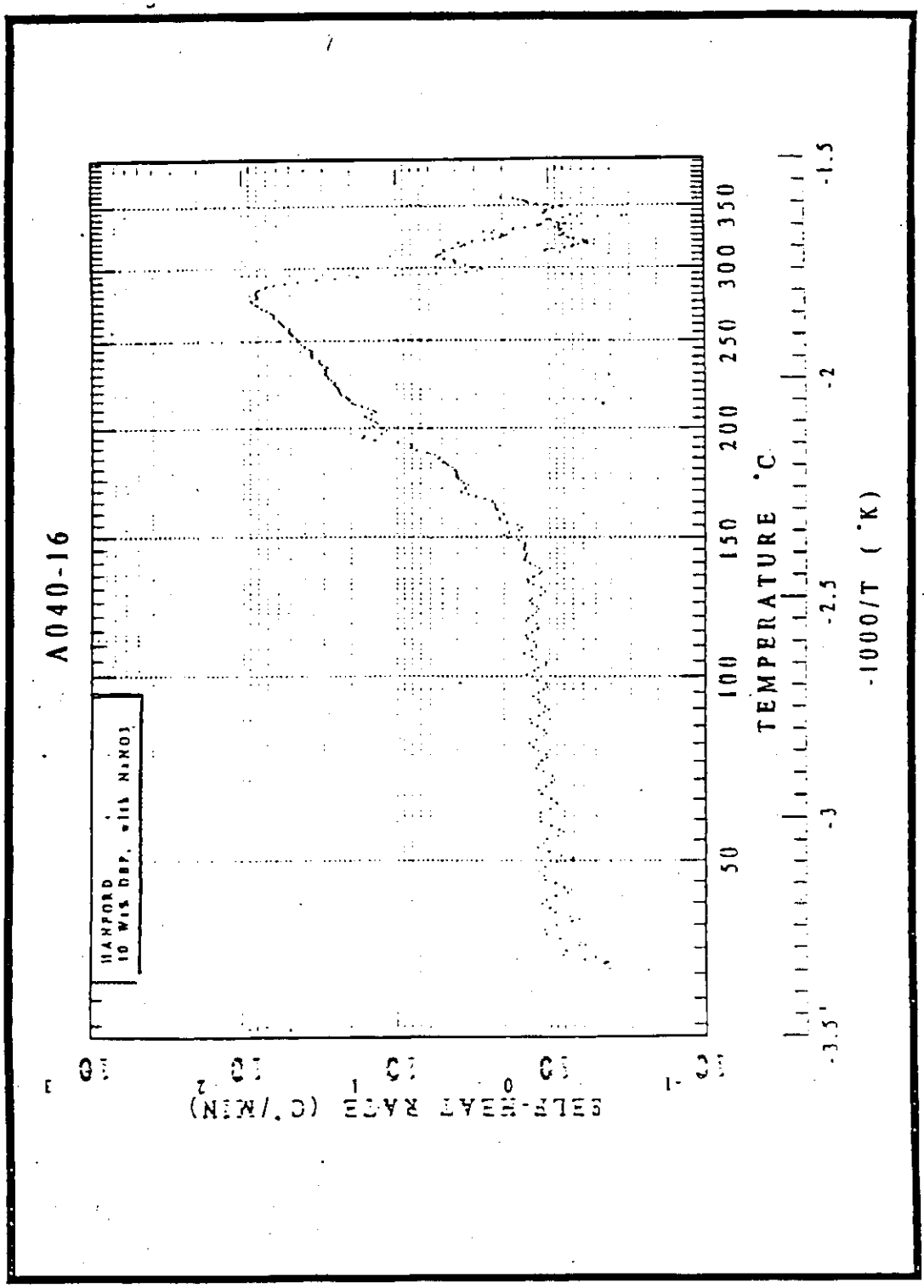

Figure 2-7 Self-heat rate data with 22.6 wt.% TOC 30% TBP - 70% NPH/104-BY salt case simulant.

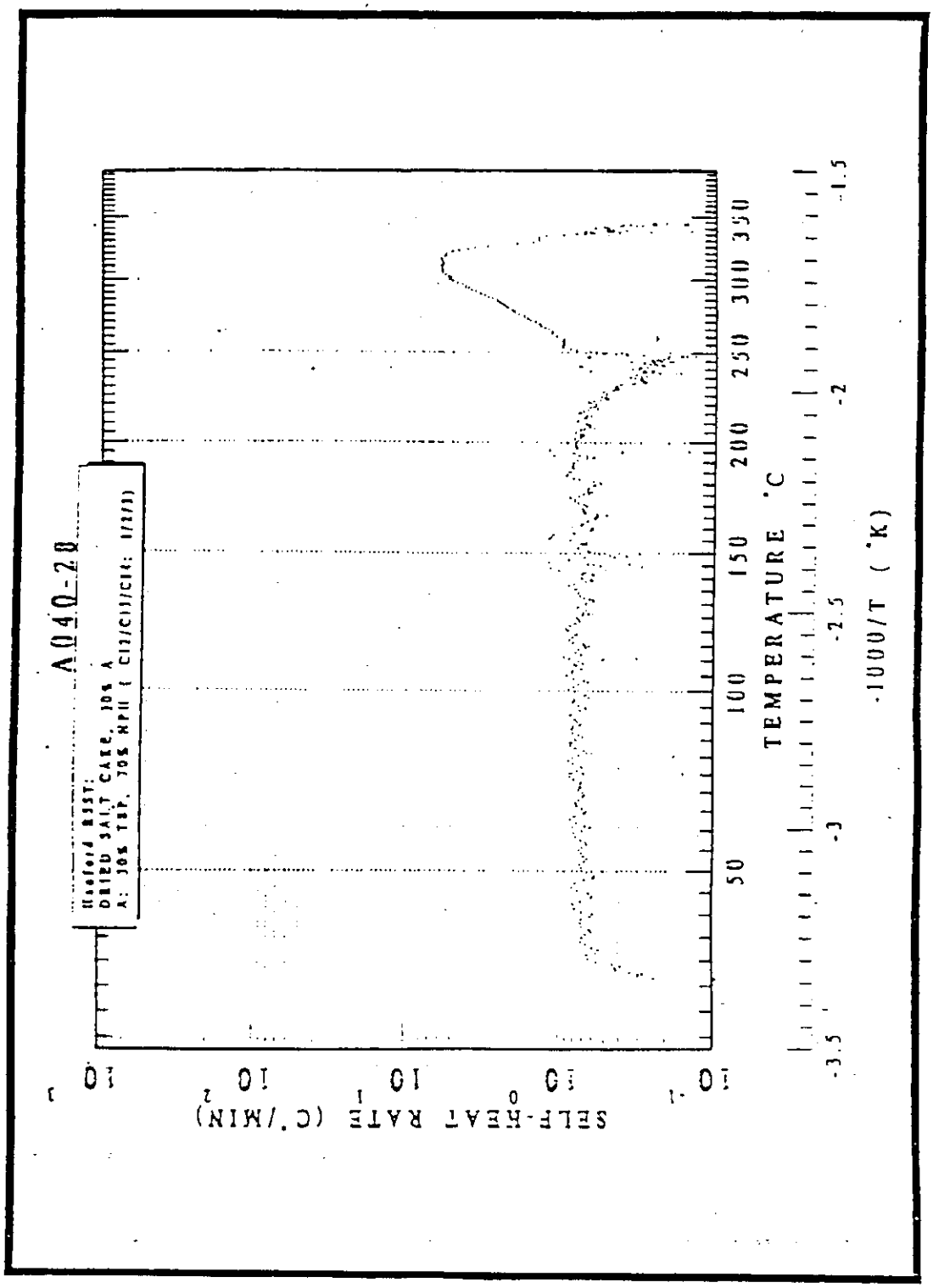

2.2 Tube Propagation Tests

Dedicated tube propagation tests are being carried out that provide measurements of combustion temperature and rate of combustion in connection with sustained propagation through cold material when subjected to a large ignition source. In these tests (see Figure 2-8) a confined low heat capacity stainless steel cylinder containing simulated waste (50-70 gm) is ignited at the upper end and the rate of propagation (if any) is measured by noting the time when the reaction front passes imbedded thermocouples. The ignition energy is about 20 watts and the igniter is left on until sustained propagation is observed (~ 15-20 seconds). In case of no propagation, the igniter is usually left on for at least 1-3 minute. Not shown in Figure 2-8, a heavy 4-liter steel containment vessel and various instrumentation and data acquisition equipment. These data also provide the necessary fuel concentration to sustain propagating reactions, i.e. the lower propagation limit (LPL) in absence of free water, as well as the moisture content that will inhibit propagations including stoichiometric fuel-oxidizer mixtures at ambient waste temperature.

An example of the relevant temperature data for a successful propagation test is illustrated in Figure 2-9 with the non-volatile complexant sodium citrate. The lower propagation limit (LPL) for this material is about 8 wt.% TOC and results in a combustion temperature of about 800°C.

Consistent with the RSST observations, sustained condensed-phase combustion with $NaNO_3$ as oxidizer, were not observed with the volatile organic solvents or representative salts.

The temperature data shown in Figure 2-10 represents 15 wt.% of the 30% TBP - 70% NPH mixture and corresponds to a TOC content of 11.3%. Higher concentrations could not be tested since the samples became liquid-like. The ignition source (~ 20 w) was kept on for about 3 min. and corresponds to the turnaround in temperature noted in Figure 2-10.

The results from two tests (one repeat test) with samples consisting of 8% TOC AℓDBP powder mixed with $NaNO_3$ are shown in Figures 2-11 and 2-12. The igniter on-time corresponding to Figure 2-11 was 62 s (~ 1.6 KJ), and for Figure 2-12 about 120 s (~ 3.1 KJ).

Similar data with no clear evidence of sustained combustion for 5 and 6 wt.% TOC NaButyrate/$NaNO_3$ mixtures are shown in Figures 2-13 and 2-14, respectively. The igniter on-times for these tests were about 200 s (~ 4.5 KJ). It is noted that based on previous test with non-volatile organic surrogates such as NaAcetate, the theoretical energy threshold for sustained combustion (~ 1600 J/gm mixture) is satisfied with all the above tested samples.

Figure 2-8 Illustration of tube propagation test cell.

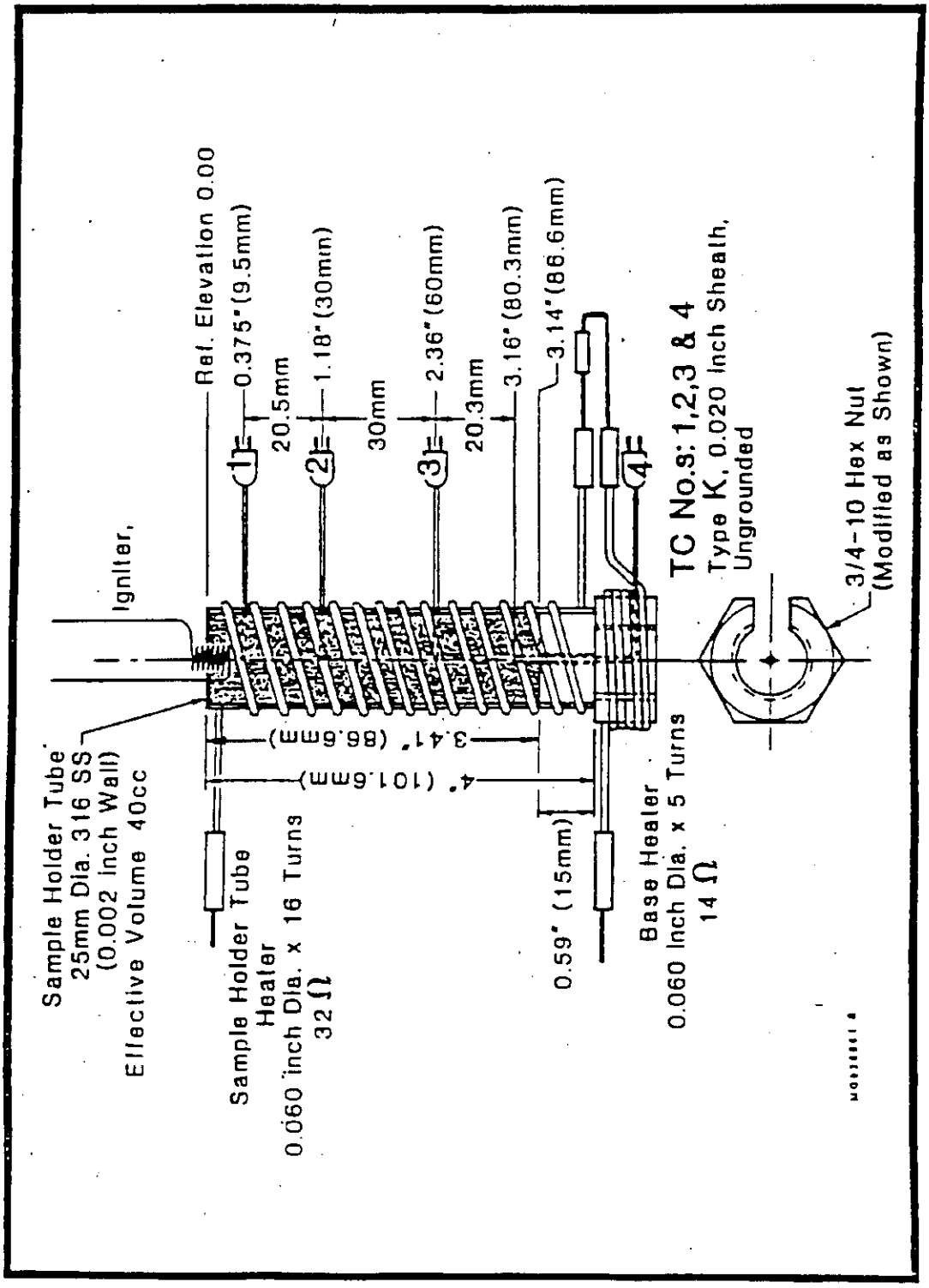

Figure 2-9 Illustration of sustained combustion with 8 wt.% TOC NaCitrate/$NaNO_3$ mixtures.

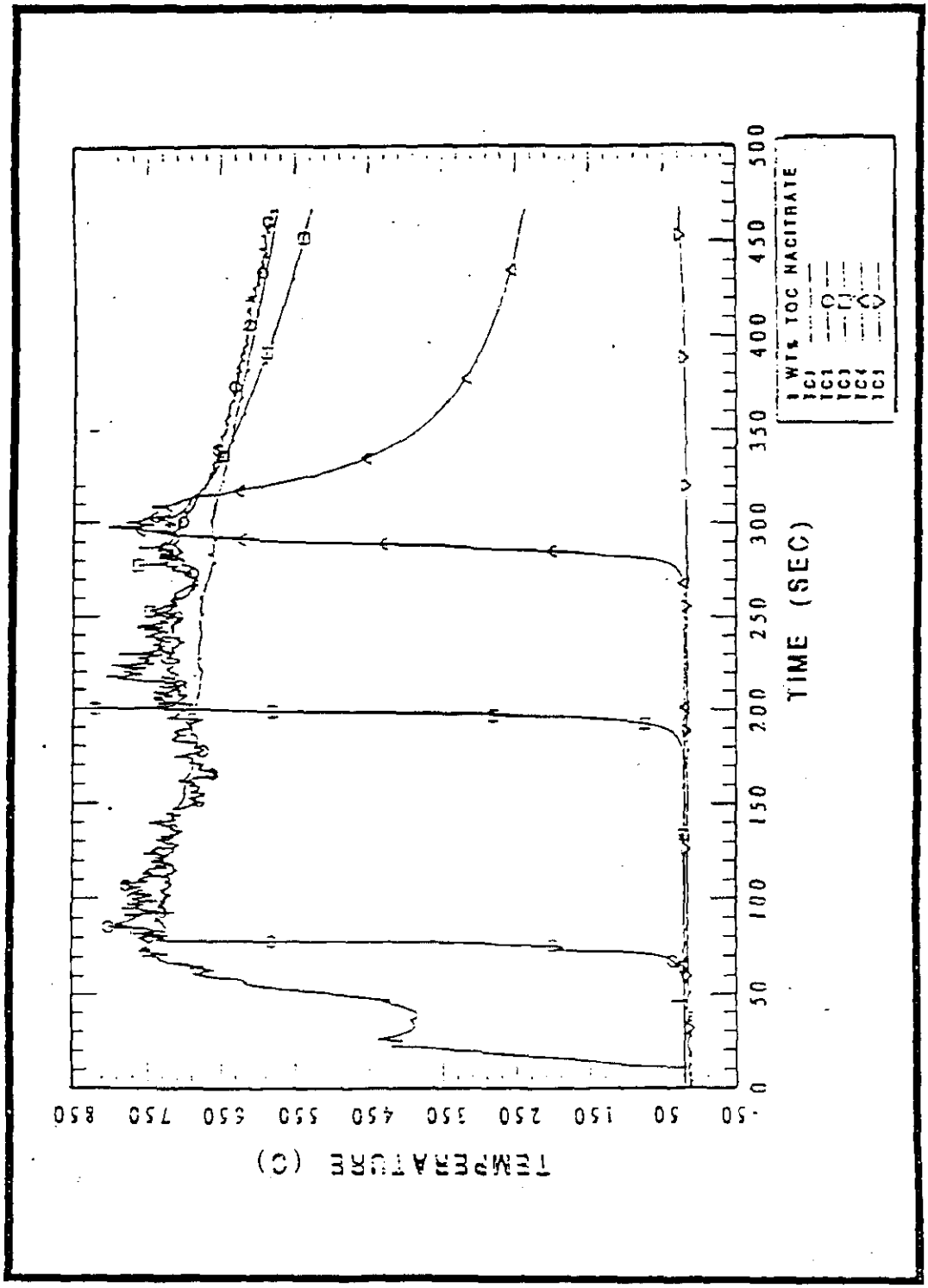

Figure 2-10 Illustration of absence of sustained combustion with 11.3 wt.% TOC 30% TBP - 70% NPH/$NaNO_3$ mixture.

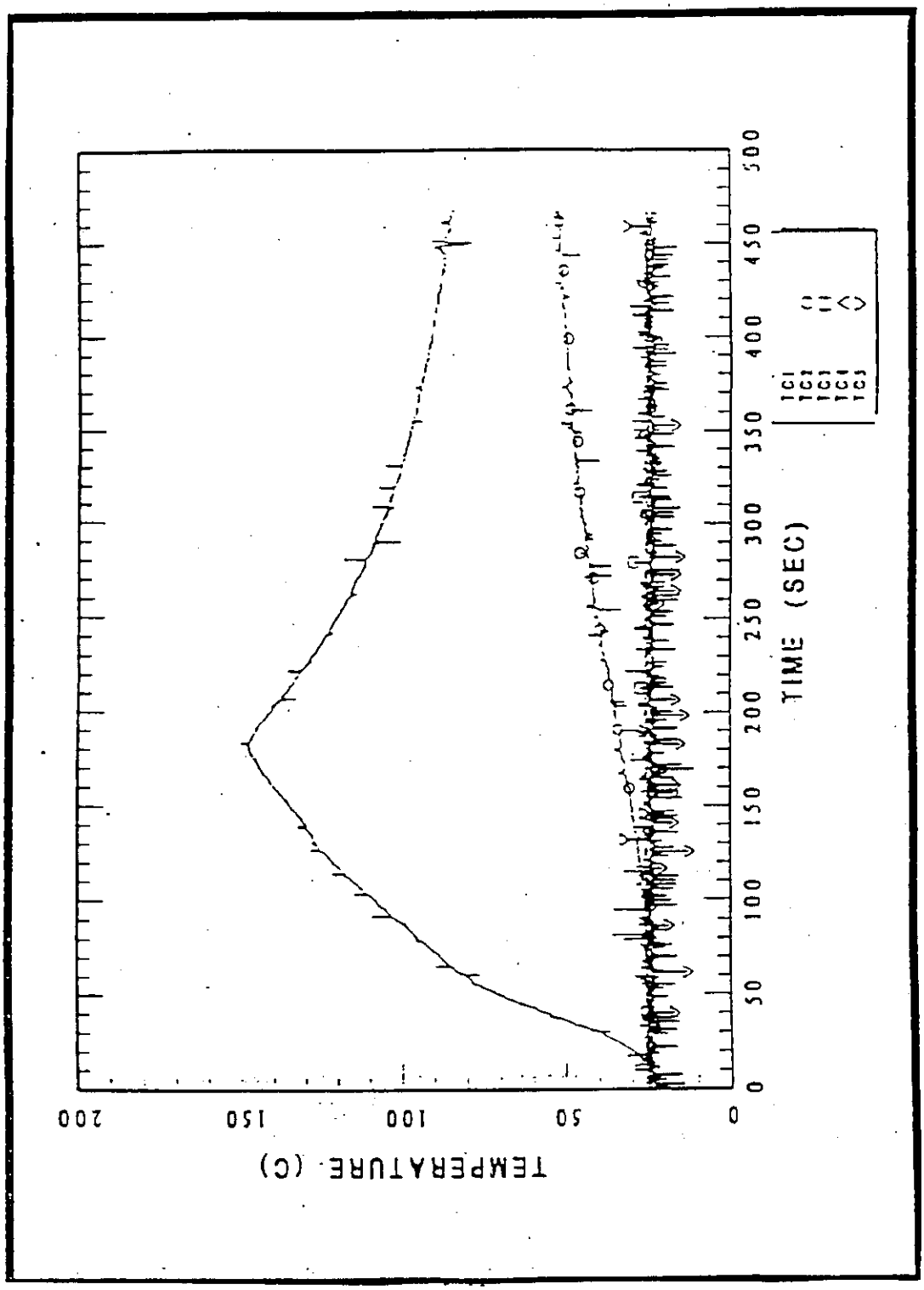

Figure 2-11 Illustration of absence of condensed-phase combustion with 8% TOC AℓDBP/$NaNO_3$ mixture.

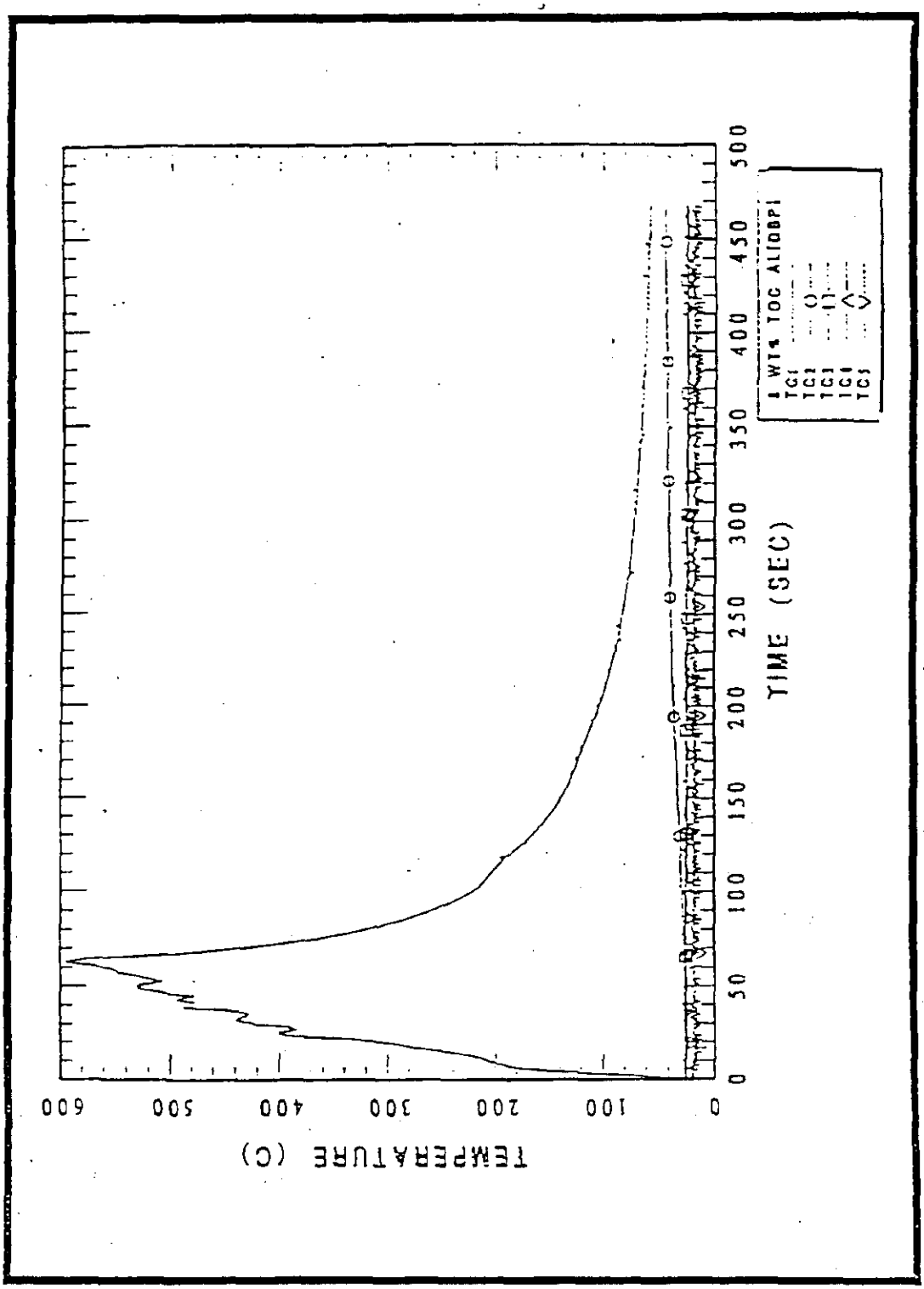

Figure 2-12 Repeat test; illustration of absence of condensed-phase combustion with 8% TOC AℓDBP/$NaNO_3$ mixture.

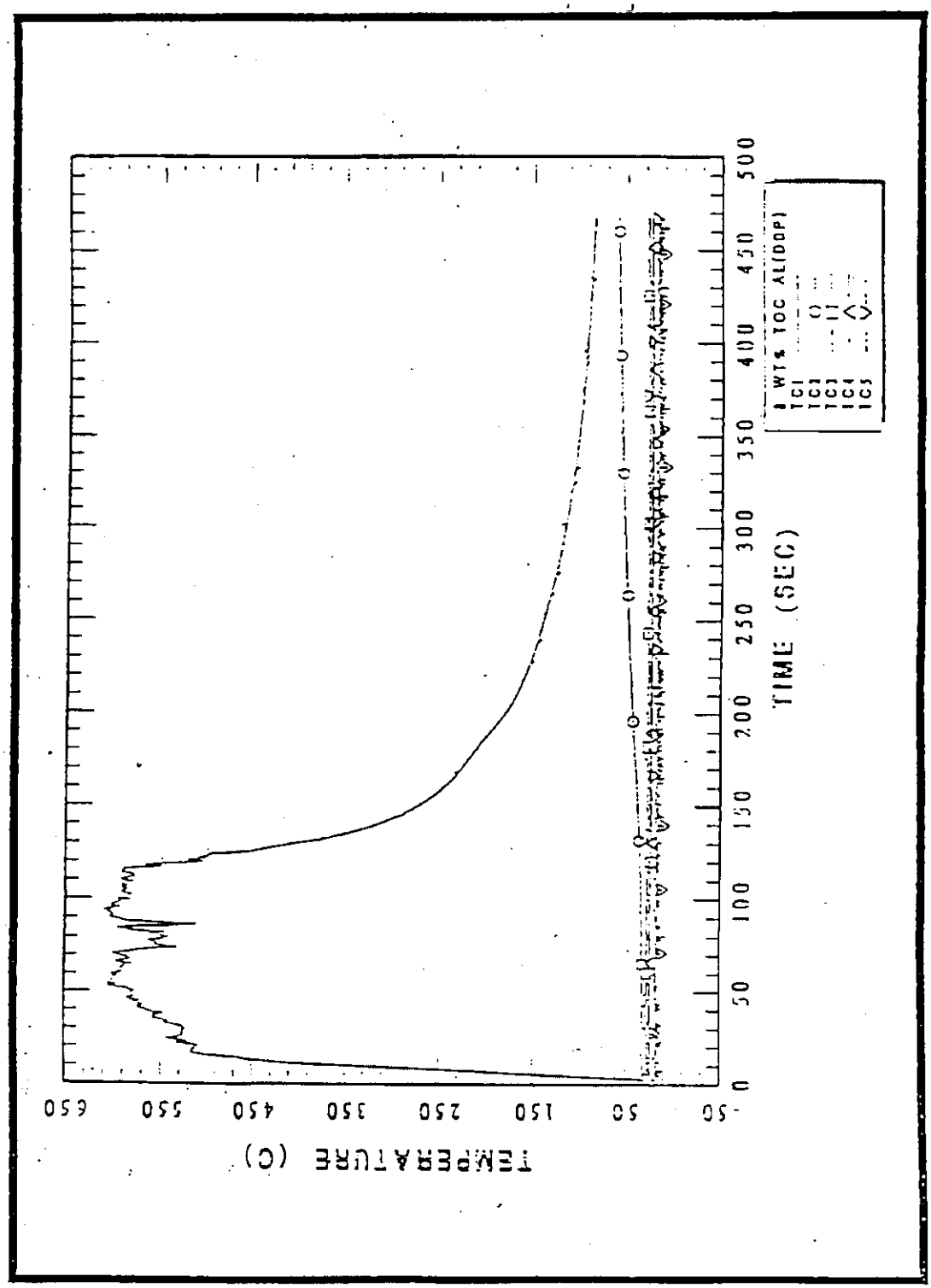

Figure 2-13 Illustration of temperature data with 5 wt.% TOC NaButyrate/$NaNO_3$ mixture. Igniter on-time ~ 200 s.

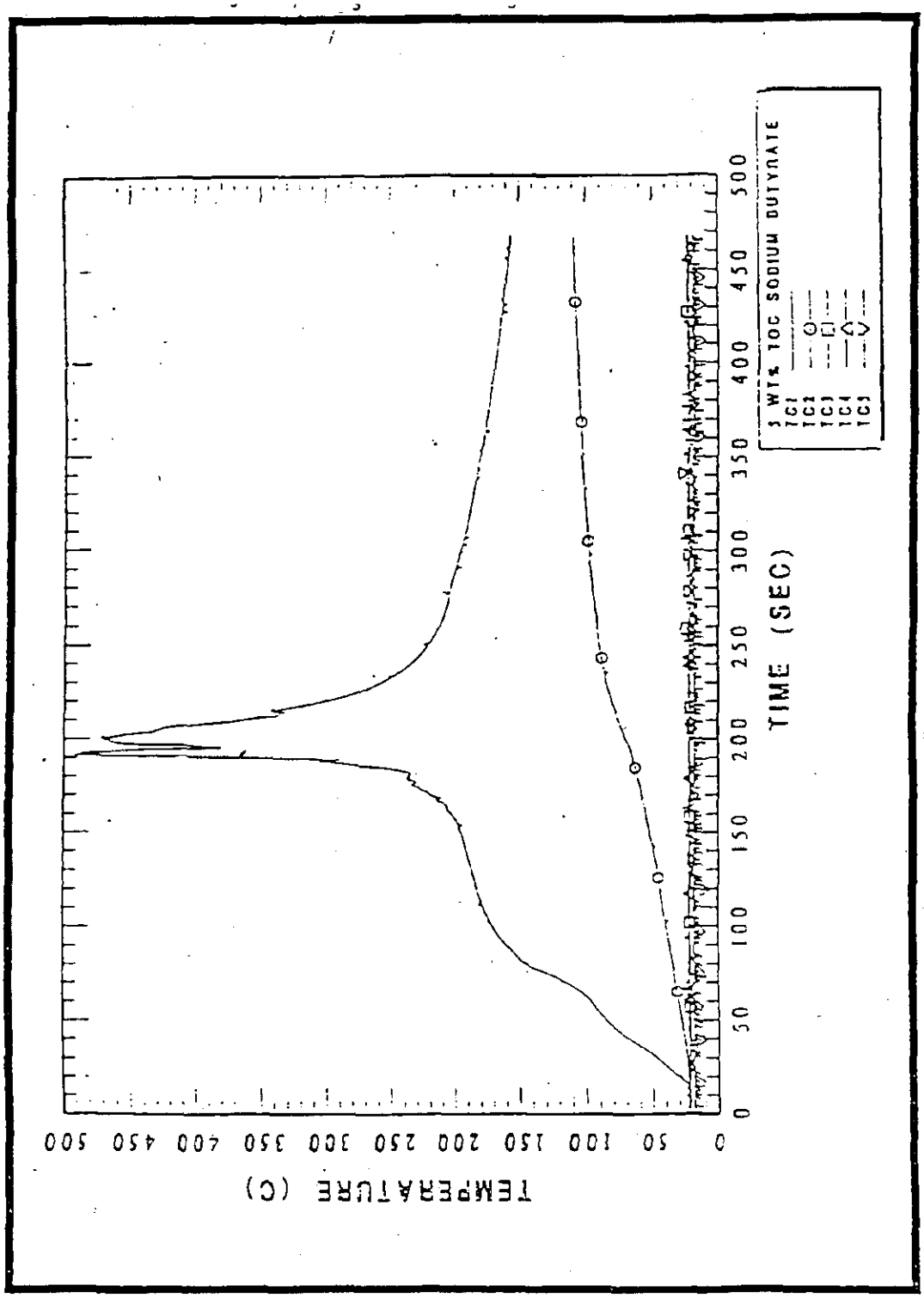

Figure 2-14 Illustration of temperature data with 6 wt.% TOC NaButyrate/$NaNO_3$ mixture.

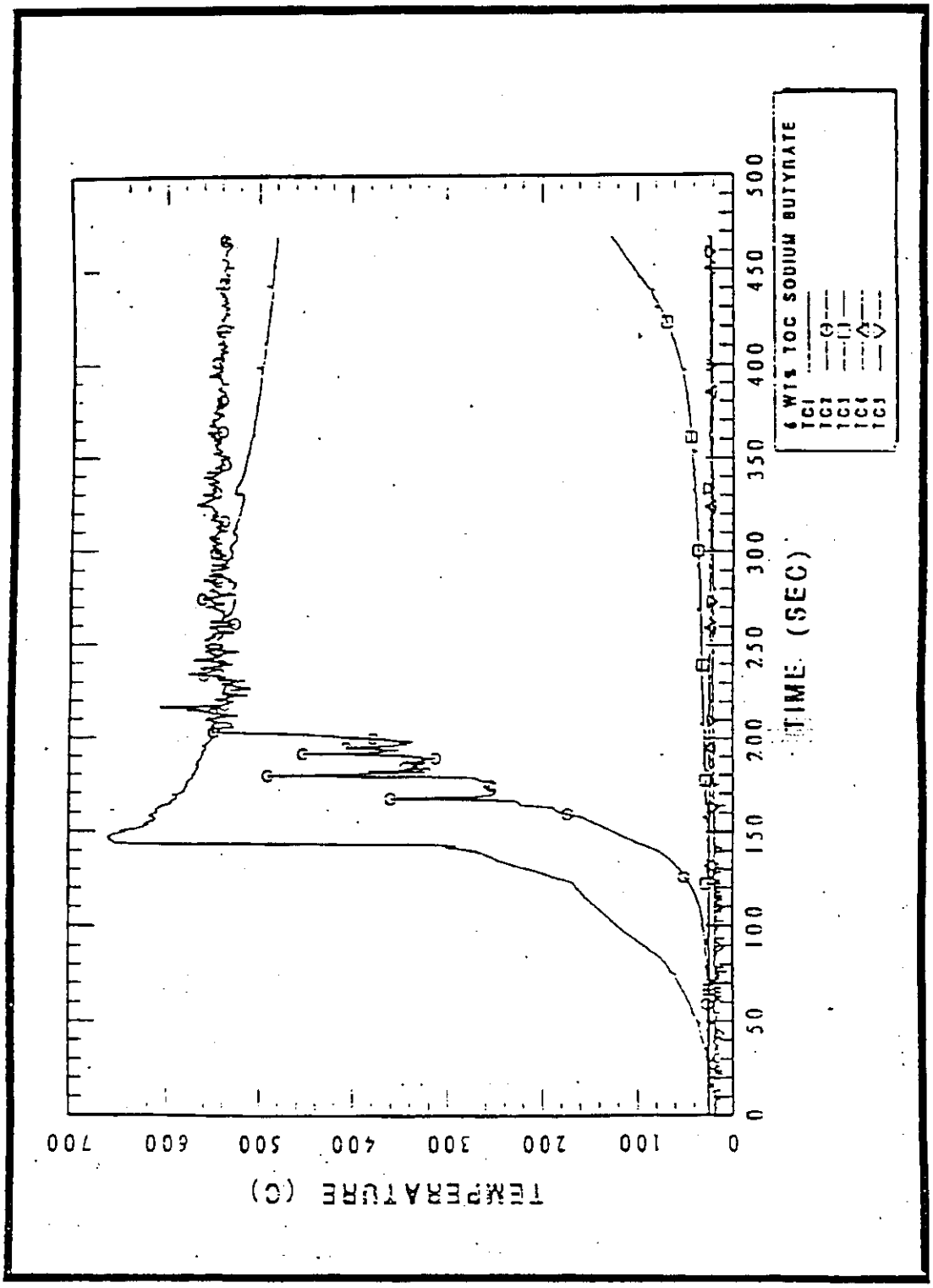

3.0 THE POTENTIAL FOR ORGANIC SOLVENTS OR THEIR SALTS AS SUPPLEMENTAL FUEL TO COMPLEXANT-NITRATE PROPAGATING REACTIONS

As to be expected from the previous discussions, adding organic solvents or their salts do not make an otherwise non-reactive waste (too little non-volatile organic complexant) into a combustible condition given an adequate ignition source.

The absence of sustained combustion is illustrated by the temperature data in Figure 3-1 representing a total TOC content of 6 wt.% made up of 3 wt.% TOC from NaCitrate and 3 wt.% TOC from AℓDBP. With $NaNO_3$ as the oxidizing medium, this mixture has an estimated theoretical heat of reaction value of about 1840 J/gm mixture (assuming the value for AℓDBP is the same as for NaDBP), which is well in excess of 1600 J/gm required for sustained combustion of NaCitrate/$NaNO_3$ mixture (see Figure 2-9).

Similar observations have been made when lack of sufficient organic complexant is supplemented with organic solvent. As an example, a mixture with a total TOC content of 15.5% made up of 7 wt.% TOC NaCitrate and 8.5 wt.% TOC dodecane, did not experience sustained condensed-phase combustion but did exhibit a limited surface vapor-phase combustion of dodecane with air. The absence of condensed-phase combustion is consistent with the requirement of at least 8 wt.% TOC NaCitrate for sustained combustion given an adequate ignition source (see Figure 2-9). In these visual bench top tests no temperature data were taken but the experiments were videotaped. The tests samples were typical 30 cm^3. The test cell is constructed from 100 mℓ glass graduated cylinder, which is cut off at about the 30 mℓ mark. The igniter used for these tests is the same as used for the previously described enclosed tube propagation tests.

Figure 3-1 Illustration of absence of condensed-phase combustion with 6 wt.% TOC (3% NaCitrate + 3% AℓDBP)/$NaNO_3$ mixture.

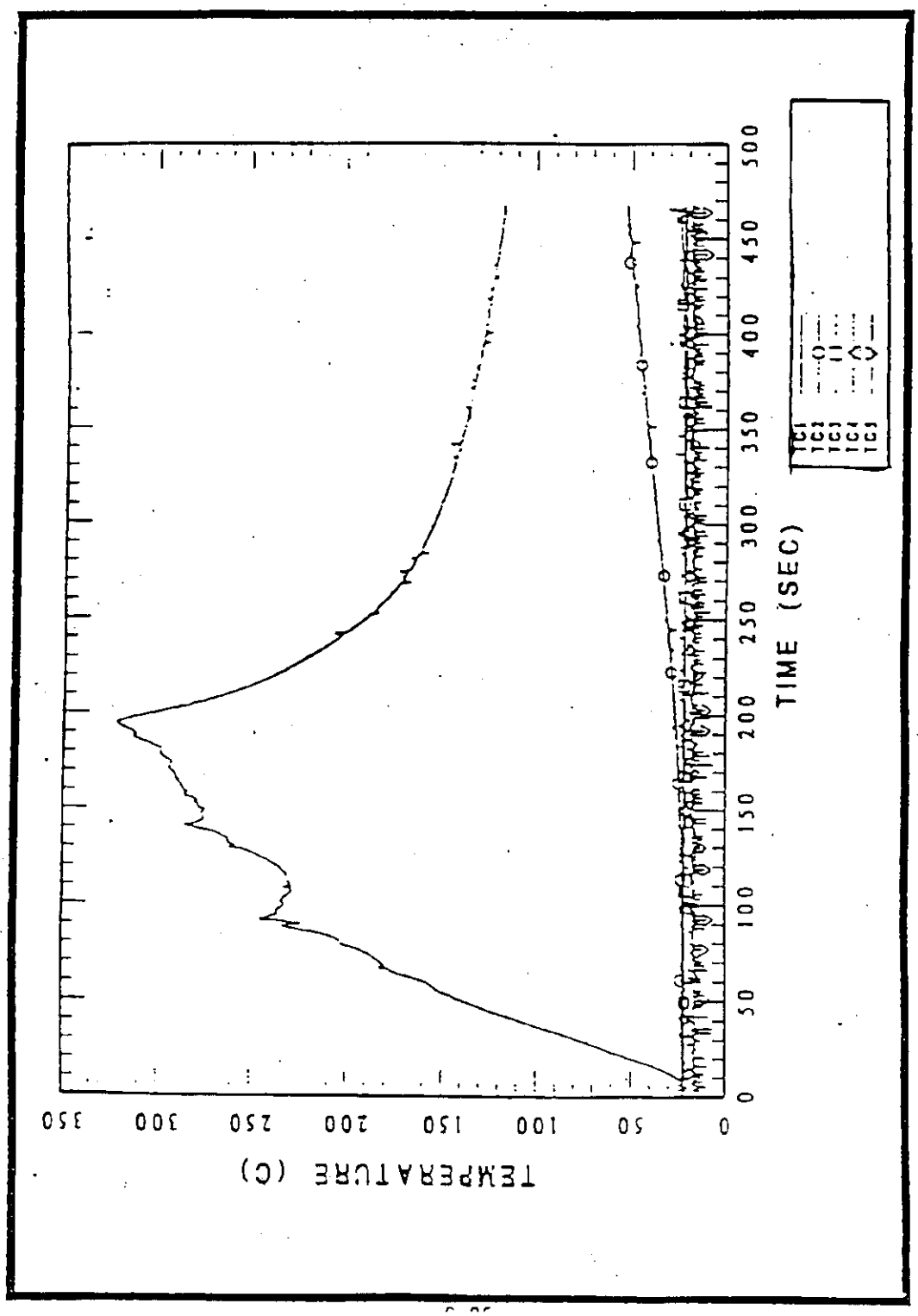

4.0 THE POTENTIAL FOR SURFACE VAPOR COMBUSTION TRANSITION TO CONDENSED-PHASE COMBUSTION

The above example of 15.5 TOC content made up of 7 wt.% TOC NaCitrate and 8.5 wt.% TOC dodecane illustrates the absence of transition to condensed-phase combustion where the organic complexant concentration is less than that required for sustained combustion in absence of organic solvent.

However, if the complexant concentration requirement is satisfied, given surface vapor combustion transition to condensed-phase combustion will eventually take place. Visual bench top tests with a mixture of 11 wt.% TOC NaCitrate/$NaNO_3$ and soaked with dodecane including a liquid pool of dodecane on the surface illustrated repeatable transition to condensed-phase combustion following vapor-phase burning of the dodecane pool. Dodecane-air burning was achieved by applying a torch to the dodecane pool. It is noted that sustained vapor-phase combustion in the absence of condensed-phase combustion appears to be maintained as long as the liquid pool exists, i.e., the pool temperature remains below the required ignition temperature for condensed-phase combustion. Only after vapor production takes place within the organic complexant-nitrate mixture, will surface vapor combustion result in high enough temperature to satisfy initiation of condensed-phase combustion. Again these experiments were videotaped.

This page intentionally left blank.

5.0 ORGANIC SOLVENT IGNITABILITY TESTS

Laboratory tests have been performed to study the minimum ignition energies required to initiate organic solvent vapor-phase combustion as well as condensed-phase combustion in the presence of organic solvents. Ignition sources utilized to date include a pyrotechnic "electrical match" which supplied with 110 VAC releases about 138 J over a 3-5 ms period, and various size steel particles (1/16, 3/32 and 3/16 inch) heated to about 1300°C (corresponding energy contents of 10, 35 and 270 J).

Initial tests with the "electrical match" have demonstrated that the presence of a volatile organic solvent actually prevents the initiation of condensed-phase combustion. The test samples were typically about 25 cm^3. The test cell is constructed from a 100 mℓ glass graduated cylinder, which is cut off at about the 35 mℓ mark. The match is placed either on the surface of the sample or immersed in the sample to a depth of about 1 inch (see Figure 5-1). Apparently, the absence of condensed-phase combustion initiation is caused by the organic solvent absorbing most of the energy release, thereby keeping the temperature below the ignition level. Similar observations are made with the presence of small quantities of moisture (see Figure 5-2). The above tests were repeated using hot steel particles (1300°C) as the ignition source. Again sustained ignition was absent in the presence of organic solvent or free moisture. On the other hand, in the complete absence of organic solvent or free moisture, the 1/16-inch steel particle (~ 10 J) was sufficient to initiate condensed-phase combustion with a stoichiometric mixture of NaCitrate and $NaNO_3$.

Tests related to ignitability of small organic solvent puddles and solvent soaked or saturated salt cakes have also been completed. Subjecting 2.5 inch diameter dodecane puddles and 2.5 inch dodecane saturated salt cakes ($NaNO_3$ powder) to hot steel particles heated to about 1300°C (energy contents ranging from 10 to 270 J) did not result in sustained ignition. Applying the 138 J match to the same conditions also resulted in no sustained ignition.

The above ignition sources would appear to envelope all credible ignition sources (in-tank instrumentation, welding and grinding, hot filament and shorting electrical wires*) with the possible exception of lightning.

---

*This source is simulated as part of the electrical match following the main energy release.

Figure 5-1 Ignition potential and effect of volatile organic.

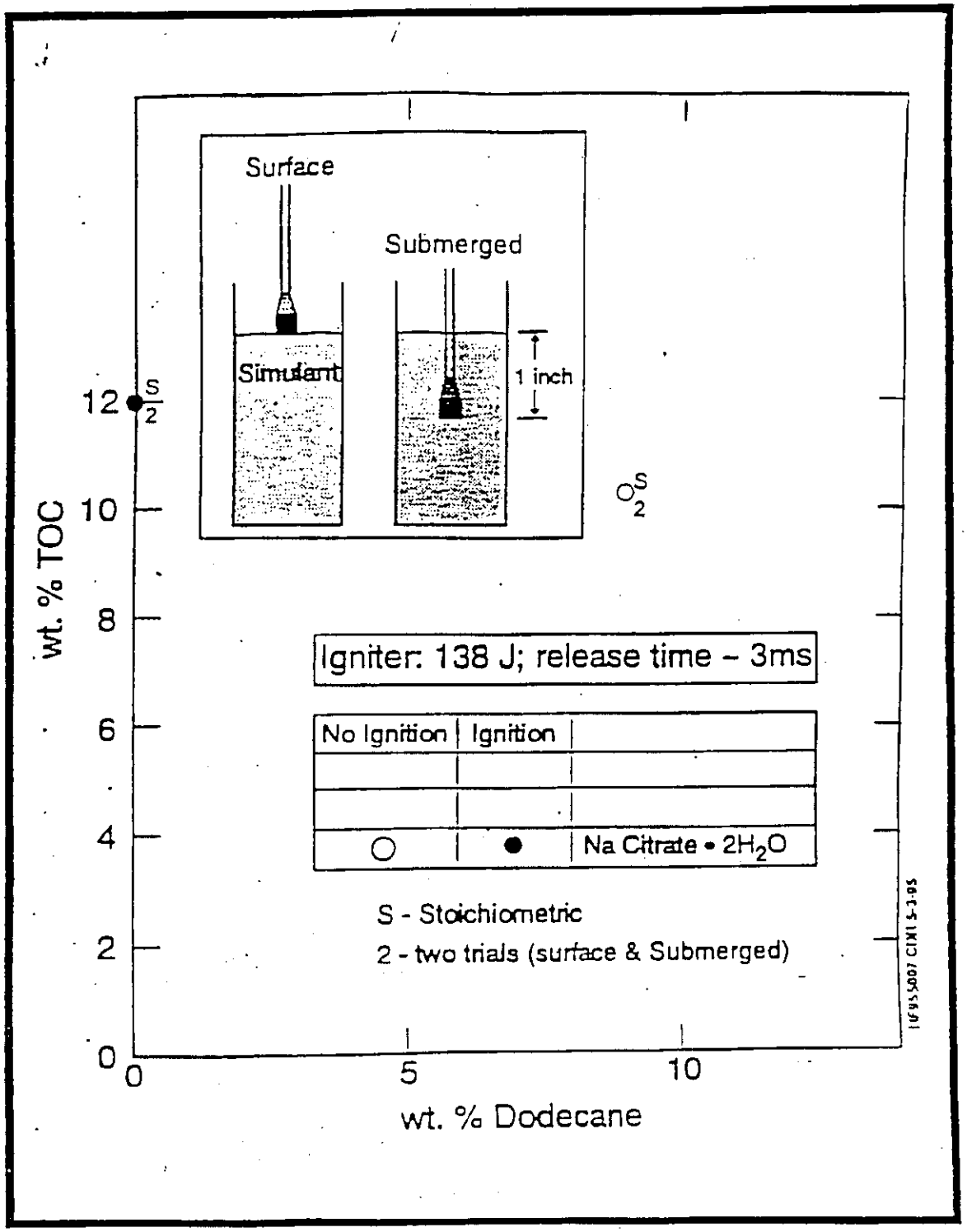

Figure 5-2 Ignition potential and the effect of free water.

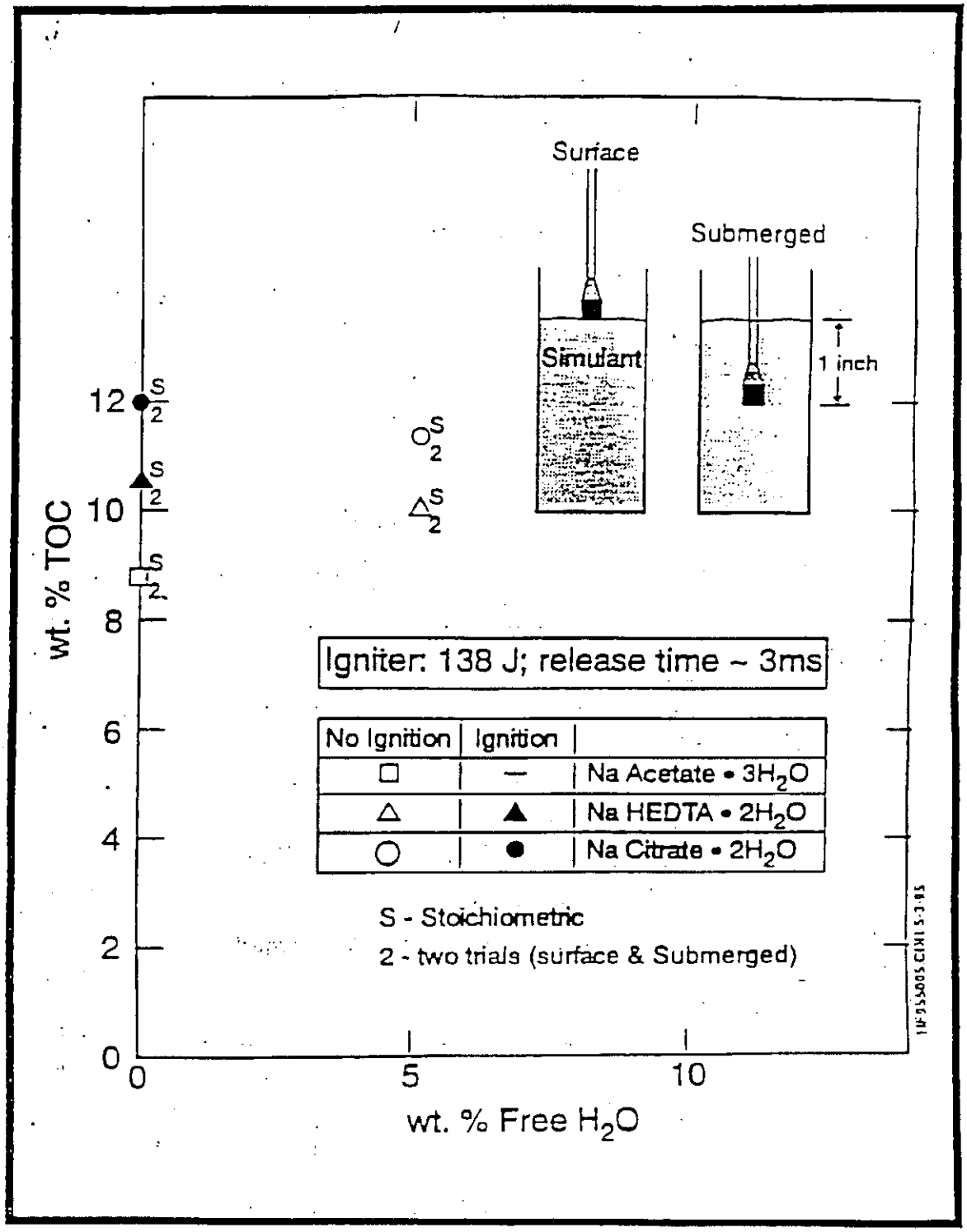

This page intentionally left blank.

APPENDIX F

POWER REQUIRED TO IGNITE A SUSTAINABLE POOL

This page intentionally left blank.

Formerly Appendix D of
HNF-SD-WM-SARR-036 REV 1A

Fauske & Associates, Inc.

DATE: June 21, 1995

TO: Mike Grigsby Westinghouse Hanford Company
FAX: (509) 628-2025

FROM: Mike Epstein Fauske & Associates, Inc.

SUBJECT: *POWER REQUIRED TO IGNITE A SUSTAINABLE POOL FIRE*

Robust Heating of a Free Pool Surface

As a result of previous analytical and experimental work (FAI, 1994) we have the following relationship for the maximum temperature increase $T_{max} - T_\infty$ at the liquid fuel surface caused by an overlying, concentrated heat source of radius r_o and transmitted heat flux q_o:

$$\frac{h(T_{max} - T_\infty)}{q_o} = 0.819 \left(\frac{r_o^4 h^3}{k_e \delta q_o^2} \right)^{0.231} \tag{1}$$

where T_∞ is the ambient temperature far from the source, h is the heat transfer coefficient for natural convection cooling of the liquid surface by overlying air, δ is the depth of the fuel layer, and k_e is a transport coefficient which incorporates the combined effects of thermogravitational and thermocapillary convection within the fuel layer. The expression for k_e is

$$k_e = \frac{\rho c_p (\sigma')^2 \delta^4}{1680 \alpha \mu^2} \left[1 + \frac{7}{24} Bo \frac{19}{864} Bo^2 \right] \tag{2}$$

where ρ, c_p, α, μ, and σ' are the density, specific heat, thermal diffusivity, viscosity, and absolute variation of surface tension with temperature of the liquid fuel material, respectively. The parameter Bo in Eq. (2) is the Bond number, defined by

16W070 West 83rd Street · Burr Ridge, Illinois 60521 · (708) 323-8750
Telefax (708) 986-5481

$$Bo = \frac{g\rho\beta\delta^2}{\sigma'} \tag{3}$$

where g is the gravitational constant and ß is the volumetric expansion coefficient of the liquid fuel.

In order for the surface of the liquid fuel (within the heated zone of radius r_o) to produce a flame, the surface must be high enough in temperature to be over the so-called flash point temperature T_{fp}. If T_{max} exceeds T_{fp} the fuel/vapor air mixture above the liquid surface is rich enough in combustible content to make a flame possible. By setting $T_{max} = T_{fp}$ in Eq. (1) and solving the result for q_o we obtain the heat source strength required to bring the underlying liquid surface temperature up to T_{fp}:

$$\frac{q_o}{h(T_{fp} - T_\infty)} = 1.45 \left[\frac{k_e\ \delta\,(T_{fp} - T_\infty)^2}{r_o^4\ h}\right]^{0.429} \tag{4}$$

In addition to a high fuel surface temperature, there are two other conditions that the fuel layer/heater system must satisfy in order for the fuel surface to support a propagable flame. From the experimental work and theoretical considerations presented by Epstein et al. (1995) we know that (i) ignition of a propagable flame on a fuel layer less than 2.0 mm deep is not credible and (ii) the heat source (or ignited flame) must be at least 10 cm in diameter before ignition of a propagable flame becomes possible. Thus the minimum power required to ignite a fire that can spread beyond the influence of the heat source is predicted by inserting $\delta = 2 \times 10^{-3}$ m and $r_o = 0.05$ m into Eq. (4).

To estimate this minimum power from Eq. (4) we consider a fuel layer having a flash point $T_{fp} = 120°C$ in a waste tank environment at $T_\infty = 40°C$. The physical properties of the fuel layer are assumed to be the same as those of dodecane at 80°C, which is the arithmetic average of T_{fp} and T_∞. These properties are: $\rho = 706$ kg m^{-3}, $c_p = 2417$ J kg K^{-1}, $\mu = 6.38 \times 10^{-4}$ kg m^{-1} s^{-1}, $k = 0.139$ W m^{-1} K^{-1}, $\alpha = 8.16 \times 10^{-8}$ m^2 s^{-1}, $\sigma' = |d\sigma/dT| = 9.74 \times 10^{-5}$ N m^{-1} K^{-1}, and $\beta = 1.05 \times 10^{-3}$ K^{-1}. With regard to a numerical choice for the heat-transfer coefficient h, combined natural convection and radiation from the surface of a "rigid" organic layer to quiescent ambient air is predicted with a standard heat-transfer correlation for turbulent natural convection (from an upward facing surface) and with a linearized form of the Stefan-Boltzmann radiation law to yield $h = 15.0$ W m^{-2} K^{-1}. We regard this prediction as a lower bound estimate of h since air drawn toward the heater and thermocapillary driven flow at the fuel surface will act to enhance the fuel-surface heat-loss rate.

Table 1 gives the k_e values and the effective power requirements ($\pi r_o^2 q_o$) for a propagable flame for two fuel layer thicknesses and heater radius $r_o = 0.05$ m.

Table 1

Power Requirements for a Propagable Flame

δ (mm)	k_e (W m K^{-3})	$\pi r_o^2 q_o$ (W)
2.0	4.11×10^{-3}	206
5.0	0.249	1780

Heating and Ignition of a Confined Region

The minimum sustained energy required to produce a propagable flame can be calculated by imagining the following sequence of events; a 10-cm diameter, 2-mm deep fuel layer is confined and heat losses to the surroundings are cut off, bulk heated to the flash point and ignited, and finally the confinement barrier is removed to "free" the resulting flame. Recall that propagable flames only exist on fuel layers deeper then 2.0 mm and initially must be at least 10 cm in diameter. This sequence results in a minimum predicted initiator energy Q given by

$$Q = \pi R_o^2 \delta \rho c_p (T_{fp} - T_\infty)$$

Using c_p = 2417 J kg K^{-1} and ρ = 706 kg m^{-3} (for dodecane), T_{fp} = 120°C and T_∞ = 40°C, we get

$$Q = 2.1 \text{ kJ}$$

References

1. Epstein, M., Burelbach, J. P., Plys, M. G., and Fauske, H. K., 1995, "Ignitability of Organic Solvent in Hanford Tank C-103 Following Interim Stabilization," Fauske & Associates, Inc. Report FAI/95-17 (February).

2. Fauske & Associates, Inc., 1994, "Hazard Assessment Techniques for Hanford Waste Tanks Presently or Previously Containing Liquid Organic Layers," FAI/94-91 (September).

ME:lak

cc: H. K. Fauske
M. G. Plys

This page intentionally left blank.

APPENDIX G

FAI/95-17
IGNITABILITY OF ORGANIC SOLVENT IN HANFORD TANK C-103 FOLLOWING INTERIM STABILIZATION

This page intentionally left blank.

Formerly Appendix B of
HNF-SD-WM-SARR-036 REV 1A

FAI/95-17
IGNITABILITY OF ORGANIC SOLVENT IN HANFORD TANK C-103 FOLLOWING INTERIM STABILIZATION

Submitted To:
Westinghouse Hanford Company
Richland, Washington

Prepared By:
M. Epstein, J. P. Burelbach, M. G. Plys, and H. K. Fauske
Fauske & Associates, Inc.
16W070 West 83rd Street
Burr Ridge, Illinois 60521
TEL: (708) 323-8750
FAX: (708) 986-5481

February, 1995

This page intentionally left blank.

TABLE OF CONTENTS

Page

1.0 INTRODUCTION G-9

2.0 ORGANIC SOLVENT CONFIGURATION FOLLOWING INTERIM STABILIZATION G-11

2.1 Problem Statement G-11
2.2 Preliminary Conclusions G-11
2.3 Kerosene/Water Weir-Flow Draining Experiments G-11
2.4 Theory of Water Wave Formation Beneath a Weir Flow of Floating Organic Liquid G-12

3.0 IGNITABILITY OF RESIDUAL ORGANIC MATERIAL G-19

3.1 Organic Liquid Pools G-19

3.1.1 Issue and summary G-19
3.1.2 Critical organic layer depth for flame extinction . G-20
3.1.3 Experiments on the initiation of flame spreading on an organic fuel layer G-22
3.1.4 Theory of the spark source initiator G-27

3.2 Organic Liquid in Cracks G-31

3.2.1 Issue and summary G-31
3.2.2 Experiments on liquid convection in an open channel heated non-uniformly from above G-32
3.2.3 Experiments on flame spreading in an open channel . G-35

3.3 Organic Liquid Embedded in Sludge G-35

3.3.1 Issue and summary G-35
3.3.2 Experiments on ignitability of TBP/NPH in kaolin sludge surrogate G-36

4.0 CONCLUSIONS G-57

5.0 REFERENCES G-59

TABLE OF CONTENTS - (Continued)

Page

APPENDIX FAI/95-17A: A Steady-State Theory for Radial Flame Spread on an Organic Liquid Layer G-61

APPENDIX FAI/95-17B: Thermal Response of Semi-Infinite Region to Surface Heat Flux Given by Eq. (3-14) in Section 3.1.4 . . G-71

APPENDIX FAI/95-17C: Thermocapillary and Thermogravitational Liquid Convection in an Open Channel Subject to a Surface Heat Flux G-77

LIST OF TABLES

Page

Table 2-1 Weir Flow Draining Tests G-13

Table 3-1 Results of Pool Fire Spreading Tests, Fire Centered in Pan . . G-23

Table 3-2 Results of Pool Fire Spreading Tests, Fire Near Pan Wall . . . G-24

Table 3-3 Summary of Channel Convection Experiments G-34

Table 3-4 Dodecane Properties at 30°C G-34

Table 3-5 Results of Sludge Burning Tests G-38

Table A-1 Physical Properties Used in Numerical Calculations G-68

LIST OF FIGURES

		Page
Figure 2-1	Schematic of experimental apparatus for observing wave disturbances and water entrainment during weir flow of floating organic layer on water	G-17
Figure 2-2	Model sketch of stationary, broad crested water wave behind weir	G-18
Figure 3-1	Flame spread apparatus	G-39
Figure 3-2	Liquid surface temperatures for Test #23	G-40
Figure 3-3	Flame diameter versus organic fuel-layer thickness map for dodecane at approximately 20°C, showing the (unshaded) region in which spreading of a centrally-located flame is impossible. The dashed curves represent theoretical results for two flame radiation efficiencies η	G-41
Figure 3-4	Flame diameter versus organic fuel-layer thickness map for dodecane at approximately 20°C, showing the (unshaded) region in which spreading of a flame initially located near the pool boundary is impossible	G-42
Figure 3-5	Radiation from a "surface element" of spark to a surface element of liquid	G-43
Figure 3-6	Schematic diagram of apparatus for measuring surface temperature versus distance profile produced by thermocapillary channel flow	G-44
Figure 3-7	Thermocapillary channel convection Test 1	G-45
Figure 3-8	Thermocapillary channel convection Test 2	G-46
Figure 3-9	Thermocapillary channel convection Test 3	G-47
Figure 3-10	Thermocapillary channel convection Test 4	G-48
Figure 3-11	Thermocapillary channel convection Test 5	G-49
Figure 3-12	Test 1 temperature histories	G-50
Figure 3-13	Test 2 temperature histories	G-51
Figure 3-14	Test 3 temperature histories	G-52
Figure 3-15	Test 4 temperature histories	G-53
Figure 3-16	Test 5 temperature histories	G-54

LIST OF FIGURES - (Continued)

		Page
Figure 3-17	Organic liquid intrusion results for kaolin/water sludge and T-plant flowsheet	G-55
Figure A-1	Schematic diagram of standing flame fed by layer of organic-liquid fuel. Flame spreading condition achieved when T_{cd} equals or exceeds fuel flash point . .	G-69
Figure C-1	Schematic diagram of semi-infinite liquid layer in a channel subject to a surface heat flux at the closed end. The countercurrent, horizontal velocity profile is produced by combined thermocapillary and thermo-gravitational convection	G-82

1.0 INTRODUCTION

This report is provided to Westinghouse Hanford Company (WHC) to support the safety analysis report (SAR) entitled "Risk from Organic Solvent Fires in C-103 Following Interim Stabilization." The background and nature of the hazard are familiar to WHC and will not be repeated here in detail, i.e., this report assumes the reader is familiar with the current configuration of Hanford tank C-103, the process of interim stabilization, and previous hazard analyses, which will be reiterated in the target SAR. Specific aspects of the hazard investigated by Fauske & Associates, Inc. (FAI) and documented here are the possible configurations of organic materials after interim stabilization and the conditions under which organic material may be ignited. Section 2 is an experimental and theoretical determination of the amount of organic material that might remain upon the C-103 sludge surface after interim stabilization. Section 3 combines experimental and analytical means to determine the size of an initiating energy (power) source required to ignite various organic configurations including residual layers and material embedded in sludge. Additional details are provided in the appendices.

This page intentionally left blank.

2.0 ORGANIC SOLVENT CONFIGURATION FOLLOWING INTERIM STABILIZATION

2.1 Problem Statement

Tank C-103 currently contains an organic layer floating upon an aqueous salt solution layer overlying aqueous-saturated sludge. Interim stabilization of C-103 to remove pumpable liquid will allow the floating organic layer to contact the sludge surface. The relative impermeability of the water-saturated sludge implies that the organic layer will always drain away from the uneven sludge surface, i.e., the hydraulic resistance to flow through sludge is orders of magnitude higher than friction on the sludge surface. Given this assumption, if the organic/aqueous interface remains stable and horizontal, then indeed all the organic will drain into the saltwell during pumping. However, if the interface becomes unstable and wavy, then some organic material may be left behind in local depressions of the sludge surface. The potential for such an instability is investigated here theoretically and experimentally.

2.2 Preliminary Conclusions

The flow from a local sludge depression over a local sludge ridge was assumed to behave like flow over a sharp-crested weir and our experimental and theoretical program on this topic addressed the possibility of wave disturbances forming behind the weir that would result in the loss of the aqueous phase and the collection of organic liquid behind the weir. A broad-crested stationary wave of water was observed to form just beneath an overlying weir flow of draining kerosene. As a result of the wave, water was transported together with the kerosene over the weir and a residual layer of kerosene was left behind at the completion of the draining process. Based on a limited number of experiments with the kerosene/water system and an accompanying theoretical effort, we tentatively conclude that measurable quantities of organic material may be left behind in sludge surface depressions.

2.3 Kerosene/Water Weir-Flow Draining Experiments

A weir flow draining apparatus was constructed as follows. Polycarbonate sheet was used to construct a transparent open-top box, or trough, with inside dimensions measuring 123 cm long by 10 cm wide by 29 cm deep, as illustrated in Fig. 2-1. One end of the box was permanently closed, but the other end was provided with a drop gate that was hinged at the bottom. An insert at the bottom of the gate end of the channel served as a weir. The top of the weir measured 3.8 cm above the channel floor, and the outer edge was beveled at a 45° angle. The drop gate could be latched closed, in which case a rubber O-ring sealed the gate end of the box.

Three tests were performed with the apparatus configured as described above. In each case the trough was partially filled with kerosene and water. Food coloring was added to the water to distinguish the interface position for purposes of observation. Once the two liquid layers had stabilized the drop gate was released and the liquid was drained down to the top of the weir. In all cases a broad-crested near-stationary wave of water was observed to form

beneath the floating organic layer just upstream of the weir, and this wave was responsible for the flow of water over the weir during kerosene draining. A residual layer of kerosene remained when the draining process was over. The residual layer thicknesses were measured and are recorded in Table 2-1. The thickness of the residual layer was found to be about 25 percent of the initial thickness of the floating kerosene layer. This result is rationalized theoretically in the next section.

In order to assure ourselves that the wave form is not an artifact of the weir-controlled draining process, the apparatus was reconfigured so that the flow out of the channel is initially controlled by a drain line valve. The apparatus was modified by the addition of a second 5.1 cm tall weir and a 2.5 cm ID drain line (see Fig. 2-1). Subsequent tests were performed with the drop gate latched closed. Four additional tests were performed using the reconfigured apparatus and different valve opening rates, the results of which are also recorded in Table 2-1.

2.4 Theory of Water Wave Formation Beneath a Weir Flow of Floating Organic Liquid

The experimental observations reported in the previous section clearly show the existence of a wave of water just behind the weir. During most of the time period in which the channel drains by gravity flow over the weir, the crest of the water wave exceeds the height of the weir and the water is carried over the weir together with the overlying organic liquid. Ultimately, however, enough water is removed from the channel to lower the water level to the point where the crest of the wave now coincides with the height of the weir. After this occurs water is no longer transported through the wave and over the weir. It is postulated here that the amplitude of the motionless wave that remains behind the weir, i.e. after the basic water flow is brought to rest with respect to the weir, is approximately equal to the depth of the organic liquid layer left behind after the completion of the draining process (see below). Thus it is of interest to attempt to predict the amplitude of the standing water wave that forms beneath a weir flow of overlying organic liquid.

The picture we wish to analyze is shown in Fig. 2-2. The interface between the floating organic layer and the underlying water just behind the weir is defined by the shape of the broad-crested water wave. Since the crest of the wave of amplitude δ is just below the top of the weir the water flow on the average is zero while the organic liquid above continues to flow over the weir. It is obvious from Fig. 2-2 that the wave amplitude δ is approximately equal the depth of the organic liquid that will be left behind when the weir flow of organic liquid ends.

Table 2-1

Weir Flow Draining Tests

TEST ID #	LAYER THICKNESSES BEFORE DRAINING (cm)		LAYER THICKNESSES AFTER DRAINING (cm)	
	WATER	ORGANIC	WATER	ORGANIC
Drop Gate Tests				
1	5.0	5.0	2.6	1.2
2	4.4	2.7	3.0	0.8
3	4.0	1.3	3.4	0.4
Drain Line Tests				
4	5.3	1.3	4.8	0.3
5	5.4	0.9	4.9	0.2
6	5.4	2.5	4.4	0.7
7	19.0	2.6	4.7	0.4

The average organic liquid velocity at position 1 upstream of the wave is denoted by u_1. The pressure at this location is denoted by P_1. The organic liquid flows over the weir at position 2 with average velocity u_2 and pressure P_2. The depth H of the organic liquid as it flows over the weir is assumed to be a known constant. The depths of the water layer upstream of the wave and at the weir are H_1 and H_2, respectively.

Assuming that energy is conserved in the flow system shown in Fig. 2-2, we can write the following momentum equations for the organic liquid layer and the motionless water layer:

$$P_1 + \frac{1}{2}\rho_o u_1^2 - (H + \delta)\rho_o g = P_2 + \frac{1}{2}\rho_o u_2^2 - H\rho_o g \tag{2-1}$$

$$P_1 + H_1\rho_w g = P_2 + H_2\rho_w g \tag{2-2}$$

In the above equations ρ_o and ρ_w are, respectively, the densities of the organic liquid and water, and g is the gravitational constant. The mass continuity equation gives the following additional relation

$$u_1(H + \delta) = u_2 H \tag{2-3}$$

Eliminating u_1 between Eqs. (2-1) and (2-3) and $P_1 - P_2$ between Eqs. (2-1) and (2-2) yields

$$\frac{1}{2}\left[1 - \left(\frac{H}{H + \delta}\right)^2\right]\rho_o u_2^2 = (\rho_w - \rho_o)\, g\delta \tag{2-4}$$

At this point it is convenient to introduce the definition of the Froude number:

$$F = \frac{\rho_o u_2^2}{(\rho_w - \rho_o)\, gH} \tag{2-5}$$

Introducing this definition into Eq. (2-4) and rearranging terms results in a quadratic relationship between the wave amplitude δ (normalized by the organic-liquid-layer head H) and the Froude number; namely

$$\left(\frac{\delta}{H}\right)^2 + \left(2 - \frac{1}{2}F\right)\frac{\delta}{H} - (F - 1) = 0 \tag{2-6}$$

Solving this expression explicitly for δ/H gives the sought result

$$\frac{\delta}{H} = \left[\left(1 - \frac{1}{4} F\right)^2 + F - 1\right]^{1/2} - \left(1 - \frac{1}{4} F\right) \tag{2-7}$$

The above equation suggests that a wave will form only when $F \geq 1.0$. Thus we come to the tentative conclusion that a measurable depth of organic fuel will be left behind when the flow (pumping) process is over, providing that

$$F = \frac{\rho_o u_2^2}{(\rho_w - \rho_o)\ gH} \geq 1.0 \tag{2-8}$$

Early in the interim-stabilization-pumping process the flow from a local sludge depression over a local sludge weir (ridge) will be controlled by the salt well pumping rate. In this case the velocity u_2 must be estimated from the known pumping rate and assumed organic layer depth H and sludge-ridge width. Late in the stabilization process, however, when H is small, the flow over a sludge ridge will be limited by the ridge itself. The average discharge velocity for flow over a sharp-crested ridge (weir) is (Streeter, 1958)

$$u_2 = 0.59\,(gH)^{1/2} \tag{2-9}$$

The appropriate Froude number for weir-controlled flow is then, from Eqs. (2-5) and (2-9),

$$F = \frac{0.348\ \rho_o}{\rho_w - \rho_o}\ , \tag{2-10}$$

which, interestingly enough, is only a function of the water-to-organic density ratio. Thus the condition for the appearance of floating residual organic layers at the end of the tank pumping process is

$$\frac{\rho_o}{\rho_w} > 0.742 \tag{2-11}$$

Unfortunately, this criterion is satisfied for the waste tank application, as the ratio ρ_o/ρ_w falls within the range 0.76-0.83.

For the kerosene/water liquid pair employed in our weir flow experiments (ρ_o/ρ_w = 0.8), the Froude number F = 1.39. Inserting this value into

Eq. (2-7) we predict a wave amplitude or, equivalently, a residual organic layer thickness δ that is 25 percent of the organic-layer-liquid head; that is

$$\frac{\delta}{H} = 0.25 \tag{2-12}$$

This theoretical result compares reasonably well with the kerosene/water weir-controlled flow experiments. However, additional experiments are needed, including experiments in which the ratio of the densities of the two liquids are varied, before it can be concluded that the theory is entirely satisfactory.

Figure 2-1 Schematic of experimental apparatus for observing wave disturbances and water entrainment during weir flow of floating organic layer on water.

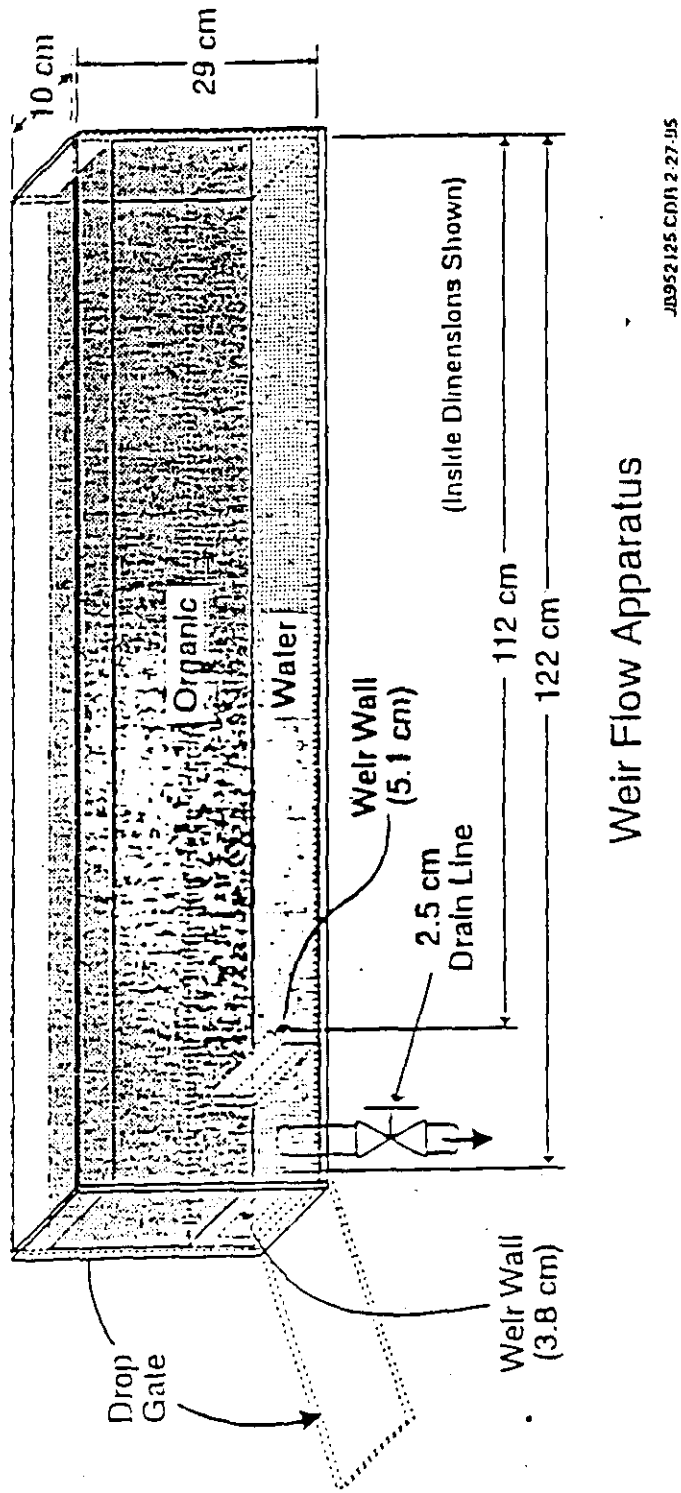

Figure 2-2 Model sketch of stationary, broad crested water wave behind weir.

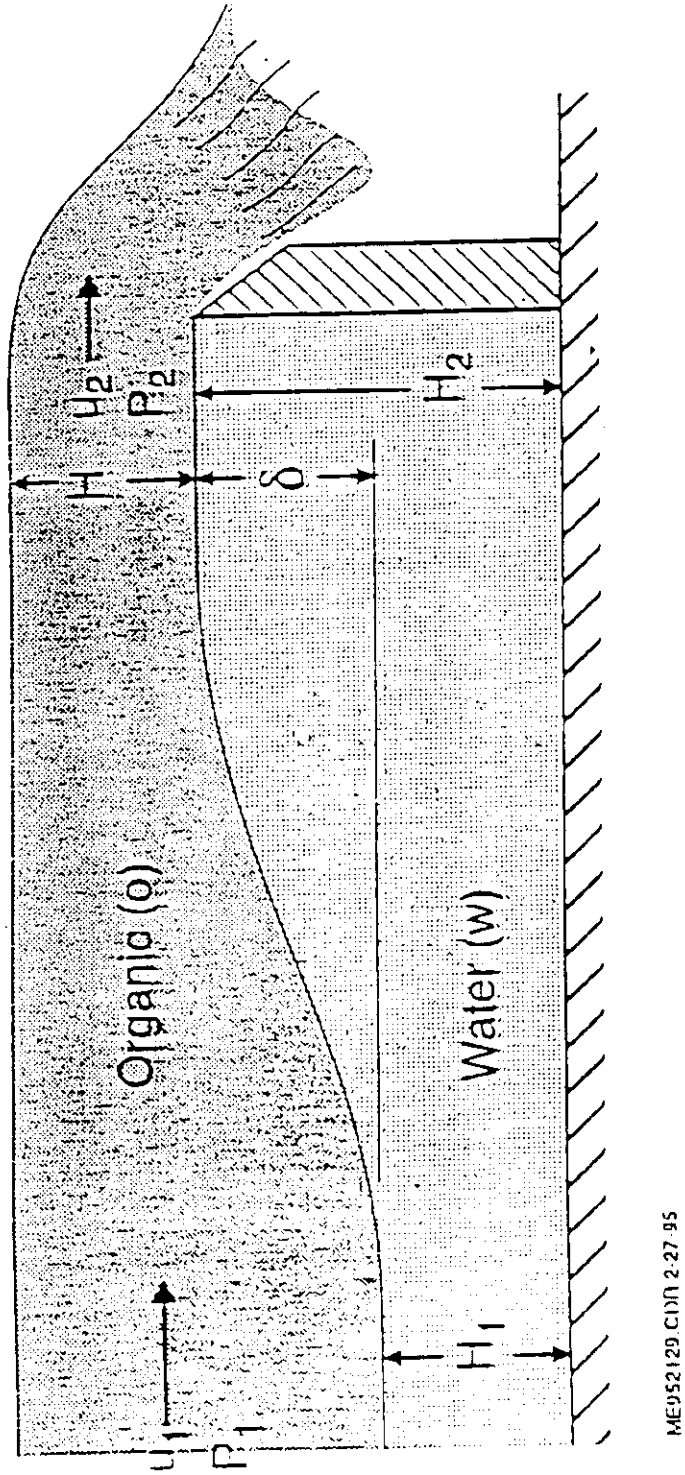

3.0 IGNITABILITY OF RESIDUAL ORGANIC MATERIAL

Liquid organic materials such as those present in C-103 can only be made to burn with great difficulty when the initial liquid temperature is well below the flash point. The question posed here is the required initiating source necessary to cause ignition of an initially cool organic liquid layer or organic liquid embedded in sludge, where "cool" means many tens of degrees below the flashpoint. To put this in perspective, the current C-103 liquid layer is presently about 80°C or more below its flashpoint of nearly 120°C.

Essential background is that local heating of a liquid layer induces liquid convection due to changes in the surface tension with temperature. Strong convective flows at and near the liquid surface carry heat away from the source (assumed at or above the liquid surface), losing heat by convection and radiation to the atmosphere above. The liquid which flows away from the source is continually replaced by a submerged current of cooler liquid. Therefore, bulk heating of an organic layer of large extent is incredible for C-103 because of the large heat losses. Local heating must be at least able to bring the local surface to a temperature above the flashpoint, so that ignition can locally occur. Furthermore, the ignited region must be large enough to cause flame spreading. These aspects of ignitability are discussed below.

When liquid organic is embedded in sludge, this convective heat removal mechanism is not effective so ignition by local heating is certainly easier. However, ignition is hindered or prevented by the presence of water in sludge as discussed below.

3.1 Organic Liquid Pools

3.1.1 Issue and summary - The conditions for ignition of organic liquid pools, as residual layers atop either sludge or water, have been investigated experimentally and analytically. Ignition of a pool requires that an energy source locally heat the liquid to a temperature above its flash point and ignite the vapors, and that the size of this locally heated region be large enough to sustain combustion, i.e., prevent flame extinction. Since either flame extinction or flame spreading will occur, depending on the region size, the latter condition is equivalent to stating that the energy source must locally heat and ignite a region of sufficient size to allow flame spreading on the remaining cool pool liquid.

Only a few scenarios exhibit the conditions for ignition of a cool pool:

(1) Heating and ignition of a confined region. A region of the pool must be confined to prevent convective heat losses to the remaining liquid, it must be bulk heated to at least the liquid flash point to be ignited, and the radiant heat from this region must be sufficient to allow flame spread to the neighboring pool area. This latter condition implies that the confined region must be sufficiently large that its radiant heat loss causes ignition nearby, an unlikely event unless the barrier responsible for fuel layer confinement is removed.

(2) Sustained burning of a large object. A burning object, producing radiant energy equivalent to the burning confined region described above, would also be sufficient to cause ignition of the adjacent pool. The burning object is thus considered to have the same characteristic dimension as the burning confined region.

(3) Spark initiation. This differs from the previous initiators by timescale. A spark deposits a large amount of power in a local area over a brief period of time, whereas the other initiators are more sustained.

Our investigation, described in the following subsections, has led to the following conclusions pertinent to C-103 organic material:

(1) Organic fuel layers less than about 2.0 mm in depth will completely retreat away from an energy source and hence will not support a propagating flame.

(2) Centrally located standing (or wick-stabilized) flames will not spread on pools covered by organic layers of depths greater than 2.0 mm unless the diameter of the flame exceeds about 15 cm. If the flame is located at the edge of the pool it will not spread unless its diameter exceeds about 10 cm.

(3) A conservative initiator energy criterion for confined regions from which flame spreading is possible now follows from Conclusion 2 above; namely that the region must be 10 cm in diameter and 2.0 mm in depth and uniformly heated to its flashpoint. The result is that 3 kJ is a reasonable bounding minimum energy for such a layer. Actual initiator energies are somewhat larger due to heat losses from the layer.

(4) It also follows from Conclusion 2 that a floating burning object must be at least 10 cm in diameter to cause flame spreading.

(5) A spark source initiator must be very large and therefore any spark source other than lightning may be a priori ruled out.

3.1.2 Critical organic layer depth for flame extinction - It is appropriate to begin the subject of flame spreading on unconfined organic liquid layers by noting that below a critical layer depth, δ_{cr}, ignition of the layer is impossible. It follows, of course, that flame spreading will not occur if the layer depth is less than δ_{cr}. Our own observations (see below) as well as those of others (see, e.g., Ross, 1994) show that the depth of the layer near the heat source (ignitor or flame) is less than at regions far from the source. The heat source causes a local rise in temperature of the free surface which, owing to the effect of surface tension, results in a net surface flow away from the source and a corresponding depression of the liquid

surface. If the liquid layer far from the source is thin to begin with then its thickness in the vicinity of the source decreases to practically zero and "dry" spots (fuel-free regions) form below the source. In the case of a standing flame on a thin organic layer this flow isolates the flame from the surrounding organic fuel and the flame is ultimately extinguished.

An approximate relationship for the extinction depth δ_{cr} is obtained by postulating that a dry spot will form beneath a standing flame when the thermocapillary force at the edge of a liquid fuel layer that has withdrawn from the flame is equal to the hydrostatic force that tends to drive the liquid fuel back beneath the flame. The temperature at the edge of the fuel layer must at least be equal to the flash point temperature, T_{fp}, of the fuel material. The temperature at the surface of the liquid layer far from the flame must be equal to the ambient temperature T_∞. Thus the thermocapillary force acting along the surface of the liquid layer and directed away from the flame is

$$F_\sigma = \sigma' \, (T_{fp} - T_\infty) \, W \tag{3-1}$$

where W is the width of the layer and σ' is the absolute value of the variation of surface tension with temperature for the organic liquid material, namely $|d\sigma/dT|$. The quantity σ' is assumed to be a known constant. The hydrostatic force that is directed from the liquid to the dry spot beneath the flame is

$$F_{hy} = \frac{1}{2} \rho g \delta^2 W \tag{3-2}$$

where ρ and δ are the density and depth of the liquid organic material, respectively, and g is the gravitational constant. By forming the equality $F_\sigma = F_{hy}$ and solving the result for δ we obtain the extinction depth

$$\delta_{cr} = \left[\frac{2\sigma' (T_{fp} - T_\infty)}{\rho \, g} \right]^{1/2} \tag{3-3}$$

This expression can also be obtained from the surface deformation theory reported by Torrance and Mahajan (1975) for a liquid layer subject to a concentrated heat source, although with a slightly different numerical coefficient of $(3/2)^{1/2}$. The flame spreading experiments of Mackinven et al. (1970) provide convincing evidence that flame spread will not occur on layers of n-decane thinner than 1.5 mm. In their experiments T_∞ = 23.0°C and, since, T_{fp} = 46°C for n-decane, we estimate from Eq. (3-3) that δ_{cr} = 0.79 mm (using σ' = 9.56 x 10^{-5} N m^{-1} K^{-1} and ρ = 720 kg m^{-3} at 34°C). Thus in order to bring Eq. (3-3) in line with the experimental result δ_{cr} = 1.5 mm an increase in the

numerical coefficient of about a factor of 2.0 is required. Thus Eq. (3-3) for the flame extinction depth becomes

$$\delta_{cr} = 2.8 \left(\frac{\sigma' (T_{fp} - T_\infty)}{\rho_g} \right)^{1/2} \tag{3-4}$$

The flash point of dodecane is T_{fp} = 74°C and using T_∞ = 20°C, along with the pertinent physical properties $\sigma' = 9.04 \times 10^{-5}$ N m^{-1} K^{-1}, ρ = 730 kg m^{-3}, we predict that flames will not spread on dodecane layers of depths less than δ_{cr} = 2.3 mm. A similar value of the extinction depth is predicted for the C-103 organic liquid layer ($\sigma' = 7 \times 10^{-5}$ N m^{-1} K^{-1}, $\rho = 10^3$ kg m^{-3}, $T_{fp} - T_\infty$ = 80°C). We shall see below that this prediction for the flame extinction depth is in good agreement with our experimental results on spreading (extinction) of flames on layers of dodecane.

3.1.3 Experiments on the initiation of flame spreading on an organic fuel layer - The pool convection apparatus employed in previous experiments on ignition limits (FAI Report, 1994) has been used to explore the onset of flame spread on a layer of liquid fuel. Specifically, a series of tests has been performed to investigate whether a small initially confined fire will be sustained and propagate once it is no longer confined. Steel rings with diameters ranging from 5 cm to 19 cm were used to isolate a portion of a dodecane layer contained in a larger 59 cm diameter pan, as illustrated in Fig. 3-1. The confined layer was ignited by prolonged exposure to an oxyacetylene torch. For the larger ring sizes, it was expedient to use several smaller concentric rings to "build up" the burning area by igniting the smallest contained area first, and then removing the rings from smallest to largest. Once the fire was well-established (say, after burning vigorously for 5 to 10 seconds), the final ring barrier was removed. Dodecane layers ranged between one and six millimeters thick, and in each case, the initial fuel temperature was about 20°C (roughly 50°C below its flashpoint of 74°C). Tests were run both with and without a water sublayer, and the rings were either concentric to the pan or spaced 3 cm from the side of the pan.

The rings were constructed of thin steel sheets and therefore do not represent a significant resistance to radial heat transport from the organic beneath the flame to the adjacent organic outside the ring. Moreover, at incipient flame spread conditions obtained with the larger rings the fire burns for some time (see below) before either flame spreading or quenching takes place and the fire "forgets" its initial confined state.

Tables 3-1 and 3-2 summarize the experimental conditions and results for centrally located flames and flames near the pan wall, respectively. Sustained burning and propagation (i.e., spreading of the fire to the pan side, leading to burning of the entire pool surface) did not occur for concentrically located fires of 15 cm diameter or less. Fires positioned near the pan side did not spread for diameters of 10 cm or less. For these non-propagating cases the fire did expand somewhat (in the form of a blue flame very close to the surface of the fuel and surrounding the initially well developed flame), burned briefly, and went out. As the fire disappeared, a low blue flame flickered around the circular area where the fire had been.

Table 3-1: Results of Pool Fire Spreading Tests, Fire Centered in Pan

est ID #	Fuel Thickness (mm)	Water Thickness (mm)	Ring Diameter (cm)	Burn Duration (sec)
15	2.1	0	13	Dryout
16	2.8	0	15	Dryout
19	3.3	0	15	12
10	5.0	0	15	10
2	2.1	5.2	6	2
1	1.3	5.3	11	6
3	2.1	5.1	11	5
4	3.0	5.1	11	6
5	3.7	5.0	11	7
6	4.2	5.1	11	6
7	5.1	5.0	11	5
8	5.1	5.0	13	8
22	2.1	5.3	15	11
23	2.7	5.3	15	14
33	3.9	4.7	15	16
36	4.6	4.6	15	13
9	5.0	5.0	15	10
25	1.7	4.6	17	9
31	2.6	4.8	17	24
24	2.9	5.3	17	Spread
26	3.4	4.8	17	19
39	3.5	4.3	17	26
32	4.0	4.7	17	Spread
38	4.5	4.6	17	26
30	2.0	4.5	19	16
46	2.2	4.1	19	16
47	2.3	4.3	19	20
29	2.5	4.8	19	Spread
27	3.3	4.8	19	Spread
28	4.5	4.7	19	Spread

Table 3-2: Results of Pool Fire Spreading Tests, Fire Near Pan Wall

est ID #	Fuel Thickness (mm)	Water Thickness (mm)	Ring Diameter (cm)	Burn Duration (sec)
12	5.0	0	8	3
17	3.8	0	10	5
13	5.0	0	10	8
18	3.8	0	13	Spread
14	5.0	0	13	Spread
11	5.0	0	15	Spread
34	3.9	4.7	11	7
35	4.6	4.7	11	7
50	2.0	4.2	13	8
48	2.4	4.3	13	7
41	3.1	4.2	13	9
40	3.5	4.3	13	10
20	3.6	8.6	13	10
37	4.5	4.7	13	Spread
51	2.0	4.2	15	42
49	2.1	4.2	15	Spread
45	2.3	4.1	15	Spread
44	2.7	4.1	15	Spread
42	3.1	4.2	15	Spread
21	3.6	8.6	15	Spread
54	1.6	4.1	17	20
53	1.7	4.2	17	Spread
52	1.9	4.2	17	Spread
55	1.6	4.1	19	Spread

The time to quench (i.e., no longer a visible flame) increased with increasing ring diameter until a sustainable (spreadable) flame size was reached. Clearly, fires near the sidewall were more easily sustained. In general, the burn duration did not depend strongly on the fuel layer thickness.

For layers less than 2 or 3 mm thick, a noticeable surface depression or "hydraulic jump" was observed beneath the burning area and remained for several seconds after quenching. The fire appeared to "push away" the bulk fuel layer and feed off of the remaining fuel microlayer until it was either fuel-starved or overwhelmed by heat losses. In the absence of a water sublayer, the thin burning region broke up into tiny puddles or droplets, which continued to burn on the substrate surface (thus the "dryout" designation in Table 3-1). Flame propagation from a centrally located flame was not observed on layers less than about 2.3 mm thick, in excellent agreement with the prediction δ_{cr} = 2.3 mm obtained from Eq. (3-4). Flame propagation was observed to occur from a flame initially located near the pan wall when the organic layer depth was as thin as 1.6 mm. However such flames were very difficult to establish and were not capable of propagating across the pan (pool). We will return to the issue of thin-fuel-layer ignition later on in this section.

Liquid temperatures were measured for one test (#23 in Table 3-1), mainly to confirm that the edge of the fuel layer remained close to the ambient temperature prior to removal of the final ring barrier. Figure 3-2 illustrates the surface temperature histories for the center of the layer (i.e., the center of the ring fire) and for three roughly equally spaced locations around the edge of the layer. Three concentric rings were initially placed in the liquid, and torch-heating of the center ring began at about 15 seconds. A weak flame was sustained once the liquid was heated to near its flashpoint (74°C), but premature removal of the center ring extinguished the flame at about 65 seconds. (Also, one of the "edge" thermocouples fell out of the pan at about this time.) The ring was replaced and the torch was reapplied, eventually leading to a vigorous flame and a surface temperature near 100°C. (Note the presence of a water sublayer may moderate surface temperatures for thin organic layers.) The small ring was removed again at about 215 seconds, after which the temperature dipped briefly while the (slightly larger) fire established itself. The second ring was removed at about 255 seconds, again resulting in a brief drop in surface temperature. The last (15 cm diameter) ring was removed at about 290 seconds, by which time the edge temperature had only risen a few degrees. (Thus the scale of the apparatus was appropriate for this test.) The center surface temperature dropped to the dodecane flashpoint in about 14 seconds, which coincided with flame quenching, and the edge temperature jumped about 10°C before gradually cooling off. Temperature spikes which occurred when each ring was removed may have been caused by sudden radial movement of the unconfined fluid, briefly exposing the thermocouple tip to hotter gas temperatures. Lastly, the scale of the apparatus is conservative in that a larger pool would tend to decrease the burn duration and make flame spreading more difficult.

The experimental data together with Eq. (3-4) allows us to construct a flame size (diameter D) versus organic fuel-layer thickness (δ) map showing the region in which flame spreading is impossible. Such a map for a centrally located flame is shown in Fig. 3-3. Also shown in the figure are two dashed curves which are the results of a theoretical analysis directed at predicting

the conditions for the onset of spreading of a pre-existing steady flame. The details of the analysis are presented in Appendix FAI/95-17A. Flame spreading is predicted to occur in the D versus δ spaces that lie above the theoretical curves. The parameter η that distinguishes one theoretical spreading threshold curve from the other is the fraction of the total flame heat release rate that is radiated away. Thus η is essentially a flame radiation efficiency parameter. Increasing the value of η increases the amount of heat transferred forward of the flame to raise the fuel-layer-surface temperature toward the flash point. Thus flames with high values of η can spread more easily than flames with relatively small values of η. Unlike the theoretical curves for incipient flame spreading, the experimentally determined boundary of the flame spreading regime (horizontal solid line in Fig. 3-3) does not show a dependence on the fuel layer thickness. This fact and the fact that the experimental data points for the onset of spreading lie between the two theoretical curves suggest that the surface emissive power of small flames must increase with flame size. From what is known about radiation from fires (De Ris, 1979) this is not an unreasonable conclusion. It would seem then that the model presented in Appendix FAI/95-17A could well be improved by accounting for an increased radiation intensity with increasing flame size.

A flame spreading map for standing flames located close to the edge of an organic layer pool is presented in Fig. 3-4. Note that for thin organic layers (say, less than 2 mm thick) it was very difficult to ignite the dodecane contained within the smallest (5 cm diameter) concentric ring. Application of the torch jet caused the organic to pull away from the hottest zone, leaving a very thin film of fuel on top of water. For these cases ignition was accomplished by focusing the torch at the capillary region next to the ring wall. Thus the ring acted as a wick to draw fuel to the hot area, and the ring itself was likely locally heated above the dodecane flashpoint. For the thinnest layers even this technique did not suffice. Rather, a 1.5 cm diameter open-sided "ring" of aluminum foil (i.e. a "C" shape) was placed inside the 5 cm steel ring and near the ring wall. The torch jet was focused on the capillary liquid enclosed by the foil. The foil served as a wick, and the opening in the foil ring allowed liquid flow to carry heat to the surrounding liquid. Once a flame had started to spread along the (steel) ring wall, the foil was removed, but the torch was left in place until the fire was established within the 5 cm ring. Fires established in this way did not survive at the pool center, but for two cases near the pool edge such fires did attach to the pan wall (where capillary forces are responsible for a thick accumulation of fuel) and spread slowly along the pan wall. To emphasize that these "sustained" fires were extremely difficult to ignite, a "half-solid triangle" symbol is employed in Fig. 3-4.

The implications of the experimental results presented in Figs. 3-3 and 3-4 are significant with respect to the potential for igniting a propagable flame on a layer of dodecane. For example, the lateral scale D of an initially combustible fuel vapor/air mixture above a layer of dodecane must exceed 10.0 cm before the ignition of this mixture will result in a spreadable flame. Wick-stabilized flames are not likely to be this large and, therefore, are incapable of spreading on room temperature dodecane. In addition, realistic spark energies expected from discharges of electrically conducting objects are not high enough to produce flammable fuel vapor/air mixtures of this size (see next section). The results displayed in Figs. 3-3 and 3-4 are directly applicable to the organic layer in Tank C-103.

3.1.4 Theory of the spark source initiator - In this section we examine the thermal response of the surface of a liquid organic layer to an electric spark discharged across a small air gap located a distance H above the liquid surface. Figure 3-5 illustrates the situation. It is assumed that the instantaneous rate of energy emitted from the spark, $\dot{E}$ in units of Joules (J) per second, is transmitted to the underlying liquid surface by thermal radiation. This assumption is reasonable in view of the fact that the local gas temperatures generated by a spark discharge may exceed 10,000 K. Krauss and Krempl (1963) measured a peak gas temperature of 50,000 K in a 1.0 J spark of discharge duration 2.0 μs. Spark gaps typically vary between roughly 0.1 and 2.0 mm. Thus on the scale of the liquid organic surface the spark may be regarded as a near-point source of energy.

To begin with we are interested in determining the radiant heat transfer between a pair of surface elements dA_s and dA that see each other, where dA_s is an element on the "surface" of the spark discharge and dA is an element on the surface of the liquid organic (see Fig. 3-5). According to Lambert's cosine law, the increment of energy radiated per unit time, dQ, from dA_s and intercepted by dA is

$$dQ = \frac{q_s}{\pi R^2} \cos \theta_s \, dA_s \cos\theta \, dA \tag{3-5}$$

where q_s is the radiant energy emitted per unit area per unit time from the spark. The elements dA_s and dA are separated by the distance R along a straight line which makes an angle θ_s with the normal to dA_s and an angle θ with the normal to dA.

Now the local instantaneous heat flux q impinging on the liquid surface at a distance R from the spark is

$$q = \frac{dQ}{\cos\theta \, dA} = \frac{q_s}{\pi R^2} \int \cos \theta_s \, dA_s \tag{3-6}$$

where the integral $\int \cos \theta_s \, dA_s$ is the projected area of the spark as seen from the liquid surface at a distance R. Since the spark is a near point source this projected area is nearly πr_s^2, where r_s is the diameter of the spark discharge. Thus

$$q = \frac{q_s \, \pi r_s^2}{\pi \, R^2} \tag{3-7}$$

The total instantaneous energy emission rate from the spark $\dot{E}$ can be related to the instantaneous radiant energy flux emitted from the spark by the formula

$$\dot{E} = 4\pi r_s^2 q_s \tag{3-8}$$

Thus from Eqs. (3-7) and (3-8) we have the following formula for the local heat flux produced at the liquid surface during the spark discharge:

$$q = \frac{\dot{E}}{4\pi R^2} = \frac{\dot{E}}{4\pi (H^2 + r^2)} \tag{3-9}$$

where r is the distance from the spark measured along the liquid surface (see Fig. 3-5).

The rate of energy emitted $\dot{E}$ from a spark discharge is not a constant but, instead, varies with time. The energy emission rate $\dot{E}(t)$ is not a quantity which has been measured but, fortunately, the spark current $I_s(t)$ has been measured and $\dot{E}(t)$ can be related to $I_s(t)$. The relationship between the air gap resistance and the current flowing through the gap during a capacitive spark discharge has been determined from laboratory data. Eckhoff (1991) recommends the following empirical correlation of all the data:

$$R_s = 40\ L_s\ I_s^{3/2} \tag{3-10}$$

where R_s is the gap resistance in ohms, I_s is the current in amps, and L_s is the spark-gap width in millimeters. Actually the exponent on I_s reported by Eckhoff is -1.47 rather than -3/2. The latter value, however, is more convenient to work with mathematically and we give up little in the way of accuracy to gain this convenience.

The rate of energy emitted from the spark can be related to the spark gap current I_s and voltage V_s by using the equation

$$\dot{E}(t) = I_s V_s \tag{3-11}$$

From Ohm's law we have the additional equation

$$V_s = R_s I_s \tag{3-12}$$

Combining Eqs. (3-10) to (3-12) yields $\dot{E}$ solely as a function of I_s and L_s:

$$\dot{E}(t) = 40\ L_s\ I_s(t)^{1/2} \tag{3-13}$$

From Eqs. (3-9) and (3-13) the instantaneous heat flux impinging on the surface of the liquid organic is

$$q(t) = \frac{10\ L_s\ I_s(t)^{1/2}}{\pi(H^2 + r^2)} \tag{3-14}$$

In principal one can now proceed to solve for the temperature profile history in, say, cylindrical r,z space within the organic liquid region subject to the surface heat flux given by Eq. (3-14). The solution to this problem is given in Appendix FAI/95-17B of this report, where it is shown that as long as the duration t of the spark discharge transient is short enough so that the inequality

$$\frac{\alpha t}{H^2} \ll 1.0 \tag{3-15}$$

is obeyed the radial spread of heat (in the r-direction) within the liquid organic can be ignored. In Eq. (3-15) α is the thermal diffusivity of the liquid material, which is typically of the order 10^{-7} m^2 s^{-1}. For a 100 μs spark discharge located 5 mm above the liquid surface the left-hand side of Eq. (3-15) is 4×10^{-7}. Indeed during the time period of interest it is only necessary to consider one-dimensional conduction in the direction perpendicular to the surface of the liquid.

The short time solution for the surface temperature of a semi-infinite region of liquid organic initially at temperature T_o and subject to the surface heat flux given by Eq. (3-14) is (see Eq. G-27 in Appendix FAI/95-17B)

$$T(r,0,t) - T_o = \frac{10\ L_s \alpha^{1/2}}{\pi^{3/2}\ k(H^2 + r^2)} \int_0^t \left[\frac{I_s(t-\tau)}{\tau}\right]^{1/2} d\tau \tag{3-16}$$

In order to evaluate the above equation, we will assume the following rather simple spark current versus time "ramp function".

$$I_s(t) = \begin{cases} I_{max} t/t_{max} & 0 < t < t_{max} \\ 0 & t_{max} < t < \infty \end{cases} \tag{3-17}$$

Note that current flows in the spark gap at a linear rate with time for time t_{max}. At time t_{max} the current achieves its maximum value I_{max} and the current suddenly stops. The maximum temperature, T_{max}, of the liquid surface (z = 0)

occurs at t_{max} and it is obtained by inserting Eq. (3-17) into Eq. (3-16) and integrating the result from t = 0 to t = t_{max}:

$$T(r,0,t_{max}) - T_o = \frac{10\ L_s \alpha^{1/2}}{\pi^{3/2} k (H^2 + r^2)} \left(\frac{I_{max}}{t_{max}}\right)^{1/2} \int_0^{t_{max}} \left(\frac{t_{max} - \tau}{\tau}\right)^{1/2} d\tau = \frac{5\ L_s (\alpha}{\pi^{1/2}\ k} \tag{3-18}$$

Usually L_s and I_{max} are not known for a given spark discharge. Thus we choose to replace these quantities with the total energy E emitted by the spark. Referring to Eq. (3-13), the spark energy is

$$E = 40\ L_s \int_0^{t_{max}} I_s(t)^{1/2}\ dt \tag{3-19}$$

By substituting Eq. (3-17) into Eq. (3-19), we get

$$E = \frac{80}{3}\ L_s (I_{max} t_{max})^{1/2}\ t_{max}^{1/2} \tag{3-20}$$

Finally, eliminating $L_s(I_{max}\ t_{max})^{1/2}$ between Eqs. (3-18) and (3-20) gives the desired result

$$T(r,0,t_{max}) - T_o = 0.106\ \frac{E(\alpha/t_{max})^{1/2}}{k(H^2 + r^2)} \tag{3-21}$$

It is important to note that while the above equation was derived for a specific spark current versus time function $I_s(t)$, the result for T_{max} is not too sensitive to the assumed functional form of $I_s(t)$. For example, suppose we chose the following sine function to represent the spark current pulse:

$$I_s(t) = \begin{cases} I_{max} \sin\left(\pi\ \dfrac{t}{t_{max}}\right) & 0 < t < t_{max} \\ 0 & t_{max} < t < \infty \end{cases} \tag{3-22}$$

Omitting the integrations, the result is Eq. (3-21) with a numerical coefficient of 0.077. Had we chosen the step function current transient

$$I_s(t) = \begin{cases} I_{max} & 0 < t < t_{max} \\ 0 & t_{max} < t < \infty \end{cases} \tag{3-23}$$

we would recover Eq. (3-21) with a numerical coefficient 0.09.

As an example of the use of Eq. (3-21), we consider an organic layer having physical properties similar to dodecane ($k = 0.15\ W\ m^{-1}\ K^{-1}$, $\alpha = 8.7 \times 10^{-8}\ m^2\ s^{-1}$). A hypothetical situation may involve a small metal container with accumulated charge accidentally falling into a waste tank and suddenly releasing its charge to an "earthed object" located just above the surface of the organic covered waste, say at $H = 10.0$ mm. The maximum theoretical spark energy of such a container is about $E \approx 10.0$ mJ (Eckhoff, 1991). A typical spark duration is roughly $t_{max} = 10.0\ \mu s$. By substituting these parameter values into Eq. (3-21) we predict a maximum temperature rise at the surface of the organic liquid vertically below the spark of $T(0,0,t_{max}) - T_o = 6.5°C$. This is well below the temperature rise of 80°C required to reach the flash point of the organic liquid. Of course, by postulating larger spark energies E and/or smaller spark discharge heights H predicted liquid surface temperatures $T(0,0,t_{max})$ may well exceed the flash point temperature. However, merely raising the temperature of the segment of the surface of the liquid located vertically below the spark is not likely to result in a large-scale pool fire. We know from the previously reported theoretical and experimental work (see Section 3.1.3) that the size of a standing flame must exceed 10 cm in diameter before it can spread by overcoming the heat drained away by radial thermocapillary and thermogravitational convection in the surrounding organic liquid. Thus the spark must produce a flammable fuel vapor/air mixture of this size before it can be regarded as a hazardous ignition source.

By solving Eq. (3-21) for E as a function of $T(r,0,t_{max})$ we can determine the spark energy required to raise the temperature of the organic liquid surface above the flash point temperature over a circular region of radius r (measured from the vertical line that passes through the spark). Referring to our previous example with $H = 5.0$ mm, $t_{max} = 10\ \mu s$, we find that E must exceed 2.0 J (0.2 MW spark power) in order to produce a 10-cm diameter, potentially flammable zone. This energy is well in excess of the maximum theoretical spark energies expected from discharge of various types of electrically conducting objects that may accidentally enter a waste tank, considering that Eckhoff (1991) estimates that a road tanker (truck) could conceivably produce a static discharge of 0.45 J.

3.2 Organic Liquid in Cracks

3.2.1 Issue and summary - Organic solvent in cracks or channels in a sludge surface are confined to essentially one-dimensional convective flow for heat rejection and therefore a priori we expect that ignition and flame spreading is easier in a narrow channel than in an open pool. Indeed this is demonstrated here by a one-dimensional version of the previously reported thermocapillary convection analysis (FAI, 1994) and by some quantitative and qualitative experiments on convection and flame spreading, respectively. However, propagation of a fire from a narrow channel into an open pool is subject to the same flame size constraints discussed before in Section 3.1.3. On the other hand, fuel in a large pool connected to a burning channel may continuously supply fuel to the channel. These observations may be summarized as follows:

(1) relatively small initiators may possibly start fires in narrow cracks filled with C-103 solvent, and

(2) these fires may continue as fuel from the pool flows back to the cracks, but

(3) fires in cracks or channels cannot propagate into open pool areas unless the characteristic crack size exceeds the pool fire spreading threshold criterion, and

(4) consequence analysis may be used to show conditions when fires in cracks, with therefore limited surface area, could threaten tank integrity, or if this is possible at all.

3.2.2 Experiments on liquid convection in an open channel heated non-uniformly from above - The experimental apparatus which was previously used to study pool convection (FAI, 1994) has been reconfigured to study convection in a shallow channel. Figure 3-6 illustrates the new geometry. The channel was constructed from a flat strip of polycarbonate plastic measuring 1 cm thick x 5 cm wide x 50 cm long. A 6.4 mm (0.25 in.) deep flat-bottomed channel was cut along the centerline on the upper face using a 1.27 cm diameter (0.5 in.) router bit. A small hole was drilled through the channel bottom at one end to allow a thermocouple (TC2) to pass through from below. The positionable thermocouple device used in the pool convection tests was mounted at this end of the channel. Three other TCs were placed in the channel from above. The plastic strip was wrapped in glass wool insulation so that only the channel cut-out was exposed.

The channel assembly was fastened to a wooden block, which in turn was attached to a metal support plate. Positioning screws in the support plate were used to level the channel. Dodecane was then added to the channel until the layer depth was about 3 mm, as determined with the positionable thermocouple. The four TCs were then adjusted so that their tips just contacted the liquid surface midway between the channel walls.

A small radiant heater previously used in the pool convection tests was also used as the heat source for the channel tests. However, a small aluminum foil screen was placed between the heater coil and the target liquid to restrict the effective radiant heat transfer area. A rectangular cutout in the foil screen provided for a 0.5 cm wide heated zone which extended across the 1.27 cm wide channel and which was centered above the positionable thermocouple TC2.

The problem of one-dimensional, combined thermocapillary and thermogravitational convection in an organic liquid-filled channel subject to a local radiant heat source has been solved in closed form and the solution procedure can be found in Appendix FAI/95-17C. In the model as well as in the experiment the heater is placed at one end of the channel (see Figs. 3-6 and C-1). At the heated end of the channel the liquid surface temperature achieves its maximum value T_{max}. The theory yields two pertinent equations for comparison with the experimental results. The first equation is the expression for T_{max}:

$$T_{max} = T_\infty + \frac{3}{4}\left(\frac{q_o x_o^4}{\delta\ k_e}\right)^{1/3} + \left(\frac{q_o x_o}{\delta\ k_e}\right)^{2/3}\left(\frac{3\ \delta\ k_e}{2h}\right)^{1/2} \tag{3-24}$$

where T_∞ is the ambient temperature, q_o is the radiant heat flux transmitted from the heater to the liquid surface, x_o is the axial length of liquid surface over which the heat flux q_o is applied, δ is the thickness of the organic layer, h is the heat transfer coefficient for heat transport from the liquid surface to the ambient air, and k_e is the effective conductivity of the organic liquid material which accounts for both thermocapillary and thermogravitational convection (see Eqs. A-11 or C-2). The second equation of interest gives the liquid-surface temperature profile as a function of distance x measured from the heated end of the channel:

$$T(x) = \begin{cases} T_{max} - \frac{3}{4}\left(\frac{q_o}{\delta\ k_e}\right)^{1/3} x^{4/3} & 0 < x < x_o \\ T_\infty + \left[\left(\frac{q_o x_o}{\delta\ k_e}\right)^{1/3}\left(\frac{3\ \delta\ k_e}{2h}\right)^{1/4} - \frac{1}{2}\left(\frac{2h}{3\ \delta\ k_e}\right)^{1/4}(x - x_o)\right]^2 & x_o < x \end{cases} \tag{3-25}$$

A series of five experiments have been performed using the above-described apparatus. The layer thickness δ ranged from 2.7 to 3.0 mm and the heat flux q_o transmitted from the heater to the liquid layer ranged from 13 to 38 kW/m^2. As mentioned above, the axial length of the heated zone was x_o = 5.0 mm. Test results for the quasi-steady peak surface temperature difference $T_{max} - T_\infty$ are shown in Table 3-3. Also shown are results predicted with Eq. (3-24) using dodecane properties at 30°C (Table 3-4) and effective natural convection heat transfer coefficients h of 15 and 30 W/m^{2}K. Steady-state surface temperatures measured at various points along the channel are presented in Figs. 3-7 through 3-11, including plots of profiles predicted with Eq. (3-25). (The "extra" data in Tests 4 and 5 were obtained by manually translating TC3 along the channel toward the heated zone.) The temperature depression beneath the heater (see Figs. 3-10 and 3-11) may not be an artifact; it is likely due to the cold back flow of organic liquid rising up in this region. Temperature histories for the five tests, shown in Figs. 3-12 through 3-16, indicate that up to 7000 seconds (2 hrs.) were typically

Table 3-3

Summary of Channel Convection Experiments

TEST ID #	1	2	3	4	5
q_o (kW/m^2)	38	13	21	26	14
δ (mm)	2.8	2.9	2.9	3.0	2.7
$T_{max} - T_\infty$ (Experiment)	80	25	40	45	30
$T_{max} - T_\infty$ (Theory, h = 15 W/m^{2}K)	80	34	46	52	38
$T_{max} - T_\infty$ (Theory, h = 30 W/m^{2}K)	57	24	33	37	27

Table 3-4

Dodecane Properties at 30°C

ρ (kg/m^3)	742
c_p (J/kgK)	2210
μ (kg/ms)	1.29×10^{-3}
α (m^2/s)	9.15×10^{-8}
β (K^{-1})	9.4×10^{-4}
σ' (kg/s^{2}K)	9.2×10^{-5}

required for the measured temperatures to "level out" to steady-state conditions. Note that in each test the temperature T_∞ at the cool end of the channel, about 40 cm (16 in.) from the heated zone, remained essentially unchanged at about 20°C.

Experimental measurements are generally bounded by theoretical predictions using a heat transfer coefficient based on combined natural convection and radiation heat transfer to quiescent ambient air of 15 W/m^2K, but the predictions are not overly conservative. Apparently some heat was lost through the insulation and/or strong buoyant gas flow of ambient air was generated by the heater suggesting that a higher effective h may be appropriate. Also, in Test 1, which was the only case where the liquid temperature exceeded its flashpoint of 74°C, a channel fire did not occur despite a brief flash when the heater/screen assembly was removed. The example problem presented at the end of Appendix FAI/95-17C illustrates how difficult it is for an organic-filled crack or channel to dissipate the heater power compared to the heat rejection capability of a liquid pool of organic material.

3.2.3 Experiments on flame spreading in an open channel - Two additional tests were performed using a channel configuration. A simulated "crack" was created by forming kaolin paste to make a rectangular channel about 1.5 cm wide and 30 cm long. This channel was filled with dodecane to a few millimeters depth. One end of the channel was first isolated using a small piece of aluminum as a barrier. Repeated attempts to ignite this confined region (about 1.5 cm x 1.5 cm square) using the oxyacetylene torch were unsuccessful. The barrier was then removed and a small wafer of wood was used to create a wick stabilized flame. This configuration continued to burn (on the wick only) for several minutes before it was intentionally extinguished. This failure to propagate is consistent with the previously discussed channel tests using a radiant heat source (see Section 3.2.2). In those tests, a few tens of centimeters length was sufficient to dissipate more than 30 kW/m^2 radiant heating applied at one end of a 1.3 cm wide channel.

One end of the channel was then reconfigured to form a circular puddle about 6 cm in diameter. A 5 cm diameter steel ring was placed in this end puddle, which was ignited as before for the pool fire spreading tests. Once the fire was established, the ring was removed and the fire remained in the end puddle. Within 3 minutes, the fire had grown in strength and began to move down the channel. After another minute, the flame had reached the far end of the channel. This channel fire burned for several minutes before it was extinguished. Clearly, the channel wall and significant preheating of the organic liquid within the finite channel helped sustain and propagate a much smaller fire than would have survived in the middle of a puddle, much as the pan sidewall did in earlier tests.

3.3 Organic Liquid Embedded in Sludge

3.3.1 Issue and summary - It is anticipated that there is limited potential for organic layer intrusion into C-103 sludge during interim stabilization. Sludge samples retrieved from Tank C-103 (Weiss and Schull, 1986) from two different locations within the tank had mean particle diameters by volume of 11.5 μm and 49.5 μm. The rheological properties of such fine-

particulate/water-saturated sludge mixtures prevent significant penetration of organic liquid material into the sludge. (The rheological properties are dictated mainly by particle size.) Indeed an experiment performed at FAI (1994) demonstrated that a heavy organic liquid was incapable of displacing water from an underlying lighter sludge of water saturated kaolin. The kaolin used in this experiment had a mean particle diameter by volume of 24 μm, which is within the mean particle size range expected for Tank C-103. Simulant ingression experiments conducted by Gerber (1995) with an organic layer atop sludge simulant indicate that no more than 5 weight percent organic may have been entrained into sludge, which is far less than the sludge water content of about 65 weight percent. Gerber used two simulant sludges with 50 percent volume particle diameters of 4.4 μm and 15.78 μm - mean sizes similar to those measured for kaolin and C-103 sludge. Also the chemical compositions of the simulant sludges and organic used in Gerber's experiments were based on the chemical composition data of C-103 sludge and organic samples.

Because of the preponderance of water over solvent, it is intuitively anticipated that such a sludge mixture would be impossible to ignite. Solvent ingression experiments conducted at FAI using tetradecane/TBP organic atop water-saturated kaolin (FAI, 1994) generated sample materials ideal for testing this hypothesis. Samples with nominal TOC contents in excess of those reported by Gerber required prolonged heating with an oxyacetylene torch to establish a self-sustained flame, which subsequently died out within seconds upon removal of the torch, as described in more detail below.

We conclude that C-103 sludge containing more than 20% water will not ignite.

3.3.2 Experiments on ignitability of TBP/NPH in kaolin sludge surrogate - Organic intrusion experiments reported previously (FAI, 1994) have been revisited to evaluate ignitability of embedded organic in aqueous sludge.

Recall that one set of intrusion tests used water/kaolin mixtures of various moisture content as a sludge surrogate. That test series began with an initial sludge mixture of 51% water in kaolin (mass basis). Sludge samples were allowed to air-dry to various reduced moisture levels, assumed to be uniform within a given sample. An organic liquid mixture of 70% TBP and 30% tetradecane (C_{14}) was then added to each sample and left in place for about two weeks. Organic which did not soak into the partially dried sludge was subsequently poured off. The difference between the mass of organic added and the amount poured off was interpreted as the amount absorbed by and embedded in the sludge, assuming that water remained completely immiscible in the organic and neglecting residual organic liquid. (Note that TBP is sparingly soluble in water.) A second test series, using T-plant flowsheets, was similarly performed. Figure 3-17 presents a plot of organic intrusion (wt % organic on a dry basis) versus initial moisture content for each test. The flowsheet data, although showing more scatter than do the kaolin/water data, indicate a similar trend (i.e., curve slope) of increasing organic intrusion with decreasing initial moisture content.

The sludge samples described above have remained intact (in jars) for the past eight months. During that time the kaolin/water/organic samples lost between 1.5 and 1.8 g each, or between 5.3 and 6.6% of the liquid content, due to evaporation and vapor leakage. A control sample of 51% water in kaolin

lost 1.2 g over the same period. It is likely that most of the mass lost was water, particularly since the normal boiling points of C_{14} and TBP are 252°C and 289°C, respectively. In any case, the mass loss can be used to bound the mass of organic in the sludge by assuming that all of the mass lost was water (organic) and calculating the corresponding maximum (minimum) amount of organic remaining. Table 3-5 summarizes the estimated bounds on the embedded organic content in the sludge, both on a dry mass basis and in terms of percentage TOC. Note that the sludge samples were uniform in color (tan) and appearance (moist), and there was no free liquid on the sample surface or in cracks within the (partially consolidated) sludge.

Having characterized the surrogate sludge samples in terms of embedded organic content (assumed to be uniform within the samples), an attempt was made to ignite the sludge. The top portion of each sample (generally a single chunk weighing between 8 and 21 g) was removed from its sample jar and placed on a small glass saucer. (No variations in color or appearance were observed within the samples.) Ignition was attempted using an oxyacetylene torch with a small visible jet flame measuring about 3 mm in diameter and about 2 cm long.

In general, the samples with the most organic (and the least moisture) were the easiest to ignite, but even the sample with 17% TOC (nominal) required some effort (prolonged heating) to establish a self-sustained flame. Even then, the flame self-extinguished after about 15 seconds, and samples with nominal TOC contents of 14, 12, and 8.5% only burned independently for about 5, 3, and 1 second, respectively. With the torch in place, these samples showed visible signs of fuel burning in the vicinity of the torch jet, particularly for higher fuel contents. A self sustained flame could not be established on the samples with 4.5 and 2% TOC, and even with the torch in place there was little if any visual evidence of fuel burning. Samples with 14% TOC and less tended to sputter, ejecting kaolin particles as trapped water was vaporized.

In summary, the samples which sustained burning did so only briefly, consuming only a fraction of the available fuel before self-extinguishing. Re-applying the torch jet allowed the process to repeat itself. Samples which contained more than 20% water did not ignite at all. The presence of water is likely the most important factor in preventing sustained burning of organic in sludge.

Table 3-5

Results of Sludge Burning Tests

Test ID	3	7	6	2	5	4
Initial Conditions						
Kaolin (g)	66.0	67.3	68.5	66.5	65.1	69.5
Water (g)	27.7	22.0	17.2	11.9	7.2	3.6
Organic (g)	2.8	6.0	11.5	16.0	20.0	25.9
Liquid net (g)	30.5	28.0	28.7	27.9	27.2	29.5
After 8 Months						
Mass Lost (g)	1.6	1.7	1.8	1.7	1.8	1.6
Liquid Net (g)	28.9	26.3	26.9	26.2	25.4	27.9
Sample Net (g)	94.8	93.6	95.4	92.7	90.5	97.4
% Kaolin	70	72	72	72	72	71
% Water (max/min)	29/27	23/22	18/16	13/11	8/6	4/2
Organic Content (Wet Basis)						
% Organic (min/max)	1/3	5/6	10/12	15/17	20/22	25/27
% TOC (min/max)	1/2	3/4	6/8	9/11	13/14	16/17
Organic Content (Dry Basis)						
% Organic (min/max)	2/4	6/8	12/15	17/20	21/24	25/28
% TOC (min/max)	1/3	4/5	7.5/9.5	11/13	13/15	16/18
Nominal % TOC	2	4.5	8.5	12	14	17
Ignitability						
Short-Duration Flame	N	N	Y	Y	Y	Y
Burn Duration (sec)	--	--	1	3	5	15

Figure 3-1 Flame spread apparatus.

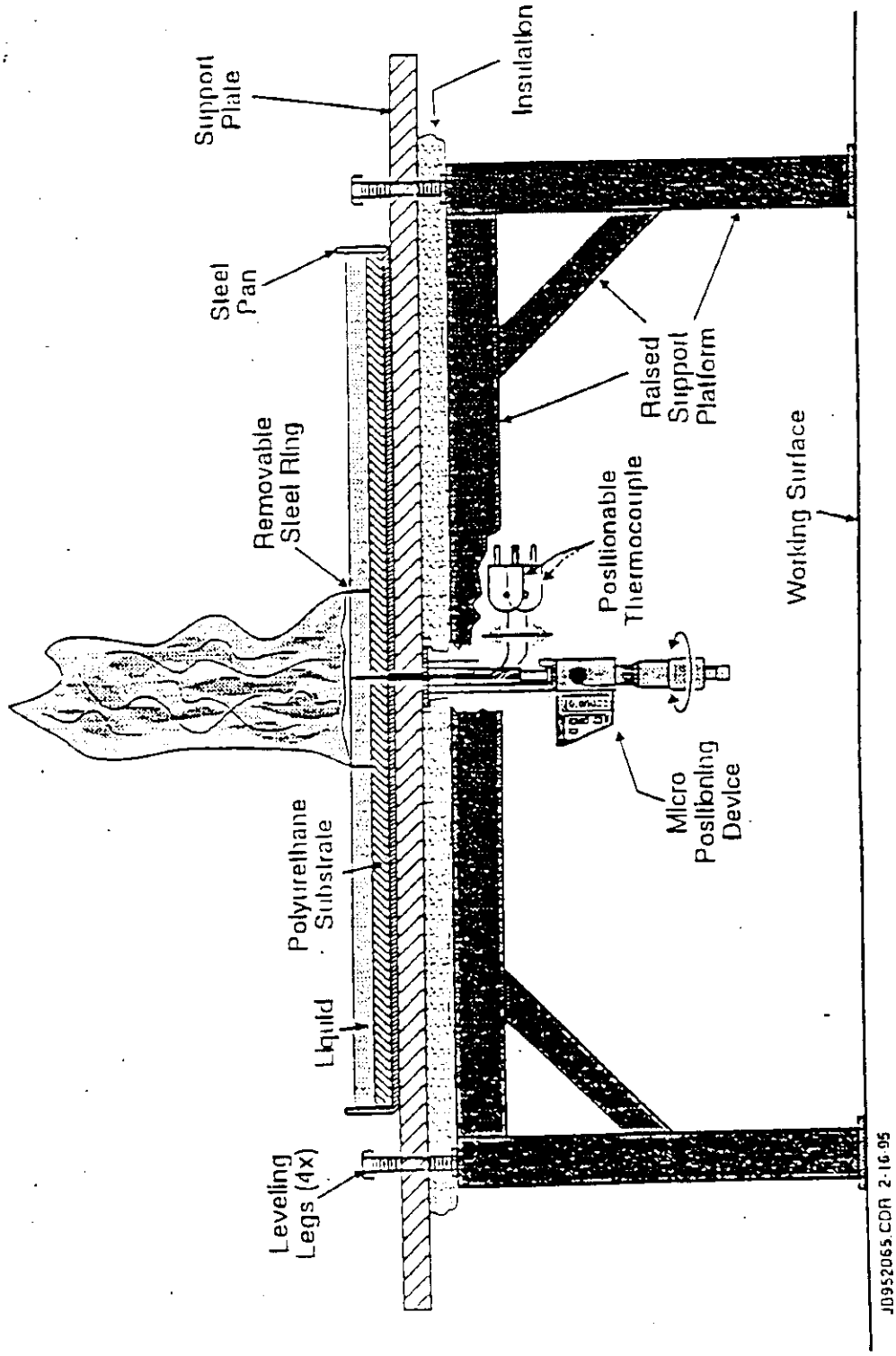

Figure 3-2 Liquid surface temperatures for Test #23.

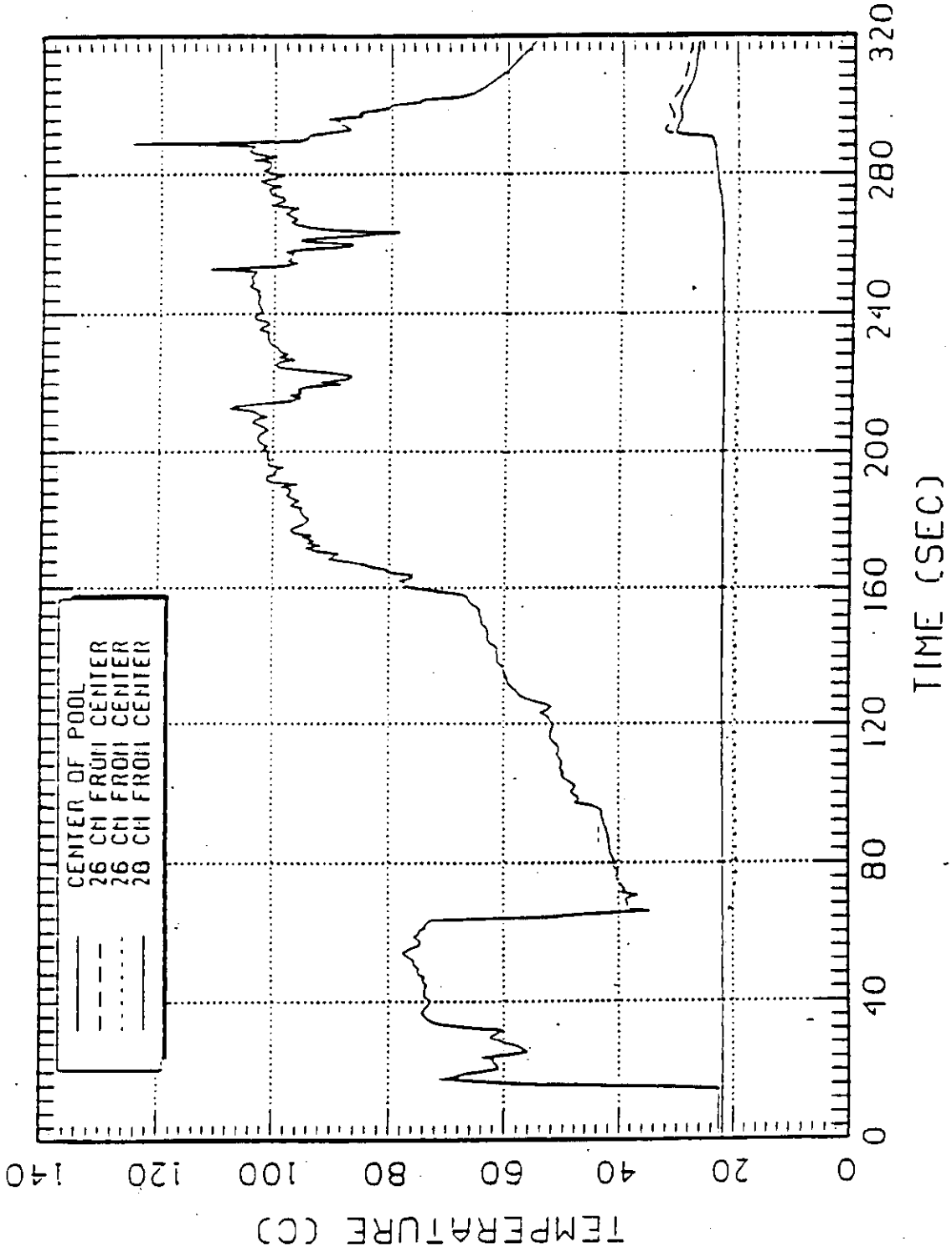

Figure 3-3 Flame diameter versus organic fuel-layer thickness map for dodecane at approximately 20°C, showing the (unshaded) region in which spreading of a centrally-located flame is impossible. The dashed curves represent theoretical results for two flame radiation efficiencies η.

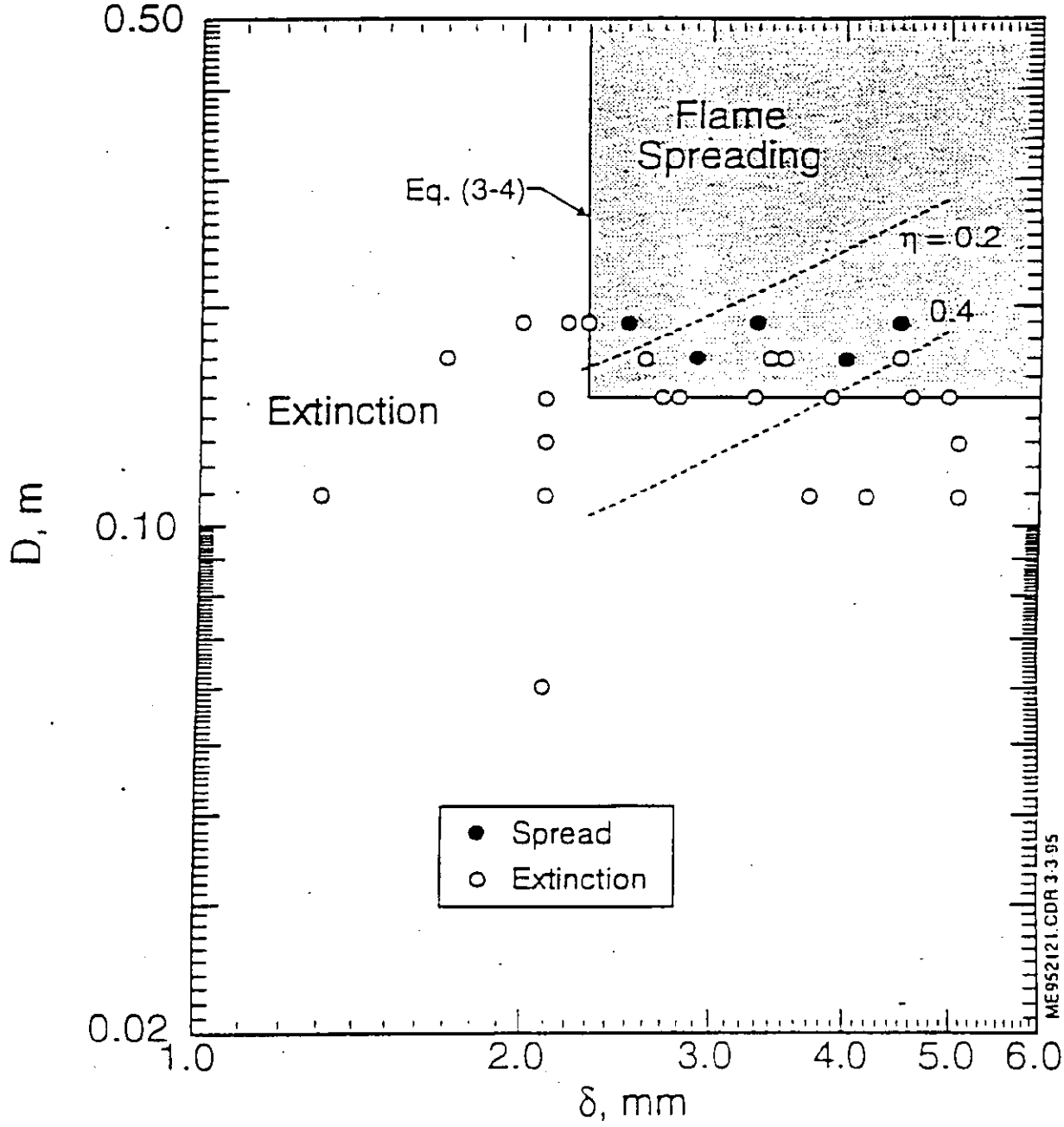

Figure 3-4 Flame diameter versus organic fuel-layer thickness map for dodecane at approximately 20°C, showing the (unshaded) region in which spreading of a flame initially located near the pool boundary is impossible.

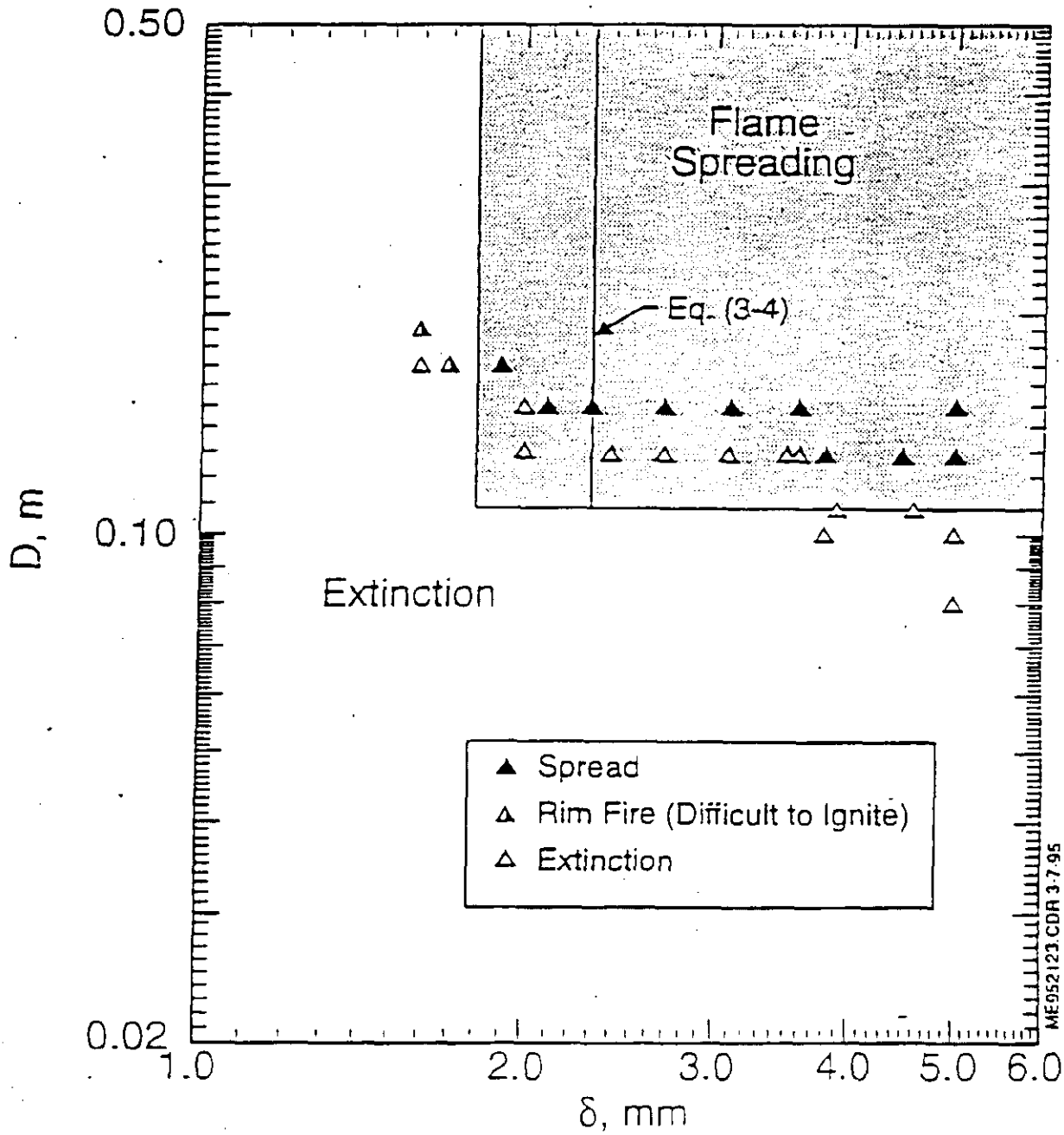

Figure 3-5 Radiation from a "surface element" of spark to a surface element of liquid.

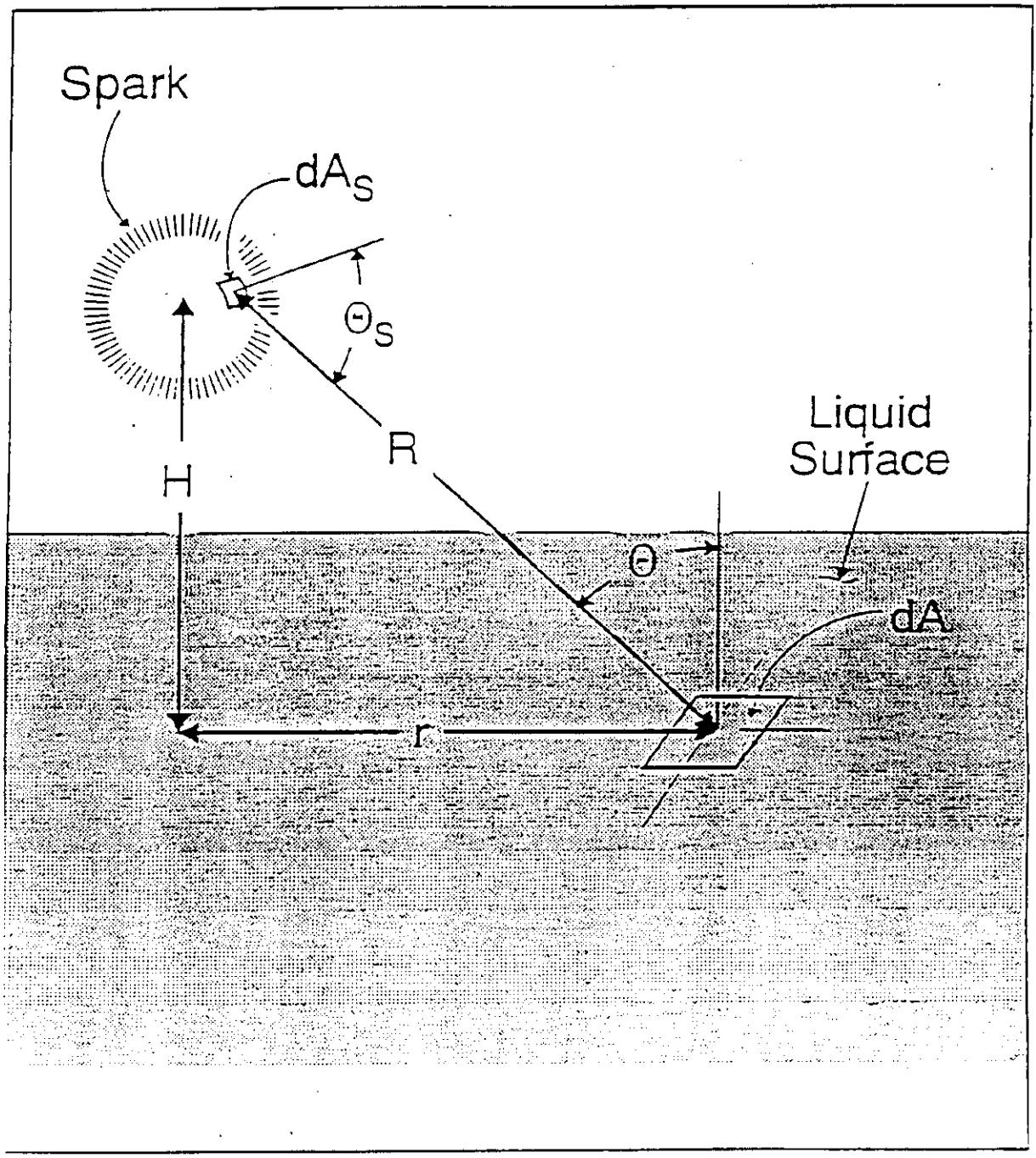

ME94N097.CDR 11-23-94

Figure 3-6 Schematic diagram of apparatus for measuring surface temperature versus distance profile produced by thermocapillary channel flow.

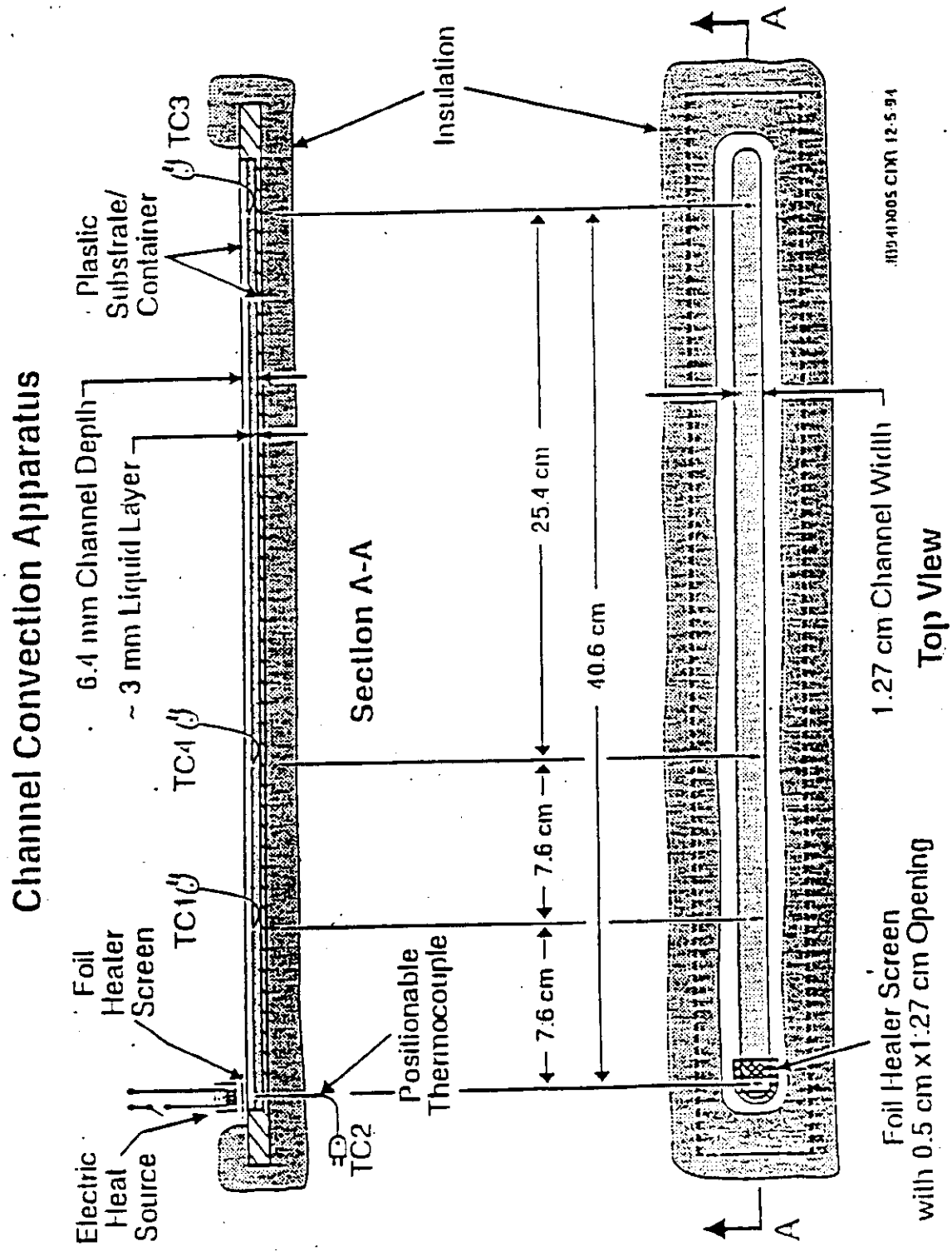

Figure 3-7 Thermocapillary channel convection Test 1.

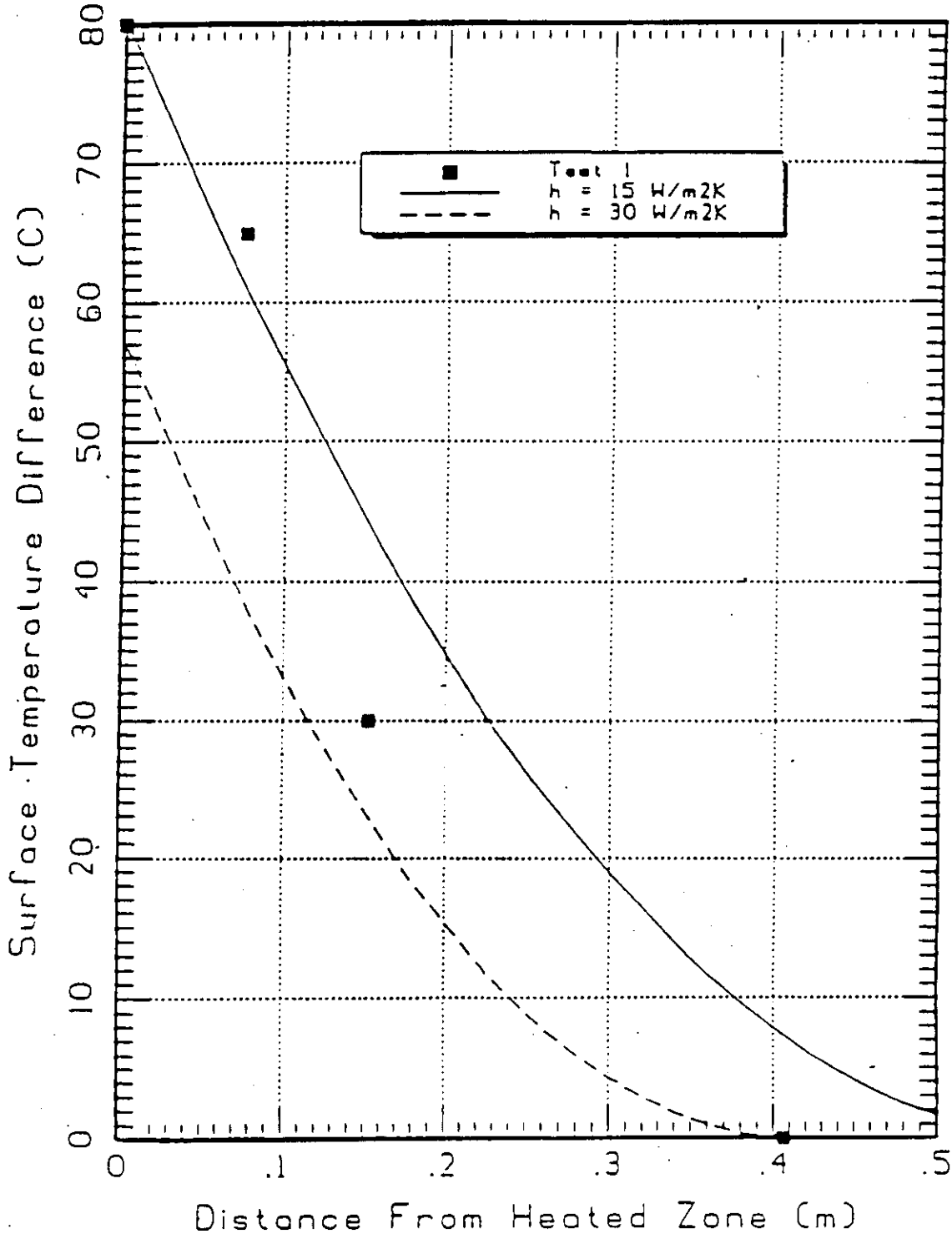

Figure 3-8 Thermocapillary channel convection Test 2.

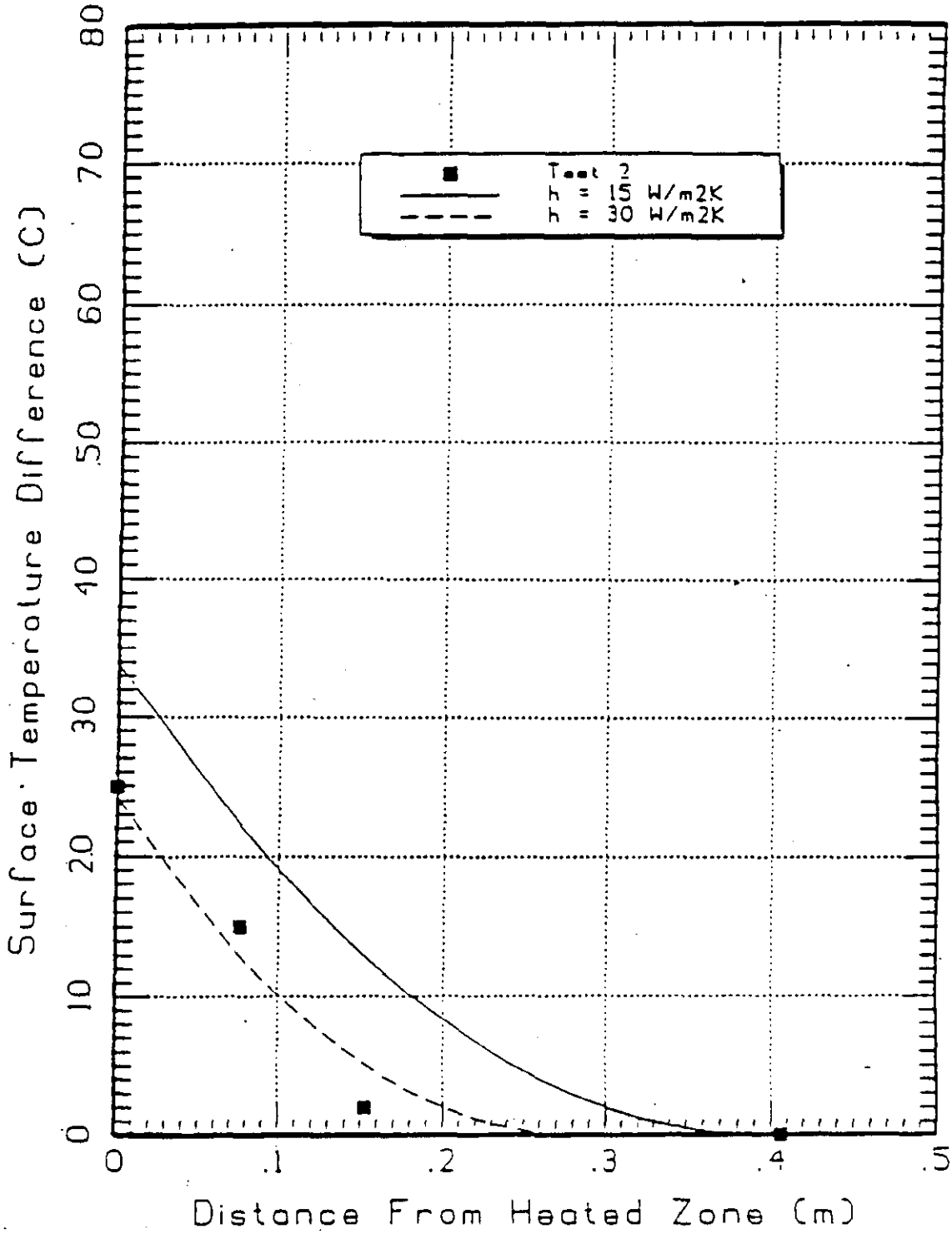

Figure 3-9 Thermocapillary channel convection Test 3.

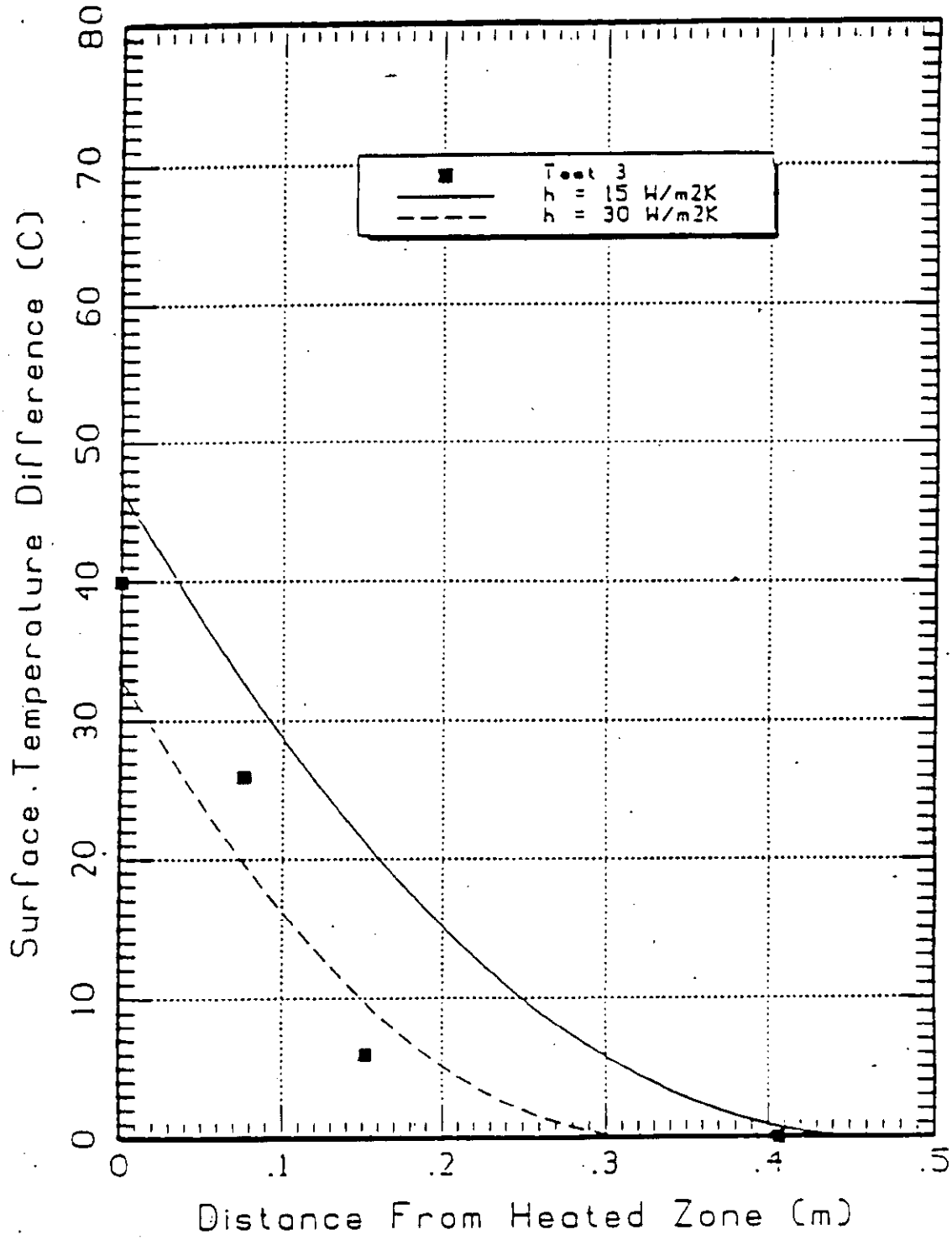

Figure 3-10 Thermocapillary channel convection Test 4.

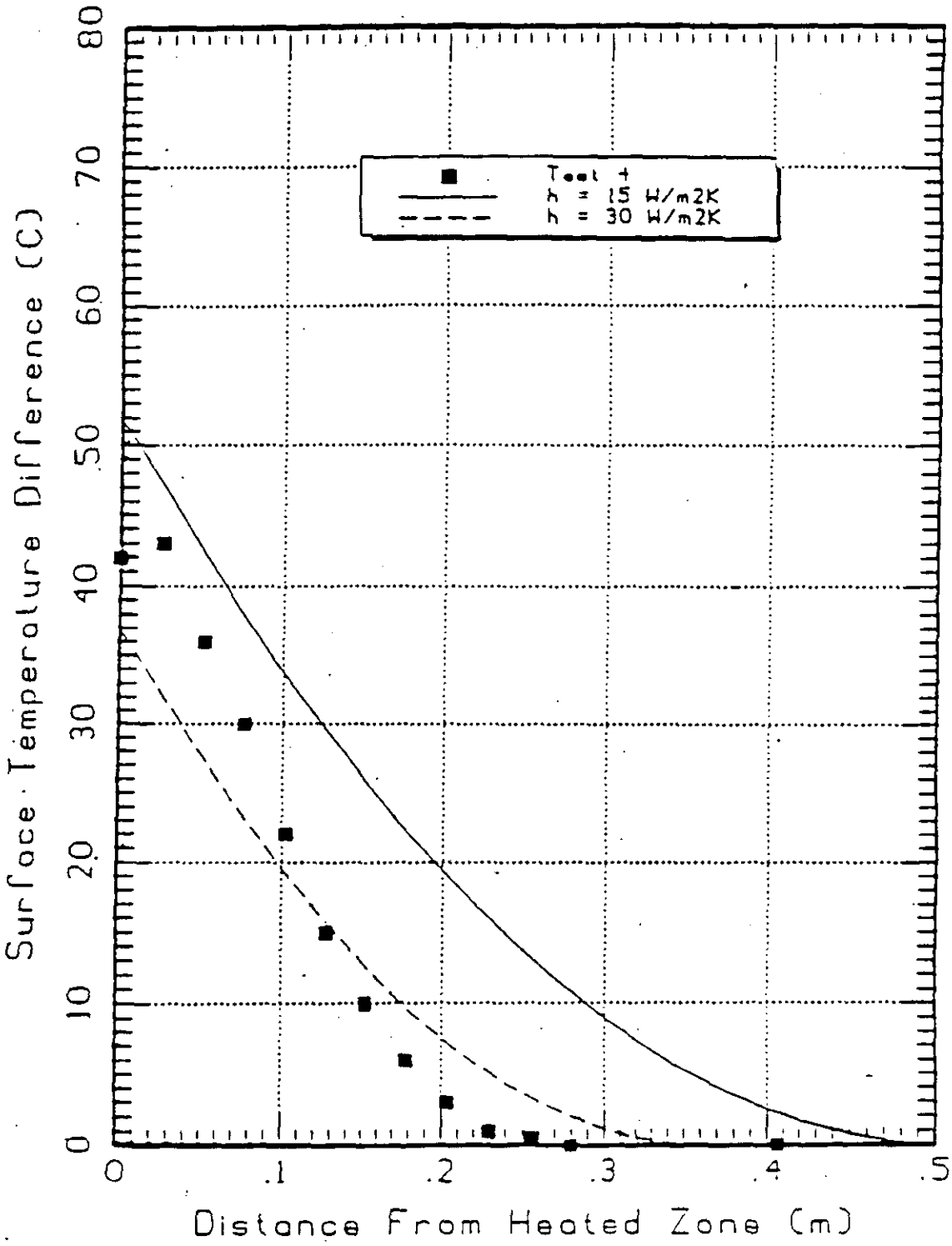

Figure 3-11 Thermocapillary channel convection Test 5.

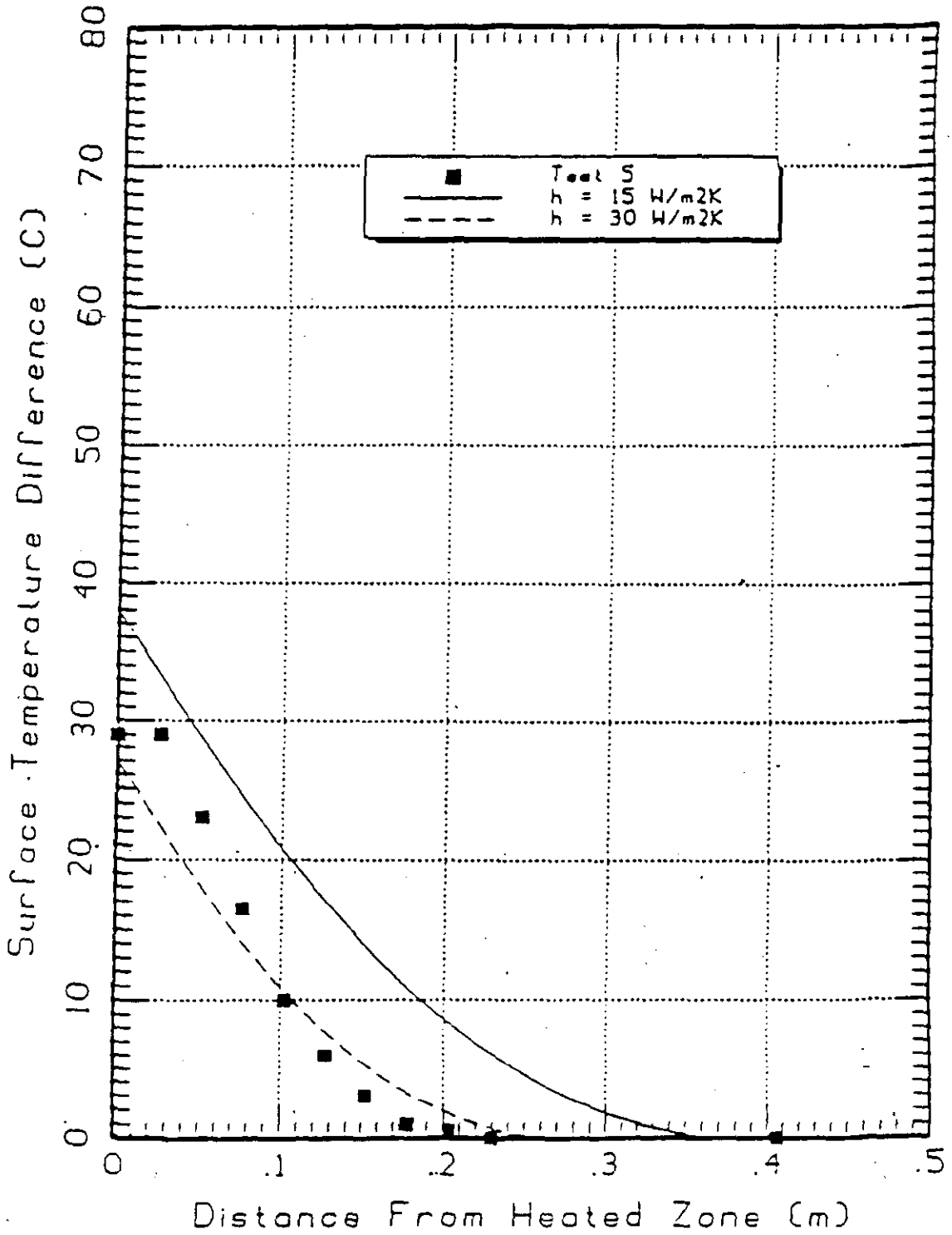

Figure 3-12 Test 1 temperature histories.

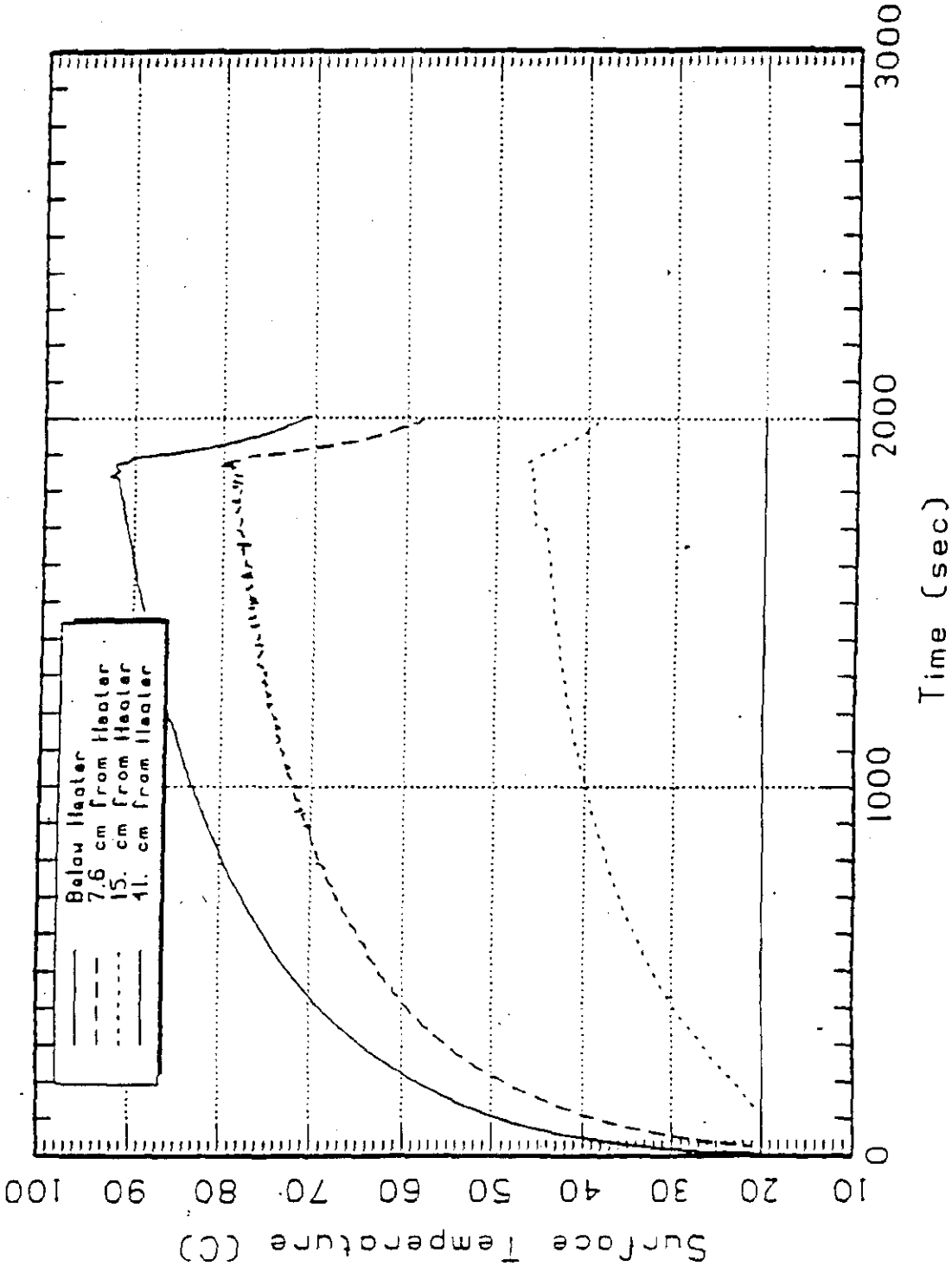

Figure 3-13 Test 2 temperature histories.

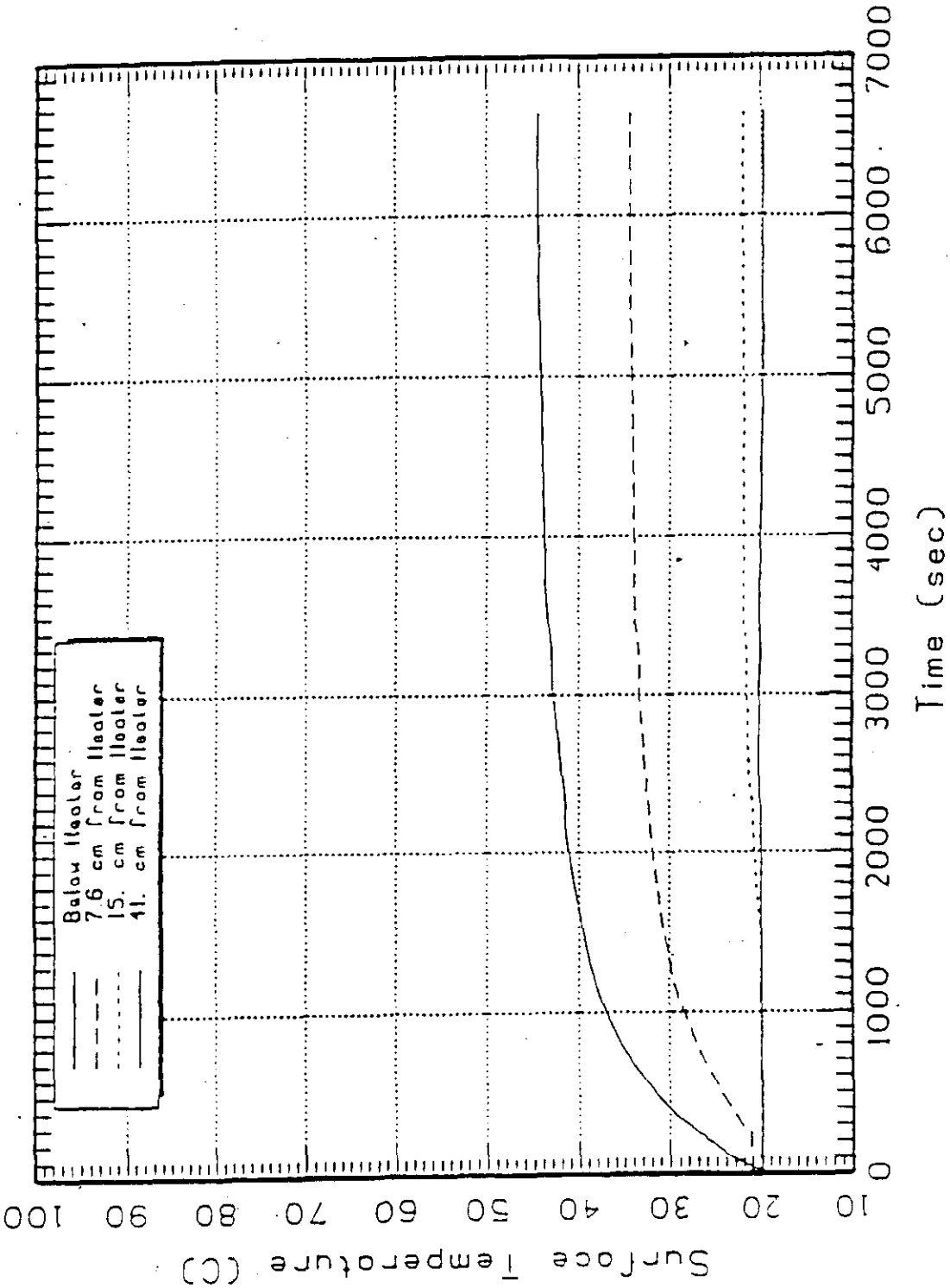

Figure 3-14 Test 3 temperature histories.

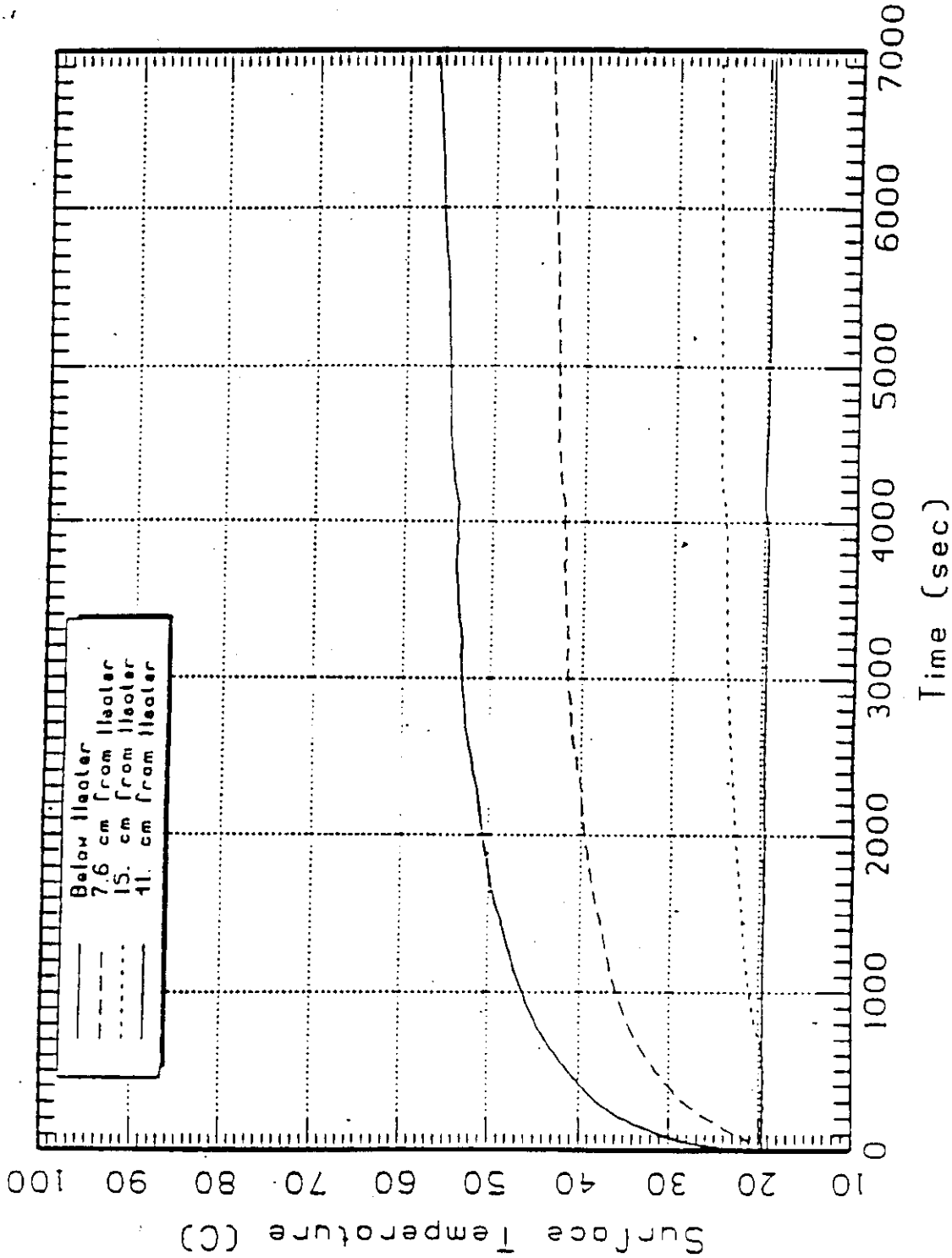

Figure 3-15 Test 4 temperature histories.

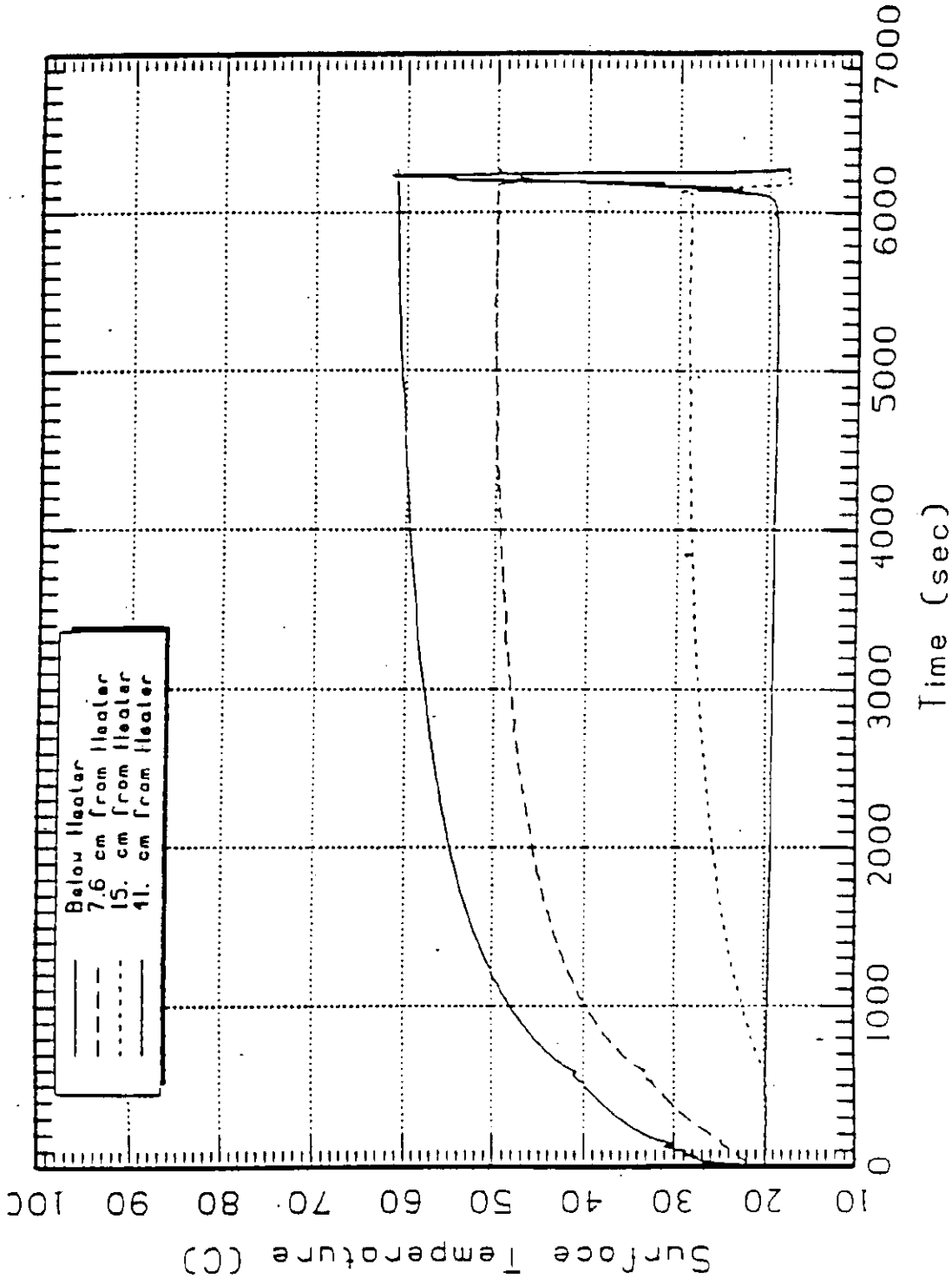

Figure 3-16 Test 5 temperature histories.

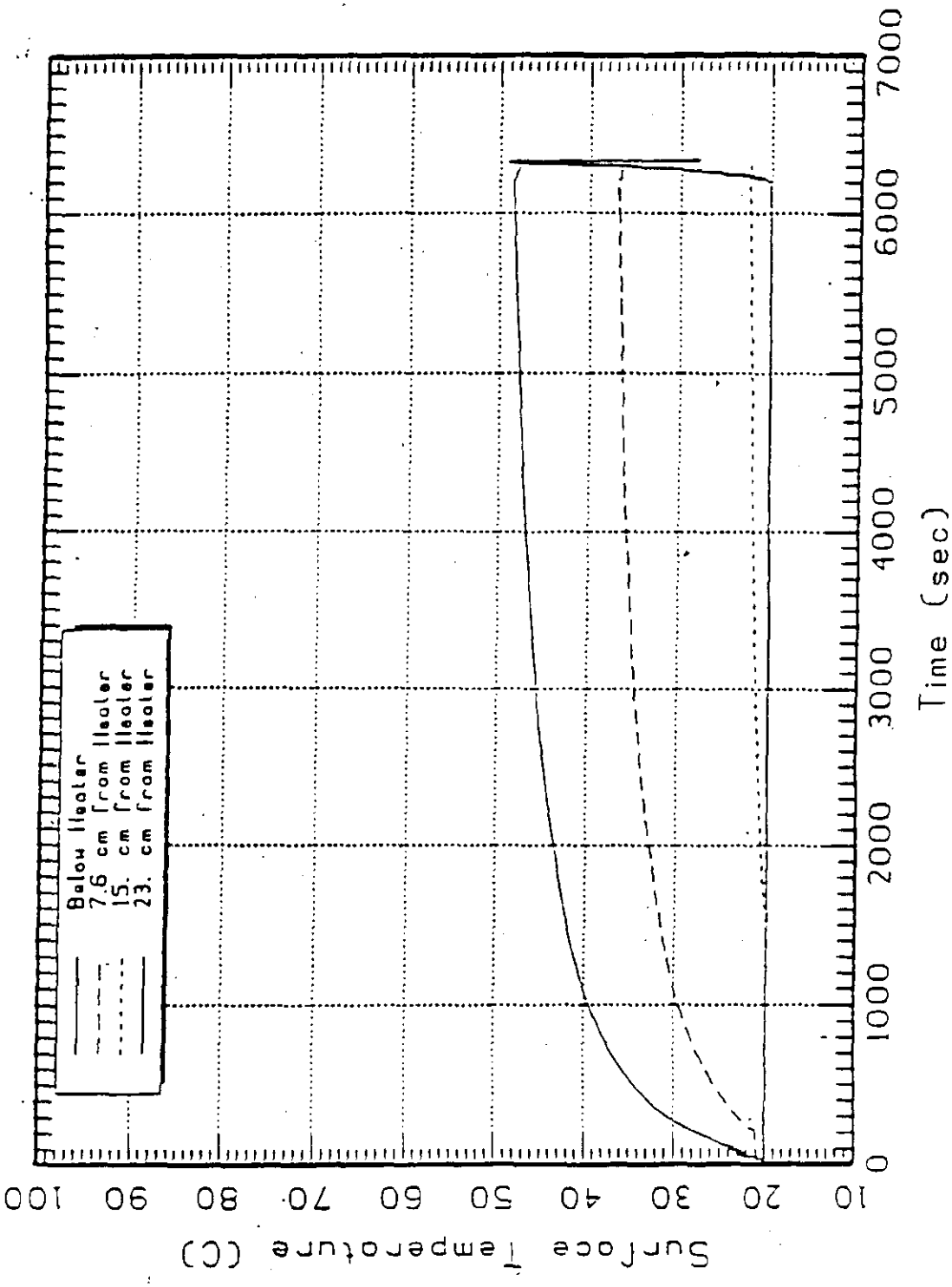

Figure 3-17 Organic liquid intrusion results for kaolin/water sludge and T-plant flowsheet.

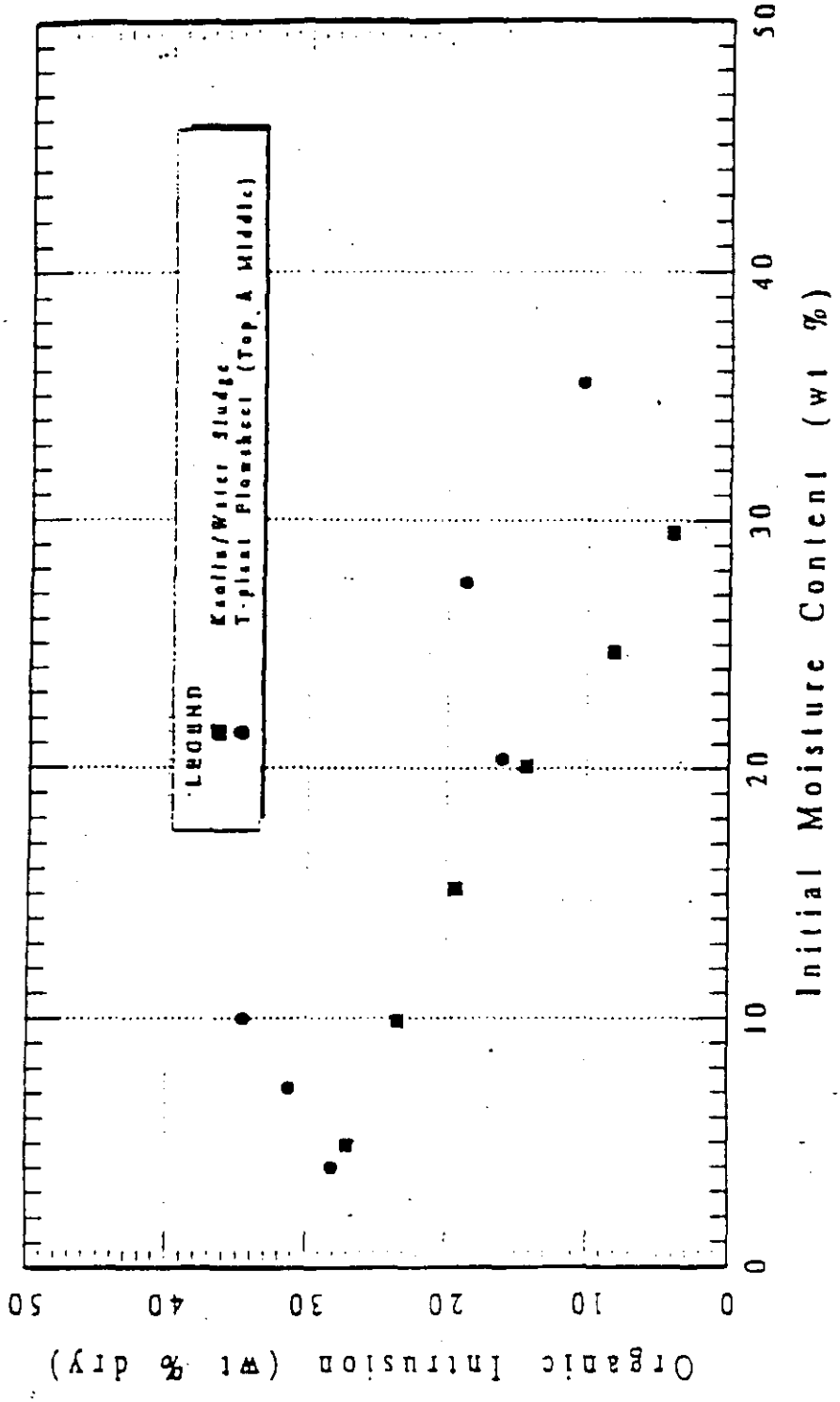

This page intentionally left blank.

4.0 CONCLUSIONS

1. Due to a wave-like instability at the floating organic layer/aqueous phase interface, some organic material may be left behind in sludge surface depressions at the completion of the interim stabilization tank pumping process.

2. An ignition source must be capable of bringing the surface of the floating organic layer to a temperature above its flash point over a surface segment wider than 10 cm before ignition of a propagable flame becomes possible.

3. It follows from Conclusion 2 that fires in cracks or channels cannot propagate into open pools unless the crack width exceeds 10 cm.

4. Ignition of a propagable flame on an organic layer less than 2.0 mm deep is not credible.

5. The minimum sustained initiator energy required to produce a propagable flame can be calculated by imagining the following, unlikely sequence of events: a 10-cm diameter, 2-mm deep zone of the organic layer is confined to cutoff convective heat losses to the surrounding organic liquid, bulk heated to at least the flash point and ignited, and finally the confinement barrier is removed to "free" the resulting flame. This sequence results in a minimum predicted initiator energy of approximately 3 kJ.

6. All realistic short-duration spark-source type of ignitors other than lightning will not cause flame spreading.

7. Sludge containing more than 20% water will not ignite.

This page intentionally left blank.

5.0 REFERENCES

Burgess, D. S., Strasser, A., and Grumer, J., 1961, "Diffusive Burning of Liquid Fuels in Open Trays," Fire Research Abs. and Revs. 3, 177-192.

De Ris, J., 1979, "Fire Radiation - A Review," 17th Symposium on Combustion, The Combustion Institute, 1003-1016.

Eckhoff, 1991, Dust Explosions in the Process Industries, Butterworth-Heinemann, Oxford, pp. 412-413.

Fauske & Associates, Inc., 1994, "Hazard Assessment Techniques for Hanford Waste Tanks Presently or Previously Containing Liquid Organic Layers," Fauske & Associates, Inc. Report FAI/94-91 (September).

Gear, C. W., 1971, Numerical Initial Value Problems in Ordinary Differential Equations, Prentice Hall, Englewood Cliffs, New Jersey.

Gerber, M. A., 1995, "Permeation of Tank C-103 Sludge Simulant by Organic Solvent", PNL-10412, UC-601 (January).

Hagglund, B. and Persson, 1976, "The Heat Radiated from Petroleum Fires," FOA Report, Forsvarets Forskningsanstalt, Stockholm.

Heskestad, G., 1988, "Fire Plumes," in SFPE Handbook of Fire Protection Engineering, National Fire Protection Association, Quincy, MA, Section 1, 107-115 (see also Fire Safety Journal, 1984, 7, 25).

Hindmarsh, A. C., 1972, "Linear Multistep Methods for Ordinary Differential Equations: Method Formulations, Stability, and the Methods of Nordsieck and Gear," Lawrence Livermore National Laboratory Report UCRL-51185, Rev. 1 (March).

Krauss, L. and Krempl, H., 1963, "uber das Temperaturabklingen in Funken 50,000 bis 5,000 Grad.," Zeitschrift fur angewandte Physik 16, 243-247; see also R. K. Eckhoff, 1991, Dust Explosions in the Process Industries, Butterworth-Heinemann, Oxford, p. 417.

Mackinven, R., Hansel, J. G., and Glassman, I., 1970, Combust. Sci. Technol., 1, 293.

Raj, P. K., Mudan, K. S., and Moussa, A. N., 1979, "Experiments Involving Pool and Vapour Fires from Spills of LNG on Water," Report No. CG-D-55-79, NTIS AD77073, U.S. Coast Guard.

Ross, H. D., 1994, "Ignition and Flame Spread over Laboratory-Scale Pools of Pure Liquid Fuels," Prog. Energy Combust. Sci. 20, 17-16.

Streeter, V. L., 1958, Fluid Dynamics, 2nd ed., McGraw-Hill, New York.

Torrance, K. E. and Mahajan, R. L., 1975, Combust. Sci. Technol. 10, 125.

Weiss, R. L. and K. E. Schull, 1986, "Data Transmittal Package for 241-C-103 Waste Tank Characterization," SD-RE-TI-203, Westinghouse Hanford Company, Richland Washington.

APPENDIX FAI/95-17A

A Steady-State Theory for Radial Flame Spread on an Organic Liquid Layer

Here we develop a theory for the onset of flame spread on an organic layer of liquid fuel. Suppose, owing to a sustained energy source (e.g., resistive heater) or to a finite duration energy source (e.g., spark discharge), a near circular segment of the surface of the organic liquid is heated above the flash point of the organic-liquid material, thereby producing a combustible air/organic vapor mixture above the heated surface segment. The question of interest is whether or not this premixed air/fuel vapor region, if ignited, will give rise to a sustained and propagable flame. It seems clear that if the energy transmitted from the growing flame to the liquid surface below is not strong enough to raise the temperature of the surrounding liquid surface up to the flash point, the flame would simply "flash" through the initial air/fuel vapor mixture, consume the combustibles in its sweep and then go out. In the analysis that follows it is assumed that the heated surface segment can support a sustained and propagable flame only if the radiant heat flux from the flame is sufficient to overcome the heat carried radially away by combined thermogravitational and thermocapillary convection within the surrounding organic liquid so that the temperature of the surface of the liquid at the outer edge of the flame equals or exceeds the flash point temperature.

The situation of interest is illustrated in Fig. A-1. Due to excessive localized heating of a circular portion of diameter D of the surface of an organic liquid layer a flammable organic vapor/air mixture forms above the heated region of the surface. The flammable mixture ignites and bursts into a flame of instantaneous diameter D and height H. We allow the flame to remain in place as a sustained and, perhaps, propagable flame until a steady temperature versus radial distance r profile is established along the underlying liquid surface. Thus for given organic layer material and flame dimensions D,H there is a unique steady-state, maximum organic-layer surface temperature T_{max} beneath the center of the flame and a steady-state organic-layer surface temperature T_{ed} beneath the radial edge of the flame. If T_{ed} is less than the flash point temperature our initial assumption of a sustained, propagable flame is incorrect and the actual situation is the flashing of the organic vapor/air mixture followed by extinction. On the other hand if T_{ed} exceeds the flash point temperature surface flame spread is possible.

Obviously from the discussion given in the foregoing we desire to determine the steady-state properties of a flame of given diameter D. In particular we desire to calculate the thermal energy output of the flame and then apply this knowledge to estimate the steady-state radial temperature distribution along the underlying surface of the organic layer that feeds the steady-state flame. It is important to emphasize that the flame diameter D is regarded as a known input quantity to the model; it is identified with the diameter of the circular surface segment of the organic layer that is heated by the ignition source.

We begin the construction of the model with the following expression that relates the organic layer evaporation rate (flux) $\dot{m}''_{ev}$ to the diameter D of the overlying flame:

$$\dot{m}''_{ev} = \dot{m}''_{ev,\infty} [1 - \exp(-\kappa D)] \tag{A-1}$$

where $\dot{m}''_{ev,\infty}$ is the asymptotic fuel layer evaporation (burning) flux for a very large flame and κ is an empirical constant that is a function of the fuel type. Apparently this burning rate expression was first proposed by Burgess et al. (1961); it is based on measurements of liquid fuel burning rates in open pans of various diameters D and is applicable to pool fires larger than about 0.1 m in diameter. In these so-called pool fire tests, the fire is confined by the barrier represented by the side wall of the pan. By employing Eq. (A-1) we are implicitly assuming that the unconfined, but finite size flame of diameter D illustrated in Fig. A-1 consumes fuel at the same rate as a contained pool fire of diameter D. For large diameter pool fires (D 1.0 m), Burgess et al. (1961) have shown that the burning rate of liquid organic fuel can be accurately correlated by the simple expression

$$\dot{m}''_{ev,\infty} = 1.27 \times 10^{-6} \frac{\rho_{bp} \Delta H_c}{\Delta H^*_{ev}} \quad (\mathrm{kg\ m^{-2}\ s^{-1}}) \tag{A-2}$$

where ρ_{bp} is the density of the liquid fuel (in kg m^{-3}) at its boiling point, ΔH_c is the heat of combustion of the organic fuel (in Joules per kg of fuel), and ΔH^*_{ev} is the fuel heat of evaporation (in Joules per kg) evaluated at the fuel boiling point plus the integrated heat capacity of the fuel from the ambient temperature T_∞ to the boiling point.

Now the total heat release rate of the flame is

$$\dot{Q} = \frac{\pi D^2}{4} \bullet \Delta H_c \bullet \dot{m}''_{ev} \tag{A-3}$$

Several semi-empirical expressions that relate mean flame height H to $\dot{Q}$ have been proposed. The correlation of Heskestad (1988) is convenient and sufficiently accurate for our purposes; it is

$$H = -1.02\ D + 1.483 \times 10^{-2} (\dot{Q})^{0.4} \tag{A-4}$$

where H and D are in units of meters and $\dot{Q}$ is in units of Watts. The total heat release rate $\dot{Q}$ of a flame is transported away from the combustion region by combined radiation and natural convection. The convective component of $\dot{Q}$ is carried away by the plume that exists above the flame, while the remainder of the total energy is radiated away in all directions. Thus the heat transmitted from the flame to the underlying surface of the organic fuel layer is largely radiative.

The shape of flames under actual conditions is arbitrary and time dependent, which makes detailed radiation analysis very difficult. In most calculations, flames are idealized as simple steady-state shapes such as planes, cylinders, or cones. A cylindrical geometry will be used here (see Fig. A-1) and the flame will be assumed to be homogeneous in the sense that it emits radiation uniformly over its cylindrical surface at the flux level $\dot{q}''_{rad,s}$ (see Fig. A-1). Then if η represents the fraction of the total flame heat release rate that is radiated away we have (see Eq. A-3)

$$\dot{q}''_{rad,s} = \frac{\eta\ \dot{Q}}{2\pi D^2/4 + \pi DH} = \frac{\eta\ \Delta H_c\ \dot{m}''_{ev}}{2 + 4H/D} \tag{A-5}$$

The radiative fraction of the total heat released from flames is rarely measured at more than 30 to 40 percent of the total heat released (see, e.g., Burgess et al., 1961; Raj et al., 1979, and Hagglund and Persson, 1976). The radiation fraction could be as low as 10 percent, especially for small flames. Thus there is considerable uncertainty in the radiation fraction parameter η.

The liquid fuel surface just beneath the flame (i.e. in the interval $0 < r < D/2$, see Fig. A-1) receives the radiation intensity $\dot{q}''_{rad,s}$. The thermal radiation intensity $\dot{q}''_{rad}$ (see Fig. A-1) to an organic fuel surface element outside of the flame envelope (i.e. in the semi-infinite interval $D/2 < r < \infty$) is calculated by the equation

$$\dot{q}''_{rad} = F(r)\ \dot{q}''_{rad,s} \tag{A-6}$$

where F(r) is the view factor for radiation exchange between the flame cylinder and the horizontal surface segment. The view factor is

$$\pi \bullet F(r) = \tan^{-1}Z - \frac{A^2 + B^2 - 1}{X \bullet Y} \tan^{-1} \frac{X}{Y \bullet Z} \tag{A-7}$$

where

$$A = \frac{2H}{D} \quad , \quad B = \frac{2r}{D} \quad , \quad Z = \left(\frac{B + 1}{B - 1}\right)^{1/2} \tag{A-8}$$

and

$$X = [A^2 + (B + 1)^2]^{1/2} \quad , \quad Y = [A^2 + (B - 1)^2]^{1/2} \tag{A-9}$$

For a given flame diameter D, we can now calculate the heat loads imposed on the liquid organic surface by the overlying flame. Thus it is time to turn our attention to the governing energy equation for heat flow within the organic layer itself. Here we make use of the simple FAI (1994) non-linear Fourier conduction-type expression that relates the outward radial heat flux q within the liquid organic layer to the radial temperature gradient along the surface of the liquid; namely,

$$q = - k_e \left(\frac{dT}{dr}\right)^3 \tag{A-10}$$

where k_e is an effective conductivity coefficient which accounts for both thermocapillary and thermogravitational convection:

$$k_e = \frac{\rho c_p (\sigma')^2 \delta^4}{1680 \alpha \mu^2} \left(1 + \frac{7}{24} Bo + \frac{19}{864} Bo^2\right) \tag{A-11}$$

The meanings of the symbols are given in the nomenclature section at the end of this appendix (see also, Table A-1).

An energy balance for a circular surface-segment of the organic layer outside the flame envelope, receiving radiant energy from the flame and losing heat to the atmosphere in accord with Newton's law of cooling, is

$$\frac{1}{r} \frac{d}{dr} \left[r \left(\frac{dT}{dr}\right)^3\right] = \frac{1}{\delta k_e} \left[- F(r) \dot{q}''_{rad,s} + h(T - T_\infty)\right] \qquad D/2 < r < \infty \tag{A-12}$$

In the above differential equation T(r) is the surface temperature distribution outside the flame zone. The last term in Eq. (A-12) is the heat-loss rate from the surface of the organic to the overlying atmosphere. The heat-transfer coefficient h is taken to be a known constant. At the location on the surface of the organic layer that coincides with the radial edge of the flame we have the boundary condition:

$$T = T_{ed} \quad \text{at} \quad r = D/2 \tag{A-13}$$

Far from the flame at some location $r = r_1$, where $r_1 >> D/2$, we have the boundary conditions

$$T \rightarrow T_\infty \quad , \quad \frac{dT}{dr} \rightarrow 0 \quad \text{as} \quad r = r_1 \tag{A-14}$$

It is known that surface tension effects are generally of finite extent, so that the liquid-surface temperature T will be reduced to the ambient value at the location $r = r_1$. This location is unknown and must be determined as part of the solution. Therefore, in order to close the problem an additional boundary condition must be imposed on the temperature of the liquid surface beneath the radial edge of the flame (i.e. at $r = D/2$). If the temperature of the liquid surface beneath the flame is spatially uniform and close to the boiling point of the organic liquid material, the thermocapillary flow should be weak beneath the flame and relatively strong just outside the flame envelope. While some liquid must be transported to the zone beneath the flame from outside the flame in order to supply fuel to maintain the flame, we will assume that the convective energy exchange between the organic liquid beneath the flame and the liquid just outside the flame zone is small and that the adiabatic condition

$$\frac{dT}{dr} = 0 \quad \text{at} \quad r = D/2 \tag{A-15}$$

is justified. In other words we are assuming that a rotating eddy exists in the organic liquid layer just outside the flame zone which carries cold liquid to the surface which almost completely replaces the thermocapillary-driven outward surface flow.

Equation (A-12) can not be solved analytically and we must seek a numerical solution of this equation. For purposes of numerical integration with the GEAR integrator subroutine (Gear, 1971, and Hindmarsh, 1972), Eq. (A-12) was converted to a system of two first-order ordinary differential equations. The boundary value problem represented by Eqs. (A-12) to (A-15) is treated as an initial value problem starting from $r = D/2$ and integrating towards $r = \infty$. Equations (A-13) and (A-15) serve as the initial conditions. Thus if T_{ed} is specified the initial conditions for Eq. (A-13) are known. The method of solution consists of guessing at T_{ed} in Eq. (A-13) and then systematically refining this guess until the resulting numerical solution satisfies the boundary conditions given by Eq. (A-14).

Once the organic fuel material and the temperature of the ambient are chosen, the remaining parameters to be specified are the flame diameter D and organic layer thickness δ. After assigning values to these parameters, the numerical solution to Eq. (A-12) is found and the predicted temperature T_{ed} is compared with the flash point temperature T_{fp} of the organic-fuel layer to determine whether the flame spreads or extinguishment occurs. The boundary that separates flame spreading from flame extinguishing in D versus δ space can be found by searching for combinations of D and δ that result in the condition $T_{ed} = T_{fp}$. The flame spreading/extinguishment boundary was determined numerically for the physical properties given in Table A-1 and the

results are shown by the dashed curves in Fig. 3-3 for two different values of the flame radiation efficiency parameter η. The thermophysical properties in Table A-1 correspond to those of dodecane at 47°C which is the arithmetic mean temperature of the flash point of dodecane, 74°C, and T_∞ = 20°C. The constant κ in the burning rate law (Eq. A-1) has not been reported for dodecane. We assume that κ for dodecane is similar to the measured value of κ = 2.0 m^{-1} for hexane (Burgess et al., 1961). With regard to a numerical choice for the heat-transfer coefficient h, combined natural convection and radiation from the surface of the organic liquid layer to quiescent ambient air is predicted with a standard heat-transfer correlation for turbulent natural convection to yield h = 15.0 W m^{-2} K^{-1}. However, ambient air drawn into the fire column acts to enhance the heat transfer rate off the surface of the liquid. Estimates of the fire draft velocity suggest a total predicted heat-transfer coefficient h = 30 W m^{-2} K^{-1}.

The theoretical trend shown in Fig. 3-3 indicates that the portion of the organic layer's surface that must be heated above the flash point to produce a spreadable flame increases with increasing layer thickness δ. The reason for this behavior is that the heat removal rate from the flame zone via combined thermocapillary and thermogravitational organic-layer convection increases with increasing film thickness (see Eq. A-11). The curves are not extended beyond δ = 5.0 mm because the assumptions employed in deriving Eqs. (A-10) and (A-11) are rendered invalid for thicker layers (FAI, 1994). In the thick-organic-layer region (δ 5.0 mm) the threshold value of D for flame spreading should be independent of δ. That is, the curves in Fig. 3-3 should bend to the right and approach a horizontal asymptote as δ is increased beyond 5.0 mm. In contrast with the theoretical results, the experimentally determined standing flame size D required for subsequent propagation of the flame is independent of the depth δ of the organic layer (see Fig. 3-3). As mentioned in Section 3.1.3, we believe that the model fails in this regard because it does not account for increasing radiation heat transfer from the flame to the surface of the organic layer with increasing flame size.

NOMENCLATURE FOR APPENDIX FAI/95-17A

Bo Bond number ($g\rho\beta\delta^2/\sigma'$)
c_p specific heat of the liquid
D diameter of flammable zone or standing flame
F(r) view factor for radiation from flame to organic surface
g gravitational acceleration
h heat transfer coefficient for surface cooling
H flame height
k thermal conductivity of the liquid
k_e effective conductivity transport coefficient
$\dot{m}''_{ev}$ organic layer evaporation mass flux beneath finite-size flame
$\dot{m}''_{ev,\infty}$ organic layer (asymptotic) evaporation mass flux beneath "infinite-size" flame
q heat flux transmitted horizontally through the liquid layer
$\dot{Q}''_{rad}$ radiation heat flux transmitted from flame to the liquid layer (Fig. A-1)
$\dot{Q}''_{rad,s}$ radiation heat flux emitted from surface of flame (Fig. A-1)
$\dot{Q}$ total heat release rate of flame
T temperature
T_{ed} liquid surface temperature beneath radial boundary of flame (Fig. A-1)
T_{max} maximum liquid surface temperature beneath center of flame (Fig. A-1)
r radial coordinate measured from the center of the flame (Fig. A-1)

Greek Letters

α thermal diffusivity of liquid organic
β liquid volumetric expansion coefficient
δ layer thickness (depth)
ΔH_c heat of combustion of organic fuel
ΔH^*_{ev} effective heat of evaporation of organic fuel
κ empirical constant in exponential burning rate law (Eq. A-1)
μ absolute viscosity of liquid organic
η radiative fraction of total heat released from flame
ρ density of liquid organic
ρ_{bp} density of liquid organic at boiling point
σ surface tension of liquid organic
σ' absolute variation of σ with temperature, $|d\sigma/dT|$

Subscripts

∞ locations far from the flame

Table A-1

Physical Properties Used in Numerical Calculations

$\kappa = 2.0\ m^{-1}$	(constant in pool burning rate law exponential)
$\Delta H_c = 4.41 \times 10^7\ J\ kg^{-1}$	(heat of combustion of organic)
$\Delta H^*_{ev} = 7.77 \times 10^5\ J\ kg^{-1}$	(effective heat of evaporation of organic)
$\rho_{bp} = 593.0\ kg\ m^{-3}$	(density of organic liquid at boiling point)
$T_\infty = 20°C$	(temperature of ambient)
$\rho = 730.0\ kg\ m^{-3}$	(average density of liquid organic fuel)
$c_p = 2277.0\ J\ kg^{-1}\ K^{-1}$	(specific heat of liquid organic fuel)
$\mu = 9.87 \times 10^{-4}\ kg\ m^{-1}\ s^{-1}$	(viscosity of liquid organic fuel)
$\alpha = 8.82 \times 10^{-8}\ m^2\ s^{-1}$	(thermal diffusivity of liquid organic fuel)
$\beta = 9.78 \times 10^{-4}\ K^{-1}$	(volume expansivity of liquid organic fuel)
$\sigma' = 9.03 \times 10^{-5}\ N\ m^{-1}\ K^{-1}$	(absolute value of $d\sigma/dT$ of liquid organic fuel)
$h = 30.0\ W\ m^{-2}\ K^{-1}$	(organic layer surface-to-air heat transfer coefficient)

Figure A-1 Schematic diagram of standing flame fed by layer of organic-liquid fuel. Flame spreading condition achieved when T_{ed} equals or exceeds fuel flash point.

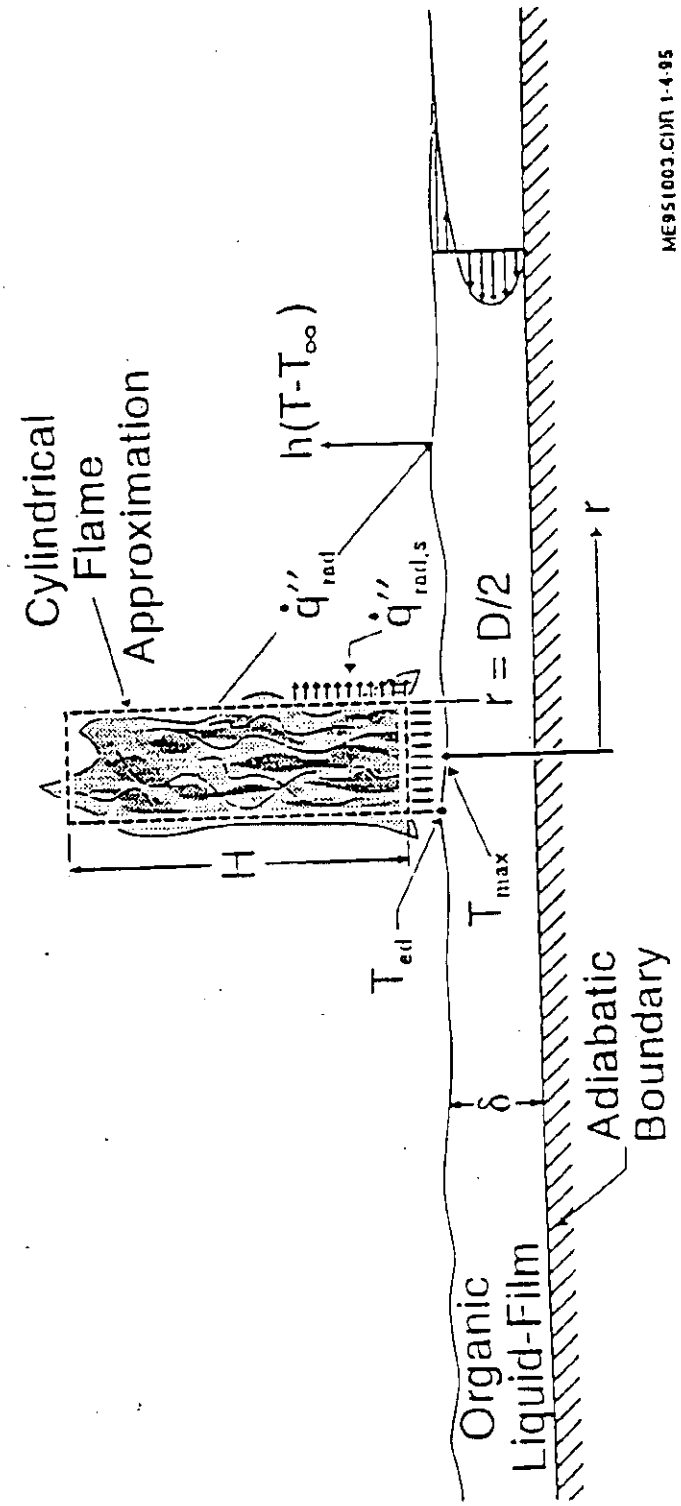

This page intentionally left blank.

APPENDIX FAI/95-17B
Thermal Response of Semi-Infinite Region to Surface Heat Flux Given by Eq. (3-14) in Section 3.1.4

An examination of Eq. (3-14) reveals that heat is supplied to the surface plane z = 0 of the semi-infinite (liquid) region at a rate depending on time and radial coordinate r only. Thus the appropriate differential equation for the temperature $\theta(r,z,t)$ is*

$$\frac{\partial\theta}{\partial t} = \alpha\left(\frac{\partial^2\theta}{\partial r^2} + \frac{1}{r}\frac{\partial\theta}{\partial r} + \frac{\partial^2\theta}{\partial z^2}\right) \tag{B-1}$$

The boundary condition at z = 0 is (see Eq. 3-14)

$$-k\left(\frac{\partial\theta}{\partial z}\right)_{z=0} = \frac{f(t)}{H^2 + r^2} \tag{B-2}$$

where

$$f(t) = \frac{10}{\pi} L_s I_s(t)^{1/2} \tag{B-3}$$

It is permissible to regard the temperature θ in the above equations as the difference between the actual local temperature T(r,z,t) and the initial temperature T_o since θ only appears in derivative terms in Eqs. (B-1) and (B-2). Thus the initial condition and the boundary condition are

$$\theta \to 0 \quad \text{as} \quad z \to \infty \tag{B-4}$$

$$\theta = 0 \quad \text{at} \quad t = 0 \tag{B-5}$$

We apply the Laplace transformation, namely

$$\theta_L(r,z,p) = \int_0^\infty e^{-pt}\,\theta(r,z,t)\,dt\ , \tag{B-6}$$

*Note that we are assuming that the spark discharge is over long before thermal convection begins in the liquid.

to Eqs. (B-1), (B-2) and (B-4) by multiplying through by e^{-pt} and integrating with respect to t from 0 to ∞. In Eq. (B-6) p is the Laplace transform variable. Equation (B-1) becomes

$$p\theta_L - \theta(r,z,0) = \alpha \left(\frac{\partial^2\theta_L}{\partial r^2} + \frac{1}{r}\frac{\partial\theta_L}{\partial r} + \frac{\partial^2\theta_L}{\partial z^2} \right) \tag{B-7}$$

Note that by virtue of Eq. (B-5) the second term in the above equation is zero. The transformed versions of Eqs. (B-2) and (B-4) are

$$-k\left(\frac{\partial\theta_L}{\partial z}\right)_{z=0} = \frac{1}{H^2 + r^2}\int_0^\infty e^{-pt} f(t)\, dt = \frac{f_L(p)}{H^2 + r^2} \tag{B-8}$$

$$\theta_L(r,z,p) \to 0 \quad \text{as} \quad z \to \infty \tag{B-9}$$

where $f_L(p)$ is the Laplace transform of f(t).

Next we introduce the Hankel transform of the Laplace transform $\theta_L(r,z,p)$:

$$\theta_{LH}(\beta,z,p) = \int_0^\infty r\, J_o(\beta r)\, \theta_L(r,z,p)\, dr \tag{B-10}$$

where $J_o(\beta r)$ is the Bessel function of order zero. Multiplying both sides of Eq. (B-7) by the product of r and $J_o(\beta r)$ and integrating with respect to r from 0 to ∞ gives

$$p\theta_{LH} = -\beta^2\alpha\, \theta_{LH} + \alpha \frac{d^2\theta_{LH}}{dz^2} \tag{B-11}$$

The second term in the above equation was obtained by integrating

$$\int_0^\infty r\, J_o(\beta r) \left(\frac{\partial^2\theta_L}{\partial r^2} + \frac{1}{r}\frac{\partial\theta_L}{\partial r} \right) dr \tag{B-12}$$

by parts. Hankel transforming the boundary conditions (B-8) and (B-9), gives

$$-k\left(\frac{d\theta_{LH}}{dz}\right)_{z=0} = f_L(p) \int_0^\infty \frac{r\, J_o(\beta r)}{H^2 + r^2}\, dr = f_L(p)\, K_o(H\beta)\ , \tag{B-13}$$

where $K_o(H\beta)$ is the modified Bessel function of order zero, and

$$\theta_{LH}(\beta, z, p) = 0 \quad \text{as} \quad z \to \infty \tag{B-14}$$

The solution to Eq. (B-11) subject to boundary condition (B-13) and (B-14) is

$$\theta_{LH} = \frac{f_L(p)\ K_o(H\beta)}{k(p/\alpha + \beta^2)^{1/2}}\ e^{-(p/\alpha + \beta^2)^{1/2} z} \tag{B-15}$$

The Hankel inversion theorem provides the following integral relationship between θ_L and θ_{LH}

$$\theta_L(r, z, p) = \int_0^\infty \beta\ J_o(r\beta)\ \theta_{LH}(\beta, z, p)\ d\beta \tag{B-16}$$

Thus, from (B-15) the Laplace transform of θ becomes

$$\theta_L(r, z, p) = \frac{1}{k} \int_0^\infty \beta\ J_o(r\beta)\ K_o(H\beta)\ f_L(p)\ \frac{e^{-(p/\alpha + \beta^2)^{1/2} z}}{(p/\alpha + \beta^2)^{1/2}}\ d\beta \tag{B-17}$$

Now the Laplace transform of

$$g_L(p) = \frac{e^{-(p/\alpha)^{1/2} z}}{(p/\alpha)^{1/2}} \tag{B-18}$$

is

$$g(t) = \left(\frac{\alpha}{\pi t}\right)^{1/2} e^{-\frac{z^2}{4\alpha t}} \tag{B-19}$$

From the Linear Transformation theorem of Laplace transforms the inversion of $g_L(p + a)$ is $e^{-at}g(t)$. Therefore the inversion of

$$h_L(p) = \frac{e^{-(p/\alpha + \beta^2)^{1/2} z}}{(p/\alpha + \beta^2)^{1/2}} \tag{B-20}$$

is

$$h(t) = e^{\alpha\beta^2 t}\, g(t) = \left(\frac{\alpha}{\pi t}\right)^{1/2} e^{-\frac{z^2}{4\alpha t}}\, e^{-\alpha\beta^2 t} \tag{B-21}$$

From the Faltung theorem of Laplace transforms the inversion of the product $f_L(p)h_L(p)$ is $\int_0^t f(t-\tau)h(\tau)d\tau$. Thus the inversion of Eq. (B-17) is

$$\theta(r,z,t) = \frac{1}{k}\int_0^\infty \beta\, J_o(r\beta)\, K_o(H\beta) \left[\int_0^t f(t-\tau)\left(\frac{\alpha}{\pi\tau}\right)^{1/2} e^{-\frac{z^2}{4\alpha\tau}}\, e^{-\alpha\beta^2\tau}\, d\tau\right] d\beta \tag{B-22}$$

Introducing the dimensionless radial distance $x = H\beta$, and the definition $\theta = T - T_o$, the above equation becomes

$$T(r,z,t) = T_o + \frac{1}{kH^2}\int_0^\infty x\, J_o\left(\frac{r}{H}x\right) K_o(x) \left[\int_0^t f(t-\tau)\left(\frac{\alpha}{\pi\tau}\right)^{1/2} e^{-\frac{z^2}{4\alpha\tau}}\, e^{-\frac{\alpha\tau}{H^2}x}\right. \tag{B-23}$$

Equation (B-23) is the general solution for the transient temperature field in a semi-infinite region with initial temperature T_o and surface heat flux given by Eq. (B-2). The integrand of Eq. (B-23) is for all practical purposes zero for values of x larger than approximately 3.0. This is because the modified Bessel function $K_o(x)$ is a rapidly decreasing function of x for all $x > 0$, as can be seen by the following numerical evaluations of K_o for several values of x: $K_o(1.0) = 0.42$, $K_o(2.0) = 0.114$, $K_o(3.0) = 0.035$, and $K_o(4.0) = 0.011$. It follows that the term $\exp(-\alpha\tau x/H^2)$ is essentially unity over the integration segment $x = 0$ to, say, $x \simeq 3.0$ in which the integrand contributes to the integral of Eq. (B-23) in a significant way, as long as the time t is short enough so that the following criterion is satisfied:

$$\frac{\alpha t}{H^2} \ll 1.0 \tag{B-24}$$

During this short-time interval we may integrate Eq. (B-23) with respect to x without difficulty since all the remaining terms containing x are independent of τ. From the well-known integral involving the product of the Bessel functions J_o and K_o, namely,

$$\int_0^\infty x\, J_o\left(\frac{r}{H}\, x\right) K_o(x)\, dx = \frac{H^2}{H^2 + r^2} \tag{B-25}$$

Eq. (B-23) becomes

$$T(r,z,t) = T_o + \frac{1}{k(H^2 + r^2)} \int_0^t f(t - \tau) \left(\frac{\alpha}{\pi\tau}\right)^{1/2} e^{-\frac{z^2}{4\alpha\tau}}\, d\tau \tag{B-26}$$

This is the solution one would obtain by ignoring the radial heat conduction terms in Eq. (B-1). Since we are only interested in the temperature history at the surface of the semi-infinite region we may set z = 0 to obtain

$$T(r,0,t) = T_o + \frac{10\, L_s\, \alpha^{1/2}}{\pi^{3/2}\, k(H^2 + r^2)} \int_0^t \left[\frac{I_s(t - \tau)}{\tau}\right]^{1/2} d\tau \tag{B-27}$$

where $f(t - \tau)$ was eliminated in favor of $I_s\ (t - \tau)$ via Eq. (B-3). Recapitulating, Eq. (B-27) is valid as long as the inequality given by Eq. (B-24) is obeyed.

This page intentionally left blank.

APPENDIX FAI/95-17C
Thermocapillary and Thermogravitational Liquid Convection in an Open Channel Subject to a Surface Heat Flux

The previous analysis of combined thermocapillary and thermogravitational convection in an organic pool subject to a local radiant heat source (FAI, 1994) can readily be extended to shallow organic-liquid-filled cracks by switching from a cylindrically symmetric flow geometry to x-directional flow in a channel formed by two parallel walls a distance W apart (see Fig. C-1). The depth of the layer is denoted by the symbol δ. We focus our attention on shallow layers such that δ is sufficiently smaller than W that the velocity profile does not depend on the z coordinate (see Fig. C-1). The channel is regarded as semi-infinite in extent and the distance x is measured from the closed end of the channel. The surface of the liquid is exposed to a heat flux q_o over the finite distance interval $0 < x < x_o$. The walls and base of the channel are assumed to be adiabatic surfaces. The heat gained by the liquid is given up to the overlying atmosphere by surface cooling within the semi-infinite interval $x_o < x < \infty$ at a rate given by Newton's law of cooling $h(T - T_\infty)$, where T is the local temperature of the surface of the organic liquid, T_∞ is the temperature of the atmosphere, and h is an effective heat transfer coefficient which accounts for both free convection and radiation heat transport off the surface of the liquid.

Much like the case of the cylindrically symmetric liquid pool (FAI, 1994), the horizontal heat flow q away from the heat source due to both thermocapillary and thermogravitational convection is assumed to be given by

$$q = - k_e \left(\frac{dT}{dx}\right)^3 \tag{C-1}$$

where k_e is

$$k_e = \frac{\rho c_p (\sigma')^2 \delta^4}{1680 \alpha \mu^2} \left(1 + \frac{7}{24} Bo + \frac{19}{864} Bo^2\right) \tag{C-2}$$

The reader should consult our previous report (FAI, 1994) for the derivation of Eq. (C-1) and a discussion of its validity when applied to macro-scale thermocapillary and thermogravitation flow fields. The meanings of the symbols are given in the nomenclature section at the end of this appendix.

We can now solve for the variation of surface temperature with distance x along the length of the channel (crack) shown in Fig. C-1 by assuming that the axial heat flow in the positive x direction follows Eq. (C-1). A thermal energy balance on a segment dx of the organic layer beneath the heat source results in

$$\frac{d}{dx}\left[\left(\frac{dT_1}{dx}\right)^3\right] = - \frac{q_o}{\delta k_e} \qquad 0 < x < x_o \tag{C-3}$$

Similarly, an energy balance for a segment of the film in the surface cooling (unheated) region is

$$\frac{d}{dx}\left[\left(\frac{dT_2}{dx}\right)^3\right] = \frac{h}{\delta\ k_e}\ (T_2 - T_\infty) \qquad x_o < x < \infty \tag{C-4}$$

In the above differential equations $T_1(x)$ is the surface temperature distribution at the surface of the organic layer under the heater and $T_2(x)$ is the surface temperature distribution at the surface of the organic layer outside the heated zone. At the intersection of these two zones we have the boundary conditions

$$T_1 = T_2 \quad , \quad \frac{dT_1}{dx} = \frac{dT_2}{dx} \quad \text{at} \quad x = x_o \tag{C-5}$$

At the closed end of the channel (x = 0) there is no heat flow in the horizontal direction and the liquid surface temperature achieves its maximum value T_{max}. At this location the boundary conditions are

$$T_1 = T_{max} \quad , \quad \frac{dT_1}{dx} = 0 \quad \text{at} \quad x = 0 \tag{C-6}$$

Note that T_{max} is an unknown quantity that we seek to determine as part of the solution. Far from the heat source we have the obvious boundary conditions

$$T_2 = T_\infty \quad , \quad \frac{dT_2}{dx} = 0 \quad \text{for large } x \tag{C-7}$$

The solution of Eq. (C-3) subject to the boundary conditions in Eq. (C-6) is

$$T_1 = T_{max} - \frac{3}{4}\left(\frac{q_o}{\delta\ k_e}\right)^{1/3} x^{4/3} \tag{C-8}$$

By applying the chain rule of differentiation Eq. (C-4) becomes

$$\frac{dT_2}{dx}\ \frac{d}{dT_2}\left[\left(\frac{dT_2}{dx}\right)^3\right] = \frac{h}{\delta\ k_e}\ (T_2 - T_\infty) \tag{C-9}$$

Integrating this equation once yields

$$\frac{3}{4}\left(\frac{dT_2}{dx}\right)^4 = \frac{h}{2\delta\ k_e}\ (T_2 - T_\infty)^2 + c_1 \tag{C-10}$$

where c_1 is a constant of integration. By virtue of the boundary conditions far from the heat source (Eq. C-7), the constant c_1 is zero and Eq. (C-10) becomes

$$\frac{dT_2}{dx} = -\left(\frac{2h}{3\delta\ k_e}\right)^{1/4} (T_2 - T_\infty)^{1/2} \tag{C-11}$$

Integrating this result gives

$$T_2 - T_\infty = \left[c_2 - \frac{1}{2}\left(\frac{2h}{3\delta\ k_e}\right)^{1/4} x\right]^2 \tag{C-12}$$

where c_2 is a constant of integration.

Now substituting the temperature profiles $T_1(x)$ and $T_2(x)$ given by Eqs. (C-8) and (C-12) in the boundary conditions of Eq. (C-5) yields the following expressions for the two desired constants c_2 and T_{max}:

$$c_2 = \left(\frac{q_o x_o}{\delta\ k_e}\right)^{1/3}\left(\frac{3\delta\ k_e}{2h}\right)^{1/4} + \frac{1}{2}\left(\frac{2h\ x_o^4}{3\delta\ k_e}\right)^{1/4} \tag{C-13}$$

$$T_{max} - T_\infty = \frac{3}{4}\left(\frac{q_o x_o^4}{\delta\ k_e}\right)^{1/3} + \left(\frac{q_o x_o}{\delta\ k_e}\right)^{2/3}\left(\frac{3\delta\ k_e}{2h}\right)^{1/2} \tag{C-14}$$

From Eqs. (C-12) and (C-13), the temperature profile in the unheated zone is

$$T_2 - T_\infty = \left[\left(\frac{q_o x_o}{\delta\ k_e}\right)^{1/3}\left(\frac{3\delta\ k_e}{2h}\right)^{1/4} - \frac{1}{2}\left(\frac{2h}{3\delta\ k_e}\right)^{1/4} (x - x_o)\right]^2 \tag{C-15}$$

By setting $T_2 - T_\infty$ in Eq. (C-15) we can solve for the distance x_∞ beyond which the thermal effects of the heater are no longer felt by the liquid; namely

$$x_\infty = x_o + 2\left(\frac{3\delta\ k_e}{2h}\right)^{1/2}\left(\frac{q_o x_o}{\delta\ k_e}\right)^{1/3} \tag{C-16}$$

The expressions for T_{max} and x_∞ when converted to dimensionless form are

$$\frac{h(T_{max} - T_\infty)}{q_o} = \frac{3}{4}\left(\frac{h^3\, x_o^4}{q_o^2\, \delta\, k_e}\right)^{1/3} + \sqrt{\frac{3}{2}}\left(\frac{x_o^4\, h^3}{k_e\, \delta\, q_o^2}\right)^{1/6} \tag{C-17}$$

$$\frac{x_\infty}{x_o} = 1.0 + 2\sqrt{\frac{3}{2}}\left(\frac{\delta\, k_e\, q_o^2}{x_o^4\, h^3}\right)^{1/6} \tag{C-18}$$

The first term on the right-hand side of Eq. (C-17) represents the dimensionless temperature decrease in the heated zone ($0 < x < x_o$) while the second term is the dimensionless temperature decrease in the unheated zone ($x_o < x < \infty$). In most practical applications the temperature decrease in the heated zone is small compared with that in the unheated zone.

As an example we consider a 5.0-mm deep crack filled with an organic liquid having physical properties similar to dodecane ($\beta = 10^{-3}$ K^{-1}, $\sigma' = 9 \times 10^{-5}$ kg s^{-2} K^{-1}, $\rho = 720$ kg m^{-3}, $\alpha = 8.7 \times 10^{-8}$ m^2 s^{-1}, $\mu = 8 \times 10^{-4}$ kg m^{-1} s^{-1}, and $c_p = 2300$ J kg K^{-1}). The corresponding value of k_e is, from Eq. (C-2), 0.15 W m K^{-3}. Our best estimate of the heat transfer coefficient for combined natural convection and radiation off the surface of the organic liquid is $h \approx 15.0$ W m^{-2} K^{-1}. Assuming a heat flux $q_o = 10^5$ W m^{-2} applied over a length $x_o = 5.0$ mm, we estimate from Eq. (C-17) a maximum temperature rise of $T_{max} - T_\infty = 66$°C. It is interesting to note that a 5.0 mm radius heat source radiating to a 5.0-mm deep pool of organic liquid at the rate 10^5 W m^{-2} produces a maximum temperature rise of only 6.7°C. From Eq. (C-18) we predict that the length of the liquid organic-filled crack would have to be at least $x_\infty = 1.5$ m in order for the liquid surface to reject heat to the atmosphere at the rate it is receiving it from the heat source.

In the above example we assumed a crack depth $\delta = 5.0$ mm and we ignored conduction heat losses in the surrounding sludge. Most cracks are likely to be considerably deeper than 5.0 mm. However, the theory is not valid for liquid organic layer depths greater than approximately this depth. Our experimental results with organic pools (FAI, 1994) indicate that the maximum temperature T_{max} becomes rather insensitive to the depth of the layer once its depth exceeds about 5.0 mm.

NOMENCLATURE FOR APPENDIX FAI/95-17C

Bo Bond number ($g\rho\beta\delta^2/\sigma'$).
c_p Specific heat of the liquid.
g Gravitational acceleration.
h Heat transfer coefficient for surface cooling.
k Thermal conductivity of the liquid.
k_e Effective conductivity transport coefficient.
q Heat flux transmitted horizontally through the liquid layer.
q_o Heat flux transmitted from heater to the liquid layer.

T Temperature.
T_{max} Maximum liquid temperature.
x Horizontal coordinate in the direction of flow.
x_o Length of heated zone.
z Coordinate perpendicular to flow direction.

Greek Letters

α Thermal diffusivity of liquid.
β Liquid volumetric expansion coefficient.
δ Layer thickness (depth).
μ Absolute viscosity of liquid.
ρ Density of liquid.
σ Surface tension.
σ' Absolute variation of σ with temperature, $|d\sigma/dT|$.

Subscripts

∞ Locations far from the heater.
1 Under the heater.
2 Outside the heated zone.

Figure C-1 Schematic diagram of semi-infinite liquid layer in a channel subject to a surface heat flux at the closed end. The countercurrent, horizontal velocity profile is produced by combined thermocapillary and thermo-gravitational convection.

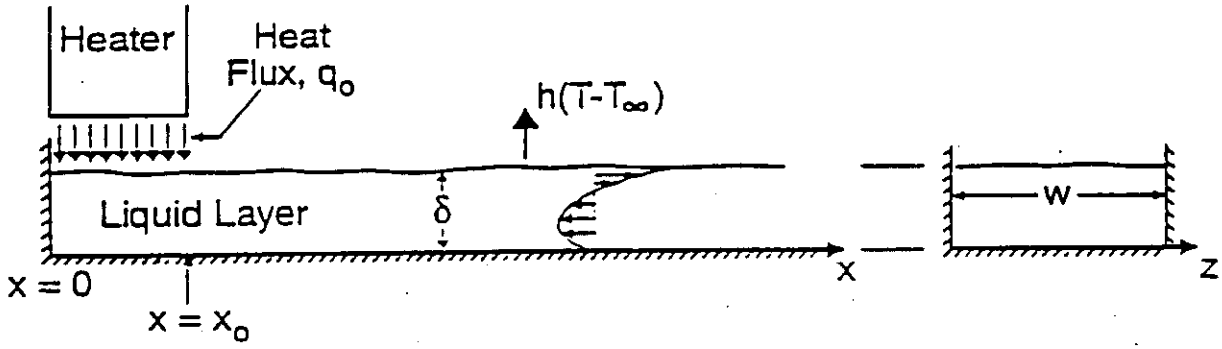

ME94N057.CDR 11-15-94

APPENDIX H

ANALYSIS OF CONSEQUENCES OF SMALL SOLVENT POOL FIRES IN ACTIVELY VENTILATED WASTE TANKS

This page intentionally left blank.

CONTENTS

1.0 SUMMARY AND CONCLUSIONS H-5
1.1 SUMMARY H-5
1.2 CONCLUSIONS H-6

2.0 STATEMENT OF THE PROBLEM H-6

3.0 ANALYSIS OF SOLVENT POOL FIRES IN ACTIVELY VENTILATED TANKS H-7
3.1 FIRE SCENARIO ANALYZED H-7
3.1.1 Event Sequence and Key Assumptions H-7
3.1.2 Comparison of Small Fire Scenario with Previously Documented Fire Analyses H-8
3.2 POOL AREA RANGE OF INTEREST H-9
3.2.1 Maximum Pool Area for a Steady-State Fire in an Actively Ventilated Tank H-9
3.2.2 Pool Area Required to Rupture HEPA Filters H-14
3.3 PREDICTED CONSEQUENCES FOR SMALL POOL FIRES IN VENTILATED TANKS H-17
3.3.1 Key Assumptions Used to Evaluate Consequences H-17
3.3.2 Predicted Toxicological Consequences H-18
3.3.3 Predicted Radiological Consequences H-19

4.0 COMPARISON OF CONSEQUENCES WITH PREVIOUSLY DOCUMENTED BOUNDING CASES H-21
4.1 TOXICOLOGICAL CONSEQUENCES H-22
4.2 RADIOLOGICAL CONSEQUENCES H-22

5.0 SUMMARY OF RESULTS OF PARAMETRIC ANALYSIS H-22

6.0 REFERENCES H-23

ATTACHMENT

A SPREADSHEETS FOR CONSEQUENCES . . . . . Att H-1

LIST OF TABLES

3-1 Peak Vent Rates Versus Pool Area H-16

5-1 Maximum Pool Area for Stable Flame H-23

H-1 Worksheet - Small Fire Analysis . . . . . Att H-3

H-2 Worksheet - Dose Summary . . . . . Att H-4

H-3 Worksheet - Toxicological Spreadsheet . . . . . Att H-5

This page intentionally left blank.

1.0 SUMMARY AND CONCLUSIONS

1.1 SUMMARY

This appendix presents an analysis of hypothetical solvent pool fires in Hanford Site waste tanks. Attention is focussed on small solvent pools in actively ventilated tanks. A review of solvent fire methodology (Postma 1996) identified the small fire case in actively ventilated tanks as deserving additional study.

At issue is whether fresh air brought into the tank by the active ventilation system could lead to appreciably more solvent burning (total mass of solvent burned during a postulated solvent fire event) than predicted in documented solvent fire analyses (Cowley et al. 1997). This issue is potentially important because predicted fire consequences could be affected by the total mass of solvent burned during an event. Thus it is important to know whether the consequences of a small fire fed by ventilation air would be bounded by fire cases already analyzed (Cowley et al. 1997).

The impact of forced ventilation on fire consequences was quantified in this study by analyzing the largest pool fire that could continue to burn <u>if</u> supplied by fresh air at 100 cfm (170 m^3/h). The methodology used in the analyses presented herein is the same as used in documented analyses (Cowley et al. 1997), extended to account for air flow into and out of a tank that is actively ventilated. Results of the analysis, in which toxicological consequences are expressed in sums of fractions of guidelines and where radiological consequences are expressed in radiation doses can thus be compared to consequences for fire cases presented in Cowley et al. 1997.

Results of the analysis indicate that consequences of a small pool fire in an actively ventilated tank would fall well below consequences for the bounding cases previously analyzed. It is shown that the HEPA filters in the ventilation system would not suffer over-pressure failure, but would trap particulate contaminants until the filters plugged. Ventilation airflow would terminate when the filters plugged with soot generated by the solvent fire, and the postulated fire would then self extinguish on low oxygen concentration.

The impact of ventilation air flow rate was evaluated parametrically. It was concluded that key results of the analysis for the 100 cfm (170 m^3/h) case apply for flow rates up to 500 cfm, a value that boundS nearly all tanks. Tank C-106 has a substantially higher flow rate (>2000 cfm) and the findings reported herein may not apply to tank C-106. Tank C-106 will have to be evaluated as a special case using tank-specific venting parameters if solvent fire risk needs to be quantified for this tank.

1.2 CONCLUSIONS

The following conclusions and summary statements are supported by the work done.

1. The overall conclusion reached from this study is that consequences of small fires in actively ventilated tanks have predicted consequences that fall well below consequences previously predicted for bounding fire cases (Cowley et al. 1997).

2. The impact of active ventilation on fire duration is significant only for small (<2 m^2 area) pools. For larger pools, headspace pressurization would prevent air inflow, and the fire would extinguish when the initially available headspace oxygen inventory was depleted by the fire.

3. HEPA filters in the ventilation train would not be ruptured by the small overpressures that could be generated by a small (<2 m^2) pool fire. The HEPA filters would trap fire-generated aerosols until they became plugged, at which time active ventilation would cease.

4. Toxicological consequences are driven primarily by the vent rate of gases from a tank following postulated fire ignition. Peak vent rates calculated herein are small in comparison to those predicted in previous analyses (Cowley et al. 1997), so toxicological consequences predicted here are small compared to those of earlier bounding cases (Cowley et al. 1997).

5. Radiological consequences are driven primarily by the mass of radioactive particulate material released from the tank. Although the mass of particulate released from waste to headspace air is predicted to be proportional to the mass of solvent burned, relatively little mass escapes from the tank and instead is captured by the HEPA filters. Therefore, radiological consequences for small fires (which could burn more solvent than predicted in cases documented earlier) are predicted to fall well below consequences for bounding cases documented earlier (Cowley et al. 1997).

2.0 STATEMENT OF THE PROBLEM

The technical issue addressed in this report is described as follows.

1. The impact of ventilation air flow on solvent fire consequences was discounted in earlier assessments (Cowley et al. 1997, Cowley and Postma 1996). The basis for discounting the impact of ventilation air flow was that fire-generated pressure in the tank headspace would prevent significant air inflow until after the fire was extinguished.

2. A review of solvent fire methodology (Postma 1996) raised the possibility that a small fire (small pool), burning at a rate limited by oxygen brought in by ventilation air, could continue to burn until available fuel was consumed.

3. The small continuing fire scenario described in (2) above could result in higher masses of solvent burned (as compared to earlier assessments) because extinguishment would be limited by fuel inventory rather than oxygen inventory. Because waste aerosolization is predicted to be proportional to the mass of fuel burned in a fire event, it is possible that aerosol release (and accident consequences) could be larger for the small continuing fire than for the larger fires previously analyzed.

4. This problem can be resolved by quantifying radiological and toxicological consequences for the small continuing fire scenario and comparing them with consequences for the bounding fire cases documented earlier (Cowley et al. 1997).

3.0 ANALYSIS OF SOLVENT POOL FIRES IN ACTIVELY VENTILATED TANKS

In this section, consequences of postulated solvent pool fires are quantified. In order to explain the basis for the predicted consequences, the following information is presented.

- Fire scenario description
- Analysis techniques
- Predicted toxicological consequences
- Predicted radiological consequences
- Comparison of scenario, methodology, and quantitative consequences with those of previously documented solvent fire analyses.

3.1 FIRE SCENARIO ANALYZED

3.1.1 Event Sequence and Key Assumptions

The following sequence of events characterizes the fire scenario analyzed herein.

1. A small solvent pool is postulated to be present in a DST or SST.

2. Local ignition of the pool is assumed to occur as a result of a low probability accidental ignition event.

3. Fire is assumed to spread at a velocity of 10 cm/s and cover the entire pool.

4. Ventilation air outflow continues at the design rate (100 cfm assumed as a base case) until intact HEPA filters plug with smoke generated by the fire. If HEPA filters are ruptured by a fire-generated pressure pulse, then outflow is assumed to continue at the design rate indefinitely.

5. Intact HEPA filters trap incoming particulate contaminants with an efficiency of 99.99% (DF = 10^4). Gaseous contaminants are assumed to pass through HEPA filters (zero retention of gases). Ruptured HEPA filters are assumed to have zero retention efficiency for all contaminants.

6. The pool fire burns until it self-extinguishes on low oxygen concentration or has consumed available fuel.

7. Gases vented from the tank are assumed to bypass the filters when gas outflow is calculated to exceed ventilation design flow rate and after the filters are predicted to be plugged with soot.

3.1.2 Comparison of Small Fire Scenario with Previously Documented Fire Analyses

Key points of comparison of the scenario described above with scenarios in previously documented analyses (Cowley et al. 1997, Cowley and Postma 1996) are the following.

1. Cowley et al. 1997 postulated rupture of HEPA filters at time zero and no trapping of contaminants by the filters. The current analysis assumes normal filter performance unless a fire-generated pressure pulse is calculated to be of a magnitude (~1 psi) that could reasonably be expected to rupture HEPA filters.

2. Cowley et al. 1997 discounted the impact of oxygen inflow to the tank caused by the ventilation system. The current analysis quantifies oxygen inflow and its predicted effect on the mass of fuel burned and thermal hydraulic parameters of headspace air.

3. The smallest pool considered by Cowley et al. 1997 was 1 m^2. The current analysis considers smaller pools because a sufficiently small pool could burn at a steady-state rate with oxygen brought into the tank by the ventilation system.

4. Analysis methodology used in the current study is, except for noted differences, identical to methodology used by Cowley et al. 1997. Burn rates, heat transfer rates, reaction energetics, aerosol formation, unit liter doses, etc., assumed in this analysis are the same as employed by Cowley et al., 1997. Thus, consequences predicted in this study can be compared with consequences for bounding cases analyzed in Cowley et al. 1997.

3.2 POOL AREA RANGE OF INTEREST

This section quantifies pool areas that can be considered "small", i.e., pools which could continue to burn at steady state if supplied by ventilation air, assuming no limitation on fuel supply. Also, pressure transients, predicted for small pools are examined to see whether HEPA rupture is probable for postulated fires on small solvent pools.

3.2.1 Maximum Pool Area for a Steady-State Fire in an Actively Ventilated Tank

At issue here is the size of fire that could continue to burn in a ventilated tank. At one extreme, one could consider a typical table candle placed inside a ventilated tank. Such a candle would consume little of the oxygen supplied by the ventilation system, and would burn until the fuel was consumed. At the other extreme, for an inflamed surface covering the whole tank cross-section, oxygen consumption is orders of magnitude greater than oxygen supplied by the ventilation system, so the fire dynamics would be unaffected by the ventilation system. In this section available information is used to relate maximum inflamed pool area for a steady-state fire to ventilation rate.

3.2.1.1 Extinguishment Criterion. Solvent pool fires self-extinguish when the oxygen concentration reaches the oxygen flammability limit for hydrocarbons. As discussed in Cowley et al. 1997, large scale tests conducted in France (Malet et al. 1983) provide a firm experimental basis for an oxygen extinguishment level of 13% by volume.

The largest inflamed solvent pool that could persist is one which reacts with all of the oxygen brought into the tank by the ventilation system. For larger pools, the oxygen reaction rate would exceed the rate of oxygen inflow, causing oxygen to fall below the extinguishment level, and the fire would go out. An oxygen material balance on headspace air allows one to relate maximum pool area for a continuing fire to flow rate.

$$O_2 \text{ input rate} = \dot{m}_{AI} X_{OI} \tag{1}$$

where

$\dot{m}_{AI}$ = mass rate of inlet air, kg/s
X_{OI} = mass fraction of O_2 in inlet air.

$$O_2 \text{ output rate} = \dot{m}_{AO} X_{oo} + R_o \tag{2}$$

where

$\dot{m}_{AO}$ = mass rate of outlet air, kg/s
X_{OO} = mass fraction of O_2 in outlet air
R_o = oxygen reaction rate, kg/s

$$O_2 \text{ accumulation rate} = \frac{d}{dt}(m_{AT}X_{OT}) \tag{3}$$

where
m_{AT} = mass of air in tank, kg
X_{OT} = mass fraction of O_2 in tank headspace air.

From the law of mass conservation,

$$\text{input rate} = \text{output rate} + \text{accumulation rate.} \tag{4}$$

At steady-state (assumed burning at the oxygen extinguishment level) the accumulation rate [Eq.(3)] is zero because headspace conditions are at steady state. Also, the mass fraction of oxygen in outlet air, assuming perfect mixing in headspace air, is X_E, the oxygen mass fraction at pool fire extinction. Equating oxygen input rate to oxygen loss rate [from Eq.(1) and Eq.(2)] one gets:

$$\dot{m}_{AI}X_{OI} = \dot{m}_{AO}X_E + R_o. \tag{5}$$

The oxygen reaction rate, R_o, may be calculated in terms of the pool burning rate:

$$R_o = \dot{m}_b A_p F \tag{6}$$

where

$\dot{m}_b$ = specific fuel burn rate, kg/s m^2,
A_p = inflamed area of pool, m^2,
F = mass oxygen reacted/mass fuel burned.

Combining equations (6) and (5) and then solving for pool area, A_p, results in:

$$A_p = \frac{\dot{m}_{AI}(X_{OI} - X_E)}{\dot{m}_b(X_E + F)} \tag{7}$$

Equation (7) defines a relationship for predicting the maximum size pool fire that can be sustained by an inlet air flow of $\dot{m}_{AI}$. A similar equation can be derived using outlet air flow in place of inlet flow. Outlet flow rate is more applicable to the present problem because it is the exhaust flow rate that is controlled by the ventilation system. At steady state, outlet air flow rate is equal to inflow rate plus fuel burning rate:

$$\dot{m}_{AO} = \dot{m}_{AI} + \dot{m}_b A_p \tag{8}$$

Using $\dot{m}_{AI}$ from Eq.(8) in Eq.(7) results in the following expression for pool area:

$$A_p = \frac{\dot{m}_{AO}(X_{OI} - X_E)}{\dot{m}_b(X_{OI} + F)} \tag{9}$$

where

A_p = maximum pool area for steady burning, m^2,
$\dot{m}_{AO}$ = mass flow rate of exhaust air, kg/s,
X_{OI} = mass fraction of oxygen in inlet air,
X_E = mass fraction of oxygen at extinction,
$\dot{m}_b$ = pool burning rate, kg/s m^2,
F = mass oxygen reacted/mass fuel burned.

3.2.1.2 Estimates of Stable Pool Fire Area Versus Ventilation Rate. Equation (9) was evaluated for a set of parameter assumptions applicable to waste tanks:

- inlet air contains water amounting to 50% humidity at 50°F (10 °C),
- inlet air, on a dry basis, contains 21% O_2 and 79% N_2,
- outlet air flow rate is 100 cfm (170 m^3/h),
- outlet air pressure is 14.5 psi (100 kPa),
- outlet air temperature is 68°F (20°C),

- X_E was evaluated for an extinction oxygen mole fraction of 0.13,
- F, the ratio of oxygen to fuel is 3.2655. This stoichiometric factor is based on oxygen reacting with NPH and TBP to form H_2O, CO_2 and P_2O_5 (Cowley and Postma 1996).

Inlet air conditions specified above are typical values at Hanford. Outlet air flow rate is a representative value for actively ventilated SSTs and DSTs. Outlet air pressure cited above is typical of atmospheric pressure at Hanford. Outlet air temperature assumed (20°C) is thought to be at the lower end of the possible range. Use of a lower end value for air outlet temperature tends to maximize $\dot{m}_{AO}$, and therefore to maximize the predicted value of A_p. X_E, based on an oxygen mole fraction of 0.13 is the same value used in previous evaluations (Cowley et al. 1997). Based on the parameters specified above, the value of A_p is calculated to be:

$$A_p = 0.125 \text{ m}^2.$$

This calculation indicates that pool fires covering areas larger than 0.125 m² would self-extinguish when the tank was ventilated with fresh air at a rate of 100 cfm (170 m³/h). Smaller pools would continue to burn as long as the ventilation rate was maintained at 100 cfm and a fuel supply was available.

This estimate of A_p is considered a best estimate because it is based in part on extinction parameters observed in the large scale tests performed by Malet et al. 1983. The large scale tests are thought to be applicable to the large waste tanks (DSTs and SSTs) considered in this report.

Japanese solvent fire tests (Ballinger et al. 1988) performed in actively ventilated cells also provide a basis for estimating maximum pool size for a stable fire. A total of 24 tests were reported in which pool area and ventilation rate were varied parametrically. For three tests, the burn period was brief because the fire self-extinguished. The ratio of pool area to ventilation rate for these tests provides an independent, experimental evaluation of the extinguishment parameter factor in Eq. (9). Equation (9) can be factored as follows:

$$A_p = \dot{m}_{AO} K_E \tag{10}$$

where

$$K_E = \frac{(X_{OI} - X_E)}{\dot{m}_b (X_{OI} + F)}.$$

K_E is an extinguishment factor that can be estimated from the Japanese tests and can be used to estimate A_p for a ventilation flow rate of 100 cfm. The fire which yielded to lowest ratio of $A_p/\dot{m}_{AI}$ and which self-extinguished was test F-2. This test used a burn area of 0.2304 m² and an inlet air flow

of 120 m^3/h. K_E can be estimated from those data, along with the following reasonable assumptions:

- inlet air temperature = 20°C,
- inlet air pressure = 1 atmosphere
- outlet air flow = inlet air flow on a mass basis.

Inlet air density is calculated from the ideal gas law to be 1.205 kg/m^3 for the temperature and pressures stated above. Thus K_E, the extinguishment factor defined in Eq.(10) is estimated as

$$K_E = \frac{A_p}{\dot{m}_{AO}} = \frac{0.2304\ m^2}{120\ \frac{m^3}{h} \times 1.205\ \frac{kg}{m^3}} = 1.59\ E\text{-}3\ m^2h/kg$$

The pool area computed for a flow rate of 100 cfm (170 m^3/h) is:

$$A_p = \dot{m}_{AO}K_E = 170\frac{m^3}{h} \times 1.19\frac{kg}{m^3} \times 1.59E\text{-}3\frac{m^2h}{kg} = 0.32m^2$$

This area is higher by a factor ~2.5 than the best estimate value of 0.125 m^2 described above, and illustrates how the extinction parameter could vary with fire conditions. The Japanese tests were conducted in a relatively small cell (20 m^3 volume, 2.6m x 3.5m x 2.2m) so air temperature in the cell would be much higher than predicted for the waste tank fire where surface area for heat loss is much greater. Higher gas temperatures would lower X_E and thereby increase the numerator of the right hand member of Eq.(10). For incomplete burning, the stoichiometric factor F, in the denominator of Eq.(10) would be lower than calculated for complete burning, as was assumed in the best estimate case. A smaller F value would lead to a higher value of K_E. Likewise, $\dot{m}_b$, a denominator factor in Eq.(10) could be lower in the Japanese tests where cell atmosphere temperatures were relatively high. The Japanese tests provide an experimental basis for the extinguishment parameter K_E that agrees reasonably well with the best estimate value based on larger scale tests and predicted parameters. The fact that K_E derived from the Japanese tests is higher than the best estimate value is as-expected on the basis of the relatively high cell air temperatures in the tests and the anticipated incomplete combustion at the extinction oxygen level.

A solvent fire test conducted at New Mexico State University (Smith et al. 1990) showed that when incoming air impinged on the burning pool from above, that fire extinction could occur at K_E values smaller than indicated above. Test KERO5 used a flow rate of 1000 cfm (1700 m^3/h) and a burn area of 0.33m. The fire extinguished, in the words of the researchers because *"...the burning caused instabilities that blew out the pool fire."* A value of K_E for this test is:

$$K_E = \frac{A_p}{\dot{m}_{AO}} \cong \frac{0.33 m^2}{1700 \frac{m^3}{h} * 0.93 \frac{kg}{m^3}} = 2.09E-4 \text{ h } m^2/kg$$

Using this value of K_E and a flow rate of 100 cfm (170 m^3/h), A_p is calculated to be

$$A_p = \dot{m}_{AO} K_E = 170 \frac{m^3}{h} \times 1.19 \frac{kg}{m^2} \times 2.09E-4 \frac{h\ m^2}{kg} = 0.0423 m^2$$

This pool area is 0.125/0.0423 or a factor of 2.96 smaller than the best estimate value for waste tanks. This smaller value of K_E is not expected to apply to waste tanks of interest here because the large size of the DSTs and SSTs, along with the low ventilation rates used, would preclude inlet air from significantly affecting the airflow patterns in the immediate vicinity of an inflamed pool surface.

In summary, a best estimate for the largest solvent pool that could be sustained indefinitely by an air flow rate of 100 cfm (170 m^3/h) is 0.125 m^2. Upper and lower bound estimates are 0.32 m^2 and 0.042 m^2. The bounding estimates are based on tests in which pool fire extinguishment was observed under known ventilation flows.

3.2.2 Pool Area Required to Rupture HEPA Filters

The potential consequences of solvent pool fires in actively ventilated tanks depends in part on whether fire-generated pressures are large enough to rupture HEPA filters. If ruptured early in the fire sequence, then ventilation flow could continue indefinitely, and a small fire could burn until fuel was exhausted. In this case, airborne contaminants would be purged from the tank headspace without efficient filtration. If, on the other hand, filters remained intact, then contaminants purged from the tank would be trapped with very high efficiency, and ventilation flow would cease when the filter became plugged. Thus it is important to know whether filter rupture is a plausible event in the small pool fire scenarios of interest in this study.

3.2.2.1 HEPA Filter Parameters Used in this Analysis. All active ventilation systems used on Hanford waste tanks employ HEPA filters protected by prefilters or de-entrainers. In all cases two HEPA filters are installed in series. In several farms, filter banks exist in parallel, so that only a fraction of the total system flow passes through any one filter. The present study considers only the case of a single filter train because this type of system would be more vulnerable to over-pressure failure than those where multiple flow paths exist.

HEPA filters used in tank farms have a nominal flow rating of 1000 cfm at a pressure drop of 1-inch water gauge. They are 24" x 24" x 12" in size (Cowley 1997)

Pressure drop across filters varies approximately linearly with flow rate. This dependency may be expressed as:

$$\Delta P = RQ \tag{11}$$

where

ΔP = pressure drop
R = resistance factor
Q = flow rate of air, volume/time.

The numerical value of R depends on the type and mass of particulate material captured by the filter.

According to Gregory et al. (1983) standard (1000 cfm) HEPA filters rupture when pressure drop exceeds 9.1 to 20 kPa. Expressed in inches of water, this is 36.5 to 80.3. Based on Eq.(11), a filter with an initial flow resistance of 1-inch of water at 1000 cfm would permit flows of 36,500 cfm to 80,300 cfm at rupture. If trapped particulate material caused the resistance factor to be double the clean value, flow rates required to generate pressure drops equal to the failure threshold would still be in the range of 18,250 cfm to 40,150 cfm. As will be shown in the next section, small pool fires do not generate outflows as large as the smallest of these values.

A fully plugged filter would presumably rupture if the static head exceeded 9.1 to 20 kPa with zero flow. If the leading filter were to rupture, the second filter would trap contaminants until it too was ruptured by overpressure.

The mass of particulate material required to plug a standard (1000 cfm) HEPA filter depends on the nature of the particulate material, but is generally in the neighborhood of 1 kg. Tests with combustion products of burning of plastic materials yielded plugging masses of 0.2 to 1.3 kg (Fenton et al. 1983). Plugging was defined by Fenton et al. 1983 as the point where the flow resistance factor had increased by a factor of 12 as compared to a clean filter.

3.2.2.2 Peak Vent Rates Predicted for Small Pool Fires. Peak vent rates are predicted to occur within minutes after fire ignition. Peak vent rates and the time of the peak were calculated for an actively ventilated DST using the POOLFIRE.4 Code. This analysis tool was employed in the analyses documented earlier in Cowley and Postma (1996) and in Cowley et al. (1997). Filter flow rates estimated by this calculation are conservatively high because outflow paths other than the ventilation duct were neglected and back pressure caused by filter resistance was neglected. Results are listed in Table 3-1.

Table 3-1. Peak Vent Rates Versus Pool Area.

Pool Area m^2	Peak Vent Rate cfm	Time of Peak s	Soot Mass Vented kg	Estimated* HEPA ΔP Inches Water
0.2	1716	106	0.0014	3.4
0.5	3708	154	0.0163	7.4
1.0	6144	173	0.066	12.3
2.0	9384	177	0.215	18.8

Note:
* Based on flow resistance factor double that of a clean filter.

The key result exhibited in Table 3-1 is that the maximum HEPA pressure drop predicted, 18.8 inches water for a 2 m^2 pool, is well below the HEPA rupture differential pressure (36.5 to 80.3 inches water). Soot mass listed in Table 3-1 was calculated on the assumption that 20% by mass of fuel burned was airborne soot, and that soot particles were transported without deposition in either the tank or in the ventilation ducting. The fractional venting of combustion products from the tank is a calculated parameter in the POOLFIRE.4 Code (Cowley and Postma 1996), and this calculated parameter, along with the soot aerosolization factor (0.20 of fuel burned) allowed the soot mass vented to the filter (the value shown in Table 3-1) to be calculated. The collected soot masses listed in Table 3-1 are small compared to HEPA loading limits (~1 kg for a single HEPA) so soot collected early in the fire transient is too small to affect HEPA pressure drop and hence would not be a significant factor in evaluating the possibility of HEPA rupture by over-pressure.

The scenario described above results in filter differential pressures of nearly 19 inches of water. The references used in this section give filter failure pressures as high as 80 inches of water. The TWRS BIO uses a filter failure pressure of 10 inches of water for accident analysis. The active ventilation systems currently used in Tank Farms (with the exception of AY and AZ farms, which do not fit this scenario) are not capable of producing a pressure change across the filters that exceed 10 inches of water. Therefore the fire burns until the filter is plugged with soot, the air flow is stopped and the fire extinguishes. Because the pressure differential never exceeds 10 inches of water, due to fan sizes, the HEPA filters never rupture.

In summary, this analysis of flow transients caused by postulated small pool fires indicates that for pools 2 m^2 and smaller, HEPA failure is not predicted. The largest pool which could continue to burn (at 100 cfm ventilation rate) was estimated to have an area of less than 0.32 m^2 (Section 3.2.1.2), so HEPA rupture for the small fire scenario is extremely unlikely, and is not considered in the calculation of consequences which follows.

3.3 PREDICTED CONSEQUENCES FOR SMALL POOL FIRES IN VENTILATED TANKS

Toxicological and radiological consequences for the case of a small fire in an actively ventilated tank are quantified in this section. Bounding consequences for the small fire case are calculated by selecting fire parameters which would lead to bounding high consequences.

3.3.1 Key Assumptions Used to Evaluate Consequences

Key assumptions and methodology used to evaluate toxicological and radiological consequences of a hypothetical small fire (stable at 100 cfm ventilation flow rate) in a waste tank are described as follows.

Methodology

The analysis tool and parameters used herein are the same as employed in documented analyses (Cowley et al. 1997, Cowley and Postma 1996). One extension of previous methodology was necessary to account for oxygen inflow caused by active ventilation: POOLFIRE.4, the thermal hydraulic model used to analyze pool fires, was modified so that outflow gas rate, on a volumetric basis, was maintained at a fixed value (a user specified input) until HEPA filters plugged.

Waste Tank Parameters

Tank properties were assigned values used for SSTs in previous studies (Cowley et al. 1997). Waste level was a minimum value so as to maximize headspace volume which also maximizes the quantity of fuel that can burn. Vent orifice size was assigned a value of 9.2 inches (0.23m) to simulate the flow resistance of a ventilation duct (Cowley and Postma 1996).

Pool Area

Solvent pool area was assigned a value of 0.32 m^2, the bounding area for a stable fire under a ventilation flow rate of 100 cfm (170 m^3/h). This area is quantified in Section 3.2.1.2. Predicted consequences increase with pool area because predicted outflow volumes which exceed ventilation rate increase with pool area. Therefore the volume and rate of unfiltered gas flow exiting from the tank (and calculated consequences) are maximized by using the bounding pool area identified above. The reader is reminded that large pool cases (up to 210 m^2) have already been considered in documented analyses (Cowley et al. 1997). For the large pool (210 m^2) case, ventilation has no significant effect on fire dynamics, and so is not of interest in the present study. Here we focus on pools that could continue to burn as a steady-state flame if supplied by fresh air at a rate of 100 cfm (170 m^3/h).

Ventilation Flow Rate

Ventilation flow rate, based on outlet volumetric rate, is set at 100 cfm (170 m^3/h) for all cases analyzed. This flow rate is believed to be representative of ventilation rates in actively ventilated tanks.

HEPA Filter Response

HEPA filters are predicted to remain intact during the analyzed small fire event. Therefore, particulate contaminants would be removed with high efficiency (assumed removal efficiency of 99.99%). The filters would also be subject to plugging by solvent fire smoke. Filter plugging was accounted for by setting ventilation rate to zero after a specified mass of solvent smoke was predicted to have accumulated on the filters. The plugging mass was specified as 1 kg in cases analyzed herein. Predicted consequences area not expected to be sensitive to the assumed plugging mass (1 kg) because the dominant atmospheric source terms for the small fire case are associated with pressure-driven ventings of gases that are assumed to bypass the filters. The HEPA plugging mass affects the calculated duration of a fire but has little effect on how much or how fast unfiltered gases are vented from the tank to the atmosphere.

3.3.2 Predicted Toxicological Consequences

Predicted toxicological consequences are sensitive to both gas vent rate and the concentration of toxins in vented gases. Vent rate is predicted to be highest during the initial few minutes whereas concentrations of fire-generated toxins would increase with burn time and reach a maximum at the time of fire extinction. Because highest vent rate occurs early and highest concentration of fire-generated toxins occurs late, two subcases were analyzed in order to determine which time period yielded the highest toxicological consequences.

Early Vent Period

Vent rate predicted by POOLFIRE.4 is highest during the first 200 s after fire ignition. 4.3 percent of the headspace gas inventory is predicted to have been vented during the time interval from zero to 200 s. Also, the mass of solvent burned is predicted to be 3.12 kg and the fraction of reaction products vented is predicted to be 0.0236. These fire response parameters were inserted into the spreadsheet used to compute consequences in previously documented analyses (Cowley and Postma 1996). This case involving the early vent period is exhibited in Row 8 of the spreadsheet exhibited as Table A-3 in Attachment A. The highest consequence is predicted for the onsite receptor at a frequency corresponding to the unlikely category. The sum of fractions for this case (Column DS) is 0.509. This value is less than unity, indicating that the risk evaluation guideline of 1.0 is met.

Late Vent Period

Highest concentrations of fire-generated toxins would occur when steady-state burning was attained. In order to bound late period concentrations of toxins it was assumed that steady-state burning was achieved, even though HEPA plugging would actually terminate vent flow before the steady state is achieved. Thus a hypothetical one-hour burn period was used to quantify toxin concentrations and release rates. For burning at the assumed extinguishment limit, the burn rate, from fire parameters described by Cowley and Postma (1996) is:

$$3\frac{kg}{min\ m^2} \times 60\frac{min}{h} \times 0.322m^2 \times 0.2236 = 12.96kg/h.$$

The fraction of headspace gas vented during the one hour period is:

$$\frac{170m^3}{4820m^3} = 0.0353.$$

All particulate materials were assumed to be trapped with an efficiency of 99.99%. Thus soot and P_2O_5 were attenuated by a factor of 10^{-4} in the calculation.

Results of the late period toxicological case are exhibited on Row 9 of the spreadsheet calculation (Table A-3). The calculated sum of fractions for the onsite receptor for the unlikely frequency category is given in column DS as 0.12. This sum of fractions is smaller than calculated for the early period, so it is concluded that early-period venting yields the bounding toxicological consequences for the small fire.

3.3.3 Predicted Radiological Consequences

Doses to onsite and offsite people were computed using fire and waste parameters that were taken from previous evaluations (Cowley et al. 1997 and Cowley and Postma 1996). However in this evaluation the HEPA filters were credited with removing aerosols with an efficiency of 99.99%, which accounts for a 99% removal efficiency for each of the two HEPAs in series.

Radiological doses are predicted to be proportional to the mass of radioactive material released from a tank to the atmosphere (Cowley and Postma 1996). For solvent fires the mass of respirable aerosol material release is calculated as the product of the mass of solvent burned (M), the aerosol release factor (ARF), the leak path factor (LPF), and the respirable fraction (RF). Values of ARF and RF used in documented analyses (Cowley et al. 1997) are assumed to apply to the small fires analyzed herein, and these factors (ARF and RF) are incorporated into the spreadsheet calculation depicted in Tables A-1 and A-2 in Attachment A. The following discussion quantifies values of solvent mass burned and leak path factors for each of four time

periods that characterize the course of a solvent pool fire. The sum of the M * LPF products are then used in the spreadsheet to compute doses using the same methodology that was used in documented pool fire analyses.

Four time periods are of interest in the fire cycle with respect to the release of radioactive aerosols. These four periods and key assumptions made in this analysis are described as follows.

Period 1. Early Vent Period

Thermal hydraulic calculations made with POOLFIRE.4 indicate that combustion energy heats headspace air and causes tank pressurization and outflow rates that exceed ventilation design flows during the first minutes of a fire. While much of this flow would be driven through the HEPAs, a fraction would exit through the normal inflow pathway to the tank. Because information needed to characterize the size of the normal inlet air path is not available, a conservative assumption is made, i.e., that all of the aerosol material released from the tank during this early period goes to the atmosphere unfiltered.

From POOLFIRE.4 calculations, outflow rate decrease to 170 m^3/h (100 cfm) at 1700 s. The mass of solvent burned in this 1700 s is calculated to be 24.81 kg and the fraction of fire-generated aerosols released (neglection depletion) is calculated to be 0.0385. The mass of fuel at risk multiplied by the leak path factor is:

$$24.81 \text{ kg} \times 0.0385 = 0.955 \text{ kg}.$$

Period 2. Filtered Vent Period

The second part of the fire cycle corresponds to the time period when ventilation at the design flow feeds fresh air into the tank and exhausts contaminated air through the HEPA filters. This period continues until the filters are plugged with soot, at which time ventilation flow would cease. The modified version of POOLFIRE.4 computes the time for HEPA plugging to be 8580 s. This flow time was based on a steady flow rate of 100 cfm (170 m^3/h), a HEPA plugging mass of 1 kg, and a soot production rate of 20% (by mass) of solvent burned. At 8580 s, the total mass of solvent burned was 92.87 kg, and the leak path factor was calculated by POOLFIRE.4 to be 0.0536. The product of solvent burned and leak path factor at 8580 s is:

$$92.87\ (0.0536) = 4.98 \text{ kg}.$$

This product applies for the total time (periods 1 and 2), so the product applicable to period 2, assuming an efficiency of 99.99% is:

$$M * LPF = (4.98 - 0.955) \times 1E\text{-}4 = 4.02E\text{-}4.$$

This quantity represents material which penetrates the filters. It is small in comparison to M * LPF for period 1.

Period 3

This period starts when HEPA filters plug and continues until the fire extinguishes on low oxygen concentration (13%). Air vented from the tank during this period is assumed to bypass the filters and carry airborne contaminants directly to the atmosphere. POOLFIRE.4 calculates fire extinguishment to occur at 16,300 s. The total mass of solvent burned is calculated to be 132 kg and the leak path factor is calculated to be 0.0380. Therefore, at 16,300 s, the product of mass burned and leak path factor is:

$$132 \times 0.0380 = 5.04 \text{ kg}$$

The M * LPF product applicable to this period is the total (5.04 kg) minus the product at the beginning of the period (4.98):

$$M * LPF = 5.04 - 4.98 = 0.06 \text{ kg.}$$

Period 4

This period starts when the fire is extinguishes. Air begins to inflow into the tank at this point because the fire is out and headspace air cools. Leakage of aerosols terminates at this time, so no release of radioactive material is predicted for period 4.

Total Release for Fire Cycle and Calculated Doses

The product of M * LPF for the entire fire cycle is the sum of the products for the three time periods:

$$\text{total } (M * LPF) = 0.955 + 0.0004 + 0.06 = 1.02 \text{ kg.}$$

Dose consequences were computed with the spreadsheet model using a burned mass of 1.02 kg and a leak path factor of unity. The dose calculations and fire parameters are listed in Row 7 of Tables A-1 and A-2 in Attachment A. Predicted dose for the onsite receptor is 3.21E-4 Sv as shown in Column K of Table A-2. Offsite dose is 2.82E-7 Sv as shown in Column L of Table A-2.

4.0 COMPARISON OF CONSEQUENCES WITH PREVIOUSLY DOCUMENTED BOUNDING CASES

Consequences for the small fire case analyzed herein are quantified in the spreadsheet presented in Attachment A. The three cases devoted to the small fire are identified as cases d1, d2, and d3 and appear on lines 7, 8, and 9 of the spreadsheet. The other fire cases listed on the spreadsheet have been copied from previously documented analyses (Cowley et al. 1997) and are presented here for comparison purposes.

4.1 TOXICOLOGICAL CONSEQUENCES

The maximum sum of fractions for the small fire case is 0.51 as listed in column DS of Table A-3. This value is small compared to the bounding case for large pools which is displayed in Tables A-3 on line 13. The sum of fractions for the previously documented bounding case is 43.3 which is nearly two orders of magnitude greater than that predicted here for the small fire. Therefore it is concluded that the small fire case studied here has toxicological consequences that fall well below those of previously documented cases.

4.2 RADIOLOGICAL CONSEQUENCES

Radiological consequences for the small fire scenario are 3.21 E-4 Sv and 2.82E-7 Sv for onsite and offsite receptors respectively. These values are listed in Columns K and L of Table A-2. The bounding radiological case previously documented had calculated doses of 5.55E-2 Sv and 4.87E-5 Sv for onsite and offsite doses respectively. These values are listed in Row 5, Columns K and L of Table A-2. Previously documented doses are larger by more than two orders of magnitude than the small fire case studied herein. Therefore it is concluded that dose consequences for the small fire case fall well below those of previously documented cases.

5.0 SUMMARY OF RESULTS OF PARAMETRIC ANALYSIS

While there is a possibility that a small pool fire (i.e., with a burning area of less than approximately 1 m^2) could burn for an extended period of time, a scenario for extended unfiltered releases is not credible. The filtered ventilation system provided these tanks mitigates the radiological and toxicological releases to values that are bounded by the unfiltered releases assumed to occur for large pool fires. This general conclusion is based on a parametric evaluation of small solvent pool fires in actively ventilated tanks.

Recent data on tank ventilation rates for actively ventilated tanks (HNF-SD-WM-CN-117 REV.0) indicate that rates vary with time and from tank to tank. Reported flow rates vary anywhere between 0 and a maximum of 2262 cfm for tank C-106. Nearly all of the tanks have maximum vent rates less than 500 cfm. Actual tank ventilation flow rates clearly differ from the nominal value of 100 cfm used to quantify consequences in Section 3.3. The impact of flow rate on predicted consequences is explored as follows.

The maximum pool area that can support a stable flame was calculated as a function of ventilation flow rate using Equation (9) with parameter values listed in Section 3.2.1.2. Results are given in Table 5-1. The largest pool listed in Table 5-1, 0.62 m^2 @ 500 cfm, is well below the size required to rupture a HEPA filter. Data of Table 3-1 indicate that pool area would have to be larger than 2 m^2 to cause HEPA rupture by overpressure. Since the largest pool in Table 5-1 is less than one-third the size required to rupture a HEPA filter, it is concluded that filter response assumed in Section 3.2.2

would apply for ventilation rates up to 500 cfm: (1) HEPA failure by overpressure is not predicted and (2) HEPAs would plug with soot, terminating ventilation air flow.

Table 5-1. Maximum Pool Area for Stable Flame.

Ventilation Flow Rate		Pool Area m^2
cfm	m^3/h	
1	1.70	0.0013
10	17.0	0.013
100	170	0.13
200	340	0.25
400	680	0.50
500	850	0.62

Very small fires, that allow ventilation systems to bring fresh air into the tank, can not challenge the HEPA filter integrity. Filtration factors for HEPA filters are sufficiently high (greater than 99.9%) that radiological and toxic material that passes through the filter is of insufficient quantity or concentration to present consequences that approach those calculated for the large pool fires where unfiltered releases are assumed to occur.

It is therefore concluded that the consequences of small pool fires in actively ventilated tanks are bounded by the consequences analyzed for large pool fires (e.g., 1 m^2 or greater) for which no filtration is assumed. Tank C-106 is an exception due to its higher ventilation rate (>2000 cfm) and the results of this analysis may not apply to tank C-106.

6.0 REFERENCES

Ballinger, M. Y., P. C. Owczarski, K. Hashimoto, G. Nishio, S. Jordan, and W. Lindner, 1987, "Aerosols Released in Accidents in Reprocessing Plants," *Nuclear Technology*, pg. 278-292, Vol.81.

Cowley, W. L., 1997, Duke Engineering and Services Corporation, Richland, Washington, Personal Communication to A.K. Postma, G&P Consulting, Inc., Richland, Washington, Feb 26, 1997.

Cowley, W. L., and A. K. Postma, 1996, *Analysis of Consequences of Postulated Solvent Fires in Hanford Site Tanks*, WHC-SD-WM-CN-032, Westinghouse Hanford Company, Richland, Washington.

Cowley, W. L., J. E. Meacham, J. M. Grigsby, and A. K. Postma, 1997, *Organic Solvent Topical*, HNF-SD-WM-SARR-036, Rev. 1A, DE&S Hanford, Inc. for Fluor Daniel Hanford, Inc., Richland, Washington.

Fenton, D. L., M. V. Gunaji, P. K. Tang and R. A. Martin, 1983, "*HEPA Filter Loading by Combustion Products*," *Proceedings of the CSNI Specialist Meeting on Interaction of Fire and Explosion with Ventilation Systems in Nuclear Facilities*, LA--9911-C-Vol.2, Los Alamos National Laboratory, Los Alamos, New Mexico.

Gregory, W. L., R. A. Martin, P. R. Smith and D. E. Fenton, 1983, "*Response of HEPA Filters to Simulated Accident Conditions*," *Proceedings of the 17th DOE Nuclear Air Cleaning Conference* (M. W. First, Ed.), CONF-820833, Harvard Air Cleaning Laboratory, Boston, MS.

Smith, P. R., I. H. Leslie, W. S. Gregory, and B. White, 1990, "*Pool Fires in a Large Scale Ventilation System*," *Proceedings of the 21st DOE/NRC Nuclear Air Cleaning Conference*, NUREG/CP--0116-Vol.2, San Diego, California.

Malet, J. C., G. Duverger de Cuy, R. Gasteiger, and K. Janberg, 1983, "Solvent Pool Fire Testing," in *CSNI Specialist Meeting on Interaction of Fire and Explosion with Ventilation Systems in Nuclear Facilities Proceedings*, April 25-28, 1983, Los Alamos, New Mexico.

Postma, A. K., December 30, 1996, "*Refinement of Solvent Fire Analysis Methodology*," LR-GP-96-068, G&P Consulting, Inc., Richland, Washington, Submitted to DE&S Hanford, Inc. for FLuor Daniel Hanford Inc., Richland, Washington.

ATTACHMENT A

SPREADSHEETS FOR CONSEQUENCES

This page intentionally left blank.

Table A-1. Worksheet - Small Fire Analysis.

	A	B	C	D	E	F	G	H	I	J	K	L	M	N	O	P	Q
1	Case	Tank Type	Solvent Pool Description	Pool Area m^2	Bounding Parameters	Ventilation Flow	Vent Description	Poolfire.4 Peak Pressure psig (kPa)	Poolfire.4 Peak Vacuum psig (kPa)	Poolfire.4 Solvent Burned kg	Solvent Aerosol Release Factor ARF	Poolfire.4 Leak Path Factor LPF	Solvent Atmosphere Release Basis kg	Aqueous Boiloff kg	Aerosol Release Factor for Aqueous ARF	Aqueous Atmospheric Release kg	Aqueous Unit Liter Dose Sv/L
3	a	SST	puddle	1.0	pressure	passive	hepa[1]	3.1 (21.4)	0.5 (3.45)	128	0.1	0.0747	9.56E-01	161.28	0.002	2.41E-02	1.10E+04
4	b	SST	puddle	1.0	vacuum	passive	hepa/flapper[2]	1.0 (6.89)	0.5 (3.45)	124	0.1	0.0399	4.95E-01	156.24	0.002	1.25E-02	1.10E+04
5	c	SST	puddle	1.0	radiological	100 cfm (0.047 m^3/s)	hepa	3.1 (21.4)	0.5 (3.45)	128	0.1	1.0	1.28E+01	161.28	0.002	3.23E-01	1.10E+04
6	d	SST	puddle	1.0	toxicological	100 cfm (0.047 m^3/s)	hepa	3.1 (21.4)	0.5 (3.45)	128	0.1	1.0	1.28E+01	161.28	0.002	3.23E-01	1.10E+04
7	d1	SST	small puddle	0.322	radiological	100 cfm (0.047 m^3/s)	vent pipe[3]	0.18(1.24)	small	1.02	0.1	1.0	1.02E-01	1.2852	0.002	2.57E-03	1.10E+04
8	d2	SST	small puddle	0.322	toxicological early	100 cfm (0.047 m^3/s)	vent pipe[3]	0.18(1.24)	small	3.12	0.1	0.024	7.36E-03	3.9312	0.002	1.86E-04	1.10E+04
9	d3	SST	small puddle	0.322	toxicological late	100 cfm (0.047 m^3/s)	vent pipe[3]	0.18 (1.24)	small	12.96	0.1	0.0001	1.30E-04	16.3296	0.002	3.27E-06	1.10E+04
10	e	SST	large	210	pressure	passive	hepa	29 (200)	0.1 (0.69)	146	0.03	0.146	6.39E-01	183.96	0.002	5.37E-02	1.10E+04
11	f	SST	large	210	vacuum	passive	hepa/flapper	1.8 (12.4)	6.8 (46.9)	84	0.03	0.3	7.56E-01	105.84	0.002	6.35E-02	1.10E+04
12	g	SST	large	210	radiological	100 cfm (0.047 m^3/s)	hepa	29 (200)	0.1 (0.69)	146	0.03	1.0	4.38E+00	183.96	0.002	3.68E-01	1.10E+04
13	h	SST	large	210	toxicological	passive	hepa/flapper	1.8 (12.4)	6.8 (46.9)	84	0.03	0.3	7.56E-01	105.84	0.002	6.35E-02	1.10E+04
14	q	SST	entrained	40.0	radiological	100 cfm (0.047 m^3/s)	hepa[1]	4.4 (30.5)	0.7 (4.8)	130	0.1	1	1.30E+01	163.8	0.002	3.28E-01	1.10E+04
15	r	SST	entrained	40.0	toxicological and vacuum	100 cfm (0.047 m^3/s)	hepa/flapper	1.0 (6.89)	2.1 (14.5)	113	0.1	1	1.13E+01	142.38	0.002	2.85E-01	1.10E+04

[1] HEPA Vent Modeled as 3.75" (9.5 mm) orifice

[2] Flapper is 50 in. (1.27 m) orifice opening at 1 psid (6.89 kPa)

[3] Vent Pipe on DST Modeled as 9.6 in. (0.24 m) orifice.

Table A-2. Worksheet - Dose Summary.

	A	B	C	D	E	F	G	H	I	J	K	L
1	Case	Tank Type	Solvent Pool Description	Pool Area m²	Bounding Parameters	Ventilation Flow	Vent Description	On Site Solvent Smoke Dose, Sv	Onsite Aqueous Boiloff Dose, Sv	HEPA Rupture Ddose Onsite Sv	Total Onsite Dose Sv	Total Offsite Dose Sv
3	a	SST	puddle	1.0	pressure	passive	hepa[1]	3.04E-05	2.98E-03	3.14E-04	3.33E-03	2.92E-06
4	b	SST	puddle	1.0	vacuum	passive	hepa flapper[2]	1.58E-05	1.54E-03	3.14E-04	1.87E-03	1.64E-06
5	c	SST	puddle	1.0	radiological	100 cfm (0.047 m^3/s)	hepa	4.08E-04	3.99E-02	1.52E-02	5.55E-02	4.87E-05
6	d	SST	puddle	1.0	toxicological	100 cfm (0.047 m^3/s)	hepa	4.08E-04	3.99E-02	1.52E-02	5.55E-02	4.87E-05
7	d1	SST	small puddle	0.322	radiological	100 cfm (0.047 m^3/s)	hepa	3.25E-06	3.18E-04	0.00E+00	3.21E-04	2.82E-07
8	d2	SST	small puddle	0.322	toxicological early	100 cfm (0.047 m^3/s)	vent pipe[3]	2.34E-07	2.30E-05	0.00E+00	2.32E-05	2.03E-08
9	d3	SST	small puddle	0.322	toxicological late	100 cfm (0.047 m^3/s)	vent pipe[3]	4.13E-09	4.04E-07	0.00E+00	4.08E-07	3.58E-10
10	e	SST	large	210	pressure	passive	hepa	2.04E-05	6.65E-03	3.14E-04	6.98E-03	6.12E-06
11	f	SST	large	210	vacuum	passive	hepa flapper	2.41E-05	7.86E-03	3.14E-04	8.20E-03	7.19E-06
12	g	SST	large	210	radiological	100 cfm (0.047 m^3/s)	hepa	1.39E-04	4.55E-02	1.52E-02	6.09E-02	5.34E-05
13	h	SST	large	210	toxicological	passive	hepa flapper	2.41E-05	7.86E-03	3.14E-04	8.20E-03	7.19E-06
14	q	SST	entrained	40.0	radiological	100 cfm (0.047 m^3/s)	hepa[1]	4.14E-04	4.05E-02	1.52E-02	5.62E-02	4.92E-05
15	r	SST	entrained	40.0	toxicological and vacuum	100 cfm (0.047 m^3/s)	hepa/flapper	3.60E-04	3.52E-02	1.52E-02	5.08E-02	4.45E-05

[1]HEPA Vent Modeled as 3.75" (9.5 mm) orifice
[2]Flapper is 50 in. (1.27 m) orifice opening at 1 psid (6.89 kPa)
[3]Vent Pipe on SST Modeled as 9.2 in. (0.23 m) orifice.

Table A-3. Worksheet - Toxicological Spreadsheet. (10 sheets)

	A	B	C	D	E	F	G	H	I	J	K	L	M	N
1	Case	Tank Type	Solvent Pool Description	Pool Area m^2	Bounding Parameters	Ventilation Flow	Vent Description	Tank Gas Volume m^3	Poolfire.4 Maximum Vent duration s	Poolfire.4 Solvent Burned in Vent kg	Poolfire.4 Reaction Gas Fraction	Poolfire.4 Headspace Gas Fraction	Source Conc. P_2O_5 mg/m^3	Source Conc. CO mg/m^3
3	a	SST	puddle	1.0	pressure	passive	hepa[1]	4.82E+03	2.50E+03	8.73E+01	1.10E-01	2.30E-01	3.75E+02	3.67E+02
4	b	SST	puddle	1.0	vacuum	passive	hepa/flapper[2]	4.82E+03	1.70E+03	6.51E+01	7.56E-02	2.40E-01	1.84E+02	1.80E+02
5	c	SST	puddle	1.0	radiological	100 cfm (0.047 m^3/s)	hepa	4.82E+03	2.50E+03	8.73E+01	1.10E-01	2.30E-01	3.75E+02	3.67E+02
6	d	SST	puddle	1.0	toxicological	100 cfm (0.047 m^3/s)	hepa	4.82E+03	2.50E+03	8.73E+01	1.10E-01	2.30E-01	3.75E+02	3.67E+02
7	d1	SST	small puddle	0.32 2	radiological	100 cfm (0.047 m^3/s)	hepa	4.82E+03	3.60E+03	1.02E+00	3.53E-02	3.53E-02	9.15E+00	8.97E+00
8	d2	SST	small puddle	0.32 2	toxicological early	100 cfm (0.047 m^3/s)	vent pipe[3]	4.82E+03	2.00E+02	3.12E+00	2.36E-02	4.30E-02	1.54E+01	1.51E+01
9	d3	SST	small puddle	0.32 2	toxicological late	100 cfm (0.047 m^3/s)	vent pipe[3]	4.82E+03	3.60E+03	5.01E+00	1.00E+00	3.53E-02	1.27E+03	1.25E+03
10	e	SST	large	210	pressure	passive	hepa	4.82E+03	1.30E+03	1.46E+02	1.46E-01	1.58E-01	1.21E+03	1.19E+03
11	f	SST	large	210	vacuum	passive	hepa/flapper	4.82E+03	6.70E+01	8.40E+01	3.00E-01	6.00E-01	3.77E+02	3.69E+02
12	g	SST	large	210	radiological	100 cfm (0.047 m^3/s)	hepa	4.82E+03	1.30E+03	1.46E+02	1.46E-01	1.58E-01	1.21E+03	1.19E+03
13	h	SST	large	210	toxicological	passive	hepa/flapper	4.82E+03	6.70E+01	8.40E+01	3.00E-01	6.00E-01	3.77E+02	3.69E+02
14	q	SST	entrained	40.0	radiological	100 cfm (0.047 m^3/s)	hepa[1]	4.82E+03	1.70E+03	1.30E+02	1.10E-01	2.10E-01	6.11E+02	5.99E+02
15	r	SST	entrained	40.0	toxicological and vacuum	100 cfm (0.047 m^3/s)	hepa/flapper	4.82E+03	1.46E+03	1.13E+02	1.00E-01	3.10E-01	3.27E+02	3.20E+02

Worksheet H-3. Toxicological Spreadsheet. (10 sheets)

	A	B	O	P	Q	R	S	T	U	V	W	X	Y	Z	AA	AB
1	Case	Tank Type	Source Conc. NO_2 mg/m^3	Aqueous Vent Rate L/s	Van's Onsite Limit Ex. Unlikely s/L	Van's Offsite Limit Ex. Unlikely s/L	Van's Onsite Limit Unlikely s/L	Van's Offsite Limit Unlikely s/L	Onsite Sum of Fractions Aqueous Boiloff	Offsite Sum of Fractions Aqueous Boiloff	Vent Rate of Gas m^3/s	Onsite Conc. P_2O_5 mg/m^3	Onsite Conc. CO mg/m^3	Onsite Conc. NO_2 mg/m^3	Onsite Normalized Conc. (1 mg/m^3)	Source Soot Conc. mg/m^3
3	a	SST	4.76E+01	1.42E-05	2.00E+02	6.20E-01	7.50E+02	8.00E+00	2.84E-03	8.80E-06	4.43E-01	5.57E+00	5.46E+00	7.08E-01	1.49E-02	1.73E+03
4	b	SST	2.34E+01	1.39E-05	2.00E+02	6.20E-01	7.50E+02	8.00E+00	2.78E-03	8.62E-06	6.80E-01	4.17E+00	4.08E+00	5.29E-01	2.27E-02	8.52E+02
5	c	SST	4.76E+01	1.42E-05	2.00E+02	6.20E-01	7.50E+02	8.00E+00	2.84E-03	8.80E-06	4.43E-01	5.57E+00	5.46E+00	7.08E-01	1.49E-02	1.73E+03
6	d	SST	4.76E+01	1.42E-05	2.00E+02	6.20E-01	7.50E+02	8.00E+00	2.84E-03	8.80E-06	4.43E-01	5.57E+00	5.46E+00	7.08E-01	1.49E-02	1.73E+03
7	d1	SST	1.16E+00	2.52E-08	2.00E+02	6.20E-01	7.50E+02	8.00E+00	5.04E-06	1.56E-08	4.72E-02	1.47E-02	1.44E-02	1.87E-03	1.61E-03	4.24E+01
8	d2	SST	1.95E+00	9.28E-07	2.00E+02	6.20E-01	7.50E+02	8.00E+00	1.86E-04	5.75E-07	1.04E+00	5.24E-01	5.13E-01	6.65E-02	3.41E-02	7.11E+01
9	d3	SST	1.62E+02	9.07E-06	2.00E+02	6.20E-01	7.50E+02	8.00E+00	1.81E-03	5.62E-06	4.72E-02	2.05E-04	2.01E+00	2.60E-01	1.61E-03	5.89E-01
10	e	SST	1.54E+02	4.13E-05	2.00E+02	6.20E-01	7.50E+02	8.00E+00	8.26E-03	2.56E-05	5.85E-01	2.37E+01	2.32E+01	3.01E+00	1.96E-02	5.60E+03
11	f	SST	4.78E+01	9.48E-04	2.00E+02	6.20E-01	7.50E+02	8.00E+00	1.90E-01	5.88E-04	4.31E+01	2.24E+02	2.20E+02	2.85E+01	5.95E-01	1.74E+03
12	g	SST	1.54E+02	4.13E-05	2.00E+02	6.20E-01	7.50E+02	8.00E+00	8.26E-03	2.56E-05	5.85E-01	2.37E+01	2.32E+01	3.01E+00	1.96E-02	5.60E+03
13	h	SST	4.78E+01	9.48E-04	2.00E+02	6.20E-01	7.50E+02	8.00E+00	1.90E-01	5.88E-04	4.31E+01	2.24E+02	2.20E+02	2.85E+01	5.95E-01	1.74E+03
14	q	SST	7.76E+01	2.12E-05	2.00E+02	6.20E-01	7.50E+02	8.00E+00	4.24E-03	1.31E-05	5.95E-01	1.21E+01	1.19E+01	1.54E+00	1.99E-02	2.83E+03
15	r	SST	4.15E+01	1.95E-05	2.00E+02	6.20E-01	7.50E+02	8.00E+00	3.90E-03	1.21E-05	1.02E+00	1.10E+01	1.08E+01	1.40E+00	3.37E-02	1.51E+03

Worksheet H-3. Toxicological Spreadsheet. (10 sheets)

	A	B	AC	AD	AE	AF	AG	AH	AI	AJ	AK	AL	AM	AN
1	Case	Tank Type	Onsite Total Particulate mg/m^3	Offsite Total Particulate mg/m^3	Particulate Limit ERPG-3 mg/m^3	Particulate Limit ERPG-2 mg/m^3	Particulate Limit ERPG-1 mg/m^3	Ex. Un. Onsite Total Particulate Fraction	Ex. Un. Offsite Total Particulate Fraction	Offsite Normalized Conc. (1 mg/m^3)	Ammonia Headspace Conc. mg/m^3	Ammonia ERPG-3 mg/m^3	Ammonia ERPG-2 mg/m^3	Ammonia ERPG-1 mg/m^3
3	a	SST	3.14E+01	2.64E-02	500	50	30	6.28E-02	5.29E-04	1.25E-05	1300	680	140	17
4	b	SST	2.35E+01	1.99E-02	500	50	30	4.69E-02	3.99E-04	1.92E-05	1300	680	140	17
5	c	SST	3.14E+01	2.64E-02	500	50	30	6.28E-02	5.29E-04	1.25E-05	1300	680	140	17
6	d	SST	3.14E+01	2.64E-02	500	50	30	6.28E-02	5.29E-04	1.25E-05	1300	680	140	17
7	d1	SST	8.28E-02	6.88E-05	500	50	30	1.66E-04	1.38E-06	1.34E-06	1300	680	140	17
8	d2	SST	2.95E+00	2.53E-03	500	50	30	5.90E-03	5.07E-05	2.93E-05	1300	680	140	17
9	d3	SST	1.15E-03	1.70E-03	500	50	30	2.30E-06	3.40E-05	1.34E-06	1300	680	140	17
10	e	SST	1.33E+02	1.13E-01	500	50	30	2.67E-01	2.26E-03	1.66E-05	1300	680	140	17
11	f	SST	1.26E+03	2.59E+00	500	50	30	2.53E+00	5.17E-02	1.22E-03	1300	680	140	17
12	g	SST	1.33E+02	1.13E-01	500	50	30	2.67E-01	2.26E-03	1.66E-05	1300	680	140	17
13	h	SST	1.26E+03	2.59E+00	500	50	30	2.53E+00	5.17E-02	1.22E-03	1300	680	140	17
14	q	SST	6.84E+01	5.79E-02	500	50	30	1.37E-01	1.16E-03	1.68E-05	1300	680	140	17
15	r	SST	6.19E+01	5.32E-02	500	50	30	1.24E-01	1.06E-03	2.89E-05	1300	680	140	17

Worksheet H-3. Toxicological Spreadsheet. (10 sheets)

	A	B	AO	AP	AQ	AR	AS	ATA	AU	AV	AW	AX	AY	AZ
1	Case	Tank Type	1,3 Buta Headspace Conc. mg/m^3	1,3 Buta ERPG-3 mg/m^3	1,3 Buta ERPG-2 mg/m^3	1,3 Buta ERPG-1 mg/m^3	meth. chl. Headspace conc. mg/m^3	meth. chl. ERPG-3 mg/m^3	meth. chl. ERPG-2 mg/m^3	meth. chl. ERPG-1 mg/m^3	TBP Headspace Conc. mg/m^3	TBP ERPG-3 mg/m^3	TBP ERPG-2 mg/m^3	TBP ERPG-1 mg/m^3
3	a	SST	0.19	11,000	110	22	21.76	17,400	3480	700	11.6	50	15	3
4	b	SST	0.19	11,000	110	22	21.76	17,400	3480	700	11.6	50	15	3
5	c	SST	0.19	11,000	110	22	21.76	17,400	3480	700	11.6	50	15	3
6	d	SST	0.19	11,000	110	22	21.76	17,400	3480	700	11.6	50	15	3
7	d1	SST	0.19	11,000	110	22	21.76	17,400	3480	700	11.6	50	15	3
8	d2	SST	0.19	11,000	110	22	21.76	17,400	3480	700	11.6	50	15	3
9	d3	SST	0.19	11,000	110	22	21.76	17,400	3480	700	11.6	50	15	3
10	e	SST	0.19	11,000	110	22	21.76	17,400	3480	700	11.6	50	15	3
11	f	SST	0.19	11,000	110	22	21.76	17,400	3480	700	11.6	50	15	3
12	g	SST	0.19	11,000	110	22	21.76	17,400	3480	700	11.6	50	15	3
13	h	SST	0.19	11,000	110	22	21.76	17,400	3480	700	11.6	50	15	3
14	q	SST	0.19	11,000	110	22	21.76	17,400	3480	700	11.6	50	15	3
15	r	SST	0.19	11,000	110	22	21.76	17,400	3480	700	11.6	50	15	3

Worksheet H-3. Toxicological Spreadsheet. (10 sheets)

	A	B	BA	BB	BC	BD	BE	BF	BG	BH	BI	BJ	BK	BL
1	Case	Tank Type	P_2O_5 Headspace Conc. mg/m^3	P_2O_5 ERPG-3. mg/m^3	P_2O_5 ERPG-2. mg/m^3	P_2O_5 ERPG-1. mg/m^3	NO_2 Headspace Conc. mg/m^3	NO_2 ERPG-3 mg/m^3	NO_2 ERPG-2 mg/m^3	NO_2 ERPG-1 mg/m^3	Acetonit. Headspace conc. mg/m^3	Acetonit. ERPG-3 mg/m^3	Acetonit. ERPG-2 mg/m^3	Acetonit. ERPG-1 mg/m^3
3	a	SST	3.75E+02	100	25	5	4.76E+01	94	47	3.8	21.81	60	20	3
4	b	SST	1.84E+02	100	25	5	2.34E+01	94	47	3.8	21.81	60	20	3
5	c	SST	3.75E+02	100	25	5	4.76E+01	94	47	3.8	21.81	60	20	3
6	d	SST	3.75E+02	100	25	5	4.76E+01	94	47	3.8	21.81	60	20	3
7	d1	SST	9.15E+00	100	25	5	1.16E+00	94	47	3.8	21.81	60	20	3
8	d2	SST	1.54E+01	100	25	5	1.95E+00	94	47	3.8	21.81	60	20	3
9	d3	SST	1.27E+03	100	25	5	1.62E+02	94	47	3.8	21.81	60	20	3
10	e	SST	1.21E+03	100	25	5	1.54E+02	94	47	3.8	21.81	60	20	3
11	f	SST	3.77E+02	100	25	5	4.78E+01	94	47	3.8	21.81	60	20	3
12	g	SST	1.21E+03	100	25	5	1.54E+02	94	47	3.8	21.81	60	20	3
13	h	SST	3.77E+02	100	25	5	4.78E+01	94	47	3.8	21.81	60	20	3
14	q	SST	6.11E+02	100	25	5	7.76E+01	94	47	3.8	21.81	60	20	3
15	r	SST	3.27E+02	100	25	5	4.15E+01	94	47	3.8	21.81	60	20	3

Worksheet H-3. Toxicological Spreadsheet. (10 sheets)

	A	B	BM	BN	BO	BP	BQ	BR	BS	BT	BU	BV	BW	BX	BY
1	Case	Tank Type	prop. nit. Headspace conc. mg/m^3	prop. nit. ERPG-3 mg/m^3	prop. nit. ERPG-2 mg/m^3	prop. nit. ERPG-1 mg/m^3	CO Headspace conc. mg/m^3	CO ERPG-3 mg/m^3	CO ERPG-2 mg/m^3	CO ERPG-1 mg/m^3	benezene Headspace conc. mg/m^3	benezene ERPG-3 mg/m^3	benezene ERPG-2 mg/m^3	benezene ERPG-1 mg/m^3	butanol Headspace conc. mg/m^3
3	a	SST	10.47	60	20	3	3.67E+02	1360	690	230	1.32	3130	1565	78	164.13
4	b	SST	10.47	60	20	3	1.80E+02	1360	690	230	1.32	3130	1565	78	164.13
5	c	SST	10.47	60	20	3	3.67E+02	1360	690	230	1.32	3130	1565	78	164.13
6	d	SST	10.47	60	20	3	3.67E+02	1360	690	230	1.32	3130	1565	78	164.13
7	d1	SST	10.47	60	20	3	8.97E+00	1360	690	230	1.32	3130	1565	78	164.13
8	d2	SST	10.47	60	20	3	1.51E+01	1360	690	230	1.32	3130	1565	78	164.13
9	d3	SST	10.47	60	20	3	1.25E+03	1360	690	230	1.32	3130	1565	78	164.13
10	e	SST	10.47	60	20	3	1.19E+03	1360	690	230	1.32	3130	1565	78	164.13
11	f	SST	10.47	60	20	3	3.69E+02	1360	690	230	1.32	3130	1565	78	164.13
12	g	SST	10.47	60	20	3	1.19E+03	1360	690	230	1.32	3130	1565	78	164.13
13	h	SST	10.47	60	20	3	3.69E+02	1360	690	230	1.32	3130	1565	78	164.13
14	q	SST	10.47	60	20	3	5.99E+02	1360	690	230	1.32	3130	1565	78	164.13
15	r	SST	10.47	60	20	3	3.20E+02	1360	690	230	1.32	3130	1565	78	164.13

Worksheet H-3. Toxicological Spreadsheet. (10 sheets)

	A	B	BZ	CA	CB	CC	CD	CE	CF	CG	CH	CI	CJ	CK
1	Case	Tank Type	butanol ERPG-3 mg/m^3	butanol ERPG-2 mg/m^3	butanol ERPG-1 mg/m^3	dodecane Headspace conc. mg/m^3	dodecane ERPG-3 mg/m^3	dodecane ERPG-2 mg/m^3	dodecane ERPG-1 mg/m^3	2-hexano Headspace conc. mg/m^3	2-hexano ERPG-3 mg/m^3	2-hexano ERPG-2 mg/m^3	2-hexano ERPG-1 mg/m^3	N2O Headspace conc. mg/m^3
3	a	SST	7500	750	75	296	7330	1450	37	2.68	5000	500	50	2340
4	b	SST	7500	750	75	296	7330	1450	37	2.68	5000	500	50	2340
5	c	SST	7500	750	75	296	7330	1450	37	2.68	5000	500	50	2340
6	d	SST	7500	750	75	296	7330	1450	37	2.68	5000	500	50	2340
7	d1	SST	7500	750	75	296	7330	1450	37	2.68	5000	500	50	2340
8	d2	SST	7500	750	75	296	7330	1450	37	2.68	5000	500	50	2340
9	d3	SST	7500	750	75	296	7330	1450	37	2.68	5000	500	50	2340
10	e	SST	7500	750	75	296	7330	1450	37	2.68	5000	500	50	2340
11	f	SST	7500	750	75	296	7330	1450	37	2.68	5000	500	50	2340
12	g	SST	7500	750	75	296	7330	1450	37	2.68	5000	500	50	2340
13	h	SST	7500	750	75	296	7330	1450	37	2.68	5000	500	50	2340
14	q	SST	7500	750	75	296	7330	1450	37	2.68	5000	500	50	2340
15	r	SST	7500	750	75	296	7330	1450	37	2.68	5000	500	50	2340

Worksheet H-3. Toxicological Spreadsheet. (10 sheets)

	A	B	CL	CM	CN	CO	CP	CQ	CR	CS	CT	CU	CV	CW
1	Case	Tank Type	N2O ERPG-3 mg/m^3	N2O ERPG-2 mg/m^3	N2O ERPG-1 mg/m^3	tridecane Headspace conc. mg/m^3	tridecane ERPG-3 mg/m^3	tridecane ERPG-2 mg/m^3	tridecane ERPG-1 mg/m^3	Ex.Unlikely Onsite Corrosives and Irritants Fraction	Ex. Unlikely Offsite Corrosives and Irritants Fraction	Unlikely Onsite Corrosives and Irritants Fraction	Unlikely Offsite Corrosives and Irritants Fraction	Ex. Unlikely Onsite Systemic Poisons Fraction
3	a	SST	36000	18000	270	388	7330	1450	37	9.52E-02	3.27E-04	3.88E-01	2.10E-03	1.20E-02
4	b	SST	36000	18000	270	388	7330	1450	37	9.59E-02	3.45E-04	4.06E-01	2.37E-03	1.52E-02
5	c	SST	36000	18000	270	388	7330	1450	37	9.52E-02	3.27E-04	3.88E-01	2.10E-03	1.20E-02
6	d	SST	36000	18000	270	388	7330	1450	37	9.52E-02	3.27E-04	3.88E-01	2.10E-03	1.20E-02
7	d1	SST	36000	18000	270	388	7330	1450	37	3.62E-03	1.40E-05	1.68E-02	1.10E-04	8.76E-04
8	d2	SST	36000	18000	270	388	7330	1450	37	7.91E-02	3.14E-04	3.66E-01	2.46E-03	1.87E-02
9	d3	SST	36000	18000	270	388	7330	1450	37	2.67E-02	8.61E-05	1.04E-01	5.05E-04	2.34E-03
10	e	SST	36000	18000	270	388	7330	1450	37	3.11E-01	1.02E-03	1.21E+00	6.01E-03	2.76E-02
11	f	SST	36000	18000	270	388	7330	1450	37	3.82E+00	3.19E-02	1.56E+01	2.05E-01	4.82E-01
12	g	SST	36000	18000	270	388	7330	1450	37	3.11E-01	1.02E-03	1.21E+00	6.01E-03	2.76E-02
13	h	SST	36000	18000	270	388	7330	1450	37	3.82E+00	3.19E-02	1.56E+01	2.05E-01	4.82E-01
14	q	SST	36000	18000	270	388	7330	1450	37	1.81E-01	6.09E-04	7.19E-01	3.75E-03	1.94E-02
15	r	SST	36000	18000	270	388	7330	1450	37	1.97E-01	6.94E-04	8.09E-01	4.53E-03	2.60E-02

Worksheet H-3. Toxicological Spreadsheet. (10 sheets)

	A	B	CX	CY	CZ	DA	DB	DC	DD	DE	DF	DG	DH	DI
1	Case	Tank Type	Ex. Unlikely Offsite Systemic Poisons Fraction	Unlikely Onsite Systemic Poisons Fraction	Unlikely Offsite Systemic Poisons Fraction	Ex. Unlikely Onsite Nervous system Fraction	Ex Unlikely Offsite Nervous system Fraction	Unlikely Onsite Nervous system Fraction	Unlikely Offsite Nervous system Fraction	Ex. Unlikely Onsite Particulate Fraction	Ex. Unlikely Offsite Particulate Fraction	Unlikely Onsite Particulate Fraction	Unlikely Offsite Particulate Fraction	Ex Unlikely Onsite HEPA Fraction
3	a	SST	2.69E-05	3.19E-02	1.55E-04	2.70E-03	1.04E-05	1.23E-02	3.69E-04	6.28E-02	5.29E-04	6.28E-01	8.81E-04	2.12E-03
4	b	SST	8.07E-05	4.25E-02	2.22E-04	4.10E-03	1.59E-05	1.87E-02	5.66E-04	4.69E-02	3.99E-04	4.69E-01	6.64E-04	2.12E-03
5	c	SST	1.78E-03	3.19E-02	1.55E-04	2.70E-03	1.04E-05	1.23E-02	3.69E-04	6.28E-02	5.29E-04	6.28E-01	8.81E-04	0.102
6	d	SST	1.78E-03	3.19E-02	1.55E-04	2.70E-03	1.04E-05	1.23E-02	3.69E-04	6.28E-02	5.29E-04	6.28E-01	8.81E-04	0.102
7	d1	SST	2.19E-06	2.62E-03	1.44E-05	2.91E-04	1.10E-06	1.33E-03	3.93E-05	1.66E-04	1.38E-06	1.66E-03	2.29E-06	0
8	d2	SST	4.85E-05	5.58E-02	3.17E-04	6.18E-03	2.42E-05	2.82E-02	8.62E-04	5.90E-03	5.07E-05	5.90E-02	8.45E-05	0
9	d3	SST	1.02E-05	5.50E-03	2.16E-05	2.91E-04	1.10E-06	1.33E-03	3.93E-05	2.30E-06	3.40E-05	2.30E-05	5.67E-05	0
10	e	SST	1.17E-04	6.52E-02	2.64E-04	3.55E-03	1.37E-05	1.62E-02	4.87E-04	2.67E-01	2.26E-03	2.67E+00	3.76E-03	2.12E-03
11	f	SST	3.24E-03	1.28E+00	1.51E-02	1.08E-01	1.01E-03	4.92E-01	3.59E-02	2.53E+00	5.17E-02	2.53E+01	8.62E-02	2.12E-03
12	g	SST	1.82E-03	6.52E-02	2.64E-04	3.55E-03	1.37E-05	1.62E-02	4.87E-04	2.67E-01	2.26E-03	2.67E+00	3.76E-03	0.102
13	h	SST	3.24E-03	1.28E+00	1.51E-02	1.08E-01	1.01E-03	4.92E-01	3.59E-02	2.53E+00	5.17E-02	2.53E+01	8.62E-02	2.12E-03
14	q	SST	1.79E-03	4.93E-02	2.25E-04	3.60E-03	1.39E-05	1.64E-02	4.95E-04	1.37E-01	1.16E-03	1.37E+00	1.93E-03	1.02E-01
15	r	SST	1.81E-03	6.99E-02	3.51E-04	6.10E-03	2.39E-05	2.78E-02	8.50E-04	1.24E-01	1.06E-03	1.24E+00	1.77E-03	1.02E-01

Worksheet H-3. Toxicological Spreadsheet. (10 sheets)

	A	B	DJ	DK	DL	DM	DN	DO	DP	DQ	DR	DS	DT
1	Case	Tank Type	Ex Unlikely Offsite HEPA Fraction	Unlikely Onsite HEPA Fraction	Unlikely Offsite HEPA Fraction	Ex. Un. Onsite Sum of Fractions Aqueous Boiloff	Ex. Un. Offsite Sum of Fractions Aqueous Boiloff	Unlikely Onsite Sum of Fractions Aqueous Boiloff	Unlikely Offsite Sum of Fractions Aqueous Boiloff	Ex. Un. Onsite Total Sum Of Fractions	Ex. Un. Offsite Total Sum Of Fractions	Unlikely Onsite Total Sum Of Fractions	Unlikely Offsite Total Sum Of Fractions
3	a	SST	3.60E-05	4.45E-02	7.00E-05	2.84E-03	8.80E-06	1.06E-02	1.14E-04	1.78E-01	9.38E-04	1.11E+00	3.69E-03
4	b	SST	3.60E-05	4.45E-02	7.00E-05	2.78E-03	8.62E-06	1.04E-02	1.11E-04	1.67E-01	8.85E-04	9.92E-01	4.01E-03
5	c	SST	1.74E-03	2.15E+00	3.37E-03	2.84E-03	8.80E-06	1.06E-02	1.14E-04	2.78E-01	4.39E-03	3.22E+00	6.99E-03
6	d	SST	1.74E-03	2.15E+00	3.37E-03	2.84E-03	8.80E-06	1.06E-02	1.14E-04	2.78E-01	4.39E-03	3.22E+00	6.99E-03
7	d1	SST	0.00E+00	0.00E+00	0.00E+00	5.04E-06	1.56E-08	1.89E-05	2.02E-07	4.95E-03	1.87E-05	2.24E-02	1.67E-04
8	d2	SST	0.00E+00	0.00E+00	0.00E+00	1.86E-04	5.75E-07	6.96E-04	7.42E-06	1.10E-01	4.38E-04	5.09E-01	3.73E-03
9	d3	SST	0.00E+00	0.00E+00	0.00E+00	1.81E-03	5.62E-06	6.80E-03	7.26E-05	3.11E-02	1.37E-04	1.17E-01	6.95E-04
10	e	SST	3.60E-05	4.45E-02	7.00E-05	8.26E-03	2.56E-05	3.10E-02	3.31E-04	6.19E-01	3.47E-03	4.03E+00	1.09E-02
11	f	SST	3.60E-05	4.45E-02	7.00E-05	1.90E-01	5.88E-04	7.11E-01	7.58E-03	7.13E+00	8.85E-02	4.33E+01	3.50E-01
12	g	SST	1.74E-03	2.15E+00	3.37E-03	8.26E-03	2.56E-05	3.10E-02	3.31E-04	7.19E-01	6.88E-03	6.14E+00	1.42E-02
13	h	SST	3.60E-05	4.45E-02	7.00E-05	1.90E-01	5.88E-04	7.11E-01	7.58E-03	7.13E+00	8.85E-02	4.33E+01	3.50E-01
14	q	SST	1.74E-03	2.15E+00	3.37E-03	4.24E-03	1.31E-05	1.59E-02	1.70E-04	4.47E-01	5.33E-03	4.32E+00	9.94E-03
15	r	SST	1.74E-03	2.15E+00	3.37E-03	3.90E-03	1.21E-05	1.46E-02	1.56E-04	4.59E-01	5.35E-03	4.31E+00	1.10E-02

[1]HEPA Vent Modeled as 3.75" (9.5 mm) orifice
[2]Flapper is 50 in. (1.27 m) orifice opening at 1 psid (6.89 kPa)
[3]Vent Pipe on SST Modeled as 9.2 in. (0.23 m) orifice.

APPENDIX I

DESCRIPTION OF POOLFIRE.4

This page intentionally left blank.

CONTENTS

1.0 INTRODUCTION I-5

2.0 FIRE SCENARIO MODELED I-5

3.0 DESCRIPTION OF KEY PARAMETERS CALCULATED I-7

4.0 CALCULATION APPROACH I-7

5.0 DETAILED CALCULATION FORMULAE I-9
5.1 GAS QUANTITY AND COMPOSITION I-9
5.2 HEATUP OF HEADSPACE AIR BY COMBUSTION I-17
5.3 GAS VENTING FROM (AND INTO) TANK I-22
5.4 HEAT TRANSFER FROM GAS TO TANK I-27
5.4.1 Heat Transport to Steel Structures I-28
5.4.2 Heat Transport to Solvent Pool I-32
5.4.3 Heat Transport to Concrete I-33
5.4.4 Heat Transport to Sludge I-37
5.5 CHANGE IN GAS TEMPERATURE DUE TO HEAT TRANSFER I-38

6.0 LISTING OF BASIC PROGRAMS I-39

7.0 EXAMPLE ANALYSIS WITH POOLFIRE.4 . . . . . I-47

8.0 CONFIRMATION OF POOLFIRE.4 . . . . . I-69

9.0 REFERENCES I-70

ATTACHMENT

A MEMO FROM M. EPSTEIN OF FAI TO A. K. POSTMA, "CONFIRMATION OF POSTMA'S SOLVENT-FIRE TANK-PRESSURE TRANSIENT MODEL, "DATED SEPTEMBER, 26, 1995 . . . . . Att I 1-1

B LETTER FROM C. L. BEYLER, HUGHES ASSOCIATES, INC. TO A. K. POSTMA . . . . . Att I 2-1

LIST OF FIGURES

2-1 Fire Scenario I-5

4-1 Calculation Method Overall Flow I-7

5-1 Normalized Burn Rate Versus Oxygen Concentration I-11

5-2 Combustion Process I-21

This page intentionally left blank.

1.0 INTRODUCTION

This appendix describes in detail the technical basis for POOLFIRE.4, a GW BASIC[1] program, which calculates a solvent fire transient in a tank. A complete listing of this program and an example run and output file are included in Sections 6.0 and 7.0 of this appendix.

2.0 FIRE SCENARIO MODELED

Figure 2-1 shows a waste tank and solvent pool that typifies the pool fire geometries studied herein.

Figure 2-1. Schematic Diagram of Solvent Pool Configuration Analyzed.

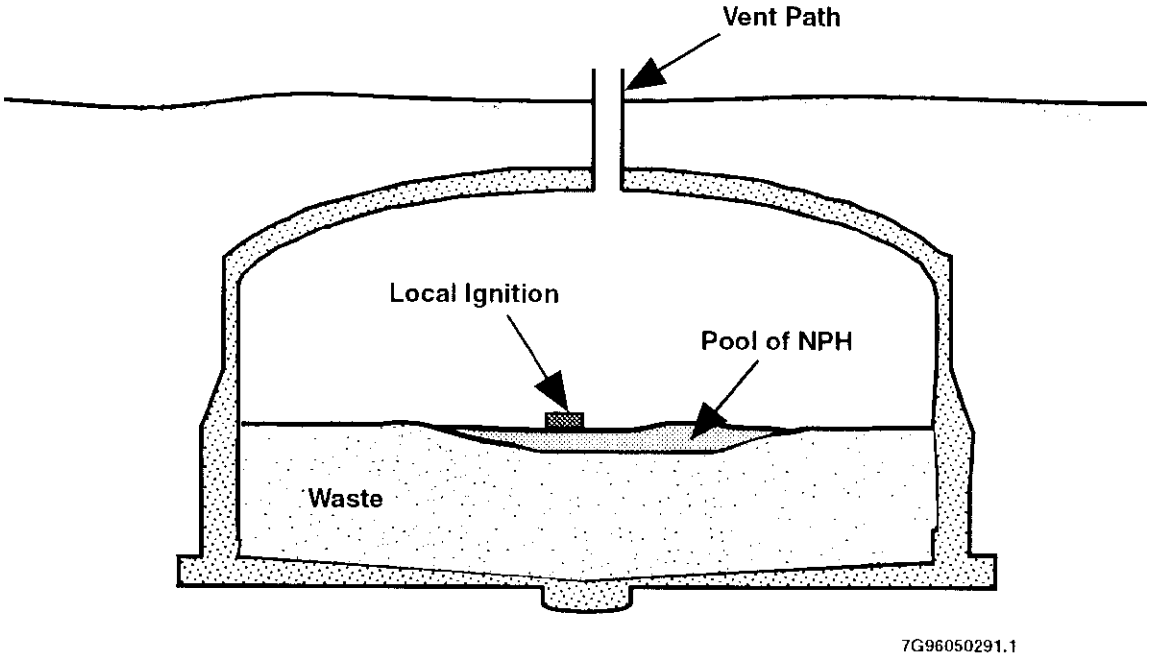

[1] GW BASIC is a trademark of Microsoft, Inc., Redmond, Washington.

Key Assumptions of Scenario

1. Local ignition of a fire is postulated without considering the probability of ignition. To consider a range of possibilities, the initial inflamed area is treated as an input parameter.

   Initial inflamed area = πR_o^2. R_o = input on line 20. Units are ft.

2. The fire spreads at a fixed velocity in the radial direction. The spread velocity is a keyboard input, SPREADV. It is input on line 240. Units are cm/s.

3. The specific burning rate is assumed to vary linearly with oxygen concentration. The initial specific burning rate (applicable for air at 21 percent oxygen) is treated as an input to permit parametric analyses. This parameter is called MDOTB and is input on line 20. Units are kg/m^2 min.

4. The combustion enthalpy is an input and is assumed constant for the fire duration. The symbol for this parameter is DELH and is input on line 80. Units are Btu/lb of organic.

5. The gas phase is assumed to be well mixed at all times. This simplifying assumption is expected to yield conservative estimates of peak pressure because heat transfer from the gas to tank walls is minimized. Actual fires would have a hot layer near the ceiling which would be higher than average temperature and would radiate ($h \sim T^4$) heat at a higher rate than calculated for the cooler, well-mixed gas case. Hörman (1983), who analyzed enclosed solvent fires, confirms that the well-mixed model yields conservative pressures.

6. The fire extinguishes when a cutoff limit in oxygen concentration is reached. This was observed in all tests on solvent fires reported by Malet et al. (1983). To perform parametric analyses, the oxygen extinguishment level is an input, on line 20. The symbol is XO2STOP, and the units are mole fraction.

7. The tank geometry is assumed to remain constant for the duration of the fire. Opening of risers caused by internal tank pressure is accounted for.

3.0 DESCRIPTION OF KEY PARAMETERS CALCULATED

The use of the pool fire calculation is to predict consequences of a fire. The following key parameters must be predicted.

- Tank internal pressure
- Quantity of organic burned
- Quantity of gas vented from tank
- Temperature of tank surfaces.

4.0 CALCULATION APPROACH

The temporal variation in pressure, temperatures, and gas inventory was computed as a result of a series of burn events in which the end state for each time step was used as the initial state for the next time step. Within each time step, mass and energy balances were made to calculate temperature changes, pressure changes, and changes in inventory.

Figure 4-1 shows the overall flow of the calculation method.

Figure 4-1. Calculation Method Overall Flow.

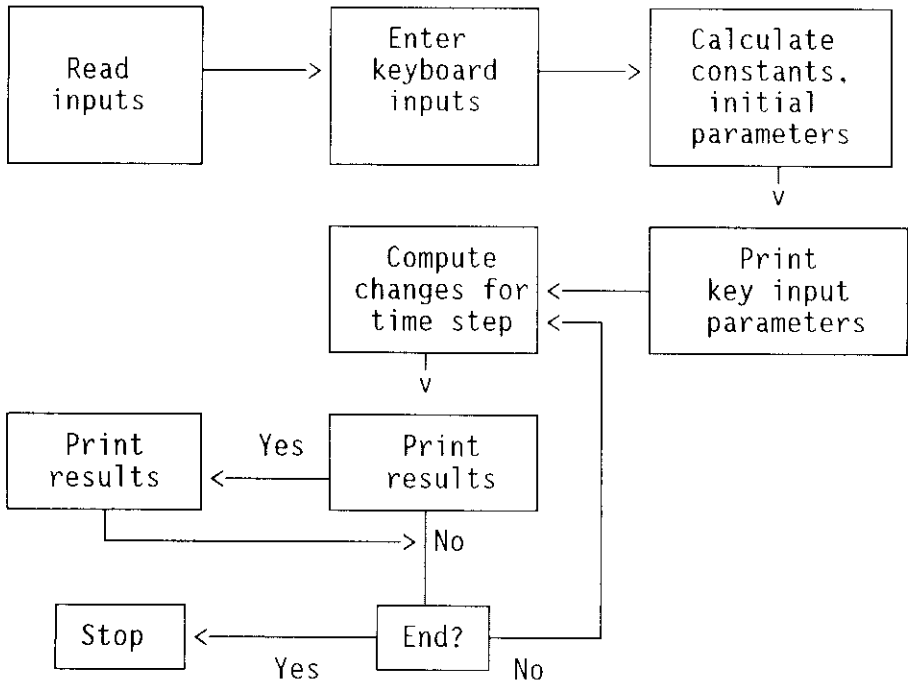

Within each time step (time steps are typically of the order of 1 sec) several thermodynamic process steps are analyzed to determine the temperature and pressure of confined gases. These are as follows:

Step 1: Combustion Energy and Stoichiometry

In step 1, the combustion energy produced by the fire is calculated, and stoichiometric calculations are made to determine gas composition at the end of the time step. These calculations are carried out in a subroutine starting at line 1800 and ending at line 1899.

Step 2: Gas Heatup at Constant Volume

In step 2, the internal energy of the gas inventory was increased by the quantity of combustion energy calculated in step 1. This heatup calculation is performed in a subroutine starting at line 1900 and ending at line 1995.

Step 3: Gas Venting and Expansion Work

The quantity of gas vented from the tank during a time step was computed on the basis of pressure difference and flow path admittance. The gas in the tank was assumed to undergo an isentropic expansion. Venting and expansion work are calculated in a subroutine starting at line 2000. For times when the tank pressure is higher than atmospheric pressure, the subroutine ends at line 2290. When internal pressure is less than atmospheric pressure, a branch of the routine (starting at line 2280) goes to a subroutine starting at line 3000 and ending at line 3290. For inflow, the step 1 calculations are bypassed, and gas composition is calculated for mixing of contained gases with inflowing atmospheric air. This mixing calculation is done in the subroutine starting at line 3000 and ending at line 3290.

Step 4: Heat Transfer to Surfaces

Heat transfer from the gas to tank surfaces was computed by accounting for radiation and convection. Gas inventory was held constant for this step. Temperature and pressure computed at the end of this step were used as initial values for the next time increment, starting again at step 1. The heat balance calculations are carried out in subroutines starting at lines 2300, 2600, 2700, and 2800. The subroutine starting at line 2300 computes heat flux from gas to concrete and organic pool areas. Similarly, the subroutine starting at line 2800 computes heat flux to sludge surfaces. The subroutine starting at line 2600 computes heat flux from gas to steel surfaces. Finally, the change in gas temperature due to heat transfer is computed in the subroutine starting at line 2700. In addition to calculating heat flux, each of the subroutines cited above also calculated the transient heatup of the surface involved.

Sequential Versus Simultaneous Processes

The four-step approach identified above treats heat transfer and outflow as sequential steps. In reality, these processes occur simultaneously. The validity of the sequential process treatment can be verified by analyzing a given problem using a series of smaller and smaller time steps. For sufficiently small steps, no significant difference in results will appear when a smaller step is used. For the cases analyzed here, little difference in calculated results was seen when time steps were reduced from 10s to 0.1s. Most runs were made with time steps in the range of 0.1s to 1s. The sequential steps work because very little change in temperature, pressure, or gas inventory occurs during the small steps.

5.0 DETAILED CALCULATION FORMULAE

This section contains the equations used to quantify the parameters included here.

5.1 GAS QUANTITY AND COMPOSITION

The quantity of gases in a tank is computed by means of the ideal gas law. Initial quantities are computed as follows.

$$MTOT = PTOT\ominus * GVOL / (R * T) \quad (1)$$

where

MTOT	=	total mols (lb mols)
PTOT⊖	=	initial absolute pressure (psia)
GVOL	=	gas volume in tank (ft^3)
R	=	gas constant (10.73 psi ft^3/°R mol)
T	=	absolute temperature (°R).

This calculation is done at line 330. PTOT⊖, GVOL, and T are input values on lines 40, 80, and 50, respectively. The initial gas temperature is specified as TG⊖ in °F on line 50.

A second step is to calculate the initial mols of water vapor on the basis of an inputted initial water vapor pressure, PWAT⊖.

$$MH_2O = PWAT\ominus * GVOL / (R * T) \quad (2)$$

where

MH_2O	=	mols of water vapor
PWAT⊖	=	initial water vapor pressure (psia).

PWATΘ is an input value on line 80.

Initial gas is assumed to be made up of water vapor and air (composed of 79 percent N_2 and 21 percent O_2). Nitrogen and oxygen moles (initially present) are computed from:

$$MN_2 = 0.79 * (MTOT - MH_2O) \quad (3)$$

and

$$MO_2 = 0.21 * (MTOT - MH_2O) \quad (4)$$

where

MN_2 = initial mols of nitrogen
MO_2 = initial mols of oxygen.

The mole fraction of oxygen in contained gases is computed as:

$$XO_2 = MO_2 / MTOT \quad (5)$$

where

XO_2 = oxygen mole fraction.

These calculations are carried out in lines 320 through 365.

The gas composition is recalculated at each time step to account for combustion and leakage. The combustion effects are computed in lines 1800 through 1899 and are described as follows.

First, a burning rate factor is computed as a function of oxygen concentration.

$$OXFACT = 9.72 * XO2 - 1.04 \quad (6)$$

This equation describes a linear relationship in which OXFACT has a value of unity at an oxygen mole fraction of 0.21 and a value 0.125 at an oxygen mole fraction of 0.12. This calculation is made at line 1807.

The basis for the assumed relationship between specific burn rate and oxygen concentration was provided by Dr. Beyler of Hughes Associates, Inc. The data provided by Beyler are shown in Figure 5-1. These data were obtained from measurements made on organic pool fires. The straight line relationship appears to be a reasonable first approximation and was recommended by Dr. Beyler.

Figure 5-1. Normalized Burn Rate Versus Oxygen Concentration.

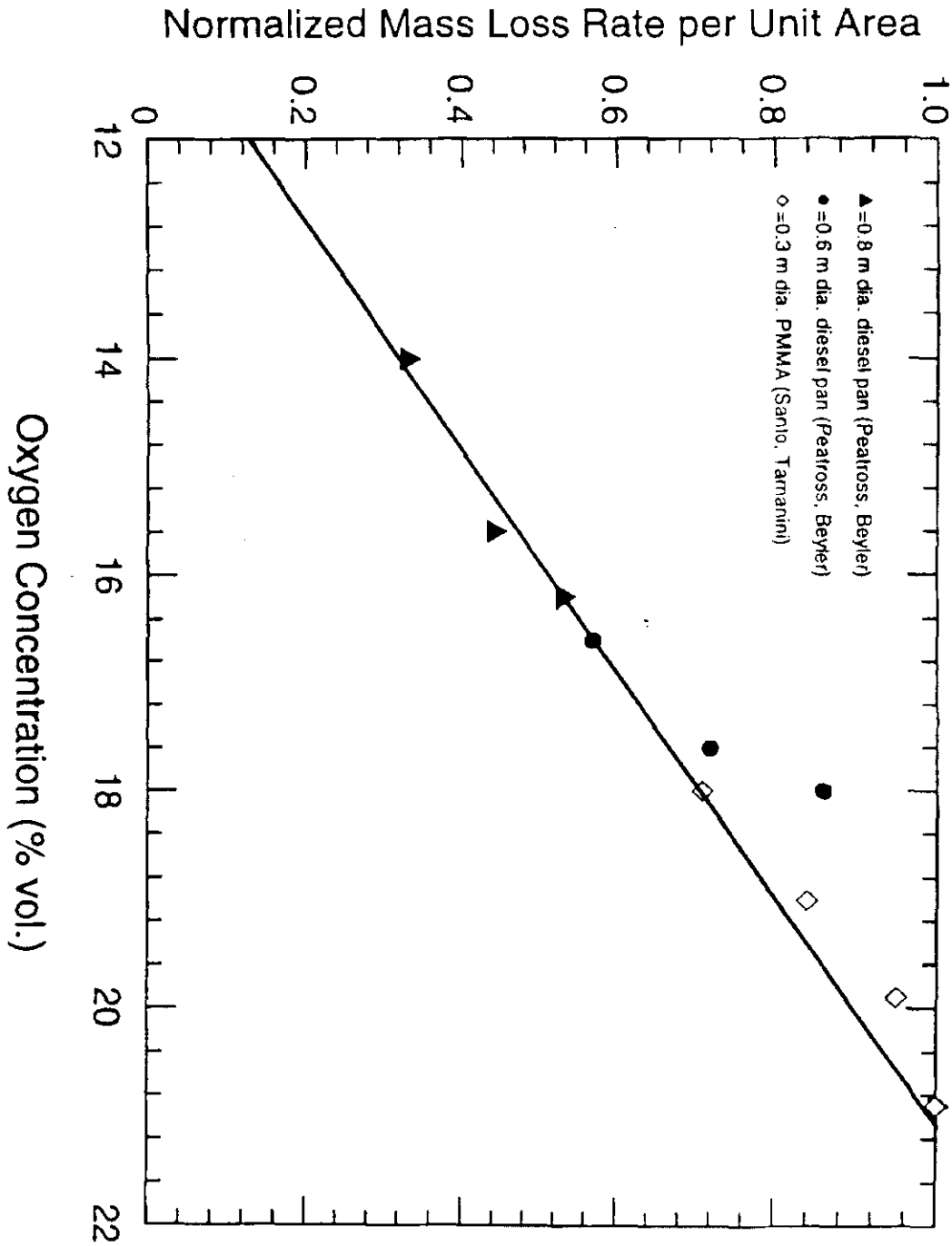

Next the average burn area is computed for the time step, at line 1810.

$$BURNAR = 3.1416 * (R\ominus + (TIM + DT/2) * (BURNR - R\ominus)/TIMS)\wedge 2 \qquad (7)$$

where

BURNAR	=	inflamed area of pool (ft^2)
R⊖	=	radius of initial inflamed area (ft)
TIM	=	time from fire initiation (sec)
DT	=	length of time step (sec)
BURNR	=	pool radius corresponding to the whole organic surface area (ft)
TIMS	=	time of fire spread across the whole organic surface (sec).

BURNR and TIMS are constants for the problem and are computed at line 310 and line 395, respectively.

The total burn rate is computed as the product of inflamed area and specific burn rate.

$$BRATE = BURNAR * MDOTB * OXFACT \qquad (8)$$

where

BRATE	=	burn rate of organic (lb/s)
MDOTB	=	specific burn rate at an oxygen mole fraction of 0.21 (lb/s ft^2)
OXFACT	=	oxygen factor computed from Eq. (6), dimensionless.

Note that MDOTB was converted to English units in line 605.

The total integrated mass of organic burned is computed from:

$$MASSBURN = BRATE * DT + MASSBURN \qquad (9)$$

where

MASSBURN	=	Total organic combusted (lb).

Combustion products are quantified on the basis of NPH and TBP reacting with O_2 to produce CO_2 and H_2O. NPH is represented by dodecane and reacts according to:

$$C_{12}H_{26} + 18.5\ O_2 = 12\ CO_2 + 13\ H_2O \tag{10}$$

TBP is assumed to react according to:

$$C_{12}H_{27}PO_4 + 18\ O_2 = 12\ CO_2 + 13.5\ H_2O + \frac{1}{2}\ P_2O_5 \tag{11}$$

Overall, stoichiometry is based on 84 percent by mass of dodecane and 16 percent by mass TBP. These mass ratios were determined experimentally for vapor equilibrium above tank 241-C-103 organic by Pool and Bean (1994) at 100 °C.

<u>Basis: 1 lb of fuel vapor</u>

$$\text{mols } C_{12}H_{26} = 0.84/170.33 = 4.932\ E\text{-}3$$

$$\text{mols TBP} = 0.16/266.32 = 6.008\ E\text{-}4$$

$$\text{Total mols} = 4.932\ E\text{-}3 + 6.008\ E\text{-}4 = 5.53\ E\text{-}3$$

$$\text{mol wt. of mixture} = 1/5.532\ E\text{-}3 = 180.8$$

<u>Basis: 1 mol of fuel (1 mol)</u>

$$\text{mols } C_{12}H_{26} = \frac{0.84\,(180.8)}{170.33} = 0.8914$$

$$\text{mols TBP} = \frac{0.16\,(180.8)}{266.32} = 0.1086$$

$$\frac{\text{mols } O_2 \text{ reacted}}{\text{mol fuel}} = 0.8914(18.5) + 0.1086(18) = 18.45$$

$$\frac{\text{mols } H_2O \text{ formed}}{\text{mol fuel}} = 0.8914(13) + 0.1086(13.5) = 13.05$$

$$\frac{\text{mols } CO_2 \text{ formed}}{\text{mol fuel}} = 0.8914(12) + 0.1086(12) = 12.0$$

The mols of fuel burned during a time step is computed in line 1840 by:

$$DMF = BRATE * DT/180.8 \tag{12}$$

where

DMF = mols fuel burned in time step.

The total inventory of combustion products is updated by adding the increment in lines 1855 through 1870.

$$1855 \quad MH_2O = MH_2O + DMF * 13.05 \tag{13}$$

$$1860 \quad MO_2 = MO_2 - 18.45 * DMF \tag{14}$$

$$1865 \quad MCO_2 = MCO_2 + 12 * DMF \tag{15}$$

$$1867 \quad TOTCO_2 = TOTCO_2 + 12 * DMF \tag{16}$$

where

$TOTCO_2$ = Total CO_2 formed by combustion.

The total CO_2 formed by combustion is used as a tracer gas to determine the fraction of combustion products vented from the tank during the course of a fire.

$$1870 \quad MTOT = MH_2O + MO_2 + MN_2 + MCO_2 \tag{17}$$

The oxygen mole fraction is calculated at each burning time step and is compared with the extinguishment level inputted as XO2STOP.

$$1880 \quad XO_2 = MO_2 \ / \ MTOT \tag{18}$$

where

XO_2 = mole fraction of O_2.

An IF statement (at line 1805) bypasses the combustion product material balance sequence for times after the fire is out.

For times when the fire is out and the tank is pressurized as compared to the outside atmosphere, the gas inventory is depleted by the fraction vented during the time step. This is done in a subroutine starting at line 2000 in lines 2170 through 2220:

$$2170 \quad MH_2O = MH_2O \ / \ VRATIO \tag{19}$$

$$2180 \quad MO_2 = MO_2 \ / \ VRATIO \tag{20}$$

$$2190 \quad MN_2 = MN_2 \ / \ VRATIO \tag{21}$$

$$2200 \quad MCO_2 = MCO_2 \ / \ VRATIO: \tag{22}$$

$$FCO_2 = MCO_2 \ / \ TOTCO_2 \tag{23}$$

$$2220 \quad MTOT = MTOT \ / \ VRATIO \tag{24}$$

In the above equation, VRATIO is the vent factor calculated in line 2120 and line 2125.

$$2120 \quad V_2 = GVOL + FVOL \tag{25}$$

$$2125 \quad VRATIO = V_2 / GVOL \tag{26}$$

where

V_2 = total of contained volume and vented volume
FVOL = volume of gas vented at tank conditions (ft^3).

When the tank internal pressure falls below that of the outside atmosphere, atmospheric air flows in through the leak path. Inflowing air is assumed to be air at 55 °F (the average annual Hanford Site temperature) and contain water vapor at 50 percent relative humidity.

<u>Basis: 1 mol of outside air</u>

H_2O vapor pressure at 55 °F = 0.222 psi

At 50 percent RH, vapor pressure = 0.5 (0.222) = 0.11 psi

For a total pressure of 14.5 psia (Hanford annual average)

$$H_2O \text{ mole fraction} = \frac{0.11}{14.5} = 0.0076$$

Dry air mole fraction = 1 - 0.0076 = 0.992

Mole fraction of N_2 = 0.79 (0.992) = 0.784

Mole fraction of O_2 = 0.21 (0.992) = 0.208.

For the inflow time period, the gas inventory is computed for each time step in lines 3180 to 3210 in a subroutine starting at line 3000.

$$3180 \quad MH_2O = MH_2O + INMOLS * 0.008 \tag{27}$$

$$3190 \quad MO_2 = MO_2 + INMOLS * 0.208 \tag{28}$$

$$3200 \quad MN_2 = MN_2 + INMOLS * 0.784 \tag{29}$$

$$3210 \quad MTOT = NEWMOLS \tag{30}$$

In equations 26 through 30, INMOLS is the quantity of air predicted to flow into the tank during a time step. The total integrated inflow is calculated in line 3120:

$$3120 \quad NEWMOLS = INMOLS + MTOT \tag{31}$$

As described, equations 1 through 31 are used to calculate the inventory and composition of headspace gases.

5.2 HEATUP OF HEADSPACE AIR BY COMBUSTION

The heatup of headspace air by combustion is treated as a constant volume process. The sensible heat gain is equated to the enthalpy of combustion:

$$\Delta T = \frac{\Delta H}{MC_v} \tag{32}$$

where

ΔT	=	increase in temperature (°F)
ΔH	=	effective enthalpy of combustion (Btu)
M	=	total mols of gas
C_v	=	average heat capacity at constant volume (Btu/mol).

This computation is carried out in a subroutine starting at line 1900 and ending at line 1995. An iterative procedure is used to account for the change in C_v with temperature.

The heat capacity of each gas was related to temperature by means of a quadratic equation:

$$C_p = A + BT + CT^2 \tag{33}$$

where

C_p	=	heat capacity at constant pressure
A,B,C	=	constants
T	=	absolute temperature.

The average heat capacity over a temperature interval can be calculated by integrating equation 32 with respect to temperature and dividing by the interval:

$$C_p(avg) = \frac{1}{(T_2 - T_1)} \int_{T_1}^{T_2} (A + BT + CT^2)\, dT \tag{34}$$

Carrying out the integration,

$$C_p(avg) = A + \frac{B}{2}(T_1 + T_2) + \frac{C}{3}(T_2^2 + T_1 T_2 + T_1^2) \tag{35}$$

Heat capacity at constant volume, C_v, can be estimated from C_p by:

$$C_v = C_p - R \tag{36}$$

where

R = ideal gas constant (1.987 cal/mole °K).

The constants, A, B, and C were taken from data presented by Hougen et al. (1954). T_1 in equation 34 is taken as the initial gas temperature and T_2 is predicted by a predictor-corrector iterative routine as described on lines 1905, 1907, 1910, 1920, 1982, 1985, and 1990.

The temperature factors in equation 34 are calculated in lines 1930 and 1940:

$$1930 \quad A = T_1 + T_2 \tag{37}$$

$$1940 \quad B = T_2^2 + T_1 * T_2 + T_1^2 \tag{38}$$

Then average heat capacities for each gas tracked is computed.

$$1950 \quad CVH2O = 5.149 + A * 0.000733 + 4.72E{-}09 * B \tag{39}$$

where CVH2O = C_v for H_2O vapor.

1955 CVN2 = 4.47 + A * 0.000386 - B * 7.1E-9 (40)

where CVN2 = C_v for nitrogen.

1960 CVO2 = 4.13 + 0.00088 * A - 1.03E-7 * B (41)

where CVO2 = C_v for oxygen.

1965 $CVCO_2$ = 4.352 + 0.00281 * A - 3.51E-7 * B (42)

where $CVCO_2$ = C_v for CO_2.

The product, MC_v (moles times heat capacity), as used in equation 32, is calculated in line 1970.

1970 MCV = MH2O * CVH2O + MN2 * CVN2 + MO2 * CVO2 + MCO2 * CVCO2 (43)

where

MCV = MC_v for headspace gas.

The temperature increase caused by combustion is calculated in line 1980:

DELTG = (DELE - FSENS) / MC_v (44)

where

DELTG = ΔT rise in °F.

The variable DELE is the total combustion energy for the time step and was computed on line 1830 in the combustion subroutine:

1830 DELE = BRATE * DELH * DT (45)

where

DELE = Btu of combustion energy.

$$\frac{lb}{s} * \frac{BTU}{lb} * s = BTU$$

As shown in equation 44, the endotherm required to heat fuel vapor from the fire point to the headspace gas temperature is deducted from combustion enthalpy.

This endotherm was calculated in a subroutine starting at line 3300.

$$3310 \quad T_1 = 758 \tag{46}$$

T_1 is the temperature of vapor leaving the pool and was based on the estimated fire point of the fuel. The fire point of the fuel was estimated by adding 30 °C to the measured flash point:

$$T_1 = 118 + 30 = 148\,^{\circ}C = 758\,^{\circ}R \tag{47}$$

$$3320 \quad T_2 = TG \tag{48}$$

T_2 is the headspace gas temperature, at which it is assumed combustion takes place. Lines 3330, 3340, and 3350 are used to compute the average heat capacity of fuel vapor, using quadratic coefficients evaluated for dodecane using a correlation from Hougen et al. (1954). The quantities A and B are temperature factors defined in equations 37 and 38. The molar heat capacity of dodecane vapor (Btu/lb mol) is calculated at line 3350:

$$3350 \quad CPFUEL = 0.478 + 0.0686 * A - 8.63E\text{-}6 * B \tag{49}$$

The sensible heat endotherm attributable to heating of fuel vapor from the firepoint to the current gas temperature is calculated in line 3360:

$$3360 \quad FSENS = (T_2 - T_1) * CPFUEL * DMF \tag{50}$$

where

FSENS = unreacted fuel vapor endotherm (Btu).

Figure 5-2 shows the combustion process modeled here.

Figure 5-2. Combustion Process.

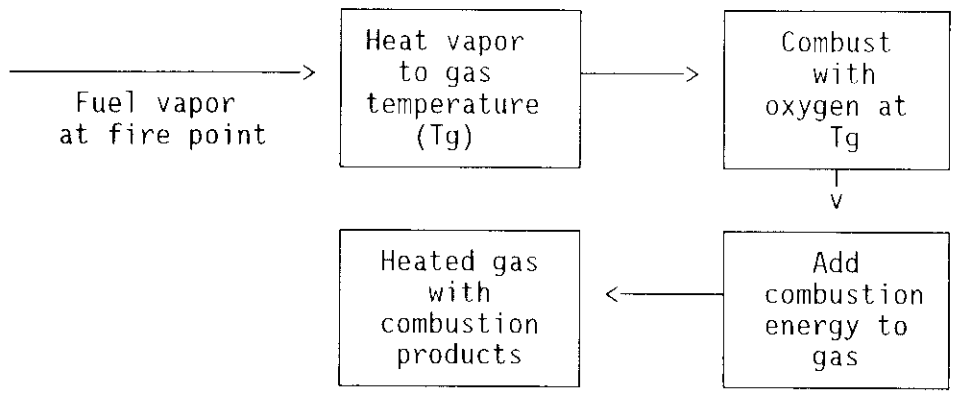

The vapor endotherm, FSENS, is small compared to combustion energy, DELE. Predicted gas pressures and temperatures are therefore not significantly affected by the FSENS term.

The combustion enthalpy, ΔH_R, varies with temperature if the products and reactants have different heat capacities. The reaction enthalpy at a temperature T, may be computed from the value at 298 °K as follows (Daniels and Alberty 1955):

$$\Delta H_T - \Delta H_{298} = \int_{298}^{T} \Delta C_p \, dT \qquad (51)$$

where

ΔH_T	=	combustion enthalpy at T
ΔH_{298}	=	combustion enthalpy at 298 °K
ΔC_p	=	Σ C_p (products) - Σ C_p (reactants)
T	=	absolute temperature.

A numerical evaluation of equation 51 indicated that the change in combustion enthalpy was less than 1 percent over the temperature range of interest. This variation is too small to significantly affect calculated temperatures and pressures and was neglected, i.e., ΔH_{298} was not corrected for temperature.

The final step in the heatup calculation is to compute the magnitude of the temperature rise for contained gases at constant volume.

```
1990   Tg = Tg + DELTG                                    (53)
```

$$1980 \quad DELTG = (DELE - FSENS) / MC_v \tag{52}$$

where

DELTG	=	rise in gas temperature (°R)
Tg	=	gas temperature (°R).

Note that the final value of DELTG is based on five iterations of heat capacity.

5.3 GAS VENTING FROM (AND INTO) TANK

The tanks are not leak-tight and will vent gas when pressurized or take in atmospheric air when at negative pressure. Two effects are:

- Gain or loss in gas inventory
- Expansion work done by gas remaining in tank.

Gas venting rates and effects are computed in a subroutine starting at line 2000.

Because relatively high internal gas pressures can theoretically develop as a result of a fire, compressible effects may be important in limiting venting velocities. Flow rates through vent paths were modeled as a gas flow through an orifice, using the American Society of Mechanical Engineers orifice equation (Perry 1950).

$$W = Q_1\rho_1 = CYS_2 \sqrt{\frac{2g_c(P_1 - P_2)/\rho_1}{1 - \beta^4}} \tag{54}$$

where

W	=	mass flow rate (lb/s)
Q	=	volumetric flow rate (ft^3/s)
ρ_1	=	density at upstream conditions (lb/ft^3)
C	=	coefficient of discharge
Y	=	expansion factor
g_c	=	gravitational constant (32.17 $lb_m ft/lb_f\ sec^2$)
P_1, P_2	=	pressures upstream and downstream (lb_f/ft^2)

β^2 = ratio of cross section area of constriction to that of upstream channel

S_2 = cross section area of discharge opening (ft^2).

Gas velocity calculated in the orifice was compared to sonic velocity, and the maximum allowed velocity was sonic velocity.

Actual vent paths are not circular orifices, so an equivalent orifice, i.e., one that delivered the same gas flow at the maximum pressure difference, was separately calculated and treated as an input parameter. The method for predicting adiabatic flow through pipes is explained in Appendix C of Grigsby et al. (1995).

A first step in the flow estimate is to compute the average value of C_v.

$$2020 \quad CVAVG = MCV/MTOT \tag{55}$$

where

CVAVG = average value of C_v
MCV = ΣMC_v (from line 1970)
MTOT = total gas mols.

Headspace gas pressure at the beginning of the time step is calculated from the ideal gas law.

$$2030 \quad P_1 = MTOT * TG * ROV \tag{56}$$

where

P_1 = initial gas pressure
ROV = gas constant/gas volume (line 380).

The ratio of downstream to upstream absolute pressure is calculated.

$$2040 \quad PRATIO = PTOTO / PAV \tag{57}$$

where

PAV = average tank pressure (line 2035).

Lines 2042, 2044, 2046, and 2048 check whether tank pressure is sufficiently high to open the salt well vent. If sufficiently high, the flow area is increased to account for the salt well vent path. The expansion factor (Y of equation 54) is computed in line 2050.

2050 YFACT = 1 - 0.315 * (1 - PRATIO) (58)

This estimate of the expansion factor is based on a formula (Perry 1950) for square-edged orifices. As a simplification, β^2 (equation 54) was set equal to zero, and the specific heat ratio was set equal to 1.3, a value applicable to air. Perry's formula for Y is:

$$Y = 1 - \left[\frac{P_1 - P_2}{P_1 K}\right] (0.41 + 0.35\beta^4) \tag{59}$$

where the terms are as defined in equation 54 with an additional term, K = specific heat ratio = C_p/C_v.

Sonic velocity in air at temperature TG is then calculated.

2060 SONIC = 47.2 * TG^0.5 (60)

where

SONIC = sonic velocity (ft/sec).

The constant in equation 60 is calculated on the basis of sonic velocity in an ideal gas (Hougen et al. 1959, p. 695):

$$a = \left[\frac{g_c KRT}{M}\right]^{\frac{1}{2}} \tag{61}$$

where

a = sonic velocity
K = specific heat ration (assumed 1.3)
R = ideal gas constant
T = absolute temperature (°R)
M = molecular weight of gas (assumed 29).

The Bernoulli velocity ($V^2 = 2g_c\Delta P/\rho$) in the orifice is calculated as a function of pressure drop.

2080 VEL = 96.3 * [(PAV - PTOTO) / RHOGAS]^0.5 (62)

where

VEL = velocity in throat (ft/sec)
RHOGAS = gas density from line 2070 (lb/ft^3)
PAV, PTOTO = pressures in psia.

The Bernoulli velocity is compared with sonic velocity in line 2090, and the lesser of these two is used as throat velocity (line 2090). Flow rate of vented gas is calculated in line 2095:

$$2095 \quad FLRATE = ORIFC * FAREA * YFACT * VEL \tag{63}$$

where

FLRATE = gas flow rate (ft^3/sec)
ORIFC = orifice coefficient (an input)
FAREA = orifice open area (ft^2).

The volume of gas expelled from the tank during the step is calculated as the product of flow rate and time.

$$2100 \quad FVOL = FLRATE * DT \tag{64}$$

where

FVOL = gas volume expelled at upstream conditions.

The ratio of specific heats, C_p/C_v, is calculated in line 2110, assuming ideal gas behavior where $C_p - C_v = R$.

$$2110 \quad KAPPA = (C_vAVG + 1.987) \ / \ C_vAVG \tag{65}$$

where

KAPPA = C_p/C_v.

The expanded volume (headspace volume plus outflow volume) is then calculated in line 2120.

$$2120 \quad V_2 = GVOL + FVOL \tag{66}$$

where

V_2 = expanded gas volume (ft^3).

The expansion ratio, V_2/GVOL, is calculated in line 2125 and used to calculate final pressure for an adiabatic, isentropic expansion:

$$2130 \quad P_2 = P_1 \ / \ VRATIO\text{^}KAPPA \tag{67}$$

This expression for P_2 derives from the formula for a reversible expansion (Hougen et al. 1959):

$$P_2 = \frac{P_1}{\left(\frac{V_2}{V_1}\right)^{\kappa}} \tag{68}$$

where

P	=	pressure
T	=	temperature
κ	=	specific heat ratio
1,2	=	indicate conditions before and after the expansion.

Temperature in the expanded gas is computed from the ideal gas law.

The volume of expelled air is summed in line 2152 and given the symbol FVOLTOT. The temperature drop caused by adiabatic expansion is calculated in line 2165 by subtracting the final temperature from the initial temperature. These two variables were calculated to aid in verifying the numerics of the program but are not used directly in consequence calculations.

The area for gas flow is computed as the open area of the equivalent orifice. The initial flow area, symbolized as FAREA⊖, is computed from the input value of orifice diameter in line 385:

$$\text{FAREA}\ominus = 0.7854 * (\text{DORF} / 12)^2 \tag{69}$$

where

FAREA⊖	=	orifice open area (ft^2)
DORF	=	diameter of orifice (in.).

DORF is a keyboard input on line 210. A second vent path is allowed for in line 215, where an input orifice diameter for a salt well vent is requested. This vent path is modeled as a path that opens when a specified internal tank pressure is exceeded. The orifice area for this vent path is computed in line 217 using the same formula indicated in equation 69. The opening of the salt well vent is computed in lines 2042 to 2048. The fraction open is computed in line 2044 by:

$$\text{FRACTION} = 2 * (\text{PAV} - \text{PLIFT}) \tag{70}$$

where

FRACTION	=	open area fraction
PAV	=	internal tank pressure (psia)
PLIFT	=	internal tank pressure at which vent begins to open.

The formula expressed in equation 70 causes the salt well vent to be fully open when internal tank pressure exceeds the PLIFT value (an input on line 15) by 0.5 psi. The vent is fully closed whenever the tank internal pressure falls to less than PLIFT.

5.4 HEAT TRANSFER FROM GAS TO TANK

Heat transfer from contained gas to exposed surfaces inside the tank is computed at each time step. Surfaces modeled include:

- Concrete dome
- Steel liner and internal structures
- Exposed sludge (waste) surface
- Solvent pool surface.

The heat flux at each surface is computed as the sum of convection and radiation:

$$w = (h_c + h_r)\ (Tg - Ts) \tag{71}$$

where

w	=	surface heat flux (Btu/sec ft^2)
h_c	=	heat transfer coefficient for convection (Btu/ft^2 sec °F)
h_r	=	radiation heat transfer coefficient (Btu/ft^2 sec °F)
Tg	=	gas temperature (°F)
Ts	=	surface temperature (°F).

The total heat loss rate is calculated by summing the product of flux times area:

$$\text{heat loss rate} = \sum_{i=1}^{i=4} W_i * A_i \tag{72}$$

Surface temperatures are computed as a function of time accounting for heat absorption. For steel and organic solvent, it was assumed that heat transport within the material was rapid enough to maintain temperature uniform with respect to depth (distance perpendicular to surface). For concrete and sludge, conduction away from the surface was calculated by dividing the solid into a number (typically 40) of one-dimensional nodes. Transient conduction from node to node was predicted by means of an explicit energy transport calculation in each node at each time step.

Details of the heat transport calculations are described as follows.

5.4.1 Heat Transport to Steel Structures

Heat transport rate from gas to steel structures by convection was computed by:

$$Q_c = h_c A_s (T_g - T_s) \tag{73}$$

where

Q_c = energy transfer rate due to convection (Btu/sec)
h_c = convection coefficient (Btu/sec °F ft^2)
A_s = surface area of steel exposed to gas (ft^2)
T_g = temperature of gas (°F)
T_s = temperature of steel (°F).

The convection coefficient was computed by means of an empirical correlation developed for natural convection (McAdams 1954):

$$\frac{h_c L}{k_f} = 0.13\ [GrPr]^{\frac{1}{3}} \tag{74}$$

where

h_c = convection coefficient (Btu/h °F ft^2)
L = characteristic length of plate
K_f = thermal conductivity of gas at film condition (Btu/h °F ft)
Gr = Grashov number (dimensionless)
Pr = Prandtl number (dimensionless).

This correlation applies for turbulent flow ($GrPr>10^9$) along vertical surfaces. The correlation of heat transfer coefficients for horizontal surfaces has the same form as equation (74), but the numerical coefficient is 0.14 versus 0.13 (McAdams 1954). The smaller coefficient is used for all areas as a simplification of the convection heat transfer package.

Inserting the parameters that define the Grashov number, equation 74, may be rearranged and solved for h_c:

$$h_c = 0.13 K_f \left[\frac{\rho_f^2 g \beta_f Pr}{\mu_f^2}\right]^{\frac{1}{3}} \Delta T^{\frac{1}{3}} \tag{75}$$

where

ρ = gas density (lb/ft^3)
g = acceleration due to gravity (ft/h^2)

β = gas expansion coefficient ($°F^{-1}$)
μ = gas viscosity (lb/ft h)
f = subscript denoting film conditions.

As a simplification, h_c was expressed as a constant multiplied by $\Delta T^{1/3}$:

$$h_c = C_1 \Delta T^{\frac{1}{3}} \tag{76}$$

C_1 changes only slowly with temperature.

Inserting physical properties of air at 1 psig and 142 F, C_1 was evaluated to be:

$$C_1 = 0.22 \text{ Btu/h °F ft}^2.$$

In the conditions cited above, 1 psig and 142 °F, were chosen to describe conditions early in a pool fire in tank 241-C-103, starting at an initial temperature of 103 °F and an initial pressure of 14.5 psia. For higher temperature and pressure and conditions, a pressure of 30 psig was judged to be a reasonable limit on the maximum contained pressures of interest. For physical properties of air at 30 psig and 1,267 °F, C, was evaluated to be:

$$C_1 = 0.318 \text{ Btu/h °F ft}^2.$$

Thus, for a postulated contained burn, h_c increases with temperature, although the change is not very large. In order to quantify the increase in C, with temperature, a power law function based on absolute temperature was derived to fit the two values of C, described above. The resulting equation is:

$$C_1 = 0.22 \left(\frac{T_R}{601.4} \right)^{0.494} \tag{77}$$

where

T_R = gas temperature (°R).

Using equation 77, equation 76 may be written as:

$$h_c = 0.22 \left(\frac{T_R}{601.4} \right)^{0.494} \Delta T$$

The heat flux caused by convection is added to radiation flux in line 2620:

$$WS = WS + (TGAV - TSTL) * 0.000061 * HT * [ABS(TGAV - TSTL)]^{0.33} \quad (78)$$

Note that the constant in equation 78 (0.000061) is 0.22/3600 and converts from h^{-1} to sec^{-1}. The variable HT is the temperature factor in equation 77 and was calculated for the current time step in line 2326. The variables listed in equation 78 are defined as follows.

WS = heat flux to steel (Btu/s ft^2)
TGAV = gas temperature (°R)
TSTL = steel temperature (°R).

TGAV is calculated in line 2310 as the average of initial temperature for a time step and the temperature achieved after combustion and expansion. TG_1 in line 2310 is the gas temperature at the end of the previous time step, and TG is the most recent estimate that accounts for heatup and expansion, but not heat loss to surfaces. TGAV typically does not vary from TG_1 by more than 1 °F because each problem is typically divided into 1,000 or more time steps. Thus, the gas heatup in any time step is small, so errors arising from an imprecise estimate of gas temperature during the heat transfer part of the cycle are also small.

Radiation heat flux from the gas to steel was computed from:

$$\frac{q_r}{A} = \sigma E_g (T_g^4 - T_s^4) E_s \quad (79)$$

where

q_r = heat transfer rate due to radiation (Btu/h)
A = surface area of steel (ft^2)
σ = Stefan-Boltzmann constant (0.1718 E-8 Btu/h ft^2 $°R^4$)
T_g = gas temperature (°R)
T_s = steel temperature (°R)
E_g = emissivity of gas (dimensionless)
E_s = emissivity of steel (dimensionless).

Equation 79 (Perry 1950) is a simplified expression of radiant heat transfer from a flame to its confinement barriers.

This expression is evaluated in line 2610:

$$WS = SB * EGAS * (TGAV^4 - TSTL^4) * ESTL \quad (80)$$

where

WS = heat flux to steel by radiation (Btu/s ft^2)
SB = Stefan-Boltzman constant (Btu/s ft^2 $°R^4$)
EGAS = emissivity of gas (dimensionless)
ESTL = emissivity of steel (dimensionless).

Note that SB, the Stefan-Boltzman constant, is an input value (line 60) that is divided by 3,600 in line 400 to convert from h^{-1} to s^{-1}. EGAS and ESTL are inputs that are constants for a given problem. EGAS is an important parameter whose value depends on geometry, size scale (beam length), and the concentration of thermally radiating species in the confined gas. For the inefficient combustion associated with solvent pool fires, the airborne soot particles are predicted to be the dominant radiators. Means for estimating values of EGAS are described in Grigsby et al. (1995).

The change in steel temperature during a time step is predicted in line 2630:

$$TSTL = TSTL + WS * DT * STLAR / MCP \tag{81}$$

where

TSTL = steel temperature (°R)
WS = total heat flux (Btu/s ft^2)
DT = time step duration (s)
STLAR = area of steel exposed to gas (ft^2)
MCP = mass of steel * heat capacity.

Equation 81 is based on an energy balance that equates heat transfer energy to the gain in sensible heat energy. STLAR is an input in line 20. MCP is computed in line 390:

$$MCP = 0.13 * MASSTL \tag{82}$$

where

MCP = product of mass and heat capacity
MASSTL = mass of steel (lb)
0.13 = heat capacity of steel (Btu/lb °F).

The numerical value of MASSTL is an input on line 20.

The energy balance shown in equation 81 is based on the assumption that steel exposed to the gas does not lose heat to other structures. This assumption is conservative in the sense that steel heatup is overpredicted, and calculated heat loss rates will be underpredicted compared to the real case. In reality, much of the steel sheeting that lines waste tanks is backed by concrete. Heat loss to concrete in contact with the back side of a steel liners would reduce the rate of heatup of steel, a factor not accounted for in the model.

The neglect of heat transfer from steel to concrete is judged to be relatively unimportant for large pool fire cases where the burn to oxygen extinguishment occurs in less than 7 minutes. During this short period, steel temperatures typically increase by 70 °F or less whereas gas temperatures increase by ~700 °F. Thus, the driving force for heat transfer (Tg-Ts) is not importantly affected by the increase in steel temperature.

For small fires, where a longer burn time could be predicted, steel heatup could be relatively more important. The effect would be an overestimate of gas temperature and therefore of pressurization caused by small fires. Because the overestimate of pressurization leads to conservative predictions of consequences of small pool fires, the neglect of heat loss from the liner to concrete would be important only if small fires were predicted to result in risks that were unacceptable.

5.4.2 Heat Transport to Solvent Pool

Heat transfer to the solvent pool by radiation and convection was accounted for. The calculations are made in a subroutine starting on line 2300. At line 2320, the heat flux attributable to radiation from bulk gas is calculated:

$$WO = SB * EGAS * (TGAV^4 - TORG^4) * EORG \tag{83}$$

where

WO = heat flux at organic solvent surface (Btu/s ft^2)
EORG = emissivity of solvent (dimensionless)
TORG = pool temperature (°R).

Convection is calculated and added in lines 2325, 2326, 2327, and 2330:

$$WO = WO + (TGAV - TORG) * H \tag{84}$$

where terms are as defined earlier.

In addition to radiation and convection from the bulk atmosphere, radiation from the flame is also added to the pool. This is done in line 2400 where the updated pool temperature is calculated.

$$TORG = TORG + (WO * ORGAR + WFLAME * BURNAR) * DT / MCPORG \tag{85}$$

where

TORG	=	temperature of pool (°R)
ORGAR	=	surface area of pool (ft^2)
WFLAME	=	radiation flux from flame (Btu/s ft^2)
BURNAR	=	inflamed area of pool (ft^2)
MCPORG	=	product of mass and heat capacity (Btu/°F).

Equation 85 is based on a heat balance for a well-mixed pool. ORGAR and WFLAME are inputs (lines 80 and 20, respectively). BURNAR is calculated in subroutine 1800 on the basis of initial inflamed area and fire spread velocity. MCPORG is calculated from input properties in line 360.

WFLAME is set equal to zero at the time of fire extinguishment. This is done at line 2761. This line is executed one time only on the basis of a flag (PRINTFLAG) whose value is set equal to two the first time oxygen falls below the inputted fire extinguishment level.

An upper limit on pool temperature is imposed at line 2410:

$$2410 \quad \text{IF TORG} > \text{BOIL THEN TORG} = \text{BOIL} \tag{86}$$

BOIL is an input variable typically chosen as the normal boiling point of tridecane. The input value (line 40) is in °F, and is converted to °R at line 315.

Pool mass, and consequently MCPORG, is a user guess or stipulation. Therefore, the predicted temperature of the pool is not likely to be an accurate valuation of temperature. Pool depth, a keyboard input is typically set at a value that leads to a desired pool temperature. For most problems, heat transfer to and from the pool is minor compared to other surfaces, so inaccuracies in pool temperature are not expected to have a major effect on predicted peak pressures and gas temperatures.

5.4.3 Heat Transport to Concrete

Heat transfer from bulk gas to concrete is calculated as the sum of that due to radiation and convection. This is done in lines 2350 and 2360. Line 2350 computes the radiation flux:

$$2350 \quad \text{WC} = \text{SB} * \text{EGAS} * (\text{TGAV}^4 - \text{TSCON}^4) * \text{ECON} \tag{87}$$

where

WC	=	heat flux to concrete (Btu/s ft^2)
TSCON	=	concrete surface temperature (°R)
ECON	=	concrete emissivity (dimensionless)
EGAS	=	gas emissivity
TGAV	=	gas temperature (°R).

ECON, the emissivity of concrete, is an input (line 60).

The convective contribution to heat flux is added to radiation in line 2360.

$$2360 \quad WC = WC + (TGAV - TSCON) * 0.0000611 * HT * [ABS(TGAV - TSCON)]^{0.33} \tag{88}$$

The convection term is identical to the formulation described in Section 5.4.1 that applies to heat transport to steel.

Concrete surface temperature is calculated at each time step by means of a one-dimensional slab model. Concrete walls are divided into a number of slices (nodes), and the change in temperature in each is computed for each time step. The algorithm used here was initially developed for an analysis of exothermic reactions in crust floating in tank 241-SY-101 (Fox et al. 1991). Heat generation terms have been deleted because the materials analyzed here do not exhibit exotherms on heating.

At the surface, heat flux is known from the heat transfer analysis described above (equation 87). The average temperature in a node is assumed to occur at its midpoint. The surface temperature is computed by equating the surface flux to conduction in the first half of the first node:

$$T_s = T_1 + \frac{XW}{2k} \tag{89}$$

where

Ts = surface temperature (°R)
T_1 = temperature at midpoint of first node
X = thickness of node (ft)
W = heat flux on surface (Btu/s ft^2)
k = thermal conductivity of concrete (Btu/°F s ft).

This calculation step is carried out in line 2477:

$$2477 \quad TSCON = TCON(1) + X * WC / (2 * KCON) \tag{90}$$

where

KCON = thermal conductivity of concrete (Btu/°F s ft).

X, node thickness, is computed by dividing the concrete wall thickness (DPTCON is an input on line 95) by the number of nodes selected. (The number of nodes is an input on line 40.) KCON, in units of Btu/h °F ft, is an input on line 40. It is converted to s^{-1} units at line 480.

Temperatures in the nodes were computed from the energy conservation equation:

energy input rate = energy output rate + energy accumulation rate. (91)

For the first node (the surface node), the increase in temperature is calculated as:

$$\Delta T_1 = \left[\frac{\alpha}{X^2} (2T_s - 3T_1 + T_2) \right] \Delta t \qquad (92)$$

where

ΔT_1 = increase in temperature in node 1 (°R)
α = thermal diffusivity of concrete (ft^2/s)
T_s = surface temperature (°R)
T_2 = temperature of node 2 (°R)
Δt = length of time step (s).

Thermal diffusivity, α, has the usual definition:

$$\alpha = \frac{k}{\rho C_p} \qquad (93)$$

where

k = thermal conductivity (Btu/°F s ft)
ρ = material density (lb/ft^3)
C_p = heat capacity (Btu/°F lb).

The term $\alpha\Delta t/X^2$ is a factor in equation 92 and all of the node heatup equations. This parameter is computed in line 570:

570 DOXCDT = DOXC * DT (94)

where

DOXCDT = $\alpha\Delta t/X^2$ (dimensionless)
DOXC = α/X^2 (s^{-1})
DT = Δt (s).

DOXC is calculated from inputs in line 465. The time step for this explicit calculation scheme is chosen so that:

$$\frac{\alpha t}{X^2} \cong 0.1 \tag{95}$$

At this value of $\alpha t/X^2$, a heat wave entering one side of a node has time to just reach the other side of the node, resulting in an approximately linear distribution of temperature across the node. This can be seen from graphical results of the exact solution to the one-dimensional transient heat conduction equations as illustrated in Carslaw and Jaeger (1959). The time step computed from equation 95 is printed on the screen at line 490, and the user is asked to enter a rounded value close to the calculated value. The length of the calculated time step can be selected by the user by changing the value of X (DPTCON) or the number of nodes (NN). Because fires normally are too brief to permit heatup of all nodes, only a portion of the concrete wall needs be modeled. Therefore, very small time steps can be used if the depth of concrete modeled is set to a relatively small value.

For internal nodes, the energy balance equation (equation 91) leads to the following equation for temperature increase during a time step:

$$\Delta T(I) = \frac{\alpha}{X^2} \{[T(I-1) - 2T(I) + T(I+1)]\}\Delta t \tag{96}$$

where

$\Delta T(I)$	=	temperature increase for Ith node (°R)
$T(I)$	=	temperature of Ith node from previous time step (°R)
$\alpha, X, \Delta t$	=	are as defined in equation 92.

This calculation is carried out in a FOR-NEXT loop in lines 2490, 2500, and 2510.

```
2500   DELT(I) = DOXCDT * [TCON(I-1) - 2 * TCON(I) + TCON(I+1)]    (97)
```

where

DELT(I)	=	temperature increase in Ith node (°R)
TCON(I)	=	temperature of Ith concrete node from previous step.

For the last node (NN), a boundary condition must be specified. This has been done by specifying the temperature of the (NN+1) th node equal to the initial concrete temperature (TSCONC). The effect is equivalent to maintaining the back side of the concrete in contact with a slab at constant temperature. The calculation is done at line 2520:

$$2520 \quad DELT(NN) = DOXCDT * [TCON(NN-1) - 2 * TCON(NN) + TSCONC] \quad (98)$$

where

TSCONC = initial concrete temperature (°R).

The variable TSCONC is set equal to the initial concrete temperature in line 315.

After temperature changes have been calculated in all nodes, node temperatures are updated in line 2540.

$$2540 \quad TCON(I) = TCON(I) + DELT(I) \quad (99)$$

The validity of this simple algorithm for predicting transient conduction in a slab was studied briefly in Fox et al. (1991).

5.4.4 Heat Transport to Sludge

Heat transport to sludge is treated similarly to heat transport to concrete. The calculations are carried out in a subroutine starting at line 2800 and ending at line 2940.

Because a common time step is used for all calculations, the node thickness for sludge was calculated to yield the same value of the parameter ($\alpha t/x^2$) (see equation 95) for sludge as for concrete. This is done in line 425.

$$425 \quad XSLUD = X * (ASLUD / ACON)^{0.5} \quad (100)$$

where

XSLUD = node thickness for sludge (ft)
X = node thickness for concrete (ft)
ASLUD = thermal diffusivity of sludge (ft/s^2)
ACON = thermal diffusivity for concrete (ft^2/s).

The thermal diffusivity for concrete and sludge are calculated from input values of thermal conductivity, density, and heat capacity in lines 410 and 415.

The area of sludge exposed to the tank atmosphere is calculated at line 305.

$$305 \quad SLUDAR = 4418 - ORGAR \tag{101}$$

where

SLUDAR	=	surface area of sludge (ft^2)
4418	=	tank cross-sectional area (ft^2)
ORGAR	=	solvent pool area (ft^2).

The numerical value of ORGAR is an input on line 80. It is assumed that the tank is 75 ft in diameter and that sludge occupies all of the cross-section except for the pool. Because this assumption is clearly incorrect for tanks that do not have the same diameter and waste configuration, the equation on line 305 must be altered appropriately for other cases.

5.5 CHANGE IN GAS TEMPERATURE DUE TO HEAT TRANSFER

The change in gas temperature during a time step is computed in a subroutine starting at line 2700 and ending at line 2790. The energy transferred is summed in line 2710:

$$2710 \quad HEATTX = WO * ORGAR + WC * CONAR + WS + STLAR + WSLUD * SLUDAR + WFLAME * BURNAR \tag{102}$$

where

HEATTX	=	thermal energy transferred to tank surfaces (Btu/s)
WO	=	heat flux to organic pool surface (Btu/s ft^2)
ORGAR	=	pool area (ft^2)
WC	=	heat flux to concrete surface (Btu/s ft^2)
CONAR	=	surface area of concrete (ft^2)
WS	=	heat flux to steel surface (Btu/s ft^2)
STLAR	=	surface area of steel (ft^2)
WSLUD	=	heat flux to sludge surface (Btu/s ft^2)
SLUDAR	=	surface area of sludge (ft^2)
WFLAME	=	heat flux from flame (Btu/s ft^2)
BURNAR	=	surface area inflamed (ft^2).

The heat transfer rate calculated in line 2710 is used to calculate a change in gas temperature for a constant volume process.

$$2720 \quad HEATTX = HEATTX * DT / MCV \tag{103}$$

where

HEATTX = temperature change (°R)
DT = time step (s)
MCV = moles of gas * mean heat capacity at constant volume (Btu/°R).

Gas temperature is updated in line 2730.

$$2730 \quad TG = TG - HEATTX \tag{104}$$

where

TG = gas temperature (°R).

Gas pressure is computed by means of the ideal gas law in line 2735.

$$2735 \quad P2 = MTOT * TG * ROV \tag{105}$$

where

P2 = gas pressure (psia)
MTOT = total moles of contained gas (lb mols)
ROV = gas constant/gas volume (psia/°R mol).

The variable ROV is computed from inputs at line 380.

6.0 LISTING OF BASIC PROGRAMS

This section contains a printout of the basic program used to analyze solvent pool fires in Hanford Site waste tanks.

A listing of the POOLFIRE.4 program is provided in the following seven pages. The input data shown on lines 15 through 96 apply to a large single-shell tank with an upper limit gas volume.

Listing of POOLFIRE.4

```
10 C10 CLS
11 REM    THIS PROGRAM IS CALLED POOLFIRE.4 (OXYGEN FACTOR CALCD.)
12 REM    INFLOW OF AIR AFTER BURN IS COMPUTED
13 REM    THIS PROGRAM ANALYZES ORGANIC POOL FIRES IN TANK C-103
14 REM
15 DATA   5.02  ,   7.4
16 READ  WFLAME ,  PLIFT
20 DATA  10.73 ,  60   ,    .6   , 246700  , 13390 ,   .5   ,  3.0   ,  .13
30 READ    R   , TSCON ,   ORIFC ,  MASSTL ,  STLAR ,   RO   ,  MDOTB ,
XO2STOP
31 REM
40 DATA  60  ,  60     ,   150   ,   50    ,    40 ,    1.05  ,  453   , 14.5
50 READ TORG ,  TGO    ,  RHOCON ,  RHOORG ,    NN  ,   KCON   , BOIL  , PTOTO
51 REM
60 DATA   .1713E-8     ,   0.20  ,  0.90   ,   0.90 ,  0.90    , .0615 , 24.7
70 READ    SB          ,  EGAS   ,  ECON   ,   ESTL ,  EORG    ,  KGAS , MOLWT
71 REM
80 DATA 14140   ,  0.11 , 187100  ,    .1   ,  10.76  ,  0.22     ,  0.5
90 READ  DELH   , PWATO ,  GVOL   ,  CONAR  ,  ORGAR  ,   CPCON   ,   CPORG
91 REM
95 DATA   60    ,  0.27 ,  120    ,  .5     ,  0.9    ,  .38    ,   55
96 READ  TSLUD  , KSLUD , RHOSLUD , CPSLUD  ,  ESLUD  ,  DPTCON ,  TGOUT
99 REM
100 DIM TCON(NN),YCON(NN),DELT(NN),TCONF(NN),TSLUD(NN),YSLUD(NN),TSLUDF(NN)
120 PRINT  "THIS PROGRAM IS CALLED  POOLFIRE.4"
122 PRINT  " "
124 PRINT  "THIS PROGRAM ANALYZES TEMPERATURE AND PRESSURE TRANSIENTS IN
C-103"
125 PRINT      "THIS VERSION COMPUTES INFLOW OF AIR AFTER FIREOUT"
126 PRINT " "
150 PRINTFLAG=0
160 PLIFT=PLIFT+PTOTO
201 PRINT " "
210 INPUT "WHAT IS THE EQUIVALENT VENT ORIFICE DIAMETER IN INCHES";DORF
211 PRINT " "
215 INPUT "WHAT IS THE EQUIV. ORIFICE DIA.  FOR SALTWELL IN INCHES";DSALT
216 PRINT " "
217 SAREA=.7854*(DSALT/12)^2
220 INPUT "TOTAL TIME FOR COMPUTATON TO CONTINUE--SEC";TIMTOT
221 PRINT" "
230 INPUT "THICKNESS OF ORGANIC POOL--FEET";DPT
231 PRINT" "
240 INPUT " ASSUMED SPREAD VELOCITY OF FIRE OVER POOL-IN CM/SEC ";SPREADV
241 PRINT" "
251 PRINT" "
300 E12=1/(1/ECON+1/EORG-1)
305 SLUDAR=4418-ORGAR
310 T=459.6+TGO :BURNR=(ORGAR/3.1416)^.5
315 TORGC=TORG+459.6:TSCONC=TSCON+459.6 : TSSLUDC=TSLUD+459.6 :BOIL=BOIL+459.6
320 MH2O=PWATO*GVOL/(R*T)
```

```
330 MTOT=PTOTO*GVOL/(R*T):MTOTO=MTOT
340 MN2=.79*(MTOT-MH2O)
350 MO2=.21*(MTOT-MH2O)
351 MO2O=MO2
355 MCO2=0
360 MCPORG=ORGAR*DPT*RHOORG*CPORG
365 XO2=MO2/MTOT
370 FOLD=0
380 ROV=R/GVOL
385 FAREAO=.7854*(DORF/12)^2
390 MCP=.13*MASSTL
395 TIMS=30.54*(BURNR-RO)/SPREADV
400 SB=SB/3600
405 FLAG=0
410 ASLUD=KSLUD/(RHOSLUD*CPSLUD*3600)
415 ACON=KCON/(RHOCON*CPCON*3600)
420 X=DPTCON/NN
425 XSLUD=X*(ASLUD/ACON)^.5
430 FOR I=1 TO NN
440 YSLUD(I)=XSLUD/2+XSLUD*(I-1)
445 YCON(I)=X/2+X*(I-1)
450 NEXT I
460 DOXS=ASLUD/XSLUD^2
465 DOXC=ACON/X^2
470 DT=.1/DOXC
475 KSLUD=KSLUD/3600
480 KCON=KCON/3600
485 DPTSLUD=NN*XSLUD
490 PRINT "THE COMPUTED TIME STEP INTERVAL IS";DT;" SEC"
500 PRINT" "
510 INPUT "ENTER A ROUNDED VALUE OF DT THAT IS CLOSE TO THE VALUE ABOVE";DT
515 PRINT" "
520 INPUT "ENTER THE TIME BETWEEN PRINTOUTS,IN SECONDS";TIMP
530 PRINT " "
531 PRINT " "
550 PRINT DATE$
560 PRINT TIME$
561 PRINT" "
565 DOXSDT=DOXS*DT
570 DOXCDT=DOXC*DT
590 GOSUB 700
600 TSCON=TSCON+459.6
605 MDOTB=MDOTB*.0034
610 TORG=TORG+459.6
612 TSLUD=TSLUD+459.6  : TSSLUD=TSLUD
615 FOR I=1 TO NN
620 TSLUD(I)=TSLUD
630 TCON(I)=TSCON
632 TSLUD(I)=TSLUD
640 NEXT I
650 TIM=0
665 TGO=TGO+459.6 : TGOUT=TGOUT+459.6
670 TG=TGO
```

```
675 TSTL=TGO
680 SUMDELE=0
699 GOTO 800
700 PRINT " KEY INPUT DATA FOR THIS PROBLEM ARE AS FOLLOWS"
710 PRINT "INITIAL CONCRETE TEMP=";TSCON;"INITIAL ORGANIC TEMP=";TORG
720 PRINT "GAS VOLUME IN HEAD SPACE=";GVOL;"  TIME STEP =";DT
730 PRINT "THICKNESS OF ORGANIC POOL=";DPT ;"IN FEET"
740 PRINT "INITIAL GAS TEMPERATURE,F=";TGO;"  INITIAL SLUDGE TEMP, F=";TSLUD
750 PRINT "COMBUSTION ENERGY IS";DELH;"BTU PER LB. OF ORGANIC BURNED"
760 PRINT "THICKNESS OF CONCRETE MODELLED=";DPTCON;"FT"
762 PRINT "THICKNESS OF SLUDGE MODELLED=";DPTSLUD;"FT"
765 PRINT "POOL BURNING RATE ASSUMED=";MDOTB;"KG/M2 MIN"
767 PRINT "FIRE SPREAD RATE =";SPREADV;"CM/SEC---TIME OF SPREAD=";TIMS;"SEC"
770 PRINT "THE OXYGEN MOLE FRACTION WHERE FIRE STOPS=";XO2STOP
780 PRINT " "
790 RETURN
800 REM THIS SECTION IS EXECUTIVE
804 SUMDELE=SUMDELE+DELE
805 GOTO 810
806 PRINT "AT TIME=";TIM;"SEC,SUMDELE=";SUMDELE;"HEAT TX DELT=";HEATTX
810 GOSUB 1800
820 GOSUB 1900
830 GOSUB 2000
840 GOSUB 2300
845 GOSUB 2800
850 GOSUB 2600
860 GOSUB 2700
1300 TIM=TIM+DT
1310 PTIM=PTIM+DT
1320 IF PTIM+.0001<TIMP GOTO 800
1330 FLAG=FLAG+1
1340 IF FLAG >1.5 GOTO 1420
1350 PRINT " "
1390 PRINT" "
1395 PRINT "FOLLOWING ARE DISTANCES FROM CONCRETE SURFACE--FT"
1400 FOR I=1 TO NN
1405 PRINT USING " ##.##### ";YCON(I);
1410 NEXT I
1411 PRINT" "
1412 PRINT "FOLLOWING ARE DISTANCES FROM SLUDGE SURFACE--FT"
1413 FOR I=1 TO NN
1414 PRINT USING " ##.##### ";YSLUD(I);
1415 NEXT I
1416 PRINT" "
1420 PRINT" "
1425 IF PRINTFLAG>1 THEN PRINT"THE POOL FIRE IS OUT AT TIME=";TIMOUT;"SEC"
1426 IF PRINTFLAG>1 THEN PRINT"PEAK PRESSURE=";PGAGEPEAK;"PSIG";" AND
TEMP=";TGFPEAK;"DEG F"
1429 PRINT" "
1430 PRINT"AT TIME=";TIM;"SEC, FLOW AREA=";FAREA;"FT^2";"  OXFACT=";OXFACT
1431 PRINT "BURN RADIUS=";BURNR;"FT";"   BURN AREA=";BURNAR;"FT^2";"
MO2O=";MO2O
1440 TGF=TG-459.6
```

```
1450 TORGF=TORG-459.6
1460 TSCONF=TSCON-459.6
1465 TSSLUDF=TSSLUD-459.6
1470 TSTLF=TSTL-459.6
1480 FOR I=1 TO NN
1495 TCONF(I)=TCON(I)-459.6
1497 TSLUDF(I)=TSLUD(I)-459.6
1500 NEXT I
1510 PRINT"GAS TEMP.=";TGF;"F";"  ORGANIC TEMP.=";TORGF;"   XO2=";XO2
1515 PGAGE=P2-PTOTO
1516 PRINT "PRESSURE IN HEADSPACE=";PGAGE;"PSIG";"    STEEL TEMP=";TSTLF
1520 PRINT"MOLES LOST= ";(MTOTO-MTOT);"   VOLUME LEAKED=";FVOLTOT;"CUBIC FT"
1530 PRINT "OUTFLOW RATE= ";FLRATE;"   GAS MOLES IN TANK=";MTOT;"
MTOTO=";MTOTO
1550 PRINT" "
1560 PRINT "CONCRETE SURFACE TEMP.=";TSCONF;"DEG F -----(FCO2=";FCO2;")"
1570 FOR I=1 TO NN
1580 PRINT USING " ####.##  ";TCONF(I);
1590 NEXT I
1592 PRINT" "
1593 PRINT"SLUDGE SURFACE TEMP=";TSSLUDF;" DEG F   --MASSBURN=";MASSBURN
1594 FOR I=1 TO NN
1595 PRINT USING " ####.##  ";TSLUDF(I);
1596 NEXT I
1600 IF TIM+.001>TIMTOT THEN END
1610 PTIM=0
1620 GOTO 800
1800 REM  THIS SUB COMPUTES MASS BURNED AND GAS COMPOSITION
1805 IF PRINTFLAG> 1.5 GOTO 1899
1807 OXFACT=9.72*XO2-1.04
1808 IF OXFACT<.125 THEN OXFACT=.125
1809 IF TIM=> TIMS GOTO 1815
1810 BURNAR=3.1416*(RO+(TIM+DT/2)*(BURNR-RO)/TIMS)^2
1811 GOTO 1820
1815 BURNAR=ORGAR
1820 BRATE= BURNAR*MDOTB*OXFACT
1825 MASSBURN=BRATE*DT+MASSBURN
1830 DELE= BRATE*DELH*DT
1840 DMF=BRATE*DT/180.8
1855 MH2O=MH2O+DMF*13.05
1860 MO2=MO2-18.45*DMF
1865 MCO2=MCO2+12*DMF
1867 TOTCO2=TOTCO2+12*DMF:FCO2=MCO2/TOTCO2
1870 MTOT=MH2O+MO2+MN2+MCO2
1880 XO2=MO2/MTOT
1885 GOSUB 3300
1899 RETURN
1900 ITER=0
1901 REM  THIS SUBROUTINE COMPUTES TEMP RISE IN GAS DUE TO COMBUSTION
1905 T1=TG
1907 TG1=TG
1910 DELTG=1
1920 T2=T1+DELTG
```

```
1930 A=T1+T2
1940 B=T2^2+T1*T2+T1^2
1950 CVH2O=5.149+A*.000733+4.72E-09*B
1955 CVN2=4.47+A*.000386-B*7.1E-09
1960 CVO2=4.13+.00088*A-1.03E-07*B
1965 CVCO2=4.352+.00281*A-3.51E-07*B
1970 MCV=MH2O*CVH2O+MN2*CVN2+MO2*CVO2+MCO2*CVCO2
1980 DELTG=(DELE-FSENS)/MCV
1982 ITER=ITER+1
1985 IF ITER<4 GOTO 1920
1990 TG=TG+DELTG
1991 REM THE PROGRAM WORKS TO HERE
1995 RETURN
2000 REM THIS SUB COMPUTES OUTFLOW EFFECTS
2002 IF FLOWFLAG>1.5 GOTO 2280
2005 ITER=0
2020 CVAVG=MCV/MTOT
2030 P1=MTOT*TG*ROV
2031 P2=P1
2035 PAV=(P1+P2)/2
2036 IF PAV<PTOTO THEN PAV=PTOTO
2040 PRATIO=PTOTO/PAV
2042 IF PAV<PLIFT THEN FAREA=FAREAO
2044 IF PAV> PLIFT THEN FRACTION=2*(PAV-PLIFT)
2046 IF FRACTION >1 THEN FRACTION=1
2048 IF PAV>PLIFT THEN FAREA=FAREAO+FRACTION*SAREA
2050 YFACT=1-.315*(1-PRATIO)
2060 SONIC=47.2*TG^.5
2070 RHOGAS=PAV*29/(R*TG)
2080 VEL=96.3*((PAV-PTOTO)/RHOGAS)^.5
2090 IF VEL>SONIC THEN VEL=SONIC
2095 FLRATE=ORIFC*FAREA*YFACT*VEL
2100 FVOL=FLRATE*DT
2110 KAPPA=(CVAVG+1.987)/CVAVG
2120 V2=GVOL+FVOL
2125 VRATIO=V2/GVOL
2130 P2=P1/VRATIO^KAPPA
2140 ITER=ITER+1
2150 IF ITER<6 GOTO 2035
2152 FVOLTOT=FVOLTOT+FVOL
2155 T1EXP=TG
2160 TG=P2*V2/(MTOT*R)
2165 DELTEXP=TG-T1EXP
2170 MH2O=MH2O/VRATIO
2180 MO2=MO2/VRATIO
2190 MN2=MN2/VRATIO
2200 MCO2=MCO2/VRATIO : FCO2=MCO2/TOTCO2
2220 MTOT=MTOT/VRATIO
2279 GOTO 2290
2280 GOSUB 3000
2290 RETURN
2300 REM THIS SECTION CALCULATES HEAT TX TO CONCRETE AND ORGANIC SURFACES
2310 TGAV=(TG1+TG)/2
```

```
2320 WO=SB*EGAS*(TGAV^4-TORG^4)*EORG
2325 H=.0000611*(ABS(TGAV-TORG))^.33
2326 HT=(TGAV/601.4)^.494
2327 H=H*HT
2330 WO=WO+(TGAV-TORG)*H
2350 WC=SB*EGAS*(TGAV^4-TSCON^4)*ECON
2360 WC=WC+(TGAV-TSCON)*.0000611*HT*(ABS(TGAV-TSCON))^.33
2380 REM AT THIS POINT HEAT FLUXES TO SURFACES HAVE BEEN CALCULATED
2390 REM  NOW COMPUTE ORGANIC LIQUID HEATUP
2400 TORG=TORG+(WO*ORGAR+WFLAME*BURNAR)*DT/MCPORG
2410 IF TORG>BOIL THEN TORG=BOIL
2420 REM THIS LIMITS TORG TO BOILING POINT OF TRIDECANE
2475 REM NOW TO CALCULATE TEMP IN CONCRETE
2477 TSCON=TCON(1)+X*WC/(2*KCON)
2480 DELT(1)=DOXCDT*(2*TSCON-3*TCON(1)+TCON(2))
2490 FOR I=2 TO NN-1
2500 DELT(I)=DOXCDT*(TCON(I-1)-2*TCON(I)+TCON(I+1))
2510 NEXT I
2520 DELT(NN)=DOXCDT*(TCON(NN-1)-2*TCON(NN)+TSCONC)
2530 FOR I=1 TO NN
2540 TCON(I)=TCON(I)+ DELT(I)
2545 NEXT I
2550 REM NODE TEMPERATURES HAVE BEEN CALCULATED
2590 RETURN
2600 REM  THIS SECTION COMPUTES HEAT LOSS TO STEEL
2610 WS=SB*EGAS*(TGAV^4-TSTL^4)*ESTL
2620 WS=WS+(TGAV-TSTL)*.000061*HT*(ABS(TGAV-TSTL))^.33
2630 TSTL =TSTL+WS*DT*STLAR/MCP
2690 RETURN
2700 REM THIS SUB COMPUTES DELTA TG DUE TO HEAT TRANSFER
2710 HEATTX=WO*ORGAR+WC*CONAR+WS*STLAR +WSLUD*SLUDAR +WFLAME*BURNAR
2720 HEATTX=HEATTX*DT/MCV
2730 TG=TG-HEATTX
2735 P2=MTOT*TG*ROV
2737 IF PMAXFLAG>1 GOTO 2744
2738 IF P2<PMAXIMUM THEN PMAXFLAG=2 :PRINT "PEAK PRESSURE =";(PMAXIMUM-PTOTO);
"AT TIME= ";(TIM)
2740 PMAXIMUM=P2
2744 IF FLOWFLAG>1.5 GOTO 2750
2745 IF (PTOTO-P2)> .1 THEN FLOWFLAG=2 :PRINT"NEGATIVE PRESSURE
AT";(TIM+DT);"SEC"
2750 IF PRINTFLAG>1.5 GOTO 2790
2755 IF XO2<= XO2STOP THEN DELE=0:PRINTFLAG=2:TIMOUT=TIM+DT:GOTO 2760
2756 GOTO 2790
2760 PGAGEPEAK=P2-PTOTO:TGFPEAK=TG-459.6
2761 WFLAME=0 :FSENS=0
2765 PRINT "  * * * * * * * * * * * * * * * *"
2770 PRINT "AT TIME=";TIMOUT;"FIRE IS OUT
-PGAGE=";PGAGEPEAK;"TG=";TGFPEAK;"DEG F"
2790 RETURN
2800 REM THIS SUB COMPUTES HEAT TRANSFER TO SLUDGE
2810 WSLUD=SB*EGAS*(TGAV^4-TSSLUD^4)*ESLUD
2820 H=.0000611*HT*(ABS(TGAV-TSSLUD))^.33
2830 WSLUD=WSLUD+(TGAV-TSSLUD)*H
```

```
2840 WSLUD=WSLUD-SB*(1-EGAS)*EI2*(TSSLUD^4-TSCON^4)
2850 TSSLUD=TSLUD(1)+XSLUD*WSLUD/(2*KSLUD)
2860 DELT(1)=DOXSDT*(2*TSSLUD-3*TSLUD(1)+TSLUD(2))
2870 FOR I=2 TO NN-1
2880 DELT(I)=DOXSDT*(TSLUD(I-1)-2*TSLUD(I)+TSLUD(I+1))
2890 NEXT I
2900 DELT(NN)=DOXSDT*(TSLUD(NN-1)-2*TSLUD(NN)+TSSLUDC)
2910 FOR I= 1 TO NN
2920 TSLUD(I)=TSLUD(I)+ DELT(I)
2930 NEXT I
2940 RETURN
3000 REM THIS SUB COMPUTES INFLOW EFFECTS
3010 ITER=0
3020 CVAVG=MCV/MTOT
3030 P1=MTOT*TG*ROV
3031 P2=P1
3035 PAV=(P1+P2)/2
3036 IF PAV>PTOTO THEN PAV=PTOTO
3040 PRATIO=PAV/PTOTO
3050 YFACT=1-.315*(1-PRATIO)
3060 SONIC=47.2*TGOUT^.5
3070 RHOGAS=PTOTO*29/(R*TGOUT)
3080 VEL=96.3*((PTOTO-PAV)/RHOGAS)^.5
3090 IF VEL>SONIC THEN VEL=SONIC
3095 FLRATE=ORIFC*FAREA*YFACT*VEL
3100 FVOL=FLRATE*DT
3110 INMOLS=FVOL*PTOTO/(R*TGOUT)
3120 NEWMOLS=INMOLS+MTOT
3130 T3=(INMOLS*4.98*TGOUT+MTOT*CVAVG*TG)/(NEWMOLS*CVAVG)
3140 P2=T3*NEWMOLS*ROV
3150 ITER=ITER+1
3160 IF ITER<6 GOTO 3035
3170 TG=T3
3180 MH2O=MH2O+INMOLS*8.000001E-03
3190 MO2=MO2+INMOLS*.208
3200 MN2=MN2+INMOLS*.784
3210 MTOT=NEWMOLS
3220 FVOLTOT=FVOLTOT-FVOL
3230 FLRATE=-FLRATE
3240 XO2=MO2/MTOT
3290 RETURN
3300 REM THIS SUB ACCOUNTS FOR FUEL SENSIBLE HEAT
3310 T1=758
3320 T2=TG
3330 A=T1+T2
3340 B=T2^2+T1*T2+T1^2
3350 CPFUEL=.478+.0686*A-8.629999E-06*B
3360 FSENS=(T2-T1)*CPFUEL*DMF
3370 RETURN
```

7.0 EXAMPLE ANALYSIS WITH POOLFIRE.4

This section gives an example analysis of a pool fire in a large (1 million gal) single-shell tank. Key inputs are those used for case E as defined in Section 10.0 of the main body of this report.

Vent Orifice Diameter

A vent orifice diameter of 3.75 in. was selected to mimic the assumed vent path, the 4-in. HEPA filter vent.

Specific Burn Rate

The initial specific burn rate was assigned a value of 3.0 kg/m^2 min. on the basis of recommendations of C. Beyler of Hughes Associates.

Fire Spread Velocity

A radial spread velocity of 10 cm/s was assigned on the basis of recommendations by C. Beyler of Hughes Associates.

Key results of this example, as documented in the 20-page output file that follows, are described as follows.

Time of Burn

The oxygen extinguishment level of 13 mole percent is reached at 80.3 s. The time of extinguishment and the pressure and temperature at the time of burn-out are printed at each printout after the burn-out time.

Mass of Solvent Burned

The mass of solvent burned is printed at each output. For this problem, the mass burned is 321.44 lb. This number is identified as "MASSBURN."

Peak Pressure

The peak pressure was reached at 79.2 seconds. This is indicated on the third page of the output file by the output "PEAK PRESSURE = 28.87708 AT TIME = 79.19936." For this case, peak pressure occurs approximately 1 sec. before the time of extinguishment, but this is not necessarily the case for other fire parameters.

Reaction Products Vented

The parameter FCO2 reaches a minimum value at approximately 1400 sec. At this time, a negative pressure has developed because of cooldown. The value of FCO2 is the fraction of CO_2 formed by combustion which is retained within the tank. For this problem, (1-0.854) or 14.6 percent of reaction products are released from the tank.

Temperature

Gas, steel, sludge, solvent, and concrete temperatures are listed for each output printing. Sludge and concrete temperatures are printed for each solid node. The distances to the center of each node is printed on page 2 of the output. For example, at 400 s, steel temperature is 163.6 °F, air temperature is 204 °F, the concrete surface temperature is 129.98 °F, and the sludge surface temperature is listed as 152.019 °F.

Other Data

Additional data that are printed are self-explanatory and will not be detailed here.

Example Run With POOLFIRE. 4

```
LIST 0-100
10 CLS
11 REM     THIS PROGRAM IS CALLED POOLFIRE.4 (OXYGEN FACTOR CALCD.)
12 REM          INFLOW OF AIR AFTER BURN IS COMPUTED
13 REM     THIS PROGRAM ANALYZES ORGANIC POOL FIRES IN TANK C-103
14 REM
15 DATA 5.02 , 7.4
16 READ WFLAME , PLIFT
20 DATA 10.73 , 60 , .6 , 148000 , 9650 , .5 , 3.0 , .13
30 READ R , TSCON , ORIFC , MASSTL , STLAR , RO , MDOTB , XO2STOP
31 REM
40 DATA 60 , 60 , 150 , 50 , 40 , 1.05 , 453 , 14.5
50 READ TORG , TGO , RHOCON , RHOORG , NN , KCON , BOIL , PTOTO
51 REM
60 DATA .1713E-8 , 1.00 , 0.90 , 0.90 , 0.90 , .0615 , 24.7
70 READ SB , EGAS , ECON , ESTL , EORG , KGAS , MOLWT
71 REM
80 DATA 14140 , 0.11 , 170000 , 4885. , 2260 , 0.22 , 0.5
90 READ DELH , PWATO , GVOL , CONAR , ORGAR , CPCON , CPORG
91 REM
95 DATA 60 , 0.27 , 120 , .5 , 0.9 , .12 , 55
96 READ TSLUD , KSLUD , RHOSLUD , CPSLUD , ESLUD , DPTCON , TGOUT
99 REM
100 DIM TCON(NN) , YCON(NN) , DELT(NN) , TCONF(NN) , TSLUD(NN) , YSLUD(NN) , TSLUDF(NN)

Ok
```

Example Run With POOLFIRE. 4

```
RUN
THIS PROGRAM IS CALLED POOLFIRE.4

THIS PROGRAM ANALYZES TEMPERATURE AND PRESSURE TRANSIENTS IN C-103

THIS VERSION COMPUTES INFLOW OF AIR AFTER FIREOUT

WHAT IS THE EQUIVALENT VENT ORIFICE DIAMETER IN INCHES? 3.75

WHAT IS THE EQUIV. ORIFICE DIA. FOR SALTWELL IN INCHES? 0

TOTAL TIME FOR COMPUTATON TO CONTINUE--SEC? 100

THICKNESS OF ORGANIC POOL--FEET? .1

ASSUMED SPREAD VELOCITY OF FIRE OVER POOL-IN CM/SEC ? 10

THE COMPUTED TIME STEP INTERVAL IS .1018286 SEC

ENTER A ROUNDED VALUE OF DT THAT IS CLOSE TO THE VALUE ABOVE? .1

ENTER THE TIME BETWEEN PRINTOUTS,IN SECONDS? 10

09-10-1997
08:07:51

KEY INPUT DATA FOR THIS PROBLEM ARE AS FOLLOWS
INITIAL CONCRETE TEMP = 60 INITIAL ORGANIC TEMP = 60
GAS VOLUME IN HEAD SPACE = 170000 TIME STEP = .1
THICKNESS OF ORGANIC POOL = .1 IN FEET
INITIAL GAS TEMPERATURE,F = 60 INITIAL SLUDGE TEMP, F = 60
COMBUSTION ENERGY IS 14140 BTU PER LB. OF ORGANIC BURNED
THICKNESS OF CONCRETE MODELLED = .12 FT
THICKNESS OF SLUDGE MODELLED = 4.512839E-02 FT
POOL BURNING RATE ASSUMED = 3 KG/M2 MIN
FIRE SPREAD RATE = 10 CM/SEC---TIME OF SPREAD = 80.38505 SEC
THE OXYGEN MOLE FRACTION WHERE FIRE STOPS = .13
```

Example Run With POOLFIRE. 4

FOLLOWING ARE DISTANCES FROM CONCRETE SURFACE--FT

0.00150	0.00450	0.00750	0.01050	0.01350	0.01650	0.01950	0.02250
0.02550	0.02850	0.03150	0.03450	0.03750	0.04050	0.04350	0.04650
0.04950	0.05250	0.05550	0.05850	0.06150	0.06450	0.06750	0.07050
0.07350	0.07650	0.07950	0.08250	0.08550	0.08850	0.09150	0.09450
0.09750	0.10050	0.10350	0.10650	0.10950	0.11250	0.11550	0.11850

FOLLOWING ARE DISTANCES FROM SLUDGE SURFACE--FT

0.00056	0.00169	0.00282	0.00395	0.00508	0.00621	0.00733	0.00846
0.00959	0.01072	0.01185	0.01297	0.01410	0.01523	0.01636	0.01749
0.01862	0.01974	0.02087	0.02200	0.02313	0.02426	0.02538	0.02651
0.02764	0.02877	0.02990	0.03103	0.03215	0.03328	0.03441	0.03554
0.03667	0.03780	0.03892	0.04005	0.04118	0.04231	0.04344	0.04456

AT TIME = 10 SEC, FLOW AREA = 7.669921E-02 FT^2 OXFACT = .9816704
BURN RADIUS = 26.82123 FT BURN AREA = 44.36798 FT^2 MO2O = 92.14253
GAS TEMP. = 70.78226 F ORGANIC TEMP. = 60.15653 XO2 = .2079798
PRESSURE IN HEADSPACE = .299469 PSIG STEEL TEMP = 60.00504
MOLES LOST = 4.248047E-02 VOLUME LEAKED = 40.4576 CUBIC FT
OUTFLOW RATE = 8.78113 GAS MOLES IN TANK = 442.0856 MTOTO = 442.1281

CONCRETE SURFACE TEMP. = 60.06955 DEG F-----(FCO2 = .9998894)

60.05	60.03	60.01	60.01	60.00	60.00	60.00	60.00
60.00	60.00	60.00	60.00	60.00	60.00	60.00	60.00
60.00	60.00	60.00	60.00	60.00	60.00	60.00	60.00
60.00	60.00	60.00	60.00	60.00	60.00	60.00	60.00
60.00	60.00	60.00	60.00	60.00	60.00	60.00	60.00

Example Run With POOLFIRE. 4

```
SLUDGE SURFACE TEMP = 60.10153     DEG F--MASSBURN = 1.72136

      60.07     60.04     60.02     60.01     60.01     60.00     60.00     60.00
      60.00     60.00     60.00     60.00     60.00     60.00     60.00     60.00
      60.00     60.00     60.00     60.00     60.00     60.00     60.00     60.00
      60.00     60.00     60.00     60.00     60.00     60.00     60.00     60.00
      60.00     60.00     60.00     60.00     60.00     60.00     60.00     60.00

AT TIME = 20.00004 SEC, FLOW AREA = 7.669921E-02 FT^2 OXFACT = .9593146
BURN RADIUS = 26.82123 FT BURN AREA = 155.368 FT 2 MO2O = 92.14253
GAS TEMP. = 128.2516 F ORGANIC TEMP. = 61.06241 XO2 = .2056531
PRESSURE IN HEADSPACE = 1.9013 PSIG STEEL TEMP = 60.08567
MOLES LOST = 8.990479E-02 VOLUME LEAKED = 190.3796 CUBIC FT
OUTFLOW RATE = 21.45095 GAS MOLES IN TANK = 442.0382 MTOTO = 442.1281

CONCRETE SURFACE TEMP. = 60.82608  DEG F-----(FCO2 = .9994886)

      60.65     60.41     60.26     60.16     60.10     60.06     60.03     60.02
      60.01     60.01     60.00     60.00     60.00     60.00     60.00     60.00
      60.00     60.00     60.00     60.00     60.00     60.00     60.00     60.00
      60.00     60.00     60.00     60.00     60.00     60.00     60.00     60.00
      60.00     60.00     60.00     60.00     60.00     60.00     60.00     60.00

SLUDGE SURFACE TEMP = 61.20206     DEG F--MASSBURN = 11.10508

      60.95     60.60     60.37     60.23     60.14     60.08     60.05     60.03
      60.02     60.01     60.01     60.00     60.00     60.00     60.00     60.00
      60.00     60.00     60.00     60.00     60.00     60.00     60.00     60.00
      60.00     60.00     60.00     60.00     60.00     60.00     60.00     60.00
      60.00     60.00     60.00     60.00     60.00     60.00     60.00     60.00

AT TIME = 30.00008 SEC, FLOW AREA = 7.669921E-02 FT 2 OXFACT = .9048483
BURN RADIUS = 26.82123 FT BURN AREA = 333.7348 FT 2 MO2O = 92.14253
GAS TEMP. = 260.6194 F ORGANIC TEMP. = 63.53501 XO2 = .2000111
PRESSURE IN HEADSPACE = 5.598814 PSIG STEEL TEMP = 60.52048
MOLES LOST = -6.866455E-03 VOLUME LEAKED = 473.0374 CUBIC FT
OUTFLOW RATE = 34.84826 GAS MOLES IN TANK = 442.135 MTOTO = 442.1281
```

Example Run With POOLFIRE. 4

```
CONCRETE SURFACE TEMP. = 64.22141  DEG F-----(FCO2 = .9987438)

      63.46     62.34     61.57     61.04     60.69     60.45     60.29     60.19
      60.12     60.08     60.05     60.03     60.02     60.01     60.01     60.00
      60.00     60.00     60.00     60.00     60.00     60.00     60.00     60.00
      60.00     60.00     60.00     60.00     60.00     60.00     60.00     60.00
      60.00     60.00     60.00     60.00     60.00     60.00     60.00     60.00

SLUDGE SURFACE TEMP = 66.12418     DEG F--MASSBURN = 33.89292

      65.03     63.39     62.27     61.51     61.00     60.65     60.43     60.27
      60.18     60.11     60.07     60.04     60.03     60.02     60.01     60.01
      60.00     60.00     60.00     60.00     60.00     60.00     60.00     60.00
      60.00     60.00     60.00     60.00     60.00     60.00     60.00     60.00
      60.00     60.00     60.00     60.00     60.00     60.00     60.00     60.00

AT TIME = 39.99996 SEC, FLOW AREA = 7.669921E-02 FT 2 OXFACT = .810496
BURN RADIUS = 26.82123 FT BURN AREA = 579.4643 FT 2 MO2O = 92.14253
GAS TEMP. = 467.3932 F ORGANIC TEMP. = 68.77042 XO2 = .1902622
PRESSURE IN HEADSPACE = 11.39094 PSIG STEEL TEMP = 62.0665
MOLES LOST = -.379303 VOLUME LEAKED = 884.0686 CUBIC FT
OUTFLOW RATE = 46.92031 GAS MOLES IN TANK = 442.5074 MTOTO = 442.1281

CONCRETE SURFACE TEMP. = 74.81931  DEG F-----(FCO2 = .9976648)

      72.43     68.75     66.13     64.27     62.96     62.04     61.40     60.95
      60.64     60.43     60.29     60.19     60.13     60.08     60.05     60.04
      60.02     60.01     60.01     60.01     60.00     60.00     60.00     60.00
      60.00     60.00     60.00     60.00     60.00     60.00     60.00     60.00
      60.00     60.00     60.00     60.00     60.00     60.00     60.00     60.00
```

Example Run With POOLFIRE. 4

SLUDGE SURFACE TEMP = 81.42252 DEG F--MASSBURN = 73.39091

77.97	72.66	68.87	66.18	64.29	62.95	62.02	61.38
60.93	60.63	60.42	60.28	60.18	60.12	60.08	60.05
60.03	60.02	60.01	60.01	60.01	60.00	60.00	60.00
60.00	60.00	60.00	60.00	60.00	60.00	60.00	60.00
60.00	60.00	60.00	60.00	60.00	60.00	60.00	60.00

AT TIME = 49.99981 SEC, FLOW AREA = 7.669921E-02 FT^2 OXFACT = .6786101
BURN RADIUS = 26.82123 FT BURN AREA = 892.557 FT^2 MO2O = 92.14253
GAS TEMP. = 708.5953 F ORGANIC TEMP. = 78.5668 XO2 = .1766605
PRESSURE IN HEADSPACE = 18.17678 PSIG STEEL TEMP = 66.24441
MOLES LOST = -1.044586 VOLUME LEAKED = 1404.934 CUBIC FT
OUTFLOW RATE = 56.71643 GAS MOLES IN TANK = 443.1727 MTOTO = 442.1281

CONCRETE SURFACE TEMP. = 99.90103 DEG F-----(FCO2 = .996272)

94.12	84.96	78.15	73.13	69.44	66.75	64.81	63.40
62.40	61.68	61.17	60.81	60.56	60.38	60.26	60.18
60.12	60.08	60.05	60.04	60.02	60.02	60.01	60.01
60.00	60.00	60.00	60.00	60.00	60.00	60.00	60.00
60.00	60.00	60.00	60.00	60.00	60.00	60.00	60.00

SLUDGE SURFACE TEMP = 117.4236 DEG F--MASSBURN = 128.7802

109.13	95.96	86.17	78.94	73.63	69.75	66.94	64.92
63.46	62.43	61.69	61.17	60.81	60.56	60.38	60.26
60.17	60.12	60.08	60.05	60.03	60.02	60.02	60.01
60.01	60.00	60.00	60.00	60.00	60.00	60.00	60.00
60.00	60.00	60.00	60.00	60.00	60.00	60.00	60.00

AT TIME = 59.99966 SEC, FLOW AREA = 7.669921E-02 FT^2 OXFACT = .5230539
BURN RADIUS = 26.82123 FT BURN AREA = 1273.014 FT^2 MO2O = 92.14253
GAS TEMP. = 919.3046 F ORGANIC TEMP. = 94.96188 XO2 = .160643
PRESSURE IN HEADSPACE = 24.14207 PSIG STEEL TEMP = 74.88077
MOLES LOST = -1.864136 VOLUME LEAKED = 2009.498 CUBIC FT
OUTFLOW RATE = 63.60703 GAS MOLES IN TANK = 443.9922 MTOTO = 442.1281

Example Run With POOLFIRE. 4

CONCRETE SURFACE TEMP. = 143.3897 DEG F-----(FCO2 = .9945812)

132.87	115.53	102.01	91.57	83.58	77.50	72.91	69.47
66.91	65.01	63.62	62.60	61.86	61.32	60.93	60.66
60.46	60.32	60.22	60.15	60.11	60.07	60.05	60.03
60.02	60.02	60.01	60.01	60.00	60.00	60.00	60.00
60.00	60.00	60.00	60.00	60.00	60.00	60.00	60.00

SLUDGE SURFACE TEMP = 179.3478 DEG F--MASSBURN = 194.4455

164.35	139.59	120.27	105.33	93.88	85.16	78.57	73.63
69.95	67.23	65.22	63.75	62.68	61.91	61.35	60.95
60.67	60.47	60.32	60.22	60.15	60.11	60.07	60.05
60.03	60.02	60.02	60.01	60.01	60.00	60.00	60.00
60.00	60.00	60.00	60.00	60.00	60.00	60.00	60.00

AT TIME = 69.99951 SEC, FLOW AREA = 7.669921E-02 FT^2 OXFACT = .3656094
BURN RADIUS = 26.82123 FT BURN AREA = 1720.836 FT^2 MO20 = 92.14253
GAS TEMP. = 1048.612 F ORGANIC TEMP. = 118.862 XO2 = .1444552
PRESSURE IN HEADSPACE = 27.83459 PSIG STEEL TEMP = 88.38809
MOLES LOST = -2.587402 VOLUME LEAKED = 2666.215 CUBIC FT
OUTFLOW RATE = 66.92511 GAS MOLES IN TANK = 444.7155 MTOTO = 442.1281

CONCRETE SURFACE TEMP. = 196.488 DEG F-----(FCO2 = .9926069)

182.05	157.15	136.68	120.04	106.66	96.00	87.58	80.99
75.88	71.94	68.92	66.63	64.90	63.60	62.63	61.92
61.39	61.00	60.72	60.51	60.36	60.26	60.18	60.13
60.09	60.06	60.04	60.03	60.02	60.01	60.01	60.01
60.00	60.00	60.00	60.00	60.00	60.00	60.00	60.00

Example Run With POOLFIRE. 4

SLUDGE SURFACE TEMP = 254.0426 DEG F--MASSBURN = 261.2897

233.64	198.39	169.36	145.73	126.69	111.50	99.50	90.09
82.78	77.13	72.82	69.53	67.05	65.19	63.79	62.76
62.00	61.44	61.04	60.74	60.53	60.37	60.26	60.18
60.13	60.09	60.06	60.04	60.03	60.02	60.01	60.01
60.01	60.00	60.00	60.00	60.00	60.00	60.00	60.00

PEAK PRESSURE = 28.87708 AT TIME = 79.19936

AT TIME = 79.99935 SEC, FLOW AREA = 7.669921E-02 FT 2 OXFACT = .2282653
BURN RADIUS = 26.82123 FT BURN AREA = 2236.021 FT^2 MO2O = 92.14253
GAS TEMP. = 1084.151 F ORGANIC TEMP. = 149.2098 XO2 = .130355
PRESSURE IN HEADSPACE = 28.86884 PSIG STEEL TEMP = 104.7179
MOLES LOST = -2.963959 VOLUME LEAKED = 3339.523 CUBIC FT
OUTFLOW RATE = 67.49219 GAS MOLES IN TANK = 445.0921 MTOTO = 442.1281

CONCRETE SURFACE TEMP. = 241.665 DEG F-----(FCO2 = .9903772)

226.10	197.99	173.55	152.61	134.89	120.07	107.81	97.77
89.63	83.09	77.87	73.75	70.51	67.99	66.04	64.54
63.39	62.52	61.87	61.38	61.01	60.74	60.53	60.39
60.28	60.20	60.14	60.10	60.07	60.05	60.04	60.03
60.02	60.01	60.01	60.01	60.00	60.00	60.00	60.00

SLUDGE SURFACE TEMP = 316.3376 DEG F--MASSBURN = 319.8886

294.59	255.21	220.88	191.39	166.39	145.44	128.09	113.85
102.29	92.98	85.55	79.67	75.05	71.45	68.66	66.51
64.87	63.63	62.69	61.98	61.45	61.06	60.77	60.56
60.40	60.29	60.21	60.15	60.10	60.07	60.05	60.04
60.03	60.02	60.01	60.01	60.01	60.00	60.00	60.00

* * * * * * * * * * * * * * * *

Example Run With POOLFIRE. 4

```
AT TIME = 80.29935 FIRE IS OUT -PGAGE = 28.862 TG = 1083.895 DEG F
THE POOL FIRE IS OUT AT TIME = 80.29935 SEC
PEAK PRESSURE = 28.862 PSIG AND TEMP = 1083.895 DEG F
AT TIME = 89.9992 SEC, FLOW AREA = 7.669921E-02 FT^2 OXFACT = .224633
BURN RADIUS = 26.82123 FT BURN AREA = 2252.518 FT 2 MO2O = 92.14253
GAS TEMP. = 905.9649 F ORGANIC TEMP. = 160.1556 XO2 = .1299824
PRESSURE IN HEADSPACE = 23.72036 PSIG STEEL TEMP = 118.0183
MOLES LOST = -1.308685 VOLUME LEAKED = 3994.632 CUBIC FT
OUTFLOW RATE = 63.17964 GAS MOLES IN TANK = 443.4368 MTOTO = 442.1281

CONCRETE SURFACE TEMP. = 244.0471  DEG F-----(FCO2 = .9866148)

     234.19    214.20    194.52    175.75    158.35    142.58    128.60    116.42
     105.99     97.17     89.80     83.72     78.76     74.73     71.50     68.92
      66.88     65.28     64.03     63.06     62.31     61.73     61.30     60.96
      60.71     60.53     60.39     60.28     60.21     60.15     60.11     60.08
      60.06     60.04     60.03     60.02     60.01     60.01     60.01     60.00

SLUDGE SURFACE TEMP = 317.4095     DEG F--MASSBURN = 321.4414

     303.92    276.41    249.18    223.09    198.80    176.74    157.11    139.98
     125.26    112.81    102.39     93.78     86.73     81.01     76.42    72.75
      69.84     67.56     65.77     64.38     63.31     62.49     61.86     61.39
      61.03     60.76     60.56     60.41     60.30     60.22     60.16     60.11
      60.08     60.06     60.04     60.03     60.02     60.01     60.01     60.00

THE POOL FIRE IS OUT AT TIME = 80.29935 SEC
PEAK PRESSURE = 28.862 PSIG AND TEMP = 1083.895 DEG F

AT TIME = 99.99904 SEC, FLOW AREA = 7.669921E-02 FT 2 OXFACT = .224633
BURN RADIUS = 26.82123 FT BURN AREA = 2252.518 FT^2 MO2O = 92.14253
GAS TEMP. = 781.9316 F ORGANIC TEMP. = 166.9057 XO2 = .1299824
PRESSURE IN HEADSPACE = 20.1242 PSIG STEEL TEMP = 126.7682
MOLES LOST = .2817993 VOLUME LEAKED = 4605.445 CUBIC FT
OUTFLOW RATE = 59.19046 GAS MOLES IN TANK = 441.8463 MTOTO = 442.1281
```

Example Run With POOLFIRE. 4

```
CONCRETE SURFACE TEMP. = 233.8812   DEG F----(FCO2 = .9830761)

     227.07    212.80    198.09    183.37    168.98    155.23    142.35    130.49
     119.76    110.20    101.80     94.51     88.27     82.98     78.54     74.86
      71.83     69.36     67.36     65.75     64.47     63.46     62.66     62.04
      61.55     61.18     60.89     60.67     60.50     60.37     60.27     60.20
      60.15     60.11     60.08     60.06     60.04     60.03     60.02    60.01

SLUDGE SURFACE TEMP = 301.538      DEG F--MASSBURN = 321.4414

     292.38    273.02    252.94    232.71    212.85    193.79    175.88    159.35
     144.35    130.95    119.14    108.89    100.09     92.62     86.35     81.14
      76.84     73.33     70.49     68.21     66.39     64.94     63.80     62.91
      62.22     61.68     61.27     60.96     60.71     60.53     60.39     60.29
      60.21     60.16     60.11     60.08     60.06     60.04     60.02     60.01

Ok
RUN
THIS PROGRAM IS CALLED POOLFIRE.4
```

Example Run With POOLFIRE. 4

```
THIS PROGRAM ANALYZES TEMPERATURE AND PRESSURE TRANSIENTS IN C-103

THIS VERSION COMPUTES INFLOW OF AIR AFTER FIREOUT

WHAT IS THE EQUIVALENT VENT ORIFICE DIAMETER IN INCHES? 3.75

WHAT IS THE EQUIV. ORIFICE DIA. FOR SALTWELL IN INCHES? 0

TOTAL TIME FOR COMPUTATON TO CONTINUE--SEC? 2000

THICKNESS OF ORGANIC POOL--FEET? .1

ASSUMED SPREAD VELOCITY OF FIRE OVER POOL-IN CM/SEC ? 10

THE COMPUTED TIME STEP INTERVAL IS .1018286 SEC

ENTER A ROUNDED VALUE OF DT THAT IS CLOSE TO THE VALUE ABOVE? .1

ENTER THE TIME BETWEEN PRINTOUTS,IN SECONDS? 200

09-10-1997
08:09:11

KEY INPUT DATA FOR THIS PROBLEM ARE AS FOLLOWS
INITIAL CONCRETE TEMP = 60 INITIAL ORGANIC TEMP = 60
GAS VOLUME IN HEAD SPACE = 170000 TIME STEP  = .1
THICKNESS OF ORGANIC POOL = .1 IN FEET
INITIAL GAS TEMPERATURE,F = 60 INITIAL SLUDGE TEMP, F = 60
COMBUSTION ENERGY IS 14140 BTU PER LB. OF ORGANIC BURNED
THICKNESS OF CONCRETE MODELLED = .12 FT
THICKNESS OF SLUDGE MODELLED = 4.512839E-02 FT
POOL BURNING RATE ASSUMED = 3 KG/M2 MIN
FIRE SPREAD RATE  = 10 CM/SEC---TIME OF SPREAD = 80.38505 SEC
THE OXYGEN MOLE FRACTION WHERE FIRE STOPS = .13
```

Example Run With POOLFIRE. 4

```
PEAK PRESSURE  = 28.87708 AT TIME = 79.19936
* * * * * * * * * * * * * * * * *
AT TIME = 80.29935 FIRE IS OUT -PGAGE = 28.862 TG = 1083.895 DEG F

FOLLOWING ARE DISTANCES FROM CONCRETE SURFACE--FT

     0.00150   0.00450   0.00750   0.01050   0.01350   0.01650   0.01950   0.02250
     0.02550   0.02850   0.03150   0.03450   0.03750   0.04050   0.04350   0.04650
     0.04950   0.05250   0.05550   0.05850   0.06150   0.06450   0.06750   0.07050
     0.07350   0.07650   0.07950   0.08250   0.08550   0.08850   0.09150   0.09450
     0.09750   0.10050   0.10350   0.10650   0.10950   0.11250   0.11550   0.11850

FOLLOWING ARE DISTANCES FROM SLUDGE SURFACE--FT

     0.00056   0.00169   0.00282   0.00395   0.00508   0.00621   0.00733   0.00846
     0.00959   0.01072   0.01185   0.01297   0.01410   0.01523   0.01636   0.01749
     0.01862   0.01974   0.02087   0.02200   0.02313   0.02426   0.02538   0.02651
     0.02764   0.02877   0.02990   0.03103   0.03215   0.03328   0.03441   0.03554
     0.03667   0.03780   0.03892   0.04005   0.04118   0.04231   0.04344   0.04456

THE POOL FIRE IS OUT AT TIME = 80.29935 SEC
PEAK PRESSURE = 28.862 PSIG AND TEMP = 1083.895 DEG F

AT TIME = 200.003 SEC, FLOW AREA = 7.669921E-02 FT^2 OXFACT = .224633
BURN RADIUS = 26.82123 FT BURN AREA = 2252.518 FT^2 MO2O = 92.14253
GAS TEMP. = 359.3661 F ORGANIC TEMP. = 187.8097 XO2 = .1299824
PRESSURE IN HEADSPACE = 7.702723 PSIG STEEL TEMP = 154.9648
MOLES LOST = 12.60202 VOLUME LEAKED = 9413.052 CUBIC FT
OUTFLOW RATE = 40.48331 GAS MOLES IN TANK = 429.5261 MTOTO = 442.1281

CONCRETE SURFACE TEMP. = 168.1103  DEG F-----(FCO2 = .9556658)

     167.03    164.59    161.82    158.77    155.45    151.90    148.17    144.27
     140.26    136.16    132.01    127.84    123.68    119.56    115.51    111.55
     107.70    103.97    100.40     96.98     93.73     90.65     87.75     85.03
      82.49     80.12     77.93     75.90     74.03     72.31     70.73     69.27
      67.94     66.71     65.58     64.53     63.54     62.61     61.72     60.85
```

Example Run With POOLFIRE. 4

```
SLUDGE SURFACE TEMP = 205.5852     DEG F--MASSBURN = 321.4414

     204.28    201.28    197.81    193.92    189.65    185.04    180.15    175.02
     169.70    164.25    158.70    153.10    147.51    141.95    136.46    131.09
     125.85    120.78    115.89    111.21    106.76    102.53     98.54     94.79
      91.28     88.01     84.98     82.17     79.57     77.18     74.99     72.97
      71.11     69.39     67.81     66.34     64.96     63.65     62.40     61.19

THE POOL FIRE IS OUT AT TIME = 80.29935 SEC
PEAK PRESSURE = 28.862 PSIG AND TEMP = 1083.895 DEG F

AT TIME = 400.0152 SEC, FLOW AREA = 7.669921E-02 FT 2 OXFACT = .224633
BURN RADIUS = 26.82123 FT BURN AREA = 2252.518 FT 2 MO2O = 92.14253
GAS TEMP. = 204.1309 F ORGANIC TEMP. = 192.7425 XO2 = .1299824
PRESSURE IN HEADSPACE = 2.819058 PSIG STEEL TEMP = 163.6486
MOLES LOST = 28.71762 VOLUME LEAKED = 15913.94 CUBIC FT
OUTFLOW RATE = 26.58642 GAS MOLES IN TANK = 413.4105 MTOTO = 442.1281

CONCRETE SURFACE TEMP. = 129.9823  DEG F-----(FCO2 = .9198121)

     129.71    129.07    128.33    127.49    126.54    125.50    124.37    123.14
     121.83    120.44    118.98    117.44    115.84    114.18    112.46    110.69
     108.87    107.01    105.12    103.19    101.23     99.24     97.24     95.21
      93.17     91.12     89.06     87.00     84.92     82.85     80.77     78.69
      76.61     74.53     72.45     70.37     68.29     66.22     64.15     62.07

SLUDGE SURFACE TEMP = 152.0193     DEG F--MASSBURN = 321.4414

     151.74    151.05    150.22    149.24    148.12    146.86    145.47    143.96
     142.32    140.57    138.71    136.75    134.69    132.54    130.31    128.01
     125.63    123.19    120.70    118.15    115.56    112.92    110.25    107.56
     104.83    102.09     99.32     96.54     93.75     90.96     88.15     85.34
      82.53     79.71     76.90     74.08     71.26     68.45     65.63     62.82

THE POOL FIRE IS OUT AT TIME = 80.29935 SEC
PEAK PRESSURE = 28.862 PSIG AND TEMP = 1083.895 DEG F
```

Example Run With POOLFIRE. 4

```
AT TIME = 600.0006 SEC, FLOW AREA = 7.669921E-02 FT 2 OXFACT = .224633
BURN RADIUS = 26.82123 FT BURN AREA = 2252.518 FT 2 MO2O = 92.14253
GAS TEMP. = 166.0481 F ORGANIC TEMP. = 192.1902 XO2 = .1299824
PRESSURE IN HEADSPACE = 1.394555 PSIG STEEL TEMP = 164.7216
MOLES LOST = 39.62659 VOLUME LEAKED = 20460.78 CUBIC FT
OUTFLOW RATE = 19.42248 GAS MOLES IN TANK = 402.5015 MTOTO = 442.1281

CONCRETE SURFACE TEMP. = 113.4432  DEG F-----(FCO2 = .8955322)

     113.27    112.88    112.43    111.90    111.32    110.67    109.96    109.18
     108.35    107.46    106.51    105.50    104.44    103.33    102.16    100.95
      99.68     98.38     97.02     95.63     94.19     92.72     91.21     89.66
      88.08     86.47     84.84     83.17     81.48     79.77     78.04     76.29
      74.52     72.74     70.94     69.14     67.32     65.50     63.67     61.83

SLUDGE SURFACE TEMP = 129.287 DEG F--MASSBURN = 321.4414

     129.12    128.70    128.19    127.60    126.92    126.15    125.29    124.35
     123.32    122.22    121.03    119.77    118.42    117.01    115.52    113.97
     112.34    110.65    108.90    107.09    105.22    103.30    101.32    99.30
      97.23     95.11     92.95     90.76     88.53     86.27     83.97     81.65
      79.31     76.94     74.56     72.16     69.74     67.32     64.88     62.44

THE POOL FIRE IS OUT AT TIME = 80.29935 SEC
PEAK PRESSURE = 28.862 PSIG AND TEMP = 1083.895 DEG F

AT TIME = 799.9518 SEC, FLOW AREA = 7.669921E-02 FT 2 OXFACT = .224633
BURN RADIUS = 26.82123 FT BURN AREA = 2252.518 FT^2 MO2O = 92.14253
GAS TEMP. = 151.3928 F ORGANIC TEMP. = 190.4638 XO2 = .1299824
PRESSURE IN HEADSPACE = .7194433 PSIG STEEL TEMP = 164.3344
MOLES LOST = 47.47827 VOLUME LEAKED = 23809.12 CUBIC FT
OUTFLOW RATE = 14.27302 GAS MOLES IN TANK = 394.6498 MTOTO = 442.1281
```

Example Run With POOLFIRE. 4

CONCRETE SURFACE TEMP. = 102.4074 DEG F-----(FCO2 = .8780703)

102.26	101.93	101.54	101.12	100.64	100.12	99.56	98.94
98.29	97.59	96.84	96.06	95.23	94.36	93.45	92.50
91.52	90.49	89.43	88.34	87.22	86.06	84.87	83.65
82.41	81.14	79.84	78.52	77.18	75.82	74.44	73.05
71.64	70.21	68.77	67.33	65.87	64.41	62.94	61.47

SLUDGE SURFACE TEMP = 114.4248 DEG F --MASSBURN = 321.4414

114.26	113.89	113.45	112.95	112.39	111.77	111.08	110.33
109.52	108.66	107.73	106.74	105.70	104.60	103.45	102.25
100.99	99.68	98.33	96.92	95.47	93.98	92.45	90.87
89.26	87.61	85.93	84.21	82.47	80.69	78.89	77.07
75.23	73.37	71.49	69.59	67.69	65.78	63.85	61.93

THE POOL FIRE IS OUT AT TIME = 80.29935 SEC
PEAK PRESSURE = 28.862 PSIG AND TEMP = 1083.895 DEG F

AT TIME = 999.9029 SEC, FLOW AREA = 7.669921E-02 FT 2 OXFACT = .224633
BURN RADIUS = 26.82123 FT BURN AREA = 2252.518 FT^2 MO2O = 92.14253
GAS TEMP. = 144.6479 F ORGANIC TEMP. = 188.3211 XO2 = .1299824
PRESSURE IN HEADSPACE = .3393822 PSIG STEEL TEMP = 163.4236
MOLES LOST = 53.03827 VOLUME LEAKED = 26223.25 CUBIC FT
OUTFLOW RATE = 9.950066 GAS MOLES IN TANK = 389.0898 MTOTO = 442.1281

CONCRETE SURFACE TEMP. = 94.47177 DEG F-----(FCO2 = .8656808)

94.32	94.00	93.65	93.26	92.83	92.38	91.89	91.36
90.80	90.21	89.59	88.94	88.25	87.54	86.79	86.02
85.22	84.39	83.53	82.65	81.74	80.81	79.85	78.88
77.88	76.86	75.82	74.77	73.70	72.61	71.51	70.40
69.27	68.14	66.99	65.84	64.68	63.51	62.34	61.17

Example Run With POOLFIRE. 4

SLUDGE SURFACE TEMP = 103.9587 DEG F--MASSBURN = 321.4414

103.79	103.41	102.98	102.51	101.99	101.43	100.83	100.18
99.49	98.75	97.98	97.16	96.30	95.40	94.45	93.47
92.46	91.40	90.31	89.19	88.03	86.83	85.61	84.36
83.08	81.77	80.44	79.08	77.70	76.30	74.88	73.44
71.99	70.52	69.04	67.55	66.05	64.54	63.03	61.52

THE POOL FIRE IS OUT AT TIME = 80.29935 SEC
PEAK PRESSURE = 28.862 PSIG AND TEMP = 1083.895 DEG F

AT TIME = 1199.854 SEC, FLOW AREA = 7.669921E-02 FT 2 OXFACT = .224633
BURN RADIUS = 26.82123 FT BURN AREA = 2252.518 FT^2 MO2O = 92.14253
GAS TEMP. = 140.9511 F ORGANIC TEMP. = 186.0644 XO2 = .1299824
PRESSURE IN HEADSPACE = .1125431 PSIG STEEL TEMP = 162.2569
MOLES LOST = 56.6275 VOLUME LEAKED = 27799.19 CUBIC FT
OUTFLOW RATE = 5.784847 GAS MOLES IN TANK = 385.5006 MTOTO = 442.1281

CONCRETE SURFACE TEMP. = 88.71792 DEG F-----(FCO2 = .8577002)

88.57	88.25	87.90	87.53	87.13	86.71	86.27	85.80
85.31	84.79	84.25	83.69	83.10	82.49	81.86	81.21
80.54	79.85	79.14	78.40	77.65	76.89	76.10	75.30
74.48	73.65	72.81	71.95	71.08	70.19	69.30	68.40
67.49	66.57	65.64	64.71	63.77	62.83	61.89	60.95

SLUDGE SURFACE TEMP = 96.52353 DEG F--MASSBURN = 321.4414

96.34	95.94	95.51	95.05	94.56	94.04	93.48	92.90
92.28	91.63	90.95	90.24	89.50	88.73	87.93	87.11
86.26	85.38	84.47	83.54	82.59	81.61	80.61	79.59
78.55	77.48	76.40	75.31	74.19	73.06	71.92	70.77
69.60	68.42	67.24	66.04	64.84	63.64	62.43	61.21

THE POOL FIRE IS OUT AT TIME = 80.29935 SEC
PEAK PRESSURE = 28.862 PSIG AND TEMP = 1083.895 DEG F

Example Run With POOLFIRE. 4

```
AT TIME = 1399.805 SEC, FLOW AREA = 7.669921E-02 FT^2 OXFACT = .224633
BURN RADIUS = 26.82123 FT BURN AREA = 2252.518 FT^2 MO2O = 92.14253
GAS TEMP. = 138.6577 F ORGANIC TEMP. = 183.759 XO2 = .1299824
PRESSURE IN HEADSPACE =-9.155273E-04 PSIG STEEL TEMP = 161.0362
MOLES LOST = 58.15436 VOLUME LEAKED = 28469.38 CUBIC FT
OUTFLOW RATE = 0 GAS MOLES IN TANK = 383.9737 MTOTO = 442.1281

CONCRETE SURFACE TEMP. = 84.53354  DEG F-----(FCO2 = .8543141)

      84.38     84.06     83.72     83.36     82.98     82.59     82.17     81.74
      81.29     80.83     80.35     79.85     79.33     78.80     78.25     77.69
      77.11     76.52     75.91     75.29     74.65     74.00     73.34     72.67
      71.98     71.29     70.58     69.87     69.14     68.41     67.67     66.93
      66.17     65.41     64.65     63.88     63.11     62.33     61.56     60.78

SLUDGE SURFACE TEMP = 91.23068     DEG F--MASSBURN = 321.4414

      91.03     90.62     90.19     89.74     89.26     88.76     88.23     87.69
      87.12     86.53     85.92     85.28     84.63     83.95     83.26     82.54
      81.81     81.05     80.28     79.49     78.68     77.85     77.01     76.16
      75.28     74.40     73.50     72.59     71.67     70.73     69.79     68.84
      67.88     66.91     65.93     64.95     63.97     62.98     61.99     60.99

THE POOL FIRE IS OUT AT TIME = 80.29935 SEC
PEAK PRESSURE = 28.862 PSIG AND TEMP = 1083.895 DEG F

AT TIME = 1599.757 SEC, FLOW AREA = 7.669921E-02 FT 2 OXFACT = .224633
BURN RADIUS = 26.82123 FT BURN AREA = 2252.518 FT 2 MO2O = 92.14253
GAS TEMP. = 136.7656 F ORGANIC TEMP. = 181.5617 XO2 = .1299824
PRESSURE IN HEADSPACE =-4.677201E-02 PSIG STEEL TEMP = 159.8026
MOLES LOST = 58.15436 VOLUME LEAKED = 28469.38 CUBIC FT
OUTFLOW RATE = 0 GAS MOLES IN TANK = 383.9737 MTOTO = 442.1281
```

Example Run With POOLFIRE. 4

```
CONCRETE SURFACE TEMP. = 81.47855  DEG F-----(FCO2 = .8543141)

      81.32     81.00     80.66     80.31     79.95     79.57     79.19     78.78
      78.37     77.94     77.50     77.05     76.58     76.11     75.62     75.12
      74.61     74.09     73.55     73.01     72.46     71.90     71.33     70.75
      70.16     69.56     68.96     68.35     67.73     67.11     66.48     65.85
      65.21     64.57     63.92     63.27     62.62     61.97     61.31     60.66

SLUDGE SURFACE TEMP = 87.43424     DEG F--MASSBURN = 321.4414

      87.23     86.81     86.38     85.93     85.46     84.98     84.48     83.96
      83.43     82.88     82.32     81.74     81.15     80.54     79.91     79.28
      78.62     77.96     77.28     76.59     75.88     75.17     74.44     73.70
      72.95     72.19     71.42     70.64     69.86     69.06     68.26     67.45
      66.64     65.82     65.00     64.17     63.34     62.51     61.67     60.84

THE POOL FIRE IS OUT AT TIME = 80.29935 SEC
PEAK PRESSURE = 28.862 PSIG AND TEMP = 1083.895 DEG F

AT TIME = 1799.708 SEC, FLOW AREA = 7.669921E-02 FT 2 OXFACT = .224633
BURN RADIUS = 26.82123 FT BURN AREA = 2252.518 FT^2 MO2O = 92.14253
GAS TEMP. = 134.8453 F ORGANIC TEMP. = 179.3645 XO2 = .1299824
PRESSURE IN HEADSPACE =-9.331131E-02 PSIG STEEL TEMP = 158.4599
MOLES LOST = 58.15436 VOLUME LEAKED = 28469.38 CUBIC FT
OUTFLOW RATE = 0 GAS MOLES IN TANK = 383.9737 MTOTO = 442.1281

CONCRETE SURFACE TEMP. = 79.2023   DEG F-----(FCO2 = .8543141)

      79.05     78.73     78.40     78.06     77.70     77.34     76.97     76.59
      76.21     75.81     75.40     74.98     74.56     74.12     73.68     73.23
      72.77     72.30     71.82     71.34     70.85     70.35     69.85     69.34
      68.82     68.30     67.77     67.24     66.70     66.16     65.61     65.06
      64.51     63.95     63.39     62.83     62.26     61.70     61.13     60.57
```

Example Run With POOLFIRE. 4

SLUDGE SURFACE TEMP = 84.6445 DEG F--MASSBURN = 321.4414

84.44	84.02	83.59	83.15	82.69	82.23	81.75	81.25
80.75	80.24	79.71	79.17	78.63	78.07	77.50	76.92
76.33	75.72	75.11	74.49	73.87	73.23	72.58	71.93
71.27	70.60	69.92	69.24	68.56	67.86	67.16	66.46
65.75	65.04	64.33	63.61	62.89	62.17	61.45	60.72

NEGATIVE PRESSURE AT 1829.8 SEC

THE POOL FIRE IS OUT AT TIME = 80.29935 SEC
PEAK PRESSURE = 28.862 PSIG AND TEMP = 1083.895 DEG F

AT TIME = 1999.659 SEC, FLOW AREA = 7.669921E-02 FT 2 OXFACT = .224633
BURN RADIUS = 26.82123 FT BURN AREA = 2252.518 FT^2 MO2O = 92.14253
GAS TEMP. = 132.8064 F ORGANIC TEMP. = 177.1672 XO2 = .1303996
PRESSURE IN HEADSPACE =-6.600094E-02 PSIG STEEL TEMP = 157.1171
MOLES LOST = 56.10242 VOLUME LEAKED = 27687.64 CUBIC FT
OUTFLOW RATE = -4.119791 GAS MOLES IN TANK = 386.0257 MTOTO = 442.1281

CONCRETE SURFACE TEMP. = 77.4476 DEG F-----(FCO2 = .8543141)

77.29	76.98	76.66	76.33	75.99	75.65	75.30	74.94
74.57	74.20	73.82	73.43	73.03	72.63	72.22	71.81
71.39	70.96	70.53	70.09	69.65	69.20	68.75	68.29
67.83	67.36	66.89	66.41	65.93	65.45	64.96	64.48
63.98	63.49	63.00	62.50	62.00	61.50	61.00	60.50

SLUDGE SURFACE TEMP = 82.52683 DEG F--MASSBURN = 321.4414

82.32	81.91	81.49	81.05	80.61	80.16	79.70	79.23
78.76	78.27	77.78	77.27	76.76	76.24	75.71	75.18
74.63	74.08	73.52	72.96	72.39	71.81	71.23	70.64
70.04	69.44	68.83	68.22	67.61	66.99	66.36	65.74
65.11	64.48	63.84	63.20	62.56	61.92	61.28	60.64

Example Run With POOLFIRE. 4

```
THE POOL FIRE IS OUT AT TIME = 80.29935 SEC
PEAK PRESSURE = 28.862 PSIG AND TEMP = 1083.895 DEG F

AT TIME = 2199.795 SEC, FLOW AREA = 7.669921E-02 FT 2 OXFACT = .224633
BURN RADIUS = 26.82123 FT BURN AREA = 2252.518 FT 2 MO2O = 92.14253
GAS TEMP. = 131.187 F ORGANIC TEMP. = 174.9699 XO2 = .1307743
PRESSURE IN HEADSPACE =-3.570652E-02 PSIG STEEL TEMP = 155.7743
MOLES LOST = 54.23188 VOLUME LEAKED = 26974.57 CUBIC FT
OUTFLOW RATE = -3.032153 GAS MOLES IN TANK = 387.8962 MTOTO = 442.1281

CONCRETE SURFACE TEMP. = 76.10616  DEG F-----(FCO2 = .8543141)

      75.95     75.65     75.33     75.01     74.69     74.35     74.02     73.67
      73.32     72.97     72.61     72.24     71.87     71.50     71.12     70.73
      70.34     69.95     69.55     69.15     68.74     68.33     67.91     67.49
      67.07     66.64     66.22     65.78     65.35     64.91     64.47     64.03
      63.59     63.14     62.70     62.25     61.80     61.35     60.90     60.45

SLUDGE SURFACE TEMP = 80.91391     DEG F--MASSBURN = 321.4414

      80.71     80.30     79.89     79.47     79.04     78.60     78.15     77.70
      77.25     76.78     76.31     75.84     75.35     74.86     74.37     73.87
      73.36     72.85     72.33     71.81     71.28     70.75     70.21     69.67
      69.12     68.57     68.02     67.46     66.90     66.33     65.77     65.20
      64.63     64.05     63.48     62.90     62.32     61.74     61.16     60.58

ok
```

8.0 CONFIRMATION OF POOLFIRE.4

An independent analysis of solvent fires was carried out at Fauske and Associates, Inc. by Epstein. The purpose was to confirm the numerical validity of pressures computed by Poolfire. Because the fire assumptions made by Epstein were consistent with those used in Grigsby et al. (1995), results could be compared on a numerical basis. Note that an earlier version of POOLFIRE.4, called POOLFIRE.3, was the program actually checked by Epstein (1995). POOLFIRE.3 differs from POOLFIRE.4 only in program lines 1807, 1808, and 1820. These lines relate specific burn rate to oxygen mole fraction in headspace air. POOLFIRE.3 used a constant specific burn rate. Because the difference between POOLFIRE.3 and POOLFIRE.4 is small and obvious, it has been assumed that Epstein's confirmation of POOLFIRE.3 applies also to POOLFIRE.4.

The memo that conveyed Epstein's analysis is included as Attachment A. The findings have been interpreted as supporting the validity of POOLFIRE.3. Differences between Epstein's model and POOLFIRE.3 are thought to be explainable in terms of different assumptions used in the two models.

In addition to Epstein's independent analysis, the methodology embodied in POOLFIRE.4 was reviewed by Dr. C. L. Beyler of Hughes Associates, Inc. Dr. Beyler's letter regarding the appropriateness of the fire analysis methodology is included as Attachment B.

9.0 REFERENCES

Carslaw, H. S., and J. C. Jaeger, 1959, *Conduction of Heat in Solids*, *Second Edition*, Oxford at the Claredon Press, London.

Daniels, F., and R. A. Alberty, 1995, *Physical Chemistry*, New York, New York.

Fox, G. L., T. E. Beaver , D. B. Bechtold, D. L. Herting, A. K. Postma, P. K. Shen, and D. D. Stepnewski, 1991, *Tank 241-SY-101 Crust Burn Analysis*, WHC-SD-WM-SAR-046, Rev. 0, Westinghouse Hanford Company, Richland, Washington.

Grigsby, J. M., J. E. Meacham, D. A. Turner, J. C. Van Keuren, M. G. Plys, M. Epstein, H. K. Fauske, J. P. Burelbach, and A. K. Postma, 1995, *Risk from Organic Solvent Fires in C-103 Following Interim Stabilization*, WHC-SD-WM-SARR-001, Supplement 1, Rev. 0A, Westinghouse Hanford Company, Richland, Washington.

Hörman, E., 1983, "Analysis of Fire and Explosion Accidents in a Fuel Reprocessing Plant," in *Proceedings of the CSNI Specialist Meeting on Interaction of Fire and Explosion with Ventilation Systems in Nuclear Facilities*, LA-9911-C-Vol. 1, April 25-28, Los Alamos, New Mexico.

Hougen, O. A., K. M. Watson, and R. A. Ragatz, 1954, *Chemical Process Principles*, *Part I*, *Material and Energy Balances*, John Wiley & Sons, Inc., New York, New York.

Hougen, O. A., K. M. Watson, and R. A. Ragatz, 1959, *Chemical Process Principles*, *Part II*, *Thermodynamics*, John Wiley & Sons, Inc., New York, New York.

Malet, J. C., G. Duverger de Cuy, R. Gasteiger, and K. Janberg, 1983, "Solvent Pool Fire Testing" in *Proceedings of the CSNI Specialist Meeting on Interaction of Fire and Explosion with Ventilation Systems in Nuclear Facilities*, LA-9911-C, Vol. II, April 25-28, Los Alamos, New Mexico.

McAdams, W. H., 1954, *Heat Transmission*, McGraw-Hill Book Company, New York, New York.

Perry, J. H., (Ed.), 1950, *Chemical Engineers' Handbook*, McGraw-Hill Book Company, Third Edition, New York, New York.

Pool, K. H., and R. M. Bean, 1994, *Waste Tank Safety Project: Analysis of Liquid Samples from Hanford Waste Tank 241-C-103*, PNL-9403, Pacific Northwest Laboratory, Richland, Washington.

ATTACHMENT A

MEMO FROM M. EPSTEIN OF FAI TO A. K. POSTMA,
"CONFIRMATION OF POSTMA'S SOLVENT-FIRE TANK-PRESSURE
TRANSIENT MODEL, "DATED SEPTEMBER, 26, 1995

This page intentionally left blank.

Fauske & Associates, Inc.

DATE: September 26, 1995

TO: Arlin Postma G & P Consulting
FAX: (503) 623-0479

FROM: Michael Epstein Fauske & Associates, Inc.

SUBJECT: *Confirmation of Postma's Solvent-Fire Tank-Pressure Transient Model*

This memo reports a model for predicting the pressure history during a postulated solvent fire in Tank C-103. The model is essentially an independently constructed version of the model reported by Postma (1995) to predict Tank C-103 pressurization. The purpose of the present model is to provide an independent calculation to confirm Postma's predicted pool-fire-induced pressure transients.

We consider a circular pool of solvent whose cross-sectional area is small compared to the total surface area of sludge. Immediately following ignition at the center of the pool a flame of initial radius r_o (measured from the center of the solvent pool) begins to spread as a cylindrically expanding surface. The flame stops spreading when it reaches a size r_p which coincides with the radius of the solvent pool. The flame goes out when the bulk oxygen concentration Y (mass fraction) in the tank headspace falls below the oxygen extinction concentration Y_{ext}. The flame may self-extinguish before it reaches the periphery of the pool. The heat generated by the flame causes the tank to pressurize. The increased pressure results in opening several flow paths (vents) from the tank headspace to the atmosphere. These vents act to reduce the pressure rise rate and the peak pressure compared to a sealed tank. After the fire goes out a cool down of headspace air occurs which produces a partial vacuum within the tank. Fresh air is then drawn into the tank and the pressure returns to atmospheric.

The approach to the calculation of the pressure-time history inside the tank headspace is based on the following set of simplifying assumptions.

(1) The physical properties of the mixture of air and combustion products are constant and taken to be those of air.

(2) The pressure P is uniform throughout the tank headspace.

(3) The temperature and oxygen concentration within the tank headspace are uniform in space.

(4) The surface of the sludge and the inside surface of the tank remain at constant temperature T_w during the pressure transient.

(5) Heat transfer from the soot-laden headspace gas to the surface of the sludge and the tank wall occurs via thermal radiation and turbulent natural convection.

(6) Flow through the vents is well-represented by incompressible flow theory.

(7) The ideal equation of state is applicable to the headspace gas.

(8) The burning rate of the solvent per unit area of inflamed pool surface $\dot{m}_b''$ is a known function of the size (diameter) of the inflamed area and the flame spreading velocity v_f is a known constant.

The equations of conservation of energy, mass of headspace gas, and mass of oxygen within the headspace are

$$\rho c_v V \frac{dT}{dt} = \dot{m}_b \Delta H - \dot{m}_v \frac{R}{M_g} T - \epsilon\sigma (T^4 - T_w^4) A_w$$

$$- 0.13\ k\ (T - T_w)\ A_w \left[\frac{g(T - T_w)}{\nu\ \alpha\ T_w}\right]^{1/3} - \dot{m}_v\ c_p\ (T_\infty - T) \tag{1}$$

$$V\ \frac{d\rho}{dt} = - \dot{m}_v \tag{2}$$

and

$$\rho V\ \frac{dY}{dt} = - r\ \dot{m}_b - \dot{m}_v\ (Y_\infty - Y) \tag{3}$$

respectively. The nomenclature list at the end of this memo gives the meanings of the symbols as well as the numerical values of the fixed parameters. The last term in Eq. (1) and the last term in Eq. (3) appear only for the suction period when the headspace pressure falls below the outside atmosphere pressure ($P < P_\infty$). Once ρ and T are determined from Eqs. (1) and (2) the tank pressure follows from the ideal gas law:

$$P = \rho\ \frac{R}{M_g}\ T \tag{4}$$

The mass flow rate through the vents is

$$\dot{m}_v = \begin{cases} A_{eff}\ [2\rho(P - P_\infty)]^{1/2} & \text{for discharge } (P \geq P_\infty) \\ - A_{eff}\ [2\rho_\infty(P_\infty - P)]^{1/2} & \text{for suction } (P < P_\infty) \end{cases} \tag{5),(6}$$

where A_{eff} is an effective vent area that appropriately accounts for all the actual vent areas and the frictional resistance associated with each vent.

Since each vent path i may be represented as an equivalent circular pipe of length L_i diameter D_i and friction factor f_i (Postma, 1995), the expression for A_{eff} is

$$A_{eff} = \frac{\pi}{8} \sum_i D_i^2 \left(\frac{D}{Lf}\right)_i \tag{7}$$

From the physical description of the vent paths and the tank pressures at which they become available (Postma, 1995), we estimate that

$$A_{eff} = \begin{cases} 4.5 \times 10^{-3}\ m^2 & \text{for} \quad P \leq 0.151\ MPa \\ 1.86 \times 10^{-2}\ m^2 & \text{for} \quad P > 0.151\ MPa \end{cases} \tag{8}$$

The burning rate of the solvent is simply the known specific burning rate $\dot{m}_b''$ multiplied by the instantaneous cross sectional area πR_f^2 of the fire, where R_f is the radius of the flame. Thus

$$\dot{m}_b = \pi R_f^2\ \dot{m}_b'' \tag{9}$$

where

$$R_f = R_{f,o} + v_f\ t \tag{10}$$

$$\dot{m}_b'' = \dot{m}_{b,\infty}''\ [1 - \exp\ (-7.0\ R_f)] \tag{11}$$

Note that $\dot{m}_b$ is set equal to zero once Y falls below Y_{ext} and R_f is not allowed to exceed R_p. Equation (11) reflects a measured reduction in the specific burning rate when the inflamed area is small (Babranskas, 1988; see Postma, 1955).

The initial conditions for Eqs. (1) to (3) are

$$T = T_w, \ \rho = \frac{M_g P_\infty}{R T_w} \quad , \quad Y = Y_\infty \ \text{ at } \ t = 0 \tag{12}$$

The equations were integrated using the simple Euler forward integration method. The parameters for the base case solvent fire are the same as those recommended by Postma; namely,

$R_{f,o}$ = 0.3 m
v_f = 0.01 m s^{-1}
R_p = 3.6 m
ϵ = 0.9
Y_{ext} = 0.142
$\dot{m}''_{b,\infty}$ = 2 x 10^{-2} kg m^{-2} s^{-1}
ΔH = 3.3 x 10^7 J kg^{-1}

The predicted best case tank-pressure history is shown in Fig. 1. The circles are Postma's predicted values. The agreement between the two calculations is good with the present result yielding a peak pressure of 0.159 MPa (8.7 psig), at t = 273 sec, versus Postma's peak pressure prediction of 0.158 MPa (8.5 psig) at 286 sec. The present model predicts a negative pressure following flame extinguishment of 0.089 MPa (-1.62 psig) at t = 426 sec. This is somewhat larger than Postma's prediction of 0.0918 MPa (-1.2 psig) at t = 540 sec.

Parameter variations that depart from the base case values were input to the model and the peak pressure results are shown in Tables 1 to 8 together with the previous results reported by Postma. In almost all cases the present model yields higher P_{max} values than those calculated by Postma. However the percentage difference between the P_{max} predictions does not exceed 15 percent.

Fig. 1

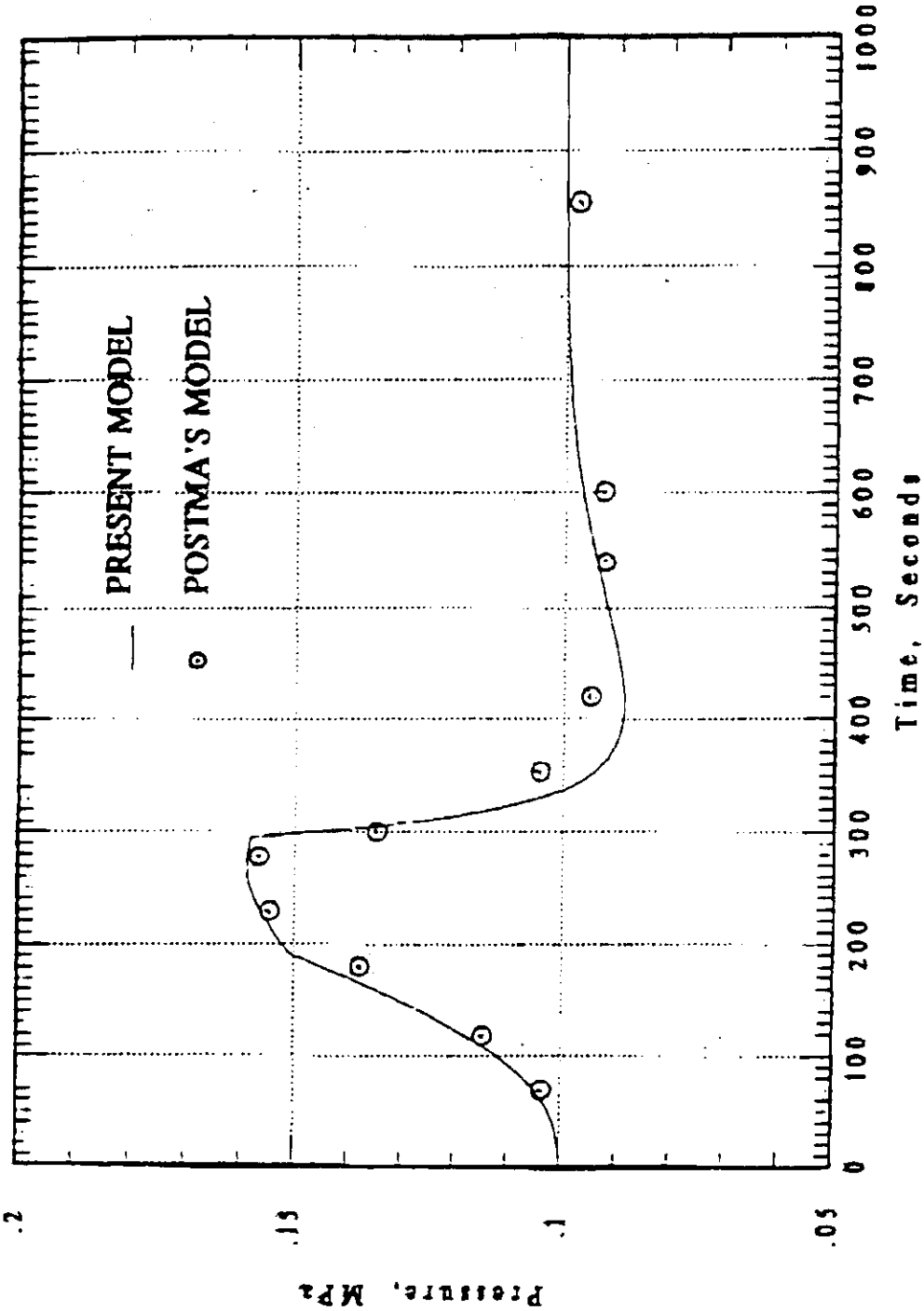

Figure 1 Tank pressure-time history for best case solvent fire.

Table 1

Effect of Initial Flame Radius on Peak Pressure

R_o (m)	P_{max} (psig)	
	PRESENT MODEL	POSTMA'S MODEL
0.15	8.66	8.5
0.31	8.67	8.5
0.62	8.73	8.5

Table 2

Effect of Flame Spread Velocity on Peak Pressure

v_f (m s^{-1})	P_{max} (psig)	
	PRESENT MODEL	POSTMA'S MODEL
0.001	2.24	1.8
0.005	7.50	7.6
0.01	8.66	8.5
0.02	12.82	11.9

Table 3

Effect of Pool Radius on Peak Pressure

R_p (m)	P_{max} (psig)	
	PRESENT MODEL	POSTMA'S MODEL
0.3	0.19	0.47
1.22	4.42	3.7
1.72	7.36	6.4
2.43	8.32	8.1
3.60	8.66	8.5
4.87	8.66	8.5

Table 4

Effect of Venting Sequence on Peak Pressure

VENT SEQUENCE	P_{max} (psig)	
	PRESENT MODEL	POSTMA'S MODEL
Salt Well Riser Opens	8.66	8.5
Salt Well Riser Does Not Open	13.79	12.0

Table 5

Effect of Emissivity on Peak Pressure

ϵ	P_{max} (psig)	
	PRESENT MODEL	POSTMA'S MODEL
1.0	8.44	8.4
0.9	8.66	8.5
0.8	8.95	8.7

Table 6

Effect of Oxygen Extinguishment Levels on Peak Pressure

Y_{ext}	P_{max} (psig)	
	PRESENT MODEL	POSTMA'S MODEL
0.12	8.66	8.5
0.142	8.66	8.5
0.19	8.30	6.5

Table 7

Effect of Specific Burning Rate on Peak Pressure

$\dot{m}''_{b,\infty}$ (kg m^{-2} s^{-1})	P_{max} (psig)	
	PRESENT MODEL	POSTMA'S MODEL
1.67×10^{-2}	8.22	8.4
2×10^{-2}	8.66	8.5
2.83×10^{-2}	9.63	9.3

Table 8

Effect of Combustion Energy on Peak Pressure

ΔH (J kg^{-1})	P_{max} (psig)	
	PRESENT MODEL	POSTMA'S MODEL
2.89×10^{7}	8.34	8.2
3.3×10^{7}	8.66	8.5
4.13×10^{7}	9.27	8.7

Nomenclature

A_{eff}	Effective area of vent paths
A_w	Heat transfer surface area in contact with headspace gas (1220 m^2)
c_p	Specific heat at constant pressure of headspace gas (1000 J kg^{-1} K^{-1})
c_v	Specific heat at constant volume of headspace gas (714 J kg^{-1} K^{-1})
D_i	Equivalent diameter of vent i
f_i	Friction factor of vent i
k	Thermal conductivity of headspace gas (0.04 W m^{-1} K^{-1})
L_i	Equivalent length of vent i
$\dot{m}_b$	Instantaneous solvent burning rate
$\dot{m}''_{b,\infty}$	Solvent burning rate per unit area of large inflamed surface
M_g	Molecular weight of headspace gas (29)
$\dot{m}_v$	Tank mass venting or suction rate
P	Instantaneous pressure of headspace gas
P_{max}	Predicted tank peak pressure
P_∞	Atmospheric pressure (0.1 MPa)
r	Mass of oxygen consumed per mass of fuel burned (3.48)
R	Ideal gas constant (8314 J kg-mole^{-1} K^{-1})
R_f	Instantaneous radius of inflamed area
$R_{f,o}$	Initial radius of inflamed area
R_p	Radius of solvent pool
t	Time measured from solvent ignition
T	Instantaneous temperature of headspace gas
T_w	Temperature of heat transfer (sinks) surfaces (43°C)
T_∞	Temperature of outside air (27°C)
V	Volume of headspace gas (2600 m^3)
v_f	Flame spreading velocity
Y	Instantaneous oxygen mass fraction in headspace gas
Y_{ext}	Oxygen extinguishment level mass fraction
Y_∞	Oxygen mass fraction in outside air (0.23)
α	Thermal diffusivity of headspace gas (5.56×10^{-5} m^2 s^{-1})
ΔH	Solvent heat of combustion
ϵ	Effective emissivity of headspace gas-tank wall system
ν	Kinematic viscosity of headspace gas (3.79×10^{-5} m^2 s^{-1})
ρ	Instantaneous density of headspace gas
ρ_∞	Density of outside air (1.16 kg m^{-3})

σ Stefan-Boltzmann constant (5.6×10^{-8} W m^{-2} K^{-4})

Reference

Postma, A. K., 1995, in "Risk from Organic Solvent Fires in C-103 Following Interim Stabilization" (et al.), Westinghouse Hanford Report WHC-SD-WM-SARR-001, Supplement 1, Revision 0-A (March).

ME:lak

cc: H. K. Fauske

ATTACHMENT B

LETTER FROM C. L. BEYLER, HUGHES ASSOCIATES, INC. TO A. K. POSTMA

This page intentionally left blank.

Hughes Associates, Inc.
Fire Science & Engineering

3610 Commerce Drive, Suite 817, Baltimore, MD 21227-1652 (410) 737-8677 FAX (410) 737-8688

10 May 1996
Via FAX 1-503-623-0479

Dr. Arlin Postma
G&P Consulting, Inc.
P.O. Box 576
Richland, WA 99352

Dear Arlin:

I have reviewed your memo of 29 March 1996 regarding the Solvent Fire Analysis for SARR-036. I concur with the resolution of the key issues raised in the memo and your proposed path forward. I very much appreciate the very open and professional manner in which both you and Dr. Grigsby have dealt with issues I had raised with regard to the modeling of the solvent fires. I feel the model as modified as indicated in the memo will be fully able to provide accurate predictions as required in this application. While no model includes every physical and chemical aspect of a problem, this model takes an excellent balanced approach very appropriate to this problem.

The fact that we were able to substantially reproduce some of your predictions using the CFAST model developed by the National Institute for Standards and Technology is significant. As you know, this model includes a two-layer environment rather than a well-stirred model as your model uses, but does not properly deal with compressible flow. The ability to reproduce your results with these differences is indicative of a relatively robust solution which is not heavily dependent on the details of the submodels used for component phenomena.

It is clear from your work and the work we have conducted that DSTs will not reach pressures where structural failure is anticipated, and the SSTs will easily exceed the structural failure limits. This conclusion seems to be quite insensitive to the details of the model and, as such, are quite robust. Of course, if significant additional vent area can be added, pressures can be limited to below the failure limit.

If I can be of further assistance, feel free to contact me. I would appreciate receiving a copy of your report when it is completed. I look forward to working with you in the future.

Sincerely,

Craig L. Beyler
Technical Director

CLB/cdp

This page intentionally left blank.

APPENDIX J

IMPACT OF MULTIPOINT IGNITION ON PREDICTED POOL FIRE CONSEQUENCES

This page intentionally left blank.

CONTENTS

1.0 INTRODUCTION J-5

2.0 OBJECTIVE AND SCOPE J-5

3.0 SUMMARY AND CONCLUSIONS J-5
3.1 SUMMARY J-5
3.2 CONCLUSIONS J-5

4.0 METHODOLOGY J-6

5.0 RESULTS OF ANALYSIS J-7
5.1 PUDDLE FIRE CASES J-7
5.2 PEAK PRESSURE IN SINGLE-SHELL TANKS FOR LARGE POOLS J-7
5.3 TOXICOLOGICAL CONSEQUENCES J-8
5.4 RADIOLOGICAL CONSEQUENCES J-9

LIST OF TABLES

5-1 Peak Pressure Predicted in a Single-Shell Tank for Multipoint Ignition of a Large Pool J-7

5-2 Key Parameters for Toxicological Impact of Multipoint Ignition . . . J-8

5-3 Impact of Multipoint Ignition on Predicted Radiological Consequences J-9

This page intentionally left blank.

1.0 INTRODUCTION

Appendix J evaluates the effects of pool fire consequences if ignition of a solvent pool occurred simultaneously at more than one location. Multipoint ignition is possible with lightning as an ignitor. Lighting strikes are typically multi-discharge events, and if successive discharges followed different paths to a solvent pool, ignition at more than one point on the pool is possible.

Figure 9-1 of the main body of this report analyzes pool fire consequences based on ignition at one pool site where subsequent radial spreading of a fire could inflame the entire pool or would last until a fire extinguished on low oxygen. Ignition at two or more points on the surface of a pool could cause the inflamed area to grow more rapidly than it would for single-point ignition. The increase in inflamed area would be reflected in an increase in pressurization rate. Increased pressures in the tank could result in more rapid venting of toxins and would impose larger structural loads on a tank. This appendix analyses the degree to which a faster spreading fire, caused by multipoint ignition, increases predicted consequences.

2.0 OBJECTIVE AND SCOPE

The objective of this study is to quantify the change in predicted pool fire consequences when ignition at more than one local region is postulated.

The scope of this study is limited to a recalculation of key pool fire cases listed in Figure 9-1 of the main body of this report which are based on single-point ignition.

3.0 SUMMARY AND CONCLUSIONS

3.1 SUMMARY

The impact of multipoint ignition of solvent pool fires on predicted consequences was quantified by analyzing bounding fire cases under the assumption that ignition occurred at three locations simultaneously. The bounding cases examined peak pressurization, toxicological consequences, and radiological consequences. Comparing consequences for single- and multipoint ignitions illustrates how multipoint ignition affects the outcome of postulated solvent fires.

3.2 CONCLUSIONS

The findings of this study are characterized by the following conclusions and summary statements.

1. Multipoint ignition increases the rate at which the surface of a solvent pool becomes inflamed. The faster burning increases peak pressurization for large pool cases. No significant effect on puddle fires is expected because even single-point ignition is predicted to cause the entire surface to become inflamed during the first seconds of a burn that continues for many minutes.

2. Peak pressures were predicted to increase from 29 psig (200 kPa) to 32.3 psig (222 kPa) when the number of simultaneous ignition areas was increased from one to three. This increase is too small to change the current evaluation of the structural response of single-shell tanks to pool fires.

3. Toxicological consequences, gauged by onsite sums of fractions for the unlikely frequency category, are calculated to increase from 0.95 to 1.10. The relative insensitivity of predicted toxicological consequences to the number of ignition points indicates that multipoint ignition is not an important issue in assessing toxicological consequences of solvent pool fires.

4. Radiological consequences for the bounding case were predicted to increase by less than one percent when the number of ignition points was increased from one to three. Therefore, multipoint ignition is not an important issue in assessing radiological consequences of solvent pool fires.

4.0 METHODOLOGY

Thermal hydraulic parameters for multipoint ignition of pool fires were quantified by means of a modified version of POOLFIRE.4. POOLFIRE.4 was modified by 1) making the number of ignition points an input variable and 2) calculating the inflamed area as the sum of spreading circles. All other aspects of the analysis used the same methodology as used for the single-point ignition scenarios described in Figure 10-1. Inflamed area is computed from:

$$A = N\pi(R_o + ut)^2 \qquad (1)$$

where

A	=	inflamed area, m^2
n	=	number of ignition sites
R_o	=	radius of initially inflamed area, m
u	=	fire spread velocity, m/s
t	=	time from ignition, s.

The inflamed area calculated in Equation 1 has an upper bound equal to the total solvent pool area, which is an input parameter in POOLFIRE.4.

Because the inflamed area predicted from Equation 1 does not account for the intersection of inflamed areas, it represents an overprediction of inflamed area after expanding circles overlap. A more realistic assessment of where multipoint ignitions would likely occur, and how inflamed areas would overlap, is beyond the scope of this study. The method used here is a conservative approximation of how inflamed area would grow with time given a number of simultaneous ignition points that spread at a specified radial velocity.

5.0 RESULTS OF ANALYSIS

5.1 PUDDLE FIRE CASES

Single-point ignition of puddle fires ($1m^2$ area) with subsequent fire spread at 10 cm/s would cause the entire pool to be inflamed in 4.1 seconds. This time is small compared to the 5,000 seconds burn times predicted for single-shell and double-shell tank puddle fires; therefore, consequences of puddle fires are insensitive to the rate of flame spread rate. On this basis, multipoint ignition would have little or no impact on puddle fire consequences; therefore, multipoint ignition is not a substantive issue for puddle fires.

5.2 PEAK PRESSURE IN SINGLE-SHELL TANKS FOR LARGE POOLS

The impact of multipoint pool ignition on predicted peak pressure in single-shell tanks was quantified by reanalyzing case e of Figure 10-1. This case postulates a large organic pool, a bounding fire spread velocity of 10 cm/s, and a minimal gas vent to maximize predicted peak pressure. As noted in column H of Figure 10-1, a peak pressure of 29 psig (200 kPa) was predicted for single-point ignition. Peak pressures predicted for multipoint ignitions are shown in Table 5-1.

Table 5-1. Peak Pressure Predicted in a Single-Shell Tank for Multipoint Ignition of a Large Pool.

Number of Ignition Points	Predicted Peak Pressure psig (kPa)
1	29 (200)
2	31 (214)
3	32.2 (222)

The data of Table 5-1 show that peak pressure is predicted to increase marginally from 29 psig to 32.2 psig when the number of ignition sites is increased from one to three. The increase in peak pressure is attributable to the faster burn predicted for three point ignition. Less time is available

for heat loss and gas venting, factors which mitigate pressure buildup. The relatively small magnitude of the increase is because heat loss and venting are relatively unimportant even for single-point ignition. For the cases in Table 5-1, peak pressures are relatively close to an upper bound defined by adiabatic isochoric conditions. Thus, increasing the number of ignition sites has a relatively small impact on predicted peak pressure.

5.3 TOXICOLOGICAL CONSEQUENCES

The impact of multiple ignition sites on calculated toxicological consequences are illustrated by reanalyzing the pool fire case that has the highest predicted consequences. Case j of Figure 10-1 applies to a large pool fire in a double-shell tank with a large flapper vent. The predicted sum of fractions for an onsite individual, for the unlikely frequency category, is 0.95. This value is displayed in row 12, column DT of the consequences spreadsheet, Figure 10-1.

Case j was reanalyzed with the modified version of POOLFIRE.4 under the assumption that ignition occurred simultaneously at three locations. Thermal hydraulic parameters for the three point ignition run were than inserted into the consequences spreadsheet to quantify total sums of fractions. Key fire parameters for Case j are listed in Table 5-2.

Table 5-2. Key Parameters for Toxicological Impact of Multipoint Ignition.

Parameter	Numerical Value	
	1 Ignition Point	3 Ignition Points
Vent duration, seconds	70.0	49.2
Solvent burned in vent, kg	92.5	96.4
Reaction gas fraction	0.31	0.37
Headspace gas fraction	0.61	0.63
Onsite sum of fractions, unlikely frequency	0.95	1.1

The data of Table 5-2 illustrate the change in predicted fire parameters when three simultaneous ignition points are assumed. For three ignition points, the fire spreads more rapidly and burns to extinction in 49.2 seconds. Slightly more solvent is predicted to burn and onsite concentrations of toxins are predicted to increase by approximately 15 percent as compared to the single-point ignition case. The predicted onsite sum of fractions is predicted to be 1.1, or 10 percent above the guideline of unity.

In summary, toxicological consequence are predicted to increase by a small fraction when multipoint ignition is postulated. The relative insensitivity of predicted toxicological consequences to the number of simultaneous ignition points indicates that multipoint ignition is not highly important in assessing the toxicological implication of solvent pool fires.

5.4 RADIOLOGICAL CONSEQUENCES

The impact of multipoint ignition sites on calculated radiological consequences are illustrated by reanalyzing the pool fire case that has the highest predicted radiological consequences. Case g of Figure 10-1 applies to a large pool fire in a SST that has a minimal vent and is actively ventilated. Active ventilation after fire extinguishment is assumed to purge airborne contaminants from the tank. This case has a predicted onsite dose of 0.0176 Sv. This dose is 35 percent of the guideline dose of 0.05 Sv for onsite individuals, for accidents in the unlikely frequency category.

Thermal hydraulic parameters for this case were quantified by means of the POOLFIRE.4 Code as modified for multipoint ignition. Aerosol depletion by in-tank sedimentation was quantified by the same methodology as used for the single ignition site case. Key fire parameters and predicted radiological consequences for one and three ignition sites are compared in Table 5-3.

Table 5-3. Impact of Multipoint Ignition on Predicted Radiological Consequences.

Parameter	Numerical Value	
	1 Ignition Point	3 Ignition Points
Fire duration, s	80	57
Solvent burned, kg	146	146.2
Aerosol depletion factor	0.231	0.233
Onsite dose, Sv	0.0176	0.0177

The data of Table 5-3 indicate that multipoint ignition has a negligible impact on predicted onsite dose. The fire is predicted to burn to extinction in less time when multiple ignition points are assumed, but the faster burn has little influence on the mass of solvent burned or the aerosol depletion factor. These results indicate that multipoint ignition has negligible impact on predicted radiological consequences of solvent pool fires.

This page intentionally left blank.

APPENDIX K

SUPPORTING CALCULATIONS FOR SECTION 9.0

This page intentionally left blank.

CONTENTS

1.0 INTRODUCTION K-4

2.0 REVISED RADIOLOGICAL CALCULATIONS K-4

3.0 REVISED TOXICOLOGICAL CALCULATIONS K-11

LIST OF FIGURES

K-1 Calculate Onsite Rad Dose K-5

K-2 Calculate New SOFs K-7

1.0 INTRODUCTION

This appendix contains two spreadsheets that support the Dose Summary and Toxicological spreadsheets found in Section 9.0 of this document. The two spreadsheets in this appendix are Calculate Onsite Rad Dose and Calculate New SOFs. Each of the spreadsheets in this appendix calculate values which are entered in the appropriate spreadsheets in Section 9.0. How and where the new values are used is explained in Section 9.0. The new spreadsheets and the changes made in Section 9.0 result from a new analysis of the ventilation system waste loadings for actively ventilated tanks. The new analysis estimates larger quantities of waste in the ventilation systems than previously used. The new analysis is contained in HNF-SD-WM-CN-099, Rev. 1A.

Because of the larger estimated waste loading, it is necessary to revise the consequence calculations in this document. The change affects the quantity of waste released by a HEPA filter rupture on actively ventilated tanks. This change does not apply to passively ventilated tanks.

While performing the changes resulting from the new data on waste volumes, it was seen that the ARF for the HEPA filters that had been used was too conservative. The ARF from Mishima (1994) for blast or vigorous banging (Sections 5.4.2.2 and 5.4.4.2) is 1E-2. An ARF of 1E-2 was used in previous revisions of this calcnote. Organic Solvent fires are less energetic and reach their peak pressure in seconds to minutes, not milliseconds as is the case for blast and banging. Section 5.4.2.1 recommends an ARF of 2E-6 for shock affects resulting from a dynamic pressure pulse. The authors decided to use an extrapolation between the two cases and selected a value of 1E-3 for the ARF for this analysis. This change applies to both active and passive ventilation systems. Therefore consequences were recalculated for the passively ventilated tanks, and the actively ventilated tanks.

2.0 REVISED RADIOLOGICAL CALCULATIONS

The new waste inventories are taken from HNF-SD-WM-CN-099, Rev. 1A, Section 4.3 (241-A-702 vent system) and Section 4.5 (296-P-16 vent system). These two vent systems are given as the bounding cases for double-shell tanks and single-shell tanks respectively. The "overpressure" case applies for both systems. Because of the way it is structured, the dose summary spreadsheet in Section 9.0 automatically calculates offsite dose and total dose based on information entered in column J. All that is needed to revise the dose calculations is to calculate a new, on-site dose and enter the dose in column J of the dose summary worksheet.

Figure K-1. Calculate Onsite Rad Dose. (2 sheets)

	A	B	C	D	E	F
1	Case	Scenario Description	Q (Waste Inventory, Liters)	ARF (Airborne Release Fraction)	ULD (Unit Liter Dose, Sieverts/Liter)	X/Q (sec/m3)
2		***ACTIVE VENTILATION***				
3	c	SST Puddle	2	1.00E-03	2.20E+05	3.41E-02
4	d	SST Puddle	2	1.00E-03	2.20E+05	3.41E-02
5	g	SST Pool	2	1.00E-03	2.20E+05	3.41E-02
6	k	DST Puddle	3.7	1.00E-03	6.10E+03	3.41E-02
7	l	DST Pool	3.7	1.00E-03	6.10E+03	3.41E-02
8	q	SST Entrained	2	1.00E-03	2.20E+05	3.41E-02
9	r	SST Entrained	2	1.00E-03	2.20E+05	3.41E-02
10	v	DST Entrained	3.7	1.00E-03	6.10E+03	3.41E-02
11						
12		***PASSIVE VENTILATION***				
13	a	SST Puddle	1.27E-02	1.00E-03	2.20E+05	3.41E-02
14	b	SST Puddle	1.27E-02	1.00E-03	2.20E+05	3.41E-02
15	e	SST Pool	1.27E-02	1.00E-03	2.20E+05	3.41E-02
16	f	SST Pool	1.27E-02	1.00E-03	2.20E+05	3.41E-02
17	h	SST Pool	1.27E-02	1.00E-03	2.20E+05	3.41E-02
18	j	DST Pool	1.27E-02	1.00E-03	6.10E+03	3.41E-02
19	n	DCRT Pool	2.27E-01	1.00E-03	1.10E+04	3.41E-02
20	o	DCRT Pool	2.27E-01	1.00E-03	1.10E+04	3.41E-02
21	p	DCRT Pool	2.27E-01	1.00E-03	1.10E+04	3.41E-02
22	s	55kgal SST Pool	1.27E-02	1.00E-03	2.20E+05	3.41E-02
23	t	55kgal SST Pool	1.27E-02	1.00E-03	2.20E+05	3.41E-02
24	u	55kgal SST Puddle	1.27E-02	1.00E-03	2.20E+05	3.41E-02
25						
26						
27						

HNF-4240 Rev. 1

Figure K-1. Calculate Onsite Rad Dose. (2 sheets)

	G	H
1	R (Breatnihg Rate, M3/sec)	HEPA Rupture Onsite Dose (Sieverts)
2		
3	3.30E-04	4.95E-03
4	3.30E-04	0.00495132
5	3.30E-04	0.00495132
6	3.30E-04	0.00025398
7	3.30E-04	0.00025398
8	3.30E-04	0.00495132
9	3.30E-04	0.00495132
10	3.30E-04	0.00025398
11		
12		
13	3.30E-04	3.14E-05
14	3.30E-04	3.14E-05
15	3.30E-04	3.14E-05
16	3.30E-04	3.14E-05
17	3.30E-04	3.14E-05
18	3.30E-04	8.72E-07
19	3.30E-04	2.81E-05
20	3.30E-04	2.81E-05
21	3.30E-04	2.81E-05
22	3.30E-04	3.14E-05
23	3.30E-04	3.14E-05
24	3.30E-04	3.14E-05
25		
26		
27		

HNF-4240 Rev. 1

Figure K-2. Calculate New SOFs. (4 sheets)

	A	B	C	D	E	F
1	Case	Scenario Description	Q(Waste Released, Liters)	Release Time (sec)	Release Rate (L/sec)	Unlikely On-site SOF Multiplier (sec/L)
2		***ACTIVE VENTILATION***				
3	c	SST Puddle	2.00E-03	60	3.33333E-05	2.10E+03
4	d	SST Puddle	2.00E-03	60	3.33333E-05	2.10E+03
5	g	SST Pool	2.00E-03	60	3.33333E-05	2.10E+03
6	k	DST Puddle	3.70E-03	60	6.16667E-05	7.50E+02
7	l	DST Pool	3.70E-03	60	6.16667E-05	7.50E+02
8	q	SST Entrained	2.00E-03	60	3.33333E-05	2.10E+03
9	r	SST Entrained	2.00E-03	60	3.33333E-05	2.10E+03
10	v	DST Entrained	3.70E-03	60	6.16667E-05	7.50E+02
11						
12		***PASSIVE VENTILATION***				
13	a	SST Puddle	1.27E-05	60	2.12E-07	2.10E+04
14	b	SST Puddle	1.27E-05	60	2.12E-07	2.10E+04
15	e	SST Pool	1.27E-05	60	2.12E-07	2.10E+04
16	f	SST Pool	1.27E-05	60	2.12E-07	2.10E+04
17	h	SST Pool	1.27E-05	60	2.12E-07	2.10E+04
18	j	DST Pool	1.27E-05	60	2.12E-07	7.50E+02
19	n	DCRT Pool	2.27E-04	60	3.78E-06	7.50E+02
20	o	DCRT Pool	2.27E-04	60	3.78E-06	7.50E+02
21	p	DCRT Pool	2.27E-04	60	3.78E-06	7.50E+02
22	s	55 kgal SST Pool	1.27E-05	60	2.12E-07	2.10E+04
23	t	56 kgal SST Pool	1.27E-05	60	2.12E-07	2.10E+04
24	u	55 kgal SST Puddle	1.27E-05	60	2.12E-07	2.10E+04
25						
26						
27						
28						
29						

Figure K-2. Calculate New SOFs. (4 sheets)

	G	H	I	J
1	Unlikely Off-Site SOF Multiplier	New Unlikely On-site SOF	New Unlikely Off-site SOF	Ex Unlikely Onsite Multiplier
2				
3	3.30E+01	7.00E-02	1.10E-03	1.00E+03
4	3.30E+01	7.00E-02	1.10E-03	1.00E+03
5	3.30E+01	7.00E-02	1.10E-03	1.00E+03
6	8.4	4.63E-02	5.18E-04	2.10E+02
7	8.4	4.63E-02	5.18E-04	2.10E+02
8	3.30E+01	7.00E-02	1.10E-03	1.00E+03
9	3.30E+01	7.00E-02	1.10E-03	1.00E+03
10	8.4	4.63E-02	5.18E-04	2.10E+02
11				
12				
13	3.30E+01	4.45E-03	6.99E-06	1.00E+03
14	3.30E+01	4.45E-03	6.99E-06	1.00E+03
15	3.30E+01	4.45E-03	6.99E-06	1.00E+03
16	3.30E+01	4.45E-03	6.99E-06	1.00E+03
17	3.30E+01	4.45E-03	6.99E-06	1.00E+03
18	8.4	1.59E-04	1.78E-06	2.10E+02
19	8	2.84E-03	3.03E-05	2.00E+02
20	8	2.84E-03	3.03E-05	2.00E+02
21	8	2.84E-03	3.03E-05	2.00E+02
22	3.30E+01	4.45E-03	6.99E-06	1.00E+03
23	3.30E+01	4.45E-03	6.99E-06	1.00E+03
24	3.30E+01	4.45E-03	6.99E-06	1.00E+03
25				
26				
27				
28				
29				

HNF-4240 Rev. 1

Figure K-2. Calculate New SOFs. (4 sheets)

	K	L	M	N
1	Ex Unlikely Off-site Multiplier	New Ex Unlikely On-site SOF	New Ex Unlikely Off-site SOF	Anticipated On-site Multiplier
2				
3	1.70E+01	3.33E-02	5.67E-04	4.00E+04
4	1.70E+01	3.33E-02	5.67E-04	4.00E+04
5	1.70E+01	3.33E-02	5.67E-04	4.00E+04
6	6.20E-01	1.30E-02	3.82E-05	1.00E+04
7	6.20E-01	1.30E-02	3.82E-05	1.00E+04
8	1.70E+01	3.33E-02	5.67E-04	4.00E+04
9	1.70E+01	3.33E-02	5.67E-04	4.00E+04
10	6.20E-01	1.30E-02	3.82E-05	1.00E+04
11				
12				
13	1.70E+01	2.12E-04	3.60E-06	4.00E+04
14	1.70E+01	2.12E-04	3.60E-06	4.00E+04
15	1.70E+01	2.12E-04	3.60E-06	4.00E+04
16	1.70E+01	2.12E-04	3.60E-06	4.00E+04
17	1.70E+01	2.12E-04	3.60E-06	4.00E+04
18	6.20E-01	4.45E-05	1.31E-07	1.00E+04
19	6.20E-01	7.57E-04	2.35E-06	9.60E+03
20	6.20E-01	7.57E-04	2.35E-06	9.60E+03
21	6.20E-01	7.57E-04	2.35E-06	9.60E+03
22	1.70E+01	2.12E-04	3.60E-06	4.00E+04
23	1.70E+01	2.12E-04	3.60E-06	4.00E+04
24	1.70E+01	2.12E-04	3.60E-06	4.00E+04
25				
26				
27				
28				
29				

Figure K-2. Calculate New SOFs. (4 sheets)

	O	P	Q
1	Anticipated Off-site Multiplier	New Anticipated On-site SOF	New Anticipated Off-site SOF
2			
3	9.40E+01	1.33E+00	3.13E-03
4	9.40E+01	1.33E+00	3.13E-03
5	9.40E+01	1.33E+00	3.13E-03
6	8.4	6.17E-01	5.18E-04
7	8.4	6.17E-01	5.18E-04
8	9.40E+01	1.33E+00	3.13E-03
9	9.40E+01	1.33E+00	3.13E-03
10	8.4	6.17E-01	5.18E-04
11			
12			
13	9.40E+01	8.47E-03	1.99E-05
14	9.40E+01	8.47E-03	1.99E-05
15	9.40E+01	8.47E-03	1.99E-05
16	9.40E+01	8.47E-03	1.99E-05
17	9.40E+01	8.47E-03	1.99E-05
18	8.4	2.12E-03	1.78E-06
19	8	3.63E-02	3.03E-05
20	8	3.63E-02	3.03E-05
21	8	3.63E-02	3.03E-05
22	9.40E+01	8.47E-03	1.99E-05
23	9.40E+01	8.47E-03	1.99E-05
24	9.40E+01	8.47E-03	1.99E-05
25			
26			
27			
28			
29			

The onsite doses are calculated using the following formula:

$$D = Q \times ARF \times ULD \times \frac{X}{Q} \times BR$$

where

BR = Breathing rate = 3.3×10^{-4} m^3/sec.

X/Q = 3.4×10^{-2} sec/m^3

ULD = Unit liter dose = different values of Sv/L for different waste.

ARF = Aerosol release factor, a dimensionless factor. Taken from Mishima (1994). Section 5.4 of Mishima (1994) gives ARFs for HEPA filters. An ARF of 1×10^{-2} is for blast effects. An ARF of 2×10^{-6} is for shock effects. The overpressure resulting from a solvent burn is best characterized as a shock effect. A conservative extrapolation between the two values is 1×10^{-3}.

Q = Liters of waste loaded on the filters taken from document HNF-SD-WM-CN-099, Rev. 1A. For these calculations, 1.98 L was rounded to 2.0 L, and 3.66 L was rounded to 3.7 L.

All values for the above terms are taken from Table 8-1 of this document. The columns of the spreadsheet Calculate Onsite Rad Dose are in the same order as the equation above. The multiplication is performed in column H and the onsite dose in Sieverts is displayed in column H.

3.0 REVISED TOXICOLOGICAL CALCULATIONS

The same waste inventories specified above are used in these calculations. The total toxicological SOFs are calculated in columns EV, EW, EX, EY, EZ, and FA of the toxicological spreadsheet in Section 9.0 of this calcnote. Each of these columns adds the SOFs for each component of the total toxicological SOFs. To change the total SOFs to reflect the new information, change columns EJ, EK, EL, EM, EN, and EO. The spreadsheet Calculate New SOFs, calculates new SOFs for HEPA filter releases in the different frequency categories. These new values are substituted into columns EJ, EK, EL, EM, EN, and EO of the toxicological spreadsheet in Section 9.0.

The SOFs are calculated using the following formula:

SOF = SOF mulitiplier x release rate

where:

SOF	=	Sum of fractions, a dimensionless number
SOF multiplier	=	Has different values in sec/L for different wastes. Values taken from Table 8-4 in this document.
Release rate	=	Calculated by dividing volume of waste released by release time. Units are L/sec. In all cases, a release time of 60 sec is used.

Release volumes are taken from document HNF-SD-WM-CN-099, Rev. 1A, and are rounded to 2.0 L and 3.7 L.

Explanation of Columns

Column C

This column is the product of the waste inventory on the filters and the ARF. The values for waste inventory and ARF are taken form the spreadsheet Calculate Onsite Rad Dose, columns C and D.

Column D

A release time of 60 sec is used for all cases. Sixty seconds is a conservative value for evaluating puff releases given in WHC-SD-WM-SARR-011, Rev. 2.

Column E

This column calculates the release rate by dividing Column C by Column D.

Column F

The appropriate multiplier from Table 8-4 of this document is entered in this column.

Column G

The appropriate multiplier from Table 8-4 is entered by hand.

Column H

New unlikely onsite SOF. This is calculated by multiplying column E (release rate) by column F (SOF multiplier).

Column I

New unlikely offsite SOF. This is calculated by multiplying column E (release rate) by column G (SOF multiplier).

Columns J, K, N, and O

Appropriate SOF multipliers are taken from Table 8-4 and entered in these columns.

Column L

New extremely unlikely onsite SOF. This is calculated by multiplying Column E (release rate) by Column J (SOF multiplier).

Column M

New extremely unlikely offsite SOF. This is calculated by multiplying Column E by Column K.

Column P

New anticipated onsite SOF. This is calculated by multiplying Column E by Column N.

Column Q

New anticipated offsite SOF. This is calculated by multiplying Column E by Column O.

4.0 REFERENCES

Mishima, J. 1994, *Recommended Values and Technical Bases for Airborne Release Fractions, Airborne Release Rates and Respirable Fractions for Materials from Accidents in DOE Fuel Cycle, Ex-Reactor Facilities*, DOW-HDBK-3010-94, Rev. 2, U.S. Department of Energy, Washington, D.C.

Himes, D.A., 1998, *Radiological and Toxicological Analyses of Tank 241-AY-102 and Tank 241-C-106*, Ventilation Systems, HNF-SD-WM-CN-099, Rev. 1A, Fluor Daniel Northwest, Inc., Richland, Washington.

Van Keuren, J.C., *1996, Toxic Chemical Considerations for Tank Farm Releases*, WHC-SD-WM-SARR-011, Rev. 2, Westinghouse Hanford Company, Richland, Washington.

This page intentionally left blank.

APPENDIX L

THE AGING OF ORGANIC SOLVENTS

Prepared by

L. M. Stock

This page intentionally left blank.

CONTENTS

L1.0 INTRODUCTION L-5

L2.0 LABORATORY INVESTIGATIONS OF AGING L-5
L2.1 HYDROCARBON AGING L-5
L2.2 PHOSPHATE ESTER AGING L-9
L2.2.1 HYDROLYSIS L-9
L2.2.2 RADIOLYSIS L-10

L3.0 FIELD EVIDENCE FOR AGING L-14
L3.1 TANK WASTE CHARACTERIZATION L-14
L3.2 DOME SPACE CHARACTERIZATION L-22
L3.3 DISPERSAL OF INTERMEDIATE COMPOUNDS L-29

L4.0 ALIPHATIC AND AROMATIC NITROSO AND NITRO COMPOUNDS L-30
L4.1 NITRO AND NITROSO COMPOUNDS IN WASTE L-30
L4.2 FORMATION OF NITRO AND NITROSO COMPOUNDS L-35
L4.3 NITRITE AND NITRATE ESTERS L-36
L4.4 NITRO COMPOUNDS L-37
L4.5 AROMATIC NITRO COMPOUNDS L-38
L4.6 ENERGY CONTENT OF INTERMEDIATE COMPOUNDS L-38

L5.0 SUMMARY L-42

L6.0 REFERENCES L-43

LIST OF FIGURES

L-1. Principal Chemical Transformations During the Radiolysis of Hydrocarbons in Tank Waste L-7

L-2. Reaction Profile for the Radiolysis of Dibutyl Phosphate L-11

L-3. Principal Chemical Transformations During the Radiolysis of Sodium Bis(2-ethylhexyl)phosphate in Tank Waste L-13

LIST OF TABLES

L-1. Concentrations of Normal Paraffin Hydrocarbons and Tributyl Phosphate in Core Composites L-16

L-2. Organic Compounds at Concentrations Greater Than 1 Milligram/Cubic Meter in the Ventilation Stack of Tank 241-C-106 During Sluicing Operations on March 7, 1999 . . . L-18

L-3. Organic Compounds at Concentrations Greater Than 1 Milligram/Cubic Meter in a Retained Gas Sample from Tank 241-SY-101 . . . . . L-20

L-4. Concentrations of Organic Compounds in Dome Spaces of Single-Shell Tanks L-23

L-5. Organic Compounds at Concentrations Greater Than 1 Milligram/Cubic Meter in Dome Space of Tank 241-C-103 . . . . L-24

L-6. Organic Compounds at Concentrations Greater Than 0.5 Milligram/Cubic Meter in Dome Space of Tank 241-BY-108 . . . L-26

L-7. Observations of Nitroso and Nitro Compounds in Dome Spaces L-31

L-8. Heat of Nitric Acid Oxidation of Methane and Ethane and Their Oxidized Derivatives in kJ/Mole at 300 °K in the Gas Phase L-40

L-9. Heat of Nitric Acid Oxidation of Nitroso and Nitro Derivatives of Methane in kJ/Mole at 300 °K in the Gas Phase L-40

L-10. Thermodynamic Heat of Nitric Acid Oxidation of Benzene and Toluene and Their Nitrated Derivatives in kJ/Mole at 300 °K in the Gas Phase L-41

L1.0 INTRODUCTION

Organic complexants and solvents, principally tributyl phosphate, bis(2-ethylhexyl)phosphoric acid and normal paraffinic hydrocarbons, were used for separations at the Hanford Site. The aqueous wastes from these operations containing these organic compounds were made alkaline and discharged to the tanks. Evaporation, chemical reactions with water, and radiolytically-initiated oxidation reactions have aged the organic solvents during interim storage.

Organic complexant aging was discussed in the recent topical report (Meacham et al. 1998). Targeted laboratory investigations established that the organic complexants were oxidized through a family of organic intermediates that led to metastable end products such as sodium formate and sodium oxalate, and eventually to sodium carbonate. Characterization work established that the concentrations of the original complexants in the tank waste were depleted and that new intermediate compounds were present together with these metastable end products. Sodium oxalate was shown to be a ubiquitous and abundant constituent of tank waste. Comparison of the quantity of organic carbon in sodium oxalate with the total organic carbon content established that aging was extensive.

Organic solvent aging by evaporation, hydrolysis, and oxidation was outlined in Section 2.3 in this document. This appendix provides additional information from targeted laboratory and field investigations for the evaporation and radiolytic oxidation of the normal paraffin hydrocarbons and the hydrolysis and radiolytic oxidation of the phosphate esters.

L2.0 LABORATORY INVESTIGATIONS OF AGING

The tanks now contain many organic compounds including the original constituents, intermediate organic compounds, and metastable products of oxidation reactions. The chemical reactions responsible for the formation of these compounds are discussed in this section to guide the interpretation of the characterization work presented in Section L3.0

L2.1 HYDROCARBON AGING

Hydrocarbons do not undergo ionic reactions in the waste tanks, consequently, only radiolytic reactions will be considered.

The radiolytic reactions of the water-insoluble hydrocarbons take place in the organic layers and dispersed organic phases. The radiolytic processes occur "directly" when the beta and gamma particles produced by the decay of radioactive nuclei in the waste interact with an organic compound and "indirectly" when the emanation first interacts with water, sodium nitrite or nitrate to produce substances such as the hydroxyl radical and its anion,

nitric oxide, nitrogen dioxide, and the nitrate dianion radical that subsequently react with the organic compounds (Meisel et al. 1993, Meisel et al. 1997, Camaioni et al. 1998).

Radiolysis of the NPH occurred during the operation of the PUREX process and has continued during storage. Specific transformations occurring during the PUREX process have been discussed by Davis (1984) and the chemical transformations of hydrocarbons during radiolysis have been discussed by Gyorgy (1981), Spinks and Woods (1990), Tabata et al. (1991), and Bugaenko et al. (1993).

Hydrocarbon radiolysis is a complex process that proceeds through an array of highly energetic ions and excited state molecules as discussed in the references cited in the previous paragraph. This discussion will highlight the reactions leading to the principal organic compounds observed in the waste rather than to describe the array of transient excited states and ions and all the products. The principal chemical transformations are outlined in Figure L-1 to guide the ensuing discussion.

The initial radiolytic formation of charged and uncharged energetic dodecane molecules is sketched in the first equation. Fragmentation reactions to form other radicals and ions occur in several different ways. Proton loss from an energetic ion can yield the 1-, 2-, 3-, 4-, 5-, and 6-dodecyl radicals; the 2- and 3-dodecyl radicals are shown in the equations.

$$C_{12}H_{26} \rightarrow \text{Excited States and Energetic Ions}$$

$$\text{Energetic Ion}]^{+} \rightarrow H^{+} + CH_3(CH_2)_6CH_2CH_2CH_2CHCH_3$$

$$\text{Energetic Ion}]^{+} \rightarrow H^{+} + CH_3(CH_2)_6CH_2CH_2CHCH_2CH_3$$

The reactions of undecane, tridecane and tetradecane form related families of intermediate free radicals.

Alkyl radicals decompose by several reaction pathways including beta scission, that is, the process in which one of the three chemical bonds on one of the two adjacent carbon atoms is broken and a double bond is formed, to produce, for example, an alkene and a hydrogen atom as illustrated for the 2-dodecyl radical,

$$CH_3(CH_2)_6CH_2CH_2CH_2CHCH_3 \rightarrow H + CH_3(CH_2)_6CH_2CH_2CH_2CH{=}CH_2$$

or to form an alkyl free radical and an alkene as illustrated for the reactions of the 2- and 3-dodecyl radicals,

$$CH_3(CH_2)_6CH_2CH_2CH_2CHCH_3 \rightarrow CH_3(CH_2)_6CH_2CH_2 + CH_2{=}CHCH_3$$

$$CH_3(CH_2)_6CH_2CH_2CHCH_2CH_3 \rightarrow CH_3(CH_2)_6CH_2 + CH_2{=}CHCH_2CH_3$$

$$CH_3(CH_2)_6CH_2CH_2CHCH_2CH_3 \rightarrow CH_3(CH_2)_8CH{=}CH_2 + CH_3$$

Figure L-1. Principal Chemical Transformations During the Radiolysis of Hydrocarbons in Tank Waste.

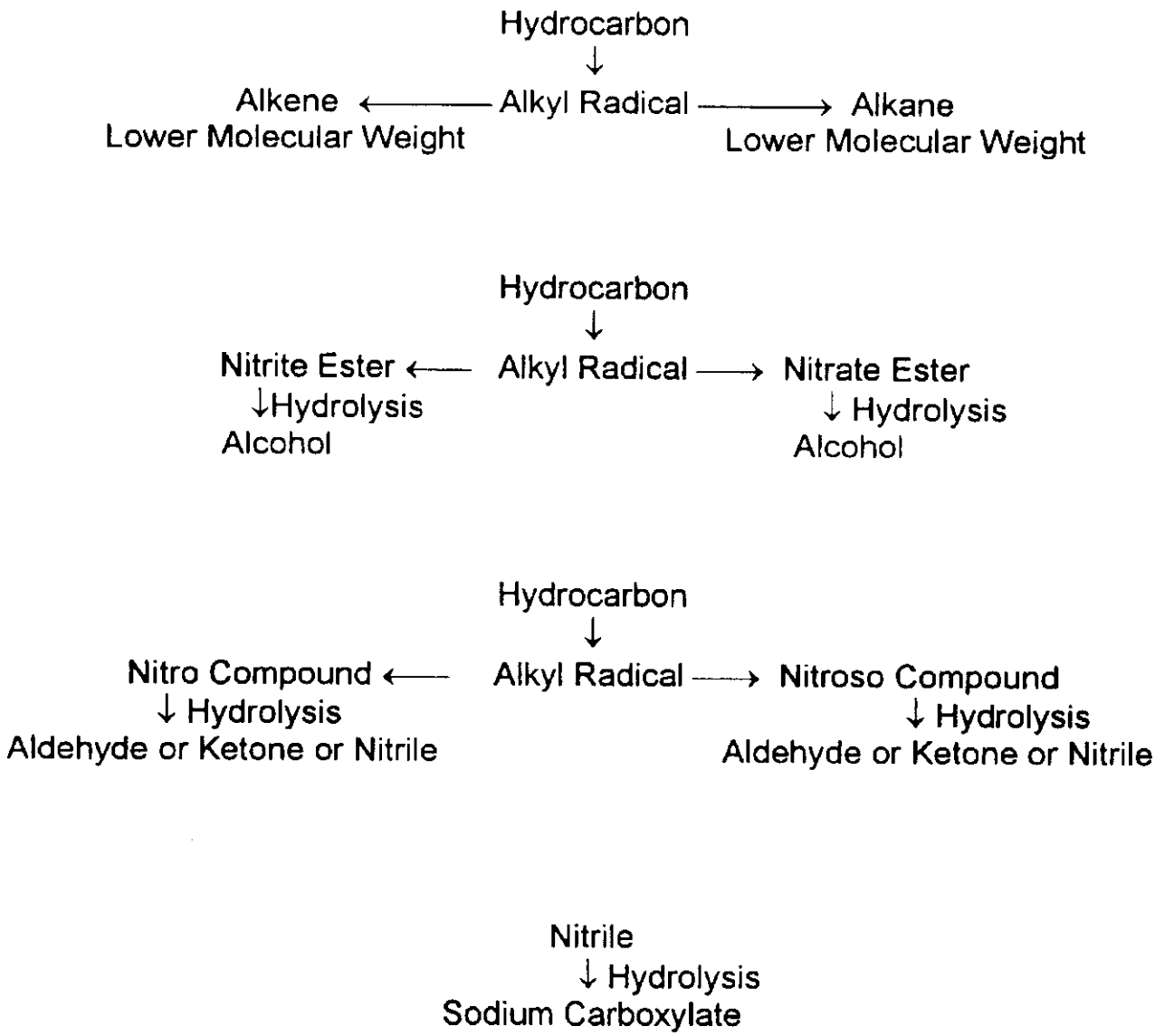

The alkanes, alkenes, alcohols, aldehydes, ketones and nitriles also undergo radiolysis to provide other lower molecular weight volatile alkanes, alkenes, alcohols, ketones and nitriles and other oxidized products leading to sodium formate, oxalate and carbonate.

The homologous series of linear radicals beginning methyl, ethyl, 1-propyl, 1-butyl, and extending to 1-decyl radical and the related linear alkenes including ethene, propene, 1-butene, 1-pentene, 1-hexene, and extending to 1-undecene are obtained from the reactions of dodecane.

One of the important reaction channels for the alkyl radicals is hydrogen atom abstraction from another molecule. The alkyl radicals, that is, methyl, ethyl, propyl, butyl, pentyl, hexyl, and so forth produce the corresponding alkanes methane, ethane, propane, butane, pentane, hexane, and so forth. The reaction pattern is conveniently illustrated by the reaction of a generic alkyl radical with the hydrogen donors,

$$\text{H Donor} + \text{Alkyl Radical} \rightarrow \text{Donor Radical} + \text{Alkane}$$

to give the homologous series of alkanes.

Radical reactions occur without structural rearrangement and the linear, that is, normal, hydrocarbons of the NPH, yield homologous series of linear radicals, alkanes and alkenes. The beta scission reactions lead to products in which the original NPH molecule is fragmented into two lower molecular weight alkanes and alkenes.

Radiolysis of the waste also yields transient radicals including nitric oxide and nitrogen dioxide. These substances combine with the alkyl radicals to produce other families of oxidized intermediate compounds. The homologous series of alkyl radicals, represented by RCH_2, produce homologous series of nitrite esters and C-nitroso and C-nitro compounds.

$$RCH_2 + NO_2 \rightarrow RCH_2ONO$$

$$RCH_2 + NO \rightarrow RCH_2NO$$

$$RCH_2 + NO_2 \rightarrow RCH_2NO_2$$

The nitrite esters react with hydroxide ion or water in conventional ionic organic reactions to give alcohols,

$$RCH_2ONO + H_2O \rightarrow RCH_2OH + HONO$$

the C-nitroso compounds react with water to produce aldehydes or nitriles,

$$RCH_2NO \rightarrow RCH{=}NOH$$

$$RCH{=}NOH + H_2O \rightarrow RCH{=}O + NH_2OH$$

$$RCH{=}NOH \rightarrow RCN + H_2O$$

and the C-nitro compounds react in aqueous solution to form aldehydes from the primary radicals and ketones from the secondary radicals.

$$2RCH_2NO_2 \rightarrow 2\ RCH{=}O + H_2N_2O_2$$

The nitrogen oxides, which are responsible for the oxidation reactions of the organic molecules, are reduced to form hydroxyl amine, NH_2OH, and hyponitrous acid, $H_2N_2O_2$. These substances are transformed into nitrous oxide, nitrogen, and ammonia in the alkaline waste (Stock and Pederson 1997, Camaioni et al. 1998).

In summary, the family of homologous linear radicals forms a homologous series of linear alcohols, aldehydes and ketones, and nitriles. The net result is that the original NPH are fragmented into lower molecular weight alkanes or oxidized to alkenes and other intermediate compounds, many of which react with water, to form alcohols, aldehydes, ketones, and nitriles. As these reactions proceed, the molecular dimensions are reduced and the reaction products become more soluble and more volatile. The intermediates and the reaction products are more mobile than the original hydrocarbons and continuously evolve from the waste into the dome space.

L2.2 PHOSPHATE ESTER AGING

L2.2.1 HYDROLYSIS

Trialkyl, dialkyl, and monoalkyl phosphates hydrolyze to liberate an alcohol and a less alkylated phosphate as shown in the equations where R_1 represents either the butyl or 2-ethylhexyl group.

$$(R_1O)_3PO + NaOH \rightarrow (R_1O)_2P(=O)ONa + R_1OH$$

$$(R_1O)_2P(=O)ONa + NaOH \rightarrow (R_1O)P(=O)(ONa)_2 + R_1OH$$

$$(R_1O)P(=O)(ONa)_2 + NaOH \rightarrow Na_3PO_4 + R_1OH$$

The hydrolysis of TBP forms 1-butanol, dibutylphosphate ion (DBP), and monobutylphosphate ion (MBP) and phosphate ion. Sodium bis(2-ethylhexyl)phosphate forms 2-ethylhexanol and (2-ethylhexyl)phosphate ion and phosphate ion. The rates of these reactions differ greatly, and solubility differences play a major role in determining the reaction rate.

The rate constants for hydrolysis of dialkyl esters are several orders of magnitude smaller than the rate constants for the hydrolysis of the corresponding trialkyl esters, and the rate constants for the hydrolysis of monoalkyl esters are also several orders of magnitude smaller than the rate constants for the dialkyl esters (Cox and Ramsay 1964, Wolfenden et al. 1998). The steric requirements of the alkyl group also influence the reaction rate. For example, the rate constant for the hydrolysis of trimethyl phosphate is about 100 times greater than the rate constant for the hydrolysis of tributyl phosphate (Camaioni et al. 1996).

The information obtained from the chemical literature has been supplemented by targeted investigations of the phosphate esters. Burger (1955) discussed the rates of hydrolysis of pure TBP under heterogeneous

conditions in the presence of 1*M* sodium hydroxide at temperatures from 30 to 100 °C. The observed rate data were fit to the following expression by Camaioni et al. (1996),

$$\ln(R) = 54.8 - 2.55 \times 10^4(1/T) + 2.69 \times 10^6(1/T)^2$$

where T is the temperature in °K and R is the rate in mg of tributyl phosphate hydrolyzed per liter per hour. The rate of disappearance of TBP was approximately 15 mg per hour per liter of 1*M* sodium hydroxide at 65 °C. The reaction rate was about 60 percent slower when kerosene, a simulant for NPH, was added to the reaction system. Burger (1955) also reported that the rate of hydrolysis of dibutylphosphate ion was negligible under the same conditions. Camaioni et al. (1996) investigated the hydrolysis of TBP and found sodium, calcium, iron (II), chromium (III), nickel, lead (II), zirconium (IV), nitrate, aluminate and stearate ions had no appreciable influence on the reaction rate.

In summary, the rate of hydrolysis of TBP is sufficient to alter its concentration during prolonged storage under alkaline conditions, but the rates of hydrolysis of the dialkyl phosphates and the monoalkyl phosphates are very slow in the aqueous phase of the waste. Butanol, which is formed in the hydrolysis reaction, is partially soluble in the aqueous phase of the waste and is transported through this phase into the dome space from which it continuously evolves.

L2.2.2 RADIOLYSIS

The radiolysis of TBP has been extensively investigated (Davis 1984) and Camaioni et al. (1996) have investigated the radiolysis of dibutyl phosphate (DBP) in alkaline solution in the presence and absence of sodium nitrate and sodium nitrite . Monobutyl phosphate forms and decomposes to phosphate ion under the same conditions. The experimental observations for DBP (•), MBP (■), phosphate (♦), other dialkyl phosphates (▲), other monoalkyl phosphates (▼) are displayed in Figure L-2.

Camaioni et al. (1996) accounted for phosphorous quantitatively by showing the product mixture contained residual DBP together with MBP, phosphate ion and families of new dialkyl and monoalkyl phosphates.

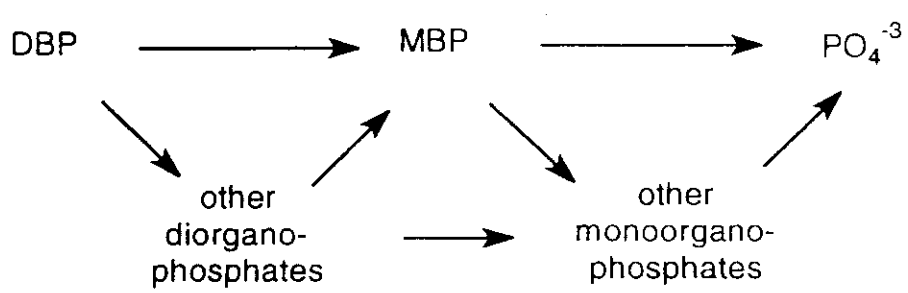

Figure L-2. Reaction Profile for the Radiolysis of Dibutyl Phosphate. (Camaioni et al. 1996)

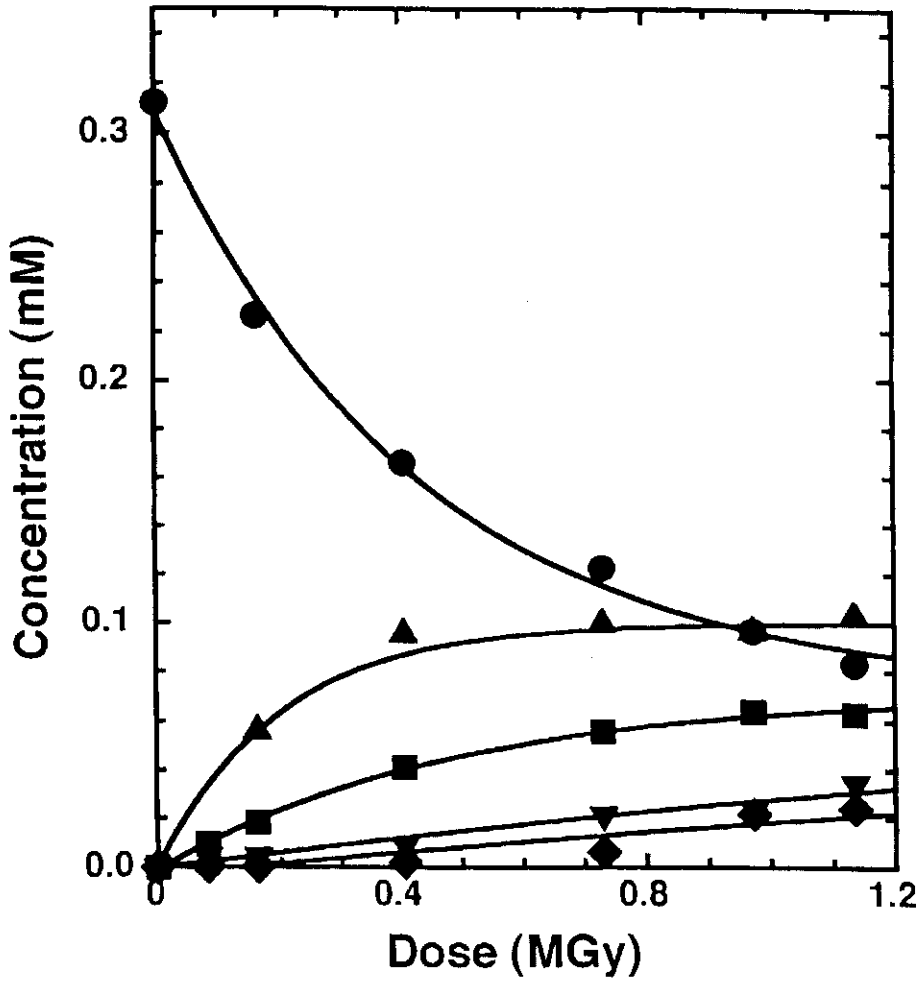

Legend:

- ● DBP
- ■ MBP
- ◆ Phosphate
- ▲ Other dialkyl phosphates
- ▼ Other monoalkyl phosphates

They concluded the new families of dialkyl and monoalkylphosphates were derivatives of the original phosphates formed by the introduction of hydroxyl or carbonyl groups into the butyl groups of DBP and MBP during radiolysis. The radiolytic oxidation of DBP could produce four hydroxy compounds and four carbonyl compounds. Two of the eight possible compounds are illustrated.

$$(CH_3CH_2CH_2CH(OH)O)(BuO)P(=O)ONa$$

$$(CH_3CH_2CH_2C(=O)O)(BuO)P(=O)ONa$$

Camaioni et al. (1996) also detected sodium acetate, formate and oxalate among the reaction products but the sum of the carbon contained in these products and in the phosphates was smaller than the amount of carbon in the starting material. This difference originates in part from the formation of sodium carbonate and in part from the formation of oxidized products and volatile alkanes and alkenes. Davis (1984) pointed out that the radiolysis of TBP produced methane, ethane, propane, ethene, and propene.

Camaioni et al. (1996) also investigated the radiolysis of two possible reaction products, 1-butanol and sodium butyrate. These substances decomposed more rapidly than the phosphate esters. The product mixture contained residual 1-butanol together with sodium formate, acetate, and propionate as well as sodium malate, malonate, and oxalate. These oxidized products account for less than 50% of the available carbon. Although these other products were not identified, it is evident from Spinks and Woods (1990) review that inorganic carbonate ion is produced and that the organic molecules are fragmented. Spinks and Woods (1990) point out the radiolysis of low molecular weight alcohols in water and in other media provides high yields of hydrogen and the corresponding aldehyde, and lower yields of alkanes, cycloalkanes, alkenes, alkynes, and other oxygen-containing compounds.

The targeted work of Burger (1955) and Camaioni et al. (1996) and the information in the literature identify the rather abundant butylphosphates and 1-butanol as sources of many volatile molecules known to be in the waste and dome spaces, that is, methane, ethane, propane, butane, ethene, propene, the butenes, cyclopropane, butadiene, ethyne, propyne, the butynes, methanol, ethanol, 1-propanol and 2-propanol, butanal, acetone, and 2-butanone.

Targeted investigations of the radiolysis of sodium bis(2-ethylhexyl)phosphate have not been carried out. But, as discussed subsequently, it is evident from the persistence of the molecule in the waste that the radiolysis proceeds slowly, presumably because sodium bis(2-ethylhexyl)phosphate is so insoluble in the brine.

Although little direct evidence is available, the radiolysis of sodium bis(2-ethylhexyl)phosphate can be formulated in accord with the information about the radiolysis of the butylphosphates and the hydrocarbons. The principal reactions are shown in Figure L-3.

When formulated in this manner, radiolysis proceeds through excited state molecules and ions and eventually leads to families of oxidized 2-ethylhexylphosphates and fragmented molecules. One initial product of radiolysis of bis(2-ethylhexyl)phosphate anion is a neutral radical.

Figure L-3. Principal Chemical Transformations During the Radiolysis of Sodium Bis(2-ethylhexyl)phosphate in Tank Waste.

Sodium Bis(2-ethylhexyl)phosphate

↓

Phosphate With Oxidized 2-Ethylhexyl Group

Sodium Bis(2-ethylhexyl)phosphate

↓

$CH_3CH_2CH_2CH_2CH(CH_2CH_3)CH_2O$

↓

C_7H_{14} ← $CH_3CH_2CH_2CH_2CH_2CHCH_3$ → C_7H_{16}

and

C_7H_{14} ← $CH_3CH_2CH_2CH_2CHCH_2CH_3$ → C_7H_{16}

Heptenes — Heptyl Radicals — Heptane

Nitrite Esters ← Heptyl Radicals → Nitrate Esters

↓Hydrolysis — ↓ Hydrolysis

Alcohols — Alcohols

Nitro Compounds ← Heptyl Radicals → Nitroso Compounds

↓ Hydrolysis — ↓ Hydrolysis

Ketone — Ketone

The phosphate ester with the oxidized 2-ethylhexyl group and heptane and the alkenes, alcohols and ketones also undergo radiolysis to provide other lower molecular weight alkanes and alkenes and other oxidized products leading to other volatile compounds and sodium formate, oxalate and carbonate.

$$(CH_3CH_2CH_2CH_2CH(CH_2CH_3)CH_2O)_2P(=O)O$$

Beta scission of this substance provides a reactive alkoxy radical,

$$CH_3CH_2CH_2CH_2CH(CH_2CH_3)CH_2O$$

which decomposes to provide 3-heptyl radical and formaldehyde.

$$CH_3CH_2CH_2CH_2CH(CH_2CH_3)CH_2O \rightarrow CH_3CH_2CH_2CH_2CHCH_2CH_3 + CH_2O$$

From this point, the chemistry follows the same pathways outlined for the NPH. For example, hydrogen atom loss produces 3-heptyl radical, which gives the 2- and 3-heptenes.

$$CH_3CH_2CH_2CH_2CHCH_2CH_3 \rightarrow H + CH_3CH_2CH_2CH_2CH{=}CHCH_3$$

$$CH_3CH_2CH_2CH_2CHCH_2CH_3 \rightarrow H + CH_3CH_2CH_2CH{=}CHCH_2CH_3$$

Reactions with the oxidizing agents lead to the same families of products as the reactions of the hydrocarbons to give 3-heptanol and 3-heptanone.

In summary, the radiolysis of the butyl and 2-ethylhexyl phosphates provide oxidized phosphate esters, 1-butene, the 1-, 2-, and 3-heptenes, and lower molecular weight alkanes, cycloalkanes, alkenes, alkynes, alkadienes, alcohols, aldehydes, ketones, and nitriles. The origins of certain reaction products of more special interest are discussed by Stauffer and Stock (1999).

L3.0 FIELD EVIDENCE FOR AGING

Studies of the organic compounds in the condensed phases of the waste and in the dome spaces of the waste tanks provide secure evidence for the aging of the organic hydrocarbons and phosphate esters. These subjects are addressed in the next two sections.

L3.1 TANK WASTE CHARACTERIZATION

The composition of the organic compounds in the liquid layer of tank 241-C-103 and the oil in tank 241-C-106 were investigated. These results are referenced below.

The sample of the organic layer from tank 241-C-103 contains about 25 wt% hydrocarbons with 10 to 15 carbon atoms, 47 wt% tributyl phosphate, 2 wt% dibutyl butylphosphonate, and 25 wt% of an inorganic material that could not be analyzed by gas chromatography (Pool and Bean 1994, Campbell et al. 1994). The NPH/TBP weight ratio was about 2.3 in the solvent used in the PUREX process and the weight ratio of these substances in the organic pool in tank 241-C-103 is about 0.5. The large decrease in the NPH/TBP ratio has already been discussed in Section 2.3 of this document and in an engineering assessment of the transfer of waste from tank 241-C-103 (Bartley et al. 1996). Bartley et al. (1996) used an engineering model to

describe the concurrent hydrolysis of TBP and the evaporation of NPH. The model adopted the rate data provided by Burger (1955) and related the evaporation rate to the temperature, ventilation rates, and related variables. The model indicates hydrocarbon evaporation is the most important factor in changing the NPH/TBP ratio for the liquid pool in tank 241-C-103.

Campbell et al. (1996a, 1996b) also investigated the composition of an oil, which was isolated by centrifugation of sludge samples from tank 241-C-106 (Campbell and Mong 1999). The organic waste in this tank originated from strontium separation operations in B Plant. The original source was a mixture of one part by weight of bis(2-ethylhexyl)phosphoric acid, 6.5 parts tributyl phosphate, and 10 parts normal paraffin hydrocarbon. The oil constitutes between 0.5 and 3.0 vol% of the sludge. Reassessment of the analytical information provided by Campbell et al.(1996a, 1996b) implies the mole fraction[1] of the constituents in the oil is about 0.45 sodium bis(2-ethylhexyl)phosphate, 0.17 butyl bis(2-ethylhexyl)phosphate, 0.13 sodium butyl (2-ethylhexyl)phosphate, 0.08 tributyl phosphate, 0.04 tris(2-ethylhexyl)phosphate, and 0.13 NPH.

The mole ratio NPH/butyl/2-ethylhexyl in the solvent mixture used for strontium separation was about 42/53/5 and the mole ratio of these substances in the residual oil is about 6/25/69. The large decreases in the NPH/butyl, NPH/2-ethylhexyl and butyl/2-ethylhexyl mole ratios show not only that the NPH have evaporated more rapidly than the phosphate esters have hydrolyzed, but also that TBP has hydrolyzed more rapidly than sodium bis(2-ethylhexyl)phosphate.

Other measurements indicate that the NPH/TBP ratio in the waste may increase. The concentrations of decane, undecane, dodecane, tridecane, tetradecane, pentadecene, and tributyl phosphate have been determined for more than 15 core composites. These observations are summarized in Table L-1.

The concentrations of dodecane and tridecane, the most abundant hydrocarbons remaining in these samples range broadly from about 10 to about 4500 μg/g, no hydrocarbons were found in the wastes from tanks 241-BY-110 and 241-C-204. The concentrations of tributyl phosphate also range widely in these samples. The amount of TBP is below the detection limit for the samples from tanks 241-B-201, 241-BY-110, 241-S-104, 241-T-104, and 241-T-111 and below 0.1 μg/g in the core from tank 241-BY-108. However, it is present in readily measurable amounts in tanks 241-B-111, 241-BX-107, 241-C-102, 241-C-110, 241-C-204, and one of the cores from tank 241-T-107.

As already mentioned, the ratio of NPH to TBP in the PUREX process was about 2.3. The values shown in the table range broadly with undefined, but high values for tanks 241-B-201, 241-S-104, 241-T-104, and 241-T-111, and values over 3 for the samples from tanks 241-B-111, 241-BX-107, 241-C-102, 241-C-110, and 241-T-107. These observations imply that TBP has hydrolyzed more rapidly than the NPH has evaporated.

---

[1] It is necessary to use mole fraction in this case because the butyl and 2-ethylhexyl groups are distributed among several molecules. Dodecane was adopted to represent the NPH in the calculation of the mole ratio.

Table L-1. Concentrations of Normal Paraffin Hydrocarbons and Tributyl Phosphate in Core Composites.

Waste Tank	Decane (µg/g)	Undecane (µg/g)	Dodecane (µg/g)	Tridecane (µg/g)	Tetradecane (µg/g)	Pentadecane (µg/g)	TBP (µg/g)	NPH/TBP (µg/g)
B-111	17	36	80	1,700	1,100	55	22	140
B-201			290	930	1,000	41		
BX-107								
Core 40			600	1,700	1,200	42	9	390
Core 41		14	620	1,400	1,100	50	6	530
BY-108	3	24	59	71	55	22		
C-102								
Sample 1	110	550	2,100	3,500	1,800		2,100	4
Sample 2	230	1300	4,500	2,500	3,700		2,700	5
C-110								
Core 38	2	19	860	2,000	1,500		9	490
Core 39	9	17	680	1,500	1,100	52	11	310
C-112		12	32	48	45	25	210	1
S-104			170	510	400	15		
T-104								
Core 45			180	670	570	26		
Core 46			95	420	390	15		
T-107								
Core 50			9	31	24		3	21
Core 52				32		28		
T-111								
Core 31	9	15	140	360	260	27		
Core 33			130	370	250	14		

General notes:

The observations were abstracted from tank characterization reports.

The Relative Standard Deviation ranges from 30 to 50% for replicate analyses.

The results are reported to two significant figures when the concentration is greater than 9 µg/g and to one significant figure when the concentration is between 1 and 9 µg/g.

The concentration of TBP in tank 241-BY-108 was reported to be 0.075 µg/g.

In contrast, the ratios for tanks 241-C-112 and 241-C-204 are significantly less than 2, comparable to the results for tanks 241-C-103 and 241-C-106. These low ratios indicate NPH has evaporated more rapidly than TBP has hydrolyzed.

According to the engineering model (Bartley et al. 1996) mentioned earlier, hydrocarbon evaporation is the most important factor in changing the NPH/Phosphate Ester ratio for the liquid pool in tank 241-C-103. But the rate of evaporation of the hydrocarbons depends upon the air flow and the evaporation rate which may be considerably slower when the organic constituents are dispersed and submerged within a sludge or saltcake. These conditions could lead to the more rapid hydrolysis of TBP.

More information about the aging of the organic solvents has been obtained from the study of the organic constituents evolving from tank 241-C-106 during sluicing operations. Before sluicing operations in December 1998, the concentrations of methanol and ethanol, the two most abundant compounds in the dome space, were about 0.4 mg/m^3. Sluicing caused the organic molecules retained in the oil distributed throughout the sludge to evolve and the concentrations of the organic molecules increased significantly. The results provide a snapshot of the composition of the organic compounds present within the sludge. The concentrations of the volatile organic compounds observed in the ventilation stack of tank 241-C-106, during active sluicing on March 7, 1999, are shown in Table L-2.

The aging of the organic constituents in this tank has led to the formation of a broad array of low molecular weight hydrocarbons and oxidized compounds including alcohols, ketones, and nitriles. The product spectrum is consistent with the aging concepts discussed in Section L2.0. In particular, the high concentrations of the heptanes, heptenes, and heptanones are directly related to the ongoing radiolysis of the most abundant organic molecule in the oil, sodium bis(2-ethylhexyl)phosphate, but the products of the radiolytic aging of the hydrocarbons are also apparent (Stauffer and Stock 1999).

Additional evidence for the aging of the NPH was obtained in a study of the organic constituents in a retained gas sample that was withdrawn from a gas rich location beneath the crust in tank 241-SY-101. These findings are shown in Table L-3.

The organic constituents in tank 241-SY-101 originated from concentrated mixtures of complexants produced during evaporator campaigns from 1977 to 1980. Many of the same fragmented and oxidized compounds appear in this sample as in the sample from tank 241-C-106. But the relative amounts of the compounds differ considerably. The concentrations of the heptanes, heptenes and heptanones are considerably smaller and the concentrations of small hydrocarbons including propane, butane, propene, butene, and butadiene are much higher. In addition, compounds such as dimethyl amine and pyrazine that are chemically related to the nitrogen-containing complexants, EDTA and HEDTA, are present in the sample from tank 241-SY-101.

In summary, analyses of the organic constituents in samples of organic liquids in the condensed phases and the vapors in the dome space indicate that aging diminishes the concentrations of the hydrocarbons and phosphate esters.

Table L-2. Organic Compounds at Concentrations Greater Than 1 Milligram/Cubic Meter in the Ventilation Stack of Tank 241-C-106 During Sluicing Operations on March 7, 1999. (2 sheets)

ALKANES	Conc. (mg/m^3)	ALKENES	Conc. (mg/m^3)	ALKADIENES AND ETHYNES	Conc. (mg/m^3)
Propane	7	Propene	8	2,3-Hexadiene	
Butane	17	2-Methyl-	5	2-Methyl-	47
2-Methyl-	2	1-Butene	35	1,5-Heptadiene	2
Pentane	9	E-2-Butene	2	1,6-Heptadiene	2
2-Methyl-	3	Z-2-Butene	2	3,4-Heptadiene	2
Hexane	13	1-Pentene	12	1,6-Octadiene	4
2-Methyl-	4	4-Methyl-	2	1-Hexyne	2
Heptane	80	E-2-Pentene	3	2-Hexyne	2
3-Methyl-	86	Z-2-Pentene	2	2-Heptyne	22
2,3-Dimethyl-	2	1-Hexene	34	**CYCLOALKANES**	**Conc. (mg/m^3)**
3-Ethyl-	9	2-Methyl-	2		
Octane	20	E-2-Hexene	2	Cyclopropane	
Nonane	19	5-Methyl-	2	Ethyl-	2
Decane	28	Z-2-Hexene	3	Butyl-	23
3-Methyl-	2	5-Methyl-	2	trans-1-Butyl-2-methyl-	11
4-Methyl-	8	E-3-Hexene		Cyclobutane	
3,7-Dimethyl-	3	2-Methyl-	2	Butyl-	2
2,6,7-Trimethyl-	2	Z-3-Hexene	3	Cyclopentane	
Undecane	44	1-Heptene	30	Ethyl-	2
2-Methyl-	3	3-Methyl-	4	Cyclohexane	
6-Methyl-	2	E-2-Heptene	160	Methyl-	2
2,6-Dimethyl-	4	Z-2-Heptene	110	Ethyl-	2
Dodecane	64	3-Methyl-	25	Pentyl-	2
6-Methyl-	6	E-3-Heptene	160	1-Methyl-3-propyl-	2
2,6,10-Trimethyl-	7	Z-3-Heptene	100	(2-Methylpropyl)-	3
Tridecane	45	5-Methyl-	13	1,1,3-Trimethyl-	3
7-Methyl-	3	3-Methyleneheptane	95	Trans-Decalin	12
Tetradecane	5	Z-2-Octene	6	2-Methyl-	6
		E-4-Octene	7	2,3-Dimethyl-	16
		Other Octenes	30	2,6-Dimethyl-	4
		1-Decene	7	**AROMATIC HYDROCARBONS**	**Conc. (mg/m^3)**
		1 or Z-3-Undecene	7		
		Cyclopentene	3	Benzene	
		Dimethyl-	5	Methyl-	2

Table L-2. Organic Compounds at Concentrations Greater Than 1 Milligram/Cubic Meter in the Ventilation Stack of Tank 241-C-106 During Sluicing Operations on March 7, 1999. (2 sheets)

ALCOHOLS AND ETHERS	Conc. (mg/m^3)	ALDEHYDES AND KETONES	Conc. (mg/m^3)	NITRILES	Conc. (mg/m^3)
1-Butanol	3	Butanol	2	Butanenitrile	2
3-Heptanol	15	Acetone	3	2-Methylene-	2
2-Ethylhexanol	100	2-Pentanone	6	Hexanenitrile	5
Dibutyl ether	12	2-Hexanone	4	Heptanenitrile	9
1,3-Diethyl-1,4-epoxybutane	65	3-Hexanone		3-Methyl-	13
		5-Methyl-	2	Octanenitrile	13
		2-Heptanone	22	Nonanenitrile	6
		3-Heptanone	170	Decanenitrile	3
		4-Heptanone	50		
		3-Methyl-	3		
		2-Octanone	4		
		3-Octanone	3		
		4-Octanone	10		

Note: [1]Bonfoey et al. (1999)

Table L-3. Organic Compounds at Concentrations Greater Than 1 Milligram/Cubic Meter in a Retained Gas Sample from Tank 241-SY-101.[1] (2 sheets)

ALKANES	Conc. (mg/m^3)	CYCLOALKANES	Conc. (mg/m^3)	ALKADIENES AND ALKYNES	Conc. (mgm^3)
Propane	160	Cyclopropane	75	1,3-Butadiene	170
Butane	160	cis-1,2-Dimethyl-	2	Propyne	11
2-Methyl-	24	**ALKENES**	**Conc. (mg/m^3)**	**AROMATIC COMPOUNDS**	**Conc. (mgm^3)**
2,2-Dimethyl-	5				
Pentane	14	Ethene		Benzene	4
2-Methyl-	6	Propene	245	**NITRO AND NITROSO COMPOUNDS**	**Conc. (mgm^3)**
3-Methyl-	4	1-Butene	75		
Hexane	3	2-Butene (E)	200	Nitromethane	4
Heptane	4	2-Methyl-1-propene	73	2-Methyl-2-nitropropane	4
Undecane	2	1-Pentene	4	N-Nitrosodimethyl amine	5
Dodecane	2	2-Methyl-1-butene	10		
Tridecane	9	2-Methyl-2-butene	4		
Tetradecane	52	1-Hexene	2		

Table L-3. Organic Compounds at Concentrations Greater Than 1 Milligram/Cubic Meter in a Retained Gas Sample from Tank 241-SY-101.[1] (2 sheets)

ALCOHOLS AND ETHERS	Conc.[3] (mg/m^3)	KETONES	Conc.[3] (mg/m^3)	AMINES	Conc.[3] (mg/m^3)
Methanol	300	Propanone	13	Methyl amine	235
Ethanol	450	2-Butanone	7	Dimethyl amine	5
2-Butoxy-	6	Pentanone		Ethyl amine	50
1-Propanol	94	4-Methyl-	2	1-Methylaziridine	17
2,2-Dimethyl-	5			Pyridine	46
2-Propanol	23			Pyrazine	4
2-Methyl-	20				
1-Butanol	195				
2-Butanol	3				
3-Heptanol	5				
Tetrahydrofuran	19				
1,4-Dioxane	10				

Notes:

[1] Evans and Mitroshkov (1999)

[2] The sample was collected below the crust in the convective layer. The sample contained approximately 45% gas by volume.

[3] The results of three analyses were averaged to obtain the information summarized in this table.

[4] Several silanes were also observed at concentrations greater than 1 mg/m^3.

The aging processes occur concurrently and, in some wastes, the evaporation of the hydrocarbons is more rapid than the hydrolysis of tributyl phosphate. In other instances, the rate of hydrolysis of tributyl phosphate is more rapid than the evaporation of the hydrocarbons. The investigations of the volatile organic compounds retained in tanks 241-C-106 and 241-SY-101 indicate the radiolysis of NPH and the phosphate esters produces new volatile organic compounds including fragmented alkanes and oxidized families of alkenes, alcohols, aldehydes, ketones, and nitriles. Other evidence for the aging of the organic compounds into more volatile and more soluble organic compounds is discussed in Section, L3.2.

L3.2 DOME SPACE CHARACTERIZATION

The tanks now contain families of compounds including the original constituents, intermediate organic compounds, and simple end products of the oxidation reactions. The oxidized remnants of the complexants and some solvents are acidic compounds and are retained in the alkaline condensed phases of the waste. However, most oxidation products of the organic solvents are neutral compounds that are volatile. These substances and the original solvents continuously evolve from the waste into the dome space. Consequently, the nature of the organic compounds in dome space reflects the nature of the organic compounds in the tank waste. The volatile organic compounds in the dome spaces of 109 single-shell tanks have been collected and analyzed.

Established procedures have been used for the collection of the organic compounds from the dome spaces in SUMMA[2] canisters and triple sorbent tubes. The samples were subsequently analyzed by gas chromatography and mass spectrometry. The analytical teams report the concentrations for "target compounds" and for "tentatively identified compounds". The substances selected for quantitative analyses according to protocols of the Environmental Protection Agency and the National Institute of Science and Technology are designated "target compounds". The concentrations of these substances are determined by comparison with independently prepared samples of pure compounds. The other substances found in the sample are designated "tentatively identified compounds". Their identification is customarily made by comparison of the mass spectrum of the substance detected in the chromatogram with the mass spectra of compounds assembled in a large library originally prepared at the National Institutes of Health.

The data, which were assembled by Huckaby et al. (1997), are included in the Tank Characterization Reports and in the Hanford Data Base. The tanks that have been sampled and the average concentrations of organic compounds are listed in Table L-4. At least two samples have been analyzed for 100 of the tanks listed in the table.

---

[2] SUMMA is a trademark of Molectric, Inc., Cleveland, Ohio.

Table L-4. Concentrations of Organic Compounds in Dome Spaces of Single-Shell Tanks. (2 sheets)

Tank	Conc. (mg/m^3)	Tank	Conc. (mg/m^3)	Tank	Conc. (mg/m^3)	Tank	Conc. (mg/m^3)
A-101	19	C-101	150	SX-107	0.5	TY-101	8.3
A-102	4.4	C-102	250	SX-108	0.8	TY-102	0.8
A-103	7.1	C-103	1,300	SX-109	0.8	TY-103	47
A-106	4.2	C-104	78	SX-110	0.4	TY-104	7.6
AX-101	2.8	C-105	3.3	SX-111	0.7	TY-105	23
AX-102	9.3	C-106	0.7	SX-112	1.0	U-102	6.8
AX-103	0.4	C-107	6.2	SX-114	0.5	U-103	9.1
AX-104	0.6	C-108	2.5	T-101	0.2	U-104	<0.6
B-102	0.1	C-109	0.9	T-104	1.9	U-105	4.0
B-103	14	C-110	19	T-107	2.7	U-106	12
B-105	2.6	C-111	0.5	T-110	0.6	U-107	11
B-107	2.2	C-112	4.2	T-111	23	U-108	9.2
B-202	0.9	C-201	6.3	TX-101	0.7	U-109	9.2
BX-102	3.3	C-202	2.5	TX-102	5.5	U-111	6.8
BX-103	49	C-204	140	TX-103	3.1	U-112	4.0
BX-104	51	S-101	12	TX-104	1.0	U-203	7.6
BX-105	4.4	S-102	28	TX-105	3.2	U-204	4.2
BX-106	2.0	S-103	7.6	TX-106	3.7		
BX-107	2.3	S-105	2.6	TX-108	2.1		
BX-110	2.6	S-106	6.6	TX-110	15		
BX--111	8.1	S-107	7.1	TX-111	15		
BY-101	51	S-108	1.8	TX-112	3.8		
BY-102	18	S-109	3.7	TX-113	4.2		
BY-103	8.6	S-110	3.4	TX-114	7.3		
BY-104	84	S-111	2.0	TX-115	1.8		
BY-105	13	S-112	6.4	TX-116	9.2		
BY-106	9.1	SX-101	0.7	TX-117	1.9		
BY-107	120	SX-102	2.5	TX-118	8.9		
BY-108	180	SX-103	0.9				
BY-109	23	SX-104	1.9				
BY-110	41	SX-106	2.1				
BY-112	10						

Tanks 241-C-103 and 241-BY-108 rank first and third in total concentration of organic material in the dome space. The concentrations of the more abundant compounds in these two tanks are assembled in Tables L-5 and L-6 to demonstrate the nature of the organic compounds observed in the wastes.

Table L-5. Organic Compounds at Concentrations Greater Than 1 Milligram/Cubic Meter in Dome Space of Tank 241-C-103.[1] (2 sheets)

Compound	Target Conc. (mg/m^3)	Target SD (mg/m^3)	TIC Conc. (mg/m^3)		Target Conc. (mg/m^3)	Target SD (mg/m^3)	TIC Conc. (mg/m^3)
ALKANES				**CYCLOALKANES**			
Butane			13	Cyclopentane			
Hexane	2.6	0.2		One other C12 cyclopentane			36
Heptane	2.5	0.5		Cyclohexane			
Octane	1.4	0.4		Four other C13 cyclohexanes			47
Nonane	1.4	0.4		One other C15 cyclohexane			1
2,6-Dimethylnonane			3	trans-Decalin			3
Decane	3.1	0.3		2-Methyl-trans-decalin			11
2,4,6-Trimethyldecane			4	Cyclotetradecane			4
Undecane	27	4		**AROMATIC HYDROCARBONS**			
2-Methyldecane			18	Biphenyl			1
3-Methyldecane			13	**ALKENES**			
4-Methyldecane			5	Propene			
5-Methyldecane			4	2-Methylpropene			3
2,4-Dimethylundecane				1-Butene			11
2,6-Dimethylundecane				1-Pentene			4
2,10-Dimethylundecane				1-Hexene			5
3,7-Dimethylundecane				1-Undecene			
Dodecane	260	50		One other C11 alkene			1
4-Methyldodecane			11	1-Dodecene			
4,6-Dimethyldodecane			35	Two other C12 alkenes			2
2,6,10-Trimethyldodecane			24	1-Tridecene			
2,6,11-Trimethyldodecane			4	One C13 alkene			5
Five other C12 alkanes			25	1-Tetradecene			1
Tridecane	370	26		Two other C14 alkenes			4
2-Methyltridecane			14	1-Pentadecene			
3-Methyltridecane			2	One other C15 alkene			9
5-Methyltridecane			4	**NITRILES**			
6-Methyltridecane			19	Acetonitrile	14	4	
One other C13 alkanes			11	Propanenitrile	6.8	0.6	
Tetradecane	75	8		Butanenitrile	6.3	2.1	
Six other C14 alkanes			30	Pentanenitrile	3.2	0.5	
Pentadecane			8	Hexanenitrile	2.9	0.4	
Three other C15 alkanes			14	Heptanenitrile	2.5	0.2	
Hexadecane			25	Octanenitrile	1.5	0.4	

Table L-5. Organic Compounds at Concentrations Greater Than 1 Milligram/Cubic Meter in Dome Space of Tank 241-C-103.[1] (2 sheets)

Compound	Target Conc. (mg/m^3)	Target SD (mg/m^3)	TIC Conc. (mg/m^3)		Target Conc. (mg/m^3)	Target SD (mg/m^3)	TIC Conc. (mg/m^3)
ALKANES (Cont'd)				**MISCELLANEOUS COMPOUNDS**			
One other C16 alkane			7	Dichloromethane	5.2	4.8	
Heptadecane			3	1,1-Dichloroethene			3
ALCOHOLS AND ETHERS				Ethyl acetate			30
1-Butanol	80	17		Butyl acetate			6
Cyclopentanol			2	Butyl butyrate			1
2-Phenyl-2-propanol			9	One other carboxylic acid ester			2
2,3 Dihydrofuran			2	One phthalate ester			2
Tetrahydrofuran			10	One alkyl nitrite ester			3
ALDEHYDES AND KETONES				One phenol			4
Butanal	3.4	2.2		Hexamethylcyclotrisiloxane			2
Nonanal			2	Octamethylcyclotetrasiloxane			1
Acetone	19	9		Tetradecanoic acid			1
2-Butanone			27	Hexadecanoic acid			1
3-Methyl-2-butanone			1				
2-Pentanone	3.6	2.1					
2-Hexanone	2.0	0.5					
3-Hexanone			11				
Two other C6 alkanones			3				
6-Methyl-2-heptanone			5				
2-Heptanone	2.5	0.5					
3-Heptanone			3				
2-Octanone	1.2	0.2					
3-Octanone			1				
Two other C8 alkanones			5				
2-Nonanone			7				
One other C9 alkanones			2				
3-Dodecanone			6				
3-Tridecanone			4				
One other C13 alkanone			6				

Note:
[1] Jenkins et al. (1994)

Table L-6. Organic Compounds at Concentrations Greater Than 0.5 Milligram/Cubic Meter in Dome Space of Tank 241-BY-108.[1]

	Target Conc, mg/m^3	Target SD mg/m^3	TIC Conc, mg/m^3		Target Conc, mg/m^3	Target SD mg/m^3	TIC Conc, mg/m^3
ALKANES				**ALKENES**			
Propane			0.91	Propene			1.8
2-Methylpropane			0.58	1-Butene			2
Butane			1.4	1-Pentene			0.69
Pentane			1.4	4-Methyl-1-pentene			0.53
2-Methylpentane			2.1	1-Hexene			0.74
Hexane	5.7	0.1		1-Heptene			1.1
3-Methylhexane			1.7	1-Undecene			
Heptane	2.3	0.1		Two other C11 alkenes			1.5
Octane			1.4	1-Tridecene			
One other C8 alkane			1.3	Two other C13 alkenes			3.4
Nonane			0.80	1-Tetradecene			
Decane	0.57	0.02		One other C14 alkene			0.91
Undecane			3.3	ALCOHOLS AND ETHERS			
One other C11 alkane			1	1-Propanol	2.1	0.4	
2,6-Dimethylundecane			4.2	1-Butanol			13
Dodecane			6.2	Tetrahydrofuran	4.2	0.1	
2,6,10-Trimethyldodecane			2.4	**ALDEHYDES AND KETONES**			
Six other C12 alkanes			3.9	Acetone	11	1	
Tridecane			5.3	2-Butanone	1.8	0.1	
Tetradecane			2	2-Pentanone			1.7
One other C14 alkane			4.9	2-Hexanone			0.66
CYCLOALKANES				3-Hexanone			
Cyclohexane	0.53	0.02		Two other C6 alkanones			
Trans-Decalin				**MISCELLANEOUS COMPOUNDS**			
2-Methyldecalin			0.67	Freon 11	0.78	0.04	
2,6-Dimethyldecalin			0.58				
Three other alkyldecalins			1.9				

Note: [1]McVeely et al. (1995)

The results for the target compounds and the standard deviation observed in replicate measurements are displayed in the first two columns to illustrate the reproducibility of the analytical measurements. The results for the tentatively identified compounds are displayed in the third column. Experience suggests the concentration of a tentatively identified compound can differ from the actual value by 100 percent.

The organic compounds in the dome space of tank 241-C-103 originate principally from the pool of organic material, which contains about 30 percent NPH and 70 percent TBP. The original alkanes including undecane, dodecane, tridecane, and tetradecane (and their isomers) are much more abundant than the other compounds. However numerous alkenes, alcohols, aldehydes, ketones, and nitriles are present. Some of the initial oxidation products including 1-dodecene, 1-tridecene, 1-tetradecene, 3-dodecanone, 3-tridecanone, and tetradecanoic acid have been detected at concentrations greater than 1 mg/m^3. Other compounds of this kind are present at lower concentrations (McVeely et al. 1995).

The organic compounds in the dome space of tank 241-BY-108 evolve from the interim stabilized saltcake. Their concentrations are significantly smaller than the concentrations of the same compounds in the dome space of tank 241-C-103. For tank 241-BY-108, the concentrations of hexane and heptane are similar to the concentrations of dodecane and tridecane. The homologous series of ketones extends only to hexanone, and the nitriles are not present at concentrations greater then 0.5 mg/m^3.

Several hundred compounds have been definitely or tentatively identified in the course of the investigations of the compounds that evolve from the waste tank during sluicing and during quiescent periods. These observations are summarized in the following paragraphs.

Alkanes ranging from propane to tetradecane and lesser amounts of branched chain hydrocarbons, principally monomethylalkanes, appear in the dome spaces. Undecane, dodecane, tridecane, tetradecane and their mono-, di- and a few trimethyl derivatives originate from unchanged NPH. The radiolytic reactions of the NPH lead to the formation of the entire family of alkanes from methane to nonane as described in Section L2.1. The linear alkanes from methane to heptane and 2-ethylhexane are also produced by the radiolysis of sodium bis(2-ethylhexyl)phosphate. The radiolysis of the butyl phosphates provides methane, ethane, and propane. The lower molecular weight compounds are more abundant than the other compounds in the dome space, not only because they are more volatile but also because they are formed from the three source molecules.

Alkenes ranging from ethene to decene are also present in the dome spaces together with alkadienes and alkynes. These oxidation products, like the alkanes, are predominantly linear molecules. The radiolytic reactions of the NPH are responsible for the formation of the family of molecules from ethene to tetradecene. The radiolysis of the sodium bis(2-ethylhexyl)phosphate gives 1-, 2- and 3-heptene as well as 3-methyleneheptane and ethene, propene, butenes, pentenes, and hexenes. The radiolysis of butylphosphates provides 1-butene and the lower molecular weight alkenes.

Hydrogen is the most abundant inorganic byproduct of the radiolytic conversion of alkanes into alkenes (Gyorgy 1981, Spinks and Woods 1990, Tabata et al. 1991).

Cycloalkanes with three, four, five and six membered rings and certain decalins with joined six-membered rings are present in low concentrations. The compounds with 10 or more carbon atoms either were originally present in the NPH or were formed from the linear NPH molecules in cyclization reactions. The lower molecular weight compounds, like the alkenes, are oxidation products of radiolytically-initiated cyclization and fragmentation reactions.

Aromatic compounds such as benzene, toluene and the xylenes are present at low concentrations. Their low concentrations are compatible with the fact that aromatic compounds were removed from the NPH during manufacture and with the fact that their formation from alkanes requires the sequential formation of several reactive intermediate compounds that can be intercepted by the oxidizing agents in the waste.

Alcohols spanning the range from methanol to heptanol are present. Only two of these compounds, 1-butanol and 2-ethyl-1-hexanol, arise by simple hydrolysis reactions of the phosphate esters. The butyl esters are certainly responsible for the high concentrations of 1-butanol. The other alcohols like the aldehydes, ketones and nitriles are produced through reaction sequences beginning with the alkyl radicals and nitric oxide and nitrogen dioxide as discussed in Section L2.2.2. The intermediates in these reactions are discussed in Section L4.0. Ethers are much less abundant than the alcohols. The structures of the more abundant compounds including the butyl ethers and the several tetrahydrofuran derivatives imply these substances were formed principally from the butyl and 2-ethylhexyl groups of the phosphate esters.

Homologous series of aldehydes and ketones with linear carbon skeletons are evident. Generally, the concentrations of the aldehydes are smaller than the concentrations of the corresponding ketones. The 2-alkanones are present in most waste tanks. Acetaldehyde and acetone are fragmentation products of the NPH and the phosphate esters. Butanal and 3-heptanone are derived from the butyl and 2-ethylhexyl groups of the phosphates as described in Section L2.2.1. The other linear aldehydes and ketones are oxidation products of the NPH. The family of ketones observed in the waste from tank 241-C-103 includes nine compounds with 8 or more carbon atoms extending to 3-tridecanone. Refer to Table L-5. These compounds are produced during the early stages of the aging process.

Homologous series of linear nitriles are also constituents of the emerging volatile organic compounds. As shown in the tables, the series from acetonitrile to nonanenitrile is present in tank 241-C-106 and members of the same series are present in the other tanks. The carbon atom of the nitrile group is in the same oxidation state as the carbon atom of the carboxylate group. Hydrolysis, as noted in Section L2.0, converts the nitrile into a soluble sodium carboxylate. Thus, the nitriles are volatile and evolve from the waste, but they also hydrolyze to provide carboxylate ions that are retained in the alkaline supernatant layer.

The nitrogen in the nitriles originates from nitrite ion. Nitrite ion is also the principal source of the nitrogen in nitrous oxide and nitrogen (Meisel et al. 1993).

Halogen compounds were included among the target analytes. These substances and other miscellaneous compounds including freons and siloxanes are found in very low concentrations. Plausible sources for these compounds have been considered in the reports, for example Huckaby and Bratzel (1995), that describe the investigations of the organic compounds in the dome spaces, but their origins have not been definitely established.

In summary, the same broad families of compounds are found in the dome spaces of many tanks and in selected samples of the condensed wastes. The distribution is dictated by the fact that normal paraffinic hydrocarbons and tributyl phosphate were used in PUREX operations and together with sodium bis(2-ethylhexyl)phosphoric acid for strontium separations. As a result, the NPH and TBP are widely distributed in the waste tanks and these two substances are primarily responsible for the appearance of volatile organic compounds in the dome spaces. Differences arise when sodium bis(2-ethylhexyl)phosphate is present. This substance provides heptanes, heptenes and heptanones that are not formed in abundance from the NPH. The presence of nitrogen-containing organic complexants in tank 241-SY-101 leads to the formation of pyrazine and dimethyl amine, and the ammonia generated by the aging of these complexants influences the product distribution from the normal paraffinic hydrocarbons and tributyl phosphate. There are therefore subtle differences in the product distribution, but the broad pattern of the aging process remains the same throughout the tank farms: the original constituents are fragmented and oxidized through the radiolytic and hydrolytic reactions eventually to form volatile organic compounds.

L3.3 DISPERSAL OF INTERMEDIATE COMPOUNDS

Several lines of evidence support the conclusion that the fragmented alkanes, alkenes, alcohols, aldehydes, ketones, nitriles and related organic intermediates produced from the solvents and complexants are dissolved and dispersed in aqueous and organic phases in the waste.

The characterization work described in Section L3.1 indicates that these organic substances are distributed throughout the waste in a similar manner to how the total organic carbon is distributed throughout the wastes. Support for this conclusion is provided by the retained gas investigations that have found the organic gases including methane, ethane, propane, and butane to be ubiquitous constituents of the retained gases.

Solubility relationships imply the paraffinic hydrocarbons and the 2-ethylhexylphosphates, which are almost completely insoluble in water, are concentrated in organic phases. The butylphosphates, which are much more soluble in water than the other solvents, are present in the water and organic phases (Camaioni et al. 1995). The products of the oxidation reactions, especially the oxygen containing compounds with one or more polar groups and four or five carbon atoms, are much more soluble in water than their precursors. These partially-water compounds and other more completely water

soluble compounds, such as methanol and ethanol, selectively emerge from the waste of tank 241-C-106 during quiescent intervals because they are transported through water to the dome space (Stauffer and Stock 1999). The oxidized organic molecules, which are formed from partially soluble molecules in the aqueous phase, presumably remain in the aqueous phase and the fragmented and oxidized organic compounds formed in the organic phase become more water soluble and redistribute between the organic and aqueous phases.

In summary, the characterization work, targeted laboratory study, and the chemical literature indicate the oxidized and intermediate organic compounds are dispersed in the waste and distributed at low concentrations between the gaseous, aqueous, and organic phases.

L4.0 ALIPHATIC AND AROMATIC NITROSO AND NITRO COMPOUNDS

Numerous oxidation products of the solvents including alkenes, alkadienes, and alkynes, alcohols and ethers, aldehydes and ketones, and nitriles appear in the dome space. Although less numerous and less abundant, organic compounds with nitro and nitroso groups have also been detected. The presence of these compounds, their chemical origins, and their energy contents are examined in this section.

L4.1 NITRO AND NITROSO COMPOUNDS IN WASTE

Nitro or nitroso compounds have been detected in the dome spaces of 60 of the tanks which have been sampled. The observations are shown in Table L-7.

In brief, twenty different esters of nitric acid have been tentatively identified. The family of primary nitrate esters from methyl to 1-decyl nitrate are much more prominent than secondary or tertiary alkyl nitrates.

Methyl nitrate	CH_3ONO_2
Ethyl nitrate	$CH_3CH_2ONO_2$
Propyl nitrate	$CH_3(CH_2)_2ONO_2$
Decyl nitrate	$CH_3(CH_2)_9ONO_2$

The other nitrate esters include primary compounds such as 2-methylpropyl (isobutyl) and 3-methylbutyl (isopentyl) nitrate.

2-Methylpropyl nitrate	$(CH_3)_2CHCH_2ONO_2$
3-Methylbutyl nitrate	$(CH_3)_2CHCH_2CH_2ONO_2$

and two secondary compounds, 1-methylethyl and 1-methylpropyl nitrate.

1-Methylethyl nitrate	$(CH_3)_2CHONO_2$
1-Methylpropyl nitrate	$CH_3CH(CH_3)ONO_2$

Table L-7. Observations of Nitroso and Nitro Compounds in Dome Spaces.[1] (3 sheets)

Tank	Nitrate Esters	Nitrite Esters	Aliphatic Nitro Compounds	Aromatic Nitro Compounds	N-Nitroso Compounds
A-101		Methyl, Unk			
A-102	Pr to Hex, 2-MePr		2-MePr		
A-103					NNDMA
AX-101			Bu		
AX-102	Et, Bu, 2-MePr, 1,4-Bu	Me, Bu	Pr, Bu, 2-MePr		
AX-103	Me, 1,4-Bu		Me, 2-MePr		
B-103	Me to Hex, 1,5-Pe, Unk	Me, Bu, Unk	2-MePr		
BX-103	Et, Hex, 1-Isopentyl				
BX-104	Me, Bu, Pe, Unk	Bu			
BY-102	Bu				
BY-104	Et				
BY-106			Unk		
BY-107	1,4-Bu				
BY-108			2-MePr		
BY-112	Pr, 1-Isopentyl	Me			
C-101	Me, MeEt, Pe, Hex, Unk				
C-102	Et, MeEt, Pr, Pe, Hex, Unk	Bu			
C-103	1,4-Bu				
C-104	Et, Bu				
C-105	Pr, Bu, 1,5-Pe				
C-106	Et, Pr	Me, Bu			
C-107	Me to Bu, Hex, 1,5-Pe, Unk		2-MePr, Unk	Chloronitrobenzene	
C-109	Me to Pr, Unk				
C-110	Bu		2-MePr		
C-112	Me to Pr, 1-Neopentyl, Unk				
C-204	Pr, Bu, 1,2-Et		Bu		
S-101		Me			NNDMA

Table L-7. Observations of Nitroso and Nitro Compounds in Dome Spaces.[1] (3 sheets)

Tank	Nitrate Esters	Nitrite Esters	Aliphatic Nitro Compounds	Aromatic Nitro Compounds	N-Nitroso Compounds
S-102					NNDMA
S-103					NNDMA
S-105	Pr		2-MePr		
S-106		Me			
S-108			2-MePr		
S-110					NNDMA
S-111			2-MePr		NNDMA
S-112					NNDMA
SX-103			2-MePr		NNDMA
SX-106			2-MePr		
T-107	Me to Hex		Bu	Nitrotoluene	
T-111	Unk				
TX-102	Me, Pr, Bu	Me	2-MePr		
TX-103		Me	2-MePr		
TX-105	Me to Hex, 2-MePr	Hept	2-MePr		
TX-106	1,2-Et				
TX-108	1,2-Et				
TX-110	Pr, Bu		2-MePr		NNDMA
TX-111	Pr, Bu, Hex, Hept				NNDMA
	1-Isopentyl, 1-Neopentyl				
TX-112			2-MePr, Unk		
TX-118	Me to Dec, 2-MePr	Me, Bu	2-MePr	Nitrobenzene	NNDMA
	1-Isobutyl, Unk				
TY-101	Pr				
TY-103	Bu				

Table L-7. Observations of Nitroso and Nitro Compounds in Dome Spaces.[1] (3 sheets)

Tank	Nitrate Esters	Nitrite Esters	Aliphatic Nitro Compounds	Aromatic Nitro Compounds	N-Nitroso Compounds
TY-104	Me to Hex, Non, 1,4-Bu, Unk		Pr, 2-MePr	Nitrobenzene	
			1-Propenyl	Nitrotoluene	
U-102			2-MePr		NNDMA
U-103			2-MePr		NNDMA
U-105					NNDMA
U-106			2-MePr		NNDMA
U-107			2-MePr		NNDMA
U-108					NNDMA
					Morpholine
U-109					NNDMA
U-111					NNDMA
U-112			Me, 2-MePr, Bu		
			1-Isobutyl, 2-Butyl		

Notes:

[1] (Huckaby 1999)

[2] Symbols for groups: Me = Methyl, Et = Ethyl, Pr= 1-Propyl, Bu = 1-Butyl, Pe = 1-Pentyl, Hex = 1-Hexyl, Hep = 1-Heptyl, Oct = 1-Octyl, Non = 1-Nonyl, Dec = 1-Decyl, 1,2-Et = OCH_2CH_2O, 1,4-Bu = $OCH_2CH_2CH_2CH_2O$, 2-MePr = 2-Methylpropyl

[3] The structure of the methyl nitrite ester is CH_3ONO, the methyl nitrate ester is CH_3ONO_2, and the methyl nitro compound is CH_3NO_2.

[4] The designation "unk" is used when the analyst did not assign the structure.

[5] The designation NNDMA is used for N-nitroso dimethyl amine, which is also referred to as N-nitroso-N-methylmethaneamine.

In contrast, tertiary alkyl nitrates are not present. Some compounds with two O-nitro groups are present. The most prominent compound of this class is the diester of 1,4-butanediol.

$$O_2NOCH_2CH_2CH_2CH_2ONO_2$$

Nitrate esters have been detected in about 30 tanks. Most of these tanks contain only one or two of these substances, but others including tanks 241-A-102, 241-B-103, 241-BX-104, 241-C-101, 241-C-102, 241-C-107, 241-C-112, 241-T-107, 241-TX-105, 241-TX-111, 241-TX-118, and 241-TY-104 contain 5 or more different nitrate esters. The concentrations of the esters of nitric acid range broadly from the threshold of about 0.001 to a maximum of 2 mg/m^3, which is the concentration of 1,4-butanediol dinitrate in the dome space of tank 241-TX-118.

The methyl and butyl esters of nitrous acid have been detected in about 15 tanks.

Methyl nitrite	CH_3ONO
Butyl nitrite	$CH_3(CH_2)_3ONO$

No other primary, secondary, or tertiary esters of nitrous acid have been reported. The highest reported concentration is less than 1 mg/m^3 for methyl nitrite in the dome space of tank 241-A-101.

Aliphatic nitro compounds including nitromethane, 1-nitropropane, 1- and 2-nitrobutane, 1-nitro-2-methylpropane, and 1-nitro-3-methylbutane have been observed in about 30 tanks.

Nitromethane	CH_3NO_2
1-Nitropropane	$CH_3(CH_2)_2NO_2$
1-Nitrobutane	$CH_3(CH_2)_3NO_2$
2-Nitrobutane	$CH_3CH_2CH(NO_2)CH_3$
1-Nitro-3-methylbutane	$CH_3CH(CH_3)CH_2CH_2NO_2$

The tertiary C-nitro compound, 2-nitro-2-methylpropane, is reported to be present in 25 tanks.

2-Nitro-2-methylpropane	$(CH_3)_3CNO_2$

The highest concentration of an aliphatic nitro compound is 2 mg/m^3 for 1-nitrobutane in the dome space of tank 241-A-101. No dinitro compounds, such as dinitromethane or dinitroethane, have been detected in the dome spaces. One trinitro compound, trinitrofluoromethane, has been tentatively identified.

One N-nitroso compounds, N-methyl-N-nitrosomethaneamine, has been observed in more than 15 tanks and N-nitrosomorpholine has been tentatively identified in the dome space of one tank.

N-Methyl-N-nitrosomethaneamine	$CH_3N(CH_3)NO$
N-Nitrosomorpholine	$O(CH_2CH_2)_2NNO$

The maximum concentration of the amine is 0.27 mg/m^3 in the dome space of tank 241-U-108.

Aromatic nitro compounds have been observed in 4 tanks. Nitrobenzene has been reported in two vapor samples, the nitrotoluenes have been observed in three samples and nitrochlorobenzene has been reported in another sample. No aromatic compounds, with two or more nitro groups, have been detected.

Nitrobenzene	$C_6H_5NO_2$
Nitrotolune	$CH_3C_6H_4NO_2$
Nitrochlorobenzene	$ClC_6H_4NO_2$

The highest concentration reported for an aromatic nitro compound was 0.015 mg/m^3 for nitrobenzene in the dome space of tank 241-TX-118.

Only one tank, 241-TX-118, contains nitrate and nitrite esters as well as aromatic compounds and the N-nitroso amine. Compounds of three of the four families are found in nine other tanks, 241-AX-102, 241-B-103, 241-C-106, 241-C-107, 241-T-107, 241-TX-102, 241-TX-105, 241-TX-110, 241-TY-104. More frequently, the dome spaces contain one or two of these compounds. Inspection of the information suggests that aliphatic nitro compounds are likely to be present in wastes that contain the N-nitroso compound, but that there is no apparent relationship between the concentrations of the nitrate and nitrite esters.

In summary, nitro or nitroso compounds appear in about half of the sampled tanks. About 30 different aliphatic and aromatic nitro and nitroso compounds have been tentatively identified. N-Nitrosodimethylamine (N-nitroso-N-methylmethane amine) appears in 15 tanks. The nitrate esters, which are present in 40 tanks, are far more prominent than methyl and butyl nitrite, which are present in 15 tanks. Aliphatic nitro compounds have been detected in 25 tanks. 2-Nitro-2-methylpropane is the most abundant compound of this type.

Aromatic nitro compounds are much less prevalent than the aliphatic nitro compounds and few such compounds have been detected. No aliphatic or aromatic molecules with two nitro groups have been detected. Only one trinitro compound, fluorotrinitromethane, has been reported.

The aliphatic nitroso and nitro compounds and the nitrate and nitrite esters, as discussed in the next section, are intermediates in the ongoing reaction sequences that convert the original complexants and solvents into alcohols, aldehydes, ketones, nitriles, and carboxylate ions. As outlined in the next sections, the nitro compounds and the inorganic esters are continuously formed in the oxidation reactions and destroyed in hydrolytic reactions.

L4.2 FORMATION OF NITRO AND NITROSO COMPOUNDS

The nitro and nitroso compounds with one and two carbon atoms can originate either from a solvent or from a complexant. In view of the fact that most of volatile nitro and nitroso compounds have more than two carbon

atoms, these compounds must originate from the organic solvents. The discussion of these chemical reactions which began in Section L2.1 and L2.2 is expanded in this section.

Direct and indirect radiolysis leads to the formation of linear alkyl free radicals and the entire family of alkyl radicals extending from methyl radical to 1-tetradecyl is present. Linear, that is, normal, radicals predominate because the NPH are linear hydrocarbons and because the principal reaction channel from sodium bis(2-ethylhexyl)phosphate leads to linear 3-heptyl radical.

$$CH_3 \quad CH_3CH_2 \quad CH_3CH_2CH_2 \quad CH_3CHCH_3 \quad CH_3(CH_2)_2CH_2, \quad CH_3CH_2CHCH_3$$

$$CH_3CH_2CH_2CH_2CHCH_2CH_3$$

Some tertiary radicals such as 2-methyl-2-propyl radical are present, but these substances are far less abundant than the linear primary and secondary radicals.

The radiolysis of water provides hydrogen atoms, hydroxyl radicals and electrons, and the ensuing chemical reactions of these substances with sodium nitrite and sodium nitrate provide nitric oxide, nitrogen dioxide, and nitrate dianion radical. Oxidized products form when the alkyl radical combines with one of the oxygen or nitrogen containing radicals to produce nitro and nitroso compounds, as illustrated for the butyl radical.

$$CH_3(CH_2)_2CH_2 + NO \rightarrow CH_3(CH_2)_2CH_2NO$$

$$CH_3(CH_2)_2CH_2 + NO_2 \rightarrow CH_3(CH_2)_2CH_2NO_2$$

$$CH_3(CH_2)_2CH_2 + NO_2 \rightarrow CH_3(CH_2)_2CH_2ONO$$

Neither the nitroso nor the nitro compounds are end products of the oxidation. These substances are converted in reactions with sodium hydroxide and water into alcohols, aldehydes, ketones, and nitriles. These compounds either evolve from the waste or are converted to the familiar sodium carboxylates including sodium formate, acetate, and sodium oxalate.

L4.3 NITRITE AND NITRATE ESTERS

Linear alkyl nitrates ranging from methyl nitrate to 1-decyl nitrate have been tentatively identified in some tanks. The wastes also contain methyl and 1-butyl nitrite. These compounds are formed in part by the processes described in the previous paragraphs. The reactions of the alcohols with nitric oxide and nitrogen dioxide provide alternative pathways for their formation. It has been known for many years that hydroxide ion reacts with nitrogen trioxide and nitrogen tetraoxide to form nitrous and nitric acid.

$$HO^- + ONONO \rightarrow HONO + ONO^-$$

$$HO^- + O_2NONO \rightarrow HONO_2 + ONO^-$$

Similar reactions with the alkoxide ions, RO^-, which are in equilibrium with the alcohols, ROH, are therefore plausible pathways for the formation of nitrite and nitrate esters. The concept that these substances are formed by the reactions of the alcohols is compatible with the fact that butyl nitrate and butyl nitrite are especially prevalent. These two substances result from the reactions of 1-butanol, the abundant product of hydrolysis of the butylphosphates.

$$ROH + HO^- \rightarrow RO^- + H_2O$$

$$RO^- + ONONO \rightarrow RONO + ONO^-$$

$$RO^- + O_2NONO \rightarrow RONO_2 + ONO^-$$

Another reaction pathway for the formation of the nitrate esters involves the reactions of hydroperoxy radical with nitrous oxide and the subsequent rearrangement of the peroxy nitrite ester into the nitrate ester.

$$R + O_2 \rightarrow RO_2$$

$$RO_2 + NO \rightarrow ROONO$$

$$ROONO \rightarrow RONO_2$$

The alkyl esters react with water and hydroxide ion to reform the alkoxide ions and the alcohols.

$$RONO + HO^- \rightarrow RO^- + HONO$$

$$RONO_2 + HO^- \rightarrow RO^- + HONO_2$$

$$RO^- + H_2O \rightarrow ROH + HO^-$$

The chemistry creates a dynamic reaction system that leads to the continuous formation and decomposition of alcohols and inorganic esters. Many different factors, including the rates of competing reaction that consume oxygen and the organic radicals, as well as the nitrogen oxides prevent the definition of the relative importance of the different reaction pathways for the formation and decomposition of the nitrite and nitrate esters. However, it is evident that the concentrations of these volatile molecules, whether alcohols or esters, are continuously reduced as they react with water or evolve into the dome space.

L4.4 NITRO COMPOUNDS

2-Methyl-2-nitropropane is present in the waste together with lesser amounts of nitromethane, nitroethane, 1-nitropropane, 2-nitropropane, 1-nitrobutane, and 2-nitrobutane.

The primary and secondary aliphatic nitro compounds, those compounds with one or two hydrogen atoms bonded to the carbon atom bonded to the nitro group, are produced during recombination reactions between the alkyl radicals and

nitrogen dioxide as already discussed. These nitro compounds react with water to produce aldehydes and ketones and nitrous oxide as illustrated for 1- and 2-nitrobutane. The balanced equations for the reactions are shown.

$$2\ CH_3(CH_2)_2CH_2NO_2 \rightarrow 2\ CH_3(CH_2)_2CHO + HON{=}NOH$$

$$2\ CH_3CH_2CH(NO_2)CH_3 \rightarrow 2\ CH_3CH_2COCH_3 + HON{=}NOH$$

$$HON{=}NOH \rightarrow H_2O + N_2O$$

The actual pathway for the formation of nitrous oxide is more complex and plausible reaction sequences for its formation have been discussed by Stock and Pederson (1997) and Camaioni et al. (1998).

There is an important distinction between the reactions of the nitrite and nitrate esters and the reactions of the aliphatic nitro compounds: the reactions of the reactions of the C-nitro compounds to give aldehydes and ketones are not reversible and the aldehydes and ketones do not reform nitro compounds.

The more frequent appearance of 2-nitro-2-methylpropane in the waste is readily explained because this tertiary nitro compound,

$$(CH_3)_3CNO_2$$

cannot directly form an aldehyde or ketone in a simple hydrolysis reaction. Consequently, this tertiary compound is decomposed more slowly than the primary and secondary nitro compounds.

L4.5 AROMATIC NITRO COMPOUNDS

Only four aromatic nitro compounds have been detected. These substances are less abundant than the aliphatic nitro compounds and the nitrate and nitrite esters because the conditions for their formation are very unfavorable. First, the concentrations of aromatic hydrocarbons are very low. Second, the alkaline and aqueous environments in the tanks prevent conventional electrophilic substitution reactions. Third, the modest rate constants for the reaction between benzene and nitrogen dioxide coupled with the very low concentrations of the aromatic compounds and nitrogen dioxide, which is competitively consumed in other reactions, obviate the formation of these substance through free radical substitution reactions. Fourth, the formation of aromatic nitro compounds during multistep cyclization reactions converting paraffinic hydrocarbons into aromatic compounds are inefficient because the unsaturated intermediates are preferentially oxidized to aldehydes, ketones, and carboxylates.

L4.6 ENERGY CONTENT OF INTERMEDIATE COMPOUNDS

Burger (1995) calculated the thermodynamic heat of reaction for the oxidation of organic complexants, selected remnants, and simple carboxylate ions by sodium nitrite and sodium nitrate in alkaline solution. His approach

could not be used for the evaluation of the heat of reaction of many intermediates formed from the hydrocarbons and the phosphate esters because the required thermodynamic data are not available.

In these circumstances, scientists and engineers have frequently used linear free energy relationships such as the Benson group increment approach for the evaluation of the physical and chemical properties of substituted organic molecules (Benson 1976, Lowry and Richardson 1987, March 1992). A variant of this approach has been applied to estimate the energy contents of the intermediates formed from complexants (Stock 1998).

The same approach will be used here to estimate the change in thermodynamic heat of reaction resulting from the replacement of a hydrogen atom in a solvent molecule by nitro and nitroso groups. Specifically, it is postulated that the difference in the heat content of an intermediate and the compound from which it was formed can be estimated with sufficient accuracy by comparing the difference in the heat content resulting from the introduction of the same substituent group into a simple molecule for which accurate data are available. To illustrate, the difference in the heat of oxidation of nonane and 1-nitrononane is equated to the difference in the heat of reaction of methane and nitromethane or ethane and nitroethane.

{[Heat of Oxidation of $C_9H_{19}NO_2$] - [Heat of Oxidation of C_9H_{20}]]}
is approximately equal to

{[Heat of Oxidation of CH_4] - [Heat of Oxidation of CH_3NO_2]}

and to

{[Heat of Oxidation of CH_3CH_3] - [Heat of Oxidation of $CH_3CH_2NO_2$]}

The approach is most accurate when the structural change is modest, as it is for substitution reactions, where, as in this illustration, a nitro group is substituted for a hydrogen atom in each case.

The necessary thermochemical information is available for the nitric acid oxidation reaction leading to carbon dioxide and nitrous oxide and this reaction was employed to model the nitrate ion-oxidation (Stock 1998).

$$4CH_3CH_3 + 14HNO_3 \rightarrow 8CO_2 + 7N_2O + 13H_2O$$

The accuracy of the approach was examined in several ways. First, Camaioni et al. (1995) showed that the heat of nitrate ion-oxidation of the organic complexants in alkaline solution evaluated by Burger (1995) were linearly related with the heat of oxidation of the same substances with oxygen in the gas phase. Second, the heat of oxidation of ethane by nitric acid for the reaction shown in the equation was compared with the heat of reaction for the same reaction with nitrate ion in alkaline solution.

$$4CH_3CH_3(g) + 14NaNO_3(aq) + 2NaOH\ (aq) \rightarrow 8Na_2CO_2(aq) + 7N_2O(g) + 13H_2O(1)$$

The heat of oxidation is -1216 kJ/mole for the liquid phase reaction compared to -1246 kJ/mole for the gas phase reaction. Similarly, the heat of

the oxidation reactions of ethanol and acetaldehyde in alkaline aqueous systems with sodium nitrate and in the gas phase with nitric acid were evaluated. The differences between the heat of reaction of ethane, ethanol and acetaldehyde in the gas and liquid phases are small compared to the difference in the heat of oxidation of ethane to ethanol and ethanol to acetaldehyde.

The observations for derivatives of methane and ethane are assembled in Tables L-8 and L-9.

Table L-8. Heat of Nitric Acid Oxidation of Methane and Ethane and Their Oxidized Derivatives in kJ/Mole at 300 °K in the Gas Phase.[1]

Compound	Heat	Compound	Heat
Methane	-693	Ethane	-1,246
Methanol	-594	Ethanol	-1,113
Methanal	-472	Ethanal	-858
Formic acid	-230	Acetic acid	-727
		Oxalic acid	-269
Carbon dioxide	0	Carbon dioxide	0

Note: [1]Stock (1998)

Table L-9. Heat of Nitric Acid Oxidation of Nitroso and Nitro Derivatives of Methane in kJ/Mole at 300 °K in the Gas Phase.

Compound	Heat	Compound	Heat
Methane	-693	Methane	-693
Nitrosomethane	-700	Methyl Nitrite	-595
Nitromethane	-586	Methyl Nitrate	-570
Trinitromethane	-521		
Tetranitromethane	-460		

The results in Table L-8 reaffirm the generally agreed upon viewpoint that oxidation reduces the energy content of organic substances in a systematic manner. The heat content of the organic molecule is reduced by more than 100 kJ/mole by oxidation of the hydrocarbon to the alcohol and by oxidation of the alcohol to the aldehyde, and by even larger amounts by oxidation of the aldehyde to the acid and the acid to carbon dioxide. The introduction of a hydroperoxy, peroxy, alkoxy, amido, or cyano group either has no influence or reduces the heat of the oxidation reaction (Stock 1998).

The replacement of a hydrogen atom by an amino group to form an alkyl amine increases the energy content as a consequence of the introduction of the additional, energetic nitrogen-hydrogen bonds (Stock 1998).

The changes resulting from the substitution of an electronegative nitro or nitroso group for a hydrogen atom are explored in Table L-9. The heat of oxidation of nitrosomethane and nitrosoethane are unchanged from the heat of oxidation of the parent hydrocarbons. The heat of oxidation of the methyl esters of nitric and nitrous acid are smaller than the heat of oxidation of the unsubstituted compound. Nitromethane has a smaller heat of oxidation than methane. This reduction is anticipated because the oxidative reaction leads to the replacement of a fuel-rich carbon-hydrogen unit by a relatively fuel-poor carbon-nitrogen group unit.

The ongoing interest in the role of C-nitro compounds in the waste prompted the consideration of the consequences of the substitution of several carbon-hydrogen bonds with nitro groups. The heat of oxidation for the compounds with one, three and four C-nitro groups in Table L-9 show the successive replacement of hydrogen systematically decreases the fuel value of these compounds.

The heat of oxidation of benzene and toluene and their nitrated derivatives are presented in Table L-10.

Table L-10. Thermodynamic Heat of Nitric Acid Oxidation of Benzene and Toluene and Their Nitrated Derivatives in kJ/Mole at 300 °K in the Gas Phase.

Compound	Heat	Compound	Heat
Benzene	-2,770	Toluene	-3,300
Nitrobenzene	-2,650	4-Nitrotoluene	-3,170
1,3-Dinitrobenzene	-2,530	2,4,6-Trinitrotoluene	-3,000
1,3,5-Trinitrobenzene	-2,430		

The thermodynamic results, which are based upon the known heat of formation of these compounds, indicate that the replacement of a carbon-hydrogen bond in benzene and toluene by a nitro group reduces the energy content of the molecule by between 100 and 130 kJ/mole. The successive replacement of carbon-hydrogen bonds reduces the energy content of the molecules.

The results indicate that the heat of the nitrate ion-oxidation of intermediate compounds should be smaller than the heat of reaction of the original paraffinic hydrocarbons and phosphate esters. The fuel content of the waste is systematically decreased during the aging process by the formation of oxidized products and the release of the lower molecular compounds from the waste together with hydrogen and ammonia.

L5.0 SUMMARY

The aqueous wastes from plant operations that contained organic solvents were made alkaline and distributed to the tanks. The organic solvents that were included in these wastes, principally normal paraffin hydrocarbons, tributyl phosphate and sodium bis(2-ethylhexyl)phosphate, evaporate, react with water, and oxidize under the influence of radiation.

The results of characterization work on samples of the organic liquids retained in the wastes and samples of volatile organic compounds from the dome space indicate that aging diminishes the concentrations of the hydrocarbons and phosphate esters. The aging processes occur concurrently with evaporation and, in some wastes, the evaporation of the hydrocarbons is more rapid than the hydrolysis of tributyl phosphate. In other instances, the rate of hydrolysis of tributyl phosphate is more rapid than the evaporation of the hydrocarbons. The investigations of the volatile organic compounds retained in tanks 241-C-106 and 241-SY-101 indicate radiolysis produces new volatile organic compounds including fragmented alkanes and oxidized families of alkenes, alcohols, aldehydes, ketones, and nitriles.

The analysis of the volatile organic compounds in the dome spaces of the single-shell tanks establish that the tanks contain the same broad families of compounds. The distribution is dictated by the fact that normal paraffinic hydrocarbons and tributyl phosphate were used in PUREX operations and together with sodium bis(2-ethylhexyl)phosphoric acid for strontium separations. As a result, the NPH and TBP are widely distributed and these two substances are primarily responsible for the volatile organic compounds in the dome spaces. Differences arise when sodium bis(2-ethylhexyl)phosphate is present because this substance provides additional heptanes, heptenes, and heptanones. Differences also arise when nitrogen-containing organic complexants are present. Although there are variations, the compounds observed in the dome spaces indicate the original constituents are fragmented, hydrolyzed, and oxidized.

Laboratory work has established the principal pathways. The NPH are decomposed by radiolysis to form lower molecular weight alkanes and oxidized to alkenes, alcohols, aldehydes, ketones, and nitriles. As these reactions proceed, the molecular dimensions are reduced and the reaction products become more soluble and more volatile. The intermediates and the reaction products are more mobile than the original hydrocarbons and continuously evolve from the waste into the dome space.

TBP undergoes hydrolysis and radiolysis. Hydrolysis yields 1-butanol, which is partially soluble in the aqueous waste and evolves into the dome space. Radiolysis leads to an array of products including DBP, MBP, and oxidized mono- and dialkylphosphates as well as low molecular weight alkanes, alkenes and related compounds.

Sodium bis(2-ethylhexyl)phosphate, which is insoluble in aqueous waste, reacts very slowly with water. Radiolysis is the main pathway for its decomposition. The radiolysis gives heptanes, heptenes, heptanones and 1-, 2-, and 3-heptenes and lower molecular weight alkanes, cycloalkanes, alkenes, alcohols, aldehydes, ketones, and nitriles.

The organic intermediates are either dissolved in the aqueous phase or in the organic phase. In either circumstance, they are present at very low concentrations in water or are minor constituents of a complex mixture of organic substances.

The laboratory work and the field work show that organic nitro and nitroso compounds are involved in the oxidation reactions. Compounds of this kind have been detected in the dome space of 60 tanks, somewhat more than 50 percent of the tanks that have been sampled. About 30 different aliphatic and aromatic nitro and nitroso compounds have been tentatively identified. N-Nitrosodimethylamine appears in 15 tanks. Nitrate esters are present in 40 tanks, and methyl and butyl nitrite are present in 15 tanks. Aliphatic nitro compounds have been detected in 25 tanks and one sample contains trinitrofluoromethane. Four nitrobenzenes have been identified. However, no dinitroalkanes or dinitrobenzenes have been found.

The nitro and nitroso compounds and the nitrate and nitrite esters are intermediates in the oxidation reactions. Like the other organic compounds they are dispersed throughout the waste and distributed among the condensed aqueous and organic phases. These substances, which are thermodynamically less energetic than the compounds from which they are formed, are produced by radiolysis, and either evaporate from the waste together with the other volatile organic compounds or react with water to give alcohols, aldehydes, ketones, and nitriles.

L6.0 REFERENCES

Bartley, P. L., G. T. Duckelow, M. J. Klem, and J. A. Reddick, 1996, *Tank 241-C-103 Systems Engineering Study: Separable Organic Phase, Skimming, Storage, Treatment and Disposal Options*, WHC-SD-WM-ES-384, Rev. 0, Westinghouse Hanford Company, Richland, Washington.

Benson, S. W., 1976, *Thermochemical Kinetics*, Second Edition, John Wiley and Sons, New York, New York.

Bugaenko, L. T., M. G. Kuzmin, and L. S. Polak, 1993, *High Energy Chemistry*, Ellis Horwood PTR Prentice Hall, New York.

Burger, L. L., 1955, *The Chemistry of Tributyl Phosphate: A Review*, HW-40910, Hanford Atomic Products Operation, Richland, Washington.

Burger, L. L., 1995, *Calculation of Reaction Energies and Adiabatic Temperatures for Waste Tank Reactions*, PNL-8557, Rev. 1, Pacific Northwest Laboratory, Richland, Washington.

Camaioni, D. M., S. A. Samuels, S. A. Clauss, W. D. Lenihan , K. L. Wahl, J. A. Campbell, and W. J. Shaw, 1995, *Organic Tank Safety Program Waste Aging Studies*, PNL-10794, Pacific Northwest Laboratory, Richland, Washington.

Camaioni, D. M., W. D. Samuels, S. A. Clauss, A. K. Sharma, and K. L. Wahl, 1996, *Alkaline Hydrolysis of Simulated Tank 241-C-103 Separable Organic Phase*, Letter Report OT: 040896, Pacific Northwest National Laboratory, Richland, Washington.

Camaioni, D. M., W. D. Samuels, J. C. Lenihan, S. T. Sharma, A. K. Autrey, M. A. Lilga, M. O. Hogan, S. A. Clauss, K. L. Wahl, and J. A. Campbell, 1998, *Organic Tanks Safety Program Waste Aging Studies Final Report*, PNNL-11909, Pacific Northwest National Laboratory, Richland, Washington.

Campbell, J. A. and G. M. Mong, 1999, *Analysis of Components in Hanford Waste Tanks*, J. Rad. Nuc. Anal. Chem., In press.

Campbell, J. A., S. A. Clauss, K. E. Grant, V. Hoopes, B. D. Lerner, R. B. Lucke, G. M. Mong, J. K. Rau, R. Steele, and K. L. Wahl, 1994, *Waste Tank Organic Safety Program Analytical Methods Development: FY 1994 Progress Report*, PNNL-10128, Pacific Northwest National Laboratory, Richland, Washington.

Campbell, J. A., M. Bean, K. L. Wahl, G. M. Mong, K. E. Bell, K. B. Werner, A. D. Rice, R. J. Ray, D. B. Bechtold, B. R. Wels, R. W. Schroeder, J. W. Ball, B. D. Valenzuela, J. M. Frye, S. L. Fitzgerald, P. P. Bachelor, B. Griffin, R. K. Fuller, A. B. Benally, and S. M. Parong, 1995, *Waste Tank Analytical Safety Project. Analysis of Samples from Hanford Waste Tanks 241-C-102, 241-BY-108, and 241-C-103*, PNNL-10531, Pacific Northwest National Laboratory, Richland, Washington.

Campbell, J. A., K. L. Wahl, S. A. Clauss, K. E. Grant, V. Hoopes, G. M. Mong, J. Rau, and R. Steele, 1996a, *Organic Tanks Safety Program: Advanced Organic Analysis FY 1996 Progress Report*, PNNL-11309, Pacific Northwest National Laboratory, Richland, Washington.

Campbell, J. A., S. A. Clauss, K. E. Grant, V. Hoopes, G. M. Mong, J. Rau, R.Steele, and K. H. Wahl, 1996b, *Flammable Gas Safety Program: Actual Waste Organic Analysis FY 1996 Progress Report*, PNNL-11307, Pacific Northwest National Laboratory, Richland, Washington.

Cox, J. R., Jr., and O. B. Ramsey, 1964, *Mechanisms of Nucleophilic Substitution in Phosphate Esters*, Chemical Reviews, 64, 317.

Davis, W., Jr., 1984, *Radiolytic Behavior in Science and Technology of Tributyl Phosphate*, W. W. Schultz and J. D. Navratil, editors, Volume I, CRC Press, Boca Raton, Florida.

Evans, J. A., A. V. Mitroshkov, and L. A. Mahonney, 1999, *SY-101 Retained Gas Vapor GC/MS Analysis*, TWS99.31, Pacific Northwest National Laboratory, Richland, Washington.

Gyorgy, I., 1981, *Aliphatic Hydrocarbons in Radiation Chemistry of Hydrocarbons*, G. Foldiak, editor, Elsevier Scientific Publishing Company, Amsterdam.

Huckaby, J. L., and D. S. Sklarew, 1997, *Screening for Organic Solvents in Hanford Waste Tanks Using Organic Vapor Concentrations*, PNNL-11688, Pacific Northwest National Laborabory, Richland, Washington.

Jenkins, R. A., A. B. Dinal, C. E. Huggins, C. Y. Ma, J. T. Skeen, and R. R. Smith, 1994, *Analysis of Tank 241-C-103 Headspace Components from Sampling Job 7b*, Oak Ridge National Laboratory, Oak Ridge, Tennessee.

Lowry, T. H. and K. S. Richardson, 1987, *Mechanism and Theory in Organic Chemistry*, Third Edition, Harper and Row Publishers, New York, New York.

March J., 1992, *Advanced Organic Chemistry: Reactions, Mechanisms, and Structure*, Fourth Edition, John Wiley and Sons, New York, New York.

Meacham, J. E., W.L. Cowley, A. B. Webb, N. W. Kirch, J. A. Lechelt, D. A. Reynolds, L. A. Stauffer, D. M. Camaioni, F. Gao, R. T. Hallen, P. G. Hessler, J. L. Huckaby, R. D. Scheele, C. S. Simmons, J. J. Toth, D. B. Bechtold, and L. M. Stock, 1998, *Organic Complexant Topical Report*, HNF-SD-CN-058, Rev. 0, Duke Engineering and Services Hanford, Inc. for Fluor Daniel Hanford, Inc., Richland, Washington.

Meisel, D., C. D. Jonah, S. Kapoor, M. S. Matheson, and M. C. Sauer, Jr., 1993, *Radiolytic and Radiolytically Induced Generation of Gases from Synthetic Wastes*, ANL-93/43, Argonne National Laboratory, Argonne, Illinois.

Meisel, D., A. Cook, D. M. Camaioni, and T. Orlando, 1997, *Chemistry, Radiation, and Interfaces in Suspensions of Nuclear Waste Simulants*, in Proceedings of the Joint International Meeting of the Electrochemical Societies, Paris, France, August 31-Sept. 5, 1997.

McVeely, B. D., T. W. Clauss, M. W. Ligotke, K. H. Pool, R. B. Lucke, G. S. Klinger, J. S. Young, M. McCulloch, J. S. Frichter, and S. C. Goheen, 1995, *Vapor Space Characterization of Waste Tank 241-BY-108: Results from Samples Collected on 10/27/94*, PNL-10495, Pacific Northwest Laboratory, Richland, Washington.

Pool, K. H., and R. M. Bean, 1994, *Waste Tank Organic Safety Project, Analysis of Liquid Samples for Hanford Waste Tank 241-C-103*, PNL-9403, Pacific Northwest Laboratory, Richland, Washington.

Spinks, J. W. T., and R. J. Woods, 1990, *An Introduction to Radiation Chemistry*, John Wiley and Sons, Inc., New York, New York.

Stauffer, L. S., and L. M. Stock, 1999, *Origins of Volatile Organic Compounds Emerging from Tank 241-C-106 during Sluicing*, HNF-4261, Rev. 0, Lockheed Martin Hanford Corp., Richland, Washington.

Stock, L. M., 1998, "The Energy Content of Intermediate Organic Compounds," *Organic Tanks Safety Program Waste Aging Studies Final Report*, Appendix C, PNNL-11909, Pacific Northwest National Laboratory, Richland, Washington.

Stock, L. M., and Pederson L. R., 1997, *Chemical Pathways for the Formation of Ammonia in Hanford Waste*, PNNL-11702, Pacific Northwest National Laboratory, Richland, Washington.

Tabata, Y., Y Ito, and S. Tagawa, 1991, *Handbook of Radiation Chemistry*, CRC Press, Boca Raton, Florida.

Wolfenden, R., C. Ridgeway, and G. Young, 1998, *Spontaneous Hydrolysis of Ionized Phosphate Monoesters and Diesters and the Proficiencies of Phosphatases and Phosphodiesterases*, J. Am. Chem. Soc., 120, 833.

INFORMATION CLEARANCE REVIEW AND RELEASE APPROVAL

Part I: Background Information

Title: Organic Solvent Topical Report

Information Category:
- ☐ Abstract ☐ Journal Article ☐ Summary
- ☐ Internet ☐ Visual Aid ☐ Software
- ☐ Full Paper ☑ Report ☐ Other

Publish to OSTI? ☐ Yes ☑ No

Trademark/Copyright "Right to Use" Information or Permission Documentation	Yes	NA
	☐	☑

Document Number: HNF-4240 Revision 1 Date: June 2000

Author: Tabor, Cindy L

Part II: External/Public Presentation Information

Conference Name:

Sponsoring Organization(s): WRPS

Date of Conference: Conference Location:

Will Material be Handed Out? ☐ Yes ☑ No Will Information be Published? ☐ Yes ☑ No *(If Yes, attach copy of Conference format instructions/guidance.)*

Part III: WRPS Document Originator Checklist

Description	*Yes*	*N/A*	*Print/Sign/Date*
Information Product meets requirements in TFC-BSM-AD-C-01?	☐	☑	
Document Release Criteria in TFC-ENG-DESIGN-C-25 completed? (Attach checklist)	☐	☑	
If product contains pictures, safety review completed?	☐	☑	

Part IV: WRPS Internal Review

Function	*Organization*	*Date*	*Print Name/Signature/Date*
Subject Matter Expert	WRPS	08/10/2020	Tabor, Cindy L Approved - IDMS data file att.
Responsible Manager	WRPS	08/04/2020	Rutland, Paul L Approved - IDMS data file att.
Other:			

Part V: IRM Clearance Services Review

Description	*Yes*	*No*	*Print Name/Signature*
Document Contains Classified Information?	☐	☒	If Answer is "Yes," ADC Approval Required Print Name/Signature/Date
Document Contains Information Restricted by DOE Operational Security Guidelines?	☐	☒	Reviewer Signature: Print Name/Signature/Date
Document is Subject to Release Restrictions? *If the answer is "Yes," please mark category at right and describe limitation or responsible organization below:*	☐	☒	Document contains: ☐ Applied Technology ☐ Protected CRADA ☐ Personal/Private ☐ Export Controlled ☐ Proprietary ☐ Procurement – Sensitive ☐ Patentable Info. ☐ OUO ☐ Predecisional Info. ☐ UCNI ☐ Restricted by Operational Security Guidelines ☐ Other (Specify)
Additional Comments from Information Clearance Specialist Review?	☐	☒	Information Clearance Specialist Approval APPROVED By Sarah Harrison at 1:35 pm, Aug 20, 2020 Print Name/Signature/Date

When IRM Clearance Review is Complete – Return to WRPS Originator for Final Signature Routing (Part VI)

INFORMATION CLEARANCE REVIEW AND RELEASE APPROVAL

Part VI: Final Review and Approvals

Description	*Approved for Release*		*Print Name/Signature*	
	Yes	*N/A*		
WRPS External Affairs	☒	☐	Mc Cune, Hal C	Approved - IDMS data file att.
WRPS Office of Chief Counsel	☒	☐	Roden, Mari L	Approved - IDMS data file att.
DOE – ORP Public Affairs/Communications	☒	☐	Levardi, Yvonne M / Tyree, Geoff T	Approved - IDMS data file att.
Other: ORP OCC	☒	☐	King, Grace J	Approved - IDMS data file att.
Other: ORP SME	☒	☐	Blackwell, Becky	Approved - IDMS data file att.

Comments Required for WRPS-Indicate Purpose of Document:

This report provides the basis for closing the organic solvent safety issue. Sufficient information is presented to conclude that risk posed by an unmitigated organic solvent fire is within risk evaluation guidelines. Added descriptive narrative to pages 2-1 and 5-29 to close comments from Oregon State Department of Ecology. Reprinted entire document and issued as Rev. 1.

APPROVED
By Sarah Harrison at 1:35 pm, Aug 20, 2020

Approved for Public Release; Further Dissemination Unlimited

Information Release Station

Was/Is Information Product Approved for Release? ☒ Yes ☐ No

If Yes, what is the Level of Releaser? ☑ Public/Unrestricted ☐ Other (Specify) _____

Date Information Product Stamped/Marked for Release: 08/20/2020

Was/Is Information Product Transferred to OSTI? ☐ Yes ☒ No

Forward Copies of Completed Form to WRPS Originator

```
- <workflow name="(SEH) Normal - HNF-4240 Rev1" id="266084640">
  - <task name="Clearance Process" id="0" date-initiated="20200804T1511"
      performer="Sarah E Harrison" performer-id="252341659"
      username="h5635746">
      <comments>Due Tuesday August 18th 2020 - COB Please approve the
        Organic Solvent Topical Report, Revision 1, submitted by Cindy Tabor for
        public external release. Thank you, Sarah Harrison Information
        Clearance</comments>
    </task>
    <task name="Add XML" id="1" date-done="20200804T1511" />
    <task name="Manager Approval" id="41" date-due="20200807T1511" date-
      done="20200804T1603" performer="Paul L Rutland" performer-id="140633218"
      username="h4494439" disposition="Approve" authentication="true" />
    <task name="Document Reviewer2" id="53" date-due="20200807T1603" date-
      done="20200806T0636" performer="Mari L Roden" performer-id="262637370"
      username="h0048955" disposition="Public Release" authentication="true" />
    <task name="Document Reviewer1" id="54" date-due="20200807T1603" date-
      done="20200806T1043" performer="Hal C Mc Cune" performer-id="226350486"
      username="h7687509" disposition="Public Release" authentication="true" />
    <task name="Document Reviewer3" id="52" date-due="20200807T1603" date-
      done="20200807T1137" performer="Rebecca I Blackwell" performer-
      id="242759597" username="h9138590" disposition="Public Release"
      authentication="true" />
    <task name="Doc Owner Clearance Review" id="13" date-due="20200810T1137"
      date-done="20200810T0709" performer="Cynthia L Tabor" performer-
      id="173738849" username="h6436378" disposition="Send On"
      authentication="true" />
    <task name="Milestone 1" id="24" date-done="20200810T0709" />
    <task name="ORP Document Reviewer2" id="58" date-due="20200812T0709"
      date-done="20200813T1007" performer="Yvonne M Levardi" performer-
      id="185346745" username="h7131303" disposition="Public Release"
      authentication="true" />
    <task name="ORP Document Reviewer1" id="57" date-due="20200812T0709"
      date-done="20200814T1240" performer="Geoff T Tyree" performer-
      id="6158846" username="h0068565" disposition="Public Release"
      authentication="true" />
    <task name="ORP Document Reviewer3" id="59" date-due="20200812T0709"
      date-done="20200819T1254" performer="Grace J King" performer-
      id="211901436" username="h9807759" disposition="Public Release"
      authentication="true" />
    <task name="Doc Owner Reviews ORP Comments" id="61" date-
      due="20200820T1254" date-done="20200819T1327" performer="Cynthia L
      Tabor" performer-id="173738849" username="h6436378" disposition="Send On"
      authentication="true" />
    <task name="Milestone 2" id="62" date-done="20200819T1327" />
    <task name="Verify Doc Consistency" id="4" date-due="20200820T1327" date-
      done="20200820T1327" performer="Sarah E Harrison" performer-
      id="252341659" username="h5635746" disposition="Cleared"
      authentication="true" />
  </workflow>
```